CROSSTALK BETWEEN MEMBRANE LIPID METABOLISM AND BACTERIAL CELL ENVELOPE HOMEOSTASIS

EDITED BY: Heidi Vitrac, Nienke Buddelmeijer, Brian J. Werth, Libin Xu and Adriana E. Rosato

PUBLISHED IN: Frontiers in Molecular Biosciences

frontiers Research Topics

ISSN 1664-8714
ISBN 978-2-88976-014-5
DOI 10.3389/978-2-88976-014-5

About Frontiers

Frontiers is more than just an open-access publisher of scholarly articles: it is a pioneering approach to the world of academia, radically improving the way scholarly research is managed. The grand vision of Frontiers is a world where all people have an equal opportunity to seek, share and generate knowledge. Frontiers provides immediate and permanent online open access to all its publications, but this alone is not enough to realize our grand goals.

Frontiers Journal Series

The Frontiers Journal Series is a multi-tier and interdisciplinary set of open-access, online journals, promising a paradigm shift from the current review, selection and dissemination processes in academic publishing. All Frontiers journals are driven by researchers for researchers; therefore, they constitute a service to the scholarly community. At the same time, the Frontiers Journal Series operates on a revolutionary invention, the tiered publishing system, initially addressing specific communities of scholars, and gradually climbing up to broader public understanding, thus serving the interests of the lay society, too.

Dedication to Quality

Each Frontiers article is a landmark of the highest quality, thanks to genuinely collaborative interactions between authors and review editors, who include some of the world's best academicians. Research must be certified by peers before entering a stream of knowledge that may eventually reach the public - and shape society; therefore, Frontiers only applies the most rigorous and unbiased reviews.
Frontiers revolutionizes research publishing by freely delivering the most outstanding research, evaluated with no bias from both the academic and social point of view. By applying the most advanced information technologies, Frontiers is catapulting scholarly publishing into a new generation.

What are Frontiers Research Topics?

Frontiers Research Topics are very popular trademarks of the Frontiers Journals Series: they are collections of at least ten articles, all centered on a particular subject. With their unique mix of varied contributions from Original Research to Review Articles, Frontiers Research Topics unify the most influential researchers, the latest key findings and historical advances in a hot research area! Find out more on how to host your own Frontiers Research Topic or contribute to one as an author by contacting the Frontiers Editorial Office: frontiersin.org/about/contact

CROSSTALK BETWEEN MEMBRANE LIPID METABOLISM AND BACTERIAL CELL ENVELOPE HOMEOSTASIS

Topic Editors:
Heidi Vitrac, Tosoh Bioscience LLC, United States
Nienke Buddelmeijer, Institut Pasteur, France
Brian J. Werth, University of Washington, United States
Libin Xu, University of Washington, United States
Adriana E. Rosato, Houston Methodist Research Institute, United States

Citation: Vitrac, H., Buddelmeijer, N., Werth, B. J., Xu, L., Rosato, A. E., eds. (2022). Crosstalk Between Membrane Lipid Metabolism and Bacterial Cell Envelope Homeostasis. Lausanne: Frontiers Media SA. doi: 10.3389/978-2-88976-014-5

Table of Contents

04 ***Alteration of Membrane Fluidity or Phospholipid Composition Perturbs Rotation of MreB Complexes in* Escherichia coli**
Keisuke Kurita, Fumiya Kato and Daisuke Shiomi

13 ***Ornithine Lipids in* Burkholderia *spp. Pathogenicity***
Luz América Córdoba-Castro, Rosalba Salgado-Morales, Martha Torres, Lourdes Martínez-Aguilar, Luis Lozano, Miguel Ángel Vences-Guzmán, Ziqiang Guan, Edgar Dantán-González, Mario Serrano and Christian Sohlenkamp

29 ***Eugene P. Kennedy's Legacy: Defining Bacterial Phospholipid Pathways and Function***
William Dowhan and Mikhail Bogdanov

51 ***Dual Regulation of Phosphatidylserine Decarboxylase Expression by Envelope Stress Responses***
Yasmine Hassoun, Julia Bartoli, Astrid Wahl, Julie Pamela Viala and Emmanuelle Bouveret

61 ***Mini Review: Bacterial Membrane Composition and Its Modulation in Response to Stress***
Jessica R. Willdigg and John D. Helmann

72 ***Phenotypic and Multi-Omics Characterization of* Escherichia coli *K-12 Adapted to Chlorhexidine Identifies the Role of MlaA and Other Cell Envelope Alterations Regulated by Stress Inducible Pathways in CHX Resistance***
Branden S. J. Gregorchuk, Shelby L. Reimer, Kari A. C. Green, Nicola H. Cartwright, Daniel R. Beniac, Shannon L. Hiebert, Timothy F. Booth, Patrick M. Chong, Garrett R. Westmacott, George G. Zhanel and Denice C. Bay

92 ***Varied Contribution of Phospholipid Shedding From Membrane to Daptomycin Tolerance in* Staphylococcus aureus**
Tianwei Shen, Kelly M. Hines, Nathaniel K. Ashford, Brian J. Werth and Libin Xu

100 ***Synergy Between Beta-Lactams and Lipo-, Glyco-, and Lipoglycopeptides, Is Independent of the Seesaw Effect in Methicillin-Resistant* Staphylococcus aureus**
Rutan Zhang, Ismael A. Barreras Beltran, Nathaniel K. Ashford, Kelsi Penewit, Adam Waalkes, Elizabeth A. Holmes, Kelly M. Hines, Stephen J. Salipante, Libin Xu and Brian J. Werth

111 ***Degradation of Components of the Lpt Transenvelope Machinery Reveals LPS-Dependent Lpt Complex Stability in* Escherichia coli**
Alessandra M. Martorana, Elisabete C. C. M. Moura, Paola Sperandeo, Flavia Di Vincenzo, Xiaofei Liang, Eric Toone, Pei Zhou and Alessandra Polissi

124 ***Cell-Free Expression to Probe Co-Translational Insertion of an Alpha Helical Membrane Protein***
Laura R. Blackholly, Nicola J. Harris, Heather E. Findlay and Paula J. Booth

frontiers in Molecular Biosciences

BRIEF RESEARCH REPORT
published: 24 November 2020
doi: 10.3389/fmolb.2020.582660

Alteration of Membrane Fluidity or Phospholipid Composition Perturbs Rotation of MreB Complexes in *Escherichia coli*

*Keisuke Kurita, Fumiya Kato and Daisuke Shiomi**

Department of Life Science, College of Science, Rikkyo University, Tokyo, Japan

Gram-negative bacteria such as *Escherichia coli* are surrounded by inner and outer membranes and peptidoglycan in between, protecting the cells from turgor pressure and maintaining cell shape. The Rod complex, which synthesizes peptidoglycan, is composed of various proteins such as a cytoplasmic protein MreB, a transmembrane protein RodZ, and a transpeptidase PBP2. The Rod complex is a highly motile complex that rotates around the long axis of a cell. Previously, we had reported that anionic phospholipids (aPLs; phosphatidylglycerol and cardiolipin) play a role in the localization of MreB. In this study, we identified that cells lacking aPLs slow down Rod complex movement. We also found that at higher temperatures, the speed of movement increased in cells lacking aPLs, suggesting that membrane fluidity is important for movement. Consistent with this idea, Rod complex motion was reduced, and complex formation was disturbed in the cells depleted of FabA or FabB, which are essential for unsaturated fatty acid synthesis. These cells also showed abnormal morphology. Therefore, membrane fluidity is important for maintaining cell shape through the regulation of Rod complex formation and motility.

Keywords: bacterial actin, peptidoglycan, anionic phospholipids, membrane fluidity, cell shape

OPEN ACCESS

Edited by:
Heidi Vitrac,
University of Texas Health Science Center at Houston, United States

Reviewed by:
Scot P. Ouellette,
University of Nebraska Medical Center, United States
William Margolin,
University of Texas Health Science Center at Houston, United States

****Correspondence:***
Daisuke Shiomi
dshiomi@rikkyo.ac.jp

Specialty section:
This article was submitted to Cellular Biochemistry, a section of the journal Frontiers in Molecular Biosciences

Received: *13 July 2020*
Accepted: *30 October 2020*
Published: *24 November 2020*

Citation:
Kurita K, Kato F and Shiomi D (2020) Alteration of Membrane Fluidity or Phospholipid Composition Perturbs Rotation of MreB Complexes in Escherichia coli. Front. Mol. Biosci. 7:582660. doi: 10.3389/fmolb.2020.582660

INTRODUCTION

Bacterial cells maintain their own shape such as rod and sphere (Young, 2003). Most bacterial cells are surrounded by peptidoglycan, a macromolecule composed of glycan strands crosslinked by short peptides, which forms the cell wall. Peptidoglycan can be purified, and electron microscopic observation of the purified peptidoglycan indicated that it determines the bacterial shape (de Pedro et al., 1997). Thus, bacterial cells have to correctly synthesize peptidoglycan to maintain cell shape. In some rod-shaped bacteria, peptidoglycan is synthesized by a supramolecular complex called Rod complex or elongasome, which contains various proteins such as a scaffold protein MreB actin, a membrane protein RodZ, a transglycosylase RodA and a transpeptidase PBP2 (den Blaauwen et al., 2008). In the rod-shaped bacterium *Escherichia coli*, peptidoglycan is synthesized at the central cylinder but not at the cell poles (de Pedro et al., 1997). This localized peptidoglycan synthesis is achieved by limited localization of Rod complex at the central cylinder (Ursell et al., 2014; Kawazura et al., 2017).

MreB is structurally and biochemically homologous to actin (van den Ent et al., 2001, 2014) and localizes at the central cylinder in *E. coli* (Ursell et al., 2014; Kawazura et al., 2017). This localization

is important for determination of cell shape and synthesis of peptidoglycan because *E. coli* cells become spherical if they lack MreB (Wachi et al., 1987; Doi et al., 1988; Bendezú and de Boer, 2008) or are treated with A22, which inhibits the assembly of MreB (Iwai et al., 2002; Kawazura et al., 2017). Rod complex or MreB rotates around the long axis of the cell and this rotational motion is coupled with peptidoglycan synthesis (Domínguez-Escobar et al., 2011; Garner et al., 2011 van Teeffelen et al., 2011).

We have shown previously that anionic phospholipids (aPLs: phosphatidylglycerol and cardiolipin), which localize at the cell poles (Mileykovskaya and Dowhan, 2000; Oliver et al., 2014), exclude MreB from cell poles in *E. coli*. Specifically, in the cells lacking aPLs (ΔaPLs), MreB localizes to cell poles as well as to the central cylinder (Kawazura et al., 2017). MreB directly binds to phospholipids through its N-terminal amphipathic helix (Salje et al., 2011). We identified that aPLs could not bind to the assembled form of MreB in the presence of ATP but could bind to a disassembled form of MreB in the absence of ATP (Kawazura et al., 2017). However, detailed molecular mechanism of interaction between MreB and aPLs is still unclear. Thus, the composition of phospholipids affects the localization of MreB (Rod complex), which in turn affects peptidoglycan synthesis (Kawazura et al., 2017). It is known that composition of phospholipids in *E. coli* affects the membrane fluidity (Pluschke and Overath, 1981; Nenninger et al., 2014), which is modulated by the amount of unsaturated fatty acids (Marr and Ingraham, 1962). Interestingly, MreB promotes membrane fluidity and affects membrane protein localization (Strahl et al., 2014). Therefore, we hypothesized that membrane fluidity also affects MreB motion.

In this study, we examined the effects of aPLs on the rotational motion of MreB and identified that aPLs affect not only the localization but also the motion of MreB. We then examined the effect of membrane fluidity on rotational motion of MreB by depleting FabA or FabB protein. When enzymes required for synthesis of unsaturated fatty acids were depleted (encoded by *fabA* or *fabB*), rotational speed of MreB was decreased, suggesting that membrane fluidity affects the rotational speed of MreB.

METHODS

Bacterial Strains and Growth Medium

All strains were derivatives of *E. coli* K-12 and are listed in **Supplementary Table 1**. MG1655 is a wild-type (WT) strain. Cells were grown in L broth (1% bacto-tryptone, 0.5% yeast extract, 0.5% NaCl) or M9 medium (0.6% Na_2HPO_4, 0.3% K_2HPO_4, 0.05% NaCl, 0.1% NH_4Cl, 0.1 mM $MgSO_4{\cdot}7H_2O$) containing 0.25% glucose at 37°C. Kanamycin (Kan; 50 μg/mL), ampicillin (Amp; 100 μg/mL), and chloramphenicol (Cm; 20 μg/mL) were added to the culture medium when necessary.

Strain and Plasmid Constructions

The primers used for strain and plasmid constructions and the plasmids used in this study are listed in **Supplementary Tables 2, 3**. Detailed methods for strain construction were described in **Supplementary Materials**.

Microscopic Observation

Cells were grown to log phase and mounted on a 2% agarose in M9 medium. The cells were observed using an Axio Observer (Zeiss, Oberkochen, Germany), and images were processed using ZEN (Zeiss), Photoshop 2020 (Adobe), and ImageJ. The objective lens was heated by a lens heater (Tokai Hit, Shizuoka, Japan) when necessary. All experiments were repeated two or more times on different days. Analyses of the rotational speed of MreB and RodZ were performed as previously described (Kurita et al., 2019).

Bacterial Two-Hybrid Assays

Bacterial two-hybrid assays were performed as described previously (Shiomi and Margolin, 2007).

SDS-PAGE and Immunoblotting

Cells were grown to log phase and samples were subjected to SDS-polyacrylamide gel electrophoresis and immunoblotting using anti-DDDDK antibody (MBL, Nagoya).

RESULTS

MreB Motion in Cells Lacking aPLs

We have previously reported that aPLs affect the subcellular localization of MreB (Kawazura et al., 2017). However, it is unknown whether aPLs affect the motion of MreB and thus, that of the Rod complex. Before we analyzed MreB rotation in ΔaPLs cells, we examined the growth of WT (RU1184) and ΔaPLs (RU1185) cells at 37°C. ΔaPLs cells (shown by a gray line) (doubling time: 144.4 ± 3.8 min, mean ± SD) grew significantly slower than WT cells (shown by a black line) (doubling time: 28.8 ± 2.4 min) (**Figure 1A**), indicating that the growth rate of ΔaPLs cells is slower than that of WT cells. We hypothesized that the slower growth rate correlated with slower peptidoglycan synthesis, which should be reflected in slower MreB and RodZ movement. To analyze the motion of MreB and RodZ, we simultaneously observed the motion of MreB-mCherry^{SW} and sfGFP (super-folder green fluorescent protein)-RodZ in WT (RU1184) and ΔaPLs cells (RU1185) (**Figures 1B,C**, **Supplementary Movies 1A–D**, and **Supplementary Table 4**). In WT cells (RU1184), MreB (14.0 ± 3.8 nm/s) and RodZ (14.1 ± 4.0 nm/s) were simultaneously rotated around the long axis, whereas in ΔaPLs cells (RU1185), the rotational speeds of both MreB (7.1 ± 4.1 nm/s) and RodZ (8.5 ± 3.8 nm/s) were clearly decreased compared to those in WT cells, suggesting that aPLs affect the motion of MreB and RodZ proteins. It is unclear whether different compositions of phospholipids or other factors, such as improper interaction between MreB and RodZ, reduced peptidoglycan synthesis, or reduced membrane fluidity, affected MreB and RodZ motion according to this result. We showed that the interaction between MreB and RodZ in ΔaPLs cells was comparable to that in WT cells (**Supplementary Figure 1**), suggesting that the decreased motion of MreB and RodZ in ΔaPLs cells may at least not be due to a lack of proper interaction between MreB and RodZ.

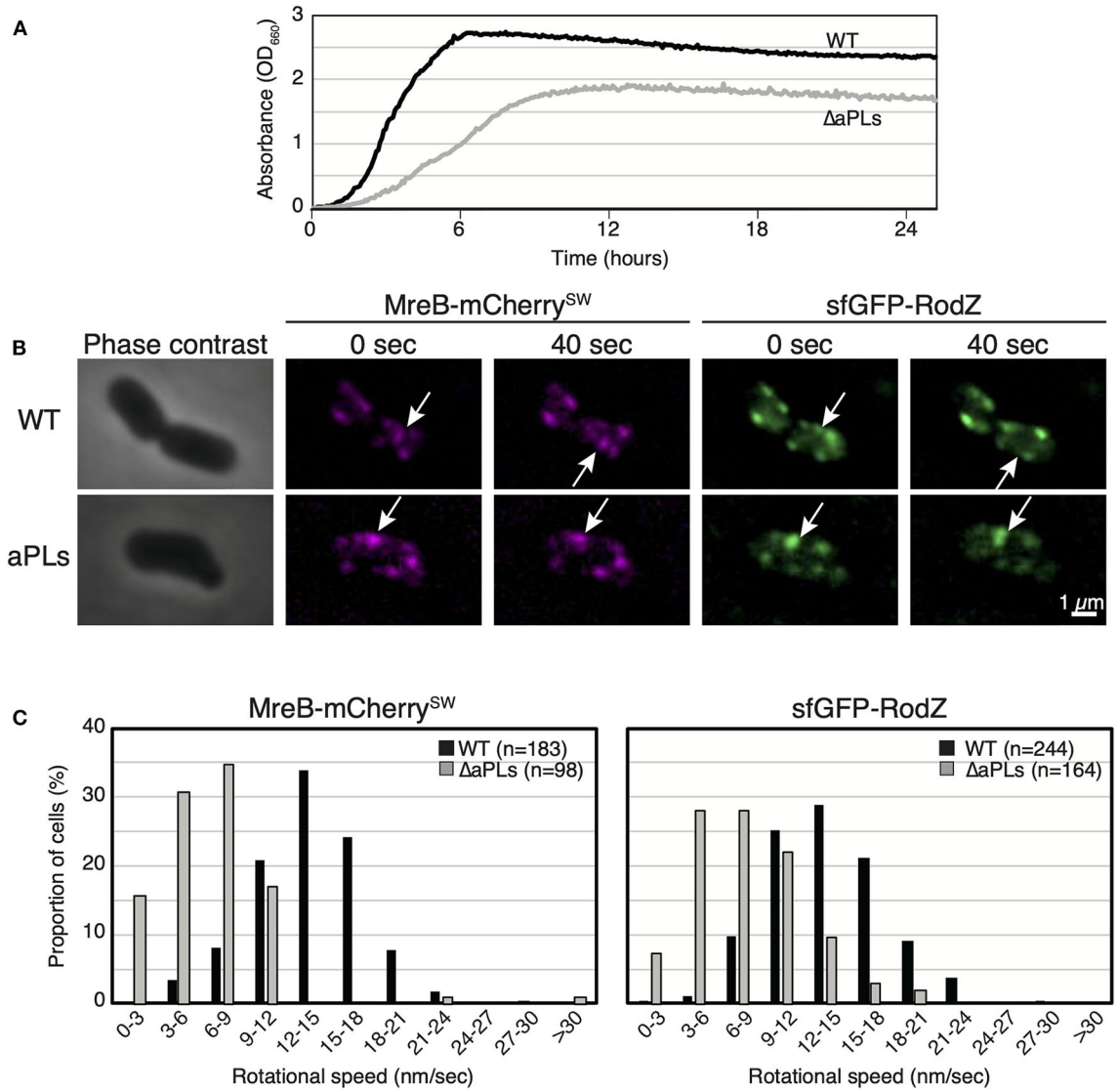

FIGURE 1 | Motion of MreB and RodZ in cells lacking anionic phospholipids (aPLs). **(A)** Growth curves of WT (solid lines) and ΔaPLs (dotted lines) at 37°C. **(B)** Time-lapse images of wild-type (WT) or ΔaPLs cells. Images were taken every 10 s on an M9 agarose pad. Phase-contrast images and fluorescent images are shown. Scale bar: 1 μm. **(C)** Histograms of rotational speeds (nm/s) of MreB and RodZ in WT and ΔaPLs cells. Black and gray bars indicate WT and ΔaPLs, respectively.

MreB Motion in Cells Lacking aPLs at Higher Temperatures

While we were examining MreB motion in the ΔaPLs mutant, we noticed that MreB rotated in the mutant at high temperatures. Thus, we analyzed the effect of temperature on MreB motion in ΔaPLs cells. ΔaPLs cells producing MreB-msfGFP^{SW} were grown to the log phase at 37°C, harvested, and mounted on an M9 agarose pad. We started the observation 5–10 min later, and the temperature was maintained at 28°C. We observed the motion of MreB at 0 and 20 min at 28°C (**Figure 2A**, **Supplementary Movies 2A,B**, and **Supplementary Table 4**). The average speeds of MreB at both time points were 8.0 ± 3.6 and 6.5 ± 2.7 nm/s, respectively. Then, we observed the motion of MreB 20 min after the objective lens was heated by a lens heater to 42°C. The speed of MreB was clearly increased (15.3 ± 6.7 nm/s). Because the increase in temperature should not increase the amount of aPLs in ΔaPLs cells (mutant that lacks the enzymes to synthesize aPLs), the results suggest a lack of aPLs; hence, different compositions of phospholipids are not a direct cause of the reduction in MreB motion. The rate of most biochemical processes generally increases with increasing temperature. In fact, it has been shown that the speed of MreB motion is dependent on temperature (van Teeffelen et al., 2011). We also examined the motion of MreB in WT cells when the temperature was increased and found that the speed of MreB motion increased 20 min after the objective lens was heated to 42°C (20.2 ± 6.3 nm/s) than that at 0 min (10.9 ± 3.7 nm/s) (**Figure 2A** and **Supplementary Table 4**). It is possible that as the temperature

increased, the cell wall synthesis rate increased, and as a result, the rotation speed of MreB increased. Therefore, we examined if growth rate affects the rotational speed of MreB. RU1558 cells producing MreB-msfGFP^{SW} was grown in L or M9 medium at 37°C. Doubling times of cells grown in L and M9 were 28.0 ± 0.6 min and 68.6 ± 1.6 min, respectively. However, the rotational speeds of MreB in rich and poor medium were similar and they were not statistically different (*P*-values was 0.077) under our conditions (19.7 ± 8.7 nm/s for L medium and 17.6 ± 7.3 nm/s for M9 medium) (**Figure 2B**, **Supplementary Movies 3A,B** and **Supplementary Table 4**). This is consistent with previous reports (van Teeffelen et al., 2011; Billaudeau et al., 2017). This result suggest that decreased rate of peptidoglycan synthesis was not the major cause of decreased rotational speed of MreB.

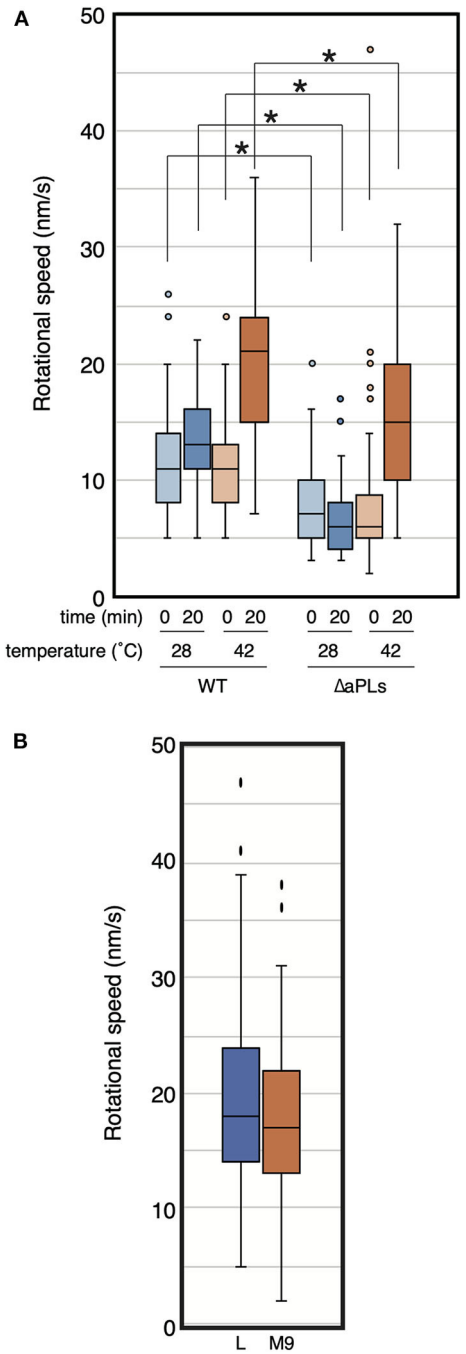

FIGURE 2 | Rotational speed of MreB at different temperatures. **(A)** The distribution of the rotational speed (nm/s) of MreB in WT (RU1558) or ΔaPL (RU1527) cells is shown. The objective lens was heated at the indicated temperature for the indicated time. *P*-values were determined by the unpaired *t*-test. *P*-values < 0.05, shown by asterisks (*), were considered significantly different from each other. **(B)** The distribution of the rotational speed (nm/s) of MreB in WT (RU1558) grown in L or M9 medium at 37°C. The objective lens was heated at 37°C.

Effect of MurG Overproduction on MreB Motion in ΔaPLs

The deletion of enzymes synthesizing cardiolipin (CL) has been shown to result in reduced activity of MurG, a GTase involved in lipid II biosynthesis, thereby causing abnormal

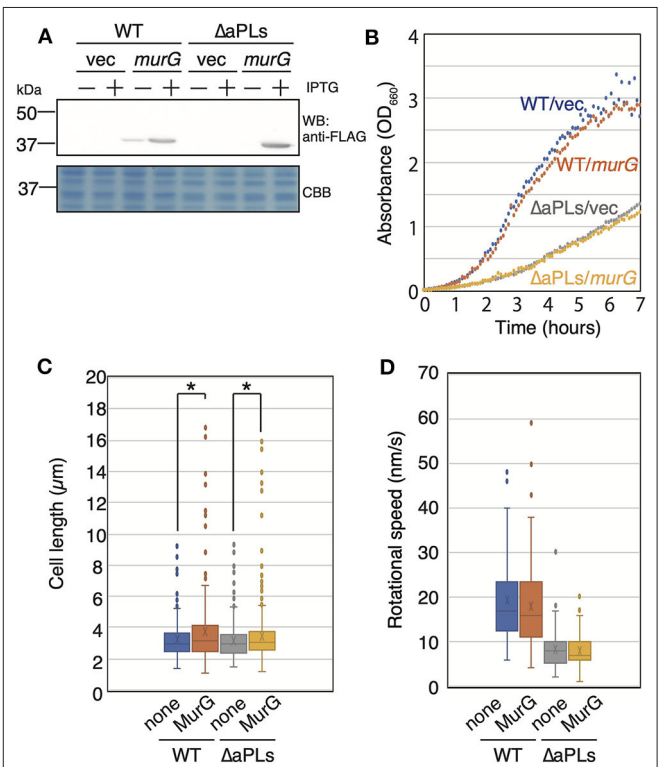

FIGURE 3 | Effect of MurG on the rotation of MreB. **(A)** Protein levels of FLAG-tagged MurG (FLAG-MurG) in WT (MG1655) and ΔaPLs (RU835) cells grown in the absence or presence of 1 mM IPTG. Samples were subjected to SDS-polyacrylamide gel electrophoresis and immunoblotting using the anti-DDDDK (FLAG) antibody. As a loading control, a CBB-stained gel is also shown. **(B)** Growth of WT (MG1655) and ΔaPLs (RU835) cells carrying a vector or a plasmid encoding *flag-murG* at 37°C. **(C)** Cell length of WT (MG1655) and ΔaPLs (RU835) cells carrying a vector (none) or a plasmid encoding *flag-murG* (MurG) grown in the presence of 1 mM IPTG to the log phase at 37°C. *P*-values were determined by the unpaired *t*-test. *P* values < 0.05, shown by asterisks (*), were considered significantly different from each other. **(D)** The distribution of the rotational speed (nm/s) of MreB in WT (RU1558) or ΔaPL (RU1527) cells carrying a vector (none) or a plasmid encoding *flag-murG* (MurG).

cell shape in *Rhodobacter sphaeroides* (Lin et al., 2019). This shape deficiency was restored by MurG overproduction. On the other hand, *murG* expression is upregulated in *E. coli* lacking CL (van den Brink-van der Laan et al., 2003). However, aPLs mutant lacks phosphatidylglycerol (PG) in addition to CL. Thus, it is possible that activity of MurG in ΔaPLs is reduced as in *R. sphaeroides* ΔCL mutant. Therefore, we examined whether MreB rotation was restored in ΔaPLs cells by MurG overproduction (and consequently by restoring peptidoglycan synthesis). If MreB rotation was restored, it is plausible to conclude that decreased MreB rotation was caused by decreased peptidoglycan synthesis in ΔaPLs. First, we cloned FLAG-tagged *murG* in a plasmid and confirmed that MurG was produced in the presence of 1 mM IPTG (**Figure 3A**). Next, we examined whether the overproduction of MurG restored the slow-growth phenotype of ΔaPLs cells and found that MurG overproduction did not improve the slow growth of ΔaPLs (**Figure 3B**). Moreover, MurG overproduction did not promote the growth of WT cells (**Figure 3B**). However, both WT and ΔaPLs cells overproducing MurG (WT: 3.69 ± 2.06 μm, ΔaPLs: 3.46 ± 1.90 μm) were slightly but significantly longer than those carrying a vector plasmid (WT: 3.21 ± 1.14 μm, ΔaPLs: 3.18 ± 1.12 μm) and the numbers of longer WT and ΔaPL cells producing MurG were increased compared to those of control cells (**Figure 3C**), suggesting that peptidoglycan synthesis in both cells was promoted by MurG overproduction. Then, we observed the rotation of MreB in MurG-overproducing cells. As seen in **Figure 3D**, **Supplementary Movies 4A,B**, and **Supplementary Table 4**, MurG overproduction did not increase the rotational rate of MreB in WT (18.0 ± 10.0 nm/s) or ΔaPLs (7.9 ± 3.9 nm/s). These results suggest that the decrease in MreB rotation in ΔaPLs did not result from reduced peptidoglycan synthesis activity but rather from reduced membrane fluidity. In fact, membrane fluidity has been shown to be decreased in ΔaPLs cells (Nenninger et al., 2014). In that study, the authors measured the diffusion coefficient of BODIPY FL-C_{12} in WT and ΔaPLs cells and showed that it is decreased in ΔaPLs (0.66 ± 0.22 μm^2/s) compared with that in WT (1.2 ± 0.3 μm^2/s). Therefore, we hypothesized that the cause of the decrease in the motion of MreB in ΔaPLs cells was the decrease in the membrane fluidity. Thus, we next examined the effect of membrane fluidity on MreB motion.

Effect of Membrane Fluidity on MreB Motion

The amount of unsaturated fatty acids is related to membrane fluidity (Marr and Ingraham, 1962). FabA and FabB are essential proteins to synthesize unsaturated fatty acids (Feng and Cronan, 2009). Moreover, it was recently shown that the depletion of FabB reduces membrane fluidity (Budin et al., 2018).

We first constructed a strain in which the expression of the *fabA* gene is controlled by arabinose to change the membrane fluidity under a constant temperature. The growth of the strain was dependent on arabinose (**Supplementary Figure 2A**), confirming that FabA is essential for viability. This result is consistent with previous reports that unsaturated fatty acids, which comprise at least 15–20% of total phospholipids, are required for growth (Cronan and Gelmann, 1973). Cells were grown in the presence of arabinose overnight, and the culture was diluted with fresh medium either in the presence (+FabA, shown by orange dots) or absence of arabinose (–FabA, shown by blue dots) (**Supplementary Figure 2A**). Then, we examined the cell shape of FabA-depleted cells in the presence and absence of arabinose at around 3 h (shown by a gray bar) (**Supplementary Figure 2B**). WT (MG1655) cells hardly exhibited any abnormal shapes such as bends (only in 1.7% of the cells, i.e., 9/553 cells). However, FabA-depleted cells grown in the absence of arabinose exhibited abnormal shapes such as bends in 29% of the cells (48/168 cells). We measured the length and width of FabA-depleted cells grown in the absence and presence of arabinose (**Supplementary Figure 2C**) and found that cell widths significantly increased when cells were grown in the absence of arabinose compared with those grown with arabinose, suggesting that the cell width was not well regulated, especially in cells grown without arabinose (**Supplementary Figures 2B,C**). These results indicate that FabA depletion affected the cell shape. It should be noted that FabA-depleted cells grown in the presence of 0.2% arabinose also showed abnormal shape in 19% of the cells (42/222 cells), suggesting that the quantity of FabA may not be optimized in the cells.

Then, we observed the localization and dynamics of MreB-mCherry^{SW} and sfGFP-RodZ in the FabA-depleted strain (RU1504). MreB and RodZ formed clusters, as in WT cells, in the presence of arabinose (+FabA) (**Figure 4A**). In contrast, in cells grown in the absence of arabinose (–FabA), MreB formed clusters that were often abnormally large and appeared to be aggregates (**Figure 4A**). We found that MreB clusters in FabA-depleted cells were larger than those in +FabA cells (**Figure 4A**). In addition, some RodZ did not form clusters but was diffused in the cells (–FabA) compared with that in the cells grown with arabinose (+FabA) (**Figure 4A**). These results suggest that membrane fluidity affects the formation of MreB and RodZ clusters and hence, the formation of the Rod complex. We found that the motion of MreB in a FabA-depleted strain (RU1504) grown in the absence of arabinose (5.5 ± 3.0 nm/s) clearly decreased compared to that in the presence of arabinose (10.8 ± 4.0 nm/s) (**Figure 4B**, **Supplementary Movies 5A,B**, and **Supplementary Table 4**). These results suggest that FabA, and thus membrane fluidity, affect the localization of MreB and RodZ and their motion. However, it is possible that FabA, not membrane fluidity, somehow directly affects the localization and motion of MreB.

Thus, we constructed a FabB-depleted strain. FabB is also an essential protein and functions downstream of FabA in the synthesis pathway of unsaturated fatty acids. We examined the subcellular localization of MreB and RodZ in a FabB-depleted strain grown in the presence (+FabB) or absence (–FabB) of arabinose. As in FabA-depleted cells, some MreB and RodZ formed large clusters (indicated by white arrows), and MreB and RodZ did not colocalize (indicated by green and magenta

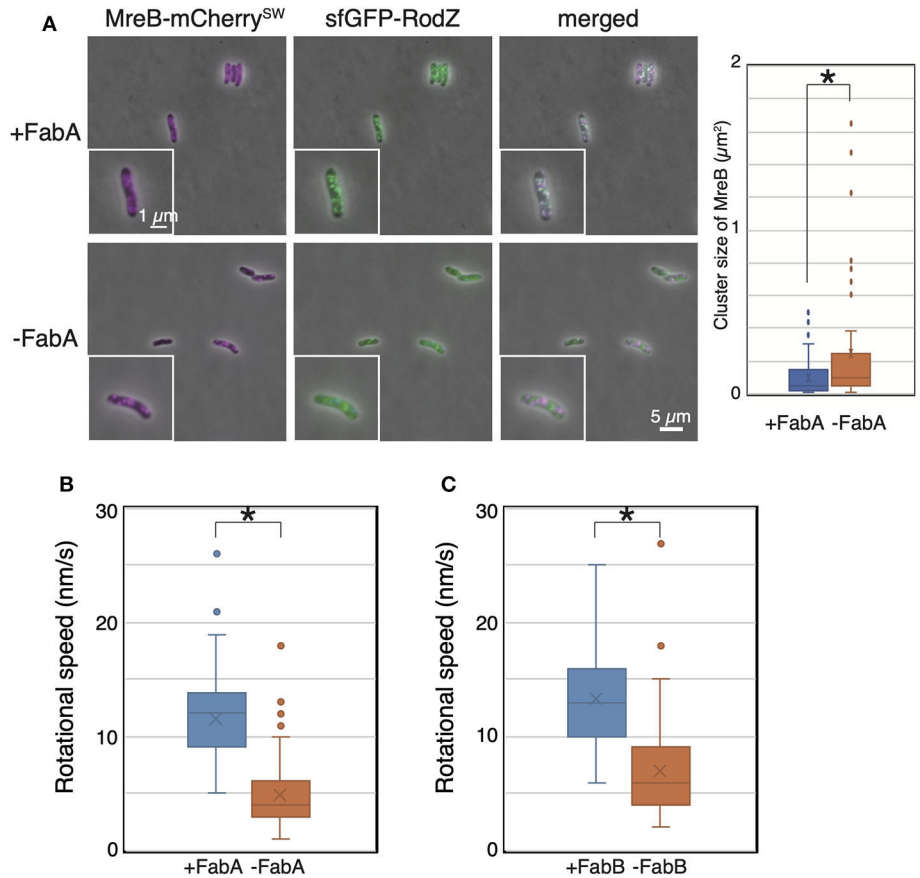

FIGURE 4 | Localization and motion of MreB and RodZ in cells depleted of FabA or FabB. **(A)** Localization of MreB and RodZ in FabA-depleted cells in the presence (+FabA) and absence (–FabA) of arabinose. Merged images of phase-contrast and fluorescent images are shown. A magnified cell is shown in the inset. Scale bar: 5 μm. **(B)** The distribution of the rotational speed (nm/s) of MreB in FabA-depleted cells in the presence (+FabA) and absence (–FabA) of arabinose is shown. **(C)** The distribution of the rotational speed (nm/s) of MreB in FabB-depleted cells in the presence (+FabB) and absence (–FabB) of arabinose is shown. *P*-values were determined by the unpaired *t*-test. *P*-values < 0.05, shown by asterisks (*), were considered significantly different from each other.

arrows) in cells grown in the absence of arabinose (–FabB) (**Supplementary Figure 3**). Interestingly, there were cells in which MreB did not form clusters but RodZ did (shown by green arrows in **Supplementary Figure 3**) and vice versa (shown by magenta arrows in **Supplementary Figure 3**). These results combined with the results obtained by FabA-depleted cells suggest that membrane fluidity affects the formation of the Rod complex. We observed the motion of MreB-msfGFP^{SW} in the FabB-depleted strain RU1822 (MG1655 *mreB-msfGFP*^{SW} Δ*fabB::kan*/pBAD-*fabB*). In the presence of arabinose (+FabB), MreB formed clusters, as in WT, and moved around the short axis of the cell (11.9 ± 4.0 nm/s) (**Figure 4C**, **Supplementary Movie 5C**, and **Supplementary Table 4**). However, in the absence of arabinose (–FabB), MreB formed clusters, as in WT cells, but the rotational speed of MreB was decreased (6.9 ± 3.9 nm/s) (**Figure 4C**, **Supplementary Movie 5D**, and **Supplementary Table 4**). These results indicate that depletion of either FabA or FabB resulted in decreased motility of MreB, and that membrane fluidity plays a key role in MreB motion.

DISCUSSION

In this study, we found that speeds of the rotational motion of MreB and RodZ significantly decreased in cells lacking aPLs, indicating that aPLs affect the motion of MreB and RodZ (Rod complex). We showed that the interaction between MreB and RodZ in ΔaPLs was comparable with that in WT cells, suggesting that the composition of phospholipids did not affect the interaction between MreB and RodZ.

The rotational speed of MreB has been shown to be dependent on temperature (van Teeffelen et al., 2011). We also showed that the rotational speed increased when the temperature was increased in WT and ΔaPLs cells, indicating that the decreased speed of MreB in ΔaPLs cells did not result from the lack of aPLs. The rotation of the Rod complex is coupled with the activity of peptidoglycan synthesis and is dependent on temperature (Domínguez-Escobar et al., 2011; Garner et al., 2011; van Teeffelen et al., 2011). Membrane fluidity is also dependent on temperature (Zhang and Rock, 2008). Therefore, the cause of the influence of temperature on rotational speed might be the change in peptidoglycan synthesis activity or membrane fluidity.

Inhibition of peptidoglycan synthesis suppresses the dynamics of the Rod complex, indicating that the movement of the Rod complex is coupled with peptidoglycan synthesis (Domínguez-Escobar et al., 2011; Garner et al., 2011; van Teeffelen et al., 2011). Therefore, it is possible that the decrease in the membrane fluidity did not directly cause the inhibition of the dynamics of the Rod complex but decreased the peptidoglycan synthetic activity, and consequently, the motion of the Rod complex was inhibited. To clarify this, we conducted two experiments; (1) MreB rotation in cells grown in rich and poor medium at the same temperature and (2) MreB rotation in cells overproducing MurG which should promote peptidoglycan synthesis. However, the rotational speed of MreB was similar whether cells were grown in rich or poor medium. This is consistent with previous reports (van Teeffelen et al., 2011; Billaudeau et al., 2017). Deletion of CL has been shown to result in reduced activity of MurG, which is a GTase involved in peptidoglycan synthesis, and therefore, it caused abnormal shape in *Rhodobacter sphaeroides* (Lin et al., 2019), while it was shown that expression of *murG* was upregulated in *E. coli* ΔCL cells (van den Brink-van der Laan et al., 2003). This abnormal shape in *R. sphaeroides* was restored to a normal rod shape by inducing *murG* expression because MurG overproduction improved peptidoglycan synthesis. This expression level of *murG* did not affect doubling time of ΔCL cells but possibly increased peptidoglycan synthesis. Therefore, to distinguish whether the reduced motion of MreB in ΔaPLs was due to reduced peptidoglycan synthesis or reduced membrane fluidity, MurG was overproduced in ΔaPLs, and we examined its effect on MreB motion. We found that the overproduction of MurG resulted in the elongation of cells but did not affect MreB rotation. These results suggest that decreased peptidoglycan synthesis was not the major cause of reduced rotational speed of MreB. However, elongation of the cells overproducing MurG was very subtle. Therefore, it is possible that overproduction of MurG did not significantly increase peptidoglycan synthesis but inhibited cell division, and hence, rational speed of MreB was not increased. In fact, it is difficult to distinguish following possibilities; (1) overproduction of MurG enhanced peptidoglycan synthesis but did not affect the rotational speed of MreB, and (2) overproduction of MurG inhibited cell division and did not affect the rotational speed of MreB. Further experiments will be needed to clarify the possibilities by examination of peptidoglycan synthesis in ΔaPLs overproducing MurG.

Nevertheless, we hypothesized that membrane fluidity is one of the important factors for the rotation of MreB because it has been shown that phosphatidylglycerol exhibits relatively higher fluidity (Pluschke and Overath, 1981), the membrane fluidity of ΔaPLs cells is lower than that of WT cells (Nenninger et al., 2014), and MreB influences membrane fluidity (Strahl et al., 2014). To decrease membrane fluidity by means other than decreasing the temperature, we depleted FabA or FabB, which are essential in the synthesis of unsaturated fatty acids determining membrane fluidity (Marr and Ingraham, 1962). When either FabA or FabB was depleted, some cells showed aberrant shapes, such as a bend or elongation. In addition, in FabA- or FabB-depleted cells, MreB apparently formed clusters, and some MreB formed larger clusters similar to aggregates. However, some MreB did not completely colocalize with RodZ in those cells. Thus, membrane fluidity affects the formation and motion of the Rod complex, and therefore, FabA- or FabB-depleted cells show an aberrant cell shape. During the preparation of this manuscript, a manuscript by Gohrbandt et al. was uploaded in bioRxiv, in which a clear defect of divisome assembly was observed upon depletion of unsaturated fatty acids in the *E. coli fabA* (Ts) mutant, while MreB still formed clusters in the mutant as in WT cells (Gohrbandt et al., 2019). However, they did not study the localization of other proteins in the Rod complex, such as RodZ. Thus, membrane fluidity affects protein complex formation during cell division and elongation.

We showed the inhibition of MreB motion in ΔaPLs cells and FabA-/FabB-depleted cells and aberrant formation of Rod complexes only in FabA-/FabB-depleted cells. It is possible that the reduced membrane fluidity independently affected the motion and formation of the Rod complex. As ΔaPLs cells can still produce FabA and FabB, the decrease in the membrane fluidity of aPLs cells may not be as great as that of FabA-/FabB-depleted cells. Thus, there is a smaller effect on the formation of the Rod complex, but the impact on complex dynamics may be significant in ΔaPLs cells. While this manuscript was under review, it was reported that membrane fluidity controls MreB motion in *Bacillus subtilis* (Zielińska et al., 2020). Thus, membrane fluidity controls the motion of the Rod complex in both gram-positive and gram-negative bacteria. Therefore, the mechanism would be widely conserved in bacterial cells. In *B. subtilis*, it has been reported that the motion of Mbl (an MreB-like protein) is inhibited by the depletion of components of the Rod complex such as RodZ and RodA, suggesting that the correct formation of the Rod complex is critical for its dynamics. In *E. coli*, the Δ*rodZ* strain (in which the morphology changes into a round shape) has been found to reduce MreB rotation (Morgenstein et al., 2015). However, when MreB carries the S14A mutation that suppresses the morphological abnormality of Δ*rodZ* cells, the motility of MreB ($MreB^{S14A}$) is restored (Hussain et al., 2018). This is probably because $MreB^{S14A}$ is able to correctly form the Rod complex without RodZ, so $MreB^{S14A}$ can rotate. This idea is consistent with the results that the formation of the Rod complex is perturbed and the motion of the Rod complex is inhibited in FabA-/FabB-depleted cells.

As membrane fluidity is modulated by external conditions such as changes in temperature and pH, cells may regulate peptidoglycan synthesis by changing membrane fluidity to survive in various harsh environments.

DATA AVAILABILITY STATEMENT

The raw data supporting the conclusions of this article will be made available by the authors, without undue reservation.

AUTHOR CONTRIBUTIONS

KK, FK, and DS made contributions to the design of the study, the acquisition, analysis, and interpretations of the data. KK and

DS made contributions to writing of the manuscript. All authors contributed to the article and approved the submitted version.

FUNDING

This work was supported by NIG-JOINT (61A2017, 57A2018, and 60A2019).

ACKNOWLEDGMENTS

We are grateful to Dr. Hironori Niki (National Institute of Genetics, Japan) for his critical comments on this work. We also thank Dr. Taishi Kasai for helping image analyses and Risa Ago for constructing the plasmid pRU1276 and all members of the Shiomi lab for their helpful discussions and suggestions. We would like to thank Editage (www.editage.com) for English language editing.

SUPPLEMENTARY MATERIAL

The Supplementary Material for this article can be found online at: https://www.frontiersin.org/articles/10.3389/fmolb.2020.582660/full#supplementary-material

REFERENCES

Bendezú, F. O., and de Boer, P. A. J. (2008). Conditional lethality, division defects, membrane involution, and endocytosis in mre and mrd shape mutants of *Escherichia coli*. *J. Bacteriol.* 190, 1792–1811. doi: 10.1128/JB.01322-07

Billaudeau, C., Chastanet, A., Yao, Z., Cornilleau, C., Mirouze, N., Fromion, V., et al. (2017). Contrasting mechanisms of growth in two model rod-shaped bacteria. *Nat. Commun.* 8, 15370–15311. doi: 10.1038/ncomms15370

Budin, I., de Rond, T., Chen, Y., Chan, L. J. G., Petzold, C. J., and Keasling, J. D. (2018). Viscous control of cellular respiration by membrane lipid composition. *Science* 362, 1186–1189. doi: 10.1126/science.aat7925

Cronan, J. E., and Gelmann, E. P. (1973). An estimate of the minimum amount of unsaturated fatty acid required for growth of *Escherichia coli*. *J. Biol. Chem.* 248, 1188–1195.

de Pedro, M. A., Quintela, J. C., Höltje, J. V., and Schwarz, H. (1997). Murein segregation in *Escherichia coli*. *J. Bacteriol.* 179, 2823–2834. doi: 10.1128/JB.179.9.2823-2834.1997

den Blaauwen, T., de Pedro, M. A., Nguyen-Distèche, M., and Ayala, J. A. (2008). Morphogenesis of rod-shaped sacculi. *FEMS Microbiol. Rev.* 32, 321–344. doi: 10.1111/j.1574-6976.2007.00090.x

Doi, M., Wachi, M., Ishino, F., Tomioka, S., Ito, M., Sakagami, Y., et al. (1988). Determinations of the DNA sequence of the mreB gene and of the gene products of the mre region that function in formation of the rod shape of *Escherichia coli* cells. *J. Bacteriol.* 170, 4619–4624. doi: 10.1128/JB.170.10.4619-4624.1988

Domínguez-Escobar, J., Chastanet, A., Crevenna, A. H., Fromion, V., Wedlich-Söldner, R., and Carballido-Lopez, R. (2011). Processive movement of MreB-associated cell wall biosynthetic complexes in bacteria. *Science* 333, 225–228. doi: 10.1126/science.1203466

Feng, Y., and Cronan, J. E. (2009). *Escherichia coli* unsaturated fatty acid synthesis: complex transcription of the fabA gene and *in vivo* identification of the essential reaction catalyzed by FabB. *J. Biol. Chem.* 284, 29526–29535. doi: 10.1074/jbc.M109.023440

Garner, E. C., Bernard, R., Wang, W., Zhuang, X., Rudner, D. Z., and Mitchison, T. (2011). Coupled, circumferential motions of the cell wall synthesis machinery and MreB filaments in *B. subtilis*. *Science* 333, 222–225. doi: 10.1126/science.1203285

Gohrbandt, M., Lipski, A., Baig, Z., Walter, S., Kurre, R., Strahl, H., et al. (2019). Low membrane fluidity triggers lipid phase separation and protein segregation *in vivo*. *bioRxiv* 180:852160. doi: 10.1101/852160

Hussain, S., Wivagg, C. N., Szwedziak, P., Wong, F., Schaefer, K., Izoré, T., et al. (2018). MreB filaments align along greatest principal membrane curvature to orient cell wall synthesis. *Elife* 7:1239. doi: 10.7554/eLife.32471.052

Iwai, N., Nagai, K., and Wachi, M. (2002). Novel S-benzylisothiourea compound that induces spherical cells in *Escherichia coli* probably by acting on a rod-shape-determining protein(s) other than penicillin-binding protein 2. *Biosci. Biotechnol. Biochem.* 66, 2658–2662. doi: 10.1271/bbb.66.2658

Kawazura, T., Matsumoto, K., Kojima, K., Kato, F., Kanai, T., Niki, H., et al. (2017). Exclusion of assembled MreB by anionic phospholipids at cell poles confers cell polarity for bidirectional growth. *Mol. Microbiol.* 104, 472–486. doi: 10.1111/mmi.13639

Kurita, K., Shin, R., Tabei, T., and Shiomi, D. (2019). Relation between rotation of MreB actin and cell width of *Escherichia coli*. *Genes Cells* 24, 259–265. doi: 10.1111/gtc.12667

Lin, T.-Y., Gross, W. S., Auer, G. K., and Weibel, D. B. (2019). Cardiolipin alters *Rhodobacter sphaeroides* cell shape by affecting peptidoglycan precursor biosynthesis. *mBio* 10:187. doi: 10.1128/mBio.02401-18

Marr, A. G., and Ingraham, J. L. (1962). Effect of temperature on the composition of fatty acids in *Escherichia coli*. *J. Bacteriol.* 84, 1260–1267. doi: 10.1128/JB.84.6.1260-1267.1962

Mileykovskaya, E., and Dowhan, W. (2000). Visualization of phospholipid domains in Escherichia coli by using the cardiolipin-specific fluorescent dye 10-N-nonyl acridine orange. *J. Bacteriol.* 182, 1172–1175. doi: 10.1128/jb.182.4.1172-1175.2000

Morgenstein, R. M., Bratton, B. P., Nguyen, J. P., Ouzounov, N., Shaevitz, J. W., and Gitai, Z. (2015). RodZ links MreB to cell wall synthesis to mediate MreB rotation and robust morphogenesis. *Proc. Natl. Acad. Sci. U. S. A.* 112, 12510–12515. doi: 10.1073/pnas.1509610112

Nenninger, A., Mastroianni, G., Robson, A., Lenn, T., Xue, Q., Leake, M. C., et al. (2014). Independent mobility of proteins and lipids in the plasma membrane of *Escherichia coli*. *Mol. Microbiol.* 92, 1142–1153. doi: 10.1111/mmi.12619

Oliver, P. M., Crooks, J. A., Leidl, M., Yoon, E.J., Saghatelian, A., and Weibel, D. B. (2014). Localization of anionic phospholipids in Escherichia coli cells. *J. Bacteriol.* 196, 3386–3398. doi: 10.1128/JB.01877-14

Pluschke, G., and Overath, P. (1981). Function of phospholipids in Escherichia coli. Influence of changes in polar head group composition on the lipid phase transition and characterization of a mutant containing only saturated phospholipid acyl chains. *J. Biol. Chem.* 256, 3207–3212.

Salje, J., van den Ent, F., de Boer, P., and Löwe, J. (2011). Direct membrane binding by bacterial actin MreB. *Mol. Cell* 43, 478–487. doi: 10.1016/j.molcel.2011.07.008

Shiomi, D., and Margolin, W. (2007). Dimerization or oligomerization of the actin-like FtsA protein enhances the integrity of the cytokinetic Z ring. *Mol. Microbiol.* 66, 1396–1415. doi: 10.1111/j.1365-2958.2007.05998.x

Strahl, H., Bürmann, F., and Hamoen, L. W. (2014). The actin homologue MreB organizes the bacterial cell membrane. *Nat. Commun.* 5, 3442–3411. doi: 10.1038/ncomms4442

Ursell, T. S., Nguyen, J., Monds, R. D., Colavin, A., Billings, G., Ouzounov, N., et al. (2014). Rod-like bacterial shape is maintained by feedback between cell curvature and cytoskeletal localization. *Proc. Natl. Acad. Sci. U. S. A.* 111, E1025–E1034. doi: 10.1073/pnas.1317174111

van den Brink-van der Laan, E., Boots, J.-W. P., Spelbrink, R. E. J., Kool, G. M., Breukink, E., Killian, J. A., et al. (2003). Membrane interaction of the glycosyltransferase MurG: a special role for cardiolipin. *J. Bacteriol.* 185, 3773–3779. doi: 10.1128/JB.185.13.3773-3779.2003

van den Ent, F., Amos, L. A., and Löwe, J. (2001). Prokaryotic origin of the actin cytoskeleton. *Nature* 413, 39–44. doi: 10.1038/35092500

van den Ent, F., Izoré, T., Bharat, T. A., Johnson, C. M., and Löwe, J. (2014). Bacterial actin MreB forms antiparallel double filaments. *Elife* 3:e02634. doi: 10.7554/eLife.02634

van Teeffelen, S., Wang, S., Furchtgott, L., Huang, K. C., Wingreen, N. S., Shaevitz, J. W., et al. (2011). The bacterial actin MreB rotates, and rotation depends on cell-wall assembly. *Proc. Natl. Acad. Sci. U. S. A.* 108, 15822–15827. doi: 10.1073/pnas.1108999108

Wachi, M., Doi, M., Tamaki, S., Park, W., Nakajima-Iijima, S., and Matsuhashi, M. (1987). Mutant isolation and molecular cloning of mre genes, which determine cell shape, sensitivity to mecillinam, and amount of penicillin-binding proteins in *Escherichia coli*. *J. Bacteriol.* 169, 4935–4940. doi: 10.1128/JB.169.11.4935-4940.1987

Young, K. D. (2003). Bacterial shape. *Mol. Microbiol.* 49, 571–580. doi: 10.1046/j.1365-2958.2003.03607.x

Zhang, Y.-M., and Rock, C. O. (2008). Membrane lipid homeostasis in bacteria. *Nat. Rev. Microbiol.* 6, 222–233. doi: 10.1038/nrmicro1839

Zielińska, A., Savietto, A., de Sousa Borges, A., Martinez, D., Berbon, M., Roelofsen, J. R., et al. (2020). Flotillin-mediated membrane fluidity controls peptidoglycan synthesis and MreB movement. *Elife* 9, 938–921. doi: 10.7554/eLife.57179

Conflict of Interest: The authors declare that the research was conducted in the absence of any commercial or financial relationships that could be construed as a potential conflict of interest.

frontiers in Molecular Biosciences

ORIGINAL RESEARCH
published: 05 January 2021
doi: 10.3389/fmolb.2020.610932

Ornithine Lipids in *Burkholderia* spp. Pathogenicity

*Luz América Córdoba-Castro[1,2], Rosalba Salgado-Morales[3], Martha Torres[1], Lourdes Martínez-Aguilar[1], Luis Lozano[1], Miguel Ángel Vences-Guzmán[1], Ziqiang Guan[4], Edgar Dantán-González[3], Mario Serrano[1] and Christian Sohlenkamp[1]**

[1] Centro de Ciencias Genómicas, Universidad Nacional Autónoma de México, Cuernavaca, Mexico, [2] Programa de Doctorado en Ciencias Biomédicas, Universidad Nacional Autónoma de México, Centro de Ciencias Genómicas, Cuernavaca, Mexico, [3] Centro de Investigación en Biotecnología, Universidad Autónoma del Estado de Morelos, Cuernavaca, Mexico, [4] Department of Biochemistry, Duke University Medical Center, Durham, NC, United States

The genus *Burkholderia* sensu lato is composed of a diverse and metabolically versatile group of bacterial species. One characteristic thought to be unique for the genus *Burkholderia* is the presence of two forms each (with and without 2-hydroxylation) of the membrane lipids phosphatidylethanolamine (PE) and ornithine lipids (OLs). Here, we show that only *Burkholderia* sensu stricto strains constitutively form OLs, whereas all other analyzed strains belonging to the *Burkholderia* sensu lato group constitutively form the two forms of PE, but no OLs. We selected two model bacteria to study the function of OL in *Burkholderia* sensu lato: (1) *Burkholderia cenocepacia* wild-type which constitutively forms OLs and its mutant deficient in the formation of OLs and (2) *Robbsia andropogonis* (formerly *Burkholderia andropogonis*) which does not form OL constitutively, and a derived strain constitutively forming OLs. Both were characterized under free-living conditions and during pathogenic interactions with their respective hosts. The absence of OLs in *B. cenocepacia* slightly affected bacterial growth under specific abiotic stress conditions such as high temperature and low pH. *B. cenocepacia* lacking OLs caused lower mortality in *Galleria mellonella* larvae while *R. andropogonis* constitutively forming OLs triggers an increased formation of reactive oxygen species immediately after infection of maize leaves, suggesting that OLs can have an important role during the activation of the innate immune response of eukaryotes.

Keywords: pathogenicity, reactive oxygen species, *Burkholderia cenocepacia*, ornithine lipids, *Robbsia andropogonis*

OPEN ACCESS

Edited by:
Heidi Vitrac, University of Texas Health Science Center at Houston, United States

Reviewed by:
Surasakdi Wongratanacheewin, Khon Kaen University, Thailand
Dwijendra K. Gupta, Jai Prakash Vishwavidyalaya, India

***Correspondence:**
Christian Sohlenkamp
chsohlen@ccg.unam.mx

Specialty section:
This article was submitted to Cellular Biochemistry, a section of the journal Frontiers in Molecular Biosciences

Received: *27 September 2020*
Accepted: *07 December 2020*
Published: *05 January 2021*

Citation:
Córdoba-Castro LA, Salgado-Morales R, Torres M, Martínez-Aguilar L, Lozano L, Vences-Guzmán MÁ, Guan Z, Dantán-González E, Serrano M and Sohlenkamp C (2021) Ornithine Lipids in Burkholderia spp. Pathogenicity. Front. Mol. Biosci. 7:610932. doi: 10.3389/fmolb.2020.610932

INTRODUCTION

One major function of amphiphilic lipids is to form the lipid bilayer of membranes which serve as semipermeable barriers and limit a cell. The best-known examples are glycerophospholipids such as phosphatidylglycerol (PG), phosphatidylethanolamine (PE), cardiolipin (CL), and phosphatidylcholine (PC). However, depending on the class of organism and the growth conditions, other lipids such as cholesterol, hopanoids, sphingolipids, sulpholipids, glycolipids, betaine lipids, or ornithine lipids (OLs), can be present in membranes in different concentrations. Especially prokaryotic membranes have been shown to contain a large diversity of lipids, some of which are only formed by specific groups of bacteria or under specific stress conditions (Geiger et al., 2010; Sohlenkamp and Geiger, 2016). OLs are phosphorus-free acyloxyacyl aminolipids

which have been found only in bacteria and are apparently absent in eukaryotes or archaea. Their basic structure is composed of a 3-hydroxylated fatty acid linked by an amide bond to the α-amino group of ornithine and a second fatty acid linked by an ester bond to the 3-hydroxyl group of the first fatty acid (Geiger et al., 2010; Sohlenkamp and Geiger, 2016). These lipids can be formed by the OlsBA acyltransferases originally described in *Sinorhizobium meliloti* (Weissenmayer et al., 2002; Gao et al., 2004) or by the bifunctional acyltransferase OlsF first described in *Serratia proteamaculans* (Vences-Guzmán et al., 2015). The OlsBA pathway is present in several α- and β-proteobacteria, in a few γ-proteobacteria and several actinomycetes. Genes encoding OlsF are present in a few γ-proteobacteria, δ- and ε-proteobacteria and in bacteria belonging to the Cytophaga-Flavobacterium-Bacteroidetes (CFB) group. Based on the analysis of genomic DNA sequences, it has been estimated that about 50% of the bacterial species can form OLs at least under specific growth conditions (Vences-Guzmán et al., 2015; Sohlenkamp and Geiger, 2016). Interestingly, in some bacteria, for example *S. meliloti* or *Pseudomonas* sp., OLs are only formed under phosphate-limiting conditions (Minnikin and Abdolrahimzadeh, 1974; Geiger et al., 1999; López-Lara et al., 2005), while in other bacteria, like many species of the genus *Burkholderia* or in *Rhizobium tropici* CIAT899, OLs are formed constitutively (Rojas-Jiménez et al., 2005; González-Silva et al., 2011). In some examples, the presence of OLs or an increased accumulation of OLs have been related to resistance to abiotic stress conditions or to a function during interactions with eukaryotic hosts like an increased persistence (Kim et al., 2018).

The genus *Burkholderia* sensu lato (s.l.) contains more than 100 diverse and versatile bacterial species, which can be found in different environments such as soil or fresh water, but also frequently in association with a number of eukaryotic hosts including humans, animals (vertebrates and invertebrates), plants or fungi. These bacteria-host interactions can be beneficial, pathogenic or both (Depoorter et al., 2016; Estrada-de Los Santos et al., 2018). In recent years, *Burkholderia* s.l. was divided into several genera and it is currently classified into *Burkholderia* sensu stricto (s.s.), *Paraburkholderia* (Sawana et al., 2014), *Caballeronia* (Dobritsa and Samadpour, 2016), *Robbsia* (Rojas-Rojas et al., 2019) and the recently proposed additional genera *Mycetohabitans* and *Trinickia* (Estrada-de Los Santos et al., 2018).

One characteristic that was thought to be unique and common to the species of the genus *Burkholderia* s.l was the presence of two forms of PE and OLs (Yabuuchi et al., 1992). However, when the membrane lipids of a few strains were examined in detail, OLs were present only in some species of the genus (Palleroni, 2015), but were absent in others such as *B. andropogonis* (now classified as *R. andropogonis*). The latter synthesizes PE and hydroxylated PE (2-OH-PE), but lacks OLs and hydroxylated OL (2-OH-OL). The biological roles played by OLs in the genus *Burkholderia* s.l. are not clear yet. As in other bacterial groups, the presence of hydroxylated OLs might be part of the response to environmental stresses. The amount of hydroxylated lipids (2OH-PE and 2OH-OL) was increased in *B. cepacia* strain NCTC 10661 when exposed to a temperature of 42°C, which can be interpreted as a response to thermal stress (Taylor et al., 1998). *B. cenocepacia* J2315 formed a new hydroxylated OL when the strain was exposed to pH 4.0 (González-Silva et al., 2011). Also, rhamnolipids and OLs from *B. pseudomallei* strain K96243 induced an immune response in goats, inducing IFN-γ required for the expression of secreted cytokines (González-Juarrero et al., 2013). Finally, antibacterial activity against *Bacillus megaterium* and *Escherichia coli* has been ascribed to OLs in *B. gladioli* pv. *agaricicola* strain ICMP 11096 (Elshafie et al., 2017).

In this study, we wanted to understand the function of OLs in the genus *Burkholderia* s.l. First, we studied the membrane lipid compositions of a representative set of bacterial species of this group to find out how widespread the presence of OLs and the hydroxylated forms of PE and OL is. *B. cenocepacia* and *R. andropogonis* were selected as models for the second part of this study. *B. cenocepacia* wild-type forms OLs in a constitutive manner and was compared to a mutant unable to synthesize OLs. *R. andropogonis* does not form OLs when grown in normal complex medium and we compared it to a constructed *R. andropogonis* strain constitutively forming OLs. The absence of OLs affected the growth of *B. cenocepacia* under acid stress conditions and it decreased its virulence in a *Galleria mellonella* L (Lepidoptera: Pyralidae) model. The constitutive presence of OLs in *R. andropogonis* caused a stimulation of the plant innate immune response by increasing the production of reactive oxygen species. Both observations highlight the importance of OLs during the interactions between bacteria and their hosts.

MATERIALS AND METHODS

Bacterial Strains, Plasmids, and Growth Conditions

The bacterial strains and plasmids used in this study are listed in the Supporting Material (**Supplementary Table 1**). Bacteria were grown in Luria–Bertani broth (LB; 5 g yeast extract, 10 g peptone, 10 g NaCl per liter and adding 1.5 % agar (w/v) for solid medium) or in a minimal medium designed for growth under phosphate-limiting conditions. The composition of the latter was based on M9 medium (Miller, 1972) and sodium citrate medium (Simmons, 1926) (2 g Sodium succinate dibasic hexa-hydrated, 1 g NH_4Cl, 0.2 g $MgSO_4 \times 7H_2O$, 0.5 g NaCl and 0.1 M K-phosphate buffer prepared with K_2HPO_4 and KH_2PO_4). Bacterial growth was determined by measuring the optical density of the cultures at 620 nm (OD620). When required, antibiotics were added to the medium at the following concentrations: 20 μg/ml tetracycline and 50 μg/ml kanamycin for *R. andropogonis* (LMG2129.pRK404.pET9a and LMG2129.pRK404.pET9a.olsF) and 300 μg/ml chloramphenicol for *B. cenocepacia* mutant NG1.

Construction of the Phylogenetic Tree

The GET_HOMOLOGUES program (Contreras-Moreira and Vinuesa, 2013) was used to obtain families of orthologs from 43 *Burkholderia* s.l. genomes that were downloaded from the NCBI RefSeq database (**Supplementary Table 2**). In this analysis, each ortholog family had 43 genes. Subsequently, with the help of the GET_PHYLOMARKERS program (Vinuesa et al., 2018), the families of orthologs were analyzed to obtain optimal markers for

phylogenomic reconstruction. Finally, with the PHYML program (Guindon et al., 2010), the phylogenetic tree was constructed based on the concatenated alignments of ortholog gene families using the GTR + G evolutionary model.

Determination of the Membrane Lipid Composition

The lipid compositions of bacterial strains were determined following labeling with [1-^{14}C]acetate (Amersham Biosciences). Cultures (1 ml) of *Burkholderia* s.l. strains were inoculated from precultures grown in the same medium. After addition of 1 μCi of [^{14}C]acetate (60 mCi mmol-1) to each culture, the cultures were incubated overnight. Cells were harvested by centrifugation, washed with 500 μl water once, resuspended in 100 μl water, and then lipids were extracted according to Bligh and Dyer (Bligh and Dyer, 1959). Aliquots of the lipid extracts were spotted on high performance TLC silica gel 60 plates (Merck, Poole, UK) and separated in two dimensions using chloroform/methanol/water (16:4:1, v/v/v) as a mobile phase for the first dimension and chloroform/methanol/acetic acid (15:3:2, v/v/v) as a mobile phase for the second dimension (Tahara and Fujiyoshi, 1994). To visualize membrane lipids, developed two-dimensional TLC plates were exposed to autoradiography film (Kodak) or to a PhosphorImager screen (Amersham Biosciences). The individual lipids were quantified using ImageQuant software (Amersham Biosciences) (Vences-Guzmán et al., 2011).

Construction of a *R. andropogonis* Strain Constitutively Producing Ornithine Lipids

The bifunctional acyltransferase OlsF was expressed in the type strain *R. andropogonis* LMG2129. The plasmid pRK404.pET9a.OlsF containing the *olsF* gene from *S. proteamaculans* was mobilized by conjugal transfer from *E. coli* S17-1 into the recipient strain *R. andropogonis* LMG2129 (Simon et al., 1983). Precultures with an OD620 of 0.5 of donor and recipient cells were harvested by centrifugation and washed twice with LB medium to remove residual antibiotics. Subsequently, the cell suspensions were mixed, dropped onto LB agar plates without antibiotics and incubated overnight at 30°C. The cells were scraped from the plates, suspended, and serial aliquots were plated on sodium citrate agar (Simmons, 1926) supplemented with tetracycline and kanamycin. Incubation continued for 2–5 days to select for the presence of the plasmid in the transconjugants. Transconjugant colonies were transferred to plates with LB medium supplemented with tetracycline and kanamycin and were grown at 30°C for 3 days. Strains were conserved in glycerol at a final concentration of 30% (w/v) and were stored at −80°C.

Liquid Chromatography/Tandem Mass Spectrometry Analysis of Lipid Samples

The three different *R. andropogonis* strains (LMG2129.pRK404.pET9a.olsF-expressing the acyltransferase OlsF, LMG2129-wild-type, and LMG2129.pRK404.pET9a-empty vector control) were grown to an OD of 1.2 at 620 nm in LB medium or in LB medium with tetracycline in case of the plasmid-harboring strains. Cells were harvested by centrifugation and lipids were extracted according to Bligh and Dyer (Bligh and Dyer, 1959). Normal phase LC-ESI MS of the lipid extracts was performed using an Agilent 1200 Quaternary LC system coupled to a high resolution TripleTOF5600 mass spectrometer (Sciex, Framingham, MA). Chromatographic separation was performed on an Ascentis Silica HPLC column, 5 μm, 25 cm × 2.1 mm (Sigma-Aldrich, St. Louis, MO). Lipids were eluted with mobile phase A, consisting of chloroform/methanol/aqueous ammonium hydroxide (800:195:5, v/v/v), mobile phase B, consisting of chloroform/methanol/water/aqueous ammonium hydroxide (600:340:50:5, v/v/v/v) and mobile phase C, consisting of chloroform/methanol/water/aqueous ammonium hydroxide (450:450:95:5, v/v/v/v), over a 40 min-long run, performed as follows: 100% mobile phase A was held isocratically for 2 min and then linearly increased to 100% mobile phase B over 14 min and held at 100% B for 11 min. The mobile phase composition was then changed to 100% mobile phase C over 3 min and held at 100% C for 3 min, and finally returned to 100% A over 0.5 min and held at 100% A for 5 min. The LC eluent (with a total flow rate of 300 μl/min) was introduced into the ESI source of the high resolution TF5600 mass spectrometer. MS and MS/MS were performed in negative ion mode, with the full-scan spectra being collected in the *m/z* 200–2,000 range. The MS settings are as follows: ion spray voltage (IS) = −4,500 V (negative ion mode), curtain gas (CUR) = 20 psi, ion source gas 1 (GS1) = 20 psi, de-clustering potential (DP) = −55 V, and focusing potential (FP) = −150 V. Nitrogen was used as the collision gas for tandem mass spectrometry (MS/MS) experiments. Data analysis was performed using Analyst TF1.5 software (Sciex, Framingham, MA).

Identification of Putative Pho Boxes in *Burkholderia* sensu latu

The program INFO-GIBBS (Defrance and van Helden, 2009) was used for the construction of a position specific scoring matrix (PSSM) matrix. Pho box sequences from *Agrobacterium tumefaciens, Sinorhizobium meliloti,* and *Mesorhizobium loti* identified in the promoter sequences of genes involved in the biosynthesis of glycolipid and OL membrane lipids were used (**Supplementary Table 3**) (Yuan et al., 2006; Geske et al., 2013). The following parameters were used: Matrix length was fixed to 18 bp, the expected number of sites per sequence was one, and the number of motifs to extract was one. As background model the sequences upstream of genes in the *Burkholderiaceae* taxon were used and the Markov order used was one. Then the program MATRIX-SCAN (Turatsinze et al., 2008) was used to search for putative Pho boxes in the regions upstream of the genes encoding OlsB homologs in the genomes of the 43 *Burkholderia* s.l. species analyzed. This search was performed for both strands.

Growth Experiments Under Abiotic Stress Conditions

Pre-cultures of *R. andropogonis* and *B. cenocepacia* were grown at 30°C at 250 rpm overnight in LB medium supplemented with the respective antibiotics if required. Cells were harvested

by centrifugation at 6,000 rpm and washed with 1% NaCl (w/v) solution, except for the salinity tests for which cells were washed in LB medium without salt. The optical density data collection was measured in the Synergy 2.0 Biotek, measuring every 3 h for 24 h, performing 3 independent repetitions. For temperature stress experiments, the cultures were grown in LB medium in 96-well microplates, inoculated with an OD620 of 0.05 and incubated at 30, 37, or 42°C. For acid stress experiments, the cultures were grown in 96-well microplates in LB medium adjusted to pH 4 buffered with 50 mM Homopipes [Homopiperazine-*N,N′*-bis-2-(ethanesulfonic acid)] or to pH 7 with 50 mM Pipes [piperazine-*N,N′*-bis(2-ethanesulfonic acid)]. Cultures were inoculated at an OD620 of 0.05 and incubated at 30°C with medium shaking. For salinity stress experiments, the cultures were grown in 96-well microplates in LB medium with salt concentrations of 0.05, 0.5, and 1 M NaCl. Cultures were inoculated at an OD620 of 0.05 and incubated at 30°C with medium shaking.

B. cenocepacia Virulence Assays Using *Galleria mellonella* Larvae

The virulence of the *B. cenocepacia* strains was evaluated in *G. mellonella* larvae. Starting from bacterial cultures grown to an OD620 of 1, serial dilutions were made in 10 mM $MgSO_4$ that corresponded to 3×10^7, 3×10^6, 3×10^5, and 2×10^4 CFU/ml. As negative controls, a simple puncture of the larvae, the injection of saline solution, or the injection of *E. coli* DH5α (Hanahan, 1983) at 3×10^6 CFU/ml were used. This strain is innocuous for *G. mellonella* (Alghoribi et al., 2014; Jonsson et al., 2017). Assays were carried out using the injection method with *G. mellonella* larvae in the sixth stage and 10 μl bacterial suspensions were injected into the dorsal region of the third anterior abdominal segment of the larvae using insulin syringe of 31G (gauge). Each bacterial suspension was tested using 10 insect larvae placed individually in 55 mm petri dishes without diet and incubated at 30°C. The mortality was evaluated every 24 h for 5 days after injection. Five independent experiments were performed. For statistical testing, experimental data ($n = 50$) were plotted using the Kaplan-Meier method and differences in survival were calculated by using the log-rank test with a $p \leq 0.05$ indicating statistical significance. The statistical analyses were performed using GraphPad Prism, version 8.4.3 (GraphPad Software Inc., San Diego, CA, USA).

Infiltration of Maize Plants With *R. andropogonis* Strains

R. andropogonis assays were carried out in corn plants using a native maize variety ("criollo de Hidalgo"). Seed sterilization and germination were performed as previously described (Matus-Acuña et al., 2018), and sterilized seeds were incubated for 48 h at 30°C in the dark. Subsequently, germinated seedlings were transplanted to pots containing sterile vermiculite and were grown under greenhouse conditions irrigating every 3 or 4 days with water or Fahraeus solution for 40 days before infection with the bacterial strains (Fahraeus, 1957). Maize leaves were infiltrated on the bottom of the leaves with a 1 ml needleless syringe containing a 1×10^5 CFU/ml bacterial suspension (corresponding to an OD620 of about 0.02) of the wild-type strain LMG2129 or the transconjugants (LMG2129.pRK404.pET9a, LMG2129.pRK404.pET9a.olsF). As mock control a 10 mM $MgCl_2$ solution was used. Approximately 10 μl were infiltrated into the leaf at each site. Forty healthy 40 day-old maize plants were used. Ten potted plants were inoculated with each isolate and the development of symptoms was followed for 15 days. The bacteria were isolated using a methodology previously described (Katagiri et al., 2002). Briefly, treated maize leaves were macerated with pistil, washed with 10 mM $MgCl_2$ twice and finally resuspended in LB medium. The suspension was serially diluted, plated on LB medium and incubated at 30°C for 72 h. Colonies were counted and colony forming units determined. For statistical analyses the one-tailed *t*-test was used with a $p \leq 0.05$ indicating statistical significance. Statistical analyses were performed using GraphPad Prism, version 8.4.3 (GraphPad Software Inc., San Diego, CA, USA).

Detection of Reactive Oxygen Species (ROS)

ROS were detected using the fluorescent probe 2′,7′-Dichlorodihydrofluorescein diacetate (DCFH-DA; Sigma-Aldrich, www.sigmaaldrich.com) as previously described (L'Haridon et al., 2011). Leaves were rapidly rinsed in DCFH-DA medium and observed under UV light with a LEICA DMR fluorescence microscope (Leica, www.leica.com). Microscope images were saved as TIFF files and processed for quantification of the pixels with Image J version 1.51 (NIH). For statistical analyses the one-tailed *t*-test was used with a $p \leq 0.05$ indicating statistical significance. Statistical analyses were performed using GraphPad Prism, version 8.4.3 (GraphPad Software Inc., San Diego, CA, USA).

RESULTS

Burkholderia sensu lato Strains and Their Membrane Lipid Compositions: Only sensu strictu Strains Form OL Constitutively

We wanted to study if there is a correlation between the membrane lipid composition of the species and their phylogenic positions within the *Burkholderia* sensu lato (s.l.) supergenus. An analysis performed with the genomes of 43 *Burkholderia* s.l. species indicated that 780 gene families, representing groups of orthologs, were present in each of the 43 genomes. Next, using the Get Phylomarkers software (Vinuesa et al., 2018), 411 families of orthologs were considered optimal markers for a phylogenomic reconstruction of the *Burkholderia* s.l. supergenus. The phylogeny showed that *Burkholderia* s.l. was separated into five different lineages (**Figure 1**). These corresponded to *Burkholderia* s.s., *Trinickia*, *Paraburkholderia*, *Caballeronia,* and *Robbsia*. We analyzed the membrane lipid composition of 35 *Burkholderia* s.l. strains to which we had access in the laboratory when they were grown in complex medium. Liquid cultures of the selected strains were grown, lipids were labeled with [^{14}C]acetate, extracted and separated by two dimensional

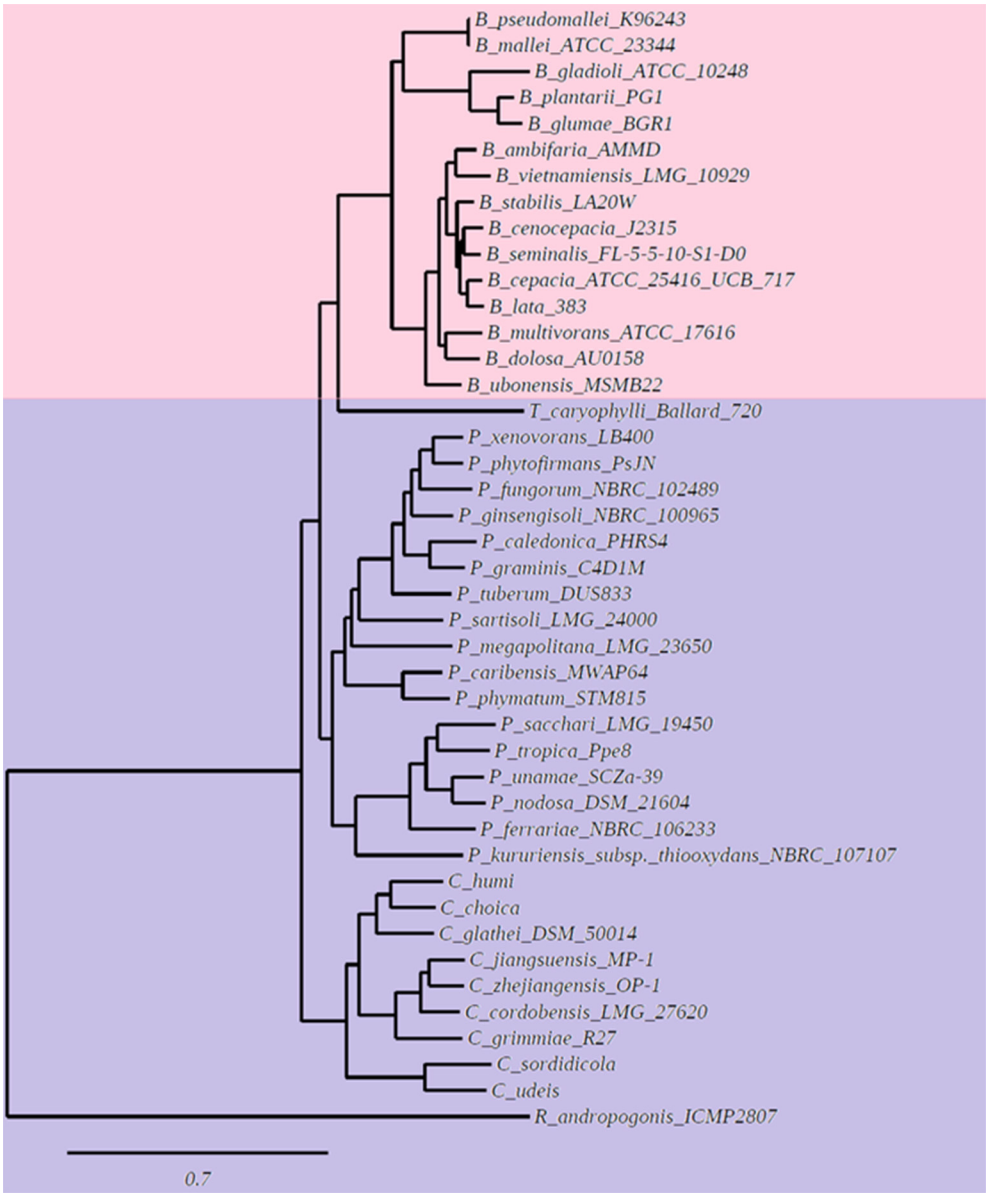

FIGURE 1 | Phylogenetic tree based on a pangenome analysis of *Burkholderiales*. The first clade (indicated with pink color) groups species of the genus *Burkholderia* sensu stricto (s.s.) that synthesize unmodified and modified OLs when grown in complex LB medium. The second clade (marked in purple color) groups species of the genera *Trinickia, Paraburkholderia, Caballeronia*, and *Robbsia*, that do not synthesize OLs when grown in complex LB medium.

thin-layer chromatography (**Figure 2**, six representative strains are shown). In all strains, the lipids phosphatidylglycerol (PG), cardiolipin (CL), phosphatidylethanolamine (PE), and 2-hydroxylated PE (2OH-PE) were detected. However, under the evaluated growth condition OLs be it unmodified and/or modified were only detected in the strains of the genus *Burkholderia* s.s. (**Figures 2A,B**). The species included in the *Burkholderia* s.s. clade (indicated in pink, **Figure 1**), are generally species that correspond to pathogens of humans, plants or animals (Depoorter et al., 2016). The clade that groups the genera *Trinickia*, *Paraburkholderia*, *Caballeronia,* and *Robbsia* (marked in purple, **Figure 1**) includes species that do not synthesize OLs when grown in complex medium, and several of these bacteria are plant beneficial and environmental bacteria, or can be involved in an N_2-fixing symbiosis with legume plants (Estrada-de Los Santos et al., 2018). An exception is the genus *Robbsia* which is formed by plant pathogens.

Bacterial species belonging to the genus *Burkholderia* form OLs by the OlsBA pathway. The presence of a gene encoding an OlsB homolog is considered a good indicator for the capacity of the bacteria to form OLs (Geiger et al., 2010). We wanted to know if the absence of OLs in the species classified as *Paraburkholderia*,

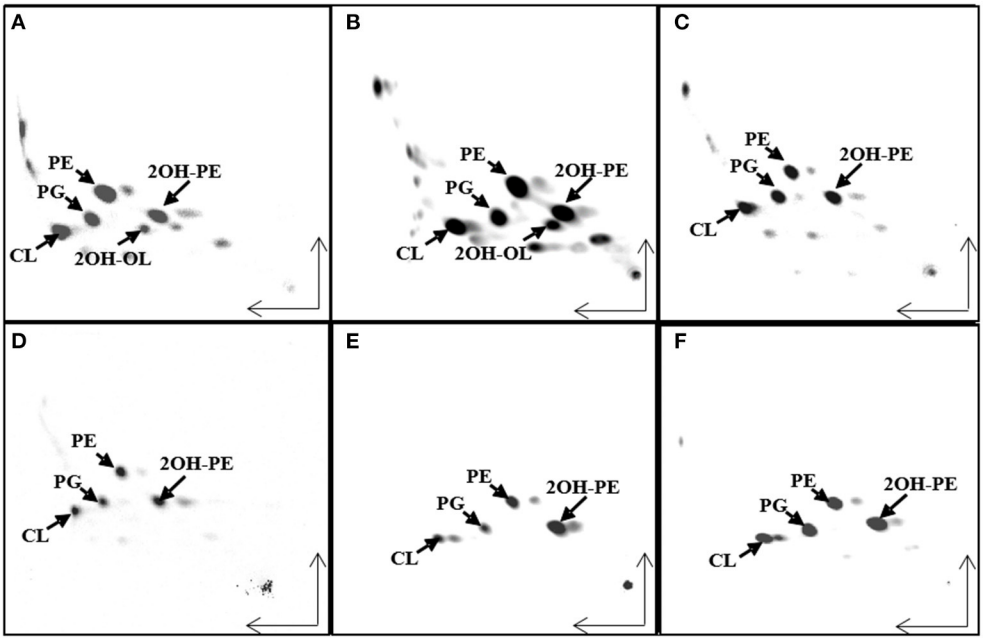

FIGURE 2 | Ornithine lipid (OL) synthesis is constitutive in strains belonging to the genus *Burkholderia* sensu stricto (s.s), but not in the other analyzed strains. Separation of [^{14}C]acetate-labeled lipids by two dimensional thin-layer chromatography (TLC) from different *Burkholderia* sensu latu (s.l) strains grown in LB medium at 30°C. **(A)** *Burkholderia cenocepacia* J2315, **(B)** *B. dolosa*, **(C)** *Paraburkholderia sortisoli*, **(D)** *P. xenovorans,* **(E)** *Caballeronia glathei*, and **(F)** *Robbsia andropogonis*. CL, cardiolipin; PG, phosphatidylglycerol; PE, phosphatidylethanolamine; 2OH-PE, hydroxylated phosphatidylethanolamine; OL, unmodified ornithine lipid; 2OH-OL, ornithine lipid 2-hydroxylated within ester-bound fatty acid.

Caballeronia, *Robbsia*, *Mycetohabitans*, and *Trinickia* was caused by the absence of a gene encoding an OlsB homolog or if it was due to a difference in gene regulation. We searched the genomes of *Paraburkholderia, Caballeronia, Robbsia, Mycetohabitans*, and *Trinickia* species for genes encoding homologs of the *N*-acyltransferase OlsB (Bcal1281) responsible for the first step in OL synthesis in *B. cenocepacia* (González-Silva et al., 2011). We found that all analyzed species possessed a gene coding for an OlsB homolog in their genome and that the genomic context around the respective genes was usually conserved in *Burkholderia* s.l. (data no shown). Bacterial species such as *Sinorhizobium meliloti*, *Rhodobacter sphaeroides*, *Pseudomonas fluorescens*, *Pseudomonas diminuta*, *Desulfovibrio alaskensis*, *Serratia proteamaculans,* and *Vibrio cholerae* do not form OL when the bacteria are grown in complex media (which are usually rich in phosphate), but induce the synthesis of OLs or/and other phosphorus-free lipids under phosphate-limiting growth conditions and replace some of their membrane phospholipids (Minnikin and Abdolrahimzadeh, 1974; Benning et al., 1995; Geiger et al., 1999; Lewenza et al., 2011; Bosak et al., 2016; Barbosa et al., 2018). In some of these bacteria, gene expression in response to phosphate limitation is known to be regulated by the two-component system PhoBR. At low phosphate concentrations, the response regulator PhoB is phosphorylated and binds to a highly conserved nucleotide motif called the Pho box in the promoter region of regulated genes (Geske et al., 2013). We would expect to find Pho boxes preceding the homologs of *olsB* genes if the synthesis of OLs can be induced at low phosphate concentrations and is regulated by PhoB. Using the sequences of identified Pho boxes from *Agrobacterium tumefaciens, S. meliloti, and Mesorhizobium loti* (Yuan et al., 2006; Geske et al., 2013) present in the promoter sequences of the genes encoding enzymes involved in the biosynthesis of glycolipids and OLs formed under conditions of phosphate limitation (**Supplementary Table 3**), a consensus sequence was obtained (**Figure 3A**). The genomes of 43 *Burkholderia* s.l. species were searched for the presence of Pho boxes upstream of the genes encoding OlsB homologs. Putative Pho boxes were detected in 21 of the analyzed genomes (**Supplementary Table 4**) and corresponded to fourteen species of the genus *Paraburkholderia*, two species of the genus *Caballeronia* (both genera do not constitutively synthesize OLs), and five species corresponding to the genus *Burkholderia* s.s. that constitutively synthesize OLs. Due to the evolutionary distance between α-proteobacteria and β-proteobacteria it is possible that we missed the Pho boxes in some genomes, but alternatively, OL formation might be regulated differently in these species. Using the putative Pho boxes of *Burkholderiales* (**Supplementary Table 4**), a new matrix was obtained (**Figure 3B**). When searching with this new matrix, putative Pho boxes were detected in the upstream regions of the genes encoding OlsB homologs in all 43 *Burkholderia* s.l genomes (data not shown).

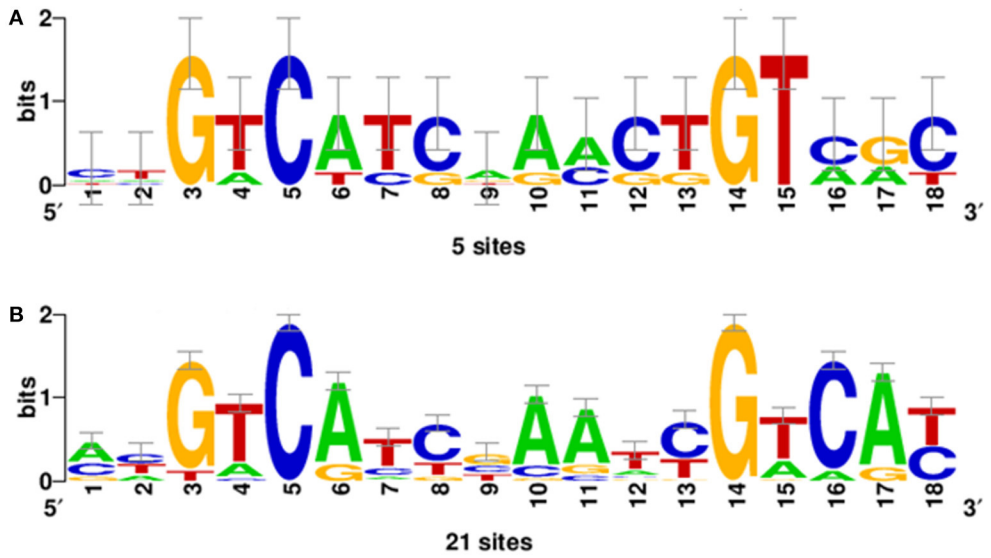

FIGURE 3 | Position-specific scoring matrix (PSSM) of Pho boxes obtained using the INFO-GIBBS program. **(A)** The PSSM derived from the sequences of Pho boxes of *A. tumefaciens*, *S. meliloti,* and *M. loti* present in the promoter sequences of the genes involved in the lipid biosynthesis of glycolipids and OLs (**Supplementary Table 3**). **(B)** PSSM obtained of putative Pho boxes from *Burkholderiales* (**Supplementary Table 4**) that constitutively synthesize OLs or not.

OlsF Expression Causes Constitutive OL Formation in *Robbsia andropogonis*

OL synthesis is constitutive in the *Burkholderia* s.s., but probably inducible in the other genera forming part of *Burkholderia* s.l., and an open question is if the presence or absence of OL affects the abiotic stress resistance of the bacteria and if it affects how the bacteria interact or how they are perceived by their eukaryotic hosts. Therefore, we wanted to study two pairs of strains either forming OLs or not, under abiotic stress conditions and during interactions with their eukaryotic hosts: (1) *B. cenocepacia* J2315 (Vandamme et al., 2003), which forms OL constitutively and its corresponding mutant deficient in OL formation NG1 (González-Silva et al., 2011) and (2) *R. andropogonis* (formerly *B. andropogonis*) which does not form OL constitutively and *R. andropogonis* constitutively forming OLs due to the presence of a plasmid harboring the gene *olsF* from *S. proteamaculans* (Vences-Guzmán et al., 2015).

R. andropogonis contains both forms of PE but no OLs when grown in complex medium (**Figure 2F**). To create a *R. andropogonis* strain constitutively forming OL, the bifunctional acyltranferase OlsF from *S. proteamaculans* (Vences-Guzmán et al., 2015) was expressed in the type strain *R. andropogonis* LMG2129 (Gillis et al., 1995). When analyzing the lipid composition of the OlsF-expressing strain using LC-MS, we observed the formation of two new lipids that were absent in the vector control strain (**Figures 4A,B**) and the lipid profile of the vector control strain is similar to the wild-type strain. These new lipids were identified as unmodified and hydroxylated OLs (**Figures 4C,D**), with the $[M\text{-}H]^-$ ions of their major species being observed at *m/z* 649.5 and 665.5, respectively. A comparison of the MS/MS spectra of *m/z* 649.5 and 665.5 (**Figures 4C,D**) indicates that the hydroxylation is located within the secondary fatty acyl chain. Specifically, the carboxylic anion of C18:1 fatty acid is observed at *m/z* 281 (**Figure 4C**), and the carboxylic anion of hydroxylated C18:1 fatty acid is observed at *m/z* 297 (**Figure 4D**). This result suggests that the hydroxylase responsible for 2-hydroxylation of OL is constitutively expressed whereas OL synthesis is inducible in the wild-type strain.

The Absence of OLs Slows the Growth of *B. cenocepacia* Under Acid Stress Conditions

Earlier reports had shown that *B. cepacia* induces OL formation under conditions of heat stress (Taylor et al., 1998). An importance of the presence of OL for heat and acid stress resistance had been also described in *R. tropici* (Rojas-Jiménez et al., 2005; Vences-Guzmán et al., 2011). We wondered if the absence of OL in *B. cenocepacia* NG1 (González-Silva et al., 2011) would negatively affect the stress tolerance of this strain in comparison with its respective wild-type J2315 or if the *R. andropogonis* strain constitutively forming OL would be more resistant to abiotic stress than the corresponding wild-type. Strains were exposed to various abiotic stresses such as variations in temperature (30, 37, or 42°C), in acidity (pH 4 or pH 7) or osmotic stress conditions (0.05 M, 0.5 M, or 1 M NaCl).

With respect to the temperature stress experiments, we observed that *R. andropogonis* strains grew best at 30°C (**Figure 5A**), and their growth was drastically affected at 37°C. The *R. andropogonis* strain constitutively forming OLs grows a little less than that of the wild-type strain at 37°C (**Figure 5B**). At 42°C, the *R. andropogonis* strains do not grow, apparently because they are lysed. No growth differences were observed between both *B. cenocepacia* strains at 30 and 37°C, but, at 42°C the absence of OL in *B. cenocepacia* NG1 apparently mildly

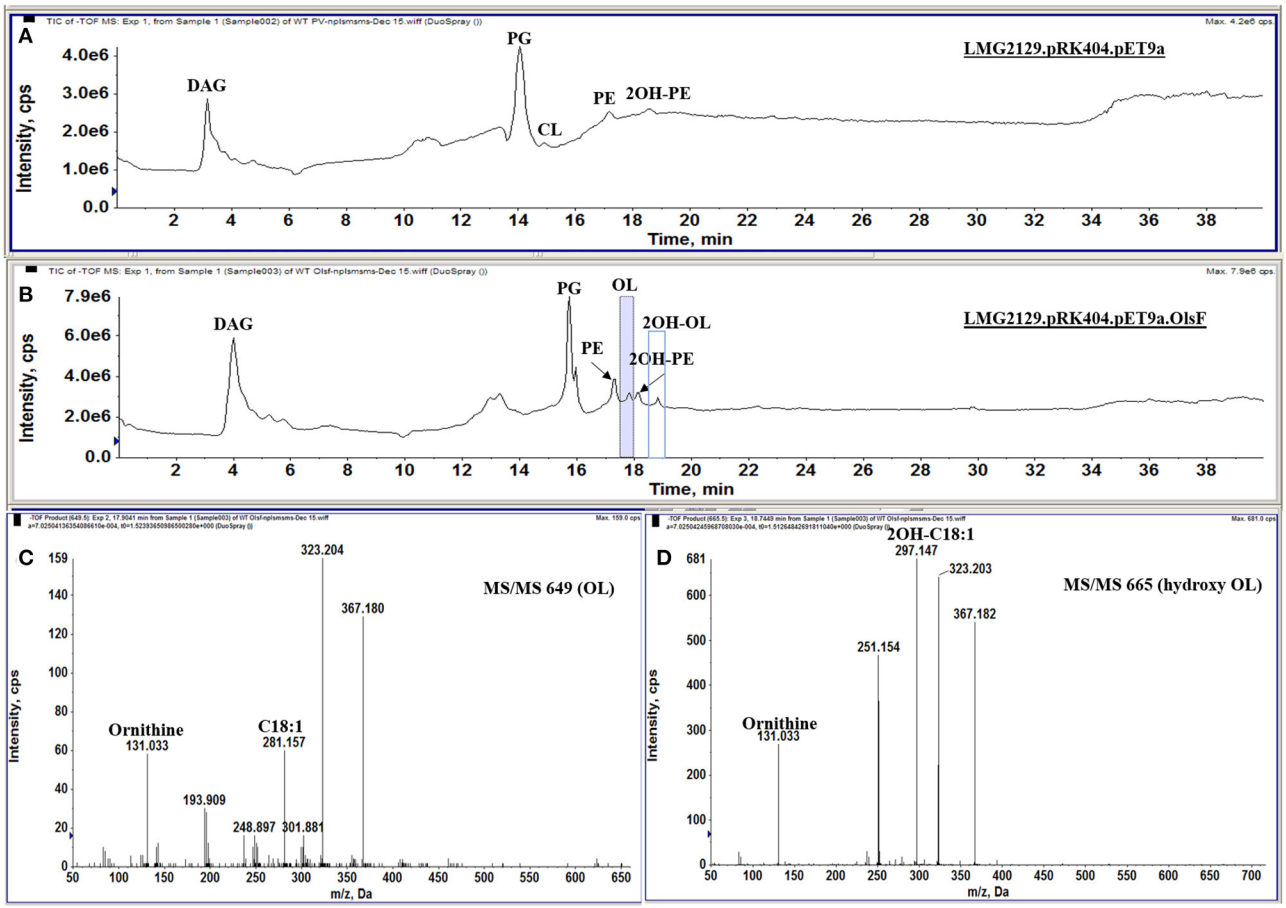

FIGURE 4 | *R. andropogonis* LMG2129 expressing OlsF forms OLs and 2OH-OLs. Shown are total ion chromatograms of the LC-MS analysis of total lipid extracts from **(A)** *R. andropogonis* LMG2129.pRK404.pET9a, and **(B)** *R. andropogonis* LMG2129.pRK404.pET9a.olsF. **(C)** Negative ion collision-induced dissociation mass spectra of [M-H]−ions at *m/z* 649 identifying OL and **(D)** *m/z* 665 showing that it is 2OH-OLs. The masses of major fragment ions indicate that the hydroxyl group is located in the secondary fatty acyl chain.

affected the growth of this strain compared to the wild-type J2315 (**Figure 5C**).

With respect to acid stress, we observed that the presence of OL did not affect the growth of the *R. andropogonis* strains. In contrast, the absence of OL in *B. cenocepacia* NG1 mildly affected the stress tolerance of this strain in comparison with its respective wild-type J2315. Also, it was observed that *R. andropogonis* strains were more resistant to pH 4 than the strains of *B. cenocepacia* (**Figures 5D,E**).

Osmotic stress is a common environmental stress for *B. cenocepacia,* to which it is exposed for example in the lungs of patients with cystic fibrosis (CF) or in soil (Smith et al., 1996). Behrends et al. (2011), investigated the tolerance to osmotic stress of five isolates of *B. cenocepacia* and elucidated the metabolic changes associated with osmotic stress when the isolates were exposed to 0.5 M NaCl. When exposing the strains to NaCl concentrations of 0.05, 0.5, and 1 M, we observed that there was no difference between the strains that synthesized OLs with those that did not (**Figures 5F–H**). *R. andropogonis* did not grow under osmotic stress conditions, whereas *B. cenocepacia* strains grow well in medium supplemented with 0.5 M NaCl, but did not grow in medium supplemented with 1 M NaCl.

The Absence of OLs in *B. cenocepacia* Reduces Their Virulence in a *Galleria mellonella* Infection Model Under Specific Conditions

Non-mammalian model systems of infection such as *G. mellonella* have been used to study the virulence of human pathogens such as *Candida albicans*, *Pseudomonas aeruginosa, Acinetobacter baumannii, Staphylococcus aureus, Enterococcus faecalis, Yersinia pseudotuberculosis*, and species of the genus *Burkholderia* (Fedhila et al., 2010). *G. mellonella* is a relatively cheap infection model, small in size, and possesses a short life cycle, the organisms can be handled easily and only small quantities of test compounds are required for injection. It has been used as a model for clinical infections as it can be maintained at physiological temperatures (37°C) for up to 5 days and its innate response to infections is structurally and

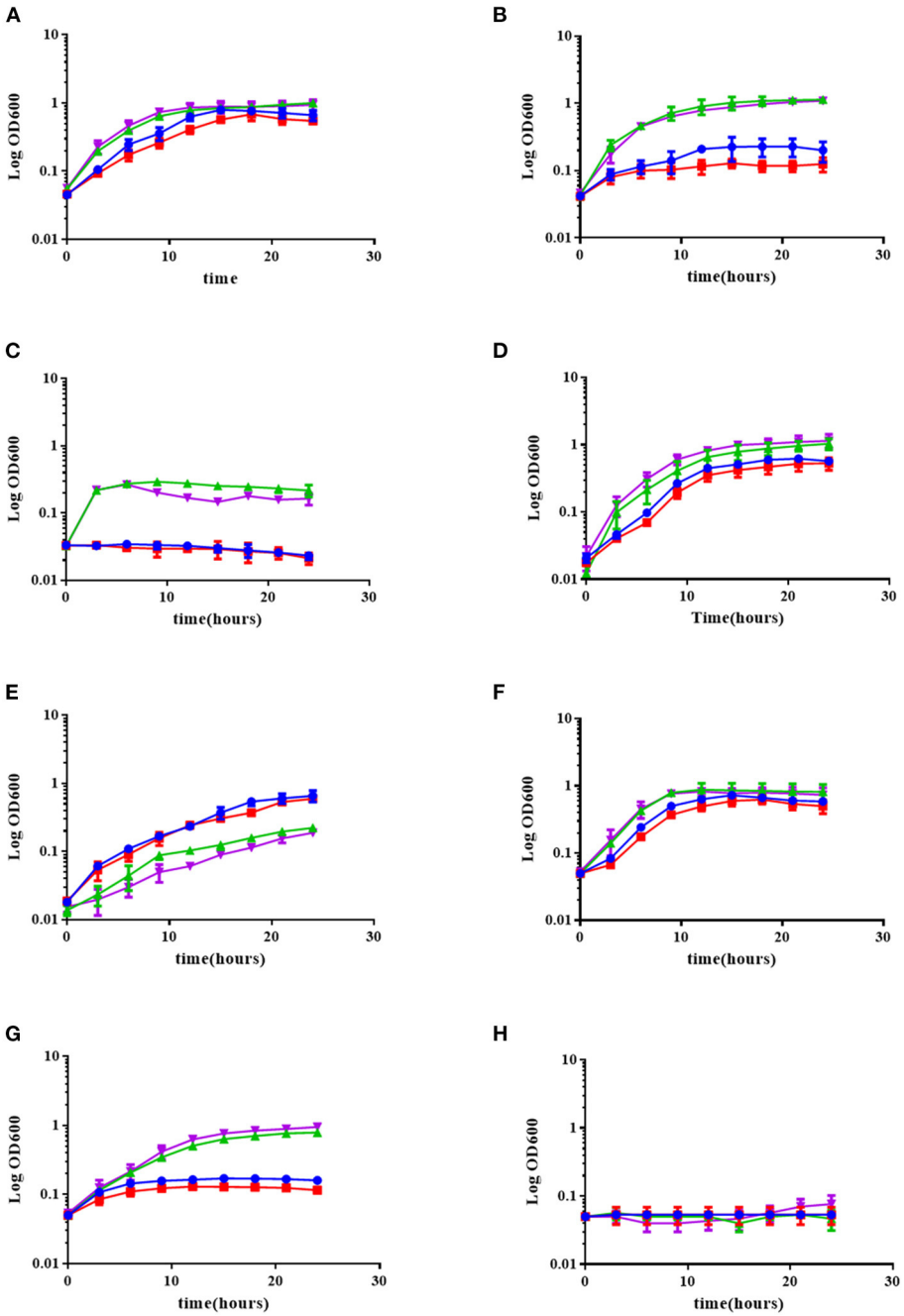

FIGURE 5 | The absence of OLs in the *B. cenocepacia* mutant deficient in *olsB* slightly affects its growth under low pH and temperature stress conditions, but the presence of OLs in *R. andropogonis* does not increase tolerance to environmental stress conditions. The strains were grown in complex LB medium at 30°C **(A)**, 37°C **(B)**, or 42°C **(C)**, or in complex LB medium adjusted to pH 7.0 **(D)**, or pH 4.0 **(E)**, and in complex LB medium supplemented with 0.05 M NaCl **(F)**, 0.5 M NaCl **(G)**, or 1 M NaCl **(H)** at 30°C. Growth kinetics were determined in a Synergy 2.0 Biotek, with medium shaking in 96-well microplates measuring every 3 h for 24 h, performing three independent repetitions. ▲ (green triangle up) *B. cenocepacia* J2315, ▼ (purple triangle down) *B. cenocepacia* NG1, • (blue circle) *R. andropogonis* LMG2129.pRK.pET9a, ■ (red square) *R. andropogonis* LMG2129.pRK.pET9a.olsF.

functionally similar to that of mammals. The release of reactive oxygen species and antimicrobial peptides into the hemolymph is triggered by humoral responses. Hemolymph clotting, equivalent to mammalian blood clotting, is followed by melanization. The cellular response results in the encapsulation of the infecting pathogen and phagocytosis (McCloskey et al., 2019). When control larvae were infiltrated with saline solution, with *E. coli* or simply picketed, they were asymptomatic and neither death

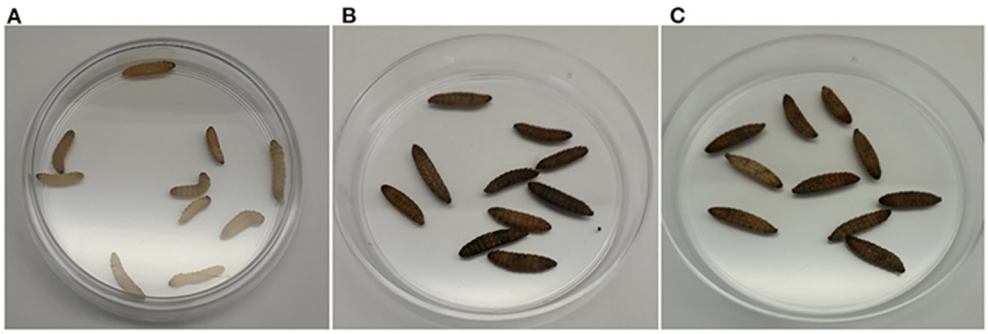

FIGURE 6 | Melanization in *Galleria mellonella* larvae infected with strains of *B. cenocepacia* occurs in the presence of the pathogen and does not depend on the presence of OLs. **(A)** Control larvae infiltrated with 10 mM $MgSO_4$, **(B)** Larvae infected with *B. cenocepacia* wild-type J2315, and **(C)** larvae infected with the *B. cenocepacia* mutant strain NG1. The pathogenicity assays were carried out using 10 insect larvae placed individually in 55 mm Petri dishes without diet and incubated at 30°C, evaluating mortality every 24 h after injection for 5 days before moving to the next larval growth stage. The melanization in *G. mellonella* larvae occurred along with larva death. Five independent experiments were performed.

nor melanization were observed until day 5 (**Figure 6A**). When evaluating the virulence of the *B. cenocepacia* wild-type J2315 and the mutant NG1 in larvae of *G. mellonella*, both strains caused the typical melanization (**Figures 6B,C**). When larvae of *G. mellonella* were infected with high concentrations of 3×10^7 CFU/ml and 3×10^6 CFU/ml, no differences between the larvae infected with the wild-type or the mutant strain were observed (**Figure 7**). However, at lower bacterial concentrations such as 3×10^5 CFU/ml, lower mortalities were observed in the case of the mutant lacking OLs. At this concentration, the wild-type strain *B. cenocepacia* J2315 caused a mortality rate of 44% after 5 days, while the mortality rate of the mutant strain NG1 was 28% after the same time. The minimum dose for larval mortality was 2×10^3 CFU/ml and only those larvae infected with the wild-type strain (2% mortality) presented larval death. Our results indicate that the presence of OLs causes an increase in mortality in the *G. mellonella* infection model under a cell density of 3×10^5 CFU/ml.

The Presence of OLs Induces an Increased Accumulation of Reactive Oxygen Species (ROS)

Plant innate immunity is the first line of defense against multiple pathogens. An important part of these immune responses is the production of extracellular reactive oxygen species (ROS). ROS can be present as impermeable superoxide (O_2^-) or as permeable hydrogen peroxide (H_2O_2) and it can be readily translocated from one cell to another (Ghosh et al., 2019). *B. andropogonis* LMG2129 has been described as bacterial stripe pathogen in maize and other plants (Moffett et al., 1986; Cother et al., 2004; Li and De Boer, 2005; Eloy and Cruz, 2008). We wanted to study if the presence or absence of OLs could modify the plant immune responses, in particular the ROS production by the plant upon infection with *R. andropogonis*. ROS formation in infiltrated plant leaves was quantified using the fluorescence emitted by the compound diacetate 2′, 7′-dichlorodihydrofluorescein (DCFH-DA) when it is oxidized by ROS (Lehmann et al., 2015). Directly after infection (0 days post infection (dpi) ROS formation is detected in leaves infected with *R. andropogonis* (**Figure 8**). Interestingly, ROS production was much higher in leaves infected with the strain LMG2129.pRK.pET9a.olsF constitutively forming OLs compared to mock-treated samples ($MgCl_2$) and to the wild-type strain (**Figures 8A–C**). To study the progression of ROS accumulation over time, ROS was quantified at 0, 3, 7, and 15 dpi (**Figure 8D**). Immediately after infection (0 dpi), ROS levels were twice as high in the strain constitutively forming OLs than the wild-type strain. ROS levels decreased at 3, 7, and 15 dpi, and no significant differences were detected between the different treatments at the later time points. Wounding caused by infiltration has been also described to induce ROS accumulation (Benikhlef et al., 2013). We observed that the possible damage by infiltrating the mock solution only slightly induces ROS formation (**Figures 8A,D**). Our results indicate that the presence of OLs triggers a strong ROS accumulation.

Constitutive OL Formation Does Not Modify the Progression of Infection Caused by *Robbsia andropogonis* on Its Host Maize

Based on the increased accumulation of ROS caused by the OL-forming *R. andropogonis* strain on maize (**Figure 8**), we wanted to characterize if the presence of OLs would modify the progression of the infection of *R. andropogonis*. Disease symptoms (dark-red lesions and chlorosis) and the number of living bacteria present inside the leaves were evaluated (**Figure 9**). Maize leaves were inoculated with the *R. andropogonis* strains and 3 days post-inoculation (dpi) disease symptoms were observed at the point of inoculation. These lesions continued to advance along the veins during the following days, while control plants infiltrated with the mock solution were asymptomatic (**Figure 9A**). Remarkably, the lesions caused by strains constitutively expressing OlsF were similar to the ones produced by the wild-type strain *B. andropogonis* LMG2129 (**Figures 9B–D**). Bacteria were isolated from leaves and colony-forming units (CFU) were determined at 0, 3, 7, and 15

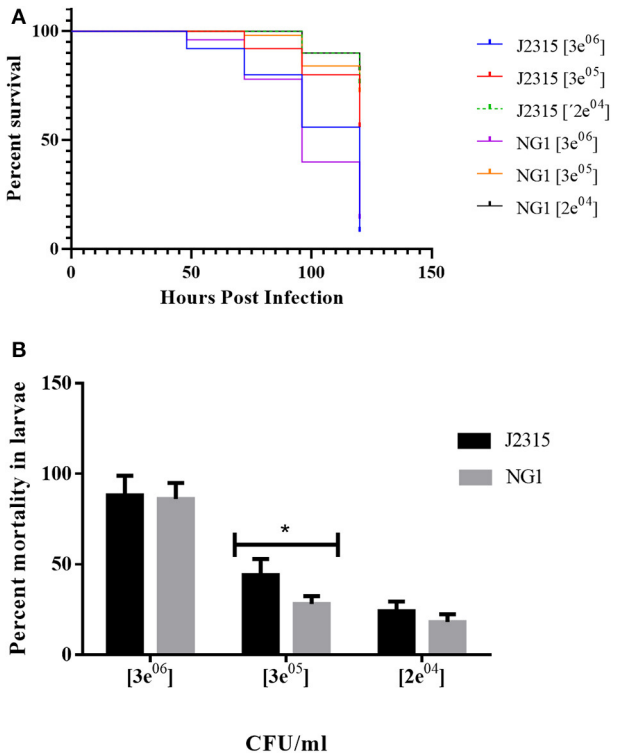

FIGURE 7 | *B. cenocepacia* lacking OLs caused lower mortality in *Galleria mellonella* larvae. **(A)** Kaplan-Meier survival curves: Larvae were injected with wild-type cells of *B. cenocepacia* J2315 or the mutant strain NG1 that does not synthesize OLs at concentrations of 3×10^7, 3×10^6, 3×10^5, and 2×10^4 CFU/ml. Survival was evaluated every 24 h for 5 days. At the highest concentration of 3×10^7 CFU/ml, the mortality for both strains was 100 %. **(B)** Strain J2315 (black columns) caused increased mortality after 5 days in the infection model of *G. mellonella* larvae compared with the mutant NG1 that lacking OLs (gray columns) at a concentration of 3×10^5 CFU/ml and was significantly different (*) with an analysis tailed *t*-test with a *P*-value: 0.0349. The experiment was repeated five times with similar results using fifty larvae in total for each treatment.

dpi. Bacterial numbers increased over time in infected plants and no significant differences could be observed between both strains (**Figure 9E**). These results suggest that the increased ROS accumulation induced by the overexpression of OLs did not influence the progression of the infection on maize.

DISCUSSION

The genus *Burkholderia* s.l. contains pathogenic, phytopathogenic, symbiotic and non-symbiotic species from a very wide range of environmental (soil, water, plants, fungi) and clinical (animal, human) habitats (Estrada-de Los Santos et al., 2018). One characteristic that was thought to be unique for the genus *Burkholderia* was the presence of the membrane lipids phosphatidylethanolamine and ornithine lipids (OLs), both in a hydroxylated and in a non-hydroxylated form (Yabuuchi et al., 1992). Here, we show that only *Burkholderia* s.s. species which often correspond to pathogens of humans, plants or animals constitutively form OLs and that these lipids are absent (or at least not constitutively formed) in the recently proposed genera *Paraburkholderia*, *Caballeronia*, *Robbsia*, *Trinickia*, and *Mycetohabitans* that are related to beneficial bacteria or that do not cause pathogenicity in humans. However, the absence of OLs is probably not caused by the absence of a copy of the *olsB* gene because we found that all analyzed species possessed a gene encoding a homolog of the *N*-acyltransferase OlsB (Bcal1281) responsible for the first step in OL synthesis in *B. cenocepacia* (González-Silva et al., 2011). The genomic context around the respective genes was usually conserved throughout *Burkholderia* s.l. (data not shown). The synthesis of OLs in the recently proposed genera is probably induced at low phosphate concentrations and regulated by PhoB as seen in a variety of other bacteria such as for example *Sinorhizobium meliloti*, *Rhodobacter sphaeroides*, *Serratia proteamaculans,* and *Vibrio cholerae*. This idea is supported by our prediction of Pho boxes preceding the respective putative *olsB* genes in 21 of the 43 genomes analyzed. The majority of these 21 genomes corresponded to genomes of bacteria that do not constitutively synthesize OLs (*Paraburkholderia* and *Caballeronia*), and five corresponded to bacterial species of the genus *Burkholderia* s.s. which constitutively synthesize OLs (**Supplementary Table 4**). It is possible that we did not detect the Pho boxes in some genomes, because of the evolutionary distance between α-proteobacteria and β-proteobacteria or alternatively that the genes responsible for OL formation are regulated differently in the other species. The presence of a Pho box in front of *olsB* in strains forming OLs constitutively might mean that expression of the respective *olsB* copies is increased further under phosphate-limiting conditions and that this leads to an increase in OL formation. Among the species that we identified with predicted Pho boxes was *P. xenovorans* and we cultured the strain LB400 (Goris et al., 2004) in minimal medium supplemented under low phosphate conditions. We observed that when cultivated in growth medium with 0 or 0.02 mM phosphate the strain was able to replace the phospholipids PE and 2OH-PE by modified and unmodified OLs (data not shown).

OLs can be modified by hydroxylations, either in the head group or in the fatty acid chains or by *N*-methylations (Sohlenkamp and Geiger, 2016). These modifications can play an important role in response to environmental stresses, and it has been observed that the amount of hydroxylated lipids (2OH-PE and 2OH-OL) increases at high temperatures in *B. cepacia* (Taylor et al., 1998) and that the hydroxylated OL NL1 is formed under acid stress in *B. cenocepacia* (González-Silva et al., 2011). In this study, we noticed that the absence of OLs in *B. cenocepacia* strain NG1, slightly affected tolerance to high temperature and acidic pH compared to its respective wild-type J2315 (**Figures 5C,E**) and we believe that the slight decrease in growth could be caused by the absence of the hydroxylated OL NL1. This observation is consistent with the earlier observations in *R. tropici*, where the presence of (hydroxylated) OLs conferred resistance to acid stress conditions and increased temperatures (Vences-Guzmán et al., 2011), although the effect observed in *B. cenocepacia* is clearly not as strong as in *R. tropici*. A possible explanation is that the presence/absence of OLs in *B. cenocepacia*

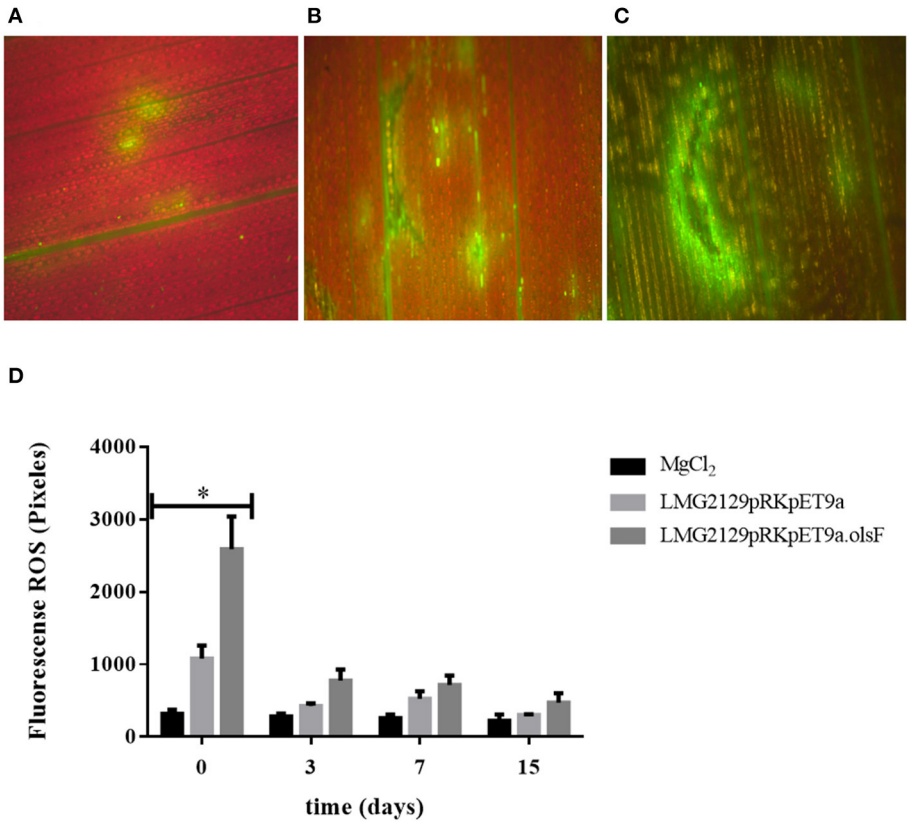

FIGURE 8 | The presence of ornithine lipids in *R. andropogonis* drastically increases the formation of reactive oxygen species (ROS) directly after infiltration into leaves of maize plants. ROS detection as DCFH-DA fluorescence **(A)** in maize leaves treated with mock solution, **(B)** treated with LMG2129.pRK404.pET9a, or **(C)** treated with LMG2129.pRK404.pET9a.olsF. **(D)** Densitometric quantification of ROS production by measuring DCFH-DA fluorescence showed that immediately after infection (0 dpi) the ROS levels were two times higher in leaves infiltrated with the strain constitutively forming OLs compared to leaves infiltrated with the wild-type strain, and were significantly different (*) determined by the analysis tailed *t*-test with a *P*-value: 0,0263 at 0 dpi. ROS concentration was lower on later times at 3, 7, and 15 dpi, and no differences were detected between the treatments. The experiment was repeated three times with similar results.

is not a main factor for stress resistance as seems to be the case in *R. tropici*, but a secondary factor contributing on a smaller scale to resistance to the stress conditions studied. In the case of the *R. andropogonis* strains, the strain expressing OlsF constitutively is growing slower under all conditions and it does not contribute to an increased resistance to abiotic stress conditions under the chosen expression conditions.

Membrane lipids can play a role in bacteria-host relationships during pathogenicity. Bartholomew et al. (2019), described that a 2-hydroxylation in lipid A contributes to virulence in *Acinetobacter baumannii* using *G. mellonella* as an infection model. They could show that only 10 % of the larvae survived when challenged with the wild-type and the complemented mutant. In contrast, 50 % of the larvae survived when inoculated with the *lpxO* mutant. A recent study by Kim et al. (2018) concluded that an increased formation of OLs might play a role in increasing persistence, while at the same time reducing the virulence of *Pseudomonas aeruginosa* on *Tenebrio molitor* (an insect) and in *Caenorhabditis elegans* (nematode). In our study, we observed that the mean of the mortalities after 5 days caused by the *B. cenocepacia* mutant deficient in OL seems to be lower at different cell densities tested, but a statistically significant reduction of mortality in the *G. mellonella* model was only observed at a cell density of 3×10^5 CFU/ml. A possible explanation is that OLs are not the main factor contributing to mortality in this experimental system, and that the effect of the absence of OLs might be covered by other unknown factors. Older studies by other groups about the immunogenicity of OLs have been contradictory and a probable reason is that OLs are not the only or main factor in all the bacteria studied, although they probably contribute to immunogenicity by interfering with or contributing to the effects of other virulence factors. We also observed that the resistance to a selected set of antibiotics and microbial peptides was not affected by the presence of OLs (data not shown). However, although OLs seem to affect the bacterial-host interaction, there are clearly additional factors present in *B. cenocepacia* affecting its virulence.

Plants have elaborate multilayered defense mechanisms to survive the constant attack of pathogens. The first line of defense is innate immunity, which is triggered by molecular components of microbes, called Microbe-Associated Molecular Patterns (MAMPs), including components of the bacterial membrane

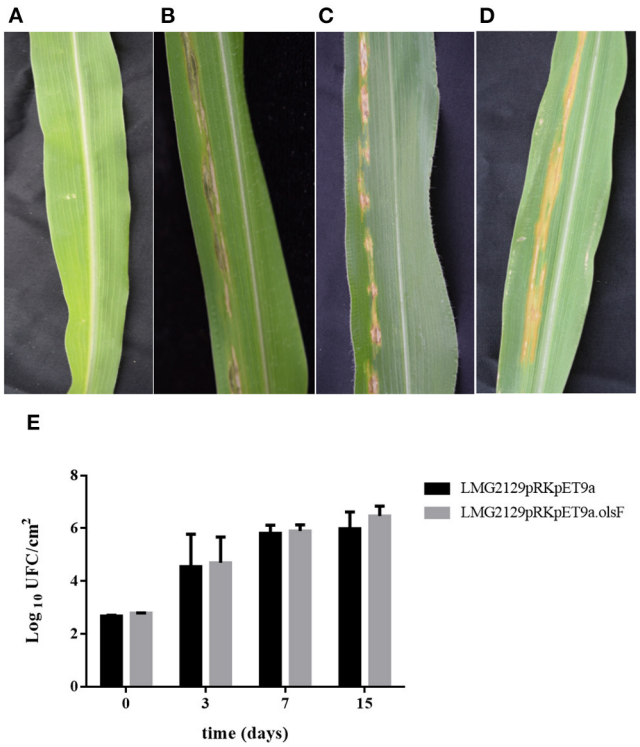

FIGURE 9 | The presence of OLs does not modify the progression of the infection of *R. andropogonis* in maize leaves. When infiltrated with *R. andropogonis* strains, maize leaves showed dark-red lesions and chlorosis, while control plants infiltrated with the mock solution were asymptomatic. **(A)** Mock solution, **(B)** wild-type LMG2129, **(C)** LMG2129.pRK404.pET9a, and **(D)** LMG2129.pRK404.pET9a.olsF. **(E)** The number of bacteria isolated from the maize leaves at 0, 3, 7, and 15 dpi, increased over time in infected plants, and no significant differences could be observed between the strains. The experiment was repeated three times with similar results using thirty corn plants in total for each treatment.

(Boller and Felix, 2009). Once MAMPs are recognized, the Pattern-Triggered Immunity (PTI) is activated, inducing a strong accumulation of ROS, MAPK signaling cascades and transcriptional activation of early defense response genes (Tsuda and Somssich, 2015). After this initial response, plants can induce the Effector-Triggered Immunity (ETI), which is based on the specific recognition of pathogen effectors by the *R* genes that leads to a local programmed cell death or hypersensitive response (HR) (Boller and Felix, 2009). The combined effect of PTI and ETI can block the invasion of pathogens, both locally at the infection site and systemically in uninfected leaves (Craig et al., 2009; Tsuda and Somssich, 2015). However, although PTI and ETI share similar molecular defense response elements, they have different dynamics in the activation and intensity (Katagiri and Tsuda, 2010). It was demonstrated that bacterial polar lipids can stimulate specific immune responses in the host (Melian et al., 2000; Roura-Mir et al., 2005). For instance, polar lipids of *B. pseudomallei* (e.g., ornithine lipids and rhamnolipids) induce antibody production and several polar lipids stimulate cellular immune responses (González-Juarrero et al., 2013). Here we show that *R. andropogonis* constitutively forming OLs causes an increased formation of ROS directly after infection of maize leaves (**Figure 8**), suggesting that plants can recognize OLs as MAMPs, inducing the PTI. As signaling molecules and as toxic compounds, ROS have been described to play multiple roles during plants life, including modulation of growth and development and response to abiotic and biotic stimuli (Camejo et al., 2016). The constitutive presence of OLs in *R. andropogonis* does not affect the number of bacteria growing inside the leaves (**Figure 9**), which suggests that a possible recognition of OLs and subsequent accumulation of ROS are not sufficient to stop the infection. One possibility to explain this phenomenon, is that the infection inflicted by *R. andropogonis* can be inhibited by activating the ETI but no PTI. This is in agreement with the observation that expression of the R gene Rxo1 controls the resistance against *R. andropogonis* in maize and rice (Zhao et al., 2005). Another possibility is that during the infection, *R. andropogonis* can produce scavenger molecules or detoxifying enzymes that can inhibit ROS, which has been previously described as invading strategy for multiple plant pathogens (Lehmann et al., 2015).

In conclusion, the presence of OLs in both bacteria-host interactions we studied affects how the pathogen is perceived and it may affect in some cases the outcome of the infection. Further work is required to determine the role of OLs in *Burkholderia* spp. during plant-pathogen and animal-pathogen interactions.

DATA AVAILABILITY STATEMENT

The raw data supporting the conclusions of this article will be made available by the authors, without undue reservation.

AUTHOR CONTRIBUTIONS

LAC-C, MS, and CS designed the study. LAC-C, RS-M, MT, LM-A, MÁV-G, and ZG carried out the experiments. LAC-C, LL, ZG, ED-G, MS, and CS carried out the data analysis and discussed the results. LAC-C and CS were involved in drafting the manuscript and all authors read and approved the final manuscript.

FUNDING

LAC-C is a Ph.D. student from Programa de Doctorado en Ciencias Biomédicas (PDCB), Universidad Nacional Autónoma de México (UNAM) and received fellowship 295964 from the Consejo Nacional de Ciencia y Tecnología (CONACyT). Research in our lab was supported by grants PAPIIT-UNAM (IN202413, IN208116, IN208319) and CONACyT-Mexico (153200, 237713). ZG and the mass spectrometry facility in the Department of Biochemistry, Duke University Medical Center, were supported by a LIPID MAPS glue grant (GM-069338) from the National Institutes of Health.

ACKNOWLEDGMENTS

We thank Irma Martínez Flores from CCG's Evolutionary Genomics program for her support in using the Synergy 2.0 Biotek equipment to measure the growth kinetics carried out in this work, and we thank the students Nahomy Donaji Rojas Sánchez and Naomi Astrid Mojica Quintana, who carried out its social service of the UAEM Clinical Laboratory Technician program supporting the execution of pathogenicity tests in plants and larvae.

SUPPLEMENTARY MATERIAL

The Supplementary Material for this article can be found online at: https://www.frontiersin.org/articles/10.3389/fmolb.2020.610932/full#supplementary-material

REFERENCES

Alghoribi, M. F., Gibreel, T. M., Dodgson, A. R., Beatson, S. A., and Upton, M. (2014). *Galleria mellonella* infection model demonstrates high lethality of ST69 and ST127 uropathogenic *E. coli*. *PLoS ONE* 9:e101547. doi: 10.1371/journal.pone.0101547

Barbosa, L. C., Goulart, C. L., Avellar, M. M., Bisch, P. M., and von Kruger, W. M. A. (2018). Accumulation of ornithine lipids in *Vibrio cholerae* under phosphate deprivation is dependent on VC0489 (OlsF) and PhoBR system. *Microbiology* 164, 395–399. doi: 10.1099/mic.0.000607

Bartholomew, T. L., Kidd, T. J., Sa Pessoa, J., Conde Alvarez, R., and Bengoechea, J. A. (2019). 2-Hydroxylation of *Acinetobacter baumannii* Lipid A contributes to virulence. *Infect. Immun.* 87:e00066-19. doi: 10.1128/IAI.00066-19

Behrends, V., Bundy, J. G., and Williams, H. D. (2011). Differences in strategies to combat osmotic stress in *Burkholderia cenocepacia* elucidated by NMR-based metabolic profiling. *Lett. Appl. Microbiol.* 52, 619–625. doi: 10.1111/j.1472-765X.2011.03050.x

Benikhlef, L., L'Haridon, F., Abou-Mansour, E., Serrano, M., Binda, M., Costa, A., et al. (2013). Perception of soft mechanical stress in *Arabidopsis* leaves activates disease resistance. *BMC Plant Biol.* 13:133. doi: 10.1186/1471-2229-13-133

Benning, C., Huang, Z. H., and Gage, D. A. (1995). Accumulation of a novel glycolipid and a betaine lipid in cells of *Rhodobacter sphaeroides* grown under phosphate limitation. *Arch. Biochem. Biophys.* 317, 103–111. doi: 10.1006/abbi.1995.1141

Bligh, E. G., and Dyer, W. J. (1959). A rapid method of total lipid extraction and purification. *Can. J. Biochem. Physiol.* 37, 911–917. doi: 10.1139/o59-099

Boller, T., and Felix, G. (2009). A renaissance of elicitors: perception of microbe-associated molecular patterns and danger signals by pattern-recognition receptors. *Annu. Rev. Plant Biol.* 60, 379–406. doi: 10.1146/annurev.arplant.57.032905.105346

Bosak, T., Schubotz, F., de Santiago-Torio, A., Kuehl, J. V., Carlson, H. K., Watson, N., et al. (2016). System-wide adaptations of *Desulfovibrio alaskensis* G20 to phosphate-limited conditions. *PLoS ONE* 11:e0168719. doi: 10.1371/journal.pone.0168719

Camejo, D., Guzman-Cedeno, A., and Moreno, A. (2016). Reactive oxygen species, essential molecules, during plant-pathogen interactions. *Plant Physiol. Biochem.* 103, 10–23. doi: 10.1016/j.plaphy.2016.02.035

Contreras-Moreira, B., and Vinuesa, P. (2013). GET_HOMOLOGUES, a versatile software package for scalable and robust microbial pangenome analysis. *Appl. Environ. Microbiol.* 79, 7696–7701. doi: 10.1128/AEM.02411-13

Cother, E. J., Noble, D., Peters, B. J., Albiston, A., and Ash, G. J. (2004). A new bacterial disease of jojoba (*Simmondsia chinensis*) caused by *Burkholderia andropogonis*. *Plant Pathol.* 53, 129–135. doi: 10.1111/j.0032-0862.2004.00982.x

Craig, A., Ewan, R., Mesmar, J., Gudipati, V., and Sadanandom, A. (2009). E3 ubiquitin ligases and plant innate immunity. *J. Exp. Bot.* 60, 1123–1132. doi: 10.1093/jxb/erp059

Defrance, M., and van Helden, J. (2009). Info-gibbs: a motif discovery algorithm that directly optimizes information content during sampling. *Bioinformatics* 25, 2715–2722. doi: 10.1093/bioinformatics/btp490

Depoorter, E., Bull, M. J., Peeters, C., Coenye, T., Vandamme, P., and Mahenthiralingam, E. (2016). *Burkholderia*: an update on taxonomy and biotechnological potential as antibiotic producers. *Appl. Microbiol. Biotechnol.* 100, 5215–5229. doi: 10.1007/s00253-016-7520-x

Dobritsa, A. P., and Samadpour, M. (2016). Transfer of eleven species of the genus Burkholderia to the genus Paraburkholderia and proposal of *Caballeronia* gen. nov. to accommodate twelve species of the genera *Burkholderia* and *Paraburkholderia*. *Int. J. Syst. Evol. Microbiol.* 66, 2836–2846. doi: 10.1099/ijsem.0.001065

Eloy, M., and Cruz, L. (2008). A new bacterial disease of carnation in Portugal caused by *Burkholderia andropogonis*. *Rev. Ciências Agrárias* 31, 89–95.

Elshafie, H. S., Viggiani, L., Mostafa, M. S., El-Hashash, M. A., Camele, I., and Bufo, S. A. (2017). Biological activity and chemical identification of ornithine lipid produced by *Burkholderia gladioli* pv. agaricicola ICMP 11096 using LC-MS and NMR analyses. *J. Biol. Res. Boll. Soc. Ital. Biol. Sperimentale* 90, 96–103. doi: 10.4081/jbr.2017.6534

Estrada-de Los Santos, P., Palmer, M., Chavez-Ramirez, B., Beukes, C., Steenkamp, E. T., Briscoe, L., et al. (2018). Whole genome analyses suggests that *Burkholderia* sensu lato contains two additional novel genera (*Mycetohabitans* gen. nov., and *Trinickia* gen. nov.): implications for the evolution of diazotrophy and nodulation in the *Burkholderiaceae*. *Genes* 9:389. doi: 10.3390/genes9080389

Fahraeus, G. (1957). The infection of clover root hairs by nodule bacteria studied by a simple glass slide technique. *J. Gen. Microbiol.* 16, 374–381. doi: 10.1099/00221287-16-2-374

Fedhila, S., Buisson, C., Dussurget, O., Serror, P., Glomski, I. J., Liehl, P., et al. (2010). Comparative analysis of the virulence of invertebrate and mammalian pathogenic bacteria in the oral insect infection model *Galleria mellonella*. *J. Invertebr. Pathol.* 103, 24–29. doi: 10.1016/j.jip.2009.09.005

Gao, J. L., Weissenmayer, B., Taylor, A. M., Thomas-Oates, J., López-Lara, I. M., and Geiger, O. (2004). Identification of a gene required for the formation of lyso-ornithine lipid, an intermediate in the biosynthesis of ornithine-containing lipids. *Mol. Microbiol.* 53, 1757–1770. doi: 10.1111/j.1365-2958.2004.04240.x

Geiger, O., González-Silva, N., López-Lara, I. M., and Sohlenkamp, C. (2010). Amino acid-containing membrane lipids in bacteria. *Prog. Lipid Res.* 49, 46–60. doi: 10.1016/j.plipres.2009.08.002

Geiger, O., Röhrs, V., Weissenmayer, B., Finan, T. M., and Thomas-Oates, J. E. (1999). The regulator gene *phoB* mediates phosphate stress-controlled synthesis of the membrane lipid diacylglyceryl-*N,N,N*-trimethylhomoserine in *Rhizobium* (*Sinorhizobium*) *meliloti*. *Mol. Microbiol.* 32, 63–73. doi: 10.1046/j.1365-2958.1999.01325.x

Geske, T., Vom Dorp, K., Dörmann, P., and Hölzl, G. (2013). Accumulation of glycolipids and other non-phosphorous lipids in *Agrobacterium tumefaciens* grown under phosphate deprivation. *Glycobiology* 23, 69–80. doi: 10.1093/glycob/cws124

Ghosh, S., Malukani, K. K., Chandan, R. K., Sonti, R. V., and Jha, G. (2019). "How plants respond to pathogen attack: interaction and communication," in *Sensory Biology of Plants*, ed S. Sopory (Singapore: Springer), 537. doi: 10.1007/978-981-13-8922-1_20

Gillis, M., Van, T. V., Bardin, R., Goor, M., Hebbar, P., Willems, A., et al. (1995). Polyphasic taxonomy in the genus *Burkholderia* leading to an emended description of the genus and proposition of *Burkholderia vietnamiensis* sp. nov. for N_2-fixing isolates from rice in Vietnam. *Int. J. Syst. Evol. Microbiol.* 45, 274–289. doi: 10.1099/00207713-45-2-274

González-Juarrero, M., Mima, N., Trunck, L. A., Schweizer, H. P., Bowen, R. A., Dascher, K., et al. (2013). Polar lipids of *Burkholderia pseudomallei* induce different host immune responses. *PLoS ONE* 8:e80368. doi: 10.1371/journal.pone.0080368

González-Silva, N., López-Lara, I. M., Reyes-Lamothe, R., Taylor, A. M., Sumpton, D., Thomas-Oates, J., et al. (2011). The dioxygenase-encoding *olsD* gene

from *Burkholderia cenocepacia* causes the hydroxylation of the amide-linked fatty acyl moiety of ornithine-containing membrane lipids. *Biochemistry* 50, 6396–6408. doi: 10.1021/bi200706v

Goris, J., De Vos, P., Caballero-Mellado, J., Park, J., Falsen, E., Quensen, J. F., et al. (2004). Classification of the biphenyl- and polychlorinated biphenyl-degrading strain LB400T and relatives as *Burkholderia xenovorans* sp. nov. *Int. J. Syst. Evol. Microbiol.* 54(Pt. 5), 1677–1681. doi: 10.1099/ijs.0.63101-0

Guindon, S., Dufayard, J. F., Lefort, V., Anisimova, M., Hordijk, W., and Gascuel, O. (2010). New algorithms and methods to estimate maximum-likelihood phylogenies: assessing the performance of PhyML 3.0. *Syst. Biol.* 59, 307–321. doi: 10.1093/sysbio/syq010

Hanahan, D. (1983). Studies on transformation of *Escherichia coli* with plasmids. *J. Mol. Biol.* 166, 557–580. doi: 10.1016/S0022-2836(83)80284-8

Jonsson, R., Struve, C., Jenssen, H., and Krogfelt, K. A. (2017). The wax moth *Galleria mellonella* as a novel model system to study Enteroaggregative *Escherichia coli* pathogenesis. *Virulence* 8, 1894–1899. doi: 10.1080/21505594.2016.1256537

Katagiri, F., Thilmony, R., and He, S. Y. (2002). The *Arabidopsis thaliana-Pseudomonas syringae* interaction. *Arabidopsis Book* 1:e0039. doi: 10.1199/tab.0039

Katagiri, F., and Tsuda, K. (2010). Understanding the plant immune system. *Mol. Plant Microbe Interact.* 23, 1531–1536. doi: 10.1094/MPMI-04-10-0099

Kim, S. K., Park, S. J., Li, X. H., Choi, Y. S., Im, D. S., and Lee, J. H. (2018). Bacterial ornithine lipid, a surrogate membrane lipid under phosphate-limiting conditions, plays important roles in bacterial persistence and interaction with host. *Environ. Microbiol.* 20, 3992–4008. doi: 10.1111/1462-2920.14430

Lehmann, S., Serrano, M., L'Haridon, F., Tjamos, S. E., and Métraux, J. P. (2015). Reactive oxygen species and plant resistance to fungal pathogens. *Phytochemistry* 112, 54–62. doi: 10.1016/j.phytochem.2014.08.027

Lewenza, S., Falsafi, R., Bains, M., Rohs, P., Stupak, J., Sprott, G. D., et al. (2011). The *olsA* gene mediates the synthesis of an ornithine lipid in *Pseudomonas aeruginosa* during growth under phosphate-limiting conditions, but is not involved in antimicrobial peptide susceptibility. *FEMS Microbiol. Lett.* 320, 95–102. doi: 10.1111/j.1574-6968.2011.02295.x

L'Haridon, F., Besson-Bard, A., Binda, M., Serrano, M., Abou-Mansour, E., Balet, F., et al. (2011). A permeable cuticle is associated with the release of reactive oxygen species and induction of innate immunity. *PLoS Pathog.* 7:e1002148. doi: 10.1371/journal.ppat.1002148

Li, X., and De Boer, S. H. (2005). First report of *Burkholderia andropogonis* causing leaf spots of *Bougainvillea* sp. in Hong Kong and Clover in Canada. *Plant Dis.* 89:1132. doi: 10.1094/PD-89-1132A

López-Lara, I. M., Gao, J. L., Soto, M. J., Solares-Pérez, A., Weissenmayer, B., Sohlenkamp, C., et al. (2005). Phosphorus-free membrane lipids of *Sinorhizobium meliloti* are not required for the symbiosis with alfalfa but contribute to increased cell yields under phosphorus-limiting conditions of growth. *Mol. Plant Microbe Interact.* 18, 973–982. doi: 10.1094/MPMI-18-0973

Matus-Acuña, V., Caballero-Flores, G., Reyes-Hernández, B. J., and Martínez-Romero, E. (2018). Bacterial preys and commensals condition the effects of bacteriovorus nematodes on *Zea mays* and *Arabidopsis thaliana*. *Appl. Soil Ecol.* 132, 99–106. doi: 10.1016/j.apsoil.2018.08.012

McCloskey, A. P., Lee, M., Megaw, J., McEvoy, J., Coulter, S. M., Pentlavalli, S., et al. (2019). Investigating the *in vivo* antimicrobial activity of a self-assembling peptide hydrogel using a *Galleria mellonella* infection model. *ACS Omega* 4, 99–106. doi: 10.1021/acsomega.8b03578

Melian, A., Watts, G. F., Shamshiev, A., De Libero, G., Clatworthy, A., Vincent, M., et al. (2000). Molecular recognition of human CD1b antigen complexes: evidence for a common pattern of interaction with alpha beta TCRs. *J. Immunol.* 165, 4494–4504. doi: 10.4049/jimmunol.165.8.4494

Miller, J. (1972). "Experiments in molecular genetics," in *Experiments in Molecular Biology,* eds J. Miller and J. B. Miller (Cold Spring Harbor, NY: Cold Spring Harbor Laboratory Press), 431–433.

Minnikin, D. E., and Abdolrahimzadeh, H. (1974). The replacement of phosphatidylethanolamine and acidic phospholipids by an ornithine-amide lipid and a minor phosphorus-free lipid in *Pseudomonas fluorescens* NCMB 129. *FEBS Lett.* 43, 257–260. doi: 10.1016/0014-5793(74)80655-1

Moffett, M. L., Hayward, A. C., and Fahy, P. C. (1986). Five new hosts of *Pseudomonas andropogonis* occurring in eastern Australia: host range and characterization of isolates. *Plant Pathol.* 35, 34–43. doi: 10.1111/j.1365-3059.1986.tb01978.x

Palleroni, N. J. (2015). "Burkholderia," in *Bergey's Manual of Systematics of Archaea and Bacteria*, eds M. Trujillo, P. DeVos, B. Hedlund, P. Kämpfer, F. Rainey, and W. B. Whitman, 1–50. doi: 10.1002/9781118960608

Rojas-Jiménez, K., Sohlenkamp, C., Geiger, O., Martínez-Romero, E., Werner, D., and Vinuesa, P. (2005). A ClC chloride channel homolog and ornithine-containing membrane lipids of *Rhizobium tropici* CIAT899 are involved in symbiotic efficiency and acid tolerance. *Mol. Plant Microbe Interact.* 18, 1175–1185. doi: 10.1094/MPMI-18-1175

Rojas-Rojas, F. U., López-Sánchez, D., Meza-Radilla, G., Méndez-Canarios, A., Ibarra, J. A., and Estrada-de Los Santos, P. (2019). The controversial *Burkholderia cepacia* complex, a group of plant growth promoting species and plant, animals and human pathogens. *Rev. Argent. Microbiol.* 51, 84–92. doi: 10.1016/j.ram.2018.01.002

Roura-Mir, C., Wang, L., Cheng, T. Y., Matsunaga, I., Dascher, C. C., Peng, S. L., et al. (2005). *Mycobacterium tuberculosis* regulates CD1 antigen presentation pathways through TLR-2. *J. Immunol.* 175, 1758–1766. doi: 10.4049/jimmunol.175.3.1758

Sawana, A., Adeolu, M., and Gupta, R. S. (2014). Molecular signatures and phylogenomic analysis of the genus *Burkholderia*: proposal for division of this genus into the emended genus *Burkholderia* containing pathogenic organisms and a new genus *Paraburkholderia* gen. nov. harboring environmental species. *Front. Genet.* 5:429. doi: 10.3389/fgene.2014.00429

Simmons, J. S. (1926). A culture medium for differentiating organisms of typhoid-colon aerogenes groups and for isolation of certain fungi: with colored plate. *J. Infect. Dis.* 39, 209–214. doi: 10.1093/infdis/39.3.209

Simon, R., Priefer, U., and Pühler, A. (1983). A broad host range mobilization system for *in vivo* genetic engineering - transposon mutagenesis in gram-negative bacteria. *Biotechnology* 1, 784–791. doi: 10.1038/nbt1183-784

Smith, J. J., Travis, S. M., Greenberg, E. P., and Welsh, M. J. (1996). Cystic fibrosis airway epithelia fail to kill bacteria because of abnormal airway surface fluid. *Cell* 85, 229–236. doi: 10.1016/S0092-8674(00)81099-5

Sohlenkamp, C., and Geiger, O. (2016). Bacterial membrane lipids: diversity in structures and pathways. *FEMS Microbiol. Rev.* 40, 133–159. doi: 10.1093/femsre/fuv008

Tahara, Y., and Fujiyoshi, Y. (1994). A new method to measure bilayer thickness: cryo-electron microscopy of frozen hydrated liposomes and image simulation. *Micron* 25, 141–149. doi: 10.1016/0968-4328(94)90039-6

Taylor, C. J., Anderson, A. J., and Wilkinson, S. G. (1998). Phenotypic variation of lipid composition in *Burkholderia cepacia*: a response to increased growth temperature is a greater content of 2-hydroxy acids in phosphatidylethanolamine and ornithine amide lipid. *Microbiology* 144(Pt. 7), 1737–1745. doi: 10.1099/00221287-144-7-1737

Tsuda, K., and Somssich, I. E. (2015). Transcriptional networks in plant immunity. *New Phytol.* 206, 932–947. doi: 10.1111/nph.13286

Turatsinze, J. V., Thomas-Chollier, M., Defrance, M., and van Helden, J. (2008). Using RSAT to scan genome sequences for transcription factor binding sites and cis-regulatory modules. *Nat. Protoc.* 3, 1578–1588. doi: 10.1038/nprot.2008.97

Vandamme, P., Holmes, B., Coenye, T., Goris, J., Mahenthiralingam, E., LiPuma, J. J., et al. (2003). *Burkholderia cenocepacia* sp. nov.–a new twist to an old story. *Res. Microbiol.* 154, 91–96. doi: 10.1016/S0923-2508(03)00026-3

Vences-Guzmán, M. A., Guan, Z., Escobedo-Hinojosa, W. I., Bermúdez-Barrientos, J. R., Geiger, O., and Sohlenkamp, C. (2015). Discovery of a bifunctional acyltransferase responsible for ornithine lipid synthesis in *Serratia proteamaculans*. *Environ. Microbiol.* 17, 1487–1496. doi: 10.1111/1462-2920.12562

Vences-Guzmán, M. A., Guan, Z., Ormeno-Orrillo, E., González-Silva, N., López-Lara, I. M., Martínez-Romero, E., et al. (2011). Hydroxylated ornithine lipids increase stress tolerance in *Rhizobium tropici* CIAT899. *Mol. Microbiol.* 79, 1496–1514. doi: 10.1111/j.1365-2958.2011.07535.x

Vinuesa, P., Ochoa-Sánchez, L. E., and Contreras-Moreira, B. (2018). GET_PHYLOMARKERS, a Software package to select optimal orthologous clusters for phylogenomics and inferring pan-genome phylogenies, used for a critical geno-taxonomic revision of the genus *Stenotrophomonas*. *Front. Microbiol.* 9:771. doi: 10.3389/fmicb.2018.00771

Weissenmayer, B., Gao, J. L., López-Lara, I. M., and Geiger, O. (2002). Identification of a gene required for the biosynthesis of ornithine-derived lipids. *Mol. Microbiol.* 45, 721–733. doi: 10.1046/j.1365-2958.2002.03043.x

Yabuuchi, E., Kosako, Y., Oyaizu, H., Yano, I., Hotta, H., Hashimoto, Y., et al. (1992). Proposal of *Burkholderia* gen. nov. and transfer of seven species of the genus *Pseudomonas* homology group II to the new genus, with the type species *Burkholderia cepacia* (Palleroni and Holmes 1981) comb. nov. *Microbiol. Immunol.* 36, 1251–1275. doi: 10.1111/j.1348-0421.1992.tb02129.x

Yuan, Z. C., Zaheer, R., Morton, R., and Finan, T. M. (2006). Genome prediction of PhoB regulated promoters in *Sinorhizobium meliloti* and twelve proteobacteria. *Nucleic Acids Res.* 34, 2686–2697. doi: 10.1093/nar/gkl365

Zhao, B., Lin, X., Poland, J., Trick, H., Leach, J., and Hulbert, S. (2005). A maize resistance gene functions against bacterial streak disease in rice. *Proc. Natl. Acad. Sci. U.S.A.* 102, 15383–15388. doi: 10.1073/pnas.0503023102

Conflict of Interest: The authors declare that the research was conducted in the absence of any commercial or financial relationships that could be construed as a potential conflict of interest.

frontiers in Molecular Biosciences

REVIEW
published: 25 March 2021
doi: 10.3389/fmolb.2021.666203

Eugene P. Kennedy's Legacy: Defining Bacterial Phospholipid Pathways and Function

William Dowhan†* and *Mikhail Bogdanov*†

Department of Biochemistry and Molecular Biology, McGovern Medical School, University of Texas Health Science Center, Houston, TX, United States

In the 1950's and 1960's Eugene P. Kennedy laid out the blueprint for phospholipid biosynthesis in somatic cells and *Escherichia coli*, which have been coined the Kennedy Pathways for phospholipid biosynthesis. His research group continued to make seminal contributions in the area of phospholipids until his retirement in the early 1990's. During these years he mentored many young scientists that continued to build on his early discoveries and who also mentored additional scientists that continue to make important contributions in areas related to phospholipids and membrane biogenesis. This review will focus on the initial *E. coli* Kennedy Pathways and how his early contributions have laid the foundation for our current understanding of bacterial phospholipid genetics, biochemistry and function as carried on by his scientific progeny and others who have been inspired to study microbial phospholipids.

Keywords: *Escherichia coli*, phospholipid metabolism, membrane proteins, Gram-negative, charge balance rule, lipid asymmetry, protein folding

OPEN ACCESS

Edited by:
Nienke Buddelmeijer, Institut Pasteur, France

Reviewed by:
Charles Rock, St. Jude Children's Research Hospital, United States
Will Prinz, National Institute of Diabetes and Digestive and Kidney Diseases, National Institutes of Health (NIH), United States

***Correspondence:**
William Dowhan
william.dowhan@uth.tmc.edu

†These authors have contributed equally to this work and share senior authorship

Specialty section:
This article was submitted to Cellular Biochemistry, a section of the journal Frontiers in Molecular Biosciences

Received: *09 February 2021*
Accepted: *01 March 2021*
Published: *25 March 2021*

Citation:
Dowhan W and Bogdanov M (2021) Eugene P. Kennedy's Legacy: Defining Bacterial Phospholipid Pathways and Function. Front. Mol. Biosci. 8:666203. doi: 10.3389/fmolb.2021.666203

INTRODUCTION

Studies of lipid metabolism were first initiated in plants and mammals in the 1920 followed by the establishment of the Kennedy Pathway for phospholipid synthesis in mammalian cells in the 1950's (Kennedy, 1992). It was not until the 1960's that serious studies of bacterial lipid metabolism began largely in the laboratory of Eugene Kennedy at Harvard Medical School. During this decade Kennedy's laboratory defined the pathways for the synthesis of the major phospholipids [phosphatidylethanolamine (PE), phosphatidylglycerol (PG) and cardiolipin (CL)] in *Escherichia coli*. With this blueprint in hand, the following two decades experienced an explosion in *E. coli* glycerol-based phospholipid metabolism, enzymology, genetics and function largely by Kennedy and his scientific progeny. Lipid A-base lipopolysaccharide (LPS) is the other phospholipid of Gram-negative that forms the outer lipid leaflet of the outer membrane of Gram-negative bacteria. The biochemistry, enzymology and genetics of Lipid A were largely defined by Chris Raetz (Dowhan et al., 2013; Whitfield and Trent, 2014), a trainee of the Kennedy lab. These initial findings laid the foundation for continuing studies in *E. coli* and other microbial systems including yeast providing excellent model systems for studying lipid involvement in bacterial antibiotic resistance and function of lipids in both prokaryotic and eukaryotic systems. The current state of pathways, enzymology, and genetics of glycerol-based phospholipid biosynthesis in *E. coli* will be reviewed followed by how this collective information has been used to establish specific functions for individual phospholipids in bacteria. Membrane bilayer phospholipid asymmetry studies are well advanced in eukaryotic cells but only beginning to be extensively studied in bacteria. Methods

for determining and perturbing lipid bilayer asymmetry in Gram-negative bacteria will be reviewed as a prerequisite for determining the role of such asymmetry in cell function. Hopefully this review will provide a basis for extended studies of phospholipids in other bacteria and lay the foundation for further studies in *E. coli*.

CURRENT STATE OF THE BACTERIAL KENNEDY PATHWAY

In *E. coli* (see **Figure 1**) and other γ-proteobacteria phosphatidic acid (PA) biosynthesis begins by acylation at the 1-position of *sn*-glycerol-3-phosphate (G3P) by either a long chain fatty acid- (primarily palmitic acid) acyl carrier protein (ACP) or CoA derivative catalyzed by PlsB (Ray et al., 1970). Many Gram-negative bacteria and all Gram-positive bacteria utilize PlsY (Lu et al., 2006), which use acyl-phosphate derivatives of long chain fatty acids. Acylation at the 2-position is catalyzed by PlsC (Coleman, 1990), which uses both ACP and CoA fatty acids (mainly long chain unsaturated) derivatives in γ-proteobacteria and only ACP derivatives in most other bacteria. The two-step acylation process generates membrane-residing PA followed by conversion of this short-lived intermediate precursor to CDP-diacylglycerol (CDP-DAG), which functions as a donor of phosphatidyl moieties to the primary hydroxyl groups of either L-serine or G3P to form phosphatidylserine (PS) or phosphatidylglycerol phosphate (PGP), respectively. The latter is dephosphorylated to form PG and the former is decarboxylated to form PE. Some of the PG pool is further converted to CL. PE, PG, and CL are the major end products of the Kennedy Pathway and the primary lipid components of the inner membrane and periplasmic leaflet of the outer membrane. The levels of the intermediates PA, CDP-DAG, PS, and PGP are extremely low in wild-type *E. coli*, representing less than 0.1–0.3% of the total cellular phospholipid. These intermediates are found in higher levels in *E. coli* lipid mutants as will be discussed below. In *E. coli* diacylglycerol (DAG) derived from transfer of *sn*-glycerol-1-phosphate from PG in the formation of membrane derived oligosaccharide (MDO) (Schneider et al., 1979; Goldberg et al., 1981) is phosphorylated by DgkA to generate PA in the inner membrane (Pieringer and Kunnes, 1965; Raetz and Newman, 1978). MDO is a periplasmic oligosaccharide osmoregulatory decorated by *sn*-glycerol-1-phosphate and ethanolamine-phosphate derived from PE (Kennedy et al., 1976). The gene for the latter decoration has not been identified. Interestingly, details of the synthesis of PA came well after most of the Kennedy Pathway was worked out for *E. coli*.

Several differences exist in phospholipid biosynthetic pathways between prokaryotes and eukaryotes and within prokaryotes. Two *de novo* biosynthetic routes, collectively also known as the Kennedy Pathway were elucidated over 60 years ago and are responsible for the production of the majority of phosphatidylcholine (PC) and PE in most eukaryotic cells (Kennedy, 1992). CDP-choline or CDP-ethanolamine is formed by condensation of CTP with choline-phosphate or ethanolamine-phosphate followed by reaction with DAG to form phosphatidylcholine (PC) or PE, respectively (Kennedy and Weiss, 1956). Although *E. coli* does not contain PC, many Gram-negative bacteria contain PC made either by methylation of PE or phosphatidyl transfer from CDP-DAG to choline (Lopez-Lara and Geiger, 2017).

Somatic cells synthesize PS by headgroup exchange between PE or PC with L-serine (Stone and Vance, 2000). Bacteria (Kanfer and Kennedy, 1962) and most fungi (Bae-Lee and Carman, 1984) utilize the prokaryotic pathway where L-serine displaces CMP from CDP-DAG to form PS. Psd, which is highly homologous between eukaryotes and prokaryotes (Voelker, 1997), catalyzes the decarboxylation of PS to PE (Kanfer and Kennedy, 1964). The decarboxylation pathway is the sole route for PE biosynthesis in *E. coli* and the major one in *Saccharomyces cerevisiae*.

A single PgsA catalyzes the displacement of CMP by G3P to form PGP in *E. coli* (Kanfer and Kennedy, 1964) and the mitochondria of somatic cells (Kiyasu et al., 1963; Kawasaki et al., 1999, 2001) and yeast (Chang et al., 1998). Eukaryotes utilize a single essential mitochondrial-localized PGP phosphatase (Zhang et al., 2011) while prokaryotes have multiple activities (Icho and Raetz, 1983; Funk et al., 1992) with PgpA (Chang and Kennedy, 1967) being the primary phosphatase. Most prokaryotes express multiple CL synthases with ClsA being the primary activity in *E. coli* with little understanding of the function of the other enzymes. ClsA is present under all growth conditions while ClsB and ClsC are induced during late log and stationary phases of growth (Tan et al., 2012). In bacteria synthesis of CL proceeds by a non-energy requiring condensation of two PG molecules with one PG acting as phosphatidyl donor and the other as a phosphatidyl acceptor with the release of glycerol (Hirschberg and Kennedy, 1972). Interestingly, ClsB also catalyzes headgroup exchange between PE and glycerol to form low amounts of PG and free ethanolamine (Li et al., 2016).

In mitochondria the formation of CL is energy dependent utilizing a transfer of PA from CDP-DAG to the terminal hydroxyl of PG (Hostetler et al., 1972). This irreversible reaction exhausts the pool of PG to maintain high CL and low PG levels in mitochondria. In contrast bacteria exhibit higher levels of PG versus CL. Since the bacterial energy independent reaction is fully reversible, the PG/CL ratio can change with an increase in CL levels in the stationary phase (Hiraoka et al., 1993) or after abiotic osmotic or thermal insults (Luevano-Martinez et al., 2015). The line between eukaryotic and prokaryotic Cls enzymes has become blurred by identification of a eukaryote-type CDP-DAG-dependent-Cls in *Streptomyces coelicolor* (Sandoval-Calderon et al., 2009) and a potentially PG condensing-Cls in the protozoan *Trypanosoma brucei* (Serricchio and Bütikofer, 2012).

The diversity of membrane lipid compositions within the Eubacterial (Lopez-Lara and Geiger, 2017) and Archaebacterial (Matsumi et al., 2011). Kingdoms is as diverse as the number of organisms; the latter phospholipids are characterized by containing *sn*-glycerol-1-phosphate in ether linkage to long chain isoprenoid alcohols. However, the pathways for generating the hydrophilic headgroups of the major phospholipids are very similar to that in Eubacteria. Covering this diversity is well beyond the scope of this review. The Kennedy Pathway

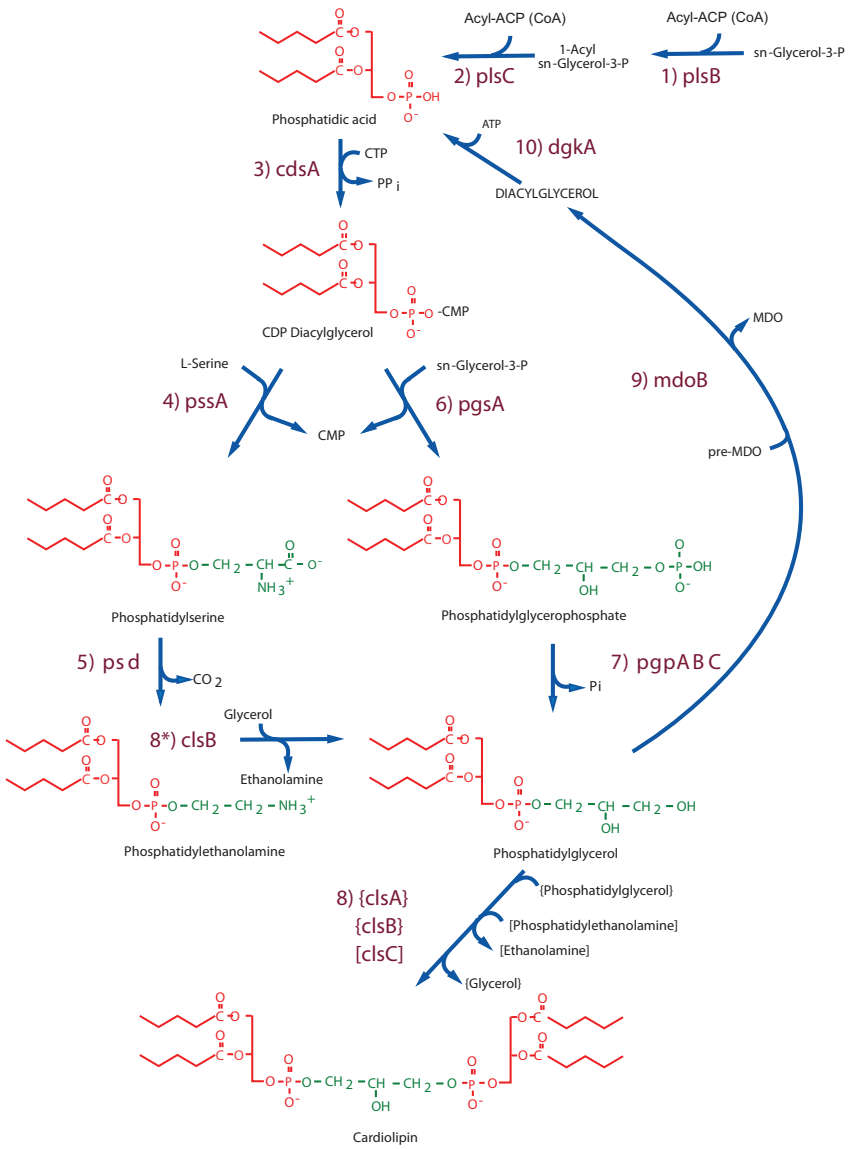

FIGURE 1 | Kennedy Pathway for synthesis of phospholipids in *Escherichia coli*. The following enzymes with their respective genes named carry out: (1) G3P acyltransferase (PlsB); (2) 1-Acyl-G3P acyltransferase (PlsC); (3) CDP-DAG synthase (CdsA); (4) phosphatidylserine synthase (PssA); (5) phosphatidylserine decarboxylase (Psd); (6) phosphatidylglycerophosphate synthase (PgsA); (7) phosphatidylglycerophosphate phosphatases (PgpABC) encoded by three genes; (8) cardiolipin synthase (Cls) encoded by three genes. ClsA and ClsB condense 2 PGs while ClsC condenses PG and PE. ClsB (8*) can also displace ethanolamine from PE using glycerol to make PG, which can be utilized to make CL in *pgsA* null strains. (9) PG pre-membrane derived oligosaccharide (MDO) *sn*-glycerol-1-*P* transferase (MDO synthase); 10. DAG kinase (DgkA). Figure (modified) and legend reprinted by permission from Elsevier (Dowhan, 2013): Copyright 2013.

phospholipid biosynthetic blueprint for *E. coli* has provided a starting point for elucidating lipid biosynthetic pathways throughout these kingdoms where differences and similarity to that of *E. coli* have been detailed.

GENETICS OF PHOSPHOLIPID METABOLISM

All the genes encoding the pathways depicted in **Figure 1** have been identified and their sequences are available either from direct sequencing or the sequence of the *E. coli* genome. Furthermore, there are mutants available for each gene. The first mutants reported in *E. coli* phospholipid synthesis were in PlsB (Bell, 1974, 1975) and PssA (Okonogi et al., 1971; Ohta et al., 1974; Ohta and Shibuya, 1977). However, a major advance in phospholipid biosynthetic enzyme genetics can be contributed to Chris Raetz, a disciple of the Kennedy lab. Since it was initially thought that null mutants in genes encoding these enzymes would be lethal, Raetz isolated conditionally lethal temperature sensitive mutants using a novel filter paper assay method (Raetz, 1975). Using this technique mutants were isolated in *pssA*

(Raetz et al., 1977), *pgsA* (Raetz, 1975), *pgpAB* (Icho and Raetz, 1983; Icho, 1988a,b), *cdsA* (Ganong et al., 1980; Icho et al., 1985b) and *dgkA* (Raetz and Newman, 1978; Lightner et al., 1983).

A *psd* temperature sensitive mutant was isolated by a modified brute force scanning after mutagenesis (Hawrot and Kennedy, 1976). A glycerol auxotroph turned out to encode a PlsB mutant with a 10-fold higher Km for G3P (Bell, 1974, 1975; Lightner et al., 1980). A mutation in *mdoB* (Jackson et al., 1984) was isolated as a suppressor of the large accumulation of DAG in a *dgkA* mutant. A screen of temperature sensitive mutants that were sensitive to deoxycholate (indicative of a defect in outer membrane integrity) turned out to be mutants in *plsC* (Coleman, 1990). Null mutants in the *dgkA* gene result in a 20-fold accumulation of DAG, which in an osmotically challenging environments is lethal (Raetz and Newman, 1978) due to failure of cells to divide (Kawashima et al., 2008). Therefore, DgkA acts as a salvage enzyme to permit the reutilization of DAG molecules for phospholipid synthesis in wild-type cells (Kennedy, 1982). MDO biogenesis accounts for only 2/3 of the DAG that accumulates upon *dgkA* inactivation (Rotering and Raetz, 1983). Most likely the remaining DAG results from LPS modification by transfer of ethanolamine-phosphate from PE catalyzed by the *eptA* gene product (Reynolds et al., 2005; Samantha and Vrielink, 2020).

The *pgpAB* double null strain still contains PGP phosphatase activity and grows normally. The original screening for phosphatase mutants missed PgsC, which is temperature sensitive at 42°C (Funk et al., 1992). Screening for increased PGP phosphatase activity in the *pgpAB* double null mutant expressing a plasmid library of the *E. coli* genome led to identifying and cloning of the *pgpC* gene (Lu et al., 2011). A mutant in *clsA* was originally identified by brute force screening of strains defective in phospholipid metabolism (Pluschke et al., 1978; Ohta et al., 1985). Informatic analysis led to identifying two paralogs of ClsA and identifying of *clsB* (Guo and Tropp, 2000) and *clsC* (Tan et al., 2012).

With the availability of plasmid-borne genetic libraries of the *E. coli* genome and the sequence of the complete genome, the remainder of the genetic map of phospholipid metabolism became available. With some exceptions the isolation of mutants and subsequent cloning of the genes was mostly done by Kennedy and his scientific descendants.

THE ENZYMES OF PHOSPHOLIPID SYNTHESIS

Most of the enzymes encoded by the genes listed in **Figure 1**, with exception of PlsC, PgpAC, ClsB, ClsC, and MdoB, have been purified to near homogeneity. Once the respective genes were cloned and expressed from multi-copy plasmids, sufficient amounts of purified enzymes were available for mechanistic and structural studies. All enzymes in the pathway except PssA are integral membrane proteins and are associated with the inner membrane of *E. coli*. The combination of the genetic and biochemical studies has validation of the Kennedy Pathway at the molecular level.

Synthesis of PA

Purification of PlsB to near homogeneity (Larson et al., 1980; Green et al., 1981) was facilitate using *E. coli* strains carrying plasmids overexpressing the *plsB* gene (Clark et al., 1980). Sequencing of isolated clones revealed the amino acid sequence of PlsB (91,381 Da). PlsC (27, 500 Da) has been partially purified (Coleman, 1992) and from informatic analysis of its sequence, PlsC appears to be similar to the catalytic properties of PlsB (Coleman, 1990; Yao and Rock, 2013). Although saturated and unsaturated long chain fatty acids are substrates, PlsB favors the former while PlsC favors the latter consistent with the acyl chain species of phospholipids found in *E. coli* (Goelz and Cronan, 1980). Orthologs of PlsB are found in several γ-proteobacteria. For more information on bacterial fatty acid synthesis (see Rock and Jackowski, 2002). PlsB and PlsC produce *de novo* PA while DgkA (13,245 Da) (Lightner et al., 1983) functions in recycling DAG generated in the synthesis of MDO. Crystal (Li et al., 2013) and NMR (Van Horn et al., 2009) structures of DgkA are available.

CDP-DAG Synthase

CdsA catalyzes the activation of PA with CTP to generate CDP-DAG which serves as a precursor at the branch point of the Kennedy Pathway for the formation of zwitterionic PE and anionic PG plus CL. Cloning of the *cdsA* gene and expression from multicopy plasmids (Icho et al., 1985b) facilitated the purification of the synthase (27,570 Da) (Sparrow and Raetz, 1985). The enzyme utilizes equally only dCTP and CTP, favors PA with at least one unsaturated fatty and requires a divalent metal ion for activity. Like many integral membrane enzymes, purified CdsA requires its lipid substrate to be dispersed in detergent micelles and exhibits substrate dilution kinetics (Warner and Dennis, 1975; Carman et al., 1995). At a fixed lipid substrate concentration, the activity increases with increasing detergent concentration until all substrate is integrated into detergent micelles. Continued increase in detergent results in progressive decrease in apparent activity due to dilution of the substrate in the surface of the micelle. CdsA has affinity for detergent-phospholipid mixed micelles and once incorporated its activity is dependent on the mole fraction of substrate within the mixed micelle. The enzyme does not catalyze either CDP-diacylglycerol hydrolase activity or exchange activity between substrates and products. Bacterial and eukaryotic synthases display significant homology throughout nature (Dowhan, 1997a), which was used to clone the respective synthase genes encoding endoplasmic reticulum Cds1 (Shen et al., 1996) and mitochondrial Tam41 (Tamura et al., 2013) from *S. cerevisiae*, and the *Drosophila* (Wu et al., 1995) and human (Weeks et al., 1997) genes.

PS Synthase

PssA's in Gram-negative bacteria including *E. coli* (Raetz and Kennedy, 1972, 1974) are unique in that they are not associated with the membrane in cell free extracts but are tightly associated with ribosomes (Dutt and Dowhan, 1977). In *Bacillus subtilis* (Okada et al., 1994), *Bacillus licheniformis* (Dutt and Dowhan, 1981) and *S. cerevisiae* (Bae-Lee and Carman, 1984), the enzyme

is an integral membrane protein requiring a divalent cation for activity, which the *E. coli* enzyme does not. The *B. subtilis* enzyme can fully substitute for the *E. coli* enzyme when expressed in a *pssA* null strain (Okada et al., 1994). The *E. coli* enzyme has been functionally expressed in wild type *B. subtilis* (Zhang et al., 2009), but it is not known whether it can substitute for native enzyme.

The affinity of *E. coli* PssA for ribosomes may not be physiological (Louie et al., 1986; Louie and Dowhan, 1980). Both termini sequences of PssA (52,817 Da) are enriched in positively charged amino acids, which may explain its strong affinity for polyphosphate surfaces such as the ribosome (DeChavigny et al., 1991). Although dissociation from the ribosomal fraction requires 5 M NaCl (Raetz and Kennedy, 1974), physiological levels of polyamines such as spermidine or mixed micelles of detergent plus the CDP-diacylglycerol substrate are sufficient to dissociate the enzyme from ribosomes. *E. coli* membranes enriched in CDP-diacylglycerol or PG result in transfer of the enzyme from the ribosomal to the membrane fraction in cell lysates. Interestingly, the association with PG is ionic being prevented by high ionic strength buffers while the association with lipid substrate is insensitive to salt levels suggesting physiological importance of different modes of membrane association and existence of potential feedback mechanism to provide anionic and zwitterionic membrane content homeostasis as discussed latter.

The affinity for polyphosphate surfaces was capitalized in the purification of the enzyme. The enzyme was first bound to phosphocellulose and specifically eluted using mixed micelles of detergent and lipid substrate (Larson and Dowhan, 1976). This affinity purification method coupled with enzyme overproduction using high copy number plasmids carrying the *pssA* gene (Raetz et al., 1977; Ohta et al., 1981a) made available increased amounts of enzyme for study.

Although PssA presents as a "soluble" enzyme, it aggregates in the absence of detergents. and as noted above, has high affinity for its membrane associated substrate even in the presence of ribosomes. This is consistent with its requirement for a lipid substrate-detergent mixed micelle and display of substrate dilution kinetics (Carman et al., 1995). PssA follows a Ping-Pong reaction mechanism (Raetz and Kennedy, 1974; Larson and Dowhan, 1976) with retention of configuration at the PA-linked phosphate in the CDP-DAG substrate indicating that the reaction path proceeds through a substrate-enzyme covalent intermediate (Raetz et al., 1987). This mechanism is also consistent with low hydrolase activity toward its lipid substrate and product and very low transfer rates of the PA moiety of CDP-DAG to glycerol and G3P.

Pss enzymes belong to two different families: type I (non-integral membrane form) in the phospholipase D-like family and type II (integral membrane form) in the CDP-alcohol phosphotransferase family (Sohlenkamp et al., 2004). PssA from *E. coli* is a type I enzyme whereas the integral membrane associated Pss enzymes from *Bacillus* and *S. cerevisiae* are type II enzymes. The yeast enzyme shows no homology with the bacterial enzymes. However, the *B. licheniformis* (Dutt and Dowhan, 1981) and yeast enzymes exhibit sequential ordered Bi–Bi kinetics with no hydrolase activities. In fact, the yeast enzyme proceeds with inversion of configuration at the PA-linked phosphate of the CDP-DAG substrate (Raetz et al., 1987) consistent with a Bi-Bi mechanism in which the formation and release of CMP from CDP–DAG is dependent on L-serine.

PS Decarboxylase

Enzymes in phospholipid biosynthetic pathways are in very low amounts requiring several thousand-fold purifications from wild type cells. The first enzyme in the *E. coli* pathway to be purified was Psd (Dowhan et al., 1974), which was at the time among one of the few functional integral membrane proteins available in purified form. This purification demonstrated that it was possible to isolate functional phospholipid biosynthetic enzymes, which was followed in the next few years in other bacteria, yeast and somatic cells. The *E. coli* enzyme is a heterodimer derived from a proenzyme through autocatalytic serinolysis at Ser-254 resulting in two subunits of 28,579 and 7332 Da with the latter subunit containing an amino-terminus blocked by pyruvate (Li and Dowhan, 1988, 1990). During catalysis a Schiff's base is formed between the L-serine α-amino group of PS and the pyruvate prosthetic group followed by decarboxylation. The crystal structure of the enzyme shows a dimer of the heterodimer with the hydrophobic N-terminal α-helices most likely inserted into the lipid bilayer (Watanabe et al., 2020). This face of the dimer displays a lipid substrate binding pocket into which covalently bound PE was resolved after reduction of the substrate-enzyme Schiff's base. Thus far all Psd's in nature are pyruvate-dependent enzymes (Voelker, 1997). The *B. subtilis* enzyme (Matsumoto et al., 1998) and the mitochondrial somatic cell (Kuge et al., 1991, 1996) and *S. cerevisiae* (Trotter et al., 1993) enzymes show significant homology to the *E. coli* enzyme, although yeast also contains a divergent Psd localized to the Golgi/vacuole (Trotter and Voelker, 1995). *E. coli* Psd exhibits substrate dilution kinetics (Warner and Dennis, 1975; Carman et al., 1995). The enzyme is specific for the diacyl and G3P back bone as well as the L-serine headgroup (Dowhan et al., 1974). Psd's are very efficient in converting PS into PE resulting in levels of 0.1% or less of total phospholipid in membranes containing a Psd. In eukaryotic cells PS is synthesized in the endoplasmic reticulum from where it is trafficked to other cell membranes where levels can reach 10% except in the mitochondria where Psd completely converts PS to PE (Voelker, 1997).

PGP Synthase

All PgsA's described so far belong to the CDP-alcohol phosphotransferase family. A gene encoding a putative PgsA is present in almost all bacterial genomes, but there are and will be increasing exceptions (Makarova et al., 2001; Radka et al., 2020). The enzyme was initially purified from wild type *E. coli* using a novel CDP-DAG affinity column (Hirabayashi et al., 1976). Once the cloned and sequenced *pgsA* gene was available, overproduction of the enzyme (20,701 Da) facilitated purification in high amounts (Ohta et al., 1981b; Gopalakrishnan et al., 1986). Functionally, the enzyme is similar to *B. subtilis* and yeast Pss in that it is an integral membrane protein, requires a divalent metal ion for

activity and proceeds via a sequential Bi-Bi mechanism. The homologous somatic cell PgsA, when engineered for expression in *E. coli*, exhibits overproduction of synthase activity (Kawasaki et al., 1999), although it is unknown whether it suppresses a *pgsA* null strain.

PGP Phosphatases

The three phosphatase of *E. coli*, PgpA (19,400 Da) (Icho and Raetz, 1983; Icho, 1988a), PgpB (29,021 Da) (Icho and Raetz, 1983; Icho et al., 1985a), and PgpC (24,439 Da) (Funk et al., 1992; Lu et al., 2011) show no sequence homology, all dephosphorylate PGP efficiently and have different specificities toward other phosphorylated lipids. A triple *pgpABC* null mutant is not viable, demonstrating that no additional PGPs exist in wild type *E. coli.* PgpAC are specific for PGP and require Mg^{2+} for active. PgpB is divalent metal ion independent and possesses a broad substrate spectrum as shown by its capacity to dephosphorylate PGP, PA, lyso-PA, undecaprenyl pyrophosphate (C55-PP) (Touze et al., 2008) and DAG-pyrophosphate (Dillon et al., 1996). In contrast to PGP hydrolysis, which relies on a His/Asp/His catalytic triad of PgpB, the mechanism of C55-PP hydrolysis only requires the His/Asp diad (Tian et al., 2020). Potential orthologs of the three phosphatases are found throughout other bacteria, but they are not homologous to any eukaryotic lipid phosphatases.

PgpB has been purified to near homogeneity (Touze et al., 2008). High resolution crystal structures have been determined for PgpB, which detail catalytically important residues (Fan et al., 2014) and a PE binding site that stabilizes the enzyme (Tong et al., 2016). Strict concentration dependence of activity on PE may allow PgpB activity to remain at a physiologically required threshold providing an attractive mechanism on how membrane proteins achieve two competing requirements, stability and flexibility both required for function (Guo et al., 2020).

CL Synthases

The bacterial CL synthases were originally thought to use CDP-DAG as substrate until definitive evidence confirmed that condensation of two PG molecules is catalyzed at least for what we know to be ClsA (Hirschberg and Kennedy, 1972). ClsA is the primary source of CL during exponential growth. The *clsA* gene was cloned, the enzyme overproduced and partially purified (Ohta et al., 1985; Hiraoka et al., 1991). The enzyme appears to follow substrate dilution kinetics (Hiraoka et al., 1991). Although the *clsA* DNA sequence indicates a protein of 54,822 Da, the mature protein is about 46,000 Da (Hiraoka et al., 1991; Quigley and Tropp, 2009). There appears to be a posttranslational shortening of the protein. High overproduction of the enzyme is lethal due to compromised cell membrane barrier function presumable due to overproduction of CL (Hiraoka et al., 1991). Interestingly, the active site of ClsA faces the periplasm of *E. coli* (Shibuya et al., 1985).

ClsB (47,634 Da) and ClsC (53,666 Da) were first identified as products of genes *ybhO* and *ymdC*, respectively, which encode proteins with high homology to ClsA (Guo and Tropp, 2000). *In vivo* studies originally missed the presence of ClsBC because these activities contribute low amounts to the CL pool and only at late exponential to stationary phases of growth (Tan et al., 2012). ClsAB both condense two molecules of PG to form CL, but ClsC transfers a phosphatidyl moiety from PE to PG (Tan et al., 2012). Clones of *clsC* containing the adjacent *ymdB* gene encode increased levels of ClsC by an unknown mechanism. Although a *clsABC* null strain contains no detectible CL, a *pgsA* null strain contains trace amounts of CL. It turns out that ClsB also replaces ethanolamine in PE with glycerol to make PG, which then is converted to CL (Tan et al., 2012).

Many questions remain unanswered with regards to CL synthesis in bacteria. Why are there multiple synthases and what are their function? What is the mechanism of *ymdB* amplification of ClsC? What is the topological orientation of the active sites of ClsBC and how are the membrane orientation of the three synthases related to their function? Is the ability of ClsB to make PG from PE of physiological significance?

WHICH ENZYME ACTIVITIES ARE ESSENTIAL?

Determining "essential" lipid genes is dependent on growth conditions. In the longer term evolution has selected genes necessary for optimal growth under a variety of conditions. Laboratory strains allow the identification of genes that are required for normal function but can be eliminated under artificial conditions leading to the identification of lipid dependent functions. No conditions have been identified to suppress the lethality of null mutants in genes encoding enzymes prior to and including the synthesis of CDP-DAG. Interestingly, growth conditions or secondary suppressor mutations have been identified to support null mutations in genes beyond the branch point. Therefore, *E. coli* stains are available completely lacking either PE and PS (DeChavigny et al., 1991), PG and CL (Asai et al., 1989; Kikuchi et al., 2000) or CL (Tan et al., 2012). However, no conditions have been found to support growth of strains lacking simultaneously PE, PS, and CL (DeChavigny et al., 1991).

The first null mutant in phospholipid synthesis in *E. coli* resulted from the interruption of the *pgsA* gene (Heacock and Dowhan, 1987, 1989). Lethality was suppressed by a plasmid copy of *pgsA* or a chromosomal copy of *pgsA* under *lacOP* promoter control in the presence its inducer (Heacock and Dowhan, 1989). Although *pgsA* is absolutely required in a wild type strain, transfer of the null allele into several genetic backgrounds had little effect on growth. The lethal effect in wild type strains is due to a requirement for PG as a DAG donor to the N-terminal cysteine thiol group of the major outer membrane lipoprotein (Lpp) in a reaction catalyzed by prolipoprotein DAG transferase (Lgt) (Asai et al., 1989; Kikuchi et al., 2000). This modification occurs in the inner membrane and is required prior to translocation of Lpp to the outer membrane. Accumulation of the precursor results in disruption of the inner membrane and cell lysis. A double null *pgsA lpp*

strain still grows poorly at 37°C and lyses at 42°C. There are several other lipoproteins requiring the same modification whose defective maturation results in membrane stress and induction of the two-component Rcs phosphorelay signal transduction system making cells thermosensitive. Disruption of the *rcsA* gene suppresses the poor growth and temperature sensitivity of the *pgsA lpp* null strain (Nishijima et al., 1981; Shiba et al., 2004; Nagahama et al., 2006; Shiba et al., 2012). Therefore, in this complex suppressor strain PG and CL are not required for near normal growth. However, there are still several phenotypes of strains completely lacking PG and CL as discussed below.

The *pgsA* null viable strains still contain about 10% anionic phospholipids mainly PA, CDP-DAG and *N*-acyl-PE (Mileykovskaya et al., 2009). Accumulated PA and CDP-DAG in the mutant can also serve as DAG donors for thiol modification of lipoprotein precursors but only inefficiently (Tao et al., 2012). Therefore, these negatively charged lipids can also compensate for loss of PG and CL so one cannot conclude that there is no requirement for anionic phospholipids in *E. coli*.

As noted earlier, a *pgpABC* null mutant is not viable unless covered by a plasmid expressing one of the phosphatase genes (Lu et al., 2011). This is probably due to accumulation of PGP in the membrane since feeding a phosphonate analog of G3P to *E. coli*, which results in the accumulation of the non-hydrolysable phosphonate analog of PGP, is bacteriostatic (Tyhach et al., 1976).

Interruption of the *pssA* gene prevents the synthesis of PS and PE thus the strains lack all amino-containing and zwitterionic phospholipids (DeChavigny et al., 1991). PS is barely detectible in *E. coli,* so PE is the major zwitterionic net neutral lipid making the cell membranes highly anionic in its absence. Null *pssA* strains are viable in media containing 10–50 mmolar divalent cations Ca^{2+}, Mg^{2+}, or Sr^{2+}, but not Ba^{2+} (DeChavigny et al., 1991; Rietveld et al., 1993, 1994; Killian et al., 1994) consistent with earlier reports of divalent metal ion suppression of temperature sensitive mutations in *pssA* (Raetz, 1976; Ohta and Shibuya, 1977) and *psd* (Hawrot and Kennedy, 1978). Removal of divalent cations from the growth medium results in rapid lysis. Null mutants require supplementation of minimal defined medium with all the amino acids. Even under optimal conditions the null mutant growth rate is two- to three-times slower and the cells are filamentous with multiple genomes (DeChavigny et al., 1991; Mileykovskaya and Dowhan, 2000). Therefore, lack of PE is essential for normal cell viability.

Construction of strains with an interrupted *psd* gene was unsuccessful even though supplementation of medium with divalent cations suppressed the lethality of temperature sensitive mutants. An interrupted chromosomal copy of the *psd* gene could be rescued by a plasmid carrying the *psd* gene along with surrounding genes suggesting a polar effect of the interruption on expression of essential genes in this region of the chromosome (Li, 1989).

Escherichia coli has a marked redundancy in CL synthesis with none of three gene products being essential under laboratory conditions. However, as noted later CL-deficient strains display several deficiencies, which would limit their survival or vitality under stressed conditions.

FUNCTIONS OF THE MAJOR PHOSPHOLIPIDS BEYOND BARRIER MAINTENANCE

Membrane associated processes account for half or more of all cellular functions. Membranes are complex structures composed primarily of proteins and lipids stabilized by dynamic cooperative non-covalent interactions. Historically, studies of membrane associated functions have focused on the protein component while ignoring the role of membrane lipids in defining function. A primary role for lipids in forming the permeability barrier of cells and organelles was first proposed by Ernest Overton in 1895 (Overton, 1895). However, a lipid bilayer as opposed to a protein barrier was not accepted until many years later (Danielli and Dańson, 1935; Robertson, 1957) but still envisioned a lipid bilayer covered with a protein layer on each side. The fluid mosaic model of membrane structure (Singer and Nicolson, 1972), where laterally mobile proteins are embedded in a sea of lipids, combined many studies on membrane structure and remains a widely accepted representation of membrane structure (Nicolson, 2014). Minor lipids as cellular signaling molecules gained recognition in the 1970s and 1980s (Horrobin et al., 1977; Hokin, 1985) and remain a heavily studied area. Interestingly, it was Kennedy that first reported the synthesis of a phosphorylated phosphatidylinositol, an important lipid signaling molecule, in brain that underwent rapid formation and dephosphorylation (Paulus and Kennedy, 1960). There are few strong examples of lipid signaling in *E. coli*. One example is the outer membrane phospholipase A that deacylates phospholipids in the LPS rich outer leaflet of the outer membrane. The generated free fatty acids act as second messages in the CoA form that prevent the degradation of a central enzyme (LipC) in Lipid A biosynthesis thus maintaining synthesis of LPS precursors (May and Silhavy, 2018). However, recognition that the major membrane lipids affect membrane protein function and affect cellular function is more recent. Lack of focus on the importance of membrane lipid composition as a factor in cell function is due to a protein centric view (Popot and Engelman, 2016) driven by the ability of detergents to substitute for lipids in supporting the function of many purified membrane proteins.

How can the function of lipids beyond providing a permeability barrier be determined? A classical genetic approach to defining multiple functions for the major membrane lipids presents several barriers. Since lipids are not encoded directly by genes, mutants must be made in biosynthetic pathways, which can result in cell death due to loss of barrier function before a specific function is recognized. Pleiotropic effects on many cellular processes, particularly in multi-organelle cells, due to buildup of precursors or lack of final products complicates interpretation. Lipids have neither inherent catalytic activity nor obvious functions in isolation. Since we still do not know how to translate the physical and chemical properties of a

single or complex mixture of lipid(s) into *in vivo* function, *in vitro* studies are prone to many artifacts especially when employing idealized lipid mixtures. Fortunately, at least in bacteria, it has been possible to establish conditions to support the growth of strains completely lacking the major phospholipid classes as noted above for *E. coli*. These strains are still compromised for cell growth and show recognizable phenotypes that provide clues to important roles for these lipids in normal cell growth.

A set of viable *E. coli* "lipid mutants" (**Figure 2**) has been constructed in which native lipid composition can be systematically controlled at steady state (Wikström et al., 2004, 2009; Xie et al., 2006; Dowhan and Bogdanov, 2009; Bogdanov et al., 2010b), titrated in a dose-dependent manner (Bogdanov et al., 2008; Bogdanov and Dowhan, 2012; Dowhan, 2013) or varied temporally during the cell cycle (Zhang et al., 2003; Bogdanov et al., 2008, 2010a,b, 2014; Bogdanov and Dowhan, 2012). Lipids foreign to *E. coli* have been introduced as replacement of native lipids to understand the functional interchangeability and essential structural and charge properties of native lipids (Xia and Dowhan, 1995b; Wikström et al., 2004, 2009; Xie et al., 2006; Bogdanov et al., 2010a,b). Since membrane proteins and lipid environment have co-evolved, roles for the major lipids in membrane protein assembly and function only became evident when lipid composition was varied *in vivo*. *In vitro* biochemical characterization of the resulting phenotypes has differentiated direct from indirect effects of lipid-protein interactions and defined roles for lipids in membrane protein structure and function at the molecular level.

Properties of Mutants Lacking PS and PE

Null *pssA* strains require mmolar levels of a select set of divalent cations and supplementation of minimal media with amino acids to support growth, display a filamentous growth phenotype, and are incompatible with a null *clsA* gene (DeChavigny et al., 1991). The requirement for a divalent cation and CL maybe related to the physical properties of the lipid bilayer. CL in the presence of a subset of divalent cations and PE are non-bilayer prone lipids due to their small hydrophilic headgroup versus their larger hydrophobic domain. This shape when present within a lipid bilayer causes local discontinuity and disruption, which appears to be universally required in natural bilayers. The minimum required concentration of divalent cations in the growth medium of a *pssA* null strain mirrors the strength of these ions to induce the non-bilayer phase for CL as follows: $Ca^{2+} > Mg^{2+} > Sr^{2+}$ and Ba^{2+} is ineffective (DeChavigny et al., 1991; Rietveld et al., 1993, 1994; Killian et al., 1994). The temperature dependent mid-point of the transition from bilayer to non-bilayer phase for phospholipids extracted from wild type *E. coli* is about 55°C. The mid-point for phospholipids extracted from a *pssA* null strain grown under optimal concentrations of each of the above ions and suspended in the same concentration of ions is also 55°C. Phospholipids from cells grown in 10 mM Ca^{2+} have a lower CL content than those grown in 50 mM Mg^{2+} so when phospholipids extracted from cells grown in Ca^{2+} are suspended in Mg^{2+}, the mid-point transition is well above 55°C. Conversely, when phospholipids extracted from cells grown in Mg^{2+} are suspended in Ca^{2+}, the mid-point transition is well below 55°C. The growth dependence on Sr^{2+} shows a bell-shaped curve with a maximum at 12 mM, which is the same for the extracted phospholipids. The divalent cation requirement is extracellular since cytoplasmic Mg^{2+} levels are near 100 mM while Ca^{2+} levels are μM in *E. coli*. This close correlation between growth requirements and the phase properties of CL and PE strongly suggests a physical rather than chemical property of these lipids. Additionally, high monovalent or trivalent cations do not substitute for the divalent ions. The mechanism by which *E. coli* adjusts its CL level in apparent response to the divalent metal ion induced physical properties of CL is unknown. The fact that over production of CL by a plasmid borne copy of *clsA* under a non-native promoter results in cell lysis suggests the presence of some mechanism to regulate the physical properties of the membrane via the level of CL (Hiraoka et al., 1991).

Wild type *E. coli* do not require amino acids for growth and can utilize lactose as an energy source at μmolar levels. However, *pssA* null strains require mmolar levels of lactose as an energy source and all the amino acids. These requirements are due to mis-folding, as discussed in more detail later, of secondary transporters, which couple substrate accumulation to the proton electrochemical potential, for probably all amino acids and as well as lactose (DeChavigny et al., 1991; Zhang et al., 2003, 2005; Hariharan et al., 2018; Vitrac et al., 2020). It had been well known that PE is required for reconstitution of energy dependent uphill transport of substrate by the secondary transporter lactose permease (LacY) in proteoliposomes (Newman and Wilson, 1980; Newman et al., 1981). Cells lacking PE still transport lactose by energy independent downhill facilitated transport but cannot accumulate lactose against a concentration gradient due to a loss of coupling of transport to the proton electrochemical gradient, which is unaffected in *pssA* null strains (Bogdanov and Dowhan, 1995). Therefore, *pssA* null strains require higher levels of lactose in the growth medium to support growth. Similarly, in *pssA* null strains secondary amino acid transporters become facilitated transporters, which allows equilibration of endogenously synthetized amino acids with the growth medium thus reducing internal levels below that required to maintain growth. Primary transporters that utilize direct phosphorylation of substrates to achieve accumulation of substrate appear to be less affected in *pssA* null strains.

Filamentous growth is common among many mutations in membrane related processes. Null *pssA* mutants organize early cell division proteins at the FtsZ ring within multiple genomes but appear to have lost synchrony between cell growth and a late stage of cell division prior to constriction (Mileykovskaya et al., 1998). It is interesting that PE movement is required from the inner to the outer leaflet of the plasma membrane at the septum of yeast (Iwamoto et al., 2004) and somatic cells (Emoto and Umeda, 2000) prior to cell division followed by movement back to the inner leaflet during cell division. This suggests a universal requirement for PE in cell division.

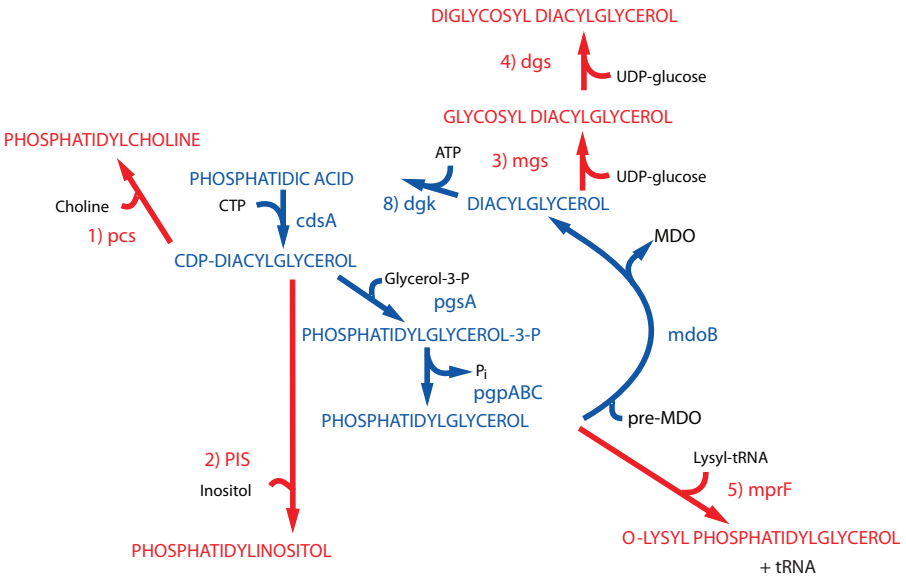

FIGURE 2 | Synthesis of foreign lipids in *E. coli*. The native pathways in *E. coli* noted in *blue* are detailed in **Figure 1**.The enzymes with their respective genes named catalyze the following steps for synthesis of foreign phospholipids in *E. coli* noted in *red*: (1) phosphatidylcholine synthase [*Legionella pneumophila* (Conover et al., 2008; Bogdanov et al., 2010a)]; (2) phosphatidylinositol synthase [*Saccharomyces cerevisiae* (Xia and Dowhan, 1995b)]; (3) glucosyl diacylglycerol synthase [*Acholeplasma laidlawii* (Xie et al., 2006)]; (4) diglucosyl diacylglycerol synthase [*Acholeplasma laidlawii* (Wikström et al., 2009)]; (5) lysyl t-RNA phosphatidylglycerol lysine transferase [*Staphylococcus aureus* (Oku et al., 2004)]. Figure (modified) and legend reprinted by permission from Elsevier (Dowhan, 2013): Copyright 2013.

PE Acts as a Lipochaperone in a Late Stage of Membrane Protein Folding

Assisting late stage folding of proteins has been restricted to protein chaperones. However, the misfolding of proteins in *E. coli* lacking PE demonstrated that lipids also act as chaperones (Bogdanov et al., 1996, 1999; Bogdanov and Dowhan, 1998, 1999). LacY from wild type cells maintains sufficient conformational memory even after SDS PAGE, which completely delipidates LacY, to be recognized by monoclonal antibody (mAb) 4B1; the 4B1 epitope lies within extramembrane domain (EMD) P7 of LacY (**Figure 3**) (Sun et al., 1996). However, LacY from PE-lacking cells is not recognized by mAb4B1 but is still recognized by mAb4B11, which recognizes native and denatured LacY; the 4B11 epitope is comprised of EMDs C8 and C10 of LacY (Sun et al., 1997). However, renaturation of LacY from *pssA* null cells after SDS PAGE in the presence of PE re-established recognition by mAb4B1. This was accomplished using the Eastern–Western technique where proteins separated by SDS PAGE are blotted onto a solid support layered with a test phospholipid. As SDS is electrophoresed away in the presence of PE, renaturation occurs as evidenced by recognition by mAb4B1. PE containing at least one saturated fatty acid (the predominant species in *E. coli*) but not PS restored recognition by mAb4B1; this is consistent with lack of uphill transport of lactose at the restrictive temperature in a *psd2* temperature sensitive mutant (Hawrot and Kennedy, 1978), which accumulates PS in the place of PE. Later it was found that PC containing at least one saturated fatty acid and neutral glycolipids (**Figure 2**) restored wild type conformation and function to LacY (Vitrac et al., 2013b). The earlier *in vitro* report that PC did not support uphill transport function of LacY reconstituted into proteoliposomes was due to the use of PC species containing only unsaturated fatty acids. Expression of PC (Bogdanov et al., 2010a) or neutral glycolipids (Xie et al., 2006; Vitrac et al., 2013b) in *E. coli* in the absence of PE or reconstitution *in vitro* in these lipids supports full function of LacY. Further demonstration of the involvement of PE in a late stage folding event was confirmed by restoration of mAb4B1 recognition of LacY initially assembled in PE-lacking *E. coli* membrane vesicles following *in vitro* synthesis of PE in these vesicles (Bogdanov and Dowhan, 1998). Therefore, PE fulfills the requirement of a lipochaperone by being required for proper protein folding during a late stage of protein maturation and no longer required once the protein is properly folded. PE is recognized as a lipochaperone supporting the function of several membrane associated processes in somatic cells (Patel and Witt, 2017).

Charge Balance Rule for Membrane Protein Assembly

What is the molecular basis for LacY mis-folding in cells lacking PE? Prior to determination of the atomic structure of LacY (Abramson et al., 2003; Kumar et al., 2018), the substituted cysteine accessibility method to determine TMD orientation (SCAM^{TM}) (Bogdanov, 2017) was used to establish a low-resolution structure of LacY that revealed the number and orientation of transmembrane domains (TMDs) and EMDs (Kaback et al., 2001) as shown in **Figure 3**. In this method the exposure of single cysteine residues in an otherwise cysteine-less protein to a membrane impermeable sulfhydryl reagent is used to map EMDs on the outside of cell membranes, isolated

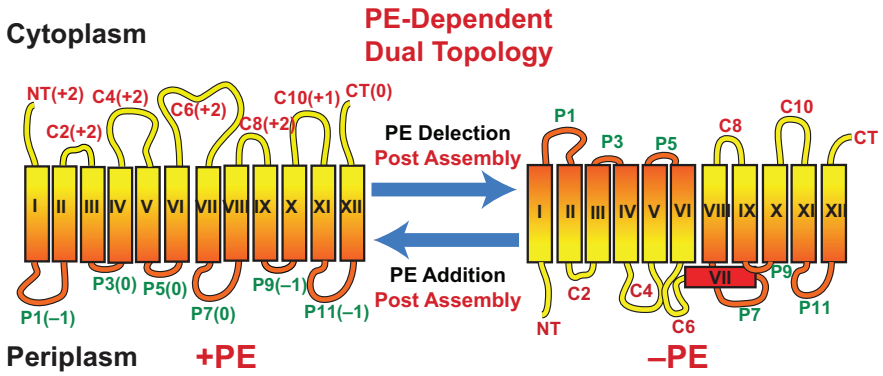

FIGURE 3 | Topological organization of LacY as a function of membrane lipid composition. TMDs (Roman numerals) and EMDs (Arabic numerals) are sequentially numbered from the N-terminus to C-terminus with EMDs exposed to the periplasm (P) or cytoplasm (C) as in wild type cells. Net charge of EMDs is shown. Topology of LacY is shown after initial assembly in PE-containing cells (+PE) or after initial assembly in PE-lacking cells (–PE). The interconversion of topological conformers and the ratio of native to inverted conformer are reversible in both directions depending on the dynamic level of PE in membranes. Figure was modified and legend reprinted by permission from Springer Nature (Dowhan et al., 2017): Copyright 2017.

membrane vesicles and proteoliposomes or facing the lumen after membrane disruption. In PE-lacking cells (Bogdanov et al., 2002) the N-terminal six TMD-helical bundle is inverted with respect to the plane of the membrane bilayer and the C-terminal five TMD- helical bundle (**Figure 3**). In addition, TMD VII, which is of low hydrophobicity due to two Asp residues, is exposed to the periplasm. Disruption of LacY structure in the vicinity of EMD P7 and retention of structure in EMDs C8 and C10 is consistent with the mAb studies. The ratio of topological conformers (Dowhan et al., 2019), which is fully reversible *in vivo* (Bogdanov and Dowhan, 2012; Bogdanov et al., 2008) and *in vitro* (Vitrac et al., 2013a, 2015) is dependent on PE levels at the time of initial membrane assembly and is proportional post-assembly to changes in PE levels. There is no rapid interconversion of conformers at a fixed PE level but rather a change in PE level post-assembly drives interconversion. Inversion in the absence of PE is prevented by position-independent increases in the positive charge of EMDs C1–C6 or increasing the hydrophobicity of low hydrophobic TMD VII (necessary hinge point between the C- and N-helical bundles). The hydrophobic block can be reversed by increasing the negative charge of EMDs C1–C6. Inversion is induced in the presence of PE by increasing the negative charge of EMDs C1-C6. Phosphorylation of EMD C6 induces inversion, which is reversed by dephosphorylation (Vitrac et al., 2017, 2019). This was the first evidence that phosphorylation of a membrane protein can change its topological organization and possibly its function post-assembly. TMD flipping in proteoliposomes occurs on a time scale of seconds without the aid of any other cellular component and is rapid enough to be physiologically significant (Vitrac et al., 2013a, 2017). Since changes in topology only require a change in membrane lipid composition or a change in the net charge of an EMD, such interconversions can occur in any cellular membrane throughout nature without requiring any additional cellular components.

The vast majority of polytopic membrane proteins insert into membranes according to Positive Inside Rule with net positively charged EMDs facing the cytoplasm (von Heijne, 1986, 1989, 1992; Nilsson and von Heijne, 1990). However, the Positive Inside Rule cannot explain (Bogdanov et al., 2018; Dowhan et al., 2019): (1) cytoplasmic orientation of 20% of EMDs that are net negative or neutral; (2) post-assembly dynamic changes in membrane protein topological organization; (3) co-existence of membrane proteins with dual or multiple topologies; (4) why basic amino acids generally dominant as cytoplasmic retention signals over acidic amino acids as membrane translocation signals; (5) why increasing the membrane content of anionic phospholipids does not favor cytoplasmic retention of positively charged EMDs but rather increases the membrane translocation potential of EMDs containing acidic residues.

The Charge Balance Rule (Dowhan et al., 2019) as an extension of the Positive Inside Rule was formulated to address the above shortcomings and the influence of membrane lipid composition on the dynamic topological orientation of membrane proteins (Bogdanov et al., 2018; Dowhan et al., 2019). The charge density of the membrane surface and the charge character of EMDs act in concert to determine TMD orientation at the time of initial membrane protein assembly and dynamically after initial assembly. Net zero charged PE and PC and uncharged cholesterol and glycolipids (Wikström et al., 2004, 2009; Xie et al., 2006; Vitrac et al., 2013a; Bogdanov et al., 2014), which dilute the high negative charge of anionic PG and CL, appear to dampen the translocation potential of negative residues in favor of the cytoplasmic retention potential of positive residues. Since the ratio of properly oriented to inverted LacY is dependent on the ratio of PE to PG plus CL, topological heterogeneity can arise simply through perturbations of the lipid-sensitive kinetic and thermodynamic equilibria resulting in either complete interconversion or a mixture of topological conformers.

The studies originated in *E. coli* strains lacking PE demonstrated that membrane protein-folding and dynamic post-assembly rearrangements are thermodynamically driven processes dependent on inherent lipid-protein interactions that may not require other cellular factors. These results provide a

thermodynamic basis for how changes in lipid composition and post-translational modifications of proteins can change the ratio of topologically distinct populations of native and non-native conformers or explain the existence of proteins with dual or multiple topologies (Dowhan et al., 2019). Therefore, membrane protein structural organization is not static but potentially highly dynamic after initial assembly.

Several other secondary transporters also undergo topological inversions in the absence of PE or show local structural changes that affect their function (Zhang et al., 2003, 2005; Hariharan et al., 2018; Vitrac et al., 2011, 2020). Others using different approaches, have reported similar effects of lipid environment and EMD charge on MP structural organization (Bowie, 2006, 2013; Hickey and Buhr, 2011; Tunuguntla et al., 2013; McIlwain et al., 2015).

If membrane lipid composition changes have such a dramatic effect on membrane protein organization, why are PE lacking strains still viable? Thus far the changes in structure of secondary transporters do not completely inactivate the transporters but render them as facilitated rather than active transporters. The same maybe true of other proteins whose function is compromised but not completely lacking. Replacing PE with PC or other net neutral lipids does not suppress the filamentous growth phenotype or divalent metal requirement of PE-lacking strains so there are addition functions requiring specifically PE (Bogdanov et al., 2010a). PE-lacking cells fail to induce formation of pili (Shi et al., 1993), show upregulation of the Cpx stress response system and display an increase in the outer membrane protease DegP (Mileykovskaya and Dowhan, 1997). These additional phenotypes have not been extensively investigated to determine their molecular basis.

The Requirement for Anionic Phospholipids

Strains lacking PG and CL or CL, although viable when coupled with suppressor mutations, display several phenotypes supporting a role for wild type levels of these lipids. Phospholipids are not evenly distributed within the inner membrane of *E. coli*. Using the fluorescent dye 10-*N*-nonyl acridine orange (NAO), anionic lipid domains were first visualized at the cell poles and potential division sites of wild type and *pssA* null mutants (Mileykovskaya and Dowhan, 2000). The former domain is derived from the latter domain after cell division. NAO displays strong green fluorescence when bound to anionic lipids such as PG, PA, and CL but also shows red fluorescence when bound only to CL. The above domains show both red and green fluorescence indicating the domains are enriched in CL and possibly PG. This appears to be the case since *clsA* null strains treated with NAO during exponential growth only show green-fluorescent domains. In addition, PG and CL content increases with increasing osmolarity and in stationary phase (Romantsov et al., 2007), which is probably related to induction of *clsB* or *clsC*. In a *clsA* null strain red fluorescence was observed after reaching stationary phase in high osmolarity medium (Romantsov et al., 2007) but not during exponential growth. *E. coli* appears to have a mechanism for enriching the poles and the septum with anionic lipids. Minicells, which are derived from the cell poles, isolated from a *pgsA* null strain (thus lacking PG and CL), are enriched in PA and the minor anionic lipid *N*-acyl-PE (Mileykovskaya et al., 2009).

What role do these anionic lipids play in cell function and is there a preference for CL? Several proteins localize to the cell poles, the septal region or interact globally with the membrane surface via interaction with anionic lipids (Matsumoto et al., 2006). ProP is an osmosensory transporter whose level increases with medium osmolarity to adjust cellular levels of solutes in response to osmotic stress. ProP co-localizes with NAO fluorescence at the cell poles (Romantsov et al., 2007, 2008). This localization is considerably reduced in a *clsA* null strain and appears to be sensitive to the level of total cell CL, which also increases with medium osmolarity, independent of the level of ProP. Additionally, *clsA* null strains are sensitive to growth in high osmolarity medium. The mechanosensitive channel MscS also localizes to the cell poles in a CL-dependent manner while LacY and several mechano- and osmosensitive cell components localize to the poles in a mostly CL-independent manner (Romantsov et al., 2010). Further studies are required in a *pgsA* null strain to determine if any of the CL-independent proteins localize to the poles via anionic lipids.

The MinCDE system is required for localization of the FtsZ ring at the cell center onto which the remaining cell division proteins organize (Margolin, 2001). In the absence of the Min system the FtsZ ring localizes with the cell center and poles resulting in the budding of mini-cells from the poles. Binding of ATP to the peripheral membrane protein MinD exposes an amphitropic helix with one face being positively charged and the opposite face being hydrophobic (Zhou and Lutkenhaus, 2003). This helix partially inserts into acidic membrane domains at the cell poles. MinE binding to MinD induces ATPase activity of the latter with release of MinD from the membrane. MinC also binds to MinD and is an inhibitor of FtsZ association with the membrane. The result is that MinCD oscillate from pole to pole with significant dwell time at the poles, which restricts FtsZ localization to the cell center. In PE-lacking cells containing only anionic lipids, MinD localizes with increased dwell time to NAO fluorescent domains randomly distributed over the filamentous cell rather than at the poles (Mileykovskaya et al., 1998; Mileykovskaya and Dowhan, 2000). The preference for anionic lipids over zwitterionic PE or PC was verified in binding of Min-ATP to zwitterionic liposomes with and without PG or CL (Mileykovskaya et al., 2003). Although increased anionic lipid content in the absence of PE disrupts oscillation of MinD between anionic lipid domains (Mileykovskaya et al., 1998), complete lack of PG and CL has little effect on this oscillation presumably due to increased levels of PA and NAPE, which localize to the poles (Mileykovskaya et al., 2009).

The peripheral membrane protein DnaA is required for initiation of DNA replication at the *oriC* locus of *E. coli*. The protein is active in the ATP-bound form but after initiation of replication it is converted to the inactive ADP bound form, which does not localize to *oriC*. It was initially

determined *in vitro* that anionic phospholipids induced release of ADP and facilitated ATP binding and activation of DnaA (Sekimizu and Kornberg, 1988; Crooke et al., 1992). Downregulation of expression of *pgsA* using a *lacOP* inducible promoter reduces both PG and CL levels by about 75%. Evidence for an *in vivo* anionic lipid requirement for DnaA initiation of DNA replication is supported by suppression of the lack of growth on agar plates of the *lacOP-pgsA* strain in the absence of inducer by a *rnhA1* null mutation (Xia and Dowhan, 1995a). This mutation allows DnaA-independent initiation of DNA replication at the alternative *oriK* site (Kogoma and von Meyenburg, 1983).

Phosphatidylglycerol can provide a conformational constraint for the conjugative *E. coli* F pilus, which is assembled from protein-phospholipid units, in which TraA pilin subunits interact with five PG's based on cryo-electron microscopic reconstructions at 3.6–5.0 Å resolution (Costa et al., 2016). Stoichiometrically arranged PG molecules line the pilus lumen with their solvent exposed head groups directed to the interior of the pilus and the acyl chains entirely buried between subunits. PG molecules could facilitate pilus dynamics and lubricate re-insertion of pilus subunits within the inner membrane during pilus retraction/depolymerization. Alternatively, PG could lubricate naked electronegative ssDNA transport and provide directionality by maintaining appropriate electrostatics of the pilus interior. A viable *pgsA* null mutant should be used to test this hypothesis further to see whether without PG the overwhelmingly positive inside of the pilus is still able to translocate negatively charged ssDNA substrate.

Efficient insertion of proteins into the membrane and export of proteins from the cytoplasm also requires anionic phospholipids. The translocation of secreted proteins across the inner membrane of *E. coli* is significantly compromised when PG and CL levels are reduced using a promoter regulated *pgsA* strain (de Vrije et al., 1988; Kusters et al., 1991). This observation coincides with the *in vitro* data demonstrating that SecA ATPase activity, required for protein translocation, is stimulated by anionic phospholipids (Lill et al., 1990). Recent evidence implicates CL more specifically as a requirement for efficient membrane translocation of periplasmic proteins and membrane insertion of integral membrane proteins (Ryabichko et al., 2020). Both processes were severely compromised in a *clsABC* null strain. The dimeric SecYEG complex and association of SecA with the complex are required for efficient function in both processes. In the *clsABC* null strain SecYEG was mostly monomeric with minimal associated SecA supporting a more specific requirement for CL over PG.

Other anionic phospholipids appear to partially replace CL resulting in normal cell growth under optimal conditions. However, lack of CL under stressed conditions should be further investigated since CL-lacking strains display several phenotypes that might compromise growth under less optimal conditions, as summarized below (Rowlett et al., 2017). Cls expression and CL biosynthesis are highly regulated and modulated during abiotic stress in both Gram-positive and Gram-negative microorganisms (Luevano-Martinez and Kowaltowski, 2015), which respond to many abiotic stressors by increasing the proportion of CL. Expression of *clsA* is increased several-fold (Heber and Tropp, 1991) and the amount of CL increases as PE decreases irrespective to how osmotic stress is imposed (Tsatskis et al., 2005). Stepwise increase in CL content of the bacterial membrane due to growth in media of increasing osmolarity results in conformational changes of ProP, which transports the osmoprotectants proline and glycine betaine (Tsatskis et al., 2005). Due to its unique conformational properties, CL could be considered a stress responsive molecule required to adjust physical properties of bacterial membrane (Luevano-Martinez and Kowaltowski, 2015).

Comparing PE-Lacking and CL-Lacking Cells

As already noted above, lack of PE or CL is not lethal under specific growth conditions, but the cells are not normal. In fact, a systematic scanning of cell morphology and cell function revealed multiple deficiencies in these mutants (Rowlett et al., 2017). Elimination of either lipid results in alteration in cell morphology and structural organization of the cell envelope, the ability to form biofilms, the tolerance to environmental stress, and reduced cellular robustness. CL-lacking cell growth characteristics were largely the same as wild type cells. However, cell viability was compromised in stationary phase, which may be related to the requirement for increased CL levels in stationary phase. Transfer of cells to defined minimal medium resulted a long lag in initiation of growth for PE-lacking cells and a significant increase in the doubling time for CL-lacking strains. For both mutants irrespective of growth medium, cell length heterogeneity was greater than for wild type cells. Envelope ultrastructure was disrupted in both mutants but greater for the PE-lacking cells. The periplasmic width was greatly increased, and considerable amounts of electron dense material accumulated in PE-lacking cells. In both mutants there was considerable extracellular material indicative of cell lysis or loss of envelope material. CL-lacking cells displayed twisted and spiral cell envelope structures in minimal medium. The outer membrane of PE-lacking cells is leaky to periplasmic macromolecules as evidenced by extracellular periplasmic RNAse (Wikström et al., 2004). This may be due to the lack of PE as the major lipid of the inner leaflet of the outer membrane, the lack of decoration of LPS by ethanolamine-P derived from PE (Schnaitman and Klena, 1993; Kanipes et al., 2001), or the significant shortening of the *O*-antigen repeats of the outer leaflet LPS (Rowlett et al., 2017). On the other hand, CL-lacking cells have an extended *O*-antigen repeat. Surface adhesion and biofilm formation was also adversely affected in cells lacking PE or CL. Tolerance to both osmotic and oxidative stress was also significantly reduced as PE levels were reduced in a dose dependent manner. Lack of CL also reduced tolerance to osmotic stress but increased tolerance to oxidative stress. The above results clearly demonstrate that large adverse changes occur in cell structure and physiology

when the evolutionary determined optimal membrane lipid composition is perturbed.

REGULATION OF PHOSPHOLIPID COMPOSITION

E. coli membrane phospholipid composition and content remain within a narrow range under a broad range of growth conditions (Dowhan, 1997b). Small variation in phospholipid composition occurs with growth conditions and between strains, but composition remains at 70–80% zwitterionic PE and 20–30% anionic PG, CL, and phospholipid precursors. Except for the reversible formation of CL from PG by Cls's, all steps in the pathway are irreversible under physiological conditions. PG ranges from 20–25% and CL 5–10% with this variability due to increased conversion of PG to CL as cell growth slows, media osmolarity increases or cells approach stationary phase.

How the ratio of zwitterionic to anionic phospholipid is regulated is still not well understood, although it must occur at the branchpoint in the biosynthetic pathway following the formation of CDP-DAG. A conditionally lethal *cdsA* mutant accumulates PA mostly at the expense of PG and CL rather than PE suggesting that affinity for CDP-DAG may be higher for the PssA than for PgsA (Ganong and Raetz, 1982). Massive 150-fold overproduction of PssA (Ohta et al., 1981a) resulted in no change in the above ratio of PE to PG plus CL while a 40-fold overproduction of PgpA (Ohta et al., 1981b) resulted in a change in the PE to anionic lipid ratio from 75/25 to 65/35 but nowhere in proportion to enzyme overproduction. A possible reason for lack of a response to overproduction of PssA lies in the peripheral membrane association of the enzyme and its membrane association dependent on binding to its lipid substrate CDP-DAG or anionic lipids (Carman and Dowhan, 1979; Louie and Dowhan, 1980). CDP-DAG remains constant and at barely detectible levels while an increase in the anionic lipid would increase PssA membrane association resulting in normalizing the ration of PE to PG plus CL. The overall control mechanism is supported by replacement of the *E. coli* PssA with the integral membrane enzyme from *B. subtilis*. In this case the level of PE increased with increasing amounts of the latter enzyme (Matsumoto, 1997).

Successful expression and function of the Kennedy Pathway enzymes from *E. coli* inside of large unilamellar lipid vesicles (Blanken et al., 2020) composed of controlled ratios of PG to PE largely supports regulation of PssA activity by PG content. PE synthesis was dependent on the PG content of the liposomes independent of the level of expression of the PG-synthesizing branch. This result indicates that the regulatory mechanism is not solely dependent on competition between the two branches of the pathway for CDP-DAG but relies on the association of PssA with anionic lipids as predicted from the earlier reconstitution experiments (Louie and Dowhan, 1980; Louie et al., 1986).

PlsB initiates phospholipid synthesis utilizing G3P as a substrate. PlsB activity is coordinated with other macromolecular synthesis via guanosine pentaphosphate (ppGpp), and the *plsB* gene is induced by the σ^E stress response regulator (Wahl et al., 2011; Yao and Rock, 2013). Thus, PlsB levels respond to coordinate down regulation of macromolecular synthesis under nutrient limiting conditions via ppGpp inhibition, and the enzyme level is increased in response to increases in envelope stress. Since PlsB produces a new PA while DgkA salvages PA using existing pools of DAG, these enzymes would be expected to be regulated in a reciprocal manner by σ^E and ppGpp, which in fact is the case (Wahl et al., 2011). PlsB activity is promoted by PG implying that PG is involved in a positive feedback loop that produces PA and thus all membrane lipids (Ishinaga et al., 1976; Scheideler and Bell, 1989).

The high Km PlsB mutant is dependent on glycerol for growth and phospholipid synthesis (McIntyre et al., 1977). Removal of glycerol from the medium results in immediate cessation in phospholipid synthesis and cell growth. However, membrane protein synthesis continues until the ratio of membrane protein to phospholipid increases about twofold. Re-supply of glycerol initiates new phospholipid synthesis immediately but membrane protein synthesis and cell growth lag until the membrane protein to phospholipid ratio returns to normal levels. Therefore, the cell senses and regulates this ratio maintaining membrane capacity for protein well below the maximum.

Overproduction of PlsB results in filamentation and massive accumulation of intracellular tubular membrane structures (Wilkison et al., 1986). The isolated structures were highly enriched in PlsB, contained an increased protein to lipid ratio compared to the cell membrane and a wild type phospholipid composition. Similar results have been observed with overproduction of other membrane proteins except that in many cases CL levels were also elevated (Arechaga, 2013; Jamin et al., 2018). Depletion of CL in a *clsABC* triple null mutant disrupts formation of these intracytoplasmic membranes in a strain overproducing F-ATPase subunit *b* (Carranza et al., 2017). This result implies a physical requirement supplied by CL in forming these intracellular structures. However, clear understanding at the molecular level of how cells coordinate phospholipid synthesis, membrane protein levels and cell growth are not well understood.

MEMBRANE PHOSPHOLIPID ASYMMETRY

Most if not all biological membranes display an asymmetric distribution of lipid species on each side of the bilayer (Marquardt et al., 2015). Such asymmetry in biological membranes is entropically disfavored and expected to be in a non-equilibrium thermodynamic state. This non-equilibrium situation appears to be maintained by membrane proteins known as phospholipid translocators (flippases and floppases), which use ATP to mediate the net transfer of specific phospholipids from one leaflet of a membrane to the other. Scramblases equilibrate lipids in both directions across the membrane and can abolish lipid asymmetry. Several candidate flippases have been identified in eukaryotes that catalyze translocation of different classes of lipids (Pomorski and Menon, 2006; Sharom, 2011; Lopez-Marques et al., 2014).

MsbA is the only bacterial phospholipid flippase identified in *E. coli*. Conditionally lethal *msbA* mutants accumulate phospholipids and LPS in the cytoplasmic leaflet of the inner membrane upon a shift to non-permissive conditions (Doerrler et al., 2004). Unfortunately, MsbA has never been demonstrated to promote translocation of phospholipids *in vitro*. Thus, either MsbA alone is necessary but not sufficient for distribution of phospholipids among lipid monolayers *in vitro* or unknown accessory proteins are required for MsbA to perform efficient phospholipid translocation. It is also possible that MsbA is involved only in LPS lipid A transport but not responsible for phospholipid distribution within the cell envelope.

Eukaryotic cell plasma membrane lipid asymmetry is well established, and loss of asymmetry is associated with an array of cellular malfunctions (Doktorova et al., 2020). However, the importance of lipid asymmetry is not fully understood especially in bacteria. In Gram-positive *Bacillus megaterium* 68% of the PE resides in the cytoplasmic leaflet of the single cell membrane (Rothman and Kennedy, 1977a). The outer membrane lipid bilayer of *E. coli* is asymmetric with LPS exclusively in the outer leaflet and primarily PE in the inner leaflet (Ganong et al., 1980). Determination of the transbilayer lipid distribution of the inner membrane of Gram-negative bacteria has been complicated by contamination with the outer membrane enrichment in PE.

Recent isolation of uniformly oriented inside-out inner membrane vesicles of *E. coli* and *Yersinia pseudotuberculosis* essentially free of outer membrane made possible the determination of the distribution of PE within the inner membrane lipid bilayer of these bacteria (Bogdanov et al., 2020). Inside-out inner membrane vesicles were treated sequentially with a membrane impermeable primary amine probe followed by a membrane permeable amine probe. The probes had different chromogenic properties so that after solvent extraction of the vesicle lipid derivatives, spectral determination was used to determine the amounts of periplasmic and cytoplasmic leaflet PE. The cytoplasmic/periplasmic leaflet distribution of PE in these two Gram-negative bacteria is 75/25 using 3 independent methods of determination (Bogdanov et al., 2020). Although *E. coli* PE is about 75% of total phospholipid, the outer membrane periplasmic leaflet is about 90% PE (Ganong et al., 1980). Thus, the inner membrane bilayer phospholipid is about 65% PE (Ganong et al., 1980; Bogdanov et al., 2020). The remaining phospholipids are anionic PG, CL, and phospholipid precursors. Currently the transmembrane distribution of the individual anionic phospholipids is not known. Using these numbers, the periplasmic leaflet of the inner membrane is composed of a near equal amount of zwitterionic and anionic phospholipid and the cytoplasmic leaflet contains a 75/25 enrichment of PE over anionic phospholipids.

Although the inner membrane bilayer distribution of PE is similar to that reported for *B. megaterium* (Rothman and Kennedy, 1977a), there is a major difference in the appearance of newly synthesized PE between these organisms. In *B. megaterium*, which contains a single lipid bilayer, newly synthesized PE appears in the cytoplasmic leaflet followed by distribution to the outer leaflet (Rothman and Kennedy, 1977b). In *E. coli* both newly synthesized PE and its precursor PS (traced in a *psd2* temperature sensitive mutant) first appear in the periplasmic leaflet followed by distribution to the cytoplasmic leaflet (Langley et al., 1982; Bogdanov et al., 2020). This is quite surprising in that PssA is a peripheral membrane protein that associates with the cytoplasmic surface of the inner membrane (Louie and Dowhan, 1980; Louie et al., 1986). Interestingly, PS synthesis initiated on the luminal leaflet of large unilamellar lipid vesicles is also immediately translocated to the outer leaflet, where it is detected by a bulky PS-specific fluorescent reporter probe (Blanken et al., 2020). Since PE is required in both the outer and inner membrane, initial appear in the periplasmic leaflet of the inner membrane may allow efficient distribution to both membranes. Upon induction of PE synthesis in a PE-lacking strain of *E. coli*, PE also initially appears in the periplasmic leaflet of the inner membrane (Bogdanov et al., 2020). As the PE content increases from 0 to 75%, the distribution between the inner membrane leaflets approaches wild type levels. Inducement of filamentation of wild type *E. coli* also reverses the distribution of PE to favor the periplasmic leaflet at steady state.

How PE distributes dynamically as its level is increased through regulated synthesis of PE in cells initially lacking PE coupled with mutants in CL synthesis was used to determine how PE and CL affect lipid order in the bilayer. Using fluorescent sensors of lipid order, it was determined that the increase in packing order driven by PE is countered by the increase in disorder driven by CL (Bogdanov et al., 2020). This *in vivo* affect mimics the results of studies done in artificial membranes free of proteins. The driving force for inner membrane lipid asymmetry can arise from the packing requirements imposed upon the system by the opposing forces of two negatively curved phospholipids in both leaflets. Therefore, percentage and localization of PE and CL appears to be adjusted to satisfy lipid packing requirements in order to maintain a stable bilayer and proper membrane morphology.

Clearly phospholipids are in constant flux within the inner membrane and between the outer and inner membranes (Langley et al., 1982; Bogdanov et al., 2020) in Gram-negative bacteria. This flux may be necessary to maintain entropically disfavored asymmetric transmembrane arrangement of lipids in both membranes by continuous retrograde transport of phospholipids from the outer to the inner membrane (Malinverni and Silhavy, 2009; Powers and Trent, 2018) and anterograde trafficking back to outer membrane (Hughes et al., 2019; Grimm et al., 2020). Membrane growth and continuous emergence of lipids in the periplasmic leaflet of the inner membrane for translocation to the outer membrane requires a constant supply of phospholipids in the cytosolic leaflet. Thus, asymmetry within the inner membrane may be regulated metabolically driven by insertion of PE in the periplasmic leaflet of the inner membrane followed by a balance between transfer to the outer membrane and the cytoplasmic leaflet of the inner membrane, which would relieve the lateral pressure within the periplasmic monolayer (Bogdanov et al., 2020). The shape difference between rod-shaped and filamentous cells may perturb the normal rates of distribution of PE within the cell envelope suggesting that PE distribution may facilitate or result from changes in bacterial shape. Indeed, the gradual changes in distribution of PE/CL amounts between the inner

FIGURE 4 | The Kennedy "Clan" on the occasion of his 90th birthday. Eugene Kennedy (1919–2011) is 3rd from the left in the front row. The gathering was in October 2009 at Harvard Medical School. Pictured are former graduate students, postdoctoral fellows and scientific associates of Eugene Kennedy. Figure and legend reprinted by permission from Elsevier (Dowhan, 2013): Copyright 2013.

membrane leaflets during *de novo* PE biosynthesis in *E. coli* cells initially lacking PE coincides with progressive reduction of cell size as PE is progressively accumulated and CL is removed from the cytoplasmic leaflet of the inner membrane (Bogdanov et al., 2020). See **Figure 4** for Kennedy associates who attended his 90th birthday celebration.

SUMMARY AND PERSPECTIVES

Prior to laying the foundation for bacterial phospholipid metabolism and enzymology in the 1960's and 1970's, Eugene Kennedy did the same for the somatic cell phospholipid field (Dowhan, 2013). Dennis Vance, Jean Vance, Claudia Kent, and Suzanne Jackowski extended Kennedy's work in somatic cells by detailing the genetics and enzymology. Susan Henry and George Carman defined the genetics and biochemistry of phospholipid metabolism in *S. cerevisiae*. There were other major contributors to the microbial phospholipid field. Roy Vagelos, John Cronan, Robert Bell, and Charles Rock defined microbial fatty acid synthesis and the synthesis of PA. The Dutch group initially formed by Laurens van Deenen made major contributions to lipid enzymology and metabolism. Japanese laboratories of Isao Shibuya, Kouji Matsumoto, and Akinori Ohta not only contributed to the *E. coli* phospholipid field but extended studies to Gram-positive bacteria. Many of Kennedy's trainees from the late 1960's to 1970's went on to make seminal contributions in areas related to cell membranes and lipids as have many of their trainees: Chris Raetz in phospholipid genetics and Lipid A studies in Gram-negative bacteria; William Wickner in membrane protein assembly; Edward Dennis in phospholipases and lipid second messengers; Carlos Hirschberg in mammalian nucleotide sugar transporters; Dennis Voelker in *S. cerevisiae* and lung phospholipid metabolism; and Nobel Laureate James Rothman in intracellular trafficking of secreted proteins.

There is still much to understand and study. Methods for determining anionic lipid bilayer asymmetry are required in order to develop a full picture of the importance of this asymmetry in microbial physiology. How is bilayer lipid asymmetry generated and controlled? What processes are responsible for transmembrane and intramembrane movement of phospholipids in Gram-negative bacteria? How is phospholipid synthesis and composition regulated and coordinated with other macromolecular synthesis? Thus, identification of the mechanism (flippase-free or flippase-guided) controlling the asymmetric distribution of lipids within the cell envelop of Gram-negative bacterial should be a high priority goal.

Given the defects in mutants lacking the major phospholipid classes, metabolic reactions with mechanisms unique to bacteria need to be exploited as antimicrobial targets. In particular PssA and ClsA fall into this category. Clearly, lipid and lipid enzyme inspired therapeutics and chemical targeting of the bacterial lipid synthesis is in its infancy, and it remains to be seen whether the significant challenges in protein biochemistry and drug design can be overcome to target essential lipid enzymes. Such studies will be aided by high resolution structural studies of phospholipid biosynthetic enzymes. Significant effort should be made to identify potential contribution of genes that are not exclusively engaged in antibiotic resistance but are involved in regulation of cell envelope synthesis, morphology and remodeling.

Many phenotypes have been observed for the current set of null mutants that need more detailed studies to expand the understanding of the role of membrane lipids in specific cell functions. Information on the biosynthesis of phospholipids in bacteria has been derived from a relatively small set of easily culturable bacteria. Studies in many pathological microorganisms are complicated due to defining appropriate growth conditions. Very few studies of bacterial phospholipid metabolism and function have been carried out under anaerobic conditions, which may more closely mimic conditions for both symbiotic and pathological presence of bacteria in mammalian systems. Given the complexity and challenges of defining functions of lipids in multi-organelle somatic cells, clues from bacterial studies will provide valuable information on the role of lipids in all cell types.

AUTHOR CONTRIBUTIONS

All authors listed have made a substantial, direct and intellectual contribution to the work, and approved it for publication.

FUNDING

This work was supported in whole or in part by National Institutes of Health Grant GM R01 121493 and the John Dunn Research Foundation both to WD. This work was also supported by the NATO Science for Peace and Security Programme-SPS 985291 and the European Union's Horizon 2020 Research and Innovation Programme under the Marie Skłodowska-Curie grant agreements no. 690853 (both to MB).

REFERENCES

Abramson, J., Smirnova, I., Kasho, V., Verner, G., Kaback, H. R., and Iwata, S. (2003). Structure and mechanism of the lactose permease of *Escherichia coli*. *Science* 301, 610–615. doi: 10.1126/science.1088196

Arechaga, I. (2013). Membrane invaginations in bacteria and mitochondria: common features and evolutionary scenarios. *J. Mol. Microbiol. Biotechnol.* 23, 13–23. doi: 10.1159/000346515

Asai, Y., Katayose, Y., Hikita, C., Ohta, A., and Shibuya, I. (1989). Suppression of the lethal effect of acidic-phospholipid deficiency by defective formation of the major outer membrane lipoprotein in *Escherichia coli*. *J. Bacteriol.* 171, 6867–6869. doi: 10.1128/jb.171.12.6867-6869.1989

Bae-Lee, M. S., and Carman, G. M. (1984). Phosphatidylserine synthesis in *Saccharomyces cerevisiae*. Purification and characterization of membrane-associated phosphatidylserine synthase. *J. Biol. Chem.* 259, 10857–10862. doi: 10.1016/s0021-9258(18)90592-2

Bell, R. M. (1974). Mutants of *Escherichia coli* defective in membrane phospholipid synthesis: macromolecular synthesis in an sn-glycerol 3-phosphate acyltransferase Km mutant. *J. Bacteriol.* 117, 1065–1076. doi: 10.1128/jb.117.3.1065-1076.1974

Bell, R. M. (1975). Mutants of *Escherichia coli* defective in membrane phospholipid synthesis. Properties of wild type and Km defective sn-glycerol-3-phosphate acyltransferase activities. *J. Biol. Chem.* 250, 7147–7152. doi: 10.1016/s0021-9258(19)40921-6

Blanken, D., Foschepoth, D., Serrao, A. C., and Danelon, C. (2020). Genetically controlled membrane synthesis in liposomes. *Nat. Commun.* 11:4317.

Bogdanov, M. (2017). Mapping of membrane protein topology by substituted cysteine accessibility method (SCAM). *Methods Mol. Biol.* 1615, 105–128. doi: 10.1007/978-1-4939-7033-9_9

Bogdanov, M., and Dowhan, W. (1995). Phosphatidylethanolamine is required for *in vivo* function of the membrane-associated lactose permease of *Escherichia coli*. *J. Biol. Chem.* 270, 732–739. doi: 10.1074/jbc.270.2.732

Bogdanov, M., and Dowhan, W. (1998). Phospholipid-assisted protein folding: phosphatidylethanolamine is required at a late step of the conformational maturation of the polytopic membrane protein lactose permease. *EMBO J.* 17, 5255–5264. doi: 10.1093/emboj/17.18.5255

Bogdanov, M., and Dowhan, W. (1999). Lipid-assisted protein folding. *J. Biol. Chem.* 274, 36827–36830. doi: 10.1074/jbc.274.52.36827

Bogdanov, M., and Dowhan, W. (2012). Lipid-dependent generation of a dual topology for a membrane protein. *J. Biol. Chem.* 287, 37939–37948. doi: 10.1074/jbc.m112.404103

Bogdanov, M., Dowhan, W., and Vitrac, H. (2014). Lipids and topological rules governing membrane protein assembly. *Biochim. Biophys. Acta* 1843, 1475–1488. doi: 10.1016/j.bbamcr.2013.12.007

Bogdanov, M., Heacock, P., Guan, Z., and Dowhan, W. (2010a). Plasticity of lipid-protein interactions in the function and topogenesis of the membrane protein lactose permease from *Escherichia coli*. *Proc. Natl. Acad. Sci. U.S.A.* 107, 15057–15062. doi: 10.1073/pnas.1006286107

Bogdanov, M., Heacock, P. N., and Dowhan, W. (2002). A polytopic membrane protein displays a reversible topology dependent on membrane lipid composition. *EMBO J.* 21, 2107–2116. doi: 10.1093/emboj/21.9.2107

Bogdanov, M., Heacock, P. N., and Dowhan, W. (2010b). Study of polytopic membrane protein topological organization as a function of membrane lipid composition. *Methods Mol. Biol.* 619, 79–101. doi: 10.1007/978-1-60327-412-8_5

Bogdanov, M., Pyrshev, K., Yesylevskyy, S., Ryabichko, S., Boiko, V., Ivanchenko, P., et al. (2020). Phospholipid distribution in the cytoplasmic membrane of Gram-negative bacteria is highly asymmetric, dynamic, and cell shape-dependent. *Sci. Adv.* 6:eaaz6333. doi: 10.1126/sciadv.aaz6333

Bogdanov, M., Sun, J., Kaback, H. R., and Dowhan, W. (1996). A phospholipid acts as a chaperone in assembly of a membrane transport protein. *J. Biol. Chem.* 271, 11615–11618. doi: 10.1074/jbc.271.20.11615

Bogdanov, M., Umeda, M., and Dowhan, W. (1999). Phospholipid-assisted refolding of an integral membrane protein. Minimum structural features for phosphatidylethanolamine to act as a molecular chaperone. *J. Biol. Chem.* 274, 12339–12345. doi: 10.1074/jbc.274.18.12339

Bogdanov, M., Vitrac, H., and Dowhan, W. (2018). "Flip-flopping membrane proteins: how the charge balance rule governs dynamic membrane protein topology," in *Biogenesis of Fatty Acids, Lipids and Membranes*, ed. O. Geiger (Cham: Springer). doi: 10.1007/978-3-319-43676-0_62-1

Bogdanov, M., Xie, J., Heacock, P., and Dowhan, W. (2008). To flip or not to flip: lipid-protein charge interactions are a determinant of final membrane protein topology. *J. Cell Biol.* 182, 925–935. doi: 10.1083/jcb.200803097

Bowie, J. U. (2006). Flip-flopping membrane proteins. *Nat. Struct. Mol. Biol.* 13, 94–96. doi: 10.1038/nsmb0206-94

Bowie, J. U. (2013). Structural biology. Membrane protein twists and turns. *Science* 339, 398–399. doi: 10.1126/science.1228655

Carman, G. M., Deems, R. A., and Dennis, E. A. (1995). Lipid signaling enzymes and surface dilution kinetics. *J. Biol. Chem.* 270, 18711–18714. doi: 10.1074/jbc.270.32.18711

Carman, G. M., and Dowhan, W. (1979). Phosphatidylserine synthase from *Escherichia coli*. The role of Triton X-100 in catalysis. *J. Biol. Chem.* 254, 8391–8397. doi: 10.1016/s0021-9258(19)86903-x

Carranza, G., Angius, F., Ilioaia, O., Solgadi, A., Miroux, B., and Arechaga, I. (2017). Cardiolipin plays an essential role in the formation of intracellular membranes in *Escherichia coli*. *Biochim. Biophys. Acta Biomembr.* 1859, 1124–1132. doi: 10.1016/j.bbamem.2017.03.006

Chang, S. C., Heacock, P. N., Clancey, C. J., and Dowhan, W. (1998). The PEL1 gene (renamed PGS1) encodes the phosphatidylglycero-phosphate synthase of *Saccharomyces cerevisiae*. *J. Biol. Chem.* 273, 9829–9836. doi: 10.1074/jbc.273.16.9829

Chang, Y. Y., and Kennedy, E. P. (1967). Phosphatidyl glycerophosphate phosphatase. *J. Lipid Res.* 8, 456–462. doi: 10.1016/s0022-2275(20)38902-1

Clark, D., Lightner, V., Edgar, R., Modrich, P., Cronan, J. E. Jr., and Bell, R. M. (1980). Regulation of phospholipid biosynthesis in *Escherichia coli*. Cloning of the structural gene for the biosynthetic sn-glycerol-3-phosphate dehydrogenase. *J. Biol. Chem.* 255, 714–717. doi: 10.1016/s0021-9258(19)86238-5

Coleman, J. (1990). Characterization of *Escherichia coli* cells deficient in 1-acyl-sn-glycerol-3- phosphate acyltransferase activity. *J. Biol. Chem.* 265, 17215–17221. doi: 10.1016/s0021-9258(17)44891-5

Coleman, J. (1992). Characterization of the *Escherichia coli* gene for 1-acyl-sn-glycerol-3-phosphate acyltransferase (plsC). *Mol. Gen. Genet.* 232, 295–303. doi: 10.1007/bf00280009

Conover, G. M., Martinez-Morales, F., Heidtman, M. I., Luo, Z. Q., Tang, M., Chen, C., et al. (2008). Phosphatidylcholine synthesis is required for optimal function of *Legionella pneumophila* virulence determinants. *Cell. Microbiol.* 10, 514–528.

Costa, T. R. D., Ilangovan, A., Ukleja, M., Redzej, A., Santini, J. M., Smith, T. K., et al. (2016). Structure of the Bacterial Sex F Pilus reveals an assembly of a stoichiometric protein-phospholipid complex. *Cell* 166, 1436–1444.e10.

Crooke, E., Castuma, C. E., and Kornberg, A. (1992). The chromosome origin of *Escherichia coli* stabilizes DnaA protein during rejuvenation by phospholipids. *J. Biol. Chem.* 267, 16779–16782. doi: 10.1016/s0021-9258(18)41849-2

Danielli, J. F., and Dańson, H. A. (1935). A contribution to the theory of permeability of thin films. *J. Cell. Comp. Physiol.* 5, 495–500. doi: 10.1002/jcp.10300050409

de Vrije, T., de Swart, R. L., Dowhan, W., Tommassen, J., and de Kruijff, B. (1988). Phosphatidylglycerol is involved in protein translocation across *Escherichia coli* inner membranes. *Nature* 334, 173–175. doi: 10.1038/334173a0

DeChavigny, A., Heacock, P. N., and Dowhan, W. (1991). Sequence and inactivation of the pss gene of *Escherichia coli*. Phosphatidylethanolamine may not be essential for cell viability. *J. Biol. Chem.* 266, 5323–5332. doi: 10.1016/s0021-9258(19)67791-4

Dillon, D. A., Wu, W. I., Riedel, B., Wissing, J. B., Dowhan, W., and Carman, G. M. (1996). The *Escherichia coli* pgpB gene encodes for a diacylglycerol pyrophosphate phosphatase activity. *J. Biol. Chem.* 271, 30548–30553. doi: 10.1074/jbc.271.48.30548

Doerrler, W. T., Gibbons, H. S., and Raetz, C. R. (2004). MsbA-dependent translocation of lipids across the inner membrane of *Escherichia coli*. *J. Biol. Chem.* 279, 45102–45109. doi: 10.1074/jbc.m408106200

Doktorova, M., Symons, J. L., and Levental, I. (2020). Structural and functional consequences of reversible lipid asymmetry in living membranes. *Nat. Chem. Biol.* 16, 1321–1330. doi: 10.1038/s41589-020-00688-0

Dowhan, W. (1997a). CDP-diacylglycerol synthase of microorganisms. *Biochim. Biophys. Acta* 1348, 157–165. doi: 10.1016/s0005-2760(97)00111-2

Dowhan, W. (1997b). Molecular basis for membrane phospholipid diversity: why are there so many lipids? *Annu. Rev. Biochem.* 66, 199–232. doi: 10.1146/annurev.biochem.66.1.199

Dowhan, W. (2013). A retrospective: use of *Escherichia coli* as a vehicle to study phospholipid synthesis and function. *Biochim. Biophys. Acta* 1831, 471–494. doi: 10.1016/j.bbalip.2012.08.007

Dowhan, W., and Bogdanov, M. (2009). Lipid-dependent membrane protein topogenesis. *Annu. Rev. Biochem.* 78, 515–540. doi: 10.1146/annurev.biochem.77.060806.091251

Dowhan, W., Bogdanov, M., Mileykovskaya, E., and Vitrac, H. (2017). "Functional roles of individual membrane phospholipids in *Escherichia coli* and *Saccharomyces cerevisiae*," in *Biogenesis of Fatty Acids, Lipids and Membranes. Handbook of Hydrocarbon and Lipid Microbiology*, ed. O. Geiger (Cham: Springer). doi: 10.1007/978-3-319-43676-0_36-1

Dowhan, W., Nikaido, H., Stubbe, J., Kozarich, J. W., Wickner, W. T., Russell, D. W., et al. (2013). Christian Raetz: scientist and friend extraordinaire. *Annu. Rev. Biochem.* 82, 1–24. doi: 10.1146/annurev-biochem-012512-091530

Dowhan, W., Vitrac, H., and Bogdanov, M. (2019). Lipid-assisted membrane protein folding and topogenesis. *Protein J.* 38, 274–288. doi: 10.1007/s10930-019-09826-7

Dowhan, W., Wickner, W. T., and Kennedy, E. P. (1974). Purification and properties of phosphatidylserine decarboxylase from *Escherichia coli. J. Biol. Chem.* 249, 3079–3084. doi: 10.1016/s0021-9258(19)42640-9

Dutt, A., and Dowhan, W. (1977). Intracellular distribution of enzymes of phospholipid metabolism in several gram-negative bacteria. *J. Bacteriol.* 132, 159–165. doi: 10.1128/jb.132.1.159-165.1977

Dutt, A., and Dowhan, W. (1981). Characterization of a membrane-associated cytidine diphosphate-diacylglycerol-dependent phosphatidylserine synthase in bacilli. *J. Bacteriol.* 147, 535–542. doi: 10.1128/jb.147.2.535-542.1981

Emoto, K., and Umeda, M. (2000). An essential role for a membrane lipid in cytokinesis. Regulation of contractile ring disassembly by redistribution of phosphatidylethanolamine. *J. Cell Biol.* 149, 1215–1224. doi: 10.1083/jcb.149.6.1215

Fan, J., Jiang, D., Zhao, Y., Liu, J., and Zhang, X. C. (2014). Crystal structure of lipid phosphatase *Escherichia coli* phosphatidylglycerophosphate phosphatase B. *Proc. Natl. Acad. Sci. U.S.A.* 111, 7636–7640. doi: 10.1073/pnas.1403097111

Funk, C. R., Zimniak, L., and Dowhan, W. (1992). The pgpA and pgpB genes of *Escherichia coli* are not essential: evidence for a third phosphatidylglycerophosphate phosphatase. *J. Bacteriol.* 174, 205–213. doi: 10.1128/jb.174.1.205-213.1992

Ganong, B. R., Leonard, J. M., and Raetz, C. R. (1980). Phosphatidic acid accumulation in the membranes of *Escherichia coli* mutants defective in CDP-diglyceride synthetase. *J. Biol. Chem.* 255, 1623–1629. doi: 10.1016/s0021-9258(19)86078-7

Ganong, B. R., and Raetz, C. R. (1982). Massive accumulation of phosphatidic acid in conditionally lethal CDP-diglyceride synthetase mutants and cytidine auxotrophs of *Escherichia coli*. *J. Biol. Chem.* 257, 389–394. doi: 10.1016/s0021-9258(19)68376-6

Goelz, S. E., and Cronan, J. E. Jr. (1980). The positional distribution of fatty acids in *Escherichia coli* phospholipids is not regulated by sn-glycerol 3-phosphate levels. *J. Bacteriol.* 144, 462–464. doi: 10.1128/jb.144.1.462-464.1980

Goldberg, D. E., Rumley, M. K., and Kennedy, E. P. (1981). Biosynthesis of membrane-derived oligosaccharides: a periplasmic phosphoglyceroltransferase. *Proc. Natl. Acad. Sci. U.S.A.* 78, 5513–5517. doi: 10.1073/pnas.78.9.5513

Gopalakrishnan, A. S., Chen, Y. C., Temkin, M., and Dowhan, W. (1986). Structure and expression of the gene locus encoding the phosphatidylglycerophosphate synthase of *Escherichia coli*. *J. Biol. Chem.* 261, 1329–1338. doi: 10.1016/s0021-9258(17)36095-7

Green, P. R., Merrill, A. H. Jr., and Bell, R. M. (1981). Membrane phospholipid synthesis in *Escherichia coli*. Purification, reconstitution, and characterization of sn-glycerol-3-phosphate acyltransferase. *J. Biol. Chem.* 256, 11151–11159. doi: 10.1016/s0021-9258(19)68570-4

Grimm, J., Shi, H., Wang, W., Mitchell, A. M., Wingreen, N. S., Huang, K. C., et al. (2020). The inner membrane protein YhdP modulates the rate of anterograde phospholipid flow in *Escherichia coli*. *Proc. Natl. Acad. Sci. U.S.A.* 117, 26907–26914. doi: 10.1073/pnas.2015556117

Guo, D., and Tropp, B. E. (2000). A second *Escherichia coli* protein with CL synthase activity. *Biochim. Biophys. Acta* 1483, 263–274. doi: 10.1016/s1388-1981(99)00193-6

Guo, R., Cang, Z., Yao, J., Kim, M., Deans, E., Wei, G., et al. (2020). Structural cavities are critical to balancing stability and activity of a membrane-integral enzyme. *Proc. Natl. Acad. Sci. U.S.A.* 117, 22146–22156. doi: 10.1073/pnas.1917770117

Hariharan, P., Tikhonova, E., Medeiros-Silva, J., Jeucken, A., Bogdanov, M. V., Dowhan, W., et al. (2018). Structural and functional characterization of protein-lipid interactions of the *Salmonella typhimurium* melibiose transporter MelB. *BMC Biol.* 16:85. doi: 10.1186/s12915-018-0553-0

Hawrot, E., and Kennedy, E. P. (1976). Conditional lethal phosphatidylserine decarboxylase mutants of *Escherichia coli*. Mapping of the structural gene for phosphatidylserine decarboxylase. *Mol. Gen. Genet.* 148, 271–279. doi: 10.1007/bf00332901

Hawrot, E., and Kennedy, E. P. (1978). Phospholipid composition and membrane function in phosphatidylserine decarboxylase mutants of *Escherichia coli*. *J. Biol. Chem.* 253, 8213–8220. doi: 10.1016/s0021-9258(17)34384-3

Heacock, P. N., and Dowhan, W. (1987). Construction of a lethal mutation in the synthesis of the major acidic phospholipids of *Escherichia coli*. *J. Biol. Chem.* 262, 13044–13049. doi: 10.1016/s0021-9258(18)45164-2

Heacock, P. N., and Dowhan, W. (1989). Alteration of the phospholipid composition of *Escherichia coli* through genetic manipulation. *J. Biol. Chem.* 264, 14972–14977. doi: 10.1016/s0021-9258(18)63798-6

Heber, S., and Tropp, B. E. (1991). Genetic regulation of cardiolipin synthase in *Escherichia coli*. *Biochim. Biophys. Acta* 1129, 1–12. doi: 10.1016/0167-4781(91)90206-2

Hickey, K. D., and Buhr, M. M. (2011). Lipid bilayer composition affects transmembrane protein orientation and function. *J. Lipids* 2011:208457.

Hirabayashi, T., Larson, T. J., and Dowhan, W. (1976). Membrane-associated phosphatidylglycerophosphate synthetase from *Escherichia coli*: purification by substrate affinity chromatography on cytidine 5'-diphospho-1,2-diacyl-sn-glycerol sepharose. *Biochemistry* 15, 5205–5211. doi: 10.1021/bi00669a002

Hiraoka, S., Matsuzaki, H., and Shibuya, I. (1993). Active increase in cardiolipin synthesis in the stationary growth phase and its physiological significance in *Escherichia coli*. *FEBS Lett.* 336, 221–224. doi: 10.1016/0014-5793(93)80807-7

Hiraoka, S., Nukui, K., Uetake, N., Ohta, A., and Shibuya, I. (1991). Amplification and substantial purification of cardiolipin synthase of *Escherichia coli*. *J. Biochem.* 110, 443–449. doi: 10.1093/oxfordjournals.jbchem.a123600

Hirschberg, C. B., and Kennedy, E. P. (1972). Mechanism of the enzymatic synthesis of cardiolipin in *Escherichia coli*. *Proc. Natl. Acad. Sci. U.S.A.* 69, 648–651. doi: 10.1073/pnas.69.3.648

Hokin, L. E. (1985). Receptors and phosphoinositide-generated second messengers. *Annu. Rev. Biochem.* 54, 205–235. doi: 10.1146/annurev.bi.54.070185.001225

Horrobin, D. F., Manku, M. S., Karmali, R. A., Ally, A. I., Karmazyn, M., and Morgan, R. O. (1977). The relationships between cyclic AMP, calcium and prostaglandins as second messengers. *Med. Hypotheses* 3, 276–282. doi: 10.1016/0306-9877(77)90038-x

Hostetler, K. Y., van den Bosch, H., and van Deenen, L. L. (1972). The mechanism of cardiolipin biosynthesis in liver mitochondria. *Biochim. Biophys. Acta* 260, 507–513. doi: 10.1016/0005-2760(72)90065-3

Hughes, G. W., Hall, S. C. L., Laxton, C. S., Sridhar, P., Mahadi, A. H., Hatton, C., et al. (2019). Evidence for phospholipid export from the bacterial inner membrane by the Mla ABC transport system. *Nat. Microbiol.* 4, 1692–1705. doi: 10.1038/s41564-019-0481-y

Icho, T. (1988a). Membrane-bound phosphatases in *Escherichia coli*: sequence of the pgpA gene. *J. Bacteriol.* 170, 5110–5116. doi: 10.1128/jb.170.11.5110-5116.1988

Icho, T. (1988b). Membrane-bound phosphatases in *Escherichia coli*: sequence of the pgpB gene and dual subcellular localization of the pgpB product. *J. Bacteriol.* 170, 5117–5124. doi: 10.1128/jb.170.11.5117-5124.1988

Icho, T., Bulawa, C. E., and Raetz, C. R. (1985a). Molecular cloning and sequencing of the gene for CDP-diglyceride hydrolase of *Escherichia coli*. *J. Biol. Chem.* 260, 12092–12098. doi: 10.1016/s0021-9258(17)38990-1

Icho, T., and Raetz, C. R. (1983). Multiple genes for membrane-bound phosphatases in *Escherichia coli* and their action on phospholipid precursors. *J. Bacteriol.* 153, 722–730. doi: 10.1128/jb.153.2.722-730.1983

Icho, T., Sparrow, C. P., and Raetz, C. R. (1985b). Molecular cloning and sequencing of the gene for CDP-diglyceride synthetase of *Escherichia coli*. *J. Biol. Chem.* 260, 12078–12083. doi: 10.1016/s0021-9258(17)38988-3

Ishinaga, M., Nishihara, M., Kato, M., and Kito, M. (1976). Function of phosphatidylglycerol molecular species in membranes. Activation of membrane-bound sn-glycerol 3-phosphate acyltransferase in *Escherichia coli*. *Biochim. Biophys. Acta* 431, 426–432. doi: 10.1016/0005-2760(76)90209-5

Iwamoto, K., Kobayashi, S., Fukuda, R., Umeda, M., Kobayashi, T., and Ohta, A. (2004). Local exposure of phosphatidylethanolamine on the yeast plasma membrane is implicated in cell polarity. *Genes Cells* 9, 891–903. doi: 10.1111/j.1365-2443.2004.00782.x

Jackson, B. J., Bohin, J. P., and Kennedy, E. P. (1984). Biosynthesis of membrane-derived oligosaccharides: characterization of mdoB mutants defective in phosphoglycerol transferase I activity. *J. Bacteriol.* 160, 976–981. doi: 10.1128/jb.160.3.976-981.1984

Jamin, N., Garrigos, M., Jaxel, C., Frelet-Barrand, A., and Orlowski, S. (2018). Ectopic neo-formed intracellular membranes in *Escherichia coli*: a response to membrane protein-induced stress involving membrane curvature and domains. *Biomolecules* 8:88. doi: 10.3390/biom8030088

Kaback, H. R., Sahin-Toth, M., and Weinglass, A. B. (2001). The kamikaze approach to membrane transport. *Nat. Rev. Mol. Cell Biol.* 2, 610–620. doi: 10.1038/35085077

Kanfer, J., and Kennedy, E. P. (1964). Metabolism and function of bacterial lipids. Ii. Biosynthesis of Phospholipids in *Escherichia Coli*. *J. Biol. Chem.* 239, 1720–1726.

Kanfer, J. N., and Kennedy, E. P. (1962). Synthesis of phosphatidylserine by *Escherichia coli*. *J. Biol. Chem.* 237, C270–C271.

Kanipes, M. I., Lin, S., Cotter, R. J., and Raetz, C. R. (2001). Ca2+-induced phosphoethanolamine transfer to the outer 3-deoxy-D-manno-octulosonic acid moiety of *Escherichia coli* lipopolysaccharide. A novel membrane enzyme dependent upon phosphatidylethanolamine. *J. Biol. Chem.* 276, 1156–1163. doi: 10.1074/jbc.m009019200

Kawasaki, K., Kuge, O., Chang, S. C., Heacock, P. N., Rho, M., Suzuki, K., et al. (1999). Isolation of a chinese hamster ovary (CHO) cDNA encoding phosphatidylglycerophosphate (PGP) synthase, expression of which corrects the mitochondrial abnormalities of a PGP synthase-defective mutant of CHO-K1 cells. *J. Biol. Chem.* 274, 1828–1834. doi: 10.1074/jbc.274.3.1828

Kawasaki, K., Kuge, O., Yamakawa, Y., and Nishijima, M. (2001). Purification of phosphatidylglycerophosphate synthase from Chinese hamster ovary cells. *Biochem. J.* 354, 9–15. doi: 10.1042/0264-6021:3540009

Kawashima, Y., Miyazaki, E., Muller, M., Tokuda, H., and Nishiyama, K. (2008). Diacylglycerol specifically blocks spontaneous integration of membrane proteins and allows detection of a factor-assisted integration. *J. Biol. Chem.* 283, 24489–24496. doi: 10.1074/jbc.m801812200

Kennedy, E. P. (1982). Osmotic regulation and the biosynthesis of membrane-derived oligosaccharides in *Escherichia coli*. *Proc. Natl. Acad. Sci. U.S.A.* 79, 1092–1095. doi: 10.1073/pnas.79.4.1092

Kennedy, E. P. (1992). Sailing to byzantium. *Annu. Rev. Biochem.* 61, 1–28.

Kennedy, E. P., Rumley, M. K., Schulman, H., and Van Golde, L. M. (1976). Identification of sn-glycero-1-phosphate and phosphoethanolamine residues linked to the membrane-derived Oligosaccharides of *Escherichia coli*. *J. Biol. Chem.* 251, 4208–4213. doi: 10.1016/s0021-9258(17)33282-9

Kennedy, E. P., and Weiss, S. B. (1956). The function of cytidine coenzymes in the biosynthesis of phospholipids. *J. Biol. Chem.* 222, 193–214. doi: 10.1016/s0021-9258(19)50785-2

Kikuchi, S., Shibuya, I., and Matsumoto, K. (2000). Viability of an *Escherichia coli* pgsA null mutant lacking detectable phosphatidylglycerol and cardiolipin. *J. Bacteriol.* 182, 371–376. doi: 10.1128/jb.182.2.371-376.2000

Killian, J. A., Koorengevel, M. C., Bouwstra, J. A., Gooris, G., Dowhan, W., and de Kruijff, B. (1994). Effect of divalent cations on lipid organization of cardiolipin isolated from *Escherichia coli* strain AH930. *Biochim. Biophys. Acta* 1189, 225–232. doi: 10.1016/0005-2736(94)90069-8

Kiyasu, J. Y., Pieringer, R. A., Paulus, H., and Kennedy, E. P. (1963). The biosynthesis of phosphatidylglycerol. *J. Biol. Chem.* 238, 2293–2298.

Kogoma, T., and von Meyenburg, K. (1983). The origin of replication, oriC, and the dnaA protein are dispensable in stable DNA replication (sdrA) mutants of *Escherichia coli* K-12. *EMBO J.* 2, 463–468. doi: 10.1002/j.1460-2075.1983.tb01445.x

Kuge, O., Nishijima, M., and Akamatsu, Y. (1991). A cloned gene encoding phosphatidylserine decarboxylase complements the phosphatidylserine biosynthetic defect of a Chinese hamster ovary cell mutant. *J. Biol. Chem.* 266, 6370–6376. doi: 10.1016/s0021-9258(18)38127-4

Kuge, O., Saito, K., Kojima, M., Akamatsu, Y., and Nishijima, M. (1996). Post-translational processing of the phosphatidylserine decarboxylase gene product in Chinese hamster ovary cells. *Biochem. J.* 319, 33–38. doi: 10.1042/bj3190033

Kumar, H., Finer-Moore, J. S., Jiang, X., Smirnova, I., Kasho, V., Pardon, E., et al. (2018). Crystal Structure of a ligand-bound LacY-Nanobody Complex. *Proc. Natl. Acad. Sci. U.S.A.* 115, 8769–8774. doi: 10.1073/pnas.1801774115

Kusters, R., Dowhan, W., and de Kruijff, B. (1991). Negatively charged phospholipids restore prePhoE translocation across phosphatidylglycerol-depleted *Escherichia coli* inner membranes. *J. Biol. Chem.* 266, 8659–8662. doi: 10.1016/s0021-9258(18)31493-5

Langley, K. E., Hawrot, E., and Kennedy, E. P. (1982). Membrane assembly: movement of phosphatidylserine between the cytoplasmic and outer membranes of *Escherichia coli*. *J. Bacteriol.* 152, 1033–1041.

Larson, T. J., and Dowhan, W. (1976). Ribosomal-associated phosphatidylserine synthetase from *Escherichia coli*: purification by substrate-specific elution from phosphocellulose using cytidine 5'-diphospho-1,2-diacyl-sn-glycerol. *Biochemistry* 15, 5212–5218. doi: 10.1021/bi00669a003

Larson, T. J., Lightner, V. A., Green, P. R., Modrich, P., and Bell, R. M. (1980). Membrane phospholipid synthesis in *Escherichia coli*. Identification of the sn-glycerol-3-phosphate acyltransferase polypeptide as the plsB gene product. *J. Biol. Chem.* 255, 9421–9426. doi: 10.1016/s0021-9258(19)70579-1

Li, C., Tan, B. K., Zhao, J., and Guan, Z. (2016). *In vivo* and *in vitro* synthesis of phosphatidylglycerol by an *Escherichia coli* cardiolipin synthase. *J. Biol. Chem.* 291, 25144–25153. doi: 10.1074/jbc.m116.762070

Li, D., Lyons, J. A., Pye, V. E., Vogeley, L., Aragao, D., Kenyon, C. P., et al. (2013). Crystal structure of the integral membrane diacylglycerol kinase. *Nature* 497, 521–524.

Li, Q.-X. (1989). '*Structure and Biosynthesis of a Pyruvate-Dependent Enzyme: Phosphatidylserine Decarboxylase from Escherichia coli*'. Ph.D. thesis, University of Texas Health Science Center at Houston, Houston, TX.

Li, Q. X., and Dowhan, W. (1988). Structural characterization of *Escherichia coli* phosphatidylserine decarboxylase. *J. Biol. Chem.* 263, 11516–11522. doi: 10.1016/s0021-9258(18)37988-2

Li, Q. X., and Dowhan, W. (1990). Studies on the mechanism of formation of the pyruvate prosthetic group of phosphatidylserine decarboxylase from *Escherichia coli*. *J. Biol. Chem.* 265, 4111–4115. doi: 10.1016/s0021-9258(19)39709-1

Lightner, V. A., Bell, R. M., and Modrich, P. (1983). The DNA sequences encoding plsB and dgk loci of *Escherichia coli*. *J. Biol. Chem.* 258, 10856–10861. doi: 10.1016/s0021-9258(17)44354-7

Lightner, V. A., Larson, T. J., Tailleur, P., Kantor, G. D., Raetz, C. R., Bell, R. M., et al. (1980). Membrane phospholipid synthesis in *Escherichia coli*. Cloning of a structural gene (plsB) of the sn-glycerol-3-phosphate acyl/transferase. *J. Biol. Chem.* 255, 9413–9420. doi: 10.1016/s0021-9258(19)70578-x

Lill, R., Dowhan, W., and Wickner, W. (1990). The ATPase activity of SecA is regulated by acidic phospholipids, SecY, and the leader and mature domains of precursor proteins. *Cell* 60, 271–280. doi: 10.1016/0092-8674(90)90742-w

Lopez-Lara, I. M., and Geiger, O. (2017). Bacterial lipid diversity. *Biochim. Biophys. Acta Mol. Cell. Biol. Lipids* 1862, 1287–1299.

Lopez-Marques, R. L., Theorin, L., Palmgren, M. G., and Pomorski, T. G. (2014). P4-ATPases: lipid flippases in cell membranes. *Pflugers Arch.* 466, 1227–1240. doi: 10.1007/s00424-013-1363-4

Louie, K., Chen, Y. C., and Dowhan, W. (1986). Substrate-induced membrane association of phosphatidylserine synthase from *Escherichia coli*. *J. Bacteriol.* 165, 805–812. doi: 10.1128/jb.165.3.805-812.1986

Louie, K., and Dowhan, W. (1980). Investigations on the association of phosphatidylserine synthase with the ribosomal component from *Escherichia coli*. *J. Biol. Chem.* 255, 1124–1127. doi: 10.1016/s0021-9258(19)86151-3

Lu, Y. H., Guan, Z., Zhao, J., and Raetz, C. R. (2011). Three phosphatidylglycerol-phosphate phosphatases in the inner membrane of *Escherichia coli*. *J. Biol. Chem.* 286, 5506–5518. doi: 10.1074/jbc.m110.199265

Lu, Y. J., Zhang, Y. M., Grimes, K. D., Qi, J., Lee, R. E., and Rock, C. O. (2006). Acyl-phosphates initiate membrane phospholipid synthesis in Gram-positive pathogens. *Mol. Cell* 23, 765–772. doi: 10.1016/j.molcel.2006.06.030

Luevano-Martinez, L. A., Forni, M. F., dos Santos, V. T., Souza-Pinto, N. C., and Kowaltowski, A. J. (2015). Cardiolipin is a key determinant for mtDNA stability and segregation during mitochondrial stress. *Biochim. Biophys. Acta* 1847, 587–598. doi: 10.1016/j.bbabio.2015.03.007

Luevano-Martinez, L. A., and Kowaltowski, A. J. (2015). Phosphatidylglycerol-derived phospholipids have a universal, domain-crossing role in stress responses. *Arch. Biochem. Biophys.* 585, 90–97. doi: 10.1016/j.abb.2015.09.015

Makarova, K. S., Aravind, L., Wolf, Y. I., Tatusov, R. L., Minton, K. W., Koonin, E. V., et al. (2001). Genome of the extremely radiation-resistant bacterium *Deinococcus radiodurans* viewed from the perspective of comparative genomics. *Microbiol. Mol. Biol. Rev.* 65, 44–79. doi: 10.1128/mmbr.65.1.44-79.2001

Malinverni, J. C., and Silhavy, T. J. (2009). An ABC transport system that maintains lipid asymmetry in the gram-negative outer membrane. *Proc. Natl. Acad. Sci. U.S.A.* 106, 8009–8014. doi: 10.1073/pnas.0903229106

Margolin, W. (2001). Bacterial cell division: a moving MinE sweeper boggles the MinD. *Curr. Biol.* 11, R395–R398.

Marquardt, D., Geier, B., and Pabst, G. (2015). Asymmetric lipid membranes: towards more realistic model systems. *Membranes* 5, 180–196. doi: 10.3390/membranes5020180

Matsumi, R., Atomi, H., Driessen, A. J., and van der Oost, J. (2011). Isoprenoid biosynthesis in Archaea-biochemical and evolutionary implications. *Res. Microbiol.* 162, 39–52. doi: 10.1016/j.resmic.2010.10.003

Matsumoto, K. (1997). Phosphatidylserine synthase from bacteria. *Biochim. Biophys. Acta* 1348, 214–227. doi: 10.1016/s0005-2760(97)00110-0

Matsumoto, K., Kusaka, J., Nishibori, A., and Hara, H. (2006). Lipid domains in bacterial membranes. *Mol. Microbiol.* 61, 1110–1117. doi: 10.1111/j.1365-2958.2006.05317.x

Matsumoto, K., Okada, M., Horikoshi, Y., Matsuzaki, H., Kishi, T., Itaya, M., et al. (1998). Cloning, sequencing, and disruption of the *Bacillus subtilis* psd gene coding for phosphatidylserine decarboxylase. *J. Bacteriol.* 180, 100–106. doi: 10.1128/jb.180.1.100-106.1998

May, K. L., and Silhavy, T. J. (2018). The *Escherichia coli* phospholipase PldA regulates outer membrane homeostasis via lipid signaling. *mBio* 9:e00379-18.

McIlwain, B. C., Vandenberg, R. J., and Ryan, R. M. (2015). Transport rates of a glutamate transporter homologue are influenced by the lipid bilayer. *J. Biol. Chem.* 290, 9780–9788. doi: 10.1074/jbc.m114.630590

McIntyre, T. M., Chamberlain, B. K., Webster, R. E., and Bell, R. M. (1977). Mutants of *Escherichia coli* defective in membrane phospholipid synthesis. Effects of cessation and reinitiation of phospholipid synthesis on macromolecular synthesis and phospholipid turnover. *J. Biol. Chem.* 252, 4487–4493. doi: 10.1016/s0021-9258(17)40187-6

Mileykovskaya, E., and Dowhan, W. (1997). The Cpx two-component signal transduction pathway is activated in *Escherichia coli* mutant strains lacking phosphatidylethanolamine. *J. Bacteriol.* 179, 1029–1034. doi: 10.1128/jb.179.4.1029-1034.1997

Mileykovskaya, E., and Dowhan, W. (2000). Visualization of phospholipid domains in *Escherichia coli* by using the cardiolipin-specific fluorescent dye 10-N-nonyl acridine orange. *J. Bacteriol.* 182, 1172–1175. doi: 10.1128/jb.182.4.1172-1175.2000

Mileykovskaya, E., Fishov, I., Fu, X., Corbin, B. D., Margolin, W., and Dowhan, W. (2003). Effects of phospholipid composition on MinD-membrane interactions *in vitro* and *in vivo*. *J. Biol. Chem.* 278, 22193–22198.

Mileykovskaya, E., Ryan, A. C., Mo, X., Lin, C. C., Khalaf, K. I., Dowhan, W., et al. (2009). Phosphatidic acid and N-acylphosphatidylethanolamine form membrane domains in *Escherichia coli* mutant lacking cardiolipin and phosphatidylglycerol. *J. Biol. Chem.* 284, 2990–3000. doi: 10.1074/jbc.m805189200

Mileykovskaya, E., Sun, Q., Margolin, W., and Dowhan, W. (1998). Localization and function of early cell division proteins in filamentous *Escherichia coli* cells lacking phosphatidylethanolamine. *J. Bacteriol.* 180, 4252–4257. doi: 10.1128/jb.180.16.4252-4257.1998

Nagahama, H., Sakamoto, Y., Matsumoto, K., and Hara, H. (2006). RcsA-dependent and -independent growth defects caused by the activated Rcs phosphorelay system in the *Escherichia coli* pgsA null mutant. *J. Gen. Appl. Microbiol.* 52, 91–98. doi: 10.2323/jgam.52.91

Newman, M. J., Foster, D. L., Wilson, T. H., and Kaback, H. R. (1981). Purification and reconstitution of functional lactose carrier from *Escherichia coli*. *J. Biol. Chem.* 256, 11804–11808. doi: 10.1016/s0021-9258(19)68477-2

Newman, M. J., and Wilson, T. H. (1980). Solubilization and reconstitution of the lactose transport system from *Escherichia coli*. *J. Biol. Chem.* 255, 10583–10586. doi: 10.1016/s0021-9258(19)70345-7

Nicolson, G. L. (2014). The fluid-mosaic model of membrane structure: still relevant to understanding the structure, function and dynamics of biological membranes after more than 40 years. *Biochim. Biophys. Acta* 1838, 1451–1466. doi: 10.1016/j.bbamem.2013.10.019

Nilsson, I., and von Heijne, G. (1990). Fine-tuning the topology of a polytopic membrane protein: role of positively and negatively charged amino acids. *Cell* 62, 1135–1141. doi: 10.1016/0092-8674(90)90390-z

Nishijima, M., Bulawa, C. E., and Raetz, C. R. (1981). Two interacting mutations causing temperature-sensitive phosphatidylglycerol synthesis in *Escherichia coli* membranes. *J. Bacteriol.* 145, 113–121. doi: 10.1128/jb.145.1.113-121.1981

Ohta, A., Obara, T., Asami, Y., and Shibuya, I. (1985). Molecular cloning of the cls gene responsible for cardiolipin synthesis in *Escherichia coli* and phenotypic consequences of its amplification. *J. Bacteriol.* 163, 506–514. doi: 10.1128/jb.163.2.506-514.1985

Ohta, A., and Shibuya, I. (1977). Membrane phospholipid synthesis and phenotypic correlation of an *Escherichia coli* pss mutant. *J. Bacteriol.* 132, 434–443. doi: 10.1128/jb.132.2.434-443.1977

Ohta, A., Shibuya, I., Maruo, B., Ishinaga, M., and Kito, M. (1974). An extremely labile phosphatidylserine synthetase of an *Escherichia coli* mutant with the temperature-sensitive formation of phosphatidylethanolamine. *Biochim. Biophys. Acta* 348, 449–454. doi: 10.1016/0005-2760(74)90229-x

Ohta, A., Waggoner, K., Louie, K., and Dowhan, W. (1981a). Cloning of genes involved in membrane lipid synthesis. Effects of amplification of phosphatidylserine synthase in Escherichia coli. *J. Biol. Chem.* 256, 2219–2225. doi: 10.1016/s0021-9258(19)69763-2

Ohta, A., Waggoner, K., Radominska-Pyrek, A., and Dowhan, W. (1981b). Cloning of genes involved in membrane lipid synthesis: effects of amplification of phosphatidylglycerophosphate synthase in *Escherichia coli*. *J. Bacteriol.* 147, 552–562. doi: 10.1128/jb.147.2.552-562.1981

Okada, M., Matsuzaki, H., Shibuya, I., and Matsumoto, K. (1994). Cloning, sequencing, and expression in *Escherichia coli* of the Bacillus subtilis gene for phosphatidylserine synthase. *J. Bacteriol.* 176, 7456–7461. doi: 10.1128/jb.176.24.7456-7461.1994

Okonogi, K., Shibuya, I., and Maruo, B. (1971). Isolation of *Escherichia coli* mutants with temperature sensitive synthesis of phosphatidylethanolamine. *Seikagaku* 43:665.

Oku, Y., Kurokawa, K., Ichihashi, N., and Sekimizu, K. (2004). Characterization of the Staphylococcus aureus mprF gene, involved in lysinylation of phosphatidylglycerol. *Microbiology* 150, 45–51. doi: 10.1099/mic.0.26706-0

Overton, E. (1895). *Über die Osmotischen Eigenschaften der lebEnden Pflanzen- und Tierzellen*. (Zürich: Extracted from Naturforschende gesellschaft), 40, 159–201.

Patel, D., and Witt, S. N. (2017). Ethanolamine and phosphatidylethanolamine: partners in health and disease. *Oxid. Med. Cell. Longev.* 2017:4829180.

Paulus, H., and Kennedy, E. P. (1960). The enzymatic synthesis of inositol monophosphatide. *J. Biol. Chem.* 235, 1303–1311. doi: 10.1016/s0021-9258(18)69403-7

Pieringer, R. A., and Kunnes, R. S. (1965). The biosynthesis of phosphatidic acid and lysophosphatidic acid by glyceride phosphokinase pathways in *Escherichia Coli*. *J. Biol. Chem.* 240, 2833–2838. doi: 10.1016/s0021-9258(18)97255-8

Pluschke, G., Hirota, Y., and Overath, P. (1978). Function of phospholipids in *Escherichia coli*. Characterization of a mutant deficient in cardiolipin

synthesis. *J. Biol. Chem.* 253, 5048–5055. doi: 10.1016/s0021-9258(17)34655-0

Pomorski, T., and Menon, A. K. (2006). Lipid flippases and their biological functions. *Cell. Mol. Life Sci.* 63, 2908–2921. doi: 10.1007/s00018-006-6167-7

Popot, J. L., and Engelman, D. M. (2016). Membranes do not tell proteins how to fold. *Biochemistry* 55, 5–18. doi: 10.1021/acs.biochem.5b01134

Powers, M. J., and Trent, M. S. (2018). Phospholipid retention in the absence of asymmetry strengthens the outer membrane permeability barrier to last-resort antibiotics. *Proc. Natl. Acad. Sci. U.S.A.* 115, E8518–E8527.

Quigley, B. R., and Tropp, B. E. (2009). *E. coli* cardiolipin synthase: function of N-terminal conserved residues. *Biochim. Biophys. Acta* 1788, 2107–2113. doi: 10.1016/j.bbamem.2009.03.016

Radka, C. D., Frank, M. W., Rock, C. O., and Yao, J. (2020). Fatty acid activation and utilization by Alistipes finegoldii, a representative Bacteroidetes resident of the human gut microbiome. *Mol. Microbiol.* 113, 807–825. doi: 10.1111/mmi.14445

Raetz, C. R. (1975). Isolation of *Escherichia coli* mutants defective in enzymes of membrane lipid synthesis. *Proc. Natl. Acad. Sci. U.S.A.* 72, 2274–2278. doi: 10.1073/pnas.72.6.2274

Raetz, C. R. (1976). Phosphatidylserine synthetase mutants of *Escherichia coli*. Genetic mapping and membrane phospholipid composition. *J. Biol. Chem.* 251, 3242–3249. doi: 10.1016/s0021-9258(17)33429-4

Raetz, C. R., Carman, G. M., Dowhan, W., Jiang, R. T., Waszkuc, W., Loffredo, W., et al. (1987). Phospholipids chiral at phosphorus. Steric course of the reactions catalyzed by phosphatidylserine synthase from Escherichia coli and yeast. *Biochemistry* 26, 4022–4027. doi: 10.1021/bi00387a042

Raetz, C. R., and Kennedy, E. P. (1972). The association of phosphatidylserine synthetase with ribosomes in extracts of *Escherichia coli*. *J. Biol. Chem.* 247, 2008–2014. doi: 10.1016/s0021-9258(19)45483-5

Raetz, C. R., and Kennedy, E. P. (1974). Partial purification and properties of phosphatidylserine synthetase from *Escherichia coli*. *J. Biol. Chem.* 249, 5083–5045.

Raetz, C. R., Larson, T. J., and Dowhan, W. (1977). Gene cloning for the isolation of enzymes of membrane lipid synthesis: phosphatidylserine synthase overproduction in *Escherichia coli*. *Proc. Natl. Acad. Sci. U.S.A.* 74, 1412–1416. doi: 10.1073/pnas.74.4.1412

Raetz, C. R., and Newman, K. F. (1978). Neutral lipid accumulation in the membranes of *Escherichia coli* mutants lacking diglyceride kinase. *J. Biol. Chem.* 253, 3882–3887. doi: 10.1016/s0021-9258(17)34773-7

Ray, T. K., Cronan, J. E. Jr., Mavis, R. D., and Vagelos, P. R. (1970). The specific acylation of glycerol 3-phosphate to monoacylglycerol 3-phosphate in *Escherichia coli*. Evidence for a single enzyme conferring this specificity. *J. Biol. Chem.* 245, 6442–6448. doi: 10.1016/s0021-9258(18)62628-6

Reynolds, C. M., Kalb, S. R., Cotter, R. J., and Raetz, C. R. (2005). A phosphoethanolamine transferase specific for the outer 3-deoxy-D-manno-octulosonic acid residue of *Escherichia coli* lipopolysaccharide. Identification of the eptB gene and Ca2+ hypersensitivity of an eptB deletion mutant. *J. Biol. Chem.* 280, 21202–21211. doi: 10.1074/jbc.m500964200

Rietveld, A. G., Chupin, V. V., Koorengevel, M. C., Wienk, H. L., Dowhan, W., and de Kruijff, B. (1994). Regulation of lipid polymorphism is essential for the viability of phosphatidylethanolamine-deficient *Escherichia coli* cells. *J. Biol. Chem.* 269, 28670–28675. doi: 10.1016/s0021-9258(19)61957-5

Rietveld, A. G., Killian, J. A., Dowhan, W., and de Kruijff, B. (1993). Polymorphic regulation of membrane phospholipid composition in *Escherichia coli*. *J. Biol. Chem.* 268, 12427–12433. doi: 10.1016/s0021-9258(18)31407-8

Robertson, J. D. (1957). Some aspects of the ultrastructure of double membranes. *Prog. Neurobiol.* 2, 1–22; discussion 22–30. doi: 10.1016/b978-1-4832-2838-9.50007-6

Rock, C. O., and Jackowski, S. (2002). Forty years of bacterial fatty acid synthesis. *Biochem. Biophys. Res. Commun.* 292, 1155–1166. doi: 10.1006/bbrc.2001.2022

Romantsov, T., Battle, A. R., Hendel, J. L., Martinac, B., and Wood, J. M. (2010). Protein localization in *Escherichia coli* cells: comparison of the cytoplasmic membrane proteins ProP, LacY, ProW, AqpZ, MscS, and MscL. *J. Bacteriol.* 192, 912–924. doi: 10.1128/jb.00967-09

Romantsov, T., Helbig, S., Culham, D. E., Gill, C., Stalker, L., and Wood, J. M. (2007). Cardiolipin promotes polar localization of osmosensory transporter ProP in *Escherichia coli*. *Mol. Microbiol.* 64, 1455–1465. doi: 10.1111/j.1365-2958.2007.05727.x

Romantsov, T., Stalker, L., Culham, D. E., and Wood, J. M. (2008). Cardiolipin controls the osmotic stress response and the subcellular location of transporter ProP in *Escherichia coli*. *J. Biol. Chem.* 283, 12314–12323. doi: 10.1074/jbc.m709871200

Rotering, H., and Raetz, C. R. (1983). Appearance of monoglyceride and triglyceride in the cell envelope of *Escherichia coli* mutants defective in diglyceride kinase. *J. Biol. Chem.* 258, 8068–8073. doi: 10.1016/s0021-9258(20)82028-6

Rothman, J. E., and Kennedy, E. P. (1977a). Asymmetrical distribution of phospholipids in the membrane of Bacillus megaterium. *J. Mol. Biol.* 110, 603–618. doi: 10.1016/s0022-2836(77)80114-9

Rothman, J. E., and Kennedy, E. P. (1977b). Rapid transmembrane movement of newly synthesized phospholipids during membrane assembly. *Proc. Natl. Acad. Sci. U.S.A.* 74, 1821–1825. doi: 10.1073/pnas.74.5.1821

Rowlett, V. W., Mallampalli, V., Karlstaedt, A., Dowhan, W., Taegtmeyer, H., Margolin, W., et al. (2017). Impact of membrane phospholipid alterations in *Escherichia coli* on cellular function and bacterial stress adaptation. *J. Bacteriol.* 199:e849-16.

Ryabichko, S., Ferreira, V. M., Vitrac, H., Kiyamova, R., Dowhan, W., and Bogdanov, M. (2020). Cardiolipin is required *in vivo* for the stability of bacterial translocon and optimal membrane protein translocation and insertion. *Sci. Rep.* 10:6296. doi: 10.1038/s41598-020-63280-5

Samantha, A., and Vrielink, A. (2020). Lipid A phosphoethanolamine transferase: regulation, structure and immune response. *J. Mol. Biol.* 432, 5184–5196. doi: 10.1016/j.jmb.2020.04.022

Sandoval-Calderon, M., Geiger, O., Guan, Z., Barona-Gomez, F., and Sohlenkamp, C. (2009). A eukaryote-like cardiolipin synthase is present in *Streptomyces coelicolor* and in most actinobacteria. *J. Biol. Chem.* 284, 17383–17390. doi: 10.1074/jbc.m109.006072

Scheideler, M. A., and Bell, R. M. (1989). Phospholipid dependence of homogeneous, reconstituted sn-glycerol-3-phosphate acyltransferase of *Escherichia coli*. *J. Biol. Chem.* 264, 12455–12461. doi: 10.1016/s0021-9258(18)63880-3

Schnaitman, C. A., and Klena, J. D. (1993). Genetics of lipopolysaccharide biosynthesis in enteric bacteria. *Microbiol. Rev.* 57, 655–682. doi: 10.1128/mr.57.3.655-682.1993

Schneider, J. E., Reinhold, V., Rumley, M. K., and Kennedy, E. P. (1979). Structural studies of the membrane-derived oligosaccharides of *Escherichia coli*. *J. Biol. Chem.* 254, 10135–10138. doi: 10.1016/s0021-9258(19)86683-8

Sekimizu, K., and Kornberg, A. (1988). Cardiolipin activation of DnaA protein, the initiation protein of replication in *Escherichia coli*. *J. Biol. Chem.* 263, 7131–7135. doi: 10.1016/s0021-9258(18)68615-6

Serricchio, M., and Bütikofer, P. (2012). An essential bacterial-type cardiolipin synthase mediates cardiolipin formation in a eukaryote. *Proc. Natl. Acad. Sci. U.S.A.* 109, E954–E961.

Sharom, F. J. (2011). Flipping and flopping–lipids on the move. *IUBMB Life* 63, 736–746.

Shen, H., Heacock, P. N., Clancey, C. J., and Dowhan, W. (1996). The CDS1 gene encoding CDP-diacylglycerol synthase in *Saccharomyces cerevisiae* is essential for cell growth. *J. Biol. Chem.* 271, 789–795. doi: 10.1074/jbc.271.2.789

Shi, W., Bogdanov, M., Dowhan, W., and Zusman, D. R. (1993). The pss and psd genes are required for motility and chemotaxis in *Escherichia coli*. *J. Bacteriol.* 175, 7711–7714. doi: 10.1128/jb.175.23.7711-7714.1993

Shiba, Y., Miyagawa, H., Nagahama, H., Matsumoto, K., Kondo, D., Matsuoka, S., et al. (2012). Exploring the relationship between lipoprotein mislocalization and activation of the Rcs signal transduction system in *Escherichia coli*. *Microbiology* 158, 1238–1248. doi: 10.1099/mic.0.056945-0

Shiba, Y., Yokoyama, Y., Aono, Y., Kiuchi, T., Kusaka, J., Matsumoto, K., et al. (2004). Activation of the Rcs signal transduction system is responsible for the thermosensitive growth defect of an *Escherichia coli* mutant lacking phosphatidylglycerol and cardiolipin. *J. Bacteriol.* 186, 6526–6535. doi: 10.1128/jb.186.19.6526-6535.2004

Shibuya, I., Yamagoe, S., Miyazaki, C., Matsuzaki, H., and Ohta, A. (1985). Biosynthesis of novel acidic phospholipid analogs in *Escherichia coli*. *J. Bacteriol.* 161, 473–477. doi: 10.1128/jb.161.2.473-477.1985

Singer, S. J., and Nicolson, G. L. (1972). The fluid mosaic model of the structure of cell membranes. *Science* 175, 720–731. doi: 10.1126/science.175.4023.720

Sohlenkamp, C., de Rudder, K. E., and Geiger, O. (2004). Phosphatidylethanolamine is not essential for growth of *Sinorhizobium meliloti* on complex culture media. *J. Bacteriol.* 186, 1667–1677. doi: 10.1128/jb.186.6.1667-1677.2004

Sparrow, C. P., and Raetz, C. R. (1985). Purification and properties of the membrane-bound CDP-diglyceride synthetase from *Escherichia coli*. *J. Biol. Chem.* 260, 12084–12091. doi: 10.1016/s0021-9258(17)38989-5

Stone, S. J., and Vance, J. E. (2000). Phosphatidylserine synthase-1 and -2 are localized to mitochondria-associated membranes. *J. Biol. Chem.* 275, 34534–34540. doi: 10.1074/jbc.m002865200

Sun, J., Li, J., Carrasco, N., and Kaback, H. R. (1997). The last two cytoplasmic loops in the lactose permease of *Escherichia coli* comprise a discontinuous epitope for a monoclonal antibody. *Biochemistry* 36, 274–280. doi: 10.1021/bi962292f

Sun, J., Wu, J., Carrasco, N., and Kaback, H. R. (1996). Identification of the epitope for monoclonal antibody 4B1 which uncouples lactose and proton translocation in the lactose permease of *Escherichia coli*. *Biochemistry* 35, 990–998. doi: 10.1021/bi952166w

Tamura, Y., Harada, Y., Nishikawa, S., Yamano, K., Kamiya, M., Shiota, T., et al. (2013). Tam41 is a CDP-diacylglycerol synthase required for cardiolipin biosynthesis in mitochondria. *Cell Metab.* 17, 709–718. doi: 10.1016/j.cmet.2013.03.018

Tan, B. K., Bogdanov, M., Zhao, J., Dowhan, W., Raetz, C. R., and Guan, Z. (2012). Discovery of a cardiolipin synthase utilizing phosphatidylethanolamine and phosphatidylglycerol as substrates. *Proc. Natl. Acad. Sci. U.S.A.* 109, 16504–16509. doi: 10.1073/pnas.1212797109

Tao, K., Narita, S., and Tokuda, H. (2012). Defective lipoprotein sorting induces lolA expression through the Rcs stress response phosphorelay system. *J. Bacteriol.* 194, 3643–3650. doi: 10.1128/jb.00553-12

Tian, X., Auger, R., Manat, G., Kerff, F., Mengin-Lecreulx, D., and Touze, T. (2020). Insight into the dual function of lipid phosphate phosphatase PgpB involved in two essential cell-envelope metabolic pathways in *Escherichia coli*. *Sci. Rep.* 10:13209. doi: 10.1038/s41598-020-70047-5

Tong, S., Lin, Y., Lu, S., Wang, M., Bogdanov, M., and Zheng, L. (2016). Structural insight into substrate selection and catalysis of lipid phosphate phosphatase PgpB in the cell membrane. *J. Biol. Chem.* 291, 18342–18352. doi: 10.1074/jbc.m116.737874

Touze, T., Blanot, D., and Mengin-Lecreulx, D. (2008). Substrate specificity and membrane topology of *Escherichia coli* PgpB, an undecaprenyl pyrophosphate phosphatase. *J. Biol. Chem.* 283, 16573–16583. doi: 10.1074/jbc.m800394200

Trotter, P. J., Pedretti, J., and Voelker, D. R. (1993). Phosphatidylserine decarboxylase from *Saccharomyces cerevisiae*. Isolation of mutants, cloning of the gene, and creation of a null allele. *J. Biol. Chem.* 268, 21416–21424. doi: 10.1016/s0021-9258(19)36940-6

Trotter, P. J., and Voelker, D. R. (1995). Identification of a non-mitochondrial phosphatidylserine decarboxylase activity (PSD2) in the Yeast *Saccharomyces cerevisiae*. *J. Biol. Chem.* 270, 6062–6070. doi: 10.1074/jbc.270.11.6062

Tsatskis, Y., Khambati, J., Dobson, M., Bogdanov, M., Dowhan, W., and Wood, J. M. (2005). The osmotic activation of transporter ProP is tuned by both its C-terminal coiled-coil and osmotically induced changes in phospholipid composition. *J. Biol. Chem.* 280, 41387–41394. doi: 10.1074/jbc.m508362200

Tunuguntla, R., Bangar, M., Kim, K., Stroeve, P., Ajo-Franklin, C. M., and Noy, A. (2013). Lipid bilayer composition can influence the orientation of proteorhodopsin in artificial membranes. *Biophys. J.* 105, 1388–1396. doi: 10.1016/j.bpj.2013.07.043

Tyhach, R. J., Engel, R., and Tropp, B. E. (1976). Metabolic fate of 3,4-dihydroxybutyl-1-phosphonate in *Escherichia coli*. *J. Biol. Chem.* 251, 6717–6723. doi: 10.1016/s0021-9258(17)33004-1

Van Horn, W. D., Kim, H. J., Ellis, C. D., Hadziselimovic, A., Sulistijo, E. S., Karra, M. D., et al. (2009). Solution nuclear magnetic resonance structure of membrane-integral diacylglycerol kinase. *Science* 324, 1726–1729. doi: 10.1126/science.1171716

Vitrac, H., Bogdanov, M., and Dowhan, W. (2013a). *In vitro* reconstitution of lipid-dependent dual topology and postassembly topological switching of a membrane protein. *Proc. Natl. Acad. Sci. U.S.A.* 110, 9338–9343. doi: 10.1073/pnas.1304375110

Vitrac, H., Bogdanov, M., and Dowhan, W. (2013b). Proper fatty acid composition rather than an ionizable lipid amine is required for full transport function of lactose permease from *Escherichia coli*. *J. Biol. Chem.* 288, 5873–5885. doi: 10.1074/jbc.m112.442988

Vitrac, H., Bogdanov, M., Heacock, P., and Dowhan, W. (2011). Lipids and topological rules of membrane protein assembly: balance between long and short range lipid-protein interactions. *J. Biol. Chem.* 286, 15182–15194. doi: 10.1074/jbc.m110.214387

Vitrac, H., MacLean, D. M., Jayaraman, V., Bogdanov, M., and Dowhan, W. (2015). Dynamic membrane protein topological switching upon changes in phospholipid environment. *Proc. Natl. Acad. Sci. U.S.A.* 112, 13874–13879. doi: 10.1073/pnas.1512994112

Vitrac, H., MacLean, D. M., Karlstaedt, A., Taegtmeyer, H., Jayaraman, V., Bogdanov, M., et al. (2017). Dynamic lipid-dependent modulation of protein topology by post-translational phosphorylation. *J. Biol. Chem.* 292, 1613–1624. doi: 10.1074/jbc.m116.765719

Vitrac, H., Mallampalli, V., Azinas, S., and Dowhan, W. (2020). Structural and functional adaptability of sucrose and lactose permeases from *Escherichia coli* to the membrane lipid composition. *Biochemistry* 59, 1854–1868. doi: 10.1021/acs.biochem.0c00174

Vitrac, H., Mallampalli, V., and Dowhan, W. (2019). Importance of phosphorylation/dephosphorylation cycles on lipid-dependent modulation of membrane protein topology by posttranslational phosphorylation. *J. Biol. Chem.* 294, 18853–18862. doi: 10.1074/jbc.ra119.010785

Voelker, D. R. (1997). Phosphatidylserine decarboxylase. *Biochim. Biophys. Acta* 1348, 236–244.

von Heijne, G. (1986). The distribution of positively charged residues in bacterial inner membrane proteins correlates with the trans-membrane topology. *EMBO J.* 5, 3021–3027. doi: 10.1002/j.1460-2075.1986.tb04601.x

von Heijne, G. (1989). Control of topology and mode of assembly of a polytopic membrane protein by positively charged residues. *Nature* 341, 456–458. doi: 10.1038/341456a0

von Heijne, G. (1992). Membrane protein structure prediction. Hydrophobicity analysis and the positive-inside rule. *J. Mol. Biol.* 225, 487–494.

Wahl, A., My, L., Dumoulin, R., Sturgis, J. N., and Bouveret, E. (2011). Antagonistic regulation of dgkA and plsB genes of phospholipid synthesis by multiple stress responses in *Escherichia coli*. *Mol. Microbiol.* 80, 1260–1275. doi: 10.1111/j.1365-2958.2011.07641.x

Warner, T. G., and Dennis, E. A. (1975). Action of the highly purified, membrane-bound enzyme phosphatidylserine decarboxylase *Escherichia coli* toward phosphatidylserine in mixed micelles and erythrocyte ghosts in the presence of surfactant. *J. Biol. Chem.* 250, 8004–8009. doi: 10.1016/s0021-9258(19)40807-7

Watanabe, Y., Watanabe, Y., and Watanabe, S. (2020). Structural basis for phosphatidylethanolamine biosynthesis by bacterial phosphatidylserine decarboxylase. *Structure* 28, 799–809.e5.

Weeks, R., Dowhan, W., Shen, H., Balantac, N., Meengs, B., Nudelman, E., et al. (1997). Isolation and expression of an isoform of human CDP-diacylglycerol synthase cDNA. *DNA Cell Biol.* 16, 281–289. doi: 10.1089/dna.1997.16.281

Whitfield, C., and Trent, M. S. (2014). Biosynthesis and export of bacterial lipopolysaccharides. *Annu. Rev. Biochem.* 83, 99–128. doi: 10.1146/annurev-biochem-060713-035600

Wikström, M., Kelly, A. A., Georgiev, A., Eriksson, H. M., Klement, M. R., Bogdanov, M., et al. (2009). Lipid-engineered *Escherichia coli* membranes reveal critical lipid headgroup size for protein function. *J. Biol. Chem.* 284, 954–965. doi: 10.1074/jbc.m804482200

Wikström, M., Xie, J., Bogdanov, M., Mileykovskaya, E., Heacock, P., Wieslander, Ä., et al. (2004). Monoglucosyldiacylglycerol, a foreign lipid, can substitute for phosphatidylethanolamine in essential membrane-associated functions in *Escherichia coli*. *J. Biol. Chem.* 279, 10484–10493. doi: 10.1074/jbc.m310183200

Wilkison, W. O., Walsh, J. P., Corless, J. M., and Bell, R. M. (1986). Crystalline arrays of the *Escherichia coli* sn-glycerol-3-phosphate acyltransferase, an integral membrane protein. *J. Biol. Chem.* 261, 9951–9958. doi: 10.1016/s0021-9258(18)67608-2

Wu, L., Niemeyer, B., Colley, N., Socolich, M., and Zuker, C. S. (1995). Regulation of PLC-mediated signalling *in vivo* by CDP-diacylglycerol synthase. *Nature* 373, 216–222. doi: 10.1038/373216a0

Xia, W., and Dowhan, W. (1995a). *In vivo* evidence for the involvement of anionic phospholipids in initiation of DNA replication in *Escherichia coli*. *Proc. Natl. Acad. Sci. U.S.A.* 92, 783–787. doi: 10.1073/pnas.92.3.783

Xia, W., and Dowhan, W. (1995b). Phosphatidylinositol cannot substitute for phosphatidylglycerol in supporting cell growth of *Escherichia coli*. *J. Bacteriol.* 177, 2926–2928. doi: 10.1128/jb.177.10.2926-2928.1995

Xie, J., Bogdanov, M., Heacock, P., and Dowhan, W. (2006). Phosphatidylethanolamine and monoglucosyldiacylglycerol are interchangeable in supporting topogenesis and function of the polytopic membrane protein lactose permease. *J. Biol. Chem.* 281, 19172–19178. doi: 10.1074/jbc.m602565200

Yao, J., and Rock, C. O. (2013). Phosphatidic acid synthesis in bacteria. *Biochim. Biophys. Acta* 1831, 495–502. doi: 10.1016/j.bbalip.2012.08.018

Zhang, J., Guan, Z., Murphy, A. N., Wiley, S. E., Perkins, G. A., Worby, C. A., et al. (2011). Mitochondrial phosphatase PTPMT1 is essential for cardiolipin biosynthesis. *Cell Metab.* 13, 690–700. doi: 10.1016/j.cmet.2011.04.007

Zhang, W., Bogdanov, M., Pi, J., Pittard, A. J., and Dowhan, W. (2003). Reversible topological organization within a polytopic membrane protein is governed by a change in membrane phospholipid composition. *J. Biol. Chem.* 278, 50128–50135. doi: 10.1074/jbc.m309840200

Zhang, W., Campbell, H. A., King, S. C., and Dowhan, W. (2005). Phospholipids as determinants of membrane protein topology. Phosphatidylethanolamine is required for the proper topological organization of the gamma-aminobutyric acid permease (GabP) of *Escherichia coli*. *J. Biol. Chem.* 280, 26032–26038. doi: 10.1074/jbc.m504929200

Zhang, Y. N., Lu, F. P., Chen, G. Q., Li, Y., and Wang, J. L. (2009). Expression, purification, and characterization of phosphatidylserine synthase from *Escherichia coli* K12 in Bacillus subtilis. *J. Agric. Food Chem.* 57, 122–126. doi: 10.1021/jf802664u

Zhou, H., and Lutkenhaus, J. (2003). Membrane binding by MinD involves insertion of hydrophobic residues within the C-terminal amphipathic helix into the bilayer. *J. Bacteriol.* 185, 4326–4335. doi: 10.1128/jb.185.15.4326-4335.2003

Conflict of Interest: The authors declare that the research was conducted in the absence of any commercial or financial relationships that could be construed as a potential conflict of interest.

frontiers in Molecular Biosciences

ORIGINAL RESEARCH
published: 07 May 2021
doi: 10.3389/fmolb.2021.665977

Dual Regulation of Phosphatidylserine Decarboxylase Expression by Envelope Stress Responses

Yasmine Hassoun[1], Julia Bartoli[1], Astrid Wahl[1], Julie Pamela Viala[1] and Emmanuelle Bouveret[2]**

[1] LISM, Institut de Microbiologie de la Méditerranée, UMR 7255, CNRS and Aix-Marseille Université, Marseille, France,
[2] SAMe Unit, UMR 2001, Microbiology Department, Pasteur Institute, Paris, France

Bacteria adapt to versatile environments by modulating gene expression through a set of stress response regulators, alternative Sigma factors, or two-component systems. Among the central processes that must be finely tuned is membrane homeostasis, including synthesis of phospholipids (PL). However, few genetic regulations of this process have been reported. We have previously shown that the gene coding the first step of PL synthesis is regulated by σ^E and ppGpp, and that the BasRS (PmrAB) two component system controls the expression of the DgkA PL recycling enzyme. The gene coding for phosphatidylserine decarboxylase, the last step in phosphatidylethanolamine synthesis is another gene in the PL synthesis pathway susceptible of stress response regulation. Indeed, *psd* appears in transcriptome studies of the σ^E envelope stress Sigma factor and of the CpxAR two component system. Interestingly, this gene is presumably in operon with *mscM* coding for a miniconductance mechanosensitive channel. In this study, we dissected the promoter region of the *psd-mscM* operon and studied its regulation by σ^E and CpxR. By artificial activation of σ^E and CpxRA stress response pathways, using GFP transcriptional fusion and western-blot analysis of Psd and MscM enzyme production, we showed that the operon is under the control of two distinct promoters. One is activated by σ^E, the second is activated by CpxRA and also responsible for basal expression of the operon. The fact that the phosphatidylethanolamine synthesis pathway is controlled by envelope stress responses at both its first and last steps might be important for adaptation of the membrane to envelope perturbations.

Keywords: *psd*, *mscM*, SigmaE, CpxRA, envelope stress response, *E. coli*, phospholipid synthesis

OPEN ACCESS

Edited by:
Heidi Vitrac,
University of Texas Health Science Center at Houston, United States

Reviewed by:
Stanley Spinola,
Indiana University–Purdue University Indianapolis, United States
Tracy Raivio,
University of Alberta, Canada

****Correspondence:***
Julie Pamela Viala
jviala@imm.cnrs.fr
Emmanuelle Bouveret
emmanuelle.bouveret@pasteur.fr

Specialty section:
This article was submitted to Cellular Biochemistry, a section of the journal Frontiers in Molecular Biosciences

Received: *09 February 2021*
Accepted: *09 April 2021*
Published: *07 May 2021*

Citation:
Hassoun Y, Bartoli J, Wahl A, Viala JP and Bouveret E (2021) Dual Regulation of Phosphatidylserine Decarboxylase Expression by Envelope Stress Responses. Front. Mol. Biosci. 8:665977. doi: 10.3389/fmolb.2021.665977

INTRODUCTION

Phospholipids (PL) are major structural and functional components of biomembranes and play a dynamic role in many regulatory processes. The biochemistry of the PL biosynthesis pathway is well described in bacteria (Parsons and Rock, 2013). It begins by two successive acylations of the positions 1 and 2 of a glycerol 3-phosphate backbone to give phosphatidic acid. Then, the third

position of the future polar head group is activated with a CDP nucleotide. Finally, two separate pathways give rise in *Escherichia coli* to the zwitterionic phosphatidylethanolamine (PE), or to the anionic phospholipids phosphatidylglycerol (PG), and cardiolipin (CL). Bacterial species display specific membrane compositions, and the less frequent phosphatidylcholine, phosphatidylinositol, and a variety of other membrane lipids can be found in addition to the common PE, PG, and CL lipids (Sohlenkamp and Geiger, 2016).

Though the composition of the membrane is highly stable in *E. coli*, it can adapt to the growth conditions, through modification of fatty acid chains, but also of the ratio of the different lipids (Sohlenkamp and Geiger, 2016). For example, the proportion of unsaturated fatty acids varies with temperature to modify the fluidity of the membrane. Another example of adaptation is the increase of CL following increase of osmotic pressure. Also, in stationary phase, there is a relative increase in anionic phospholipids, together with the replacement of fatty acid unsaturations by cyclopropane groups. This conversion is performed by the Cfa enzyme, whose expression is activated by σ^S alternative Sigma factor (Wang and Cronan, 1994; Eichel et al., 1999). In addition, global transcriptome studies had suggested that expression of PL synthesis genes might be globally affected during the stringent response (Durfee et al., 2008), and that specific genes of PL synthesis might be regulated by envelope stress responses (De Wulf et al., 2002; Rhodius et al., 2006).

In bacteria, several regulating pathways are present to monitor and respond to envelope perturbations. In *E. coli*, the alternative Sigma factor σ^E responds to the accumulation of unfolded outer membrane proteins or altered forms of LPS in the periplasm through a proteolytic signaling cascade (Mitchell and Silhavy, 2019). In addition, two-component systems such as CpxRA, RcsBA, or BaeRS respond to various envelope perturbations such as defects in protein secretion, alterations in LPS or peptidoglycan, or exposure to toxic compounds, by a phosphorylation signaling cascade that ends up in the activation of a transcriptional regulator (Mitchell and Silhavy, 2019). We have previously shown that *plsB,* coding for the first acylation step in PL synthesis, is activated by the envelope stress response σ^E factor, and that *dgkA,* coding for a diacylglycerol kinase involved in PL recycling, is controlled by the two-component system BasRS (Wahl et al., 2011).

The *psd* gene coding for phosphatidylserine decarboxylase, the last step in phosphatidylethanolamine synthesis, appears in the regulon of σ^E like *plsB,* but also in the regulon of the CpxAR two-component system (De Wulf et al., 2002; Rezuchova et al., 2003; Rhodius et al., 2006). The *psd* gene is followed by *mscM* (previously called *yjeP*), and they probably form an operon. MscM protein is a miniconductance mechanosensitive channel of the MscS family, involved in the protection of the physical integrity of the cell during transitions from high to low osmolarity (Booth, 2014; Edwards et al., 2012).

In this study, we dissected the organization of the promoter region of the *psd-mscM* operon, and we studied the dual regulation of these genes by σ^E and the response regulator CpxR. We showed that the operon is under the control of two distinct promoters. One is activated by σ^E, the other by CpxRA. This second promoter is responsible for basal expression of the operon. Therefore, the PL synthesis pathway (and more specifically the PE pathway) is controlled by envelope stress responses at both its first and last steps, which might be important for adaptation of the membrane to envelope perturbations.

MATERIALS AND METHODS

Plasmid and Strain Constructions

pUA66 and pUA-psdP2 plasmids were obtained from the library of *E. coli* promoters fused to GFP coding sequence (Zaslaver et al., 2006). The other *psd* transcriptional fusions were constructed using primers indicated in **Supplementary Table 1**, and cloned in *Xho*I/*Bam*HI sites of pUA66. Expression plasmids for *rpoE*, *nlpE*, and $nlpE_{IM}$ were constructed using primers indicated in **Supplementary Table 1**, and cloned in *Eco*RI/*Sal*I sites of pBAD24 vector (Guzman et al., 1995). A region of 1600 base pairs encompassing *psd* promoter was cloned in pKO3 vector (Link et al., 1997). Mutations were introduced in the pKO3-*psd* vector, in the pBAD-*nlpE* and in the transcriptional fusions by PCR mutagenesis on plasmid, using the oligonucleotides indicated (**Table 1** and **Supplementary Table 1**).

In order to introduce the sequence coding for the Flag or SPA tags downstream of the coding sequences of interest on the chromosome, we amplified the corresponding cassette from the template plasmid pJL148 (Zeghouf et al., 2004). MG1655_Psd-Flag and MG1655_MscM-SPA strains were then constructed by PCR recombination at the locus followed by P1 transduction as described previously (Datsenko and Wanner, 2000) (**Table 2**). When required, the gene conferring resistance to Kanamycin was removed using the pCP20 plasmid (Cherepanov and Wackernagel, 1995), allowing the transformation by transcriptional fusion plasmids. Point mutations were introduced on the chromosome using the pKO3 vector (Link et al., 1997).

Transcriptional Fusions with GFP

We used several clones from the *E. coli* transcriptional fusions library (Zaslaver et al., 2006) and we constructed the required additional transcriptional fusions (see above for plasmid construction and **Table 1**). MG1655 wild-type *E. coli* strain or isogenic mutants were transformed with plasmids carrying the *gfp* transcriptional fusions and maintained with kanamycin. For co-transformation, compatible plasmids (pBAD24 and derivatives) were used, and ampicillin added. Selection plates were incubated at 37°C for 16 h. A total of 600 µl of LB medium supplemented with required antibiotics, and with 0.01% arabinose when necessary for pBAD-driven expression, were incubated (four to six replicate each assay) and grown for 16 h at 30°C in 96-well polypropylene plates of 2.2 ml wells under aeration and agitation. Fluorescent intensity measurement was performed in a TECAN infinite M200 plate reader. A total of 150 µl of each well was transferred into black Greiner 96-well plate for reading optical density at 600 nm and fluorescence (excitation: 485 nm; emission: 530 nm). The expression levels

TABLE 1 | Plasmids.

Lab code	Name		Description	References
pEB0794	pJL148		ampR, kanaR, SPA-FRT-kanaR-FRT cassette	Zeghouf et al., 2004
pEB0267	pKD46		ampR, ts, lambdaRed genes	Datsenko and Wanner, 2000
pEB0266	pCP20		camR, ampR, pSC101 ori, ts	Cherepanov and Wackernagel, 1995
pEB0227	pBAD24		ampR, colE1 ori, PBAD promoter	Guzman et al., 1995
pEB1470	pBAD-*nlpE*		PCR ebm981/982 (*Eco*RI/*Xho*I) in pBAD24 (*Eco*RI/*Sal*I)	This work
pEB1966	pBAD-$nlpE_{IM}$		PCR mutagenesis ebm1785/1786 on pEB1470	This work
pEB1102	pBAD-*rpoE*			Wahl et al., 2011
pEB0232	pKO3		camR, pSC101 ori, *sacB*	Link et al., 1997
pEB1973	pKO3-*psd*		PCR ebm1762/1763 (*Bgl*II/*Xho*I) in pEB0232 (*Bam*HI/*Sal*I)	This work
pEB1983	pKO3-*psd*_mutCpxR		PCR mutagenesis ebm1777/ebm1778 on pEB1973	This work
pEB1988	pKO3-*psd*_mut$P\sigma^E$		PCR mutagenesis ebm1808/ebm1809 on pEB1973	This work
pEB2021	pKO3-*psd*_mut$P\sigma^E$_mutCpxR		PCR mutagenesis ebm1777/ebm1778 on pEB1988	This work
pEB0067	pACYC184		camR, p15A ori	Chang and Cohen, 1978
pEB1975	pACYC-psd-3Flag		PCR ebm1762/968 on EB1075 (*Bgl*II/*Xho*I) in pACYC184 (*Bam*HI/*Sal*I)	This work
pEB2033	pACYC-psd(S254A)-3Flag		PCR mutagenesis ebm1911/1912 on pEB1975	This work
pEB2099	pACYC-psd		PCR ebm1762/1763 (*Bgl*II/*Xho*I) in pACYC184(*Bam*HI/*Sal*I)	This work
pEB0898	pUA66		kanaR, pSC101 ori, GFPmut2	Zaslaver et al., 2006
		Limits[a]		
pEB1120	psdBis	−391/+57	PCR ebm435/436 in pUA66 *Xho*I/*Bam*HI	This work
pEB1509	$psdP\sigma^E$	−391/−229	PCR ebm435/1023 *Xho*I/*Bam*HI in pUA66	This work
pEB1981	$psdP\sigma^E$mut		PCR mutagenesis ebm1808/1809 on pEB1509	This work
	psdP2	−196/+95		Zaslaver et al., 2006
pEB1963	psdP2mutCpxR		Mutagenesis ebm1777/ebm1778 on pUA-psdP2	This work

[a] *The limits of the transcriptional fusions are given relative to the start codon of psd.*

were calculated by dividing the intensity of fluorescence by the optical density at 600 nm, after subtracting the values of blank sample. These results are given in arbitrary units because the intensity of fluorescence is acquired with an automatic optimal gain and hence varies from one experiment to the other.

SDS-PAGE and Western Blotting

Total cell extracts were prepared by resuspending cell pellets in Laemli buffer 1X at a concentration of 0.3 $uOD_{600\ nm}$ in 10 µl, and then heating for 10 min at 95°C. After separation of 8 µl of total cell extracts on SDS-PAGE, electrotransfer onto nitrocellulose membranes was performed using Trans-Blot turbo transfer system from Bio-Rad. After blocking in PBS 1X + milk 5%, SPA-tagged or 3Flag-tagged proteins were detected with monoclonal anti-Flag M2 antibody purchased from Sigma. IscS protein was used as an internal control and revealed with polyclonal anti-IscS antibodies (Gully et al., 2003). Fluorescent secondary antibodies were respectively IRDye 800 anti-mouse and IRDye 680 anti-rabbit purchased from Li-Cor. Scanning and quantification were performed on a Li-Cor Odyssey-Fc imaging system, reading at 700 nm (for IscS detection) or 800 nm (for Flag detection).

Reverse Transcriptase – PCR

RNAs were purified using the NEB Monarch Total RNA MiniPrep Kit and further digested with Dnase I followed by clean up with the Qiagen Rneasy Mini kit. Reverse transcription was performed using Invitrogen SuperScript III First-Stand Synthesis System with random hexamers. Finally, PCR was performed using ebm446 and ebm2079 primers.

RESULTS

In a global experimental study of all the transcriptional starting sites of *E. coli* (Thomason et al., 2015), two putative promoters were identified upstream the *psd* ORF (**Figure 1**). The first one, that we will call $psdP\sigma^E$, had been already reported as a promoter activated by the alternative sigma factor σ^E (Rezuchova et al., 2003; Rhodius et al., 2006). The second one, that we will call psdP2, is located 197 nucleotides downstream $psdP\sigma^E$. It has already been reported that *psd* expression was activated by CpxR, and a putative CpxR box was proposed (De Wulf et al., 2002). This CpxR box is located 41 nucleotides upstream the predicted transcription start site of the psdP2 promoter, which is a distance in perfect agreement with CpxR acting as an activator of the psdP2 promoter (Busby, 2019).

Dissection of the Promoter Region

In order to dissect the promoter region of *psd* and to study the genetic regulation of *psd* expression, we first used transcriptional fusions with GFP, expressed from the low copy vector pUA66, which enable to follow promoter activity by measuring fluorescence directly in living cells (Zaslaver et al., 2006). A transcriptional fusion containing the upstream region of *psd* ORF was already available from a library of *E. coli* promoters

TABLE 2 | *Escherichia coli* strains.

Lab code	Name	Description	References
EB758	BW25113 Δ*cpxR*:kana^R		Baba et al., 2006
EB944	MG1655	Wild-type reference. F- λ- rph-1	Lab stock
EB425	MG1655 ppGpp°	Δ*relA*Δ*spoT*::cat	Wahl et al., 2011
EB559	MG1655Δ*dksA*		Wahl et al., 2011
EB544	MG1655 ppGpp+	MG1655Δ*relA spoT203 zib563:tetra*	My et al., 2013
EB780	MG1655 Δ*cpxR*	P1 transduction from EB758 in MG1655. kanaR cassette removed using pCP20.	This work
EB533	EH150	Mutation Gly280Asp. *psd-2*^{ts}	Hawrot and Kennedy, 1975
EB1075	psd-3Flag	PCR ebm472/448 on pJL148 recombined in MG1655pKD46, then P1 transduction in MG1655	This work
EB1078	Δ*cpxR psd*-3Flag	P1 transduction from EB1075 in EB780	This work
EB1098	Psd-3Flag_mutCpxR	Recombination pEB1983 in EB1075	This work
EB1085	Psd-3Flag_mutPσ^E	Recombination pEB1973 in EB1075	This work
EB1113	Psd-3Flag_mutCpxRmutPσ^E	Recombination pEB2021 in EB1075	This work
EB1095	MscM-SPA	PCR ebm488/489 on pJL148 recombined in MG1655pKD46, then P1 transduction in MG1655	This work
EB1081	Psd_mutCpxR	Recombination pEB1983 in MG1655	This work
EB1103	Psd_mutPσ^E	Recombination pEB1988 in MG1655	This work
EB1112	Psd_mutCpxRmutPσα^E	Recombination pEB2021 in MG1655	This work

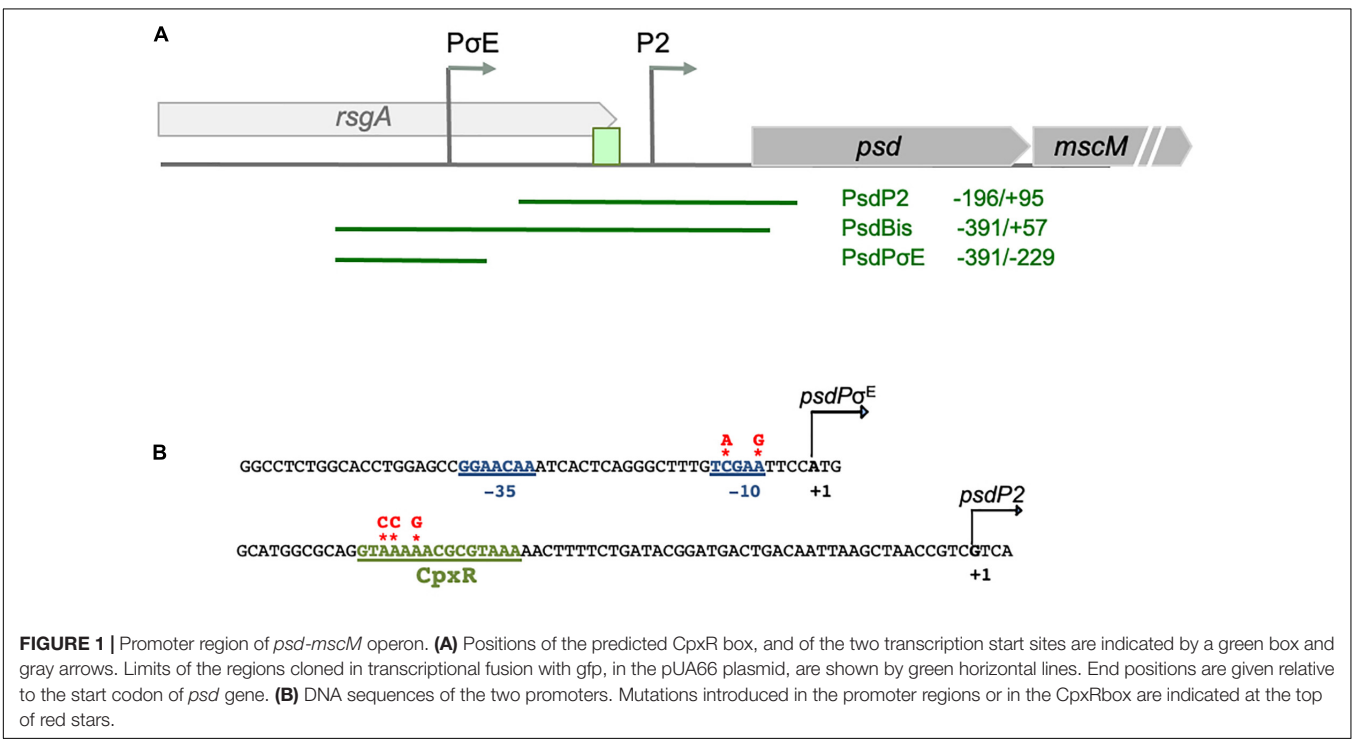

FIGURE 1 | Promoter region of *psd-mscM* operon. **(A)** Positions of the predicted CpxR box, and of the two transcription start sites are indicated by a green box and gray arrows. Limits of the regions cloned in transcriptional fusion with gfp, in the pUA66 plasmid, are shown by green horizontal lines. End positions are given relative to the start codon of *psd* gene. **(B)** DNA sequences of the two promoters. Mutations introduced in the promoter regions or in the CpxRbox are indicated at the top of red stars.

(Zaslaver et al., 2006), but it only contained the putative psdP2 promoter. Therefore, we constructed additional transcriptional fusions, containing both promoters (called psdBis) or only the psdPσ^E promoter (**Figure 1A**).

We first studied the control of *psd* expression by σ^E. We artificially induced the σ^E response, by overproducing the σ^E factor from an inducible pBAD-*rpoE* plasmid as previously described (Wahl et al., 2011). We co-transformed an *E. coli* wild-type strain with the different GFP transcriptional fusions and with the pBAD-*rpoE* plasmid. Upon σ^E overproduction, only the transcriptional fusions containing the psdPσ^E promoter (psdBis and psdPσ^E, but not psdP2) showed a strong induction (**Figure 2**). We then mutated two nucleotide positions in the predicted −10 box of the psdPσ^E promoter. These mutations completely abolished the induction of the psdPσ^E transcriptional fusion by pBAD-*rpoE* (**Figure 2**).

We then tested if CpxR was a transcriptional activator of the psdP2 promoter. We first compared the activity of the

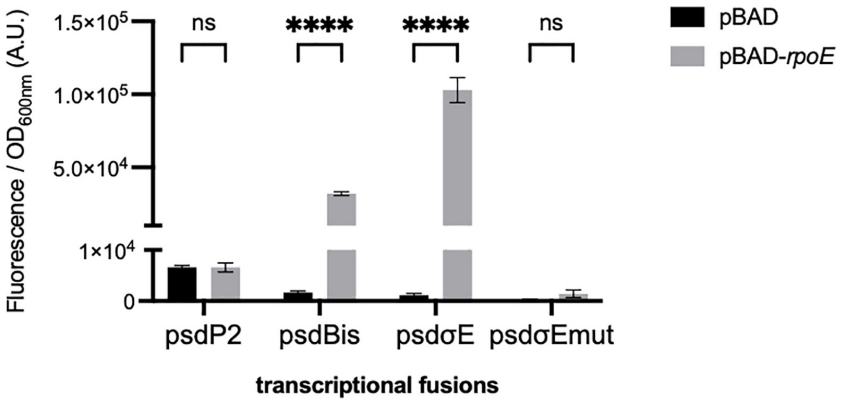

FIGURE 2 | Effect of σ^E overproduction on the psdPσ^E promoter. MG1655 strain was transformed with plasmids carrying the transcriptional fusions pUA66, pUA-psdP2, pUA-psdBis, pUA-psdPσ^E, or pUA-psdPσ^Emut together with plasmids pBAD24 or pBAD-*rpoE*. Cultures were grown overnight at 30°C in LB supplemented with ampicillin, kanamycin, and 0.01% arabinose. The values show the mean ratio of GFP fluorescence over optical density at 600 nm, after subtraction of the pUA66 negative control, in arbitrary units (A.U.). The values are the mean of six replicas and the error bars show the SEM (standard error of the mean). ns, non-significant, ****$p < 0.0001$ in a two-way ANOVA statistical analysis.

psdP2 transcriptional fusion in wild-type and Δ*cpxR* strains. This activity was reduced in the Δ*cpxR* strain (**Figure 3A**), suggesting a potential role of CpxR in the regulation of *psd* expression, even in balanced growth conditions. In reverse, in order to induce the CpxR response, we overproduced the NlpE lipoprotein or its $NlpE_{IM}$ variant that triggers an even stronger response (Delhaye et al., 2016). We co-transformed an *E. coli* wild-type strain by the different transcriptional fusions and by the pBAD-*nlpE* or -$nlpE_{IM}$ plasmids. The psdP2 transcriptional fusion showed an activation when NlpE was overproduced, and the effect was reinforced with $NlpE_{IM}$ (**Figure 3B**). Furthermore, the activation was abolished when the experiment was repeated in a Δ*cpxR* strain (**Figure 3C**), which showed that this was indeed the result of an activation of the CpxR pathway. Finally, to prove that the activation was due to direct binding of CpxR response regulator to the psdP2 promoter, we introduced point mutations that destroy the CpxR binding motif in the psdP2 transcriptional fusion (**Figure 1B**). With this mutated transcriptional fusion, the activation of psdP2 promoter was abolished (**Figure 3B**).

In conclusion, *psd* expression (and potentially *mscM* expression) is under the control of two distinct promoters. One is activated by σ^E, the other by CpxRA. Given that this promoter organization is very similar to the one we described previously for *plsB* (Wahl et al., 2011), we hypothesized that this second promoter might be regulated by ppGpp as shown for *plsB* and suggested by global study of the stringent response (Durfee et al., 2008). We tested this by measuring the activity of the transcriptional fusions in strains with modified ppGpp levels as previously described (Wahl et al., 2011). The ppGpp° (Δ*relA*Δ*spoT*) strain is devoid of ppGpp, the DksA cofactor is necessary for ppGpp action on RNAP hence a Δ*dksA* mutant mimics the absence of ppGpp, and finally the *spoT203* mutant is impaired in ppGpp degradation, leading to ppGpp accumulation in the cell. The psdP2 promoter did not show a strong dependence on ppGpp levels (**Supplementary Figure 1**). The psdP2 expression did slightly increase in a Δ*dksA* mutant, but not in the ppGpp° mutant, and it did not show a corresponding repression in the ppGpp+ mutant. Interestingly, the activity of the psdPσ^E transcriptional fusion increased in the ppGpp accumulating mutant (**Supplementary Figure 1**), which is in agreement with the known positive effect of ppGpp on σ^E (Costanzo et al., 2008).

Impact of σ^E or CpxR Regulation on Psd and MscM Protein Amounts

Because *psd* expression is controlled by two promoters, we then wanted to study the relative involvement of these two promoters in the control of the amounts of Psd in the cell. For that, we constructed a strain where Psd is fused at its C-terminus with the 3Flag tag, in order to detect the protein by western blot with a monoclonal antibody. Psd is produced as a proenzyme, which after endoproteolysis gives rise to a mature two-domains enzyme (Li and Dowhan, 1990; Choi et al., 2015). Because the tag is fused to the C-terminus of the protein, we detected as expected the small C-terminal Psdα-3Flag subdomain, indicating that the cleavage occurred normally (it migrated at a higher position than the expected 12 kDa, but this is not exceptional, and might be influenced by the pyruvoyl N-terminal modification). Furthermore, the tagged strain did not display any obvious growth defect, suggesting that the Psd-3Flag fusion was functional. However, in order to prove the functionality of the Psd-3Flag tagged protein, we also cloned this construction or the wild-type *psd* gene under its own promoter in a plasmid, and tested the complementation of a *psd*-ts mutant (Hawrot and Kennedy, 1975). Expression of *psd*-3Flag or wild-type *psd* expressed from a plasmid similarly restored growth of the psd^{ts} mutant at 42°C, showing that the recombinant Psd-3Flag protein was functional (**Figure 4**). We then tested the effect of overproducing σ^E or inducing the CpxR response through NlpE expression. The levels of Psd-3Flag protein were clearly increased when σ^E was overproduced (**Figure 5A**). Similarly,

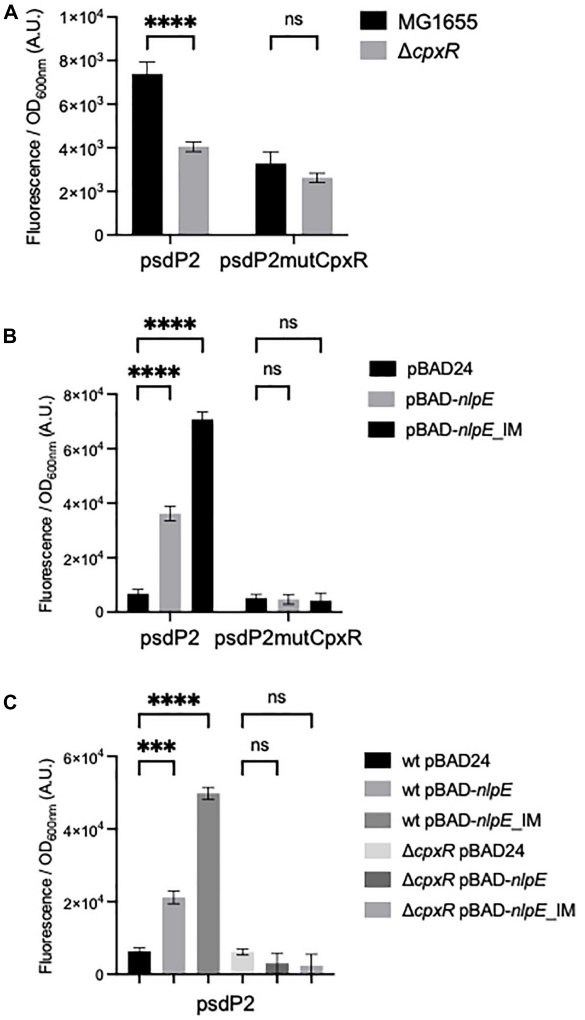

FIGURE 3 | Control of the psdP2 promoter by CpxR. **(A)** MG1655 or Δ*cpxR* strains were transformed with the indicated transcriptional fusions. Cultures were grown overnight at 30°C in LB supplemented with kanamycin. **(B,C)** MG1655 or Δ*cpxR* strains were transformed with the indicated transcriptional fusions together with pBAD24, pBAD-*nlpE*, or pBAD-*nlpE_IM* plasmids. Cultures were grown overnight at 30°C in LB supplemented with ampicillin, kanamycin and 0.01% arabinose. The values show the mean ratio of GFP fluorescence over optical density at 600 nm, after subtraction of the pUA66 negative control, in arbitrary units (A.U.). The values are the mean of 12 **(A)** or 4 **(B,C)** replicas and the error bars show the SEM (standard error of the mean). ns, non-significant, $^{***}p < 0.001$, $^{****}p < 0.0001$ in a two-way ANOVA statistical analysis.

levels of Psd-3Flag increased when NlpE or $NlpE_{IM}$ proteins were overproduced (**Figure 5B**). The increases observed when the CpxRA pathway was artificially induced were not as strong as the ones observed when σ^E was overproduced. However, they were clearly abolished when the experiment was repeated in a Δ*cpxR* genetic context (**Figure 5B**). It has to be noted that when Psd-3Flag amounts were strongly increased, a band at approximately 45 kDa was also detected (**Figure 5A**). We hypothesized that this band might correspond to the accumulation of an unmatured full length Psd-3Flag proenzyme. In order to test this, we introduced the point mutation S254A, which is known to prevent the maturation of Psd (Li and Dowhan, 1990), in the plasmid expressing *psd*-3Flag. As expected, this mutant form was detected at 45 kDa (**Supplementary Figure 2**). Interestingly, when we compared the production of Psd-3Flag with or without induction of *rpoE*, the band at 45 kDa accumulating when *rpoE* is induced migrated at the exact same size than the unmatured Psd(254A)-3Flag (**Supplementary Figure 2**), suggesting that endoproteolytic cleavage is indeed impaired when Psd-3Flag is overproduced.

On the genome of *E. coli*, *psd* ORF is followed by *mscM* ORF, suggesting an organization of these two genes as an operon. To study the involvement of σ^E and CpxR on *mscM* expression, we constructed a strain where MscM is fused at its C-terminus with the SPA tag. MscM-SPA was faintly detected on Western blot at the expected size of 130 kDa, and MscM protein levels were increased when *rpoE* or *nlpE* were artificially expressed, similarly as for Psd-3Flag (**Figure 6A**). We then performed an RT-PCR experiment, which confirmed that *psd* and *mscM* are expressed as an operon, controlled by the same two promoters (**Figure 6B**).

Characterization of Strains Devoid of *psd-mscM* Control by σ^E and CpxR

The above experiments using transcriptional fusions or following the amount of Psd and MscM proteins demonstrated the control of *psd* and *mscM* expression by the two envelope stress response pathways mediated by σ^E or CpxR. The next question was naturally to understand the physiological role of these regulations. To address this question, we chose to introduce point mutations in the promoters of *psd*, on the chromosome, in order to prevent specifically the activation of *psd-mscM* expression by σ^E, CpxR or both stress responses at the same time. We have shown above that the mutations chosen in the σ^E promoter and CpxR box completely abolished the induction of the transcriptional fusions by pBAD-*rpoE* or pBAD-*nlpE*, respectively (**Figures 2**, **3**). Note that both mutations are localized inside the ORF of the upstream *rsgA* gene. The mutation in the $PsdP\sigma^E$ promoter does not modify the amino acid sequence of RsgA, while the mutation in the CpxR box does modify residue Lys340 of RsgA in Glutamine. We introduced the mutations in wild-type MG1655 strain and in the Psd-3Flag strain using homologous recombination with the pKO3 plasmid (Link et al., 1997). The three types of mutants were readily obtained in the two strains (**Table 2**). The mutant strains did not display any obvious growth phenotype in LB (**Supplementary Figure 3**) showing that σ^E and CpxR regulations are not essential in balanced growth conditions. In the Psd-3Flag background strains, we observed that mutations in the $P\sigma^E$ promoter and CpxR box had no effect on the basal amounts of Psd-3Flag protein (**Figure 5C** and data not shown). This suggests that the decreased expression observed with the psdP2muCpxR transcriptional fusion (**Figure 3A**) does not impact protein level, and shows that these regulations are not important to control basal Psd and MscM protein levels. However, when σ^E was induced, the amounts of Psd-3Flag protein did not increase anymore in the strains containing the $P\sigma^E$ mutation (**Figure 5C**, first and

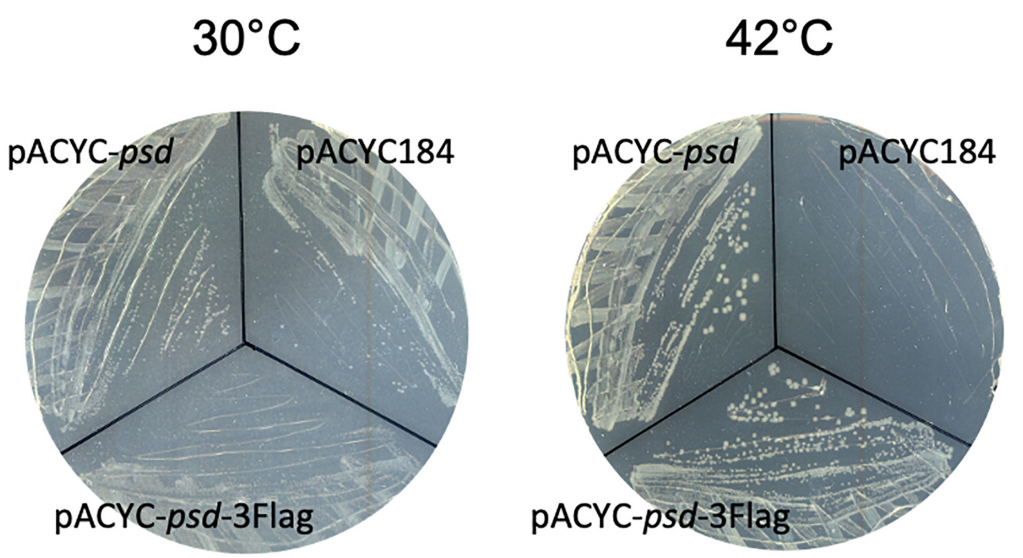

FIGURE 4 | Strain EH150 *psd2*-ts (Hawrot and Kennedy, 1975) was transformed by pACYC184, pACYC-*psd*, or pACYC-psd-3Flag plasmids and the selection was performed at 30°C. Then, colonies were spread out on LB chloramphenicol plates at 30 or 42°C for 24 h.

third panel), while Psd-3Flag still increased in the CpxRbox mutant (**Figure 5C**, second panel). When the CpxRA pathway was induced, with pBAD-*nlpE* or pBAD-*nlpE_IM* plasmids, Psd-3Flag protein amounts did not increase anymore in the strains containing the mutation in the CpxR binding site (**Figure 5C**, second and third panel), while Psd-3Flag still increased in the Pσ^E mutant (**Figure 5C**, first panel). These results confirmed what we observed with the transcriptional fusions (**Figure 3A**), and showed that the σ^E and CpxR control of *psd* promoters impact the amount of proteins produced *in vivo* upon stress induction.

DISCUSSION

The goal of this work was to decipher the genetic control of *psd-mscM* operon and its regulation by the two envelope stress responses mediated by the alternative Sigma factor σ^E and by the two-component system CpxRA. We found that *psd* promoter region comprises two promoters, confirming the +1 transcription start sites identified previously (Thomason et al., 2015): a distal σ^E promoter and a proximal P2 promoter, activated by CpxRA, which is likely to be also responsible for the basal expression of *psd*. This organization is very similar to what we observed previously for the promoter of *plsB*, which comprises a distal σ^E promoter and a proximal P2 promoter, responsible for the basal expression of *plsB* (Wahl et al., 2011). However, *plsB* expression was not controlled by CpxR (data not shown). We also systematically tested if other genes of PL synthesis were regulated by σ^E or CpxR but it was not the case (data not shown). Therefore, it appears that envelope stress responses control the first step of PL synthesis (*plsB*) and the last step of PE synthesis (*psd*). This suggests that in response to envelope stress, an increase in the pathway for PE might be important, in order to help in envelope biogenesis processes such as LPS or outer membrane proteins trafficking. An enhanced PE biosynthesis might be obtained by "pushing" from the top with PlsB and "pulling" from the bottom of the pathway with Psd. However, enzymes of PL synthesis are believed to be present in excess and it is not clear how increasing enzyme amounts might have an effect on the flux in the PL synthetic pathway. This regulation might be a long-term adaptation rather than an immediate response to the encountered stress. An alternative hypothesis is that the enzymes might be damaged during envelope stress and need to be replaced.

We previously showed that the basal promoter of the *plsB* gene was repressed by ppGpp (Wahl et al., 2011). Furthermore, it was proposed that the genes for PE pathway, including *psd*, might be downregulated during the stringent response, while the genes for PG/CL were upregulated (Durfee et al., 2008), which would be consistent with an increase in PG and CL in the membrane during growth arrest. However, we did not detect a strong regulation of psdP2 promoter by ppGpp (**Supplementary Figure 1**).

It is striking to find *psd* in operon with a gene encoding a mechanosensitive channel. There is no obvious direct functional link between these two genes, apart from a function in membrane homeostasis. Mechanosensitive channels open in response to transition from high to low osmolarity in order to protect cells from bursting (Booth, 2014). There are seven mechanosensitive channels in *E. coli*, MscL and six channels of the MscS family, including MscM. This redundancy might be explained by a need to respond to different rates or intensities in osmolarity variations (Booth, 2014). As for *psd*, a genetic regulation might

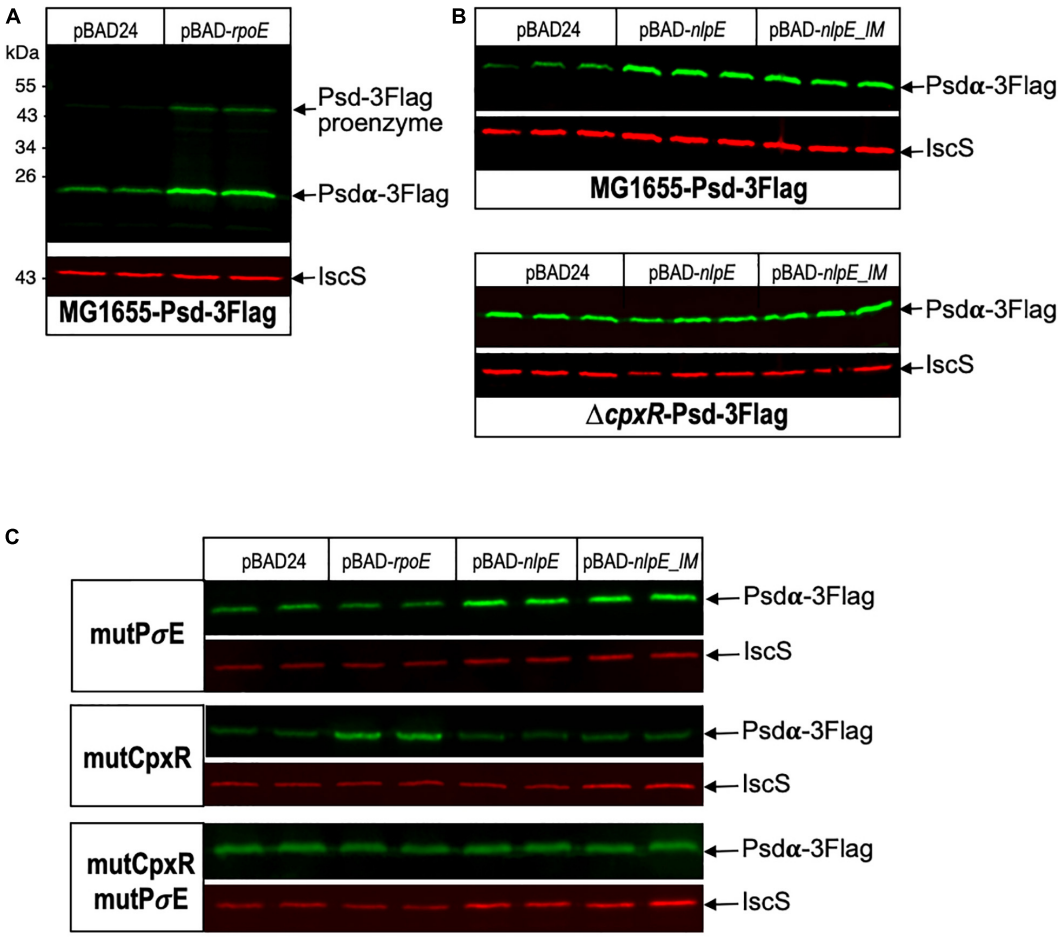

FIGURE 5 | Psd protein levels are controlled by σ^E and CpxR. **(A)** *E. coli* Psd-3Flag strain was transformed by pBAD24 or pBAD-*rpoE* plasmids. Two replicas of each transformation were grown in LB supplemented with ampicillin until $OD_{600\ nm}$ = 0.8, then cultures were induced with 0.2% arabinose for 2 h. **(B)** Psd-3Flag and Δ*cpxR*-Psd-3Flag strains were transformed by pBAD24, pBAD-*nlpE*, or pBAD-*nlpE_IM* plasmids. Three replicas of each transformation were grown in LB supplemented with ampicillin until $OD_{600\ nm}$ = 0.8, then cultures were induced with 0.2% arabinose for 2 h. **(C)** Psd-3Flag_mutPσ^E, Psd-3Flag_mutCpxR, and Psd-3Flag_mutCpxRmutPσ^E strains containing mutations in the promoter region were transformed by pBAD24, pBAD-*rpoE*, pBAD-*nlpE*, or pBAD-*nlpE_IM* plasmids. Two replicas of each transformation were grown in LB supplemented with ampicillin until $OD_{600\ nm}$ = 0.8, then cultures were induced with 0.2% arabinose for 2 h. Proteins were separated by SDS-PAGE 12% and detected by western blot using anti-Flag monoclonal antibody to detect Psd-3Flag or anti-IscS polyclonal antibody as an internal loading control. Quantification of the bands are shown in **Supplementary Figure 4**.

appear irrelevant for a rapid response to physical stress. However, the number and types of channels are important factors to determine the protective ability and cell fate (Bialecka-Fornal et al., 2015), and it has been shown that over-expression of MscM confers protection to hypo-osmotic shock in a strain otherwise devoid of all the other mechanosensitive channels (Edwards et al., 2012). Therefore, increased expression of *mscM* by σ^E and CpxR in response to envelope stress might be a bet hedging strategy, as it might confer adaptation for future additional envelope injuries. Similarly, *mscL* and *mscS* genes are regulated by the alternative Sigma factor σ^S (Stokes et al., 2003). Also, in *Pseudomonas aeruginosa*, the *cmpX* gene coding for a putative mechanosensitive channel is part of the SigX envelope stress response regulon (Gicquel et al., 2013). Furthermore, these mechanosensitive channels possess diverse periplasmic and cytoplasmic domains that might play additional functions in stress responses, which for example was suggested recently for YbdG in *E. coli* (Amemiya et al., 2019).

Unfortunately, we were not able yet to find growth conditions or stress conditions where the σ^E or CpxRA regulations on *plsB* and *psd-mscM* had a role for cell physiology. We tried to subject the mutant strains to stresses known to induce the σ^E or CpxRA pathways, i.e., osmotic stress, alkaline stress, envelope porin misfolding or mislocalization, or heat shock, but we did not detect any effects in these experiments. As mentioned above, these regulations are certainly involved in long-term adaptation rather than being an immediate response to the encountered stress. This might be why we did not detect any obvious phenotypic defects in the regulatory mutant strains when testing for immediate resistance to stress. Combining stresses, long-term, or competition experiments might be needed to be able to unravel a phenotypic advantage of the wild-type over the

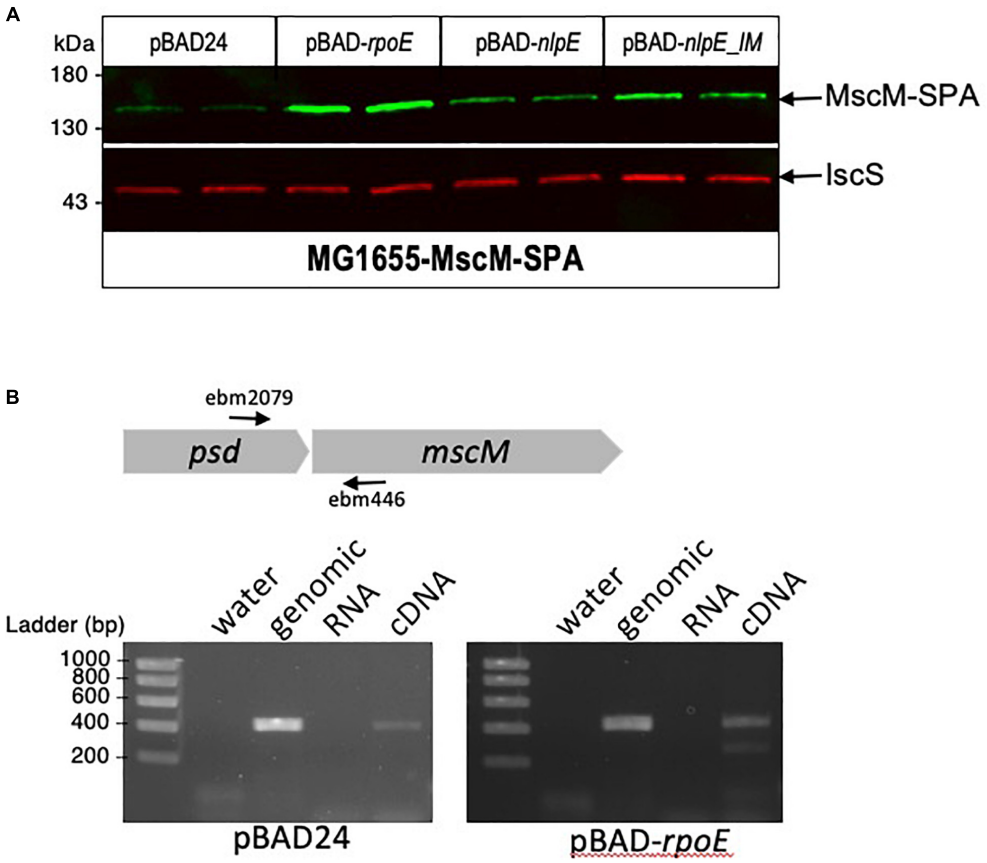

FIGURE 6 | *mscM* is in operon with *psd*, under control of the σ^E and CpxR dependent promoters. **(A)** *E. coli* MscM-SPA strain was transformed by pBAD24, pBAD-*rpoE*, pBAD-nlpE, or pBAD-*nlpE_IM* plasmids. Two replicas of each transformation were grown in LB supplemented with ampicillin until $OD_{600\ nm}$ = 0.8, then cultures were induced with 0.2% arabinose for 2 h. Proteins were separated by SDS-PAGE 10% and detected by western blot using anti-Flag monoclonal antibody for the detection of MscM-SPA or anti-IscS polyclonal antibodies as an internal loading control. **(B)** RT-PCR was performed on MG1655 strain transformed by pBAD or *pBAD-rpoE* induced in the above conditions. The black arrows indicate the positions of the primers used for the amplification. PCR controls on water, genomic DNA, and equivalent amounts of RNA as in the RT-PCR reaction were performed.

regulatory mutant strains. Interestingly, and in a reversed way, several studies have shown that PL synthesis mutants, which affect membrane composition, activate envelope stress responses, including σ^E and CpxRA signaling pathways (Mileykovskaya and Dowhan, 1997; Itou et al., 2012; Rowlett et al., 2017; Nepper et al., 2019). Therefore, the σ^E or CpxRA regulations of *plsB* and *psd-mscM* might also be part of a feedback loop involved in maintaining an optimum PL synthesis balance for membrane homeostasis.

DATA AVAILABILITY STATEMENT

The original contributions presented in the study are included in the article/**Supplementary Material**, further inquiries can be directed to the corresponding author/s.

AUTHOR CONTRIBUTIONS

YH, EB, and JV contributed to conception and design of the study. YH, JB, and AW performed experiments. EB wrote the manuscript. All authors contributed to manuscript revision, read, and approved the submitted version.

FUNDING

This work was funded by the Centre National de la Recherche Scientifique (CNRS), the Pasteur Institute, and grant ANR-19-CE13-0009-02. YH was supported by a doctoral fellowship from the French Ministry of Higher Education and Research.

ACKNOWLEDGMENTS

We thank Celia Torrielli for the construction of *E. coli* strains.

SUPPLEMENTARY MATERIAL

The Supplementary Material for this article can be found online at: https://www.frontiersin.org/articles/10.3389/fmolb.2021.665977/full#supplementary-material

REFERENCES

Amemiya, S., Toyoda, H., Kimura, M., Saito, H., Kobayashi, H., Ihara, K., et al. (2019). The mechanosensitive channel YbdG from *Escherichia coli* has a role in adaptation to osmotic up-shock. *J. Biol. Chem.* 294, 12281–12292. doi: 10.1074/jbc.ra118.007340

Baba, T., Ara, T., Hasegawa, M., Takai, Y., Okumura, Y., Baba, M., et al. (2006). Construction of *Escherichia coli* K-12 in-frame, single-gene knockout mutants: the Keio collection. *Mol. Syst. Biol.* 2:2006.0008.

Bialecka-Fornal, M., Lee, H. J., and Phillips, R. (2015). The rate of osmotic downshock determines the survival probability of bacterial mechanosensitive channel mutants. *J. Bacteriol.* 197, 231–237. doi: 10.1128/jb.02175-14

Booth, I. R. (2014). Bacterial mechanosensitive channels: progress towards an understanding of their roles in cell physiology. *Curr. Opin. Microbiol.* 18, 16–22. doi: 10.1016/j.mib.2014.01.005

Busby, S. J. W. (2019). Transcription activation in bacteria: ancient and modern. *Microbiology* 165, 386–395. doi: 10.1099/mic.0.000783

Chang, A. C., and Cohen, S. N. (1978). Construction and characterization of amplifiable multicopy DNA cloning vehicles derived from the P15A cryptic miniplasmid. *J. Bacteriol.* 134, 1141–1156. doi: 10.1128/jb.134.3.1141-1156.1978

Cherepanov, P. P., and Wackernagel, W. (1995). Gene disruption in *Escherichia coli*: TcR and KmR cassettes with the option of Flp-catalyzed excision of the antibiotic-resistance determinant. *Gene* 158, 9–14. doi: 10.1016/0378-1119(95)00193-a

Choi, J. Y., Duraisingh, M. T., Marti, M., Ben Mamoun, C., and Voelker, D. R. (2015). From Protease to Decarboxylase: the molecular metamorphosis of phosphatidylserine decarboxylase. *J. Biol. Chem.* 290, 10972–10980.

Costanzo, A., Nicoloff, H., Barchinger, S. E., Banta, A. B., Gourse, R. L., and Ades, S. E. (2008). ppGpp and DksA likely regulate the activity of the extracytoplasmic stress factor sigmaE in *Escherichia coli* by both direct and indirect mechanisms. *Mol. Microbiol.* 67, 619–632. doi: 10.1111/j.1365-2958.2007.06072.x

Datsenko, K. A., and Wanner, B. L. (2000). One-step inactivation of chromosomal genes in *Escherichia coli* K-12 using PCR products. *Proc. Natl. Acad. Sci. U.S.A.* 97, 6640–6645. doi: 10.1073/pnas.120163297

De Wulf, P., McGuire, A. M., Liu, X., and Lin, E. C. (2002). Genome-wide profiling of promoter recognition by the two-component response regulator CpxR-P in *Escherichia coli*. *J. Biol. Chem.* 277, 26652–26661. doi: 10.1074/jbc.m203487200

Delhaye, A., Collet, J. F., and Laloux, G. (2016). Fine-tuning of the Cpx envelope stress response is required for cell wall homeostasis in *Escherichia coli*. *mBio* 7:e00047-16.

Durfee, T., Hansen, A. M., Zhi, H., Blattner, F. R., and Jin, D. J. (2008). Transcription profiling of the stringent response in *Escherichia coli*. *J. Bacteriol.* 190, 1084–1096. doi: 10.1128/jb.01092-07

Edwards, M. D., Black, S., Rasmussen, T., Rasmussen, A., Stokes, N. R., Stephen, T. L., et al. (2012). Characterization of three novel mechanosensitive channel activities in *Escherichia coli*. *Channels* 6, 272–281. doi: 10.4161/chan.20998

Eichel, J., Chang, Y. Y., Riesenberg, D., and Cronan, J. E. (1999). Effect of ppGpp on *Escherichia coli* cyclopropane fatty acid synthesis is mediated through the RpoS sigma factor (sigmaS). *J. Bacteriol.* 181, 572–576. doi: 10.1128/jb.181.2.572-576.1999

Gicquel, G., Bouffartigues, E., Bains, M., Oxaran, V., Rosay, T., Lesouhaitier, O., et al. (2013). The extra-cytoplasmic function sigma factor sigX modulates biofilm and virulence-related properties in *Pseudomonas aeruginosa*. *PLoS One* 8:e80407. doi: 10.1371/journal.pone.0080407

Gully, D., Moinier, D., Loiseau, L., and Bouveret, E. (2003). New partners of acyl carrier protein detected in *Escherichia coli* by tandem affinity purification. *FEBS Lett.* 548, 90–96. doi: 10.1016/s0014-5793(03)00746-4

Guzman, L. M., Belin, D., Carson, M. J., and Beckwith, J. (1995). Tight regulation, modulation, and high-level expression by vectors containing the arabinose PBAD promoter. *J. Bacteriol.* 177, 4121–4130.

Hawrot, E., and Kennedy, E. P. (1975). Biogenesis of membrane lipids: mutants of *Escherichia coli* with temperature-sensitive phosphatidylserine decarboxylase. *Proc. Natl. Acad. Sci. U.S.A.* 72, 1112–1116. doi: 10.1073/pnas.72.3.1112

Itou, A., Matsumoto, K., and Hara, H. (2012). Activation of the Cpx phosphorelay signal transduction system in acidic phospholipid-deficient pgsA mutant cells of *Escherichia coli*. *Biochem. Biophys. Res. Commun.* 421, 296–300. doi: 10.1016/j.bbrc.2012.04.003

Li, Q. X., and Dowhan, W. (1990). Studies on the mechanism of formation of the pyruvate prosthetic group of phosphatidylserine decarboxylase from *Escherichia coli*. *J. Biol. Chem.* 265, 4111–4115. doi: 10.1016/s0021-9258(19)39709-1

Link, A. J., Phillips, D., and Church, G. M. (1997). Methods for generating precise deletions and insertions in the genome of wild-type *Escherichia coli*: application to open reading frame characterization. *J. Bacteriol.* 179, 6228–6237. doi: 10.1128/jb.179.20.6228-6237.1997

Mileykovskaya, E., and Dowhan, W. (1997). The Cpx two-component signal transduction pathway is activated in *Escherichia coli* mutant strains lacking phosphatidylethanolamine. *J. Bacteriol.* 179, 1029–1034. doi: 10.1128/jb.179.4.1029-1034.1997

Mitchell, A. M., and Silhavy, T. J. (2019). Envelope stress responses: balancing damage repair and toxicity. *Nat. Rev. Microbiol.* 17, 417–428. doi: 10.1038/s41579-019-0199-0

My, L., Rekoske, B., Lemke, J. J., Viala, J. P., Gourse, R. L., and Bouveret, E. (2013). Transcription of the *Escherichia coli* fatty acid synthesis operon fabHDG is directly activated by FadR and inhibited by ppGpp. *J. Bacteriol.* 195, 3784–3795. doi: 10.1128/jb.00384-13

Nepper, J. F., Lin, Y. C., and Weibel, D. B. (2019). Rcs phosphorelay activation in cardiolipin-deficient *Escherichia coli* reduces biofilm formation. *J. Bacteriol.* 201:e00804-18.

Parsons, J. B., and Rock, C. O. (2013). Bacterial lipids: metabolism and membrane homeostasis. *Prog. Lipid Res.* 52, 249–276. doi: 10.1016/j.plipres.2013.02.002

Rezuchova, B., Miticka, H., Homerova, D., Roberts, M., and Kormanec, J. (2003). New members of the *Escherichia coli* sigmaE regulon identified by a two-plasmid system. *FEMS Microbiol. Lett.* 225, 1–7. doi: 10.1016/s0378-1097(03)00480-4

Rhodius, V. A., Suh, W. C., Nonaka, G., West, J., and Gross, C. A. (2006). Conserved and variable functions of the sigmaE stress response in related genomes. *PLoS Biol.* 4:e2. doi: 10.1371/journal.pbio.0040002

Rowlett, V. W., Mallampalli, V. K. P. S., Karlstaedt, A., Dowhan, W., Taegtmeyer, H., Margolin, W., et al. (2017). Impact of membrane phospholipid alterations in *Escherichia coli* on cellular function and bacterial stress adaptation. *J. Bacteriol.* 199:e00849-16.

Sohlenkamp, C., and Geiger, O. (2016). Bacterial membrane lipids: diversity in structures and pathways. *FEMS Microbiol. Rev.* 40, 133–159. doi: 10.1093/femsre/fuv008

Stokes, N. R., Murray, H. D., Subramaniam, C., Gourse, R. L., Louis, P., Bartlett, W., et al. (2003). A role for mechanosensitive channels in survival of stationary phase: regulation of channel expression by RpoS. *Proc. Natl. Acad. Sci. U.S.A.* 100, 15959–15964. doi: 10.1073/pnas.2536607100

Thomason, M. K., Bischler, T., Eisenbart, S. K., Förstner, K. U., Zhang, A., Herbig, A., et al. (2015). Global transcriptional start site mapping using differential RNA sequencing reveals novel antisense RNAs in *Escherichia coli*. *J. Bacteriol.* 197, 18–28. doi: 10.1128/jb.02096-14

Wahl, A., My, L., Dumoulin, R., Sturgis, J. N., and Bouveret, E. (2011). Antagonistic regulation of dgkA and plsB genes of phospholipid synthesis by multiple stress responses in *Escherichia coli*. *Mol. Microbiol.* 80, 1260–1275. doi: 10.1111/j.1365-2958.2011.07641.x

Wang, A. Y., and Cronan, J. E. (1994). The growth phase-dependent synthesis of cyclopropane fatty acids in *Escherichia coli* is the result of an RpoS(KatF)-dependent promoter plus enzyme instability. *Mol. Microbiol.* 11, 1009–1017. doi: 10.1111/j.1365-2958.1994.tb00379.x

Zaslaver, A., Bren, A., Ronen, M., Itzkovitz, S., Kikoin, I., Shavit, S., et al. (2006). A comprehensive library of fluorescent transcriptional reporters for *Escherichia coli*. *Nat. Methods* 3, 623–628. doi: 10.1038/nmeth895

Zeghouf, M., Li, J., Butland, G., Borkowska, A., Canadien, V., Richards, D., et al. (2004). Sequential peptide affinity (SPA) system for the identification of mammalian and bacterial protein complexes. *J. Proteome Res.* 3, 463–468. doi: 10.1021/pr034084x

Conflict of Interest: The authors declare that the research was conducted in the absence of any commercial or financial relationships that could be construed as a potential conflict of interest.

frontiers in Molecular Biosciences

MINI REVIEW
published: 11 May 2021
doi: 10.3389/fmolb.2021.634438

Mini Review: Bacterial Membrane Composition and Its Modulation in Response to Stress

*Jessica R. Willdigg and John D. Helmann**

Department of Microbiology, Cornell University, Ithaca, NY, United States

Antibiotics and other agents that perturb the synthesis or integrity of the bacterial cell envelope trigger compensatory stress responses. Focusing on *Bacillus subtilis* as a model system, this mini-review summarizes current views of membrane structure and insights into how cell envelope stress responses remodel and protect the membrane. Altering the composition and properties of the membrane and its associated proteome can protect cells against detergents, antimicrobial peptides, and pore-forming compounds while also, indirectly, contributing to resistance against compounds that affect cell wall synthesis. Many of these regulatory responses are broadly conserved, even where the details of regulation may differ, and can be important in the emergence of antibiotic resistance in clinical settings.

Keywords: bacteria, membrane, lipid, cellular envelope, antimicrobial resistance, metabolism, *Bacillus subtilis*

OPEN ACCESS

Edited by:
Heidi Vitrac,
University of Texas Health Science Center at Houston, United States

Reviewed by:
Turabe M. H. U. Fazil,
Nanyang Technological University, Singapore
Leonel Malacrida,
Universidad de la República, Uruguay
Jan Maarten Van Dijl,
University Medical Center Groningen, Netherlands

***Correspondence:**
John D. Helmann
jdh9@cornell.edu
orcid.org/0000-0002-3832-3249

Specialty section:
This article was submitted to Cellular Biochemistry, a section of the journal Frontiers in Molecular Biosciences

Received: *27 November 2020*
Accepted: *13 April 2021*
Published: *11 May 2021*

Citation:
Willdigg JR and Helmann JD (2021) Mini Review: Bacterial Membrane Composition and Its Modulation in Response to Stress. Front. Mol. Biosci. 8:634438. doi: 10.3389/fmolb.2021.634438

INTRODUCTION: MEMBRANE HOMEOSTASIS AND ITS MODULATION IN RESPONSE TO STRESS

The cell envelope is a multilayered outer barrier that protects the cell from a changing environment. Cell envelope stress responses (CESRs) are regulatory pathways that sense threats and mount a protective response, often involving modification of lipopolysaccharides (in Gram-negative bacteria), teichoic acids (Gram-positive bacteria), peptidoglycan, and the inner membrane (Helmann, 2016; Radeck et al., 2017; Mitchell and Silhavy, 2019). Here, we focus on *Bacillus subtilis* as a Gram-positive model for the role of CESRs in membrane homeostasis.

The cell membrane is a dynamic, fluid mosaic comprising a lipid bilayer and associated proteins (**Figure 1**). In *B. subtilis*, the major lipid species are phospholipids, glucolipids, and the lipoteichoic acids (LTA) (Salzberg and Helmann, 2008; Nickels et al., 2017). The membrane proteome includes proteins for transport and signaling, as well as membrane synthesis, remodeling, and protection. As the innermost and last line of defense, the cell membrane is critical for viability. In *B. subtilis*, for example, collapsing the proton motive force activates autolysins resulting in rapid cell lysis (Jolliffe et al., 1981). Membrane-active compounds such as detergents, antimicrobial peptides, and pore-forming compounds often trigger stress responses that modify the lipidome and membrane proteome to confer resistance. Membrane stress responses can modify the cell membrane, by (i) modulating the length, branching, and saturation of the fatty acid (FA) acyl chains, (ii) altering membrane lipid composition, or (iii) synthesizing proteins that modify or protect the membrane (**Table 1**).

THE REGULATION OF FA SYNTHESIS DURING GROWTH

Most bacteria utilize a type II FA synthase that catalyzes repeated cycles of acyl chain elongation (Parsons and Rock, 2013). The committed step, catalyzed by acetyl-CoA carboxylase (ACC), generates malonyl-CoA and then malonyl-ACP to serve in FA chain initiation by FabH and elongation by FabF. *B. subtilis* has two isoforms of FabH, and both preferentially synthesize branched chain FAs (BCFAs) (Choi et al., 2000; Kingston et al., 2011). Acylation of glycerol-3-phosphate by the PlsX/PlsY/PlsC acyltransferase system with long chain FAs generates phosphatidic acid, the precursor to all other phospholipids (Yao and Rock, 2013).

FapR is the key transcriptional regulator of membrane lipid synthesis in *B. subtilis* and clinically relevant pathogens such as *Staphylococcus aureus*, *Bacillus anthracis*, and *Listeria monocytogenes* (Schujman et al., 2003; Fujita et al., 2007; Albanesi et al., 2013; Machinandiarena et al., 2020), and modulates the overall rate of membrane synthesis in response to precursor availability. *B. subtilis* FapR represses genes for FA and phospholipid synthesis, and this repression is relieved by allosteric interactions with malonyl-CoA or malonyl-ACP (Schujman et al., 2006; Martinez et al., 2010).

As a branchpoint enzyme, ACC is often under complex regulation (Zhang and Rock, 2009; Salie and Thelen, 2016; Machinandiarena et al., 2020). In *B. subtilis*, ACC is regulated in part by YqhY, a conserved DUF322/Asp23 protein which is highly expressed and often encoded together with ACC subunits as part of an *accB-accC-yqhY* operon (Todter et al., 2017). The namesake, *S. aureus* Asp23, is a membrane-associated protein originally linked to alkaline shock (Petersen et al., 2020). Loss of Asp23/YqhY causes cell wall stress and poor growth (Muller et al., 2014; Todter et al., 2017). In *B. subtilis*, *yqhY* null mutants acquire suppressors that decrease ACC activity, but this selective pressure is alleviated in medium supplemented with acetate (Todter et al., 2017). We suggest that ACC-dependent depletion of acetyl-CoA may contribute to wall stress by negatively affecting synthesis of UDP-N-acetylglucosamine needed for peptidoglycan synthesis. A key challenge for future research will be to understand the precise role of YqhY/Asp23 proteins and how they control ACC activity to balance FA synthesis with other cellular needs.

MODULATING FA COMPOSITION FOR HOMEOVISCOUS ADAPTATION

Tuning of FA composition provides one way in which the cell can optimize membrane properties in response to a changing environment. Even under non-stressed conditions, *B. subtilis* membranes contain ∼7 distinct FAs varying in length from C_{14} to C_{18} (indicating the number of carbon atoms) and include both branched (∼24% iso and 66% anteiso) and straight chain (∼10%) FAs (Kingston et al., 2011). Since membrane phospholipids and glucolipids each contain 2 FA chains, the lipidome contains a complex mix of species (**Figure 1B**), with a preponderance containing one C_{15} and one C_{17} FA chain (Kingston et al., 2011).

Modifications of FAs are important for regulating membrane fluidity in a process known as *homeoviscous adaptation* (de Mendoza, 2014; Ernst et al., 2016). In *B. subtilis*, temperature downshift induces a FA desaturase (Des) controlled by the DesKR two-component system (TCS) (Abriata et al., 2017). Des modifies existing membrane lipids, and is thereby suited for rapid adaptation. DesK is one of the better understood TCS sensors, with both kinase and phosphatase activity (Abriata et al., 2017; Fernandez et al., 2019). DesK lacks an extracellular sensor domain, but has multiple transmembrane segments that sense changes in the membrane physical state. DesK phosphorylates the DesR response regulator, which induces *des*, encoding a FA Δ5 desaturase (Altabe et al., 2003). The resultant unsaturated FAs increase bilayer fluidity, which restores DesK phosphatase activity in a negative feedback loop (de Mendoza, 2014). Longer term adaptation to low temperatures relies on an isoleucine-dependent switch to primarily anteiso-FAs (Weber et al., 2001). Since anteiso-FAs perturb the lateral interactions between adjacent lipids to a greater extent than iso-FAs (**Figure 1B**), this shift increases membrane fluidity (Kingston et al., 2011). This shift may result from a cold-dependent change in FabH activity (Beranova et al., 2008; Saunders et al., 2016).

Membranes must also adapt to conditions that increase fluidity. In *B. subtilis,* the ECF σ factor σ^W is activated by detergents, antibiotics, and bacteriocins active on the membrane (Cao et al., 2002b; Pietiainen et al., 2005; Butcher and Helmann, 2006; Helmann, 2006, 2016). A σ^W promoter within the *fabHA-fabF* operon plays a major role in homeoviscous adaptation (Kingston et al., 2011). Activation of σ^W leads to a decrease in FabHA levels, resulting in increased reliance on FabHB and an increase in straight chain FAs (from ∼10 to 30%). Elevated expression of the FabF elongation enzyme leads to increased FA chain length. The combined effect is a membrane with longer acyl chains and less BCFA. This increased membrane rigidity serves to protect cells against detergents and antimicrobial peptides (Kingston et al., 2011). The activation of σ^W is controlled by regulated proteolysis of its membrane-bound anti-σ^W factor (RsiW) (Schobel et al., 2004; Ellermeier and Losick, 2006; Devkota et al., 2017). However, the mechanisms by which membrane stressors trigger σ^W activation remain unclear.

To better understand the role of FA heterogeneity in controlling membrane properties, it would be desirable to study bacteria with chemically simple membranes. This has been achieved in *B. subtilis* by feeding exogenous FAs to cells with *de novo* FA synthesis blocked by cerulenin and a mutation to inhibit FA degradation (Nickels et al., 2020). Growth can be rescued with only two FA species: a straight-chain C_{16} FA (high melting) and an anteiso C_{15} FA (low melting). Even with only these two FA species, four distinct arrangements are possible upon acylation of glycerol-3-phosphate to generate phosphatidic acid. Cells compensate for this reduced FA complexity by altering the distribution of phospholipid headgroups, a modest induction of the DesRK system, apparent downregulation of the σ^W stress response, and an increase in isoprenoid lipids (Nickels et al., 2020). These results highlight the remarkable adaptability of

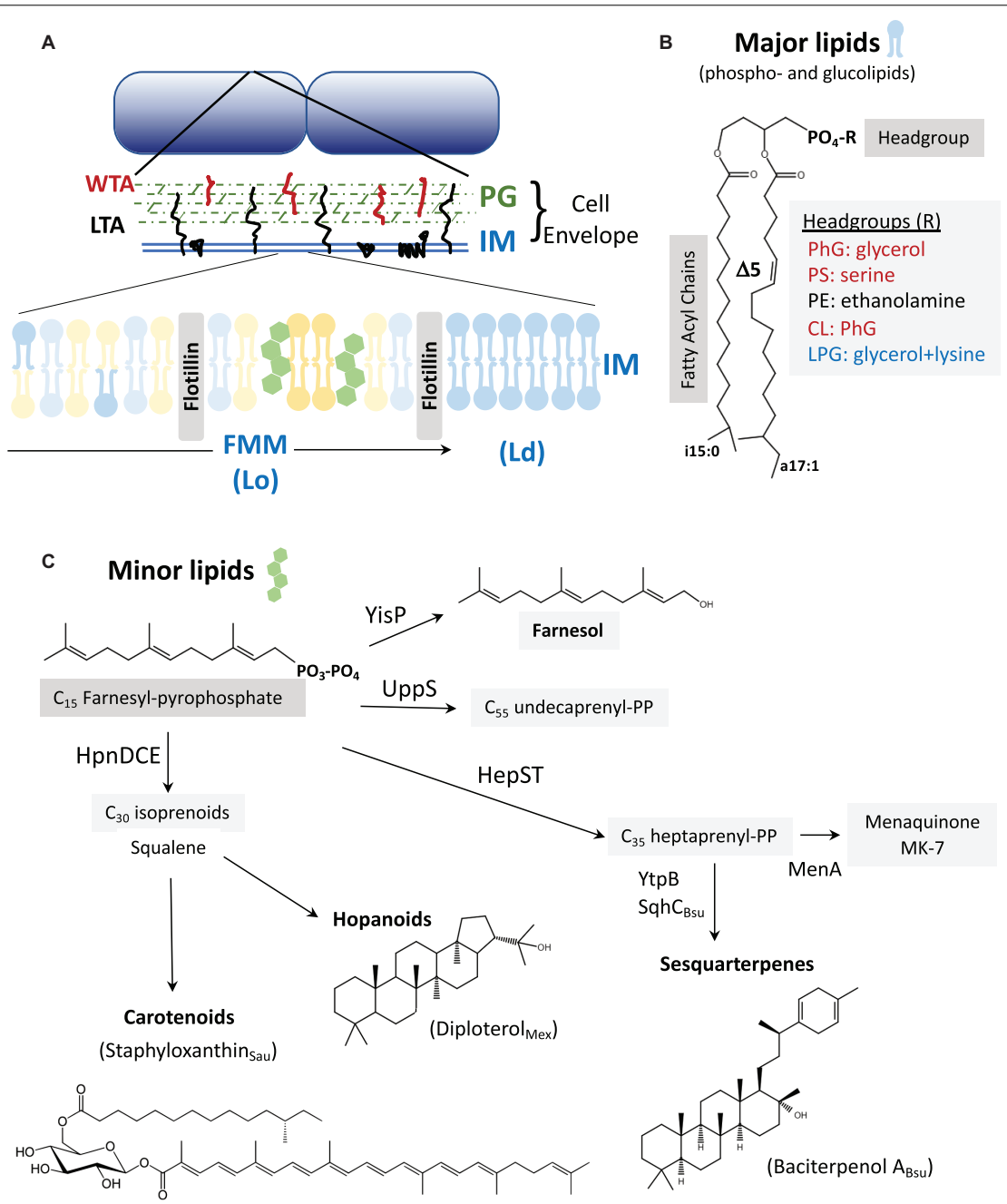

FIGURE 1 | (A) *The cell envelope*: *Bacillus subtilis* is surrounded by a cell envelope comprised of a thick peptidoglycan (PG) layer and an inner membrane (IM). The membrane-associated lipoteichoic acid (LTA) and PG-linked wall teichoic acid (WTA) are abundant anionic polymers in the envelope (Rajagopal and Walker, 2017). The IM contains lateral microheterogeneity in the form of functional membrane microdomains (FMMs), regions of liquid-ordered (Lo) membrane together with associated proteins such as flotillins (Lopez and Koch, 2017). These are flanked by regions of higher fluidity characterized as liquid-disordered (Ld). **(B)** *Major membrane lipids*: Major membrane lipids include phospholipids and glucolipids (Nickels et al., 2017). Phospholipids (shown) vary in their FA chains, which are largely branched in *B. subtilis*. Shown here are a C_{15} iso-FA and a C_{17} Δ5 (unsaturated) anteiso-FA. Other FA chain lengths (including straight chains), and the positioning of the FA chains on the 1 and 2 positions of glycerol can vary. Variations in the phospholipid headgroups modulate surface charge (red are anionic, blue cationic, and black net neutral). Glucolipids are generally neutral lipids with one or more sugar residues in place of the phosphate shown. **(C)** *Minor membrane lipids*: Many of the minor lipids in the membrane are isoprenoids and are derived from the C_{15} intermediate farnesyl-pyrophosphate (FPP). FPP is a precursor for undecaprenyl-PP (for PG synthesis) and for the C_{35} intermediate heptaprenyl-PP. The latter is a precursor for the electron carrier menaquinone (MK-7) and sesquarterpenes including baciterpenol A and its derivatives (sporulenes) (Bosak et al., 2008; Takigawa et al., 2010; Sato et al., 2011; Sato, 2013). Two FPP can also be coupled in a multistep reaction by HpnDCE to generate C_{30} squalene (Pan et al., 2015; van der Donk, 2015), which can be processed into carotenoids [such as staphyloxanthin from *S. aureus;* (Garcia-Fernandez et al., 2017; Foster, 2019)] or cyclized by squalene-hopene cyclases to generate polycyclic compounds (hopanoids) (Saenz et al., 2015; Belin et al., 2018). In *B. subtilis*, FPP can also be dephosphorylated by YisP to generate the alcohol farnesol (Bell and Chappell, 2014; Feng et al., 2014).

TABLE 1 | Representative *B. subtilis* CESRs that modify the lipidome and membrane proteome[1].

CESR	Gene(s)	Function	References
Lipidome			
σ^W	*fabHA-fabF*	Homeoviscous adaptation; Increased anteiso FA, decreased straight chain FA	Kingston et al., 2011
DesKR	*des*	Homeoviscous adaptation; Δ-5-FA desaturase	de Mendoza, 2014
σ^X, σ^V	*dltABCDE*	Surface charge modification; D-alanylation of LTA, WTA; contributes to lantibiotic resistance	Cao and Helmann, 2004; Pietiainen et al., 2005; Kingston et al., 2013
σ^X, σ^V	*pssA-ybfM-psd*	Surface charge modification; synthesis of PE (zwitterionic lipid) from anionic phosphatidylglycerol; upregulated by 1-butanol treatment	Cao and Helmann, 2004; Vinayavekhin et al., 2015
σ^M	*ytpAB*	YtpA; FA chain hydrolysis to generate lysophospholipids YtpB; initiating enzyme in sesquarterpene synthesis	Tamehiro et al., 2002; Sato et al., 2011
σ^M	*ltaSa*	Alternative LTA synthase; induced in strains lacking the primary synthase (LtaS).	Eiamphungporn and Helmann, 2008; Wormann et al., 2011; Hashimoto et al., 2013
Proteome			
σ^W	*floA* *floT*	FloA and FloT flotillins (SPFH family); integral membrane proteins implicated in lipid raft function; Induction of *yqeZ-floA-yqfB* operon provides resistance against sublancin.	Butcher and Helmann, 2006; Bramkamp and Lopez, 2015
σ^W	*pspA*	PspA; phage shock protein A (PspA/VIPP1/IM30/ESCRT III family), membrane protection and remodeling; contributes to nisin resistance.	Kingston et al., 2013; Flores-Kim and Darwin, 2016; Manganelli and Gennaro, 2017
σ^W	*yknWXYZ* *yfhLM*	YknWXYZ (transporter) and YfhLM provide protection against the SdpC "cannibalism toxin." YfhL is a paralog of the SdpI immunity protein.	Butcher and Helmann, 2006; Lamsa et al., 2012; Yamada et al., 2012; Hofler et al., 2016
σ^W	*ydbST*	YdbST provide protection against Amylocyclicin (cyclic lipopeptide).	Butcher and Helmann, 2006; Scholz et al., 2014
LiaRS	*liaIH*	LiaH; a PspA paralog, anchored by LiaI. Strongly induced by membrane-perturbing antimicrobials; induced by TAT protein export.	Mascher et al., 2004; Radeck et al., 2017; Bernal-Cabas et al., 2020
BceRS	*bceAB*	Prototype for flux-sensing TCS (BceRS) that integrates signals from the cognate ABC transporter (BceAB).	Fritz et al., 2015; Radeck et al., 2016; Kobras et al., 2020
LnrJK	*lrnLMN*	A flux-sensing system for induction of linearmycin and amphotericin (polyene antibiotic) resistance.	Stubbendieck and Straight, 2017; Stubbendieck et al., 2018; Revilla-Guarinos et al., 2020

[1] *This list includes representative systems from B. subtilis, but does not include CESRs with related functions from other organisms.*

bacterial membranes, and the interconnection between diverse stress responses.

OVERVIEW OF MEMBRANE LIPID COMPOSITION AND SYNTHESIS

One of the persistent challenges in membrane biology is to define the roles of the diverse constituent lipids (Sohlenkamp and Geiger, 2016; Dowhan et al., 2019; Chwastek et al., 2020). Although membranes have a complex and adaptable composition (the lipidome), cells are remarkably resilient to genetic alterations that remove lipid species. Because of its single membrane and ease of genetic manipulation, *B. subtilis* presents an attractive model system (Nickels et al., 2017). The *B. subtilis* lipidome comprises ∼70% phospholipids and ∼30% neutral glucolipids. The major phospholipids are phosphatidylglycerol (PhG) and phosphatidylethanolamine (PE), with minor contributions from cardiolipin and lysylphosphatidylglycerol (LPG). Variations in phospholipid headgroup size and charge modulate membrane properties (**Figure 1B**). Membranes also contain LTA anchored to neutral glucolipids, which together with peptidoglycan-linked wall teichoic acid (WTA) can account for up to 60% of the dry weight of the cell wall (Rajagopal and Walker, 2017; Sumrall et al., 2020). However, LTA fractionates with the wall during membrane lipid extraction, and is often not considered in lipidome measurements.

The only essential phospholipid in *B. subtilis* is PhG. Remarkably, the membrane can be simplified to contain close to 100% PhG with no glucolipids. Despite a greatly simplified membrane, such mutants can grow rapidly, albeit with a highly abnormal coiled filament morphology (Salzberg and Helmann, 2008). Genetic perturbations of membrane composition can lead to resistance to cationic antimicrobial peptides (CAMP). For example, gain-of-function mutations in *mprF*, encoding the LPG synthase/flippase, can confer daptomycin resistance possibly by reducing surface charge (Ernst et al., 2018; Ernst and Peschel, 2019). Consistently, *mprF* null mutants have increased daptomycin sensitivity and overexpression decreases sensitivity in *B. subtilis* (Hachmann et al., 2009). Daptomycin resistance also results from *pgsA* mutations that decrease PhG levels (Hachmann et al., 2011; Peleg et al., 2012).

In addition to the dominant phospholipids and glucolipids, membranes contain numerous other lipid species. Most prominent are the isoprenoid lipids synthesized by polymerization of C_5 isoprene units (**Figure 1C**). The key intermediate farnesyl-PP (C_{15}) can be joined (head-to-head) to generate squalene (C_{30}) (Pan et al., 2015; van der Donk, 2015), a precursor of cholesterol and other sterols in eukaryotes and of structurally related hopanoid lipids in many bacteria. One major hopanoid is diploterol (**Figure 1C**), with five fused rings that can be further modified in a variety of ways (Belin et al., 2018). Farnesyl-PP can also be extended by UppS, which sequentially adds eight isopentenyl units to generate undecaprenyl-PP, the

C_{55} carrier lipid that supports cell wall synthesis (**Figure 1C**). Alternatively, the HepST complex can extend farnesyl-PP to generate heptaprenyl (C_{35})-PP, an isoprenoid used as a lipid anchor for menaquinone (MK-7), the electron carrier for respiration. In *B. subtilis*, this same precursor can be processed to polycyclic C_{35}-sesquarterpenoids, which may be functionally similar to C_{30} hopanoids (Bosak et al., 2008; Takigawa et al., 2010; Sato et al., 2011; Sato, 2013). This process is initiated by YtpB, which generates tetraprenyl-β-curcumene, and then SqhC (a homolog of squalene-hopene cyclases) to generate the C_{35} tetracyclic product known as baciterpenol A (Sato, 2013). Although initially described in spores, and named "sporulenes" (Bosak et al., 2008), these sesquarterpenoids are found in vegetative cells (Takigawa et al., 2010). Finally, heptaprenyl-PP can be coupled to glycerol-1-phosphate by PcrB, and then further processed by an unidentified phosphatase and the YvoF acetyltranferase to generate an ether linked lipid of unknown function (Linde et al., 2016).

Lateral Heterogeneity and Functional Membrane Microdomains

In eukaryotes, cholesterol is associated with the generation of functional membrane microdomains (FMM), also called lipid rafts. These regions have relatively low membrane fluidity (a liquid-ordered, or Lo phase) and are associated with flotillins. *B. subtilis* also encodes flotillin homologs, regulated by σ^W (Huang et al., 1999; Wiegert et al., 2001). These proteins, subsequently renamed FloA and FloT, are implicated in FMM formation (**Figure 1A**). The notion of FMMs in bacteria received strong impetus from the finding that *yisP* mutants, lacking a putative squalene synthase, was defective in biofilm formation (Lopez and Kolter, 2010). Together with the finding of a punctate localization for FloT, and chemical inhibition studies with compounds that affect sterol synthesis, this led to the proposal that bacteria harbor FMMs (Bramkamp and Lopez, 2015; Wagner et al., 2017). However, subsequent work revealed that YisP is a farnesyl-PP phosphatase that generates farnesol (**Figure 1C**), rather than squalene (Feng et al., 2014). Moreover, farnesol itself complements the biofilm defect of the *yisP* mutant, suggesting that this long chain alcohol may have an ordering effect on FMMs provided in other systems by hopanoids or carotenoids (Bell and Chappell, 2014; Feng et al., 2014). *B. subtilis* FMMs are enriched in flotillins (FloA and FloT) and their associated signaling complexes, with FMM formation apparently stabilized by farnesol (YisP product). No role for the C_{35} isoprenoid lipids has yet been demonstrated in biofilm formation (Lopez and Kolter, 2010) or in FMM formation or function.

Lateral heterogeneity, including FMMs, is likely a feature of most bacterial membranes. However, the lipid species that are required to form FMMs are still poorly understood, but likely include carotenoids, hopanoids, and other polycyclic isoprenoid lipids (Lopez and Koch, 2017). Hopanoids are structurally diverse and fulfill a broad range of functions in bacterial membranes (Belin et al., 2018). The hopanoid diplopterol (**Figure 1C**) orders saturated lipids and glycolipids in the outer membrane of *Methylobacterium extorquens*, and deficient mutants are impaired in multidrug transport (Saenz et al., 2015). Hopanoids and other polycyclic isoprenoids are present in many Gram-positive bacteria as well, suggestive of a role in the plasma membrane. In methicillin-resistant *S. aureus*, the carotenoid staphyloxanthin (**Figure 1C**) colocalizes in FMMs with FloA, and disruption of these domains with isoprenoid synthesis inhibitors interferes with the function of the penicillin-binding protein required for β-lactam resistance (PBP2a) (Garcia-Fernandez et al., 2017; Foster, 2019). The formation and function of FMMs, in both the inner (plasma) and outer membrane, remains an important area for future research.

CELL ENVELOPE STRESS RESPONSES THAT MODULATE LIPID COMPOSITION

Bacteria generally have a negatively charged membrane, which contributes to their susceptibility to CAMPs, bacteriocins, and antimicrobials. In *B. subtilis*, membrane composition and properties are regulated by ECF σ factors (Eiamphungporn and Helmann, 2008; Kingston et al., 2013; Helmann, 2016). Because of their overlapping activation and promoter recognition properties, these CESRs are intertwined and referred to as an σ^{ECF} stress response (Mascher et al., 2007). In *B. subtilis*, activation of σ^X reduces the net negative charge of the membrane by increasing zwitterionic PE levels (Cao and Helmann, 2004; Ho and Ellermeier, 2019). The net negative charge of the cell wall can be further reduced by D-alanylation of teichoic acids, activated by σ^X (Cao and Helmann, 2004; Ho and Ellermeier, 2019) and σ^V, a lysozyme-responsive CESR (Guariglia-Oropeza and Helmann, 2011; Ho et al., 2011; Ho and Ellermeier, 2019). In *S. aureus*, surface membrane charge is modified by the induction of *mprF* by the GraRS TCS, thereby increasing LPG levels (Falord et al., 2011; Yang et al., 2012). In *B. anthracis*, the membrane-active compound targocil activates the EdsRS TCS, which induces expression of a cardiolipin synthase (Laut et al., 2020). Thus, many different stimuli can trigger changes in the membrane lipidome.

Bacillus subtilis σ^{ECF} factors also control other membrane-related functions, although the effects are not yet understood. For example, σ^M activates the *ytpAB* operon. The YtpA lysophospholipase cleaves FAs from the 2 position of phospholipids resulting in a lysophospholipid (bacilysocin) suggested to function as an antibiotic (Tamehiro et al., 2002). However, it is unclear if bacilysocin is ever released at levels sufficient to serve as an antibiotic, and it may instead modify membrane properties or be an intermediate in lipid remodeling. As noted above, YtpB initiates synthesis of baciterpenol (**Figure 1C**; Bosak et al., 2008; Sato et al., 2011; Sato, 2013). Genetic studies have revealed only modest phenotypes for *ytpAB* mutants, including effects on antibiotic sensitivity, sporulation, and germination (Kingston et al., 2014; Sayer et al., 2019). In the case of *ytpB*, the observed phenotype (bacitracin sensitivity) was due to the accumulation of the substrate (heptaprenyl-PP) rather than a loss of baciterpenol (Kingston et al., 2014).

Genetic perturbations of membrane composition can also trigger CESRs. For example, deletion of LTA synthases induces

σ^{ECF} factors. An *ltaS* mutation upregulates σ^{M}, which then activates expression of the alternate LTA synthase LtaSa. The absence of both *ltaS* and *ltaSa* leads to activation of additional σ^{ECF} factors (Hashimoto et al., 2013). The depletion of PhG, a building block of LTA, also activates σ^{M} and to a lesser extent σ^{V} (Hashimoto et al., 2009; Seki et al., 2019). The effects of mutations that affect glucolipids have been particularly challenging to understand. Glucolipids produced by UgtP are important membrane lipids and also serve as the lipid anchor of LTA. *ugtP* mutants lacking glucolipids are shorter and rounder, have abnormal localization of MreB, and altered assembly of FtsZ (Weart et al., 2007). Whether this abnormal morphology is due, in part, to the loss of glucolipids is unclear (Matsuoka, 2018). Mutation of *ugtP* activates a σ^{ECF} stress response and can be suppressed by production of monoglycosyldiacylglycerol (MGlcDG) using a heterologous synthase. Since this product does not function as an LTA anchor lipid, this suggests that it is the loss of glucolipids that induces the σ^{ECF} response (Matsuoka et al., 2016). The mechanistic basis for activation of σ^{ECF} factors in the absence of glucolipids is unclear, but at least for σ^{V} does not require intramembrane proteolysis of the anti-σ factor (Seki et al., 2019). One hypothesis is that glucolipids might regulate folding and function of intramembrane proteins (Matsuoka, 2018).

CELL ENVELOPE STRESS RESPONSES THAT FUNCTION THROUGH MEMBRANE PROTEINS

In addition to modulating lipid composition, CESRs also induce proteins that function in membrane protection and remodeling. In *B. subtilis*, these proteins include two flotillin homologs (FloA, FloT), two members of the phage shock protein family (LiaH, PspA), as well as antibiotic specific detoxification modules. The roles of these proteins in stabilizing and repairing the membrane are increasingly appreciated, although the precise mechanisms remain controversial.

Flotillins and Modulation of Membrane Fluidity

Flotillins are members of the widely conserved stomatin, prohibitin, flotillin, and HflK/C (SPFH) domain proteins. Flotillins localize to FMMs and are thought to be required for FMM function. In *S. aureus*, FloA colocalizes with staphyloxanthin in FMMs (Garcia-Fernandez et al., 2017; Foster, 2019). In other systems, flotillins and FMMs are associated with flagellar function and chemotaxis (Padilla-Vaca et al., 2019; Takekawa et al., 2019), type VII secretion (Mielich-Suss et al., 2017), signaling (Wagner et al., 2017), and interaction with the host during infection (Hutton et al., 2017). Ongoing efforts strive to track the mobility, oligomerization state, and interaction partners of flotillins in living cells.

Bacillus subtilis FloA and FloT are oligomeric, integral membrane proteins implicated in the formation of FMMs (Lopez and Kolter, 2010; Bach and Bramkamp, 2013; Bramkamp and Lopez, 2015; Lopez and Koch, 2017), and regulated by σ^{W} (Huang et al., 1999; Cao et al., 2002a). FloA and FloT are thought to help partition the membrane into low fluidity FMM regions that are spatially distinct from more fluid regions. A direct role for flotillins in FMM formation has been challenged, however, since *B. subtilis* FloA and FloT do not always colocalize, and form separated foci of ∼100 nm in diameter that appear spatially distinct from FMMs (Dempwolff et al., 2016). Counter-intuitively, flotillins appear to be required for regions of increased fluidity (RIFs), which are the counterpart to the FMMs. A lack of flotillins leads to a decrease in membrane fluidity and a concomitant reduction in activity of the MreB-directed elongasome complex that synthesizes peptidoglycan. This loss of membrane fluidity can be chemically complemented with fluidizing agents such as benzoyl alcohol (Zielinska et al., 2020).

Flotillins also functionally interact with DynA, a constitutively expressed dynamin homolog (Dempwolff et al., 2012; Dempwolff and Graumann, 2014). Dynamins are membrane-associated GTPases implicated in membrane remodeling, fusion and fission, and lipid mixing (Guo and Bramkamp, 2019). DynA may help repair damaged membrane regions, and contribute to resistance against antibiotics that bind membrane components, including nisin, bacitracin, and daptomycin (Sawant et al., 2016). Our understanding of flotillins and dynamins, and their roles in bacterial physiology is still incomplete and rapidly evolving.

Phage-Shock Proteins Protect Membrane Integrity

Cell envelope stress responses also support membrane stability through induction of PspA proteins, including two paralogs in *B. subtilis*: PspA an LiaH. Originally defined as part of the phage-shock protein response in *Escherichia coli* (Kobayashi et al., 2007; Flores-Kim and Darwin, 2016), PspA proteins comprise a conserved family including the vesicle-inducing protein in plastids (VIPP1/IM30) and mammalian ESCRT III (Thurotte et al., 2017; Liu et al., 2020). PspA proteins have a conserved N-terminal amphipathic helix required for membrane binding (McDonald et al., 2015, 2017), which seems to depend on anionic lipid content and regions with unfavorable packing geometries creating stored curvature elastic stress (McDonald et al., 2015). Structural studies reveal that VIPP1 forms oligomeric rings of various symmetries that stack together to form domes (Saur et al., 2017; Gupta et al., 2020). These rings are dynamic, and are thought to stabilize membranes during budding, tubulation, and fusion (Thurotte et al., 2017; Gutu et al., 2018; Junglas and Schneider, 2018). However, the role of these oligomeric structures has been questioned (Siebenaller et al., 2019). An alternative model suggests that these rings dissociate, and the resultant intrinsically disordered monomers interact with the membrane surface to form a protective protein "carpet" to stabilize the membrane and suppress proton leakage (Junglas et al., 2020).

Although PspA proteins are assumed to function in membrane protection and repair, their regulation differs markedly (Manganelli and Gennaro, 2017). *B. subtilis* PspA is regulated by σ^{W} (Wiegert et al., 2001; Cao et al., 2002a), whereas the paralog LiaH is regulated by the LiaRS TCS (Mascher et al., 2004; Jordan et al., 2006). Both paralogs

localize to the membrane in response to stress and protect against membrane-damaging antibiotics (Wolf et al., 2010; Kingston et al., 2013; Dominguez-Escobar et al., 2014; Popp et al., 2020). In the case of LiaH, membrane association is mediated by interaction with the integral membrane protein LiaI (Dominguez-Escobar et al., 2014). LiaH may also protect the membrane against proton leakage during the export of proteins through the twin-arginine translocation (TAT) system (Hou et al., 2018; Bernal-Cabas et al., 2020). While the *B. subtilis* LiaRS regulon is rather limited in scope (Jordan et al., 2006; Wolf et al., 2010), LiaRS orthologs (e.g., *S. aureus* VraRS) play an important role in stress resistance in many Gram-positive pathogens, and mutations in these regulators are associated with clinical antibiotic resistance (Tran et al., 2016). In *Mycobacterium tuberculosis*, the PspA ortholog is also under control of the ECF σ factor σ^E (Datta et al., 2015), whereas *E. coli pspA* requires the σ^{54} RNAP and PspF activator (Joly et al., 2010; Flores-Kim and Darwin, 2016). A common theme in these systems is that PspA-like proteins are often regulated by a specific CESR; they can accumulate to high levels in stressed cells, and they seem to protect the membrane against disruptions that can dissipate the proton gradient (Manganelli and Gennaro, 2017).

Antibiotic Specific Detoxification Modules

Bacillus subtilis, like many soil bacteria, can synthesize a wide range of antimicrobial compounds and also encodes diverse resistance mechanisms (Stein, 2005; Caulier et al., 2019). Many antimicrobial peptides induce the *B. subtilis* LiaRS stress response that protects cells through induction of LiaH. Induction of σ^W also leads to expression of the SppA membrane-localized protease and its regulatory protein SppI, which function to clear the membrane of embedded peptides to protect against lantibiotics (Kingston et al., 2013; Henriques et al., 2020). Other antimicrobial peptides induce specific detoxification machinery, often including ABC transporters that either export the peptide antibiotic or disassemble membrane-bound peptide complexes (Staron et al., 2011; Dintner et al., 2014).

A prototype for such systems is the BceRS TCS, which regulates the bacitracin-specific induction of the BceAB ABC transporter (Radeck et al., 2016; Piepenbreier et al., 2020). Bacitracin is a peptide antibiotic made by *Bacillus* spp. that inhibits cell wall synthesis by binding to undecaprenyl-PP. The BceAB system appears to act in disassembly of bacitracin complexes to confer resistance (Kobras et al., 2020). In addition, BceAB interacts with the BceRS TCS to allow sensing of bacitracin (Ohki et al., 2003; Dintner et al., 2014; Fritz et al., 2015; Koh et al., 2020). The BceRS-AB system provides a first line of defense against bacitracin, with higher levels of antibiotic activating the protective responses mediated by the LiaRS and σ^{ECF} regulons (Radeck et al., 2016). The detailed study of the *B. subtilis* bacitracin stress response has provided lessons relevant to the understanding of other antibiotic detoxification modules. Similar genetic modules, encoding both TCS and ABC transporter/sensors have been described for several other antimicrobial peptides (Revilla-Guarinos et al., 2014). Since induction can be quite specific, these systems provide a basis for antibiotic-inducible gene expression systems (Wolf and Mascher, 2016).

Bacillus subtilis also encodes and responds to many other secondary metabolites that can induce membrane stress (Caulier et al., 2019). For example, the toxic peptide YydF* is encoded by the *yydFGHIJ* operon, together with a radical-SAM epimerase (YydG), protease (YydH), and ABC transporter (YydIJ). Transposon insertions in the presumptive efflux pump lead to the upregulation of the LiaRS stress system (Butcher et al., 2007). Subsequent studies revealed that YydF is post-translationally processed to convert two L-amino acids to D-amino acids (Benjdia et al., 2017). The resulting epipeptide, YydF*, induces LiaRS-regulated LiaH and the FloT flotillin (Popp et al., 2020). The modified YydF* peptide kills *B. subtilis* cells by dissipating the membrane potential via membrane permeabilization. The associated concomitant decrease in membrane fluidity together with increased membrane permeabilization induces *liaIH* (Popp et al., 2020). YydF* peptides are likely synthesized by a variety of Gram-positive organisms including *Enterococcus*, *Staphylococcus*, and *Streptococcus* spp. as well as members of the human microbiome (Benjdia et al., 2017).

Bacillus subtilis also has CESRs induced by polyketide and polyene-type antimicrobials. For example, *Streptomyces* spp. produce linear polyketides (linearmycins) that depolarize the membrane (Stubbendieck and Straight, 2015, 2017; Stubbendieck et al., 2018). Linearmycins strongly activate the LnrJK TCS that regulates an ABC transporter, LnrLMN (Stubbendieck and Straight, 2017; Revilla-Guarinos et al., 2020). This ABC transporter also provides resistance against other polyenes, including the anti-fungal amphotericin (Revilla-Guarinos et al., 2020).

OUTLOOK

Here we provide a brief overview of the diverse ways in which CESRs help modify and protect the membrane in response to environmental threats (**Table 1**). This is a rapidly evolving field, and the impact of membrane composition on cell physiology is still mysterious. We have much to learn about the synthesis and roles of minor lipids (sesquarterpenes, ether lipids, lysophospholipids). There is a growing need to reconcile current models of lipid rafts, and the role that isoprenoid lipids and flotillins play in their formation. The activities of the VIPP1/IM30/PspA family of proteins in membrane repair and protection, and in particular the specific role of different oligomeric states, are still debated. Finally, the mechanisms by which diverse CESRs sense membrane perturbations are largely unknown, although considerable progress has been made in the specific cases of the DesK sensor kinase (Abriata et al., 2017), flux-sensing by peptide detoxification modules (Koh et al., 2020), and the lysozyme-mediated induction of the σ^V protein (Ho and Ellermeier, 2019). The overall picture is of the cell membrane as a complex and adaptable assemblage of many different lipid and protein species that still has many secrets to reveal.

AUTHOR CONTRIBUTIONS

Both authors listed have made a substantial, direct and intellectual contribution to the work, and approved it for publication.

FUNDING

This work was funded by the National Institutes of Health under award number R35GM122461 to JH. The content is solely the responsibility of the authors and does not necessarily represent the official views of the National Institutes of Health.

ACKNOWLEDGMENTS

We appreciate helpful comments from our Cornell colleagues, Thorsten Mascher, James Saenz, and Diego de Mendoza.

REFERENCES

Abriata, L. A., Albanesi, D., Dal Peraro, M., and de Mendoza, D. (2017). Signal sensing and transduction by histidine kinases as unveiled through studies on a temperature sensor. *Acc. Chem. Res.* 50, 1359–1366. doi: 10.1021/acs.accounts.6b00593

Albanesi, D., Reh, G., Guerin, M. E., Schaeffer, F., Debarbouille, M., Buschiazzo, A., et al. (2013). Structural basis for feed-forward transcriptional regulation of membrane lipid homeostasis in *Staphylococcus aureus*. *PLoS Pathog.* 9:e1003108. doi: 10.1371/journal.ppat.1003108

Altabe, S. G., Aguilar, P., Caballero, G. M., and de Mendoza, D. (2003). The *Bacillus subtilis* acyl lipid desaturase is a delta5 desaturase. *J. Bacteriol.* 185, 3228–3231. doi: 10.1128/jb.185.10.3228-3231.2003

Bach, J. N., and Bramkamp, M. (2013). Flotillins functionally organize the bacterial membrane. *Mol. Microbiol.* 88, 1205–1217. doi: 10.1111/mmi.12252

Belin, B. J., Busset, N., Giraud, E., Molinaro, A., Silipo, A., and Newman, D. K. (2018). Hopanoid lipids: from membranes to plant-bacteria interactions. *Nat. Rev. Microbiol.* 16, 304–315. doi: 10.1038/nrmicro.2017.173

Bell, S. A., and Chappell, J. (2014). Now playing: farnesol in the biofilm. *Chem. Biol.* 21, 1421–1422. doi: 10.1016/j.chembiol.2014.11.001

Benjdia, A., Guillot, A., Ruffie, P., Leprince, J., and Berteau, O. (2017). Post-translational modification of ribosomally synthesized peptides by a radical SAM epimerase in *Bacillus subtilis*. *Nat. Chem.* 9, 698–707. doi: 10.1038/nchem.2714

Beranova, J., Jemiola-Rzeminska, M., Elhottova, D., Strzalka, K., and Konopasek, I. (2008). Metabolic control of the membrane fluidity in *Bacillus subtilis* during cold adaptation. *Biochim. Biophys. Acta* 1778, 445–453. doi: 10.1016/j.bbamem.2007.11.012

Bernal-Cabas, M., Miethke, M., Antelo-Varela, M., Aguilar Suarez, R., Neef, J., Schon, L., et al. (2020). Functional association of the stress-responsive LiaH protein and the minimal TatAyCy protein translocase in *Bacillus subtilis*. *Biochim. Biophys. Acta Mol. Cell Res.* 1867:118719. doi: 10.1016/j.bbamcr.2020.118719

Bosak, T., Losick, R. M., and Pearson, A. (2008). A polycyclic terpenoid that alleviates oxidative stress. *Proc. Natl. Acad. Sci. U.S.A.* 105, 6725–6729. doi: 10.1073/pnas.0800199105

Bramkamp, M., and Lopez, D. (2015). Exploring the existence of lipid rafts in bacteria. *Microbiol. Mol. Biol. Rev.* 79, 81–100. doi: 10.1128/mmbr.00036-14

Butcher, B. G., and Helmann, J. D. (2006). Identification of *Bacillus subtilis* σ^W-dependent genes that provide intrinsic resistance to antimicrobial compounds produced by Bacilli. *Mol. Microbiol.* 60, 765–782. doi: 10.1111/j.1365-2958.2006.05131.x

Butcher, B. G., Lin, Y. P., and Helmann, J. D. (2007). The *yydFGHIJ* operon of *Bacillus subtilis* encodes a peptide that induces the LiaRS two-component system. *J. Bacteriol.* 189, 8616–8625. doi: 10.1128/jb.01181-07

Cao, M., and Helmann, J. D. (2004). The *Bacillus subtilis* extracytoplasmic-function σ^X factor regulates modification of the cell envelope and resistance to cationic antimicrobial peptides. *J. Bacteriol.* 186, 1136–1146. doi: 10.1128/jb.186.4.1136-1146.2004

Cao, M., Kobel, P. A., Morshedi, M. M., Wu, M. F., Paddon, C., and Helmann, J. D. (2002a). Defining the *Bacillus subtilis* σ^W regulon: a comparative analysis of promoter consensus search, run-off transcription/macroarray analysis (ROMA), and transcriptional profiling approaches. *J. Mol. Biol.* 316, 443–457. doi: 10.1006/jmbi.2001.5372

Cao, M., Wang, T., Ye, R., and Helmann, J. D. (2002b). Antibiotics that inhibit cell wall biosynthesis induce expression of the *Bacillus subtilis* σ^W and σ^M regulons. *Mol. Microbiol.* 45, 1267–1276. doi: 10.1046/j.1365-2958.2002.03050.x

Caulier, S., Nannan, C., Gillis, A., Licciardi, F., Bragard, C., and Mahillon, J. (2019). Overview of the Antimicrobial Compounds Produced by Members of the *Bacillus subtilis* Group. *Front. Microbiol.* 10:302.

Choi, K. H., Heath, R. J., and Rock, C. O. (2000). beta-ketoacyl-acyl carrier protein synthase III (FabH) is a determining factor in branched-chain fatty acid biosynthesis. *J. Bacteriol.* 182, 365–370. doi: 10.1128/jb.182.2.365-370.2000

Chwastek, G., Surma, M. A., Rizk, S., Grosser, D., Lavrynenko, O., Rucinska, M., et al. (2020). Principles of membrane adaptation revealed through environmentally induced bacterial lipidome remodeling. *Cell Rep.* 32:108165. doi: 10.1016/j.celrep.2020.108165

Datta, P., Ravi, J., Guerrini, V., Chauhan, R., Neiditch, M. B., Shell, S. S., et al. (2015). The Psp system of *Mycobacterium tuberculosis* integrates envelope stress-sensing and envelope-preserving functions. *Mol. Microbiol.* 97, 408–422. doi: 10.1111/mmi.13037

de Mendoza, D. (2014). Temperature sensing by membranes. *Annu. Rev. Microbiol.* 68, 101–116. doi: 10.1146/annurev-micro-091313-103612

Dempwolff, F., and Graumann, P. L. (2014). Genetic links between bacterial dynamin and flotillin proteins. *Commun. Integr. Biol.* 7:e970972. doi: 10.4161/cib.29578

Dempwolff, F., Schmidt, F. K., Hervas, A. B., Stroh, A., Rosch, T. C., Riese, C. N., et al. (2016). Super resolution fluorescence microscopy and tracking of bacterial flotillin (Reggie) paralogs provide evidence for defined-sized protein microdomains within the bacterial membrane but absence of clusters containing detergent-resistant proteins. *PLoS Genet.* 12:e1006116. doi: 10.1371/journal.pgen.1006116

Dempwolff, F., Wischhusen, H. M., Specht, M., and Graumann, P. L. (2012). The deletion of bacterial dynamin and flotillin genes results in pleiotrophic effects on cell division, cell growth and in cell shape maintenance. *BMC Microbiol.* 12:298. doi: 10.1186/1471-2180-12-298

Devkota, S. R., Kwon, E., Ha, S. C., Chang, H. W., and Kim, D. Y. (2017). Structural insights into the regulation of *Bacillus subtilis* σ^W activity by anti-sigma RsiW. *PLoS One* 12:e0174284. doi: 10.1371/journal.pone.0174284

Dintner, S., Heermann, R., Fang, C., Jung, K., and Gebhard, S. (2014). A sensory complex consisting of an ATP-binding cassette transporter and a two-component regulatory system controls bacitracin resistance in *Bacillus subtilis*. *J. Biol. Chem.* 289, 27899–27910. doi: 10.1074/jbc.m114.596221

Dominguez-Escobar, J., Wolf, D., Fritz, G., Hofler, C., Wedlich-Soldner, R., and Mascher, T. (2014). Subcellular localization, interactions and dynamics of the phage-shock protein-like Lia response in *Bacillus subtilis*. *Mol. Microbiol.* 92, 716–732. doi: 10.1111/mmi.12586

Dowhan, W., Vitrac, H., and Bogdanov, M. (2019). Lipid-assisted membrane protein folding and topogenesis. *Protein J.* 38, 274–288. doi: 10.1007/s10930-019-09826-7

Eiamphungporn, W., and Helmann, J. D. (2008). The *Bacillus subtilis* σ^M regulon and its contribution to cell envelope stress responses. *Mol. Microbiol.* 67, 830–848. doi: 10.1111/j.1365-2958.2007.06090.x

Ellermeier, C. D., and Losick, R. (2006). Evidence for a novel protease governing regulated intramembrane proteolysis and resistance to antimicrobial peptides in *Bacillus subtilis*. *Genes Dev.* 20, 1911–1922. doi: 10.1101/gad.1440606

Ernst, C. M., and Peschel, A. (2019). MprF-mediated daptomycin resistance. *Int. J. Med. Microbiol.* 309, 359–363. doi: 10.1016/j.ijmm.2019.05.010

Ernst, C. M., Slavetinsky, C. J., Kuhn, S., Hauser, J. N., Nega, M., Mishra, N. N., et al. (2018). Gain-of-function mutations in the phospholipid flippase MprF confer specific daptomycin resistance. *mBio* 9:e01659-18.

Ernst, R., Ejsing, C. S., and Antonny, B. (2016). Homeoviscous adaptation and the regulation of membrane lipids. *J. Mol. Biol.* 428, 4776–4791. doi: 10.1016/j.jmb.2016.08.013

Falord, M., Mader, U., Hiron, A., Debarbouille, M., and Msadek, T. (2011). Investigation of the *Staphylococcus aureus* GraSR regulon reveals novel links to virulence, stress response and cell wall signal transduction pathways. *PLoS One* 6:e21323. doi: 10.1371/journal.pone.0021323

Feng, X., Hu, Y., Zheng, Y., Zhu, W., Li, K., Huang, C. H., et al. (2014). Structural and functional analysis of *Bacillus subtilis* YisP reveals a role of its product in biofilm production. *Chem. Biol.* 21, 1557–1563. doi: 10.1016/j.chembiol.2014.08.018

Fernandez, P., Porrini, L., Albanesi, D., Abriata, L. A., Dal Peraro, M., de Mendoza, D., et al. (2019). Transmembrane prolines mediate signal sensing and decoding in *Bacillus subtilis* DesK histidine kinase. *mBio* 10:e02564-19.

Flores-Kim, J., and Darwin, A. J. (2016). The phage shock protein response. *Annu. Rev. Microbiol.* 70, 83–101. doi: 10.1146/annurev-micro-102215-095359

Foster, T. J. (2019). Can beta-lactam antibiotics be resurrected to combat MRSA? *Trends Microbiol.* 27, 26–38. doi: 10.1016/j.tim.2018.06.005

Fritz, G., Dintner, S., Treichel, N. S., Radeck, J., Gerland, U., Mascher, T., et al. (2015). A New way of sensing: need-based activation of antibiotic resistance by a flux-sensing mechanism. *mBio* 6: e00975.

Fujita, Y., Matsuoka, H., and Hirooka, K. (2007). Regulation of fatty acid metabolism in bacteria. *Mol. Microbiol.* 66, 829–839. doi: 10.1111/j.1365-2958.2007.05947.x

Garcia-Fernandez, E., Koch, G., Wagner, R. M., Fekete, A., Stengel, S. T., Schneider, J., et al. (2017). Membrane microdomain disassembly inhibits MRSA antibiotic resistance. *Cell* 171, 1354–1367.e1320.

Guariglia-Oropeza, V., and Helmann, J. D. (2011). *Bacillus subtilis* σ^V confers lysozyme resistance by activation of two cell wall modification pathways, peptidoglycan O-acetylation and D-alanylation of teichoic acids. *J. Bacteriol.* 193, 6223–6232. doi: 10.1128/jb.06023-11

Guo, L., and Bramkamp, M. (2019). Bacterial dynamin-like protein DynA mediates lipid and content mixing. *FASEB J.* 33, 11746–11757. doi: 10.1096/fj.201900844rr

Gupta, T. K., Klumpe, S., Gries, K., Heinz, S., Wietrzynski, W., Ohnishi, N., et al. (2020). Structural basis for VIPP1 oligomerization and maintenance of thylakoid membrane integrity. *BioRxiv* [Preprint]. doi: 10.1101/2020.08.11.243204

Gutu, A., Chang, F., and O'Shea, E. K. (2018). Dynamical localization of a thylakoid membrane binding protein is required for acquisition of photosynthetic competency. *Mol. Microbiol.* 108, 16–31. doi: 10.1111/mmi.13912

Hachmann, A. B., Angert, E. R., and Helmann, J. D. (2009). Genetic analysis of factors affecting susceptibility of *Bacillus subtilis* to daptomycin. *Antimicrob. Agents Chemother.* 53, 1598–1609. doi: 10.1128/aac.01329-08

Hachmann, A. B., Sevim, E., Gaballa, A., Popham, D. L., Antelmann, H., and Helmann, J. D. (2011). Reduction in membrane phosphatidylglycerol content leads to daptomycin resistance in *Bacillus subtilis*. *Antimicrob. Agents Chemother.* 55, 4326–4337. doi: 10.1128/aac.01819-10

Hashimoto, M., Seki, T., Matsuoka, S., Hara, H., Asai, K., Sadaie, Y., et al. (2013). Induction of extracytoplasmic function sigma factors in *Bacillus subtilis* cells with defects in lipoteichoic acid synthesis. *Microbiology (Reading)* 159, 23–35. doi: 10.1099/mic.0.063420-0

Hashimoto, M., Takahashi, H., Hara, Y., Hara, H., Asai, K., Sadaie, Y., et al. (2009). Induction of extracytoplasmic function sigma factors in *Bacillus subtilis* cells with membranes of reduced phosphatidylglycerol content. *Genes Genet. Syst.* 84, 191–198. doi: 10.1266/ggs.84.191

Helmann, J. D. (2006). Deciphering a complex genetic regulatory network: the *Bacillus subtilis* σ^W protein and intrinsic resistance to antimicrobial compounds. *Sci. Prog.* 89, 243–266. doi: 10.3184/003685006783238290

Helmann, J. D. (2016). *Bacillus subtilis* extracytoplasmic function (ECF) sigma factors and defense of the cell envelope. *Curr. Opin. Microbiol.* 30, 122–132. doi: 10.1016/j.mib.2016.02.002

Henriques, G., McGovern, S., Neef, J., Antelo-Varela, M., Gotz, F., Otto, A., et al. (2020). SppI forms a membrane protein complex with sppa and inhibits its protease activity in *Bacillus subtilis*. *mSphere* 5:e00724-20.

Ho, T. D., and Ellermeier, C. D. (2019). Activation of the extracytoplasmic function sigma factor σ^V by lysozyme. *Mol. Microbiol.* 112, 410–419. doi: 10.1111/mmi.14348

Ho, T. D., Hastie, J. L., Intile, P. J., and Ellermeier, C. D. (2011). The *Bacillus subtilis* extracytoplasmic function sigma factor σ^V is induced by lysozyme and provides resistance to lysozyme. *J. Bacteriol.* 193, 6215–6222. doi: 10.1128/jb.05467-11

Hofler, C., Heckmann, J., Fritsch, A., Popp, P., Gebhard, S., Fritz, G., et al. (2016). Cannibalism stress response in *Bacillus subtilis*. *Microbiology (Reading)* 162, 164–176. doi: 10.1099/mic.0.000176

Hou, B., Heidrich, E. S., Mehner-Breitfeld, D., and Bruser, T. (2018). The TatA component of the twin-arginine translocation system locally weakens the cytoplasmic membrane of *Escherichia coli* upon protein substrate binding. *J. Biol. Chem.* 293, 7592–7605. doi: 10.1074/jbc.ra118.002205

Huang, X., Gaballa, A., Cao, M., and Helmann, J. D. (1999). Identification of target promoters for the *Bacillus subtilis* extracytoplasmic function sigma factor, σ^W. *Mol. Microbiol.* 31, 361–371. doi: 10.1046/j.1365-2958.1999.01180.x

Hutton, M. L., D'Costa, K., Rossiter, A. E., Wang, L., Turner, L., Steer, D. L., et al. (2017). A *Helicobacter pylori* homolog of eukaryotic flotillin is involved in cholesterol accumulation, epithelial cell responses and host colonization. *Front. Cell Infect. Microbiol.* 7:219.

Jolliffe, L. K., Doyle, R. J., and Streips, U. N. (1981). The energized membrane and cellular autolysis in *Bacillus subtilis*. *Cell* 25, 753–763. doi: 10.1016/0092-8674(81)90183-5

Joly, N., Engl, C., Jovanovic, G., Huvet, M., Toni, T., Sheng, X., et al. (2010). Managing membrane stress: the phage shock protein (Psp) response, from molecular mechanisms to physiology. *FEMS Microbiol. Rev.* 34, 797–827. doi: 10.1111/j.1574-6976.2010.00240.x

Jordan, S., Junker, A., Helmann, J. D., and Mascher, T. (2006). Regulation of LiaRS-dependent gene expression in *Bacillus subtilis*: identification of inhibitor proteins, regulator binding sites, and target genes of a conserved cell envelope stress-sensing two-component system. *J. Bacteriol.* 188, 5153–5166. doi: 10.1128/jb.00310-06

Junglas, B., and Schneider, D. (2018). What is Vipp1 good for? *Mol. Microbiol.* 108, 1–5. doi: 10.1111/mmi.13924

Junglas, B., Orru, R., Axt, A., Siebenaller, C., Steinchen, W., Heidrich, J., et al. (2020). IM30 IDPs form a membrane-protective carpet upon super-complex disassembly. *Commun. Biol.* 3:595.

Kingston, A. W., Liao, X., and Helmann, J. D. (2013). Contributions of the σ^W, σ^M and σ^X regulons to the lantibiotic resistome of *Bacillus subtilis*. *Mol. Microbiol.* 90, 502–518. doi: 10.1111/mmi.12380

Kingston, A. W., Subramanian, C., Rock, C. O., and Helmann, J. D. (2011). A σ^W-dependent stress response in *Bacillus subtilis* that reduces membrane fluidity. *Mol. Microbiol.* 81, 69–79. doi: 10.1111/j.1365-2958.2011.07679.x

Kingston, A. W., Zhao, H., Cook, G. M., and Helmann, J. D. (2014). Accumulation of heptaprenyl diphosphate sensitizes *Bacillus subtilis* to bacitracin: implications for the mechanism of resistance mediated by the BceAB transporter. *Mol. Microbiol.* 93, 37–49. doi: 10.1111/mmi.12637

Kobayashi, R., Suzuki, T., and Yoshida, M. (2007). *Escherichia coli* phage-shock protein A (PspA) binds to membrane phospholipids and repairs proton leakage of the damaged membranes. *Mol. Microbiol.* 66, 100–109. doi: 10.1111/j.1365-2958.2007.05893.x

Kobras, C. M., Piepenbreier, H., Emenegger, J., Sim, A., Fritz, G., and Gebhard, S. (2020). BceAB-type antibiotic resistance transporters appear to act by target protection of cell wall synthesis. *Antimicrob. Agents Chemother.* 64:e02241-19.

Koh, A., Gibbon, M. J., Van der Kamp, M. W., Pudney, C. R., and Gebhard, S. (2020). Conformation control of the histidine kinase BceS of *Bacillus subtilis* by its cognate ABC-transporter facilitates need-based activation of antibiotic resistance. *Mol. Microbiol.* 115, 157–174. doi: 10.1111/mmi.14607

Lamsa, A., Liu, W. T., Dorrestein, P. C., and Pogliano, K. (2012). The *Bacillus subtilis* cannibalism toxin SDP collapses the proton motive force and induces autolysis. *Mol. Microbiol.* 84, 486–500. doi: 10.1111/j.1365-2958.2012.08038.x

Laut, C. L., Perry, W. J., Metzger, A. L., Weiss, A., Stauff, D. L., Walker, S., et al. (2020). *Bacillus anthracis* responds to targocil-induced envelope damage through EdsRS activation of cardiolipin synthesis. *mBio* 11:e03375-19.

Linde, M., Peterhoff, D., Sterner, R., and Babinger, P. (2016). Identification and characterization of heptaprenylglyceryl phosphate processing enzymes in *Bacillus subtilis*. *J. Biol. Chem.* 291, 14861–14870. doi: 10.1074/jbc.m115.711994

Liu, J., Tassinari, M., Souza, D. P., Naskar, S., Noel, J. K., Bohuszewicz, O., et al. (2020). Bacterial Vipp1 and PspA are members of the ancient ESCRT-III membrane-remodelling superfamily. *bioRxiv* [Preprint]. doi: 10.1101/2020.08.13.249979

Lopez, D., and Koch, G. (2017). Exploring functional membrane microdomains in bacteria: an overview. *Curr. Opin .Microbiol.* 36, 76–84. doi: 10.1016/j.mib.2017.02.001

Lopez, D., and Kolter, R. (2010). Functional microdomains in bacterial membranes. *Genes Dev.* 24, 1893–1902. doi: 10.1101/gad.1945010

Machinandiarena, F., Nakamatsu, L., Schujman, G. E., de Mendoza, D., and Albanesi, D. (2020). Revisiting the coupling of fatty acid to phospholipid synthesis in bacteria with FapR regulation. *Mol. Microbiol.* 114:14574.

Manganelli, R., and Gennaro, M. L. (2017). Protecting from envelope stress: variations on the phage-shock-protein theme. *Trends Microbiol.* 25, 205–216. doi: 10.1016/j.tim.2016.10.001

Martinez, M. A., Zaballa, M. E., Schaeffer, F., Bellinzoni, M., Albanesi, D., Schujman, G. E., et al. (2010). A novel role of malonyl-ACP in lipid homeostasis. *Biochemistry* 49, 3161–3167. doi: 10.1021/bi100136n

Mascher, T., Hachmann, A. B., and Helmann, J. D. (2007). Regulatory overlap and functional redundancy among *Bacillus subtilis* extracytoplasmic function sigma factors. *J. Bacteriol.* 189, 6919–6927. doi: 10.1128/jb.00904-07

Mascher, T., Zimmer, S. L., Smith, T. A., and Helmann, J. D. (2004). Antibiotic-inducible promoter regulated by the cell envelope stress-sensing two-component system LiaRS of *Bacillus subtilis*. *Antimicrob. Agents Chemother.* 48, 2888–2896. doi: 10.1128/aac.48.8.2888-2896.2004

Matsuoka, S. (2018). Biological functions of glucolipids in *Bacillus subtilis*. *Genes Genet. Syst.* 92, 217–221. doi: 10.1266/ggs.17-00017

Matsuoka, S., Seki, T., Matsumoto, K., and Hara, H. (2016). Suppression of abnormal morphology and extracytoplasmic function sigma activity in *Bacillus subtilis ugtP* mutant cells by expression of heterologous glucolipid synthases from *Acholeplasma laidlawii*. *Biosci. Biotechnol. Biochem.* 80, 2325–2333. doi: 10.1080/09168451.2016.1217147

McDonald, C., Jovanovic, G., Ces, O., and Buck, M. (2015). Membrane stored curvature elastic stress modulates recruitment of maintenance proteins PspA and Vipp1. *mBio* 6:e001188-15.

McDonald, C., Jovanovic, G., Wallace, B. A., Ces, O., and Buck, M. (2017). Structure and function of PspA and Vipp1 N-terminal peptides: insights into the membrane stress sensing and mitigation. *Biochim. Biophys. Acta Biomembr.* 1859, 28–39. doi: 10.1016/j.bbamem.2016.10.018

Mielich-Suss, B., Wagner, R. M., Mietrach, N., Hertlein, T., Marincola, G., Ohlsen, K., et al. (2017). Flotillin scaffold activity contributes to type VII secretion system assembly in *Staphylococcus aureus*. *PLoS Pathog.* 13:e1006728. doi: 10.1371/journal.ppat.1006728

Mitchell, A. M., and Silhavy, T. J. (2019). Envelope stress responses: balancing damage repair and toxicity. *Nat. Rev. Microbiol.* 17, 417–428. doi: 10.1038/s41579-019-0199-0

Muller, M., Reiss, S., Schluter, R., Mader, U., Beyer, A., Reiss, W., et al. (2014). Deletion of membrane-associated Asp23 leads to upregulation of cell wall stress genes in *Staphylococcus aureus*. *Mol. Microbiol.* 93, 1259–1268.

Nickels, J. D., Chatterjee, S., Mostofian, B., Stanley, C. B., Ohl, M., Zolnierczuk, P., et al. (2017). *Bacillus subtilis* lipid extract, a branched-chain fatty acid model membrane. *J. Phys. Chem. Lett.* 8, 4214–4217.

Nickels, J. D., Poudel, S., Chatterjee, S., Farmer, A., Cordner, D., Campagna, S. R., et al. (2020). Impact of fatty-acid labeling of *Bacillus subtilis* membranes on the cellular lipidome and proteome. *Front. Microbiol.* 11:914.

Ohki, R., Giyanto, K. T., Masuyama, W., Moriya, S., Kobayashi, K., and Ogasawara, N. (2003). The BceRS two-component regulatory system induces expression of the bacitracin transporter, BceAB, in *Bacillus subtilis*. *Mol. Microbiol.* 49, 1135–1144. doi: 10.1046/j.1365-2958.2003.03653.x

Padilla-Vaca, F., Vargas-Maya, N. I., Elizarraras-Vargas, N. U., Rangel-Serrano, A., Cardoso-Reyes, L. R., Razo-Soria, T., et al. (2019). Flotillin homologue is involved in the swimming behavior of *Escherichia coli*. *Arch. Microbiol.* 201, 999–1008. doi: 10.1007/s00203-019-01670-8

Pan, J. J., Solbiati, J. O., Ramamoorthy, G., Hillerich, B. S., Seidel, R. D., Cronan, J. E., et al. (2015). Biosynthesis of squalene from farnesyl diphosphate in bacteria: three steps catalyzed by three enzymes. *ACS Cent. Sci.* 1, 77–82. doi: 10.1021/acscentsci.5b00115

Parsons, J. B., and Rock, C. O. (2013). Bacterial lipids: metabolism and membrane homeostasis. *Prog. Lipid Res.* 52, 249–276. doi: 10.1016/j.plipres.2013.02.002

Peleg, A. Y., Miyakis, S., Ward, D. V., Earl, A. M., Rubio, A., Cameron, D. R., et al. (2012). Whole genome characterization of the mechanisms of daptomycin resistance in clinical and laboratory derived isolates of *Staphylococcus aureus*. *PLoS One* 7:e28316. doi: 10.1371/journal.pone.0028316

Petersen, I., Schluter, R., Hoff, K. J., Liebscher, V., Bange, G., Riedel, K., et al. (2020). Non-invasive and label-free 3D-visualization shows in vivo oligomerization of the staphylococcal alkaline shock protein 23 (Asp23). *Sci. Rep.* 10:125.

Piepenbreier, H., Sim, A., Kobras, C. M., Radeck, J., Mascher, T., Gebhard, S., et al. (2020). From modules to networks: a systems-level analysis of the bacitracin stress response in *Bacillus subtilis*. *mSystems* 5:e00687-19.

Pietiainen, M., Gardemeister, M., Mecklin, M., Leskela, S., Sarvas, M., and Kontinen, V. P. (2005). Cationic antimicrobial peptides elicit a complex stress response in *Bacillus subtilis* that involves ECF-type sigma factors and two-component signal transduction systems. *Microbiology (Reading)* 151, 1577–1592. doi: 10.1099/mic.0.27761-0

Popp, P. F., Benjdia, A., Strahl, H., Berteau, O., and Mascher, T. (2020). The epipeptide YydF intrinsically triggers the cell envelope stress response of *bacillus subtilis* and causes severe membrane perturbations. *Front. Microbiol.* 11:151.

Radeck, J., Fritz, G., and Mascher, T. (2017). The cell envelope stress response of *Bacillus subtilis*: from static signaling devices to dynamic regulatory network. *Curr. Genet.* 63, 79–90. doi: 10.1007/s00294-016-0624-0

Radeck, J., Gebhard, S., Orchard, P. S., Kirchner, M., Bauer, S., Mascher, T., et al. (2016). Anatomy of the bacitracin resistance network in *Bacillus subtilis*. *Mol. Microbiol.* 100, 607–620. doi: 10.1111/mmi.13336

Rajagopal, M., and Walker, S. (2017). Envelope structures of gram-positive bacteria. *Curr. Top. Microbiol. Immunol.* 404, 1–44. doi: 10.1007/82_2015_5021

Revilla-Guarinos, A., Durr, F., Popp, P. F., Doring, M., and Mascher, T. (2020). Amphotericin B specifically induces the two-component system LnrJK: development of a novel whole-cell biosensor for the detection of amphotericin-like polyenes. *Front. Microbiol.* 11:2022.

Revilla-Guarinos, A., Gebhard, S., Mascher, T., and Zuniga, M. (2014). Defence against antimicrobial peptides: different strategies in Firmicutes. *Environ. Microbiol.* 16, 1225–1237. doi: 10.1111/1462-2920.12400

Saenz, J. P., Grosser, D., Bradley, A. S., Lagny, T. J., Lavrynenko, O., Broda, M., et al. (2015). Hopanoids as functional analogues of cholesterol in bacterial membranes. *Proc. Natl. Acad. Sci. U.S.A.* 112, 11971–11976. doi: 10.1073/pnas.1515607112

Salie, M. J., and Thelen, J. J. (2016). Regulation and structure of the heteromeric acetyl-CoA carboxylase. *Biochim. Biophys. Acta* 1861, 1207–1213.

Salzberg, L. I., and Helmann, J. D. (2008). Phenotypic and transcriptomic characterization of *Bacillus subtilis* mutants with grossly altered membrane composition. *J. Bacteriol.* 190, 7797–7807. doi: 10.1128/jb.00720-08

Sato, T. (2013). Unique biosynthesis of sesquarterpenes (C_{35} terpenes). *Biosci. Biotechnol. Biochem.* 77, 1155–1159. doi: 10.1271/bbb.130180

Sato, T., Yoshida, S., Hoshino, H., Tanno, M., Nakajima, M., and Hoshino, T. (2011). Sesquarterpenes (C_{35} terpenes) biosynthesized via the cyclization of a linear C_{35} isoprenoid by a tetraprenyl-beta-curcumene synthase and a tetraprenyl-beta-curcumene cyclase: identification of a new terpene cyclase. *J. Am. Chem. Soc.* 133, 9734–9737. doi: 10.1021/ja203779h

Saunders, L. P., Sen, S., Wilkinson, B. J., and Gatto, C. (2016). Insights into the mechanism of homeoviscous adaptation to low temperature in branched-chain fatty acid-containing bacteria through modeling FabH kinetics from the foodborne pathogen *Listeria monocytogenes*. *Front. Microbiol.* 7:1386.

Saur, M., Hennig, R., Young, P., Rusitzka, K., Hellmann, N., Heidrich, J., et al. (2017). A Janus-faced IM30 ring involved in thylakoid membrane fusion is assembled from IM30 tetramers. *Structure* 25, 1380–1390.e1385.

Sawant, P., Eissenberger, K., Karier, L., Mascher, T., and Bramkamp, M. (2016). A dynamin-like protein involved in bacterial cell membrane surveillance under environmental stress. *Environ. Microbiol.* 18, 2705–2720. doi: 10.1111/1462-2920.13110

Sayer, C. V., Barat, B., and Popham, D. L. (2019). Identification of L-Valine-initiated-germination-active genes in *Bacillus subtilis* using Tn-seq. *PLoS One* 14:e0218220. doi: 10.1371/journal.pone.0218220

Schobel, S., Zellmeier, S., Schumann, W., and Wiegert, T. (2004). The *Bacillus subtilis* σ^W anti-sigma factor RsiW is degraded by intramembrane proteolysis through YluC. *Mol. Microbiol.* 52, 1091–1105. doi: 10.1111/j.1365-2958.2004.04031.x

Scholz, R., Vater, J., Budiharjo, A., Wang, Z., He, Y., Dietel, K., et al. (2014). Amylocyclicin, a novel circular bacteriocin produced by *Bacillus amyloliquefaciens* FZB42. *J. Bacteriol.* 196, 1842–1852. doi: 10.1128/jb.01474-14

Schujman, G. E., Guerin, M., Buschiazzo, A., Schaeffer, F., Llarrull, L. I., Reh, G., et al. (2006). Structural basis of lipid biosynthesis regulation in Gram-positive bacteria. *EMBO J.* 25, 4074–4083. doi: 10.1038/sj.emboj.7601284

Schujman, G. E., Paoletti, L., Grossman, A. D., and de Mendoza, D. (2003). FapR, a bacterial transcription factor involved in global regulation of membrane lipid biosynthesis. *Dev. Cell* 4, 663–672. doi: 10.1016/s1534-5807(03)00123-0

Seki, T., Furumi, T., Hashimoto, M., Hara, H., and Matsuoka, S. (2019). Activation of extracytoplasmic function sigma factors upon removal of glucolipids and reduction of phosphatidylglycerol content in *Bacillus subtilis* cells lacking lipoteichoic acid. *Genes Genet. Syst.* 94, 71–80. doi: 10.1266/ggs.18-00046

Siebenaller, C., Junglas, B., and Schneider, D. (2019). Functional implications of multiple IM30 oligomeric states. *Front. Plant Sci.* 10:1500.

Sohlenkamp, C., and Geiger, O. (2016). Bacterial membrane lipids: diversity in structures and pathways. *FEMS Microbiol. Rev.* 40, 133–159. doi: 10.1093/femsre/fuv008

Staron, A., Finkeisen, D. E., and Mascher, T. (2011). Peptide antibiotic sensing and detoxification modules of *Bacillus subtilis*. *Antimicrob. Agents Chemother.* 55, 515–525. doi: 10.1128/aac.00352-10

Stein, T. (2005). *Bacillus subtilis* antibiotics: structures, syntheses and specific functions. *Mol. Microbiol.* 56, 845–857. doi: 10.1111/j.1365-2958.2005.04587.x

Stubbendieck, R. M., and Straight, P. D. (2015). Escape from lethal bacterial competition through coupled activation of antibiotic resistance and a mobilized subpopulation. *PLoS Genet.* 11:e1005722. doi: 10.1371/journal.pgen.1005722

Stubbendieck, R. M., and Straight, P. D. (2017). Linearmycins activate a two-component signaling system involved in bacterial competition and biofilm morphology. *J. Bacteriol.* 199:JB.00186-17.

Stubbendieck, R. M., Brock, D. J., Pellois, J. P., Gill, J. J., and Straight, P. D. (2018). Linearmycins are lytic membrane-targeting antibiotics. *J. Antibiot. (Tokyo)* 71, 372–381. doi: 10.1038/s41429-017-0005-z

Sumrall, E. T., Keller, A. P., Shen, Y., and Loessner, M. J. (2020). Structure and function of *Listeria* teichoic acids and their implications. *Mol. Microbiol.* 113, 627–637. doi: 10.1111/mmi.14472

Takekawa, N., Isumi, M., Terashima, H., Zhu, S., Nishino, Y., Sakuma, M., et al. (2019). Structure of *Vibrio* FliL, a new stomatin-like protein that assists the bacterial flagellar motor function. *mBio* 10:e00292-19.

Takigawa, H., Sugiyama, M., and Shibuya, Y. (2010). C_{35}-Terpenes from *Bacillus subtilis* KSM 6-10. *J. Nat. Prod.* 73, 204–207.

Tamehiro, N., Okamoto-Hosoya, Y., Okamoto, S., Ubukata, M., Hamada, M., Naganawa, H., et al. (2002). Bacilysocin, a novel phospholipid antibiotic produced by *Bacillus subtilis* 168. *Antimicrob. Agents Chemother.* 46, 315–320. doi: 10.1128/aac.46.2.315-320.2002

Thurotte, A., Brüser, T., Mascher, T., and Schneider, D. (2017). Membrane chaperoning by members of the PspA/IM30 protein family. *Commun. Integrat. Biol.* 10:e1264546. doi: 10.1080/19420889.19422016.11264546

Todter, D., Gunka, K., and Stulke, J. (2017). The highly conserved Asp23 family protein YqhY plays a role in lipid biosynthesis in *Bacillus subtilis*. *Front. Microbiol.* 8:883.

Tran, T. T., Miller, W. R., Shamoo, Y., and Arias, C. A. (2016). Targeting cell membrane adaptation as a novel antimicrobial strategy. *Curr. Opin. Microbiol.* 33, 91–96. doi: 10.1016/j.mib.2016.07.002

van der Donk, W. A. (2015). Bacteria do it differently: an alternative path to squalene. *ACS Cent. Sci.* 1, 64–65. doi: 10.1021/acscentsci.5b00142

Vinayavekhin, N., Mahipant, G., Vangnai, A. S., and Sangvanich, P. (2015). Untargeted metabolomics analysis revealed changes in the composition of glycerolipids and phospholipids in *Bacillus subtilis* under 1-butanol stress. *Appl. Microbiol. Biotechnol.* 99, 5971–5983. doi: 10.1007/s00253-015-6692-0

Wagner, R. M., Kricks, L., and Lopez, D. (2017). Functional membrane microdomains organize signaling networks in bacteria. *J. Membr. Biol.* 250, 367–378. doi: 10.1007/s00232-016-9923-0

Weart, R. B., Lee, A. H., Chien, A. C., Haeusser, D. P., Hill, N. S., and Levin, P. A. (2007). A metabolic sensor governing cell size in bacteria. *Cell* 130, 335–347. doi: 10.1016/j.cell.2007.05.043

Weber, M. H., Klein, W., Muller, L., Niess, U. M., and Marahiel, M. A. (2001). Role of the *Bacillus subtilis* fatty acid desaturase in membrane adaptation during cold shock. *Mol. Microbiol.* 39, 1321–1329. doi: 10.1111/j.1365-2958.2001.02322.x

Wiegert, T., Homuth, G., Versteeg, S., and Schumann, W. (2001). Alkaline shock induces the *Bacillus subtilis* σ^W regulon. *Mol. Microbiol.* 41, 59–71. doi: 10.1046/j.1365-2958.2001.02489.x

Wolf, D., and Mascher, T. (2016). The applied side of antimicrobial peptide-inducible promoters from Firmicutes bacteria: expression systems and whole-cell biosensors. *Appl. Microbiol. Biotechnol.* 100, 4817–4829. doi: 10.1007/s00253-016-7519-3

Wolf, D., Kalamorz, F., Wecke, T., Juszczak, A., Mader, U., Homuth, G., et al. (2010). In-depth profiling of the LiaR response of *Bacillus subtilis*. *J. Bacteriol.* 192, 4680–4693. doi: 10.1128/jb.00543-10

Wormann, M. E., Corrigan, R. M., Simpson, P. J., Matthews, S. J., and Grundling, A. (2011). Enzymatic activities and functional interdependencies of *Bacillus subtilis* lipoteichoic acid synthesis enzymes. *Mol. Microbiol.* 79, 566–583. doi: 10.1111/j.1365-2958.2010.07472.x

Yamada, Y., Tikhonova, E. B., and Zgurskaya, H. I. (2012). YknWXYZ is an unusual four-component transporter with a role in protection against sporulation-delaying-protein-induced killing of *Bacillus subtilis*. *J. Bacteriol.* 194, 4386–4394. doi: 10.1128/jb.00223-12

Yang, S. J., Bayer, A. S., Mishra, N. N., Meehl, M., Ledala, N., Yeaman, M. R., et al. (2012). The *Staphylococcus aureus* two-component regulatory system, GraRS, senses and confers resistance to selected cationic antimicrobial peptides. *Infect. Immun.* 80, 74–81. doi: 10.1128/iai.05669-11

Yao, J., and Rock, C. O. (2013). Phosphatidic acid synthesis in bacteria. *Biochim. Biophys. Acta* 1831, 495–502. doi: 10.1016/j.bbalip.2012.08.018

Zhang, Y. M., and Rock, C. O. (2009). Transcriptional regulation in bacterial membrane lipid synthesis. *J. Lipid Res.* 50(Suppl), S115–S119.

Zielinska, A., Savietto, A., de Sousa Borges, A., Martinez, D., Berbon, M., Roelofsen, J. R., et al. (2020). Flotillin-mediated membrane fluidity controls peptidoglycan synthesis and MreB movement. *Elife* 9:e57179.

Conflict of Interest: The authors declare that the research was conducted in the absence of any commercial or financial relationships that could be construed as a potential conflict of interest.

frontiers in Molecular Biosciences

ORIGINAL RESEARCH
published: 19 May 2021
doi: 10.3389/fmolb.2021.659058

Phenotypic and Multi-Omics Characterization of *Escherichia coli* K-12 Adapted to Chlorhexidine Identifies the Role of MlaA and Other Cell Envelope Alterations Regulated by Stress Inducible Pathways in CHX Resistance

*Branden S. J. Gregorchuk[1], Shelby L. Reimer[1], Kari A. C. Green[1], Nicola H. Cartwright[1], Daniel R. Beniac[2], Shannon L. Hiebert[2], Timothy F. Booth[1,2], Patrick M. Chong[2], Garrett R. Westmacott[2], George G. Zhanel[1] and Denice C. Bay[1]**

[1] Department of Medical Microbiology and Infectious Diseases, University of Manitoba, Winnipeg, MB, Canada, [2] National Microbiology Laboratory, Public Health Agency of Canada, Winnipeg, MB, Canada

OPEN ACCESS

Edited by:
Heidi Vitrac,
University of Texas Health Science Center at Houston, United States

Reviewed by:
Luke Peter Allsopp,
Imperial College London, United Kingdom
Tanya Elizabeth Susan Dahms,
University of Regina, Canada

***Correspondence:**
Denice C. Bay
denice.bay@umanitoba.ca

Specialty section:
This article was submitted to Cellular Biochemistry, a section of the journal Frontiers in Molecular Biosciences

Received: 26 January 2021
Accepted: 09 April 2021
Published: 19 May 2021

Citation:
Gregorchuk BSJ, Reimer SL, Green KAC, Cartwright NH, Beniac DR, Hiebert SL, Booth TF, Chong PM, Westmacott GR, Zhanel GG and Bay DC (2021) Phenotypic and Multi-Omics Characterization of Escherichia coli K-12 Adapted to Chlorhexidine Identifies the Role of MlaA and Other Cell Envelope Alterations Regulated by Stress Inducible Pathways in CHX Resistance. Front. Mol. Biosci. 8:659058. doi: 10.3389/fmolb.2021.659058

Chlorhexidine (CHX) is an essential medicine used as a topical antiseptic in skin and oral healthcare treatments. The widespread use of CHX has increased concerns regarding the development of antiseptic resistance in Enterobacteria and its potential impact on cross-resistance to other antimicrobials. Similar to other cationic antiseptics, resistance to CHX is believed to be driven by three membrane-based mechanisms: lipid synthesis/transport, altered porin expression, and increased efflux pump activity; however, specific gene and protein alterations associated with CHX resistance remain unclear. Here, we adapted *Escherichia coli* K-12 BW25113 to increasing concentrations of CHX to determine what phenotypic, morphological, genomic, transcriptomic, and proteomic changes occurred. We found that CHX-adapted *E. coli* isolates possessed no cross-resistance to any other antimicrobials we tested. Scanning electron microscopy imaging revealed that CHX adaptation significantly altered mean cell widths and lengths. Proteomic analyses identified changes in the abundance of porin OmpF, lipid synthesis/transporter MlaA, and efflux pump MdfA. Proteomic and transcriptomic analyses identified that CHX adaptation altered *E. coli* transcripts and proteins controlling acid resistance (*gadE, cdaR*) and antimicrobial stress-inducible pathways Mar-Sox-Rob, stringent response systems. Whole genome sequencing analyses revealed that all CHX-resistant isolates had single nucleotide variants in the retrograde lipid transporter gene *mlaA* as well as the *yghQ* gene associated with lipid A transport and synthesis. CHX resistant phenotypes were reversible only when complemented with a functional copy of the *mlaA* gene. Our results highlight the importance of retrograde phospholipid transport and stress response systems in CHX resistance and the consequences of prolonged CHX exposure.

Keywords: chlorhexidine, retrograde phospholipid transport, disinfectant, *Escherichia coli*, MlaA, antiseptic resistance, multi-omics, antimicrobial resistance (AMR)

INTRODUCTION

Chlorhexidine (CHX) is a commonly used antiseptic and disinfectant in medical, dental, and veterinary practice and it is listed as an essential medicine by the World Health Organization (World Health Organization, 2019). CHX is the active antimicrobial ingredient used in a variety of clinical antiseptics (skin, oral, and eye washes) and daily use products (cosmetics and personal hygiene products), making CHX usage widespread. This antiseptic is a membrane-active bisbiguanide compound that consists of two cationic biguanidine moieties linked by a hexamethyl acyl-chain region (Nayyar, 2015). Similar to other hydrophobic cationic antiseptics, CHX kills and/or inhibits cell growth in a concentration dependent manner by disrupting cell membrane phospholipids by displacing divalent cations at the anionic cell membrane surface (Gilbert and Moore, 2005; Nayyar, 2015). Specifically, CHX acts by inserting itself in between phospholipid headgroup pairs gradually destabilizing cell membrane integrity by forming gaps in the phospholipid membrane bilayer that result in cell content leakage and death (Gilbert and Moore, 2005). Although bacterial resistance to CHX has not been convincingly shown at its working concentrations, Gram-negative bacterial resistance to CHX is becoming a growing concern. There are increasing reports of CHX-resistant Enterobacterales (Kampf, 2016, 2018; Cieplik et al., 2019), where CHX-resistant pathogens, *Klebsiella* spp. and *Salmonella* spp., have demonstrated cross-resistance to antibiotics, most notably the last-line polymyxin antibiotic colistin (Wand et al., 2017; Hashemi et al., 2019; Verspecht et al., 2019). Increasing resistance as well as possible antibiotic cross-resistance is very concerning given CHX's clinical importance as a medical antiseptic and, in some cases, as a last-line debridement treatment (Brookes et al., 2020). This highlights an important knowledge gap to address regarding how intrinsic CHX mechanisms of resistance develop, especially among antimicrobial resistant species deemed to be critical priority pathogens. Unfortunately, there are no clinically defined CHX breakpoint concentrations to distinguish resistant from susceptible CHX concentrations according to the Clinical Laboratory Standards Institute (CLSI[1]) or European Committee on Antimicrobial Susceptibility Testing (EUCAST[2]). Despite the absence of defined CHX breakpoints, we will refer to reduced CHX susceptibility as "resistant" rather than "tolerant" herein based on minimum inhibitory concentration values defined for antiseptics and antibiotics (Cerf et al., 2010; Brauner et al., 2016).

Previous studies have attempted to identify CHX-resistance's mechanisms of action using clinical isolates (Condell et al., 2012; Naparstek et al., 2012; Fernández-Cuenca et al., 2015; Vali et al., 2015) or laboratory adapted bacteria/isolates that were gradually exposed to increasing concentrations of CHX over numerous sub-cultures (Braoudaki and Hilton, 2004; Wand et al., 2017; Verspecht et al., 2019). These approaches have identified the involvement of intrinsically expressed or acquired efflux pumps, such as KpnEF (Abuzaid et al., 2012), CepA (Fang et al., 2002), SmvA (Wand et al., 2017), and AceI (Hassan et al., 2015) as CHX resistance mechanisms. However, based on the membrane disruptive mechanism of action by CHX and its frequent co-association with colistin resistance, there may be other overlapping membrane-specific mechanisms contributing to intrinsic CHX resistance such as lipopolysaccharide (LPS) transcriptional regulators PmrD and PhoPQ as previously identified (Wand et al., 2017). With respect to known colistin resistance mechanisms, many of these regulators are known contributors of LPS alterations that promote colistin resistance (Olaitan et al., 2014).

In this study, we performed an in-depth phenotypic and molecular analysis to identify intrinsic CHX resistance mechanisms using *Escherichia coli* K-12 BW25113 adapted to CHX. We selected this antimicrobial susceptible strain based on its well-established collection of single gene deletions known as the Keio collection (Baba et al., 2006) and gene clone ASKA library collection (Kitagawa et al., 2005). In our study, we gradually adapted *E. coli* BW25113 to CHX over 20 subcultures. We characterized these CHX-adapted *E. coli* isolates for their phenotypic alterations using antimicrobial susceptibility testing (AST) methods to determine antimicrobial cross-resistance, changes in fitness using optical growth curve experiments, scanning electron microscopy (SEM) to identify any cell morphology changes, and a recently published membrane integrity assay to detect membrane alterations. We also conducted in-depth multi-omics analyses of these isolates using whole genome sequencing (WGS), liquid chromatography tandem mass spectrometry (LC-MS/MS) proteomics techniques, and RNA-seq transcriptomic analyses. This combined "omics" approach identified single nucleotide variants (SNVs) in genes in CHX-adapted isolates as well as their associated proteomic and transcript alterations caused by prolonged CHX exposure. Genes with SNVs identified from this analysis potentially contributing to CHX resistance were also examined for their ability to phenotypically complement CHX-adapted and un-adapted isolates using ASKA plasmid library gene clones and in-frame single gene deletions in BW25113. This in-depth multi-omics study revealed the involvement of the outer membrane lipoprotein MlaA, which is a component of the retrograde phospholipid transport Mla system, that serves as an intrinsic CHX resistance contributor. We also identified alterations of other stress response pathways often involving acid regulation. Our analyses show that phospholipid removal is an important mechanism contributing to CHX resistance.

RESULTS

Gradual Adaptation of *E. coli* Isolates to Increasing CHX Concentrations Resulted in CHX-Resistant Isolates That Showed No Cross-Resistance to Any Other Antimicrobials Tested

To initiate this study, we first performed a CHX-adaptation experiment of *E. coli* K-12 BW25113 using the gradual antiseptic adaptation approach described in a previous study

[1]https://clsi.org/

[2]https://www.eucast.org/

(Bore et al., 2007). As described in this method, we repeatedly sub-cultured BW25113 (in biological triplicate) in Luria-Bertani (LB) broth containing gradually increasing concentrations of CHX-, starting at a sub-inhibitory CHX concentration 0.4 μg/mL, and the cultures that had most turbid growth were sub-cultured repeatedly into fresh media with increasing stepwise CHX concentrations (**Supplementary Table 1**). After 20 sub-cultures (20 days) with increasing CHX concentrations, we generated three gradually adapted CHX-resistant isolates (CHXR1-3) capable of growing in the presence of 2.4 μg/mL CHX, which was above the minimum inhibitory concentration (MIC) value for the susceptible un-adapted wild-type BW25113 control (WT; **Table 1**). Using the broth microdilution AST method, we determined the MIC values of each CHX-resistant isolate to CHX as well as its susceptibility to other representative antimicrobials (**Table 2**). AST results demonstrated that all three CHX-resistant isolates were only resistant to CHX at 2- to 4-fold higher concentrations when compared to the un-adapted WT (**Table 2**). Surprisingly, all three CHX-adapted isolates had no increase in resistance to the bisbiguanide antiseptic alexidine (ALX), indicating that our adaptation of *E. coli* to CHX was highly selective and did not confer cross-resistance to another commonly used bisbiguanide antiseptic. CHX-adapted isolates were susceptible to all quaternary ammonium compound (QAC) cationic antiseptics we tested based on their MIC values, as well as to all other antibiotics, including colistin (**Table 2**). It is notable that CHX-adapted isolates were more susceptible to QACs cetyldimethylethylammonium bromide (CDAB) and cetytrimethylammonium bromide (CTAB) and to the aminoglycoside antibiotic tobramycin when compared to the WT (**Table 2**). Together, our MIC data indicates that the CHX-adapted *E. coli* we generated had no significant antiseptic cross-resistance or antibiotic cross-resistance in this study. This AST result outcome permitted us to study these isolates in more depth to determine CHX-resistant phenotypes only.

CHX-Adapted *E. coli* Isolates Are Phenotypically Stable and Reach Higher Final ODs in LB, DG, and M9 Media

We examined all three CHX-resistant isolates for their CHX phenotypic stability to determine how long these isolates maintained CHX resistance after repeated growth without CHX exposure. This experiment has been performed in previous

TABLE 1 | Bacterial *E. coli* strains and plasmids used or generated in this study.

Strain name	Genotype; Description of CHX adaptation	Final concentration of CHX used for adaptation (μg/mL)	References
BW25113	F- Δ(araD-araB)567 Δ*lacZ4787*:*rrnB*-3, λ-, *rph-1* Δ(*rhaD-rhaB*)568 *hsdR514*	—	Baba et al., 2006
CHXR1	BW25113; Replicate isolate 1 adapted to CHX after 20 subcultures	2.4	This study
CHXR2	BW25113; Replicate isolate 2 adapted to CHX after 20 subcultures	2.4	This study
CHXR3	BW25113; Replicate isolate 3 adapted to CHX after 20 subcultures	2.4	This study
JW2343-KC	F-, Δ(*araD-araB*)567, Δ*lacZ*4787:*rrnB*-3, λ-, Δ*mlaA*:*kan*, *rph-1*, Δ(*rhaD-rhaB*)568, *hsdR*514	—	Baba et al., 2006
JW4276-KC	F-, Δ(*araD-araB*)567, Δ*lacZ*4787:*rrnB*-3, λ-, Δ*fimE*:, *rph-1*, Δ(*rhaD-rhaB*)568, *hsdR*514	—	Baba et al., 2006
JW5248-KC	F-, Δ(*araD-araB*)567, Δ*lacZ*4787:*rrnB*-3, λ-, Δ*marR*:, *rph-1*, Δ(*rhaD-rhaB*)568, *hsdR*514	—	Baba et al., 2006
JW5490-KC	F-, Δ(*araD-araB*)567, Δ*lacZ*4787:*rrnB*-3, λ-, Δ*yghQ*:, *rph-1*, Δ(*rhaD-rhaB*)568, *hsdR*514	—	Baba et al., 2006
JW3471-AM	F-, Δ(*araD-araB*)567, Δ*lacZ*4787:*rrnB*-3, λ-, Δ*yhiS*:, *rph-1*, Δ(*rhaD-rhaB*)568, *hsdR*514	—	Baba et al., 2006
JW3480-KC	F-, Δ(*araD-araB*)567, Δ*lacZ*4787:*rrnB*-3, λ-, Δ*gadE*:, *rph-1*, Δ(*rhaD-rhaB*)568, *hsdR*514	—	Baba et al., 2006
JW5013-KC	F-, Δ(*araD-araB*)567, Δ*lacZ*4787:*rrnB*-3, λ-, Δ*cdaR*:, *rph-1*, Δ(*rhaD-rhaB*)568, *hsdR*514	—	Baba et al., 2006
Plasmid name	**Plasmid details**	**Antimicrobial resistance marker**	**References**
pCA24N(–)	Parental; T5-*lac* promoter expression vector	CM	Kitagawa et al., 2005
pMlaA	pCA24N(–) with *mlaA* cloned with His_6-affinity tag fusions at the C-terminus	CM	Kitagawa et al., 2005
pYghQ	pCA24N(–) with *yghQ* cloned with His_6-affinity tag fusions at the C-terminus	CM	Kitagawa et al., 2005
pFimE	pCA24N(–) with *fimE* cloned with His_6-affinity tag fusions at the C-terminus	CM	Kitagawa et al., 2005
pYhiS	pCA24N(–) with *yhiS* cloned with His_6-affinity tag fusions at the C-terminus	CM	Kitagawa et al., 2005
pGadE	pCA24N(–) with *gadE* cloned with His_6-affinity tag fusions at the C-terminus	CM	Kitagawa et al., 2005
pCdaR	pCA24N(–) with *cdaR* cloned with His_6-affinity tag fusions at the C-terminus	CM	Kitagawa et al., 2005
pMarR	pCA24N(–) with *marR* cloned with His_6-affinity tag fusions at the C-terminus	CM	Kitagawa et al., 2005

CM, Chloramphenicol; His_6, hexahistidine.

gradual antiseptic laboratory-based adaptation studies (Gadea et al., 2016, 2017) and verified that CHX phenotypes are stable prior to our multi-omics analyses. To confirm that each CHX-adapted isolate had a stable CHX-resistant phenotype, we sub-cultured each isolate in LB broth without CHX over a 10-day experiment, where we performed CHX AST daily to determine any MIC value changes (**Table 3**). This CHX phenotype stability testing outcome indicated that there was no significant change in MIC values over the course of 9 days for all three CHXR isolates (**Table 3**). However, CHXR2 and CHXR3 did show a 2-fold reduction in MIC values on day 10 when compared to MIC values from Days 1–9 (**Table 3**), though these isolates were still 2-fold more resistant to CHX than the WT. CHXR1 showed the greatest CHX phenotypic stability without CHX selection over the 10-day period, where it occasionally showed higher resistance to CHX (Days 3, 4, and 9; **Table 3**), suggesting CHX resistance fluctuated within a 2-fold range. Based on this outcome, we selected CHXR1 isolates for further in-depth proteomic and transcriptomic analyses as discussed in further sections.

TABLE 2 | A summary of AST MIC values using broth microdilution for each CHX-adapted *E. coli* isolate in this study.

Antimicrobial agent tested	WT	CHXR1	CHXR2	CHXR3
ALX	2	2	2	2
BZK	18	18	9	9
CDAB	32	**8**	**8**	**8**
CEF	0.5	0.5	1	0.5
CET	30	30	30	30
CHX	2	**8**	**4**	**4**
CIP	0.25	0.25	0.25	0.25
CM	<7.5	15	15	15
COL	1	1	1	1
CPC	8	8	8	8
CTAB	32	**8**	**8**	**8**
DDAB	8	4	4	4
DOM	8	8	8	8
DOX	8	4	4	**2**
ERY	512	256	512	256
KAN	16	16	16	16
LZD	1024	1024	1024	**512**
MEM	0.03	0.03	0.03	0.03
RMP	512	512	512	512
SMX-TMP	16	16	16	16
TLN	0.25	0.25	0.25	0.25
TOB	16	**4**	**4**	**4**
VAN	256	512	512	256

Bold values indicate > 2-fold differences in MIC as compared to WT. ALX, alexidine dihydrochloride; BZK, benzalkonium chloride; CAZ, ceftazidime; CDAB, cetyldimethylethylammonium bromide; CET, cetrimide bromide; CHX, chlorhexidine digluconate; CIP, ciprofloxacin; CM, chloramphenicol; COL, colistin; CPC, cetylpyridinium chloride; CTAB, cetyltrimethylammonium bromide; DDAB, dodecyl-dimethylammonium bromide; DOM, domiphen bromide; DOX, doxycycline; ERY, erythromycin; KAN, kanamycin; LZD, linezolid; MEM, meropenem; RMP, rifampicin; SXT-TMP, sulfamethoxazole-trimethoprim; TLN, triclosan; TOB, tobramycin; VAN, vancomycin.

The growth phenotypes of each CHX-adapted isolate were also compared to the un-adapted WT using broth optical density (600 nm) growth curve experiments. We compared CHX-adapted isolate growth in various rich media, LB, LB + 0.4% w/v glucose (LB + Glc), Mueller Hinton broth (MHB), and tryptic soy broth (TSB) as well as minimal media, minimal 9 salts (M9), and Davis Glucose (DG). All growth experiments were performed with and without added CHX (at a final 0.4 μg/mL concentration) over a 24 h period at 37°C. Growth curve results helped assess if there were any significant growth delays or reductions for CHXR isolates in specific media and used to identify any changes in the overall fitness of the isolates from lag to stationary phase. To verify final OD values, final colony-forming units/mL (CFU/mL) were determined for diluted (10^{-6} and 10^{-7}) 24 h cultures from plated LB agar colonies grown at 37°C. When CHX-adapted isolates were grown without CHX selection in various rich media their final $OD_{600\ nm}$ values were significantly differed from the WT growth over 24 h in LB, MHB, and TSB (P-values of < 0.05) but not LB + Glc (**Figures 1A–D**, **Supplementary Figure 1**, and **Supplementary Table 2**) and grew similar to or slower than WT by 11.6–22.8% differences (**Supplementary Table 3**). In LB medium, independent of CHX, CHXR isolates reached significantly higher stationary phase $OD_{600\ nm}$ values after 5 h, ranging from 1.21 $OD_{600 nm}$ (±0.07 units error) to 1.37 $OD_{600\ nm}$ (±0.12 units error) than the WT (1.09 ± 0.03 to 1.11 ± 0.09; P-values < 0.05) and corresponded to higher CHXR CFU/mL counts (**Supplementary Table 3**). CHXR isolate growth in all rich media with CHX selection identified significant changes in final $OD_{600\ nm}$ values and CFU/mL cell counts when compared to WT under the same conditions in LB, LB + Glc, and MHB (P-values < 0.05) but not TSB (**Figures 1A–D**, **Supplementary Figure 1**, and **Supplementary Table 2**, **3**). In rich media with CHX selection, CHXR isolates had similar or slower growth doubling times (6.5–24.1% differences)

TABLE 3 | A summary of MIC values determined for each CHX-adapted isolate after 1–10 days of growth without CHX selection in LB growth medium.

Isolate/Strain	MIC of CHX (μg/mL) after specified days without added CHX selection									
	Day 1	Day 2	Day 3	Day 4	Day 5	Day 6	Day 7	Day 8	Day 9	Day 10
WT	2	2	2	4	4	2	2	2	2	2
CHXR1	8	8	16	16	8	8	8	8	16	8
CHXR2	8	8	8	8	8	8	8	8	8	4-8
CHXR3	8	8	8	8	8	8	8	8	8	4-8

*WT, un-adapted wild-type BW25113; CHXR1, CHX-adapted isolate 1; CHXR2, CHX-adapted isolate 2; CHXR3, CHX-adapted isolate 3 (see **Table 1**).*

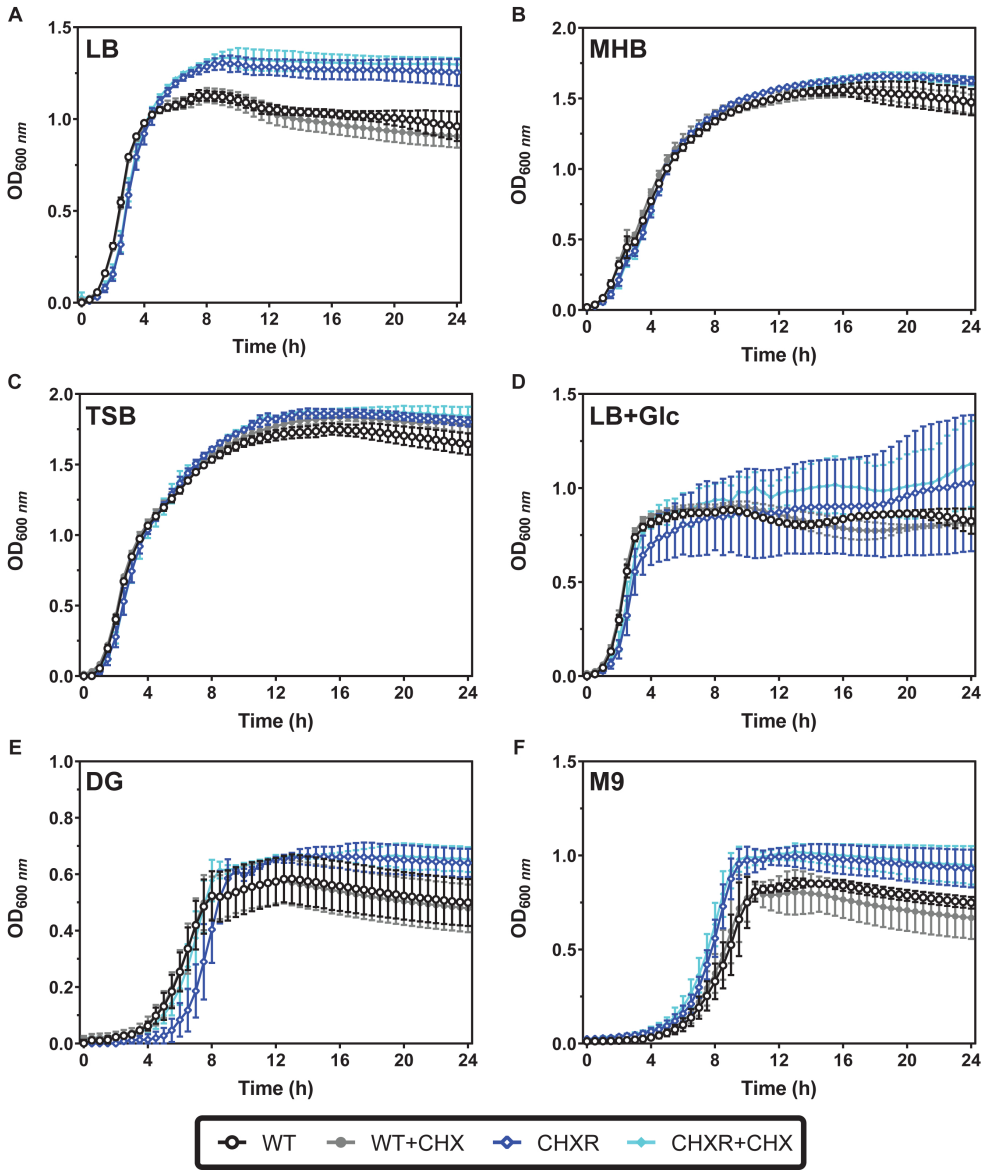

FIGURE 1 | Growth curves of WT and CHXR isolates in rich and minimal media with and without CHX selection. In all panels, growth curves were measured from optical density values at 600 nm ($OD_{600\ nm}$) in 96-well microtiter plates incubated at 37°C with shaking over 24 h. Averaged values from CHXR1-3 isolates and WT measured in biological triplicate are plotted in each panel, and error bars highlight standard deviation of $OD_{600\ nm}$ values at each timepoint. In all panels, CHXR isolates are plotted as blue shaded diamonds and WT as circles, where solid filled symbols indicate samples grown in the presence of 0.4 μm/mL CHX final concentration and unfilled symbols indicate media growth without CHX selection. Media with and without CHX addition used to measure the growth of each isolate/strain is shown in each panel: **(A)** LB, **(B)** MHB, **(C)** TSB, **(D)** LB + 0.4% w/v glucose (LB + Glc), **(E)** DG, and **(F)** M9.

than the WT (**Supplementary Table 3**). As LB was the medium used to gradually adapt all *E. coli* isolates to CHX for this study, these growth differences may reflect the isolate's adaptation not only to CHX but also the LB medium components specific to LB formulations.

Growth curves in either minimal media (DG and M9) we tested, showed lower maximum final $OD_{600\ nm}$ values for all CHXR and WT isolates as compared to their growth in rich media after 12 h (CHXR; 0.61–0.75 $OD_{600\ nm}$, WT; 0.52–0.58 $OD_{600\ nm}$), indicating that growth in defined media for all CHXR isolates and WT was reduced (**Figures 1E,F**, **Supplementary Figure 2**, and **Supplementary Table 3**). In minimal media without CHX, final $OD_{600\ nm}$ values and CFU/mL values for CHXR isolates compared to WT were only statistically different in M9 (P-value < 0.05) but not in DG medium (**Figures 1E,F**, **Supplementary Figure 2**, and **Supplementary Tables 2**, **3**) suggesting these different defined media formulations influenced CHXR growth rates. In M9 without CHX, CHXR isolates had a mean doubling time that was 33.6% slower than WT but in the presence of CHX, CHXR isolates grew 17.0% faster

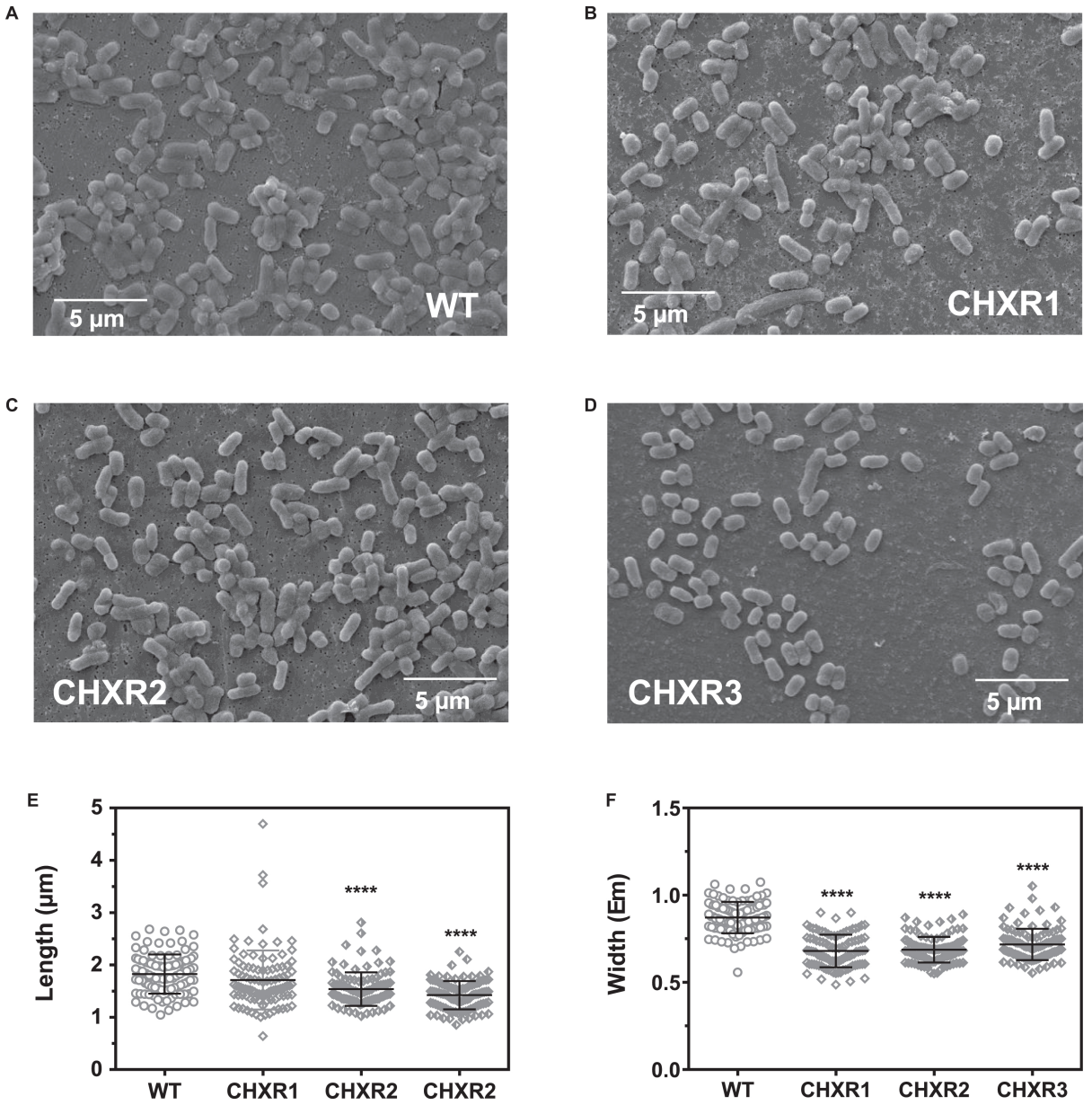

FIGURE 2 | Scanning electron microscopy (SEM) images of CHXR isolates and a summary of measured CHXR cell lengths and widths. **(A–D)** Show representative 5,000X magnification SEM images of WT **(A)**, CHXR1 **(B)**, CHXR2 **(C)**, and CHXR3 **(D)** cells. Bars shown in each panel indicate a 5 μm length as a size reference. **(E,F)** Indicate a summary cell lengths **(E)** and widths **(F)** in μm of 200 cells (n = 200) and are shown as plotted symbols. Each CHXR isolate or WT was measured from five SEM images collected from each biological replicate using ImageJ software v1.8.0 measurement tools. Bar plots overlaid on measured cells indicates the maximum, median, and minimum interquartile ranges of the cell measurement datasets and asterisks (****) indicate significant differences between the WT and each CHXR isolate median values at P-values < 0.0001.

than WT, indicating that CHX enhances CHXR growth rates (**Supplementary Table 3**). In DG without CHX addition, CHXR isolates grew faster than WT by 27.2% and in the presence of CHX, CHXR isolates had a mean doubling time that was 9.3% faster than WT (**Supplementary Table 3**). This shows that CHXR growth rates were faster in minimal media with CHX in contrast to the generally slower CHXR isolate growth rates in rich media. In minimal medium without CHX, CHXR isolates had a slightly longer lag phase of 1 h when compared to CHXR grown in the presence of CHX (**Figure 1E** and **Supplementary Figure 2**), however, when we compared final $OD_{600\ nm}$ and CFU/mL values from CHXR growth curves with and without added CHX, neither was statistically different (**Supplementary Tables 2**, **3**). These findings suggest that prolonged adaptation to CHX measurably alters their growth fitness, where CHXR isolates grew slower than the un-adapted WT in nearly all rich

media with and without CHX, whereas when CHX is added to either minimal medium tested, CHXR isolate growth rate was faster than the WT (**Figure 1**, **Supplementary Figures 1**, **2**, and **Supplementary Tables 2**, **3**). Growth curve findings for specific media conditions (LB + Glc, DG, and M9) also demonstrated that CHXR isolates were capable of growing to higher final $OD_{600\ nm}$ values and CFU/mL than WT, suggesting some growth conditions maintained or enhanced CHXR isolate fitness.

CHX-Adapted *E. coli* Isolates Have Altered Cell Morphologies, Where Cells Are Shorter and Narrower Than WT and Have More Permeable Membranes Than WT

Our final phenotypic analysis of each CHX-adapted isolate sought to identify if there were any significant alterations in cell morphology with the use of SEM and a novel membrane integrity assay that we had previously published. With SEM imagery, we assessed CHX-adapted isolates grown to mid-log phase and compared them to mid-log WT cell preparations as shown in **Figures 2A–D**. Based on a visual assessment, all CHX-adapted isolate's cell surface morphology appeared to be similar to the un-adapted WT, where all cells had the characteristic bacilliform shape (**Figures 2A–D**). A blinded cell image analysis with ImageJ (Abràmoff et al., 2007) was used determine the mean lengths and widths of 200 cells from two biological replicates of each CHXR and WT cell preparations (**Figures 2E,F** and **Supplementary Figure 3**). The analysis revealed that CHXR2 and CHXR3 isolates were significantly ($P < 0.001$) shorter in length than WT cells (WT; 1.82 ± 0.06 μm, CHXR2; 1.75 ± 0.35 μm, CHXR3; 1.42 ± 0.29 μm, **Figure 2E** and **Supplementary Figure 3**) and all three CHX-adapted isolates were significantly ($P < 0.001$) narrower in width (CHXR1; 0.68 ± 0.09 μm, CHXR2; 0.69 ± 0.09 μm, CHXR3; 0.71 ± 0.06 μm) than the WT (0.88 ± 0.08 μm) on average (**Figure 2F** and **Supplementary Figure 3**). These findings show that CHX adaptation alters cell morphology, by narrowing cell widths overall and in 2/3 isolates, reducing average cell length.

To verify if CHXR isolate membranes were significantly altered from the WT, we examined membrane permeation differences using the membrane impermeant fluorescent dye (propidium iodide). This dye increases in fluorescent emission (at 620 nm) when bound to DNA/RNA and was used to indirectly compare the membrane integrity differences of CHXR1 and WT cells. This commonly used dye is applied to measure dead bacterial cells (Stiefel et al., 2015), and we recently showed it can be used to discriminate the membrane integrity differences between antiseptic-resistant and susceptible Enterobacterial isolates (Gregorchuk et al., 2020). We monitored the relative fluorescent emission unit (RFUs) values of live and heat-treated CHXR isolates and WT cells exposed to the same concentration of dye in buffer after 30-min of exposure. We expected heat-treated (dead) cells would have the highest dye RFUs, as compared to live cells, and live cells with higher cell permeability should correspond to greater dye penetration due to more permeable cell membranes as we verified in **Supplementary Figure 4A**. A comparison of live mid-log CHXR1 to WT cell preparations showed significantly higher dye RFUs after 30-min for CHXR isolates (2.2-fold increase; mean RFU = 565 ± 248 error, $n = 9$) as compared to WT cells (mean RFU = 252 ± 122 error, $n = 9$; **Supplementary Figure 4B**). These findings show that CHXR cell membranes are more CHX-permeant than WT and suggests that CHX adaptation alters the *E. coli* membrane from WT, in agreement with our SEM images. Together, our SEM and 30-min impermeant fluorescent dye RFU analyses confirm that CHX adaptation of *E. coli* BW25113 causes phenotypic alterations that can be detected by visual as well as fluorescent techniques.

Proteomic Analysis of CHX-Adapted *E. coli* Identifies Alterations of Acid Resistance and Stress Response Systems and a Lack of MlaA Protein

To identify any alterations in protein presence and abundance between CHXR isolates and WT, we performed proteomic analysis on CHXR1 and WT. We specifically focused on CHXR1 for proteomic analysis due to its greater phenotypic CHX-resistant stability and its higher resistance to CHX (**Tables 2**, **3**). A comparison of CHXR1 and WT whole cell extracted proteomes to cytoplasmic extracted proteomes was conducted using nano LC-MS/MS to determine the relative abundances of soluble and membrane proteins that were altered in the CHXR1 isolate (**Supplementary Tables 4**, **5**). From this analysis, we identified a total of 1904 whole cell (WC) extracted proteins and 2307 cytoplasmic (CY) CHXR1 proteins, of which only 24 WC and 17 CY proteins were noted to significantly differ in abundance or detection when compared to the WT (**Figure 3** and **Supplementary Tables 4**, **5**).

Few significantly altered relative protein abundance differences were observed between CHXR1 and WT proteomes (shown as circles in **Figure 3**), where only two proteins, CadA and NfsA, were differentially accumulated in both the WC and CY extracted proteomes. Lysine decarboxylase (CadA), part of the lysine-dependent organic acid resistance system (Kanjee and Houry, 2013), was decreased in abundance (3.8-fold reduction) in both CHXR1 proteomes as compared to WT. GadE, a central transcriptional activator of glutamic acid decarboxylase (GAD) system that maintains pH homeostasis and regulates multidrug efflux pump MdtEF expression (Ma et al., 2003; Hommais et al., 2004), showed increased (4.6-fold) abundance in the CHXR1 WC proteome (**Figure 3**). Since CHX is cationic at lower acidity, it was not surprising to see upregulation of pH homeostasis systems in the CHX-adapted proteome. NfsA had significantly increased (2.0-fold) in abundance in the CHXR1 WC and CY proteomes as well as NfsB (1.8-fold) in the WC proteome (**Figure 3**). NfsA is an NADPH-dependent nitroreductase that catalyzes the reduction of nitrocompounds and is frequently upregulated in *E. coli* exposed to QACs, paraquat, and nitrofuran antimicrobials (Zenno et al., 1996; Whiteway et al., 1998). The increased abundance of NfsA and NfsB in the CHXR1 proteome suggests that this nitrogen reductive pathway may help counteract exposure to toxic nitrogen rich compounds like CHX.

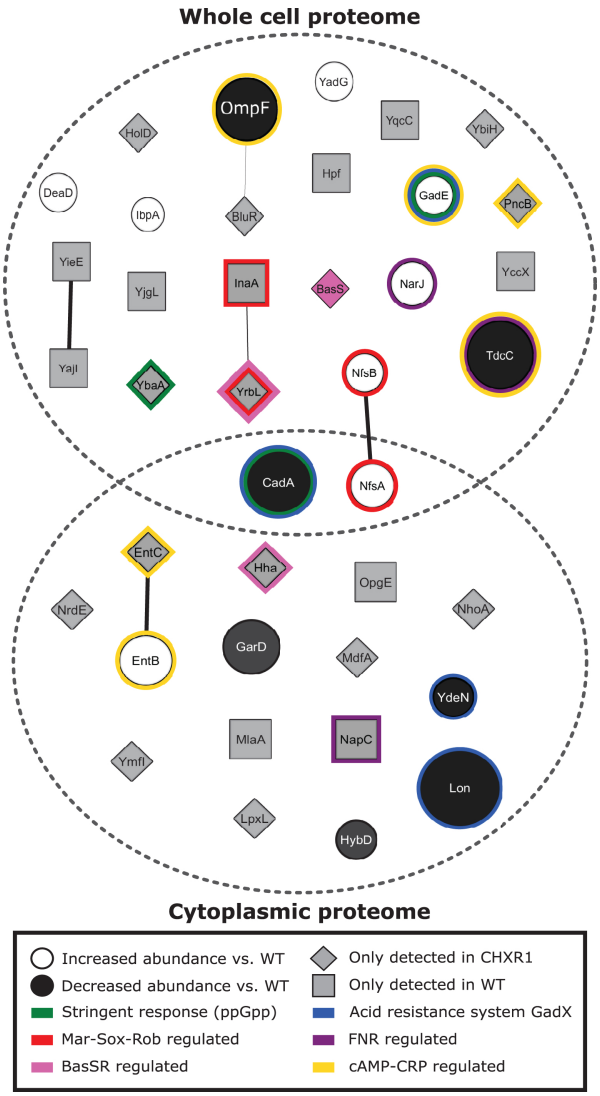

FIGURE 3 | A network diagram summary of significantly identified proteins determined from the CHXR1 isolate and WT proteomic analyses. The network diagram was generated using Cytoscape v3.7.2 (Shannon et al., 2003) using the StringApp v1.5.0 software package (Doncheva et al., 2019). As summarized in the panel legend, significantly altered protein abundances are represented as circles with protein names and indicate proteins that differed between WT and CHXR1 in both the WC and CY proteomes. The size of the protein circles represents the degree of fold change from the WT proteome, where white filled circles represent CHXR1 proteins with increased abundance and black filled circles represent CHXR1 proteins with decreased abundance. Gray filled squares and diamonds represent WT and CHXR1 proteins respectively, that were not detected in the opposite (WT or CHXR1) proteome. Known regulatory systems influencing protein accumulation are outlined by color according to the bottom panel legend.

Besides NfsAB, many other proteins with altered in abundance between the CHXR and WT were noted to be regulated by stress inducible pathways associated with antimicrobial resistance, such as the Mar-Sox-Rob regulon (Chubiz et al., 2012), the stringent response (Strugeon et al., 2016), and the fumarate and nitrate reduction (FNR) pathways (Kurabayashi et al., 2017). Lon protein, an ATP-dependent protease that degrades misfolded proteins involved in transient multidrug resistance, particularly MarA, SoxS, and GadE (Heuveling et al., 2008; Nicoloff and Andersson, 2013) was significantly reduced (5.3-fold) in abundance in the CHXR1 CY proteomes only (**Figure 3**). The reduction of Lon in CHXR1 is expected if prolonged activation of the Mar-Sox-Rob and organic acid resistance systems are induced by acidic CHX exposure.

Lastly, nearly half of all proteins we identified in WC and CY proteomes shown in **Figure 3** were detectable in either CHXR1 or WT samples (gray filled proteins). Although we cannot compare the relative abundances of these proteins, their detection in the CHX-adapted isolate or WT only were important to note. There was a noticeable absence of MlaA detection in both CHXR1 proteomes (**Figure 3**), we expected this outcome based on our WGS SNV findings of *mlaA* (**Table 4**). We also detected MdfA in the in the CHXR1 WC proteome (**Figure 3**); MdfA is an alkali-resistant chloramphenicol selective multidrug efflux pump belonging to the Major Facilitator Superfamily (MFS) (Edgar and Bibi, 1997; Bohn and Bouloc, 1998). Altered detection of this MFS alkali-resistant efflux pump in CHXR1 suggests upregulated expression of this efflux pump, possibly contributing to CHX-resistance. BasS, also known as PmrB, was detectable only in CHXR1 WC proteomes and is the sensor histidine kinase of the BasSR two-component system that regulates the expression of the *arnBCADTEF* operon which modifies LPS and is often detected in colistin resistant species (Olaitan et al., 2014). Additionally, lipid A biosynthesis enzyme, lauroyl acyltransferase (LpxL) was only detected in the CY proteome of CHXR1, suggesting that LPS biosynthesis may be altered in the CHX-adapted isolate.

Overall, CHX-adaptation resulted in the significant alteration of a small collection of proteins pivotal in acid resistance, prolonged antimicrobial stress, as well as LPS biosynthesis and transport highlighting many new and previously identified proteins involved in antimicrobial resistance that overlap with CHX-resistance.

Transcriptomic Analysis of CHX-Adapted Isolates Identifies Reductions in *mlaA* and Upregulation of Acid Regulated Genes

To determine if any CHX-adaptation resulted in any gene expression changes in addition to the proteomic changes we observed, RNA-seq transcriptome analyses was performed on mid-log cultures of CHXR1 and WT under the same growth conditions used for proteomic analyses. A total of 4490 genes had altered gene expression as detected by RNA-seq analysis, where only 505 were significantly up- or down-regulated in CHXR1 and WT transcripts (**Supplementary Table 6**). In an effort to identify significantly altered transcripts from other omics analyses performed herein (proteomic and genomic), we generated a summary heatmap of these differentially expressed gene from CHXR1 and WT (**Figure 4**). This analysis identified that 11 CHXR1 transcripts up or down regulated from RNA-seq were also similarly altered in protein abundance (bolded genes; **Figure 4**). Notably, up-regulated efflux pump *mdfA* and

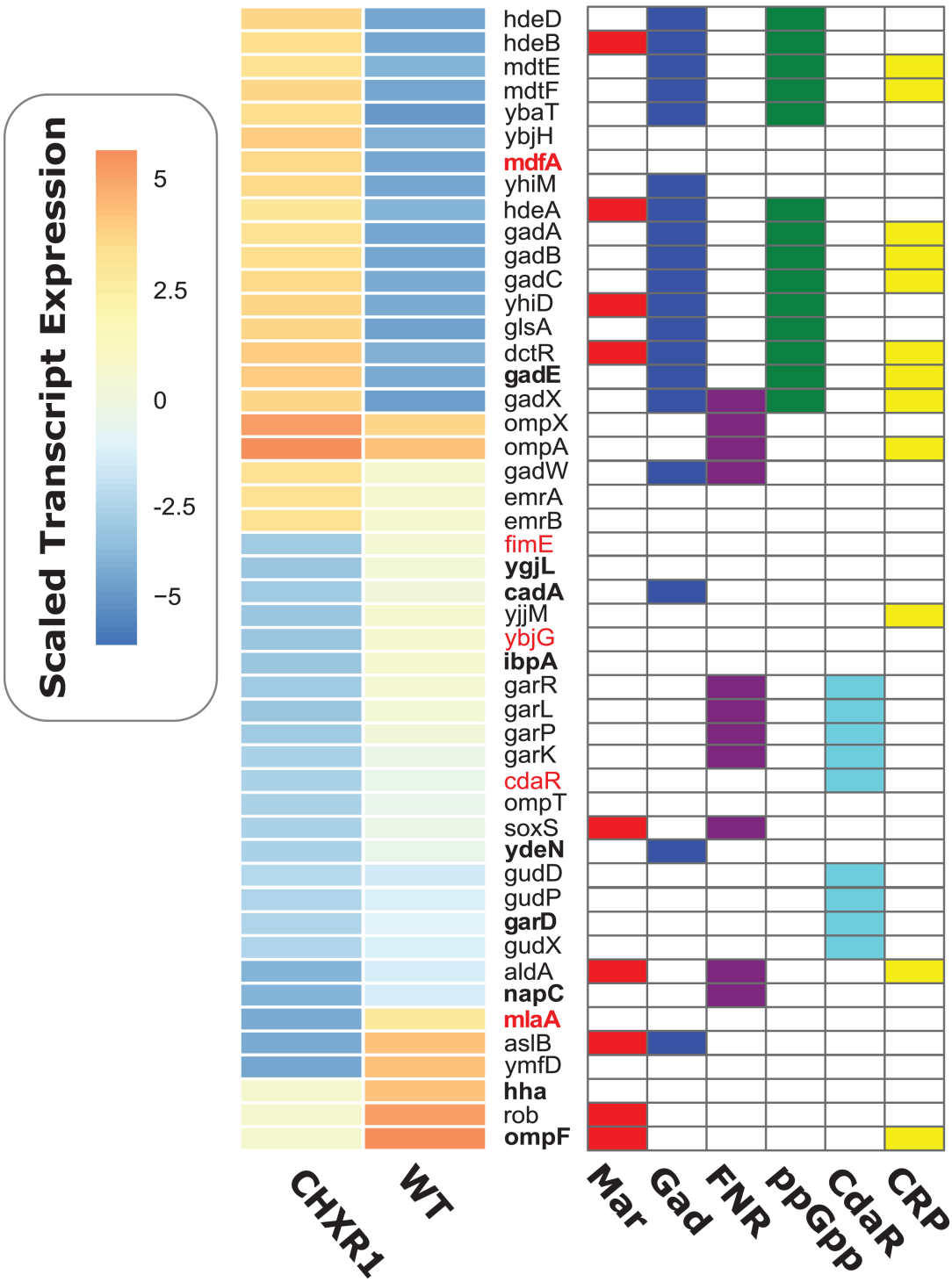

FIGURE 4 | A heatmap diagram of significantly altered gene transcripts of CHXR1 and WT *E. coli* for RNA-seq transcriptional analysis. The heatmap shown to the left of the gene names listed indicates scaled median gene expression values of CHXR1 and WT, where red to orange colors indicate genes that were up-regulated and blue to dark blue colors indicate down-regulated transcripts of CHXR1 to WT. Heat mapped expression data represents median gene expression values from three biological replicates (n = 3) of WT and CHXR1 isolates. Colored charts on the right-hand grid beside each y-axis gene name indicate whether or not the listed gene is regulated by the mar-sox-rob regulon (Mar; red), GadE/W/X (Gad; blue), fumarate and nitrate reductase regulon (FNR; purple), stringent response system (ppGpp; green), carbohydrate diacid regulator CdaR (light blue), and cyclic AMP-CRP regulon (CRP; yellow). Gene names in red font indicate genes that possessed SNVs (**Figure 5B** and **Table 4**) and genes with bolded font indicate translated protein products that were significantly altered in abundance based on proteomic analyses (**Figure 3**).

down-regulated porin *ompF* transcripts in CHXR1 (**Figure 4**), had similar accumulation differences in their translated CHXR1 proteins when compared to WT proteomes (**Figure 3**). In CHXR1 transcriptomes, efflux pump *emrAB* was up-regulated 2-fold, whereas only three additional porins *ompX* (3.1-fold up-regulated), *ompA* (2.2-fold upregulated) and *ompT* (4.3-fold down-regulated) exhibited altered expression in CHXR1 when compared to WT (**Figure 4**). Acid resistance and pH regulatory genes *cadA* and *gadE* previously identified as having altered protein accumulation also demonstrated similar alterations in transcript levels in CHXR1 transcriptomes (**Figure 4**). Up-regulation of *gadE* transcripts (8.1-fold from WT) and other GAD system transcriptional regulators *gadX* (4-fold), and *gadW* (2-fold) were detected in CHXR1 when compared to the WT transcriptome (**Figure 4**). Altered expression of GAD regulated genes were also noted and included *mdtEF*, *gadABC*, *cadA*, *hdeABD,* and *ydeN* (Mates et al., 2007) when compared to the WT transcriptome (**Figure 4**); YdeN is important to note as it was also down-regulated in CHXR1 proteomes (**Figure 3**). This suggests that *gadE* and the GAD system regulon may play a role in *E. coli* CHX resistance.

Altered expression of genes in CHXR1 that were genetically altered by SNVs based on WGS were identified for *mlaA* and the carbohydrate diacid regulator *cdaR* (**Table 4**). Reduced transcript levels of outer membrane lipoprotein *mlaA* (6.4-fold reduction) was identified in CHXR1 and this finding also corresponds with proteomic data where MlaA protein was only detectable in WT CY proteomes only, highlighting its consistent absence in CHXR isolates. The carbohydrate diacid regulator *cdaR,* which had a single frame shift mutation in *cdaR* in the CHXR1 genome, was also significantly down-regulated (6-fold) in the CHXR1 transcriptome (**Figure 4** and **Supplementary Table 6**). Many of the genes regulated by *cdaR,* such as D-glucarate degrading enzymes *gudDPX* and D-galactarate degrading enzymes *garDKPLR* (Monterrubio et al., 2000), were noticeably down-regulated in CHXR1 as well (**Figure 4** and **Supplementary Table 6**), suggesting that the reduction of each carbohydrate degrading enzyme pathway may increase these osmolytes and contribute to CHXR1 resistance.

Lastly, antimicrobial stress inducible genes *rob* and *soxS* were down-regulated 3 to 4-fold in CHXR1 (**Figure 4**). *rob* and *soxS* are part of the multiple antibiotic resistance *mar-sox-rob* regulon that directly regulates efflux pumps (*acrAB-tolC*) and indirectly *ompF* porin transcription (via *micF*) (Chubiz and Rao, 2011), however, we only detected significant *ompF* down-regulation in CHXR1 (**Figure 4** and **Supplementary Table 6**). Altogether, this indicates that antimicrobial, and pH/acid inducible stress systems are significantly altered in CHX-adapted *E. coli,* in addition to

TABLE 4 | A summary of repetitive coding and non-coding SNVs identified from CHX-adapted genomes sequenced in this study.

Coding SNVs*						
Gene	**Isolate**	**Type of SNV****	**Function**	**Location**	**Locus Tag**	**Uniprot ID[a]**
mlaA/vacJ	CHXR1	1NS, 1A	Intermembrane phospholipid transport system; outer membrane lipoprotein	Outer membrane	b2346	P76506
	CHXR2	6NS, 1T				
	CHXR3	4NS, 1T				
yghQ	CHXR1	10NS, 2F, 2S	Putative multidrug/oligosaccharidyl-lipid/polysaccharide (MOP) flippase superfamily transporter	Plasma membrane	b2983	Q46841
	CHXR3	2NS, 1S				
yhiS-2	CHXR2	1S, 1F, 3NS	Pseudogene; putative uncharacterized protein	Unknown	b3504	P37635
yhiS-1	CHXR3	7NS				
Non-coding upstream region SNVs						
Gene	**Isolate**	**Type of SNV****	**Function**	**Location**	**Locus tag**	**Uniprot ID**
mlaA	CHXR1	12	Intermembrane phospholipid transport system; outer membrane lipoprotein	Outer membrane	b2346	P76506
insH1	CHXR2	9	CP4-6 prophage; insertion sequence 5 (IS5) transposase and trans-activator	Plasma membrane	b0259	P0CE49
	CHXR3	2				
fimE	CHXR1	11	Transcriptional regulator of fimbria type 1 *fimA*	Cytosol	b4313	P0ADH7
	CHXR2	11				
	CHXR3	16				

A detailed list of SNVs and their locations is provided in **Supplementary Table 2. **The total number of SNVs is provided as well as their type and they are abbreviated as follows: synonymous (S), non-synonymous (NS), frameshifted (F), truncation due to stop codon (T), altered start codon (A). In some cases, the corresponding NS amino acid alteration is highlighted according to its translated residue number. [a]ID refers to Uniprot identification number.*

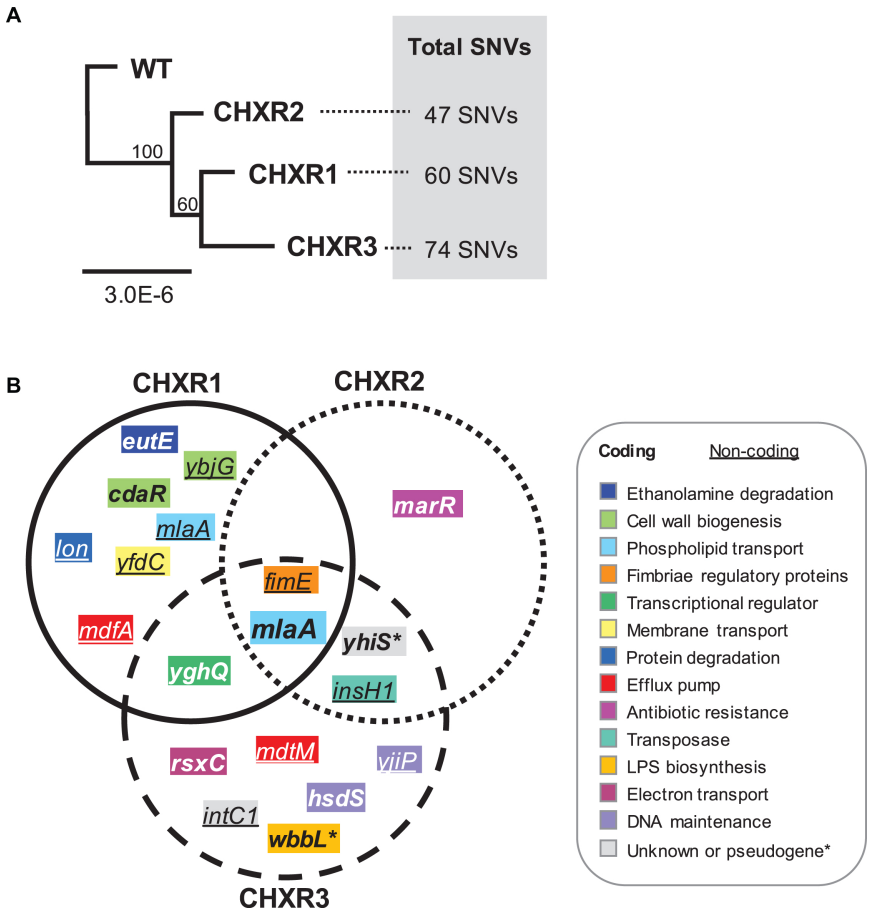

FIGURE 5 | Phylogenetic analysis of CHXR isolate genomes and a Venn diagram summary of coding and non-coding SNVs identified in each CHXR isolate. **(A)** A Maximum Likelihood dendrogram of aligned WGS WT and CHXR1-3 sequences, where bootstrap confidence values are indicated at each node. Total SNVs identified from genomic comparisons of each CHXR isolate to the WT is indicated on the right-hand side of the dendrogram. **(B)** A Venn diagram summary highlighting SNVs identified in the coding genes and non-coding upstream regions of genes (underlined) identified from CHXR isolates by WGS. The gene names shown in the diagram are color-coded according to their functional association as shown in the panel legend.

TABLE 5 | A summary of CHX MIC values from AST of plasmid transformed WT, CHXR isolates, and *E. coli* K-12 single gene deletions.

		Mean transformant CHX MIC values (μg/mL)						
Strain/isolate transformed	**pCA24N**	**pMlaA**	**pYghQ**	**pMarR**	**pFimE**	**pYhiS**	**pCdaR**	**pGadE**
BW25113 (WT)	2	1	2	2	**4**	2	2	2
CHXR1	8	**2**	8	8	8	8	**4**	8
CHXR2	8	**2**	8	8	8	8	8	8
CHXR3	8	**2**	8	8	8	8	8	8

Deletion strain	**Mean CHX MIC values (μg/mL)**
BW25113 (WT)	2
JW2343-KC (Δ*mlaA*)	**4**
JW5490-KC (Δ*yghQ*)	**4**
JW4276-KC (Δ*fimE*)	2
JW3471-KC (Δ*yhiS*)	2
JW3480-KC (Δ*gadE*)	**4**
JW5013-KC (Δ*cdaR*)	2

Bold values indicate significant >2-fold MIC changes as compared to the relevant control (pCA24N or WT).

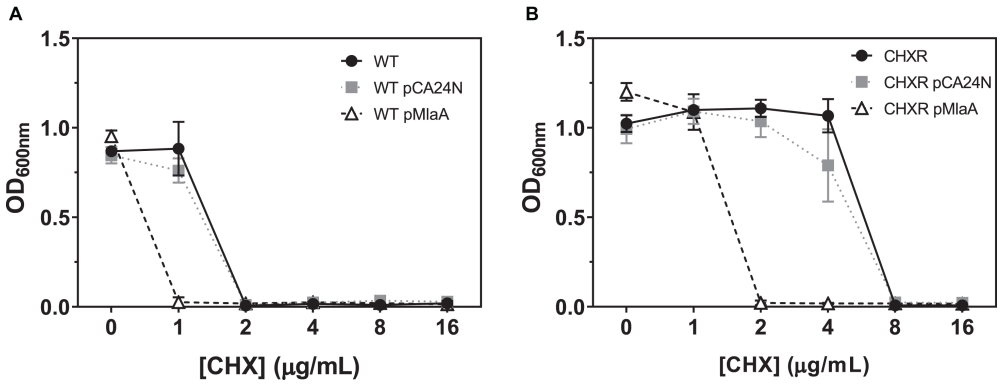

FIGURE 6 | A summary of broth microdilution AST $OD_{600\ nm}$ values for CHXR and WT pCA24N and pMlaA transformants after 18 h of growth at 37°C. **(A)** pCA24N, and pMlaA transformed CHXR1-3 isolates $OD_{600\ nm}$ values after 18 h of growth at 37°C at increasing CHX concentrations. The results of CHXR1-3 isolate $OD_{600\ nm}$ values are shown as a plotted average and error bars indicate standard deviation. **(B)** pCA24N, and pMlaA transformed WT (BW25113) isolates $OD_{600\ nm}$ values after 18 h of growth at 37°C at increasing CHX concentrations with chloramphenicol selection. Untransformed CHXR1-3 isolate **(A)** or WT **(B)** $OD_{600\ nm}$ values are shown in each panel as a negative control reference and were grown in the absence of chloramphenicol. All transformant AST $OD_{600\ nm}$ values were measured in biological triplicate.

genes corresponding to antiseptic resistance mechanisms (i.e., efflux pump, LPS modifiers, and porins).

WGS of CHX-Adapted *E. coli* Isolates Identifies Repetitive Deleterious SNVs in *mlaA* Gene in All Three Isolates

To discern the genetic consequences of CHX-adaptation, we performed WGS analysis at 30X coverage on each CHX-adapted isolate (CHXR1-3) and compared them to sequenced WT as summarized in **Supplementary Tables 7**, **8**. Findings from this analysis identified relatively few SNVs among each CHXR isolate (47–74 SNVs total), indicating that prolonged CHX-exposure did not generate numerous SNVs in this *E. coli* strain (**Figure 5A** and **Supplementary Table 8**). Maximum Likelihood phylogenetic analyses of the sequenced genomes showed that all CHX-adapted isolates grouped together and separately from the WT sequence, where CHXR1 and CHXR3 grouped more closely together than CHXR2 but at lower bootstrap confidence values (60/100; **Figure 5A**). After comparing CHXR genomic sequences to the sequenced WT reference we identified SNVs in a number of coding and non-coding regions as summarized in **Supplementary Table 8**. However, very few of these SNVs were repeatedly identified in the same gene(s) amongst all three CHXR isolates as summarized in **Figure 5B** and **Table 4**. As shown in the Venn diagram SNV summary of **Figure 5B** only a single gene *mlaA* (also known as *vacJ*), encoding for an outer membrane lipoprotein and component of the Mla retrograde phospshoplipid transport system, was repeatedly identified in all three CHXR isolates. In each CHXR isolate, the *mlaA* gene possessed deleterious SNVs that either truncated the gene, resulting in reading frameshifts (CHXR2-3) or eliminated its start codon (CHXR1) as noted in **Table 4**. Several SNVs were also repeatedly identified in 2/3 CHXR isolates, specifically, in *yghQ* a putative multidrug/oligosaccharidyl-lipid/polysaccharide (MOP) flippase superfamily transporter (Saier et al., 2016) and a pseudogene *yhiS* (*yhiS*-1, *yhiS*-2) which is disrupted by an insertion element and encodes for an as yet uncharacterized protein (**Figure 5B** and **Table 4**).

Our analysis of non-coding SNVs in repetitively occurring regions of the CHX-adapted isolates primarily focused on upstream genetic regions for their potential to disrupt coding sequence expression/regulation (**Table 4**). In all three CHXR isolates, there was only one set of repetitively identified non-coding SNVs in the upstream of *fimE*, which is a transcriptional regulator of the type 1 fimbrial gene *fimA*. FimE is a recombinase that controls the "ON-OFF" *fim*-switch (*fimS*) that regulates transcription of the type 1 fimbrial operon referred to as phase-variation (Kulasekara and Blomfield, 1999). In CHXR1 transcriptomes, *fimE* was down-regulated by 3.6-fold but no significant changes in any other *fim* operon gene expression was identified (**Figure 4** and **Supplementary Table 6**). More in-depth analysis of the *fimS* region from WGS contigs revealed that all three CHXR possessed SNVs and indel alterations of the *fimS* resembling a hybrid ON-OFF promoter sequence (**Supplementary Figure 5**), which may explain why *fimE* expression was reduced in CHXR1 when compared to WT. The only other repetitively identified non-coding SNV region was in the upstream region of *insH1* in CHXR2-3 isolates. InsH1 is a transposase and transcriptional trans-activator of the insertion sequence element IS5 and it is a stress inducible gene within the cryptic prophage (CP) 4–6 in *E. coli* K-12 (Schnetz and Rak, 1992). Transcripts of *insH1* were not shown to significantly differ between CHXR1 and WT transcriptomes (**Supplementary Table 6**). Lastly, it is worth noting that the upstream region of *mlaA* in the CHXR1 isolate had numerous nucleotide sequence substitutions and transversions that altered the putative –35 and –10 regions of the *mlaA* promoter (**Supplementary Table 8**). When this finding is combined with coding SNV data showing the start codon of *mlaA* is altered in CHXR1, all three CHXR isolates are expected to have non-functional *mla* genes. In summary, WGS revealed that relatively few genes

were repetitively altered in all CHX-adapted and suggests the involvement of *mlaA* and *fimE* in all CHXR isolates.

Complementation of CHXR Isolates With *mlaA* Reverts the CHX-Resistant Phenotype to WT

Our final aim sought to identify which genes that were confidently and repeatedly identified in our multi-omics analyses of CHX-adapted isolates, specifically contributed to overall CHX-resistance mechanisms. Using the *E. coli* ASKA plasmid clone library we transformed plasmids with cloned genes for *marR, mlaA, yghQ, yhiS, fimE, gadE,* and *cdaR* (**Table 1**), into each CHXR isolate and the WT strain to determine if there were any significant changes in CHX susceptibility using broth microdilution AST methods as previously described. The results from all plasmid complementations revealed that only CHXR isolates transformed with pMlaA showed significant 4-fold reductions in CHX MIC values as compared to the parental vector pCA24N (**Figure 6A** and **Table 5**). Complementation of the WT strain with these plasmids also demonstrated a significant reduction in CHX MIC values for pMlaA only (**Figure 6B** and **Table 5**). No changes in CHXR1-3 transformant CHX MIC values were determined for pYghQ, pFimE, or pMarR indicating that *mlaA* primarily influences the CHX-resistant phenotype (**Table 5**). It is important to note that transformation of WT with pFimE resulted in a 2-fold increase in CHX MIC when compared to the parental vector but no changes in CHX MIC were observed in any CHXR isolate transformed with pFimE (**Table 5**), indicating that FimE had no impact on CHX-resistant phenotypes. Additionally, only pCdaR CHXR1 transformants showed 2-fold CHX MIC reduction as compared to the parental vector (**Table 5**). Since CHXR1 was the only isolate to have *cdaR* mutations, the partial complementation of a functional *cdaR* gene suggests this carbohydrate diacid regulator may also contribute to CHX resistance mechanisms. However, *cdaR* likely is most effective in combination with Δ*mlaA* deletions based on the lack of CHX MIC values difference from the WT in Δ*cdaR* strain (**Table 5**).

Antimicrobial susceptibility testing of *E. coli* K-12 BW25113 Keio collection strains containing single gene deletions the same complemented genes listed above, revealed that only the deletion of Δ*mlaA* (JW2343-KC), Δ*yghQ* (JW5490-KC), and Δ*gadE* (JW3480-KC) increased CHX MIC values by 2-fold from the WT (**Table 5**). This suggests that the loss of *mlaA* in *E. coli*, as well as the individual deletion of putative polysaccharide exporter *yghQ* or the GAD transcriptional regulator *gadE* can also confer modest CHX-resistance enhancements based on MIC values. Growth curve analysis of Δ*mlaA* and WT showed no statistically significant differences in growth rate in all media tested (**Supplementary Figure 6** and **Supplementary Table 3**). However, similar to CHXR isolate growth curves, Δ*mlaA* also had significantly higher final OD_{600nm} values than WT (by 20–29%) in all media tested (LB, MHB, and DG) with and without added CHX (**Supplementary Figure 6**). These findings confirm that pMlaA complementation and *mlaA* over-expression in CHXR and WT strains is detrimental for CHX resistance and in fact even increases WT cell susceptibility to CHX. Our results also identify additional *E. coli* genes (*yghQ*, *fimE*, *gadE,* and *cdaR*) that when altered, may additively contribute toward CHX-resistant phenotypes and serve as additional CHX biomarkers with *mlaA*.

DISCUSSION

The findings from this phenotypic and multi-omics study of CHX-adapted *E. coli* isolates have revealed the importance of MlaA in intrinsic CHX resistance. Outer membrane lipoprotein MlaA forms a complex with outer membrane porins OmpF and OmpC (Chong et al., 2015), and serves as the outer membrane component linking the remaining MlaFEDBC system components in the plasma membrane and periplasm to the outer membrane. The Mla system, referred to as the maintenance of outer membrane lipid asymmetry in Gram-negative species, functions as a retrograde phospholipid transport system. This system removes phospholipids from the outer membrane back into the plasma membrane in an ATP-dependent process (Ekiert et al., 2017). Retrograde phospholipid trafficking helps maintain LPS enrichment in the outer leaflet of the outer membrane and assists in cellular phospholipid recycling. In our study of CHX-adapted *E. coli* isolates, we observed deleterious SNVs in a single gene, *mlaA* amongst all three CHXR isolates indicating its involvement in CHX resistance (**Figure 5B** and **Table 4**). This suggests that intrinsic CHX resistance by *E. coli* and potentially other Gram-negative species is enhanced when the retrograde phospholipid Mla transport system is inactivated and may be an important contributor to CHX resistance mechanisms. Since CHX acts by forming gaps between paired lipids, we speculate that CHX may be brought along with its paired lipids as they are returned back to the plasma membrane by the Mla system, this may also identify a route of entry of CHX into the cell. When the MlaA is absent, as we observed in our CHX-adapted isolates, CHX entry and potentially its membrane disruptive mechanisms of action are prevented.

Our findings related to MlaA and CHX-resistance herein appear to be novel, however, other Mla system components have been previously identified as antimicrobial resistant contributors in various proteobacterial studies (Bernier et al., 2018; Elliott et al., 2020). MlaC, a periplasmic spanning protein component of the Mla system was previously shown to confer resistance to antimicrobial peptide arenicin-3 in uropathogenic strains of *E. coli* (Elliott et al., 2020). MlaC was also shown to participate in the intrinsic resistance of *Burkholderia cepacia* complex species, where mutants were more susceptible to Gram-positive selective antibiotics (macrolides, rifampin) as well as fluoroquinolones and tetracyclines (Bernier et al., 2018). In our study, CHXR isolates were more susceptible to cationic antiseptic QACs (CTAB and CDAB) and tobramycin which is cationic antibiotic at neutral pH (**Table 2**). Although we included Gram-positive selective antimicrobials rifampin, vancomycin, and macrolide erythromycin, we did not see any significant changes in MIC values for our CHXR isolates (**Table 2**). This may suggest that *mlaA* mutants we observed in our *E. coli* isolates may

confer more selective antimicrobial resistant profiles as compared to mutations in internal *mlaFEDBC* system inter-membrane spanning components.

Our adaptation of *E. coli* K-12 to CHX did not result in colistin cross-resistant phenotypes as shown in previous studies of *Klebsiella* and *Salmonella* species (Wand et al., 2017; Hashemi et al., 2019; Verspecht et al., 2019). We did, however, identify two proteins (BasS, LpxL; **Figure 5B**) in our CHXR1 isolate that have been previously implicated as mechanistic contributors of colistin resistance and LPS modification (Olaitan et al., 2014). Based on our study, the alteration of only two proteins previously associated with colistin resistance was insufficient to confer colistin cross-resistance in CHX-adapted *E. coli*. Our findings also show that the LB growth medium we used to initially adapt *E. coli* K-12 only contained CHX, and as result, it generated adapted isolates with resistance exclusively to CHX and even excluded cross-resistance to the other bisbiguanide ALX we tested (**Table 2**). The chemical structure of ALX differs significantly from CHX as ALX possesses ethylhexane chains instead of benzene rings at the end of the biguanidine moieties. These key chemical differences likely impact how each bisbiguanide displaces or disrupts phospholipid associations and could result in different lipid-to-bisbiguanide compound configurations, thereby affecting different outer membrane systems. ALX was previously shown to have a higher affinity for LPS binding than CHX, which may be an influential factor (Zorko and Jerala, 2008). It is also important to note that species isolated from the environment are likely exposed to far more antimicrobials than the controlled conditions of our study and the lack of antimicrobial cross-resistance we observed in our CHX-adapted isolates may simply reflect controlled lab conditions. Additionally, *E. coli* K-12 lacks the *O*-antigen moiety present in most pathogenic *E. coli* strains and LPS antigens present in other Enterobacterial clinical isolates like *Klebsiella* spp. and *Salmonella* spp. (Rai and Mitchell, 2020). Future studies of *mlaA* and its role in antimicrobial resistance and antiseptic resistance can now focus on exploring other Enterobacterial species including clinical isolates, which may identify additional outer membrane contributors to intrinsic CHX-resistance and cross-resistance.

A notable finding from transcriptome and proteomic analyses show a small, but potentially important role for two acid regulatory systems in CHX resistance, specifically the GAD (*gadE*) system and carbohydrate diacid regulator (*cdaR*) (**Figures 3**, **4**). Due to the cationic charge of CHX in solution ($\leq$pH 7), CHX can decrease pH as its concentration increases, likely triggering acid resistance system requirement. The glutamate dependent GAD system transcriptional activator *gadE* had increased protein abundance and transcript levels in CHXR1 multi-omics analyses (**Figures 3**, **4**). GadE, along with GAD system regulators GadX/GadW, regulate the expression of many genes involved in pH homeostasis and acid resistance, including the efflux pump *mdtEF* gene which were shown to be transcriptionally up-regulated in CHXR1 (**Figure 4**). Complementation of pGadE in all three CHXR isolates did not alter CHX MIC values, however, deletion of Δ*gadE* in *E. coli* did increase WT resistance by 2-fold (**Table 5**). This suggests gadE deletions may partially contribute to CHX resistance mechanisms. Additionally, carbohydrate diacid regulator CdaR was another proteomically and transcriptomically diminished protein/transcript in CHXR1 (**Figures 3**, **4**), that was also mutated by a single frame shifting SNVs in the CHXR1 isolate (**Table 4**). As we observed from AST, only pCdaR CHXR1 had a 2-fold reduced CHX MIC value (**Table 5**), suggesting that the loss CdaR expression can partially rescue the CHX susceptible phenotype back to WT levels. Since CdaR regulates the D-glucarate (*gudPDX*) and D-galactarate (*garPLRK*) uptake and metabolism (Monterrubio et al., 2000), the build-up of glucarate and galactarate compounds may offset the pH and osmotic stress associated with CHX exposure. Although neither *gadE*/*cdaR* gene deletion or plasmid complementations resulted in significant CHX MIC changes on their own (**Table 5**), it is likely that *cdaR* deletion or *gadE* up-regulation may be important additive acid regulatory systems with Δ*mlaA* to confer greater intrinsic CHX resistance.

Lastly, our phenotypic analysis of CHX-adapted *E. coli* isolates herein demonstrated that these isolates had similar or enhanced growth rates as the un-adapted WT across the rich and minimal media we tested (**Figure 1**, **Supplementary Figures 1**, **2**, and **Supplementary Tables 2**, **3**). CHXR cells were also narrower and shorter than WT cells in mid-log phase based on SEM imaging (**Figure 2**) and more permeant to the dead cell stain propidium iodide (**Supplementary Figure 4**), indicating that the cell membranes of CHXR1 are more compromised than WT. Molecular explanations for these morphological alterations are likely due to expected outer membrane phospholipid distribution problems that would be caused by the loss of functional MlaA in the CHXR isolates (as discussed above). Our growth curve analyses of WT and (Δ*mlaA*) revealed that the loss of *mlaA* increased CHXR cell CFU/mL numbers and cells grew to higher final ODs than WT but CHXR isolates did not increase doubling times significantly from WT (**Supplementary Figure 6** and **Supplementary Table 3**). We speculate that the lack of phospholipid recycling caused by the deletion of *mlaA* in cells exposed to CHX, helps the cell overcome its membrane disruptive actions by providing more phospholipids for CHX to interact with, ultimately slowing CHX entry into the cell. In addition to *mlaA* mutations, we identified non-coding alterations to the promoter region of the transcriptional regulator *fimE*, which is an important type 1 fimbrial regulator (**Figure 3** and **Table 4**). Although changes in type 1 fimbrial expression primarily impacts cell attachment, previous studies have also shown that type 1 fimbrial gene (*fim*) mutants can influence bacterial colony morphology (Hasman et al., 2000). Our transcriptomic analysis of CHXR1 identified that *fimE* was significantly down regulated in CHXR1 but *fimAICDFGH* operon expression was not significantly altered as compared to WT (**Figure 4** and **Supplementary Table 6**). This might be explained by our WGS findings; all CHXR isolates had significant SNVs and indels that altered the *fimS* promoter region regulated by *fimE*, where it had a hybrid ON-OFF sequence configuration (**Supplementary Figure 5**). This hybrid promoter may explain the *fimE* and *fimAICDFGH* operon transcriptome results (**Figure 4**). Transformation of CHXR isolates with

plasmids expressing *fimE* failed to alter their CHX MIC values (**Table 5**) but deletion of *fimE* in *E. coli* (JW4276-KC) did increase CHX resistance by 2-fold as compared to WT (**Table 5**). This suggests that similar to *gadE* and *cdaR*, *fimE,* and the *fim* operon it transcriptionally regulates may also play another small but additive role when combined with the Δ*mlaA* phenotype.

In conclusion, our phenotypic and multi-omics analyses of CHX-adapted *E. coli* K-12 isolates has identified the involvement of *mlaA* as an intrinsic CHX resistance contributor. The role of MlaA, the outer membrane component of the Mla retrograde phospholipid transport system, in CHX resistance is a novel finding that may have broader implications for intrinsic CHX resistance in *E. coli* as well as other Gram-negative bacterial species. The Mla system component MlaC, was shown to contribute to antimicrobial resistance in other proteobacterial species, such as *Burkholderia* (Bernier et al., 2018) highlighting the importance of this lipid transport system as a potential therapeutic antimicrobial target. When combined with our proteomic and transcriptome analysis, the findings of our study offer greater insights into the mechanism of intrinsic CHX resistance and identify many other pertinent antiseptic resistant biomarkers (*yghQ, fimE, gadE, cdaR*) that may be helpful for future initiatives to rapidly detect CHX-resistant phenotypes.

MATERIALS AND METHODS

Chemicals and Bacterial Strains Used in This Study

Chlorhexidine digluconate (CHX), as well as all other antimicrobials and chemicals used in this study were obtained from either Tokyo Chemical Industry America (United States), Millipore Sigma (United States), Fisher Scientific (United States), or VWR (Canada). *E. coli* K-12 BW25113 (Baba et al., 2006) was obtained from the Coli Genetic Stock Centre (CGSC[3]). All cultures were grown with selection when necessary in Luria-Bertani (LB) broth at 37°C with shaking at 150 revolutions per min (RPM) (WT transformants: 30 μg/mL chloramphenicol (CM); CHXR: 2 μg/mL CHX; CHXR transformants: 2 μg/mL CHX and 30 μg/mL CM).

CHX Adaptation Experiments

Chlorhexidine adaptation experiments were performed in LB broth medium using a gradual adaptation sub-culturing method as described by Bore et al. (2007) with modifications. Briefly, *E. coli* K-12 BW25113 was initially grown overnight (18 h) from a dimethylsulfoxide (DMSO) cryopreserved stock and then diluted 10^{-2} into 5 mL LB containing 0.4 μg/mL CHX (20% of the WT MIC value) in triplicate. The next day, each individual culture was re-inoculated into 5 mL of fresh LB containing 0.4 μg/mL CHX and grown overnight until day 12 to expose the cultures to prolonged sub-inhibitory CHX. After day 12, cultures were exposed to increasing CHX above the MIC value of WT (2 μg/mL) for an additional 8 generations for a total of 20 days. This process generated three independent isolates: CHXR1, CHXR2, and CHXR3 (**Table 1**) and a summary of the CHX concentrations added to each sub-culture is shown in **Supplementary Table 1**. At the end of this process, adapted bacteria were cryopreserved in LB with 16% (v/v) glycerol and stored at −80°C.

[3]cgsc2.biology.yale.edu

Antimicrobial Susceptibility Testing (AST) to Determine MIC Values

A modified broth microdilution AST method (CLSI, 2012) was used to determine MIC values. Briefly, cryopreserved stocks of WT or CHX-adapted *E. coli* were inoculated overnight without selection, then overnight with selection. Culture turbidity was measured and standardized spectrophotometrically to obtain an optical density ($OD_{600\ nm}$) of 1.0 unit in LB with a Multiskan Spectrum microplate reader (Thermo Fisher Scientific, United States). The adjusted cultures were diluted 10^{-2} into 96-well microtiter plates containing 2-fold serial dilutions of antimicrobial in LB broth. AST for all isolates was performed in technical triplicate. A total of 22 antimicrobial compounds were included for AST and are summarized in **Table 1**. For antimicrobials that required solubilization in ethanol (linezolid; LZD, rifampicin; RMP, erythromycin; ERY), or DMSO (alexidine; ALX, trimethoprim-sulfamethoxazole; SXT), control plates containing the same concentration of these solvents only were used to assure the results were due to the antimicrobial. Once inoculated, all microplates were incubated overnight before $OD_{600\ nm}$ spectrophotometric measurement. Significant increases in MIC were defined as greater than 2-fold MIC changes when compared to the WT.

Growth Curve and CHX Resistance Stability Testing of CHX-Adapted Isolates

Bacterial fitness was assessed for CHX-adapted isolates, WT (BW25113), and JW2343-KC (Δ*mlaA*) in 96-well microplate broth cultures. Microplate growth curves were set up as described for AST testing, however, CHX concentrations used in these assays were 20% of the WT strain's MIC value (0.4 μg/mL) to compare isolates grown at identical drug exposures. Growth curves were measured spectrophotometrically over 24 h using a Synergy Neo2 Hybrid Multimode reader (Biotek, United States). Twenty-four hour growth curve experiments were repeated for each replicate tested in a variety of rich media [LB, LB plus 0.4% (w/v) glucose; LB + Glc, cation adjusted Mueller Hinton broth; MHB, Tryptic Soy broth; TSB] and minimal (minimal nine salts; M9, Davis Glucose; DG) media. To calculate the doubling time of the WT, Δ*mlaA*, and CHXR isolates in each media, $OD_{600\ nm}$ values were blank subtracted and plotted on a semi-log graph; calculated values are provided in **Supplementary Table 3**. The linear slopes of plotted $OD_{600\ nm}$ trendlines ($R^2 \geq 0.99$) were used to calculate each culture's doubling time/growth rate in 2-min intervals. Final mean colony-forming units/mL (CFU/mL) were determined from the number of colonies produced from three biological replicates of 100 μl of diluted (10^{-7}) *E. coli* 24 h culture plated on LB agar and incubated overnight (18 h) at 37°C (**Supplementary Table 3**).

The phenotypic stability of each CHX-adapted *E. coli* was assessed by repeated sub-culturing of the CHX-adapted isolates in LB without CHX over 10 days. Each day, AST against CHX was performed as described above. All stability experiments were completed in technical triplicate per isolate (**Table 3**).

Scanning Electron Microscopy

To identify morphological anomalies between WT and CHX-adapted *E. coli*, SEM was performed using conditions described by Golding et al. (2016). Briefly, bacterial samples were grown with selection to an $OD_{600\ nm}$ of 0.5 units, pelleted by microcentrifugation (30 s at 14,000 RPM) and resuspended in PBS. Once resuspended, we modified the protocol by diluting the sample 1:1000 instead of 1:10 as to not overload the filter. Each sample's filter was washed with increasing concentrations of ethanol before being allowed to dry. Samples were mounted onto a carbon disk, put onto an aluminum stud, and contact between the stud and the filter was established using flash dry silver paint. Samples were subsequently sputtered with gold using a Quorum Q150R S (Quorum Technologies, United Kingdom). Each stud was imaged with the JCM-5700 SEM (JEOL, United States), at 5,000X magnification in five different locations on the filter to help assess overall patterns in cell imaging. Twenty bacterial cell lengths and widths were measured in five separate images for each biological replicate (n = 100) where measurements were performed using ImageJ v1.8.0 (Abràmoff et al., 2007). Statistical analysis of measured cell lengths and widths were analyzed using Prism6 v6.0 (Graphpad Software, United States) and significant differences were assessed using the Student's t-test ($P < 0.001$). Two biological replicates of each WT and CHXR1-3 cells were measured by SEM, with no significant difference ($P > 0.05$) between each replicate. Differences between WT and CHXR1-3 in terms of average cell lengths and widths were assessed using a Student's t-test.

Propidium Iodide Dye Cell Permeation Assays

Propidium iodide assays were performed as described by Gregorchuk et al. (2020) using modified live-and heat-treated cell fluorescent dye emission assays. Briefly, mid-log ($OD_{600\ nm}$ = 0.5 units) cultures of CHXR1-3 and WT were grown as described for SEM, but these preparations were washed in cold phosphate buffered saline and resuspended to a final $OD_{600\ nm}$ value of 0.2 units and stored on ice. Samples were divided, where half were heat-treated at 120°C for 20 min (heat-treated) and the other were not (live samples) and added to 96-well fluorescent black-walled microtiter plates containing propidium iodide at 2 μg/ml final concentration. Plates containing heat-treated and live cell preparations of CHXR and WT in biological triplicate and technical triplicate were measured in a fluorescent microplate-reader (Polarstar Optima, BMG labtech, Germany) for 30 min at 37°C taking fluorescent emission measurements at 620 nm every 5 min. RFU values were determined for live as well as heat-treated samples, which were baseline subtracted from emission values from wells lacking cells but containing PBS and dye only. RFU values for each heat-treated and live cell reparations are plotted in **Supplementary Figures 4A,B**. Statistical analysis was performed using Prism v6.0 (Graphpad Software, United States) software to compare significantly different RFU values between WT and CHXR1 samples using Mann–Whitney tests at P-values of < 0.05.

Whole Genome Sequencing (WGS), Genome Assembly, and SNV Analysis

Genomic DNA (10–30 ng/μL) was isolated from each CHX-adapted replicate using a Purelink Microbiome DNA isolation kit (A29790, Thermo Fisher Scientific, United States) according to manufacturer's instructions for bacterial culture DNA extraction. Genome sequencing was performed by MicrobesNG[4] (United Kingdom) with an Illumina-MiSeq system (Illumina Inc., United States) at a minimum of 30X coverage. Sequencing details are found in **Supplementary Table 2**. Trimmed paired reads were generated and assembled in-house using the MicrobesNG pipeline with *E. coli* BW25113 (CP009273.1) as the mapping reference. Each sequenced CHX-adapted *E. coli* genome sequence is available as BioProject ID PRJNA646979 in NCBI GenBank. SNV analysis was performed using Geneious v11.1.5 software (Biomatters Ltd., New Zealand) to identify SNVs and compare DNA sequences from each CHX-adapted replicate to the reference genome. We controlled for genetic drift of the adapted isolates by eliminating any WT SNVs found in the CHX-adapted isolates. A multiple sequence alignment of genome assemblies was created from the mapped reads, and a Maximum Likelihood tree was constructed using *E. coli* BW25113 (NZ_CP009273) as the root sequence using PhyML v.3.3.20180621 (Guindon et al., 2010). Confidence of tree branching was determined by performing 100 bootstrap replicates and these values are indicated at each node in the dendrogram.

Proteomic Analysis and Gene Ontology

Sample Preparation

Proteomic analysis of the CHXR1 was performed on biological triplicate cultures grown in 4 L batches with CHX selection. Cultures were grown to a final $OD_{600\ nm}$ = 0.5 units and were then harvested by centrifugation at 6000 RPM for 10 min in Avanti-J-E High performance centrifuge (HPC; Beckman, United States). The pellet was resuspended by wet weight in an equal volume of isolation buffer: 50 mM 3-(*N*-morpholino) propane sulfonic acid (MOPS), 8% v/v glycerol, 5 mM ethylenediaminetetraacetic acid (EDTA), 1 mM dithiothreitol, pH 7 and WC pellets were stored frozen at –80°C. Cytoplasmic protein extractions were performed from thawed WC pellet preparations, where pellets were thawed and a final concentration of 0.1 mM phenylmethylsulfonyl fluoride was added. This cell slurry was immediately French pressed in a 4°C chilled Thermofisher Sim Aminco 30,000 lb/in^2 cylinder twice at 1,500 lb/in^2 each pressing. The pressed slurry was centrifuged at 10,000 RPM in a JA-20 Beckman rotor, where the supernatant was collected and ultracentrifuged at 40,000 RPM for 90 min in a Type 70Ti rotor in a Beckman Optima XPN-100 ultracentrifuge. The supernatant was saved as the cytosolic

[4]https://microbesng.com/

protein fraction and protein concentrations were determined using a modified Lowry assay (Shen et al., 2013). This cytoplasmic protein extraction was stored at −80°C.

Thawed WC pellets and cytoplasmic extracted protein samples were prepared similarly as detailed below. Thawed pellets were homogenized in sterile Milli-Q water, mixed with 100 µl 0.1-mm glass beads (Scientific Industries Inc., United States), and heated for 5 min at 95°C. Cells were lysed by highspeed vortex-mixing for 3 min, followed by centrifugation at 3000 RPM for 1 min. The supernatant was collected, and another aliquot of cold sterile Milli-Q water was added to the beads, followed by 1 min of vortexing and 1 min of 3000 RPM centrifugation to pool protein supernatants from the beads. This was repeated five times total to extract the remaining proteins, which was stored at –80°C. Protein was quantified using a bicinchoninic acid (BCA) protein assay kit, with bovine serum albumin (BSA) as the standard (Pierce Protein Research Products; Thermo Fisher Scientific, United States). Hundred microgram of protein was isolated from WT and CHXR1 in biological triplicate, and digested with trypsin (Promega, United States) overnight (16–18 h) using a filter-assisted sample preparation (FASP) method described previously (Wiśniewski et al., 2009). Following digestion, all samples were dried down and reconstituted using mass spectrometry grade water to a final concentration of 1 µg/µl for LC-MS/MS analysis.

Nanoflow-LC-MS/MS

Each sample was separately analyzed using a nano-flow Easy nLC 1200 connected in-line to an Orbitrap Fusion Lumos mass spectrometer with a nanoelectrospray ion source at 2.3 kV (Thermo Fisher Scientific, United States). The peptide samples were loaded (2 µl) onto a C_{18}-reversed phase Acclaim PepMap 100 trap column (2 cm × 75 µm, 3 µm particles; Thermo Fisher Scientific, United States) with 30 µL of buffer A (2% v/v acetonitrile, 0.1% v/v formic acid) and then separated on an Easy Spray column (50 cm long, 75 µm inner diameter, 2 µm particles; Thermo Fisher Scientific, United States). Peptides were eluted using a gradient of 2–30% buffer B (80% v/v acetonitrile, 0.1% v/v formic acid) over 100 min, 30–40% buffer B for 20 min, 40–100% buffer B for 5 min and a wash at 100% B for 10 min at a constant flow rate of 250 nl/min. Total LC-MS/MS run-time was about 175 min, including the loading, linear gradient, column wash, and the equilibration.

LC-MS/MS data was acquired using the settings described below. The most abundant precursor ions from each survey scan that could be fragmented in 1 second (s) were dynamically chosen, where each ion was isolated in the quadrupole (0.7 *m/z* isolation width) and fragmented by higher-energy collisional dissociation (27% normalized collision energy). The survey scans were acquired in the Orbitrap at mass over charge ratios (*m/z*) of 375–1500 with a target resolution of 240,000 at *m/z* 200, and the subsequent fragment ion scans were acquired in the ion trap at a rapid scan rate. The lower threshold for selecting a precursor ion for fragmentation was 1.5×10^4. Dynamic exclusion was enabled using a *m/z* resistance of 10 parts per million (ppm), a repeat count of 1, and an exclusion duration of 15 s.

Data Processing

All spectra were processed using MaxQuant (v1.6.7, Max Planck Institute) using the imbedded Andromeda search engine. Searches were performed against a subset of the SwissProt database set to *E. coli* K-12 (4519 sequences). The following search parameters were used: Carbamidomethyl (C) was selected as a fixed modification, Oxidation (M) and Acetyl (Protein N-term) as variable modifications, fragment ion mass resistance of 0.5 Da, parent ion resistance of 20 ppm, and trypsin enzyme with up to two missed cleavage. False discovery rates were set up using 0.01 for peptides, 0.01 for proteins, and at least 1 razor peptide per protein. Label free quantification (LFQ) was enabled for Quantitation. Resulting LFQ intensities were imported into Perseus v1.6.5 (Max Planck Institute) (Tyanova et al., 2016). In Perseus the data was Log2 transformed. All proteins that did not have a least three valid log2 LFQ intensities from ID were filtered out. Proteins present were assessed for significance using volcano plots with a modified Student's *t*-test (false discovery rate of 0.05; $S_0 = 0.1$). Enrichment analysis of protein-to-protein interactions was performed with Cytoscape v3.7.2 (Shannon et al., 2003) using the StringApp v1.5.0 software package (Doncheva et al., 2019). To analyze functional pathways involved in adaptation, significant proteins were categorized using the KEGG pathway database with ClueGO v2.5.5 (Bindea et al., 2009) application for Cytoscape. Default parameters for KEGG analysis were used, with network specificity set at "medium" and 50% overlap of genes for the group merge.

RNA-Seq Transcriptomic Analysis

Transcriptomic analyses were preformed with 10 mL WT and CHXR1 cultures grown to mid-log phase ($OD_{600\ nm}$ = 0.5 units) in biological triplicate, where CHXR1 cultures were grown with CHX selection as described for proteomic analyses. Cells reaching mid-log were immediately stored on ice and total RNA was extracted using a bacterial RiboPure RNA purification isolation kit (Ambion Inc, TX, United States) according to the manufacturer's protocol for Gram-negative bacterial extraction yielding 25–50 µg of RNA/sample. Ribosomal RNA was depleted from these samples using MICROB*Express* Bacterial mRNA Enrichment kit (Ambion Inc, TX, United States) based on the manufactures recommended standard protocol. mRNA sequencing analyses were performed by LC Sciences total RNA sequencing services (StateTexas, United States) using an Illumina NovaSeq 6000 for paired-end sequencing. RNA integrity, quality control and quantification analyses were performed using an Agilent Technologies 2100 Bioanalyzer with high sensitivity DNA chip.

Transcript sequences were bioinformatically analyzed by LC Sciences using the following workflow. Raw transcript sequence reads were assembled using Cutadapt (Martin, 2011) and in-house perl scripts to remove adaptor contaminated reads, low quality bases and undetermined bases. Sequences were verified using FastQC[5] and bowtie2 (Langmead and Salzberg, 2012) was used to map reads to the *E. coli* BW25113 genome

[5]http://www.bioinformatics.babraham.ac.uk/projects/fastqc/

(GenBank accession number CP009273.1). Mapped reads for each bioreplicate were assembled using StringTie software (Pertea et al., 2015) and transcriptome datasets were merged to reconstruct a comprehensive transcriptome using perl scripts and gffcompare (Pertea and Pertea, 2020). StringTie (Pertea et al., 2015) and R statistics package edgeR[6] were used to estimate the expression levels of all transcripts (**Supplementary Table 6**). The statistical significance (p-values < 0.05) of differentially expressed mRNAs based on their log2(fold change; FC) > 1 or log2(FC) < -1 were assessed using R statistics edgeR v3.14.0 package. Agglomerative hierarchical heatmaps of selected differentially transcribed genes listed in **Supplementary Table 6** was generated using R statistics software v 4.0.3 (R Development Core Team, 2008) using the heatmap.plus (Day, 2012) package (**Figure 5**).

Plasmid Complementation and Gene Deletion Assays of *E. coli* Strains and Isolates

Plasmid complementation assays were performed using chemical competent cell preparations of *E. coli* BW25113, Keio collection gene deletion mutants (listed in **Table 1**), and CHRX1-3 isolates using the $RbCl_2$ protocol described in Green and Rogers (2013). ASKA collection strains AG1 (ME5305; pCA24N–), JW2343-AM (pMlaA–), JW5490-AM (pYghQ–), JW5248-AM (pMarR–), JW4276-AM (pFimE), JW3480-AM (pGadE), and JW5013-AM (pCdaR) were used to extract and purify their respective plasmid clones, using plasmid DNA extraction kits and isolation protocols from BioBasic Inc (ON, Canada). pCA23N(–) plasmids add an in-frame amino-terminal hexahistidine affinity tag to each cloned gene as described by Kitagawa et al. (2005). Plasmids were individually transformed into each *E. coli* strain listed above using the protocol described by Green and Rogers (2013) and transformants were selected and grown on LB medium with 30 μg/mL CM to maintain plasmid selection. Plasmids were re-isolated from each transformant to verify proper plasmid transformation. All transformants were examined using the same broth microdilution AST methods as described in sections above, at increasing CHX concentration ranges (0.5–16 μg/mL) to calculate any differences in MIC values between the transformants. All AST experiments were performed in triplicate for each transformed isolate or strain (**Table 5**).

DATA AVAILABILITY STATEMENT

The datasets presented in this study can be found in online repositories. The names of the repository/repositories and accession number(s) can be found in the article/**Supplementary Material**.

[6] https://www.rdocumentation.org/packages/edgeR

AUTHOR CONTRIBUTIONS

DCB and NC designed the study, where NC performed the adaptation experiment. NC, KG, and BG performed the AST and evaluated MIC data. KG and BG measured the growth curve data. KG measured the stability data. NC and SR performed the Genomic DNA extractions and WGS SNV identification. SR generated and analyzed the WGS phylogenetic trees. BG and SR performed the SEM imaging with DRB, SH, and TB. BG and SR prepared all proteomic samples for nano LC-MS/MS collection by PC and GW. KG, BG, and SR extracted the transcriptome RNA. DCB conducted sequencing by LC Sciences services and analyzed the data. BG and SR performed CHXR and WT plasmid transformant and gene deletion MIC testing. BG performed impermeant fluorescent dye CHXR and WT cell experiments. BG, SR, and DCB analyzed the all data and prepared manuscript figures. DCB wrote the manuscript draft in consultation with KG, BG, and SR. DCB and GZ edited the manuscript. All the authors read and approved the final manuscript.

FUNDING

Funding for this study was provided by Natural Sciences and Engineering Research Council of Canada (NSERC) Discovery Grant (RGPIN-2016-05891) operating funds to DCB.

ACKNOWLEDGMENTS

We would like to thank Stuart McCorrister and the Mass Spectrometry and Proteomics Core Facility group (National Microbiology Laboratory, Public Health Agency of Canada, Winnipeg, MB, Canada) for help with proteomics data acquisition and analysis. Thanks to the Diagnostic Microscopy and Imaging group (National Microbiology Laboratory, Public Health Agency of Canada, Winnipeg, MB, Canada) for assistance with scanning electron microscopy experiments.

SUPPLEMENTARY MATERIAL

The Supplementary Material for this article can be found online at: https://www.frontiersin.org/articles/10.3389/fmolb.2021.659058/full#supplementary-material

REFERENCES

Abràmoff, M. D., Magalhães, P. J., and Ram, S. J. (2007). Image Processing with ImageJ. *Biophotonics Int.* 11, 36–42.

Abuzaid, A., Hamouda, A., and Amyes, S. G. B. (2012). *Klebsiella pneumoniae* susceptibility to biocides and its association with *cepA*, *qac*Δ*E* and *qacE* efflux pump genes and antibiotic resistance. *J. Hosp. Infect.* 81, 87–91. doi: 10.1016/j.jhin.2012.03.003

Baba, T., Ara, T., Hasegawa, M., Takai, Y., Okumura, Y., Baba, M., et al. (2006). Construction of *Escherichia coli* K-12 in-frame, single-gene knockout mutants: the Keio collection. *Mol. Syst. Biol.* 2:2006.0008. doi: 10.1038/msb4100050

Bernier, S. P., Son, S., and Surette, M. G. (2018). The Mla pathway plays an essential role in the intrinsic resistance of *Burkholderia cepacia* complex species to antimicrobials and host innate components. *J. Bacteriol.* 200:e00156-18. doi: 10.1128/JB.00156-18

Bindea, G., Mlecnik, B., Hackl, H., Charoentong, P., Tosolini, M., Kirilovsky, A., et al. (2009). ClueGO: a Cytoscape plug-in to decipher functionally grouped gene ontology and pathway annotation networks. *Bioinformatics* 25, 1091–1093. doi: 10.1093/bioinformatics/btp101

Bohn, C., and Bouloc, P. (1998). The *Escherichia coli cmlA* gene encodes the multidrug efflux pump Cmr/MdfA and is responsible for isopropyl-β-D-thiogalactopyranoside exclusion and spectinomycin sensitivity. *J. Bacteriol.* 180, 6072–6075.

Bore, E., Hébraud, M., Chafsey, I., Chambon, C., Skjaeret, C., Moen, B., et al. (2007). Adapted resistance to benzalkonium chloride in *Escherichia coli* K-12 studied by transcriptome and proteome analyses. *Microbiology* 153, 935–946. doi: 10.1099/mic.0.29288-0

Braoudaki, M., and Hilton, A. C. (2004). Adaptive resistance to biocides in *Salmonella enterica* and *Escherichia coli* O157 and cross-resistance to antimicrobial agents. *J. Clin. Microbiol.* 42, 73–78. doi: 10.1128/JCM.42.1.73

Brauner, A., Fridman, O., Gefen, O., and Balaban, N. Q. (2016). Distinguishing between resistance, tolerance and persistence to antibiotic treatment. *Nat. Rev. Microbiol.* 14, 320–330. doi: 10.1038/nrmicro.2016.34

Brookes, Z. L. S., Bescos, R., Belfield, L. A., Ali, K., and Roberts, A. (2020). Current uses of chlorhexidine for management of oral disease: a narrative review. *J. Dent.* 103:103497. doi: 10.1016/j.jdent.2020.103497

Cerf, O., Carpentier, B., and Sanders, P. (2010). Tests for determining in-use concentrations of antibiotics and disinfectants are based on entirely different concepts: "Resistance" has different meanings. *Int. J. Food Microbiol.* 136, 247–254. doi: 10.1016/j.ijfoodmicro.2009.10.002

Chong, Z. S., Woo, W. F., and Chng, S. S. (2015). Osmoporin OmpC forms a complex with MlaA to maintain outer membrane lipid asymmetry in *Escherichia coli*. *Mol. Microbiol.* 98, 1133–1146. doi: 10.1111/mmi.13202

Chubiz, L. M., and Rao, C. V. (2011). Role of the mar-sox-rob regulon in regulating outer membrane porin expression. *J. Bacteriol.* 193, 2252–2260. doi: 10.1128/JB.01382-10

Chubiz, L. M., Glekas, G. D., and Rao, C. V. (2012). Transcriptional cross talk within the mar-sox-rob regulon in *Escherichia coli* is limited to the *rob* and *marRAB* operons. *J. Bacteriol.* 194, 4867–4875. doi: 10.1128/JB.00680-12

Cieplik, F., Jakubovics, N. S., Buchalla, W., Maisch, T., Hellwig, E., and Al-Ahmad, A. (2019). Resistance toward chlorhexidine in oral bacteria-is there cause for concern? *Front. Microbiol.* 10:587. doi: 10.3389/fmicb.2019.00587

CLSI (2012). *Methods for Dilution Antimicrobial Susceptibility Tests for Bacteria That Grow Aerobically; Approved Standard*, 9th Edn. Wayne, PA: Clinical Laboratory Standards Institute.

Condell, O., Iversen, C., Cooney, S., Power, K. A., Walsh, C., Burgess, C., et al. (2012). Efficacy of biocides used in the modern food industry to control *Salmonella enterica*, and links between biocide resistance and resistance to clinically relevant antimicrobial compounds. *Appl. Environ. Microbiol.* 78, 3087–3097. doi: 10.1128/AEM.07534-11

Day, A. (2012). *heatmap.plus.package: Heatmap With More Sensible Behavior*. Available online at: https://cran.r-project.org/web/packages/heatmap.plus/heatmap.pdf

Doncheva, N. T., Morris, J. H., Gorodkin, J., and Jensen, L. J. (2019). Cytoscape StringApp: network analysis and visualization of proteomics data. *J. Proteome Res.* 18, 623–632. doi: 10.1021/acs.jproteome.8b00702

Edgar, R., and Bibi, E. (1997). MdfA, an *Escherichia coli* multidrug resistance protein with an extraordinarily broad spectrum of drug recognition. *J. Bacteriol.* 179, 2274–2280.

Ekiert, D. C., Bhabha, G., Isom, G. L., Greenan, G., Ovchinnikov, S., Henderson, I. R., et al. (2017). Architectures of lipid transport systems for the bacterial outer membrane. *Cell* 169, 273–285. doi: 10.1016/j.cell.2017.03.019.e17

Elliott, A. G., Huang, J. X., Neve, S., Zuegg, J., Edwards, I. A., Cain, A. K., et al. (2020). An amphipathic peptide with antibiotic activity against multidrug-resistant Gram-negative bacteria. *Nat. Commun.* 11:3184. doi: 10.1038/s41467-020-16950-x

Fang, C. T., Chen, H. C., Chuang, Y. P., Chang, S. C., and Wang, J. T. (2002). Cloning of a cation efflux pump gene associated with chlorhexidine resistance in *Klebsiella pneumoniae*. *Antimicrob. Agents Chemother.* 46, 2024–2028. doi: 10.1128/AAC.46.6.2024-2028.2002

Fernández-Cuenca, F., Tomás, M., Caballero-Moyano, F. J., Bou, G., Martínez-Martínez, L., Vila, J., et al. (2015). Reduced susceptibility to biocides in *Acinetobacter baumannii*: association with resistance to antimicrobials, epidemiological behaviour, biological cost and effect on the expression of genes encoding porins and efflux pumps. *J. Antimicrob. Chemother.* 70, 3222–3229. doi: 10.1093/jac/dkv262

Gadea, R., Fernández Fuentes, M. Á, Pérez Pulido, R., Gálvez, A., and Ortega, E. (2016). Adaptive resistance to phenolic biocides in bacteria from organic foods: effects on antimicrobial susceptibility and resistance to physical stresses. *Food Res. Int.* 85, 131–143. doi: 10.1016/j.foodres.2016.04.033

Gadea, R., Fernández Fuentes, M. Á, Pérez Pulido, R., Gálvez, A., and Ortega, E. (2017). Effects of exposure to quaternary-ammonium-based biocides on antimicrobial susceptibility and resistance to physical stresses in bacteria from organic foods. *Food Microbiol.* 63, 58–71. doi: 10.1016/j.fm.2016.10.037

Gilbert, P., and Moore, L. E. (2005). Cationic antiseptics: diversity of action under a common epithet. *J. Appl. Microbiol.* 99, 703–715. doi: 10.1111/j.1365-2672.2005.02664.x

Golding, C. G., Lamboo, L. L., Beniac, D. R., and Booth, T. F. (2016). The scanning electron microscope in microbiology and diagnosis of infectious disease. *Sci. Rep.* 6:26516. doi: 10.1038/srep26516

Green, R., and Rogers, E. J. (2013). Chemical transformation of *E. coli*. *Methods Enzymol.* 529, 329–336. doi: 10.1016/B978-0-12-418687-3.00028-8

Gregorchuk, B. S. J., Reimer, S. L., Beniac, D. R., Hiebert, S. L., Booth, T. F., Wuzinski, M., et al. (2020). Antiseptic quaternary ammonium compound tolerance by gram-negative bacteria can be rapidly detected using an impermeant fluorescent dye-based assay. *Sci. Rep.* 10:20543. doi: 10.1038/s41598-020-77446-8

Guindon, S., Dufayard, J. F., Lefort, V., Anisimova, M., Hordijk, W., and Gascuel, O. (2010). New algorithms and methods to estimate Maximum-Likelihood phylogenies: assessing the performance of PhyML 3.0. *Syst. Biol.* 59, 307–321. doi: 10.1093/sysbio/syq010

Hashemi, M. M., Holden, B. S., Coburn, J., Taylor, M. F., Weber, S., Hilton, B., et al. (2019). Proteomic analysis of resistance of gram-negative bacteria to chlorhexidine and impacts on susceptibility to colistin, antimicrobial peptides, and ceragenins. *Front. Microbiol.* 10:210. doi: 10.3389/fmicb.2019.00210

Hasman, H., Schembri, M. A., and Klemm, P. (2000). Antigen 43 and type 1 fimbriae determine colony morphology of *Escherichia coli* K-12. *J. Bacteriol.* 182, 1089–1095. doi: 10.1128/JB.182.4.1089-1095.2000

Hassan, K. A., Liu, Q., Henderson, P. J. F., and Paulsen, I. T. (2015). Homologs of the *Acinetobacter baumannii aceI* transporter represent a new family of bacterial multidrug efflux systems. *mBio* 6:e01982-14. doi: 10.1128/mBio.01982-14

Heuveling, J., Possling, A., and Hengge, R. (2008). A role for Lon protease in the control of the acid resistance genes of *Escherichia coli*. *Mol. Microbiol.* 69, 534–547. doi: 10.1111/j.1365-2958.2008.06306.x

Hommais, F., Krin, E., Coppée, J. Y., Lacroix, C., Yeramian, E., Danchin, A., et al. (2004). GadE (YhiE): a novel activator involved in the response to acid environment in *Escherichia coli*. *Microbiology* 150, 61–72. doi: 10.1099/mic.0.26659-0

Kampf, G. (2016). Acquired resistance to chlorhexidine- is it time to establish an "antiseptic stewardship" initiative? *J. Hosp. Infect.* 94, 213–227. doi: 10.1016/j.jhin.2016.08.018

Kampf, G. (2018). Biocidal agents used for disinfection can enhance antibiotic resistance in gram-negative species. *Antibiotics* 7:110. doi: 10.3390/antibiotics7040110

Kanjee, U., and Houry, W. A. (2013). Mechanisms of acid resistance in *Escherichia coli*. *Annu. Rev. Microbiol.* 67, 65–81.

Kitagawa, M., Ara, T., Arifuzzaman, M., Ioka-Nakamichi, T., Inamoto, E., Toyonaga, H., et al. (2005). Complete set of ORF clones of *Escherichia coli* ASKA library (a complete set of *E. coli* K-12 ORF archive): unique resources for biological research. *DNA Res.* 12, 291–299. doi: 10.1093/dnares/dsi012

Kulasekara, H. D., and Blomfield, I. C. (1999). The molecular basis for the specificity of *fimE* in the phase variation of type 1 fimbriae of *Escherichia coli* K-12. *Mol. Microbiol.* 31, 1171–1181. doi: 10.1046/j.1365-2958.1999.01257.x

Kurabayashi, K., Tanimoto, K., Tomita, H., and Hirakawa, H. (2017). Cooperative actions of CRP-cAMP and FNR increase the fosfomycin susceptibility of

enterohaemorrhagic *Escherichia coli* (EHEC) by elevating the expression of *glpT* and *uhpT* under anaerobic conditions. *Front. Microbiol.* 8:426. doi: 10.3389/fmicb.2017.00426

Langmead, B., and Salzberg, S. L. (2012). Fast gapped-read alignment with Bowtie 2. *Nat. Methods* 9, 357–359. doi: 10.1038/nmeth.1923

Ma, Z., Gong, S., Richard, H., Tucker, D. L., Conway, T., and Foster, J. W. (2003). GadE (YhiE) activates glutamate decarboxylase-dependent acid resistance in *Escherichia coli* K-12. *Mol. Microbiol.* 49, 1309–1320. doi: 10.1046/j.1365-2958.2003.03633.x

Martin, M. (2011). Cutadapt removes adapter sequences from high-throughput sequencing reads. *EMBnet. Journal* 17, 10–12. doi: 10.14806/ej.17.1.200

Mates, A. K., Sayed, A. K., and Foster, J. W. (2007). Products of the *Escherichia coli* acid fitness island attenuate metabolite stress at extremely low pH and mediate a cell density-dependent acid resistance. *J. Bacteriol.* 189, 2759–2768. doi: 10.1128/JB.01490-06

Monterrubio, R., Baldoma, L., Obradors, N., Aguilar, J., and Badia, J. (2000). A common regulator for the operons encoding the enzymes involved in D-galactarate, D-glucarate, and D-glycerate utilization in *Escherichia coli*. *J. Bacteriol.* 182, 2672–2674. doi: 10.1128/jb.182.9.2672-2674.2000

Naparstek, L., Carmeli, Y., Chmelnitsky, I., Banin, E., and Navon-Venezia, S. (2012). Reduced susceptibility to chlorhexidine among extremely-drug-resistant strains of *Klebsiella pneumoniae*. *J. Hosp. Infect.* 81, 15–19. doi: 10.1016/j.jhin.2012.02.007

Nayyar, A. S. (2015). Chlorhexidine: a cationic bisbiguanide, membrane active drug in periodontal medicine, structure advantages and associated adverse effects, a brief communication. *World J. Pharm. Pharm. Sci.* 4, 370–392.

Nicoloff, H., and Andersson, D. I. (2013). Lon protease inactivation, or translocation of the *lon* gene, potentiate bacterial evolution to antibiotic resistance. *Mol. Microbiol.* 90, 1233–1248. doi: 10.1111/mmi.12429

Pertea, M., and Pertea, G. (2020). GFF Utilities: GffRead and GffCompare. *F1000Res.* 9:ISCB Comm J-304. doi: 10.12688/f1000research.23297.1

Pertea, M., Pertea, G. M., Antonescu, C. M., Chang, T.-C., Mendell, J. T., Salzberg, S. L., et al. (2015). StringTie enables improved reconstruction of a transcriptome from RNA-seq reads. *Nat. Biotechnol.* 33, 290–295. doi: 10.1038/nbt.3122

Olaitan, A. O., Morand, S., and Rolain, J. M. (2014). Mechanisms of polymyxin resistance: acquired and intrinsic resistance in bacteria. *Front. Microbiol.* 26:643. doi: 10.3389/fmicb.2014.00643

Rai, A. K., and Mitchell, A. M. (2020). Enterobacterial common antigen: synthesis and function of an enigmatic molecule. *mBio* 11:e01914-20. doi: 10.1128/mBio.01914-20

R Development Core Team (2008). *R: A Language and Environment for Statistical Computing*. Available online at: http://www.r-project.org

Saier, M. H., Reddy, V. S., Tsu, B. V., Ahmed, M. S., Li, C., and Moreno-Hagelsieb, G. (2016). The Transporter Classification Database (TCDB): recent advances. *Nucleic Acids Res.* 44, D372–D379. doi: 10.1093/nar/gkv1103

Schnetz, K., and Rak, B. (1992). IS5: a mobile enhancer of transcription in *Escherichia coli*. *Proc. Natl. Acad. Sci. U.S.A.* 89, 1244–1248. doi: 10.1073/pnas.89.4.1244

Shannon, P., Markiel, A., Ozier, O., Baliga, N. S., Wang, J. T., Ramage, D., et al. (2003). Cytoscape: a software environment for integrated models of biomolecular interaction networks. *Genome Res.* 13, 2498–2504. doi: 10.1101/gr.1239303

Shen, Y. X., Xiao, K., Liang, P., Ma, Y. W., and Huang, X. (2013). Improvement on the modified Lowry method against interference of divalent cations in soluble protein measurement. *Appl. Microbiol. Biotechnol.* 97, 4167–4178. doi: 10.1007/s00253-013-4783-3

Stiefel, P., Schmidt-Emrich, S., Maniura-Weber, K., and Ren, Q. (2015). Critical aspects of using bacterial cell viability assays with the fluorophores SYTO9 and propidium iodide. *BMC Microbiol.* 15:36. doi: 10.1186/s12866-015-0376-x

Strugeon, E., Tilloy, V., Ploy, M.-C., and Da Re, S. (2016). The stringent response promotes antibiotic resistance dissemination by regulating integron integrase expression in biofilms. *mBio* 7:e00868-16. doi: 10.1128/mBio.00868-16

Tyanova, S., Temu, T., Sinitcyn, P., Carlson, A., Hein, M. Y., Geiger, T., et al. (2016). The Perseus computational platform for comprehensive analysis of (prote)omics data. *Nat. Methods* 13, 731–740. doi: 10.1038/nmeth.3901

Vali, L., Dashti, A. A., El-Shazly, S., and Jadaon, M. M. (2015). *Klebsiella oxytoca* with reduced sensitivity to chlorhexidine isolated from a diabetic foot ulcer. *Int. J. Infect. Dis.* 34, 112–116. doi: 10.1016/j.ijid.2015.03.021

Verspecht, T., Rodriguez Herrero, E., Khodaparast, L., Khodaparast, L., Boon, N., Bernaerts, K., et al. (2019). Development of antiseptic adaptation and cross-adapatation in selected oral pathogens *in vitro*. *Sci. Rep.* 9:8326. doi: 10.1038/s41598-019-44822-y

Wand, M. E. E., Bock, L. J. J., Bonney, L. C. C., and Sutton, J. M. M. (2017). Mechanisms of increased resistance to chlorhexidine and cross-resistance to colistin following exposure of *Klebsiella pneumoniae* clinical isolates to chlorhexidine. *Antimicrob. Agents Chemother.* 61:e01162-16. doi: 10.1128/AAC.01162-16

Whiteway, J., Koziarz, P., Veall, J., Sandhu, N., Kumar, P., Hoecher, B., et al. (1998). Oxygen-insensitive nitroreductases: analysis of the roles of *nfsA* and *nfsB* in development of resistance to 5-nitrofuran derivatives in *Escherichia coli*. *J. Bacteriol.* 180, 5529–5539. doi: 10.1128/jb.180.21.5529-5539.1998

Wiśniewski, J. R., Zougman, A., Nagaraj, N., and Mann, M. (2009). Universal sample preparation method for proteome analysis. *Nat. Methods* 6, 359–362. doi: 10.1038/nmeth.1322

World Health Organization (2019). *World Health Organization Model List of Essential Medicines: 21st list 2019*. Geneva: WHO.

Zenno, S., Koike, H., Kumar, A. N., Jayaraman, R., Tanokura, M., and Saigo, K. (1996). Biochemical characterization of NfsA, the *Escherichia coli* major nitroreductase exhibiting a high amino acid sequence homology to Frp, a *Vibrio harveyi* flavin oxidoreductase. *J. Bacteriol.* 178, 4508–4514. doi: 10.1128/jb.178.15.4508-4514.1996

Zorko, M., and Jerala, R. (2008). Alexidine and chlorhexidine bind to lipopolysaccharide and lipoteichoic acid and prevent cell activation by antibiotics. *J. Antimicrob. Chemother.* 62, 730–737. doi: 10.1093/jac/dkn270

Conflict of Interest: The authors declare that the research was conducted in the absence of any commercial or financial relationships that could be construed as a potential conflict of interest.

frontiers in Molecular Biosciences

ORIGINAL RESEARCH
published: 11 June 2021
doi: 10.3389/fmolb.2021.679949

Varied Contribution of Phospholipid Shedding From Membrane to Daptomycin Tolerance in *Staphylococcus aureus*

Tianwei Shen[1], *Kelly M. Hines*[1†], *Nathaniel K. Ashford*[2], *Brian J. Werth*[2*] *and Libin Xu*[1*]

[1]*Department of Medicinal Chemistry, School of Pharmacy, University of Washington, Seattle, WA, United States,* [2]*Department of Pharmacy, School of Pharmacy, University of Washington, Seattle, WA, United States*

It has been suggested that daptomycin can be inactivated by lipids released by *Staphylococcus aureus* and that this effect is antagonized by phenol soluble modulins (PSMs), which bind to the shed lipids. PSM production is regulated by the Agr system, and others have shown that loss of the Agr function enhances *S. aureus* survival in the presence of daptomycin. Here we assessed the impact of Agr function on daptomycin activity and lipid metabolism under various conditions. Daptomycin activity was evaluated against three sets of isogenic strain series with wild-type or dysfunctional Agr using static daptomycin time-kills over 24 h and against one strain pair using *in vitro* pharmacokinetic/pharmacodynamic (PK/PD) models simulating clinical daptomycin exposure for 48 h. We performed comprehensive lipidomics on bacterial membranes and the spent media to correlate lipid shedding with survival. In static time-kill experiments, two *agr*-deficient strains (SH1000- and USA300 LAC Δ*agrA*) showed improved survival for 8 h compared with their corresponding wild-type strains as seen in previous studies, but this difference did not persist for 24 h. However, four other *agr*-deficient strains (SH1001 and JE2 *agr* KOs) did not demonstrate improved survival compared to isogenic wild-type strains at any time in the time-kills. Lipidomics analysis of SH1000, SH1001, and SH1000- strains showed daptomycin exposure increased lipid shedding compared to growth controls in all strains with phosphatidylglycerols (PGs), lysylPGs and cardiolipins predominating. In the cell pellets, PGs and lysylPGs decreased but cardiolipins were unchanged with daptomycin exposure. The shed lipid profiles in SH1001 and SH1000- were similar, suggesting that the inability to resist daptomycin by SH1001 was not because of differences in lipid shedding. In the PK/PD model, the *agr* mutant SH1000- strain did not show improved survival relative to SH1000 either. In conclusion, inactivation of daptomycin by shed lipids may be dependent on genetic background, the specific *agr* mutations, or the techniques used to generate these KOs rather than the overall function of the Agr system, and its contribution to daptomycin tolerance seems to be varied, transient, and growth-condition dependent.

Keywords: lipidomics, Agr, pharmacokinetic and pharmacodynamic model, daptomycin tolerance, phospholipid release

OPEN ACCESS

Edited by:
Allen Liu,
University of Michigan, United States

Reviewed by:
Huiming Lu,
University of Texas Southwestern Medical Center, United States
Dwijendra K. Gupta,
Jai Prakash Vishwavidyalaya, India

****Correspondence:***
Brian J. Werth
bwerth@uw.edu
Libin Xu
libinxu@uw.edu

†Present address:
Department of Chemistry, University of Georgia, Athens, GA, United States

Specialty section:
This article was submitted to Cellular Biochemistry, a section of the journal Frontiers in Molecular Biosciences

Received: *12 March 2021*
Accepted: *24 May 2021*
Published: *11 June 2021*

Citation:
Shen T, Hines KM, Ashford NK, Werth BJ and Xu L (2021) Varied Contribution of Phospholipid Shedding From Membrane to Daptomycin Tolerance in Staphylococcus aureus. *Front. Mol. Biosci. 8:679949. doi: 10.3389/fmolb.2021.679949*

INTRODUCTION

Daptomycin is a lipopeptide antimicrobial that consists of a cyclic polypeptide with 13 amino acids and a decanoyl fatty acyl tail that plays an important role in the management of invasive infections caused by methicillin-resistant *Staphylococcus aureus* (MRSA). Its mechanism of action involves direct interaction with the negatively charged membrane lipids, phosphatidylglycerols (PGs), leading to loss of membrane potential and cell death (Muraih et al., 2011; Muraih et al., 2012; Pogliano et al., 2012; Bayer et al., 2013). As such, most studies on daptomycin resistance point to development of mutations in genes that control membrane lipid metabolism and/or lead to changes in surface charge, membrane fluidity, or both, such as *mprF*, *cls*, *pgsA*, and the *dlt* operon, which reduces binding of daptomycin to the cell membrane or prevents disruption of the membrane by daptomycin (Yang et al., 2009; Peleg et al., 2012; Mishra and Bayer, 2013; Mishra et al., 2013; Bayer et al., 2014; Cafiso et al., 2014; Mishra et al., 2014; Bayer et al., 2015; Hines et al., 2017; Jiang et al., 2019). Mutations in two-component regulatory systems that regulate cell wall and cell membrane metabolism, such as *vraSR* and *walKR* (Friedman et al., 2006; Mehta et al., 2012; Werth et al., 2021), have also been shown to contribute to daptomycin resistance. We previously applied a novel multi-dimensional lipidomic method to characterizing the detailed lipid profile changes associated with MRSA strains that have developed resistance to daptomycin and found overall greatly decreased levels of PGs in a resistant strain with mutations in both *pgsA* and *mprF* (Hines et al., 2017) and greatly elevated levels of lysyl-phosphatidylglycerols (lysylPGs) and cardiolipins (CLs) in a strain with only an *mprF* mutation (Hines et al., 2020). Thus, altering lipid metabolism is an important route for bacteria to acquire resistance to daptomycin.

In recent years, inactivation of daptomycin by phospholipids released by *S. aureus* upon daptomycin exposure was proposed as a novel mechanism of daptomycin tolerance (Pader et al., 2016). The authors found that this effect may be antagonized by the production of amphipathic peptides called phenol soluble modulins (PSMs), which bind released phospholipids and thus prevent inactivation of daptomycin (Otto, 2014; Pader et al., 2016). PSM production is regulated by the accessory gene regulator (Agr) system, which is encoded by a four-gene operon (*agrBDCA*) and a regulatory RNA gene (RNAIII) (Peschel and Otto, 2013). Pader et al. suggested that the loss of the Agr quorum-sensing system enhances *S. aureus* survival during daptomycin exposure since PSMs are not released, and thus there is no competition for daptomycin sequestration by the shed lipids. However, the detailed composition of membrane lipids and shed lipids by *S. aureus* strains with variable Agr activity in response to daptomycin exposure has not been elucidated and the effect of lipid shedding on daptomycin activity has not been examined under clinically relevant kinetic drug exposures. In this work, we assessed the impact of Agr function on daptomycin activity and lipid metabolism in several genetic backgrounds and in static time-kills and *in vitro* pharmacokinetic/pharmacodynamic (PK/PD) models to better understand the contribution of lipid shedding to daptomycin tolerance.

MATERIALS AND METHODS

Susceptibility Testing and Agr Functionality Testing

The susceptibility to daptomycin was evaluated by broth microdilution in accordance with CLSI guidelines (CLSI, 2017). The Agr functionality was tested on BBL™ Trypticase™ soy agar with 5% sheep blood (TSA II; Becton, Dickinson and Company, Franklin Lakes, NJ, United States) as previously described (Sakoulas et al., 2002). Briefly, a 0.5-McFarland suspension of RN4220 was streaked in a line down the center of the agar plate dividing the plate into two halves, and the test strains were streaked from the edge of the agar plate to the center line of RN4220. Hemolysis was examined after overnight incubation at 37°C.

Static Time-Kill Assay

Overnight cultures of each strain were inoculated into tryptic soy broth (TSB, Remel Lenexa, KS, United States) supplemented with 50 μg/ml of elemental calcium and 20 μg/ml of daptomycin (Merck, Kenilworth, NJ, United States) to ~10^8 CFU/ml in 50 ml conical tubes, incubated at 37°C with shaking. Samples were taken at 0, 2, 4, 6, 8, and 24 h, serially diluted and spiral plated on tryptic soy agar (TSA; Becton, Dickinson and Company, Franklin Lakes, NJ, United States) plates to evaluate the bacterial growth over time with exposure to daptomycin. Experiments were performed under lower aeration (30 ml of culture in 50 ml tube shaken at 85 rpm; SH1000 and SH1001, JE2 and JE2 Δ*agr*) and higher aeration (9 ml of culture in 50 ml tube shaken at 180 rpm; SH1000, SH1001, and SH1000-, USA300 LAC and USA300 LAC Δ*agrA*) conditions, the latter of which were more consistent with the methods by (Pader et al., 2016). All experiments were performed in duplicate.

Lipid Profiling of Static Time-kill of SH1000, SH1001, and SH1000- Overnight cultures of SH1000, SH1001, and SH1000- were inoculated into TSB containing 50 μg/ml of elemental calcium to ~10^8 CFU/ml in 50 ml conical tubes, with or without exposure to daptomycin (20 μg/ml) and incubated at 37°C and 180 rpm with a total media culture of 9 ml. Each strain was grown in triplicate for 6 h and pelleted by centrifugation, with 5 ml of the supernatant saved for lipid profiling of the broth. The pellets and the broth were dried in a SpeedVac vacuum concentrator (Thermo Fisher Savant, Waltham, MA, United States), the pellets weighed, and both stored at −80°C until analysis. Lipid extraction, hydrophilic interaction liquid chromatography-ion mobility-mass spectrometry (HILIC-IM-MS), and data analysis were performed as previously described (Hines et al., 2017; Hines et al., 2020), using a Waters Synapt G2-Si ion mobility-QTOF mass spectrometer (Waters Corp., Milford, MA, United States) equipped with an electrospray ionization (ESI) source.

TABLE 1 | The three series of isogenic *S. aureus* strain pairs of *agr* wild-type and *agr*-defective used in this study and their daptomycin minimum inhibitory concentration (MIC).

Parent	MIC (μg/ml)	Mutant	MIC (μg/ml)	Mutation	Source
SH1000	0.25	SH1001	0.25	Full *agr* KO	Dr. Alexander Horswill
		SH1000-	0.5	H174L mutation in AgrA	Dr. Andrew Edwards
USA300 LAC	0.5	USA300 LAC Δ*agrA*	0.5	Full *agrA* KO	
JE2	0.25	JE2 Δ*agrA*	0.25	Transposon KOs	Nebraska transposon mutant library
		JE2 Δ*agrB*	0.25		
		JE2 Δ*agrC*	0.5		

In Vitro Pharmacokinetic/ Pharmacodynamic Model and Lipid Profiling

A one-compartment glass model was used to test the impact of a simulated daptomycin exposure on the survival and lipid shedding profile of SH1000 and SH1000-, as previously described (Hall Snyder et al., 2016; Werth et al., 2021). The model apparatus was prefilled with cation adjusted Mueller-Hinton-II broth (MHB; Becton, Dickinson and Company, Franklin Lakes, NJ, United States) supplemented with 50 μg/ml of elemental calcium, and fresh medium was continuously added and removed from the compartment along with the drug *via* a reciprocating syringe pump network (New Era Pump Systems Inc.), set to simulate the average plasma half-life of daptomycin (8 h). The starting inoculum was ~8 $\log_{10}$ CFU/ml. Daptomycin was administered at 0 and 24 h as a bolus injection to achieve the average peak free-drug concentration (C_{max}) associated with a 10 mg/kg/day dose (11.3 mg/L) (Benvenuto et al., 2006). All models were performed in duplicate and run continuously for 48 h. All effluent (21.6 ml/h per replicate) was collected from 4 to 5 h and 28–29 h and centrifuged to remove cells. The supernatant was divided into four technical replicates, and subjected to lipid profiling as described above.

RESULTS

Not All Agr-Deficiency Slowed Down the Killing of *Staphylococcus aureus* by Daptomycin

We compared the survival of *agr* wild-type and *agr*-defective (either KO or mutant) *S. aureus* under daptomycin exposure using three series of isogenic strain pairs (**Table 1**) (Boles and Horswill, 2008; Tsompanidou et al., 2011; Fey et al., 2013; Pader et al., 2016). Some of these strains have been well characterized previously (Boles and Horswill, 2008; Tsompanidou et al., 2011; Pader et al., 2016), and we also confirmed the Agr function of SH1001 and the transposon mutants of *agrA*, *agrB*, or *agrC* by examining their hemolytic activity (**Supplementary Figure S1**). The daptomycin minimum inhibitory concentration (MIC) was 0.25–0.5 μg/ml for all strains (**Table 1**). Daptomycin time-kill curves for each strain series are illustrated in **Figures 1A–D**. The wild-type SH1000 survived similarly or better than the *agr* KO strain SH1001, under both high and low aeration for 24 h. SH1000 and SH1001 in **Figure 1A** were grown under lower aeration than in **Figure 1C**. The higher aeration allowed both strains to re-grow to a higher and similar CFU/mL at 24 h, although the aeration conditions did not impact the general trend of daptomycin killing of wild-type vs. *agr* KO strains. However, **Figure 1C** also showed that the *agr* mutant SH1000- survived better than SH1000 and SH1001 for 8 h, with 1.7- and 1.4-$\log_{10}$ CFU/ml improved survival, respectively, at the 8 h timepoint. In USA300 LAC background the *agr*-KO strain survived better than the wild-type for 8 h, with 1.5-$\log_{10}$ CFU/ml improved survival at the 8 h timepoint (**Figure 1D**). However, JE2 strains demonstrated similar growth among the wild-type and the *agr* KO's for 24 h (**Figure 1B**). Overall, SH1000- and USA300 LAC Δ*agrA* displayed a similar trend as observed previously (Pader et al., 2016), but the *agr*-KO SH1001 and transposon *agr*-KO strains did not display improved survival relative to their matching wild-type strains when exposed to 20 μg/ml daptomycin.

Lipid Profiles Released by *Staphylococcus aureus* Upon Daptomycin Exposure Did Not Correlate With Agr Genotypes and Killing Profiles by Daptomycin

SH1000, SH1001 and SH1000- were grown for 6 h in static time-kills in the presence and absence of 20 μg/ml of daptomycin, and comprehensive lipidomics were carried out on the cell pellets and the broth to profile the membrane lipids and shed lipids. Average dry pellet weights +/− standard deviations of all strains are shown in **Supplementary Table S1**. The relative abundance of all lipid species including free fatty acids (FAs), diglucosyl-diacylglycerol (DGDGs), PGs, lysylPGs, and CLs were measured and normalized to all compounds. A heatmap depicting the relative abundance of each lipid is shown in **Figure 2**. All three strains released lipids, regardless of daptomycin exposure, but the levels of shed lipids were higher in the presence of daptomycin. Specifically, the levels of shed PGs were higher with daptomycin exposure than without for all three strains. The Agr-defective strains, SH1001 and SH1000-, shed more PGs than the wild-type SH1000 strain under daptomycin exposure (see **Supplementary Table S2** for the complete list of *p* values using Student's *t*-test). The levels of shed lysylPGs followed a similar trend, except the undetected

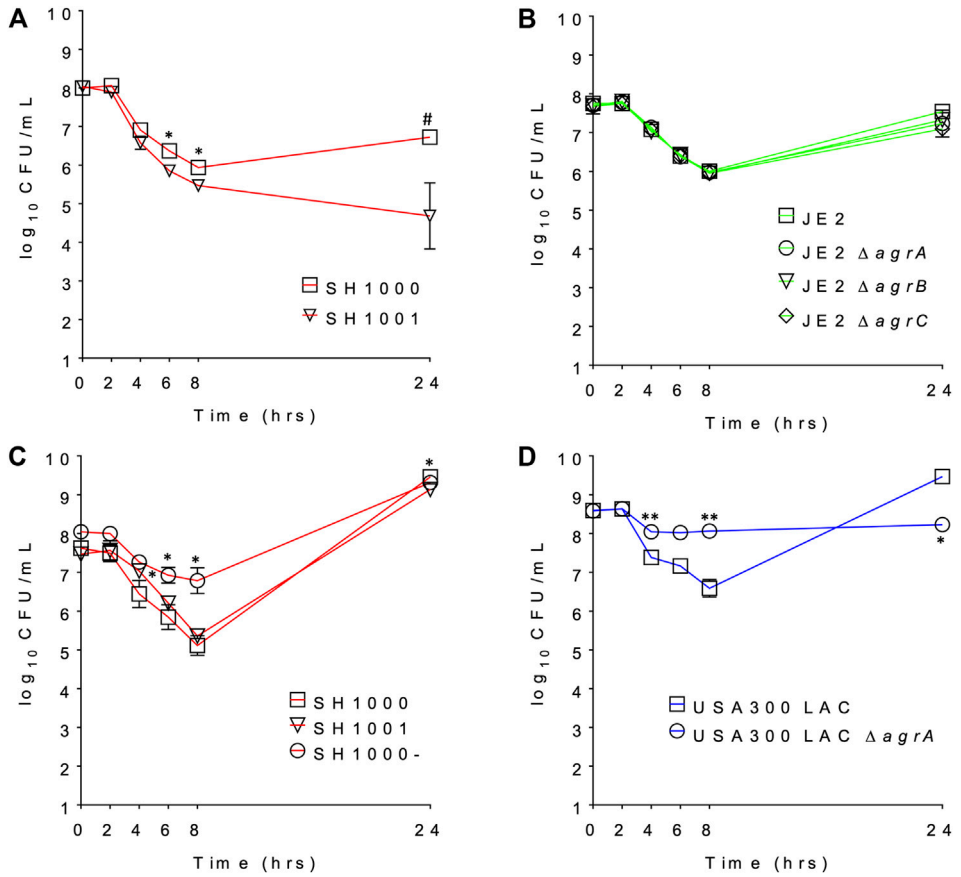

FIGURE 1 | The daptomycin time kill profile of **(A)** SH1000 and SH1001 pair under lower eration; **(B)** JE2 transposon series under low aeration; **(C)** SH1000, SH1001, and SH1000- series under higher eration; and **(D)** USA300 LAC pair under high aeration. $^{\#}p < 0.001$; $^{**}0.001 < p < 0.01$; $^{*}0.01 < p < 0.05$ (based on the percent survival at each timepoint, relative to the wild-type, Student's *t*-test, two-tailed, equal variance).

minor species lysylPG 36:0. CLs were also shed more with daptomycin exposure than without. However, the wild-type SH1000 strain released the largest amount of CLs than SH1001 and SH1000-. FAs and DGDGs were shed only slightly more with daptomycin exposure than without for all three strains, suggesting that PGs, lysylPGs, and CLs are the major lipid classes released in response to daptomycin.

Comparing the levels of shed lipids with the levels of membrane lipids in cell pellets, we found that low levels of shed lipids correlated with high level of membrane lipids, and *vice versa*, regardless of daptomycin exposure, especially for FAs, DGDGs, PGs, and lysylPGs. The same trend was observed for shed and membrane CLs when the three strains were grown under daptomycin exposure. However, when the three strains were grown without daptomycin, the levels of both shed and membrane CLs were relatively low, suggesting CLs might be synthesized and shed specifically in response to daptomycin exposure.

Overall, daptomycin exposure induced more lipids released into the broth, with PGs, lysylPGs, and CLs being the major classes, but the *agr* mutants SH1001 and SH1000- showed similar profile of released lipids, suggesting that the released lipids do not account for their differential killing profiles (**Figure 1C**).

Killing Profile in a Pharmacokinetic/Pharmacodynamic Model of Daptomycin Exposure Did Not Correlate With Agr Genotypes

The changes in bacterial densities over time during clinically meaningful kinetic exposures to daptomycin in the PK/PD model are illustrated in **Figure 3A**. To our surprise, the wild-type SH1000 appear to survive better than the *agr* mutant SH1000- up to 24 h although the difference was not statistically significant (Student's t-test, two-tailed, equal variance). Furthermore, both grew similarly after the second dose of daptomycin administered at 24 h. These data suggest that lack of Agr function does not provide meaningful advantage to the bacteria under conditions that replicate clinically relevant daptomycin exposures.

The released lipids in the effluent were evaluated at 4–5 h, when the greatest differences in survival were observed, and at

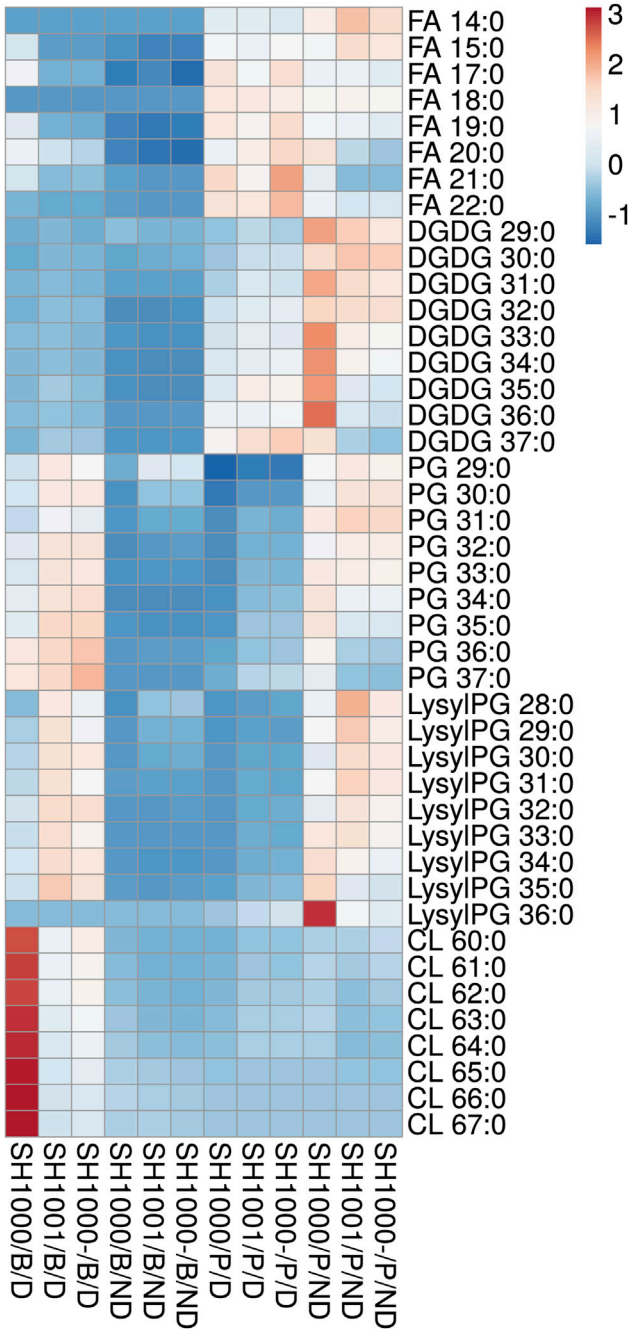

FIGURE 2 | Heatmap of the lipid profile in the broth (B) and the bacterial pellet (P) of the time-kill of SH1000, SH1001 and SH1000-, with (D) or without (ND) daptomycin exposure (row-centered; unit variance scaling applied to rows). Individual lipid species are represented as the number of carbons: the degree of unsaturation in the fatty acid chains. FA, free fatty acid; DGDG, diglucosyl-diacylglycerol; PG, phosphatidylglycerol; LysylPG, lysyl-phosphatidylglycerol; CL, cardiolipin. $N = 3$ per group. See **Supplementary Table S2** for p values from Student's t-test analysis.

28–29 h, when the wild-type and the *agr* mutant grew back to similar CFU/ml. DGDGs, PGs, lysylPGs and CLs were identified from the lipidomics analysis, as shown in **Figures 3B–E** (see **Supplementary Table S3** for the complete list of p values using Student's t-test), among which PGs were the most abundant. Both strains released more lipids at 4–5 h than at 28–29 h, and SH1000 released more than SH1000- at 4–5 h, which seems to correlate with the better survival of the SH1000 strain.

DISCUSSION

Inactivation of daptomycin by shed lipids of *S. aureus* is an intriguing potential mechanism for daptomycin tolerance. However, after examining the time-kill profiles of *agr* mutant and wild-type strains in three different genetic backgrounds, not all *agr* mutant strains displayed improved survival relative to their isogenic control strains (**Figure 1**), suggesting that the protection afforded by defective Agr and thus lack of secreted PSMs is not universal. Lipidomic profiling of SH1001 (loss of Agr function due to an *agrA* mutation) (Boles and Horswill, 2008) and SH1000- (full *agr*-KO) (Tsompanidou et al., 2011) showed that both strains released similar lipid profiles to the media (**Figure 2**) even though their time-kill profiles dramatically differed with only SH1000- displaying better survival than SH1000 (**Figure 1C**). Furthermore, although SH1001 released more PGs and lysylPGs, but less CLs, than the wild-type SH1000, SH1000 survived better or similarly relative to SH1001 depending on the aeration conditions (**Figure 1**). These observations suggest that the amount of released lipids does not correlate with the survival of *S. aureus* in the presence of daptomycin.

Comprehensive lipid profiling suggests that phospholipids, including PGs, lysylPGs, and CLs, are preferentially released by *S. aureus* relative to DGDGs and FFAs in response to daptomycin exposure. Furthermore, the lipids released to the media appear to account for relative reductions in the residual membrane lipids in the cell pellets, except CLs. The preferential release of some lipid classes suggests an active releasing process. In particular, daptomycin exposure also upregulates both the synthesis and the release of CLs. This is intriguing as gain-of-function mutation in *cls2*, which encodes cardiolipin synthase, has been associated with daptomycin resistance (Jiang et al., 2019).

In the comprehensive lipidomics analysis of the static time-kills, the average dry pellet weight of the *agr* mutants SH1000- and SH1001 was overall higher than their isogenic wild-type SH1000 with daptomycin exposure (**Supplementary Table S1**), which is seemingly contradictory to the survival profile (**Figure 1C**). However, many factors might contribute to the pellet weight, such as the degree of protein synthesis and aggregation of bacterial cells. Additionally, the lipid profile was normalized to all compounds, and hence the differences in pellet weight is unlikely to confound our results.

S. aureus and many other bacteria are known to release membrane lipids as extracellular vesicles into their surrounding environment. These released vesicles are composed of lipids, varieties of proteins, polysaccharides, and nucleic acids, and thus may contribute to a variety of biological functions including delivery of intracellular contents for quorum

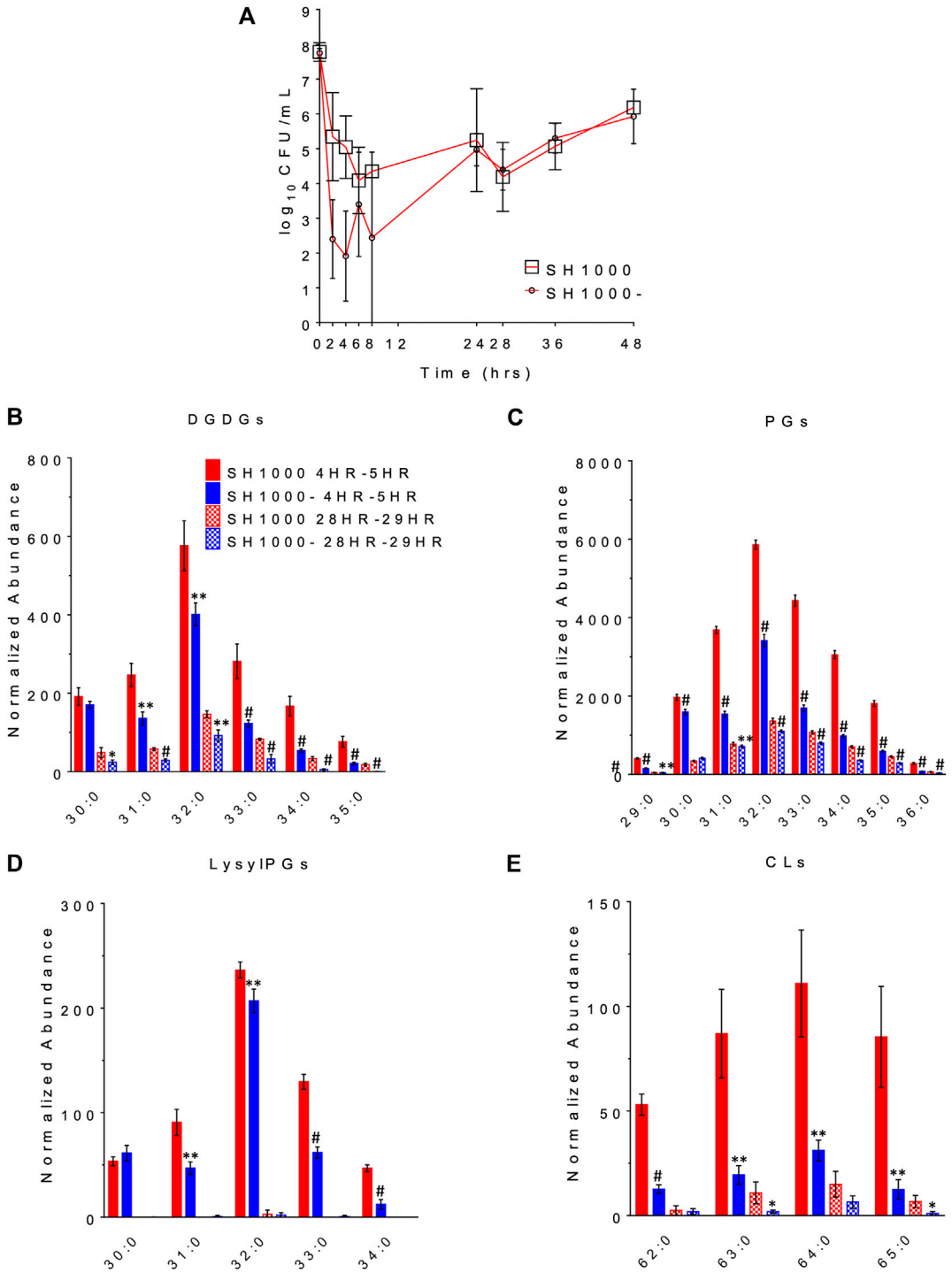

FIGURE 3 | The survival profile **(A)** and lipid profile during 4HR-5HR and 28HR-29HR **(B–E)** of SH1000 and SH1000- in the pharmacokinetics/pharmacodynamics (PK/PD) model of daptomycin exposure. Individual lipid species are represented as the number of carbons: the degree of unsaturation in the fatty acid chains. DGDGs, diglucosyl-diacylglycerols; PGs, phosphatidylglycerols; LysylPGs, lysyl-phosphatidylglycerols; CLs, cardiolipins. $^{\#}p < 0.001$; $^{**}0.001 < p < 0.01$; $^{*}0.01 < p < 0.05$ (Student's *t*-test, two-tailed, equal variance).

sensing or delivery of virulence factors to host cells (Gurung et al., 2011; Wang et al., 2018). PSMs were found to promote the biogenesis of extracellular vesicles by disrupting cytoplasmic membrane (Wang et al., 2018). *S. aureus* with *psmα*-KO was found to produce significantly less and smaller extracellular vesicles than wild-type. Other factors, such as

peptidoglycan cross-linking and autolysis enzymes, also affect the formation of extracellular vesicles. Therefore, it is possible that alternative factors other than PSMs in the extracellular vesicles released by *S. aureus* could contribute to the survival of the bacteria under daptomycin pressure. Elucidation of such factors could shed light on the discrepancy that some *agr* mutant strains resulted in improved survival against daptomycin while others did not.

CONCLUSION

In this study, we found that while daptomycin exposure indeed resulted in increased shedding of membrane lipids to the media, the amount and types of released lipids did not correlate with the survival of the bacteria against daptomycin or the genotype of the bacteria. In the cases where there is improved survival, such effect appears to be dependent on experimental conditions, such as aeration, and ultimately are transient effects. Furthermore, the role of the Agr system in counteracting this effect appears to be dependent on the nature of the Agr dysfunction and genetic backgrounds as demonstrated by the variable effects of our isogenic strains with different types of *agr* mutants.

DATA AVAILABILITY STATEMENT

The original contributions presented in the study are included in the article/**Supplementary Material**, further inquiries can be directed to the corresponding authors.

AUTHOR CONTRIBUTIONS

BW and LX conceived of and designed the study. TS and KH performed the lipidomic analysis. TS performed time-kill experiments and PK/PD models. TS and NA performed MIC measurements. TS, BW, and LX wrote the first draft and all authors reviewed the data, prepared the manuscript and approved the final version.

FUNDING

This study was supported by the National Institute of Allergy and Infectious Diseases of the National Institutes of Health under the award numbers R01AI136979 and R21AI132994, and SINGH19R0 from the Cystic Fibrosis Foundation.

ACKNOWLEDGMENTS

The authors thank the technical assistance from Dr. Rutan Zhang on mass spectrometry, Dr. Andrew Edwards at Imperial College London for providing SH1000-, USA300 LAC, and USA300 LAC Δ*agrA* strains, as well as Dr. Alexander Horswill at the University of Colorado for providing SH1000 and SH1001 strains.

SUPPLEMENTARY MATERIAL

The Supplementary Material for this article can be found online at: https://www.frontiersin.org/articles/10.3389/fmolb.2021.679949/full#supplementary-material

REFERENCES

Bayer, A. S., Mishra, N. N., Chen, L., Kreiswirth, B. N., Rubio, A., and Yang, S.-J. (2015). Frequency and Distribution of Single-Nucleotide Polymorphisms withinmprFin Methicillin-Resistant *Staphylococcus aureus* Clinical Isolates and Their Role in Cross-Resistance to Daptomycin and Host Defense Antimicrobial Peptides. *Antimicrob. Agents Chemother.* 59, 4930–4937. doi:10.1128/aac.00970-15

Bayer, A. S., Mishra, N. N., Sakoulas, G., Nonejuie, P., Nast, C. C., Pogliano, J., et al. (2014). Heterogeneity ofmprFSequences in Methicillin-Resistant *Staphylococcus aureus* Clinical Isolates: Role in Cross-Resistance between Daptomycin and Host Defense Antimicrobial Peptides. *Antimicrob. Agents Chemother.* 58, 7462–7467. doi:10.1128/aac.03422-14

Bayer, A. S., Schneider, T., and Sahl, H.-G. (2013). Mechanisms of Daptomycin Resistance inStaphylococcus Aureus: Role of the Cell Membrane and Cell wall. *Ann. N. Y Acad. Sci.* 1277, 139–158. doi:10.1111/j.1749-6632.2012.06819.x

Benvenuto, M., Benziger, D. P., Yankelev, S., and Vigliani, G. (2006). Pharmacokinetics and Tolerability of Daptomycin at Doses up to 12 Milligrams Per Kilogram of Body Weight once Daily in Healthy Volunteers. *Aac* 50, 3245–3249. doi:10.1128/aac.00247-06

Boles, B. R., and Horswill, A. R. (2008). Agr-mediated Dispersal of *Staphylococcus aureus* Biofilms. *Plos Pathog.* 4, e1000052. doi:10.1371/journal.ppat.1000052

Cafiso, V., Bertuccio, T., Purrello, S., Campanile, F., Mammina, C., Sartor, A., et al. (2014). dltA Overexpression: A Strain-independent keystone of Daptomycin Resistance in Methicillin-Resistant *Staphylococcus aureus*. *Int. J. Antimicrob. Agents* 43, 26–31. doi:10.1016/j.ijantimicag.2013.10.001

CLSI (2017). *Performance Standards for Antimicrobial Susceptibility Testing: Twenty-Fifth Informational Supplement M100-S27.*

Fey, P. D., Endres, J. L., Yajjala, V. K., Widhelm, T. J., Boissy, R. J., Bose, J. L., et al. (2013). A Genetic Resource for Rapid and Comprehensive Phenotype Screening of Nonessential *Staphylococcus aureus* Genes. *mBio.* 4, e00537. doi:10.1128/mbio.00537-12

Friedman, L., Alder, J. D., and Silverman, J. A. (2006). Genetic Changes that Correlate with Reduced Susceptibility to Daptomycin in *Staphylococcus aureus*. *Aac* 50, 2137–2145. doi:10.1128/aac.00039-06

Gurung, M., Moon, D. C., Choi, C. W., Lee, J. H., Bae, Y. C., Kim, J., et al. (2011). *Staphylococcus aureus* Produces Membrane-Derived Vesicles that Induce Host Cell Death. *PLOS ONE* 6, e27958. doi:10.1371/journal.pone.0027958

Hall Snyder, A. D., Werth, B. J., Nonejuie, P., Mcroberts, J. P., Pogliano, J., Sakoulas, G., et al. (2016). Fosfomycin Enhances the Activity of Daptomycin against Vancomycin-Resistant Enterococci in anIn VitroPharmacokinetic-Pharmacodynamic Model. *Antimicrob. Agents Chemother.* 60, 5716–5723. doi:10.1128/aac.00687-16

Hines, K. M., Waalkes, A., Penewit, K., Holmes, E. A., Salipante, S. J., Werth, B. J., et al. (2017). Characterization of the Mechanisms of Daptomycin Resistance Among Gram-Positive Bacterial Pathogens by Multidimensional Lipidomics. *mSphere* 2, e00492. doi:10.1128/msphere.00492-17

Hines, K. M., Shen, T., Ashford, N. K., Waalkes, A., Penewit, K., Holmes, E. A., et al. (2020). Occurrence of Cross-Resistance and β-lactam Seesaw Effect in Glycopeptide-, Lipopeptide- and Lipoglycopeptide-Resistant MRSA Correlates with Membrane Phosphatidylglycerol Levels. *J. Antimicrob. Chemother.* 75, 1182–1186. doi:10.1093/jac/dkz562

Jiang, J.-H., Bhuiyan, M. S., Shen, H.-H., Cameron, D. R., Rupasinghe, T. W. T., Wu, C.-M., et al. (2019). Antibiotic Resistance and Host Immune Evasion inStaphylococcus Aureusmediated by a Metabolic Adaptation. *Proc. Natl. Acad. Sci. USA* 116, 3722–3727. doi:10.1073/pnas.1812066116

Mehta, S., Cuirolo, A. X., Plata, K. B., Riosa, S., Silverman, J. A., Rubio, A., et al. (2012). VraSR Two-Component Regulatory System Contributes tomprF-Mediated Decreased Susceptibility to Daptomycin inIn Vivo-Selected Clinical Strains of Methicillin-Resistant *Staphylococcus aureus*. *Antimicrob. Agents Chemother.* 56, 92–102. doi:10.1128/aac.00432-10

Mishra, N. N., Bayer, A. S., Weidenmaier, C., Grau, T., Wanner, S., Stefani, S., et al. (2014). Phenotypic and Genotypic Characterization of Daptomycin-Resistant Methicillin-Resistant *Staphylococcus aureus* Strains: Relative Roles of mprF and Dlt Operons. *PLoS One* 9, e107426. doi:10.1371/journal.pone.0107426

Mishra, N. N., Yang, S. J., Chen, L., Muller, C., Saleh-Mghir, A., Kuhn, S., et al. (2013). Emergence of Daptomycin Resistance in Daptomycin-Naive Rabbits with Methicillin-Resistant *Staphylococcus aureus* Prosthetic Joint Infection Is Associated with Resistance to Host Defense Cationic Peptides and mprF Polymorphisms. *PLoS One* 8, e71151. doi:10.1371/journal.pone.0071151

Mishra, N. N., and Bayer, A. S. (2013). Correlation of Cell Membrane Lipid Profiles with Daptomycin Resistance in Methicillin-Resistant *Staphylococcus aureus*. *Antimicrob. Agents Chemother.* 57, 1082–1085. doi:10.1128/aac.02182-12

Muraih, J. K., Harris, J., Taylor, S. D., and Palmer, M. (2012). Characterization of Daptomycin Oligomerization with Perylene Excimer Fluorescence: Stoichiometric Binding of Phosphatidylglycerol Triggers Oligomer Formation. *Biochim. Biophys. Acta (Bba) - Biomembranes* 1818, 673–678. doi:10.1016/j.bbamem.2011.10.027

Muraih, J. K., Pearson, A., Silverman, J., and Palmer, M. (2011). Oligomerization of Daptomycin on Membranes. *Biochim. Biophys. Acta (Bba) - Biomembranes* 1808, 1154–1160. doi:10.1016/j.bbamem.2011.01.001

Otto, M. (2014). Phenol-soluble Modulins. *Int. J. Med. Microbiol.* 304, 164–169. doi:10.1016/j.ijmm.2013.11.019

Pader, V., Hakim, S., Painter, K. L., Wigneshweraraj, S., Clarke, T. B., and Edwards, A. M. (2016). *Staphylococcus aureus* Inactivates Daptomycin by Releasing Membrane Phospholipids. *Nat. Microbiol.* 2, 16194. doi:10.1038/nmicrobiol.2016.194

Peleg, A. Y., Miyakis, S., Ward, D. V., Earl, A. M., Rubio, A., Cameron, D. R., et al. (2012). Whole Genome Characterization of the Mechanisms of Daptomycin Resistance in Clinical and Laboratory Derived Isolates of *Staphylococcus aureus*. *PLoS One* 7, e28316. doi:10.1371/journal.pone.0028316

Peschel, A., and Otto, M. (2013). Phenol-soluble Modulins and Staphylococcal Infection. *Nat. Rev. Microbiol.* 11, 667–673. doi:10.1038/nrmicro3110

Pogliano, J., Pogliano, N., and Silverman, J. A. (2012). Daptomycin-mediated Reorganization of Membrane Architecture Causes Mislocalization of Essential Cell Division Proteins. *J. Bacteriol.* 194, 4494–4504. doi:10.1128/jb.00011-12

Sakoulas, G., Eliopoulos, G. M., Moellering, R. C., Jr., Wennersten, C., Venkataraman, L., Novick, R. P., et al. (2002). Accessory Gene Regulator (Agr) Locus in Geographically Diverse *Staphylococcus aureus* Isolates with Reduced Susceptibility to Vancomycin. *Aac* 46, 1492–1502. doi:10.1128/aac.46.5.1492-1502.2002

Tsompanidou, E., Sibbald, M. J. J. B., Chlebowicz, M. A., Dreisbach, A., Back, J. W., Van Dijl, J. M., et al. (2011). Requirement of the Agr Locus for colony Spreading of *Staphylococcus aureus*. *J. Bacteriol.* 193, 1267–1272. doi:10.1128/jb.01276-10

Wang, X., Thompson, C. D., Weidenmaier, C., and Lee, J. C. (2018). Release of *Staphylococcus aureus* Extracellular Vesicles and Their Application as a Vaccine Platform. *Nat. Commun.* 9(1):1379. doi:10.1038/s41467-018-03847-z

Werth, B. J., Ashford, N. K., Penewit, K., Waalkes, A., Holmes, E. A., Ross, D. H., et al. (2021). Dalbavancin Exposure *In Vitro* Selects for Dalbavancin-Non-Susceptible and Vancomycin-Intermediate Strains of Methicillin-Resistant *Staphylococcus aureus*. *Clin. Microbiol. Infect.* 27 (6), 910.e1–910.e8. In Press. doi:10.1016/j.cmi.2020.1008.1025

Yang, S. J., Kreiswirth, B. N., Sakoulas, G., Yeaman, M. R., Xiong, Y. Q., Sawa, A., et al. (2009). Enhanced Expression ofdltABCDIs Associated with the Development of Daptomycin Nonsusceptibility in a Clinical Endocarditis Isolate ofStaphylococcus Aureus. *J. Infect. Dis.* 200, 1916–1920. doi:10.1086/648473

Conflict of Interest: BW has received research grants from commercial sources, including Shionogi Inc.

The remaining authors declare that the research was conducted in the absence of any commercial or financial relationships that could be construed as a potential conflict of interest.

frontiers in Molecular Biosciences

ORIGINAL RESEARCH
published: 09 September 2021
doi: 10.3389/fmolb.2021.688357

Synergy Between Beta-Lactams and Lipo-, Glyco-, and Lipoglycopeptides, Is Independent of the Seesaw Effect in Methicillin-Resistant *Staphylococcus aureus*

Rutan Zhang[1], Ismael A. Barreras Beltran[2], Nathaniel K. Ashford[2], Kelsi Penewit[3], Adam Waalkes[3], Elizabeth A. Holmes[3], Kelly M. Hines[1†], Stephen J. Salipante[3], Libin Xu[1] and Brian J. Werth[2]**

[1]Department of Medicinal Chemistry, School of Pharmacy, University of Washington, Seattle, WA, United States, [2]Department of Pharmacy, School of Pharmacy, University of Washington, Seattle, WA, United States, [3]Department of Laboratory Medicine and Pathology, School of Medicine, University of Washington, Seattle, WA, United States

OPEN ACCESS

Edited by:
May Khanna,
University of Arizona, United States

Reviewed by:
Dwijendra K. Gupta,
Jai Prakash Vishwavidyalaya, India
Andrew David Berti,
Wayne State University, United States

***Correspondence:**
Libin Xu
libinxu@uw.edu
Brian J. Werth
bwerth@uw.edu

†Present address:
Kelly M. Hines,
Department of Chemistry, University of Georgia, Athens, GA, United States

Specialty section:
This article was submitted to Cellular Biochemistry, a section of the journal Frontiers in Molecular Biosciences

Received: *30 March 2021*
Accepted: *20 August 2021*
Published: *09 September 2021*

Citation:
Zhang R, Barreras Beltran IA, Ashford NK, Penewit K, Waalkes A, Holmes EA, Hines KM, Salipante SJ, Xu L and Werth BJ (2021) Synergy Between Beta-Lactams and Lipo-, Glyco-, and Lipoglycopeptides, Is Independent of the Seesaw Effect in Methicillin-Resistant Staphylococcus aureus. *Front. Mol. Biosci. 8:688357. doi: 10.3389/fmolb.2021.688357*

Methicillin-resistant *S. aureus* (MRSA) are resistant to beta-lactams, but synergistic activity between beta-lactams and glycopeptides/lipopeptides is common. Many have attributed this synergy to the beta-lactam-glycopeptide seesaw effect; however, this association has not been rigorously tested. The objective of this study was to determine whether the seesaw effect is necessary for synergy and to measure the impact of beta-lactam exposure on lipid metabolism. We selected for three isogenic strains with reduced susceptibility to vancomycin, daptomycin, and dalbavancin by serial passaging the MRSA strain N315. We used whole genome sequencing to identify genetic variants that emerged and tested for synergy between vancomycin, daptomycin, or dalbavancin in combination with 6 beta-lactams with variable affinity for staphylococcal penicillin binding proteins (PBPs), including nafcillin, meropenem, ceftriaxone, ceftaroline, cephalexin, and cefoxitin, using time-kills. We observed that the seesaw effect with each beta-lactam was variable and the emergence of the seesaw effect for a particular beta-lactam was not necessary for synergy between that beta-lactam and vancomycin, daptomycin, or dalbavancin. Synergy was more commonly observed with vancomycin and daptomycin based combinations than dalbavancin in time-kills. Among the beta-lactams, cefoxitin and nafcillin were the most likely to exhibit synergy using the concentrations tested, while cephalexin was the least likely to exhibit synergy. Synergy was more common among the resistant mutants than the parent strain. Interestingly N315-D1 and N315-DAL0.5 both had mutations in *vraTSR* and *walKR* despite their differences in the seesaw effect. Lipidomic analysis of all strains exposed to individual beta-lactams at subinhibitory concentrations suggested that in general, the abundance of cardiolipins (CLs) and most free fatty acids (FFAs) positively correlated with the presence of synergistic effects while abundance of phosphatidylglycerols (PGs) and lysylPGs mostly negatively correlated with synergistic effects. In conclusion, the beta-lactam-glycopeptide seesaw effect and beta-lactam-glycopeptide synergy are distinct phenomena. This suggests that the emergence of the seesaw effect may not have clinical importance in terms of predicting synergy. Further work

is warranted to characterize strains that don't exhibit beta-lactam synergy to identify which strains should be targeted with combination therapy and which ones cannot and to further investigate the potential role of CLs in mediating synergy.

Keywords: seesaw effect, beta-lactam antibacterials, lipidomic analysis, vancomycin, daptomycin, dalbavancin, synergy, membrane fluidity

INTRODUCTION

All MRSA are resistant to traditional beta-lactams, but when combined with glycopeptides, lipopeptides, or lipoglycopeptides, synergistic antimicrobial activity is commonly observed, especially among strains with reduced susceptibility to the latter antimicrobial classes (Mehta et al., 2012; Werth et al., 2013b; Xhemali et al., 2018). Some investigators have attributed this synergy to the "seesaw effect" (Renzoni et al., 2017; Molina et al., 2020), a phenomenon where the susceptibility to beta-lactams increases with declining vancomycin or daptomycin susceptibility (Sieradzki and Tomasz, 1997; Ortwine et al., 2013). While it is intuitive that the seesaw effect between beta-lactams and glyco-, lipo-, and lipoglycopeptides could be related to synergy between these agents, this association has not been rigorously tested. While the seesaw effect is assumed to be a common feature of strains with reduced susceptibility to vancomycin or daptomycin, to measure it requires the comparison between a parent strain that is initially susceptible to vancomycin or daptomycin and isogenic strains that develop reduced susceptibility. There are a few well-characterized examples of such clinical strain pairs, but this is not something that can be easily determined through routine monitoring by clinical laboratories (Vignaroli et al., 2011; Werth et al., 2013a). Not all MRSA with reduced susceptibility to vancomycin (*i.e.*, vancomycin intermediate *S. aureus*; VISA) or daptomycin exhibit the seesaw effect, and for most such clinical isolates, the emergence of the seesaw effect cannot be assessed due to absence of the parent strain.

In a previous study, we selected for a series of isogenic mutants by serial passage and identified isolates that do and do not exhibit the seesaw effect with a panel of six different beta-lactams (Hines et al., 2020). We found that lipidomic characteristics seem to correlate with the emergence or absence of the seesaw effect. In this study, we selected for a series of isogenic mutants against vancomycin, dalbavancin, or daptomycin using the well characterized MRSA strain N315, and evaluated the occurrence of seesaw effect and synergy with six different beta-lactams. The objective of this study was to determine whether the seesaw effect was necessary for synergy, to examine the changes in the lipidomic profiles after exposure to various beta-lactams, and to evaluate whether the lipidomic changes correlate with the occurrence of synergy with vancomycin, daptomycin, or dalbavancin.

MATERIALS AND METHODS

Media, Antimicrobials and Strains

Serial passage, susceptibility testing, and time–kill experiments were performed in Mueller–Hinton II broth (MHB). Tryptic soy agar (TSA) was used for subculture of organisms and colony enumeration. Beta-lactams and vancomycin were purchased commercially from Sigma-Aldrich and Thermo Fisher Scientific. Ceftaroline-2-HCl and dalbavancin were acquired from Allergan, and daptomycin was purchased from Merck. The well-characterized MRSA strain N315 and three strains derived from N315 were evaluated. These strains were selected for by serial passage in escalating concentrations of vancomycin (VAN), leading to N315-VAN8, daptomycin (DAP), leading to N315-DAP1, and dalbavancin (DAL), leading to N315-DAL0.5, as described previously (Silverman et al., 2001; Hines et al., 2020).

Reagents

LC/MS grade water and acetonitrile, ammonium acetate and brain heart infusion (BHI) media were purchased from Thermo Fisher Scientific. Phosphatidylcholines (PC) and phosphatidylethanolamines (PE) Standards for lipidomics were purchased from Avanti Polar Lipids and Nu-Chek prep and prepared as described previously (Hines K. M. et al., 2017; Hines KM. et al., 2017).

Susceptibility Testing and Time–Kills

MICs were determined by broth microdilution at an inoculum of 10^6 cfu/ml in accordance with CLSI guidelines (CLSI, 2017). MICs of vancomycin, dalbavancin, and daptomycin were also determined in the presence of 0.5x MIC (**Table 1**) of individual beta-lactams to assess the MIC lowering effects of subinhibitory beta-lactam concentrations. Time–kill experiments were performed in duplicate as previously described (Werth et al., 2013b; Werth, 2017). Briefly, 2 ml of MHB was inoculated with10^6 cfu/mL of study organism and exposed to 0.5x MIC for both single and combination drug exposures. The average free peak plasma concentration for a given drug was used instead if 0.5x the MIC was greater than this value in order to avoid over-estimating clinically relevant effects as has been done previously (Werth et al., 2015; Werth, 2017). Exposures tested are summarized in **Table 2** and included vancomycin, daptomycin, and dalbavancin each combined with nafcillin (NAF), meropenem (MEM), ceftriaxone (CRO), ceftaroline (CPT), cephalexin (LEX), and cefoxitin (FOX). Samples of 100 μL were taken at 0, 4, 8, and 24 h, diluted in sterile saline, and spiral plated for colony enumeration after 24 h incubation. Synergy was defined as a ≥2-$\log_{10}$cfu/mL reduction of the combination over the most active single agent, antagonism was defined as ≥1-$\log_{10}$cfu/mL growth compared with the most active single agent, and other interactions were considered indifferent.

Whole Genome Sequencing

DNA from N315 and antibiotic-selected derivatives was extracted using the Ultraclean microbial DNA isolation kit (Mo Bio). Sequencing libraries were prepared as described elsewhere

TABLE 1 | Strains used in this study and their antibiotic susceptibility and genetic profiles. The seesaw effect was most pronounced with cephalexin (LEX) and nafcillin (NAF) across the 3 mutant strains. Vancomycin (VAN), daptomycin (DAP), dalbavancin (DAL), nafcillin (NAF), cephalexin (LEX), meropenem (MEM), ceftriaxone (CRO), cefoxitin (FOX), ceftaroline (CPT).

Strain name	Selection drug	Cross-resistance MIC (μg/ml)										Genetic variants	
		VAN	DAP	DAL	NAF	LEX	MEM	CRO	FOX	CPT	Gene Name	Nucleotide Change	Predicted Amino Acid Change
N315	–	0.5	0.125	0.0039	16	32	16	512	128	1	–	–	–
N315-Dap1	DAP	1	1	0.0039	0.25	0.125	32	512	128	0.5	*walK* *yjbH* *vraS*	784 A → G 257 G → A 353 T → C	Lys262Glu Gly86Asp Leu118Ser
N315-Dal0.5	DAL	4	1	0.5	>32	8	16	2048	128	0.5	*walK* *vraT* *SA1741*	1278 G → A 20 C → T 242 C → A	Met426Ile Ser7Leu Ala81Asp
N315-Van8	VAN	8	1	1	0.5	1	8–16	64	64–128	0.25	*asp1* *norA*	841 A → G 737 G → C	Met281Val Gly246Ala

(Roach et al., 2015; Salipante et al., 2015), with sequencing performed using an Illumina MiSeq (Illumina, San Diego, CA, United States) with 150-bp paired-end chemistries. Sequence analysis was performed to identify single nucleotide mutations and insertion and deletion mutations in coding sequences as previously (Jorth et al., 2017), against the reference genome of N315 (GenBank Accession BA000018). Sequence variants were annotated using SnpEFF (Cingolani et al., 2012). Whole genome sequencing data from this study are available from the NCBI Sequence Read Archive (SRA; http://www.ncbi.nlm.nih.gov/sra) under BioProject number PRJNA547605.

Preparation of N315 and N315 Mutants for Lipidomics

The N315 parent strain and three N315 mutants (N315-DAP1, N315-VAN8 and N315-DAL0.5) were grown in 1 ml of BHI medium with addition of various beta-lactams targeting at different penicillin binding proteins (PBPs), including nafcillin (PBP non-specific), cephalexin (PBP3), meropenem (PBP1), ceftriaxone (PBP2), cefoxitin (PBP4), and ceftaroline (PBP2a) as shown in **Table 1**. Each strain was grown in the presence and absence of each beta-lactam in quadruplicate in subinhibitory concentrations equal to 0.5 time the MIC unless that value exceeded the maximum plasma concentration in which the average Cmax concertation was used instead.

Lipid Extraction

Briefly, bacteria broth was collected after cultivation overnight in the absence or presence of individual beta-lactams, rinsed with 1x PBS, spun and dried with a speed-vac. 150 μL of water was then added to the pelleted and dried bacteria. The resulting suspensions were sonicated in an ice bath for 30 min to dislodge the dried pellets and homogenize the suspension. A chilled solution of chloroform and methanol (1:2 v/v, 600 μL) was added to each tube, followed by 5 min of vortex and the addition of 150 μL of chilled chloroform and 150 μL of chilled water. The samples were then rigorously vortexed for 1 min and centrifuged for 10 min at 4°C and 2,000 × *g* to separate the organic and aqueous layers. The organic layers were collected to clean 1.5 ml polypropylene microcentrifuge tubes (Fisher Scientific, Waltham, MA, United States) and dried in a vacuum concentrator. The dried lipid extracts were reconstituted with 500 μL of 2:1 acetonitrile/methanol and transferred to glass vials for storage prior to LC-MS analysis.

Liquid Chromatography

Bacterial lipids were separated by a Waters UPLC (Waters Corp., Milford, MA, United States) as described previously (Hines K. M. et al., 2017; Hines KM. et al., 2017). Briefly, hydrophilic interaction liquid chromatography (HILIC) was performed with a Phenomenex Kinetex HILIC column (2.1 × 100 mm, 1.7 μm) maintained at 40°C at a flow rate of 0.5 ml/min. The solvent system consisted of: A) 50% acetonitrile/50% water with 5 mM ammonium acetate; and B) 95% acetonitrile/5% water with 5 mM ammonium acetate. The linear gradient was as follows: 0–1 min, 100% B; 4 min, 90% B; 7–8 min, 70% B; 9–12 min, 100% B. A sample injection volume of 5 μL was used for all analyses.

Ion Mobility-Mass Spectrometry

The Waters Synapt G2-XS platform was used for lipidomics analysis. Effluent from the UPLC was introduced through the electrospray ionization (ESI) source. ESI capillary voltages of +2.0 and −2.0 kV were used for positive and negative analyses, respectively. Additional ESI conditions were as follows: sampling cone, 40 V; extraction cone, 80 V; source temperature, 150°C; desolvation temperature, 500°C; cone gas, 10 L/h; desolvation gas, 1000 L/h. Mass calibration over *m/z* 50-1200 was performed with sodium formate. Calibration of ion mobility (IM) measurements was performed as previously described (Hines et al., 2016). IM separation was performed with a traveling wave height of 40 V and velocity of 500 m/s. Data was acquired for *m/z* 50-1200 with a 1 s scan time. Untargeted MS/MS (MS^E) was performed in the transfer region with a collision energy ramp of 35–45 eV. Mass and drift time correction was performed post-acquisition using the leucine enkephalin lockspray signal.

Cell Membrane Fluidity Assay

The effects of beta-lactam exposure on membrane fluidity was measured in each of the strains as previously described.(Lew et al., 2021). Briefly, the N315 parent strain and N315 mutants were grown overnight in 5 ml of BHI medium in the presence and absence of each of the beta-lactams tested in the time-kills at subinhibitory concentrations at 37°C, pelleted, and then resuspended into saline to a 0.9 McFarland suspension. CM fluidity was subsequently measured by polarizing spectrofluorometery using Synergy H1 Hybrid Multi-Mode Reader (BioTek Instrument, Inc., Winooski, VT, United States) with 1,6-diphenyl-1,3,5-hexatriene (DPH) as the probe. The detailed methods for calculating fluorescence polarization (FP) have been described previously (Lentz, 1989; Mishra et al., 2021). There is an inverse relationship between FP values and CM fluidity (Mishra et al., 2021). Each FP value was obtained based on 8 technical replicates.

Data Analysis

Data alignment, chromatographic peaks detection, and normalization were performed in Progenesis QI (Nonlinear Dynamics). A pooled quality control sample was used as the alignment reference. The default "All Compounds" method of normalization was used to correct for variation in the total ion current amongst samples. PCA analysis was performed with the online tool, MetaboAnalyst 4.0 (Chong et al., 2018). Pearson correlation coefficients were obtained using the Correlation function in the Analysis Toolpak add-in in Excel and visualized by an R package, ComplexHeatmap (Gu et al., 2016). Lipid profile heatmap was generated using ClustVis (Metsalu and Vilo, 2015). Student's t-tests for two groups were performed using a two-tailed distribution and equal variance. Lipid identifications were made based on *m/z* (within 10 ppm mass accuracy), retention time, and CCS with an in-house version of LipidPioneer, modified to contain the major lipid species observed in *S. aureus*, including free fatty acids (FFAs), DGDGs, PGs, CLs, and LysylPGs with fatty acyl compositions ranging from 25:0 to 38:0 (total carbons: total degree unsaturation), and LiPydomics (Hines KM. et al., 2017; Ulmer et al., 2017; Ross et al., 2020).

RESULTS

Susceptibility Testing and Time–Kills

Susceptibility of each of the N315-derived strains are listed in **Table 1**. As shown in the table, N315-DAP1 exhibited strong seesaw effect with cephalexin and nafcillin, with 8 and 6-$\log_2$ fold-change in MIC, respectively, compared to the N315 parent strain. N315-Van8 strain, aside from the above 2 beta-lactams inducing 5 $\log_2$ fold-change, ceftriaxone also showed significant decreases in MIC with 3 $\log_2$ fold-change relative to the parent. For N315-Dal0.5 strain, no general seesaw effect was observed in our susceptibility testing, notably, ceftriaxone and nafcillin even displayed increased MICs. Generally there was cross-resistance among VAN/DAL/DAP similar to what has been reported previously (Hines et al., 2020).

Time-kills results are summarized in **Table 2** and detailed kill curves are illustrated in **Supplementary Figures S1–S6**. Synergistic sensitivity to drug combinations of 3 peptide-based antimicrobials and 6 beta-lactams was commonly observed among all three N315-derived mutants with the exceptions that the combination of dalbavancin and 5 beta-lactams did not exhibit synergistic killing against N315-DAP1 and most combinations with cephalexin did not display synergy. In contrast, synergy was less common for the N315 parent strain. Interestingly, we found that the seesaw effect was not necessary for synergy between beta-lactams and VAN/DAP/DAL against MRSA. Although N315-DAL0.5 did not exhibit the seesaw effect (**Table 1**), this strain displayed general synergistic effect for most combinations of VAN, DAP or DAL with beta-lactams (**Table 2**); for example, with increases in killing activity up to 5.78, 6.52 and 6.11 $\log_{10}$CFU/mL, for drug combinations of vancomycin and cefoxitin, daptomycin and cefoxitin, as well as dalbavancin and ceftriaxone, respectively. It is also noteworthy that among all tested beta-lactams, cefoxitin and nafcillin were the most likely to exhibit synergistic activity, while cephalexin was the least likely to exhibit synergy.

Changes to the MICs of VAN, DAP, and DAL in the presence of sub-inhibitory concentration of individual beta-lactams relative to the MICs of the peptide-based drugs alone were also evaluated (**Table 3**). As shown in the table, most of the MICs of the three drugs significantly decreased in the presence of beta-lactams with the exception of cephalexin, indicating wide occurrence of synergy.

Whole Genome Sequencing

Whole genome sequencing (WGS) was performed on all selected strains to identify mutations which arose relative to the parental N315 (**Table 1**). Mutations affecting the *vraTSR* operon and the histidine kinase, *walK* were detected in N315-DAP1 and N315-DAL0.5 but not in N315-VAN8. Alternatively, N315-VAN8 acquired a variant in *asp1,* encoding accessory secretory system protein, and *norA*, a known contributor to quinolone resistance, neither of which has been clearly implicated in the emergence of VAN/DAL/DAP resistance previously.

Lipidomic Analysis of Beta-Lactam Exposed Strains

DAP-, VAN- and DAL-non-susceptible N315 mutants (4 replicates) as well as the N315 parent strains (4 replicates) were treated with 6 beta-lactams targeting different PBPs at the same concentrations used in the time kill experiments and combination MICs (see Experimental Section), then harvested for lipidomic analysis (**Figure 1**; NAF, MEM, CRO, CPT, LEX, FOX). Major lipids were identified as shown in **Supplementary Table S1**. PCA analysis of the lipidome in negative mode (**Supplementary Figure S7**) showed clear clustering of biological replicates, indicating good reproducibility of the sample preparation process and the LC-MS analysis of lipids. As shown in the PCA plot, the cluster of N315-VAN8 strains overlapped with the cluster of the N315 parent strains, indicating that they have similar lipidomic phenotype after being treated

TABLE 2 | Increase in killing activity (–log_{10}cfu/mL) of the combinations compared to the most active single agents from the time kills. Synergy (green) is ≤ –2 log_{10}cfu/mL; –2–1 log_{10}cfu/mL is improved activity (yellow), –1–0 log_{10}cfu/mL is no interaction (red).

N315-Parent	Nafcillin (NAF)	Meropenem (MEM)	Ceftriaxone (CRO)	Ceftaroline (CPT)	Cephalexin (LEX)	Cefoxitin (FOX)
vancomycin	-3.96	-0.81	0.17	-0.01	-0.1	-4.95
daptomycin	-6.86	-1.03	-0.25	-2.33	-0.05	-5.58
dalbavancin	0.26	0	-0.15	-0.01	-0.01	-3.91
N315-DAP1	NAF	MEM	CRO	CPT	LEX	FOX
vancomycin	-4.64	-3.38	-5.01	-1.63	-3.5	-6.01
daptomycin	-3.58	-3.61	-6.89	-3.61	-4.19	-6.38
dalbavancin	0.51	0.14	-0.09	0.02	0.06	-2.67
N315-VAN8	NAF	MEM	CRO	CPT	LEX	FOX
vancomycin	-3.94	-2.78	-4.25	-2.78	-4.42	-6.64
daptomycin	-6.59	-5.02	0.2	-7.31	-0.03	-6.64
dalbavancin	-6.66	-7.02	-6.12	-2.25	-0.13	-6.64
N315-DAL0.5	NAF	MEM	CRO	CPT	LEX	FOX
vancomycin	-3.26	-4.19	-5.57	-5.24	-0.07	-5.78
daptomycin	-4.06	0	-6.34	-2.61	0.07	-6.52
dalbavancin	-4.56	-5.58	-6.11	-0.78	-0.31	-5.52

TABLE 3 | Decrease in MIC (1/(fold change) of the combinations compared to the most active single agents from the susceptibility tests. Synergy (green) is 0.25 MIC; 0.25–0.5 MIC is improved activity (yellow), 0.5–1 MIC is no interaction (red).

N315-Parent	Nafcillin (NAF)	Meropenem (MEM)	Ceftriaxone (CRO)	Ceftaroline (CPT)	Cephalexin (LEX)	Cefoxitin (FOX)
vancomycin	0.25	0.25	1	0.5	1	0.25
daptomycin	0.25	0.125	0.25	0.25	0.25	0.25
dalbavancin	1	0.0625	0.25	0.0625	0.125	0.0312
N315-DAP1	NAF	MEM	CRO	CPT	LEX	FOX
vancomycin	0.25	0.25	1	0.25	1	0.5
daptomycin	0.25	0.0312	0.0625	0.125	0.5	0.0312
dalbavancin	1	0.0312	0.0625	0.0625	1	0.25
N315-VAN8	NAF	MEM	CRO	CPT	LEX	FOX
vancomycin	0.25	0.0625	0.5	0.0078	0.5	0.125
daptomycin	0.5	0.0625	0.25	0.25	1	0.125
dalbavancin	0.0039	0.125	0.0020	0.0078	0.5	0.0078
N315-DAL0.5	NAF	MEM	CRO	CPT	LEX	FOX
vancomycin	0.125	0.0312	0.5	0.5	0.25	0.125
daptomycin	0.125	0.0312	1	0.25	0.125	0.125
dalbavancin	0.0078	0.0156	0.0039	0.25	0.0039	0.0625

with beta-lactams. The heatmap intuitively shows the variation of major lipids observed in N315 mutant and parent strains treated with beta-lactams (**Figure 1**). Specifically, most of the cardiolipins (CLs) in N315-DAP1 strains and N315 strains were upregulated after being treated with beta-lactams, relative to the growth control (GC) strain without beta-lactam treatment. In N315-VAN8 samples treated with beta-lactams, most of the FFAs and PGs were significantly elevated, compared to VAN8 GC and N315 GC. For the N315 parent strain treated with nafcillin or meropenem, nearly all classes of lipids were highly expressed. For N315-Dal0.5, the presence of beta-lactams has only minor effect on the lipid profiles, in comparison with the GC strain.

Correlation of Lipid Levels and MICs

Using Pearson correlation analysis, the difference in individual lipid species abundance in a strain given a series of beta-lactam exposure was correlated with the changes in VAN, DAL, or DAP MIC for the same strain given the same beta-lactam exposure (**Figure 2**). In general, the MIC changes for the combination of VAN/DAP/DAL and beta-lactams had negative correlations with the levels of CLs, except for the N315-DAP1 strain and N315 parent strain treated with dalbavancin with or without beta-lactams. Conversely, the MICs changes for VAN/DAP/DAL in each strain were positively correlated with LysylPGs, except for the N315-DAP1 strain and N315 parent strain treated with vancomycin. For FFAs, there was an overall negative correlation with the MIC changes, and the correlation seemed to vary with fatty acid chain length. For DGDGs and PGs, there was no consistent trend observed for the correlation between the MIC changes and lipid levels among all four strains.

Correlation of Lipid Levels and Time-Kills

The difference in individual lipid species abundance for a strain given a series of beta-lactam exposure was also correlated with the changes in activity in time kills between VAN, DAL, or DAP alone or in combination with that same beta-lactam exposure using Pearson correlation analysis (**Figure 3**). For CLs, the correlation between lipid levels and time-kill changes showed similar trend as between lipid levels and MICs. The levels of LysylPGs and PGs were mainly positively correlated with the changes in time-kills of combo treatments relative to single VAN/DAP/DAL treatment, except for the N315-VAN8 strain treated with vancomycin and the N315 parent strain treated with vancomycin and daptomycin. For FFA, there was an overall negative correlation with the presence of synergy, and consistent with the MIC related correlations, such correlation seems to vary with fatty acid chain length. However, the correlation between synergies and the levels of DGDGs varied for specific lipid species and for the strains examined.

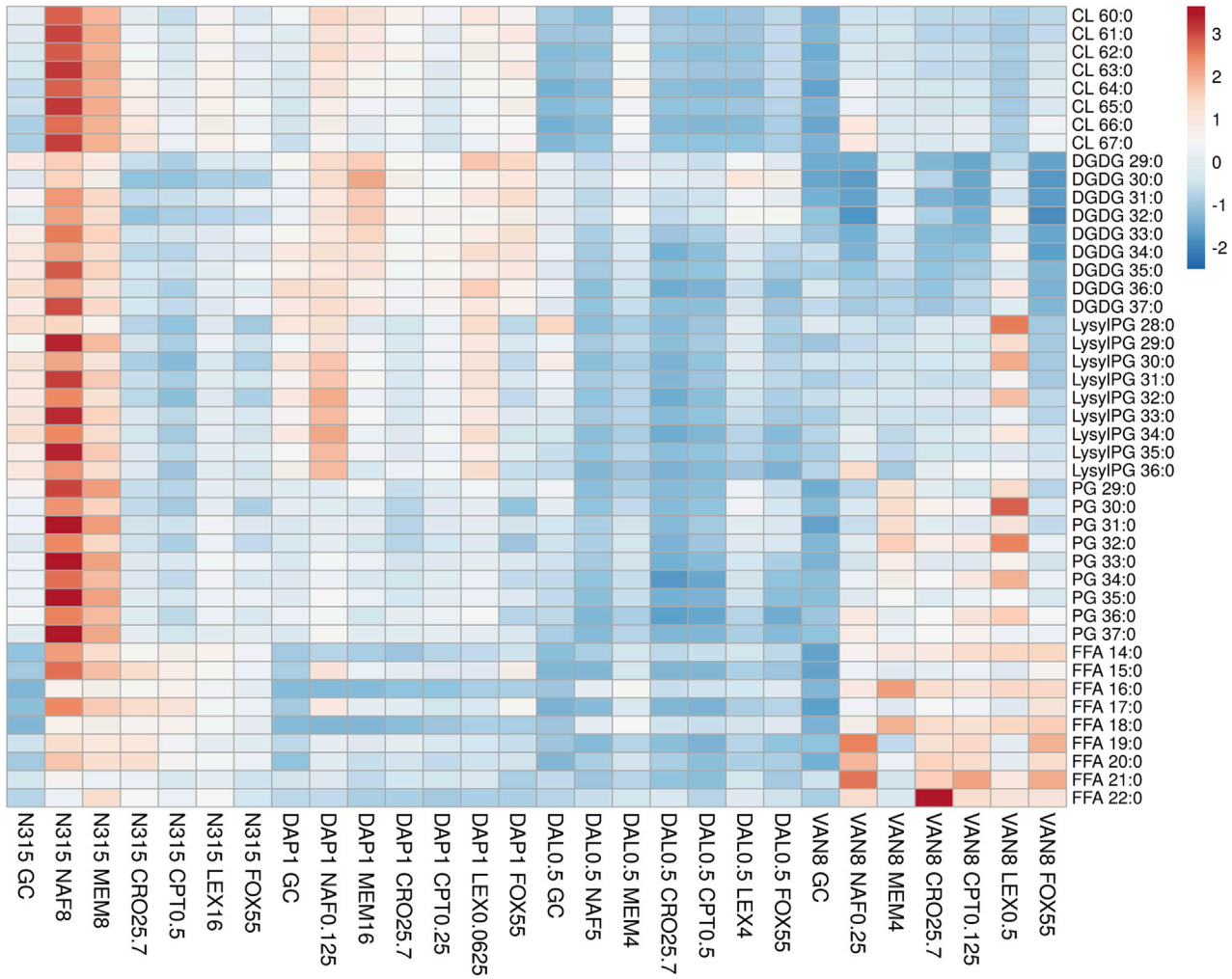

FIGURE 1 | The distribution of main lipids in N315 mutants (DAL0.5, DAP1 and VAN8) and the N315 parent strain treated with six beta-lactams. CPT, ceftaroline; CRO, ceftriaxone; FOX, cefoxitin; LEX, cephalexin; MEM, meropenem; NAF, nafcillin; GC, drug-free growth control.

DISCUSSION

In this study, we demonstrated that synergy between VAN/DAL/DAP and beta-lactams against MRSA is not dependent on the emergence of the seesaw effect. While N315-DAL0.5 did not exhibit the beta-lactam seesaw effect after becoming resistant to these peptide drugs, most combinations of VAN, DAP, or DAL with beta-lactams were still synergistic against this strain. Despite that N315-DAL0.5 and N315-DAP1 both acquired mutations in the *vraTSR* operon and *walK*, the seesaw effect phenotype was discordant. We do not know how the function of these genes was affected by the different mutations, but this discordance suggests that WalKR and/or VraTSR modulate cell envelope metabolism that favors or hinders beta-lactam susceptibility independently from any effect on VAN/DAP/DAL susceptibility. However, we also report the emergence of the seesaw effect and VAN/DAP/DAL cross resistance in a VISA strain that did not carry mutations in genes known to affect susceptibility these drugs or cell envelope metabolism. This finding reinforces the idea that beta-lactam susceptibility and VAN/DAP/DAL susceptibility are indeed closely linked metabolically.

Another pivotal finding in this research is that cefoxitin was among the least likely of the beta-lactams to show any seesaw effect but was consistently synergistic with VAN/DAL/DAP. Conversely, all strains, even N315-DAL0.5, exhibited some degree of the seesaw effect with cephalexin, but cephalexin was rarely synergistic with VAN/DAL/DAP at the concentrations tested. The PBP-nonselective nafcillin frequently exhibited the seesaw effect but also commonly exhibited synergy with VAN/DAL/DAP. Dalbavancin was less likely than vancomycin or daptomycin to be synergistic with companion agents overall, but specifically it was less likely to exhibit synergy against the parent strain and the N315-DAP1 strain, which both had very low dalbavancin MIC values. Due to these low MICs it remains possible that the time kills underestimated the synergistic effects against these strains and that greater enhancement would be seen at therapeutic concentrations. However other studies have shown

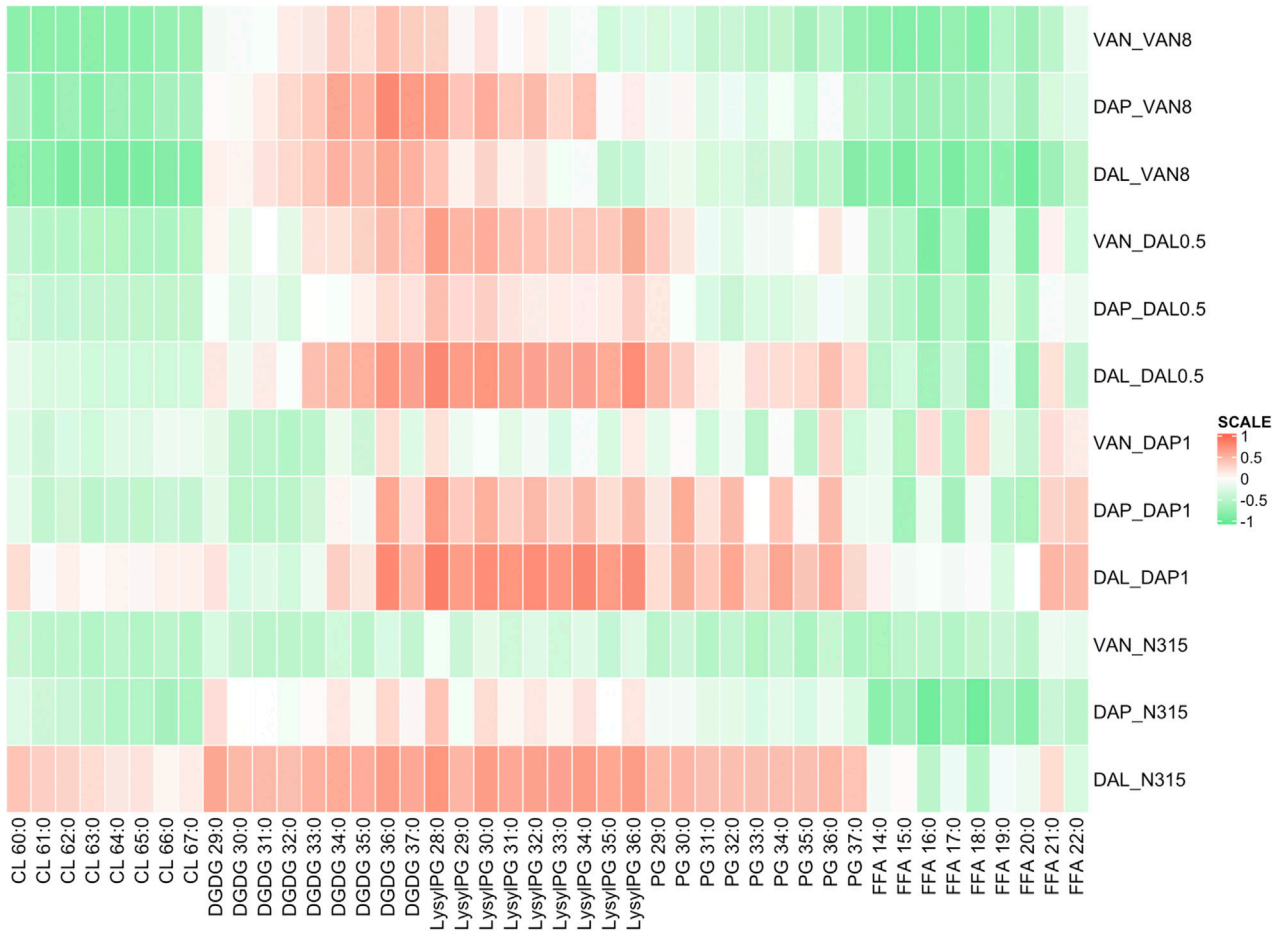

FIGURE 2 | Pearson correlation analysis showing the difference in individual lipid species abundance in a strain given a series of beta-lactam exposure vs the change in VAN, DAL, or DAP MIC given the same beta-lactam exposure. Green indicates that as an individual lipid increases, the MIC of VAN/DAP/DAL in the presence of beta-lactam decreases, while red indicates the opposite.

only modest improvement of dalbavancin in combination with ceftaroline in *in vitro* PK/PD models against dalbavancin susceptible strains (Kebriaei et al., 2019). Alternatively, synergy may be more common or more pronounced against strains with reduced susceptibility to dalbavancin. Additionally, the synergistic effects of these drug combinations were only observed in mutants from a single genetic background and only in *in vitro* time kills, so these data should not be used to select optimally synergistic combinations in the clinical setting.

Although many researchers have shown evidence that LysylPGs are increased in daptomycin-resistant MRSA, our lipidomic study (**Figure 1**), clearly showed that the expression of LysylPGs could be altered by treatment with different types of beta-lactams. The reduction in LysylPGs observed when N315-DAP1 was treated with CRO or FOX, relative to the growth control, DAP1 GC (**Figure 1** and **Supplementary Figure S8**), suggests that beta-lactam exposure reversed the changes in LysylPGs associated with the emergence of resistance. Furthermore, we found increases in the negatively charged CLs in most of the N315-DAP1 samples treated with beta-lactams (**Figure 1** and **Supplementary Figure S8**). Moreover, CLs were also highly expressed in the other beta-lactam exposed N315 derivatives compared to their respective non-treatment growth controls (**Figure 1** and **Supplementary Figures S10–S12**), indicating that beta-lactams appear to upregulate the synthesis of CLs. As shown in the **Figure 1**, it is also noteworthy that different PBP-targeting beta-lactams have different impact on the composition of cell membrane lipids for each strain derived from the common N315 ancestry.

For the three N315 mutants, synergistic activity, measured by either combination MIC or time kill, mostly (with two exceptions) positively correlated with the levels of LysylPGs. LysylPGs contain a positively charged headgroup, and increased level of LysylPGs has been associated with daptomycin resistance (Peleg et al., 2012; Jiang et al., 2019). Since LysylPGs are synthesized by lysinylation of negatively charged PGs by MprF (Peschel et al., 2001; Oku et al., 2004), the ratio of PGs/LPGs is a key indicator of charge changes. As expected, for all N315 mutants, the changes of PGs/LPGs are positively correlated with the synergies (negatively correlated with the colony counts) between DAP and beta-lactams (**Supplementary Figure S13**). However, whether such increases in positive charge

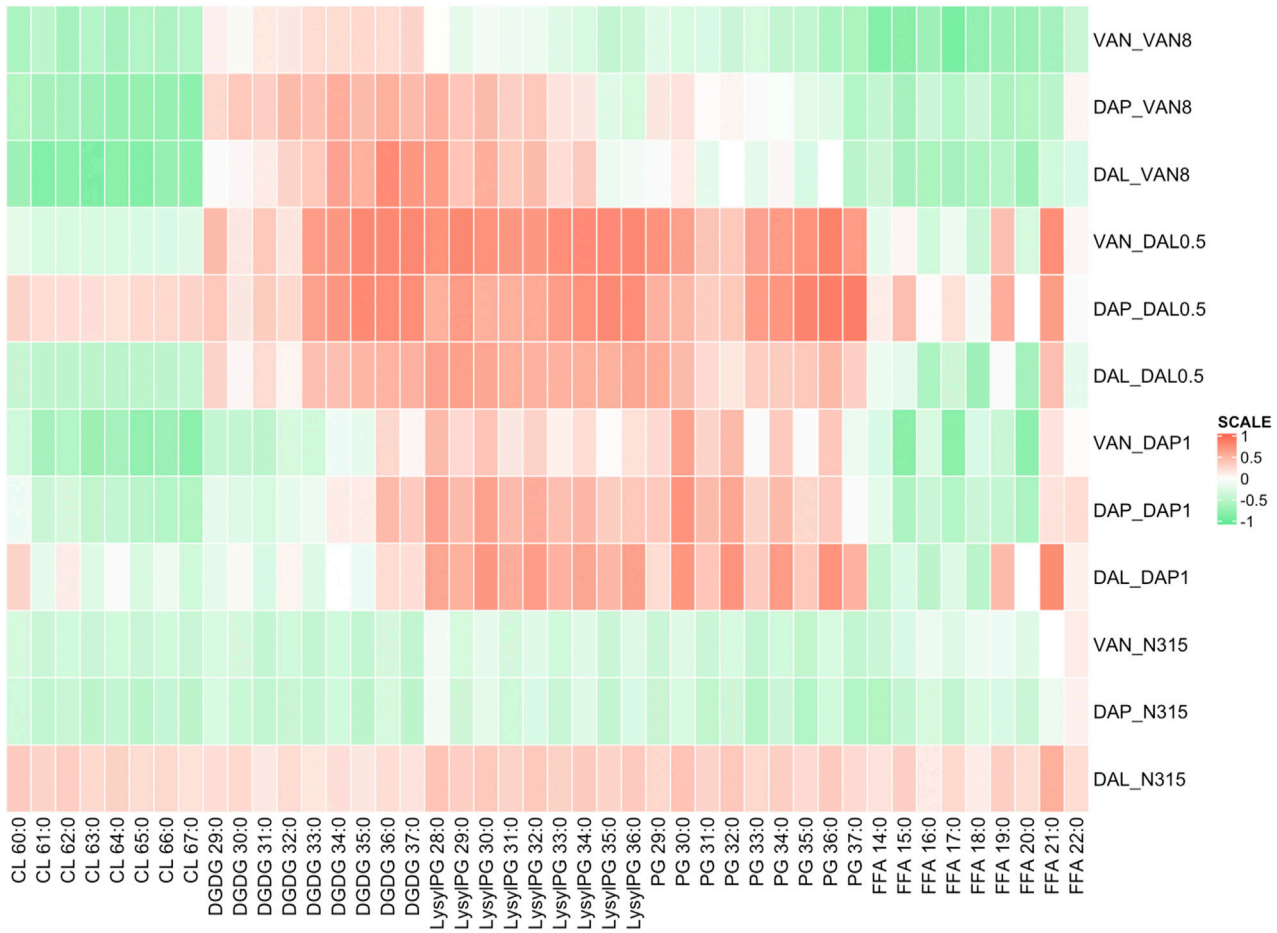

FIGURE 3 | Pearson correlation analysis showing the difference in individual lipid species abundance given a beta-lactam exposure vs the change in $\log_{10}$CFU/mL of the combination treatments of VAN, DAL, or DAP given the same beta-lactam exposure in time kills. Green indicates that as an individual lipid increases, the bacterial survival synergistically declined with beta-lactam exposure, while red indicates the opposite.

could also affect the binding of VAN or DAL is unknown. In contrast, the expression of CLs in most of the N315 mutants generally displayed negative correlation with synergistic reductions in survival or MICs, which might be related with the remodeling of cell membrane (Khan et al., 2019). Increased CL content has been found to increase fluidity and decrease mechanical stability of the lipid bilayer (Unsay et al., 2013). Mutations or downregulation in *cls* have also been associated with daptomycin resistance (Camargo et al., 2008; Peleg et al., 2012; Jiang et al., 2019; Khan et al., 2019). Interestingly, daptomycin was shown to attract fluid lipids in the membrane, causing delocalization of cell-wall synthesis-related proteins, proton leakage, and eventual death (Muller et al., 2016). For most of the N315 mutants, there was no clear correlation between DGDGs, PGs and changes in VAN/DAL/DAP MICs. However, we note that MIC synergies do not necessarily correlate with time-kill synergies as PGs showed overall positively correlated with time-kill synergies (similar to LysylPGs). As for FFAs, except some fatty acids with longer acyl chains, an overall negative correlation with changes in MIC/time-kill synergies was observed for most of the N315 mutants. It has been reported that a higher proportion of branched-chain fatty acids are associated with higher susceptibility to daptomycin (Boudjemaa et al., 2018). However, our lipidomic method does not allow the determination of straight or branched-chain fatty acids at this time, so future work is needed to validate this hypothesis.

In previous studies, beta-lactam exposure in daptomycin-resistant MRSA leads primarily to decreased cell membrane (CM) fluidity, but sometimes it is increased or unchanged (Lew et al., 2021; Mishra et al., 2021). Thus, different beta-lactam exposures and different mutations may have distinct impacts on the CM fluidity as a result of various lipids perturbations. The DPH based fluorescence polarity assay (**Supplementary Figure S14**) showed there were no general changes in CM fluidity for the majority of N315 mutants exposed to beta-lactams, which generally showed synergistic activity, indicating CM fluidity may not be the key factor in facilitating the general beta-lactam synergy. Correlation analysis between CM fluidity and synergistic killing (**Supplementary Figure S15**) did not display consistent trends

across the strains, suggesting that alteration of CM fluidity by lipids is confined to the strain level.

While MRSA elaborates 5 PBP subtypes, the seesaw effect between beta-lactams and peptide antibiotics, including daptomycin and vancomycin, usually stems from the vulnerability of PBP2a due to its dependence on functional membrane microdomains, wall teichoic acids, and the *PrsA* chaperone (Jousselin et al., 2015; Renzoni et al., 2017). Interference with any of these elements impairs PBP2a function and renders MRSA susceptible to beta-lactams (Foster, 2019). Both *walK* and *vraTSR* mutations are commonly observed in MRSA and their regulation of cell wall synthesis is well documented (Roch et al., 2017). It is likely that disruptions in cell membrane metabolism mediated by mutations in these genes could sensitize MRSA to beta-lactams by interfering with PBP2a trafficking. It's also noteworthy that the observed single nucleotide polymorphisms (SNPs) within *walK* and *vraTSR* may act as hot spots for gain-in-function phenotypes of synergies, similar with the association between SNPs within the *mprF* open reading frame and acquisition of daptomycin resistance (Bayer et al., 2015). Additionally, *yjbH* mutation observed in N315-DAP1 was also found to be associated with the acquisition of beta-lactam resistance by affecting PBP4 levels and peptidoglycan cross-linking, despite its main role in regulating oxidative burst by binding to the transcriptional regulator Spx and controlling its degradation via the proteasome-like ClpXP protease (Gohring et al., 2011; Engman et al., 2012). However, It's also possible that the inactivation of proteolysis triggered by *yjbH* mutation may directly mediate changes of susceptibility to beta-lactams by pathways regulating cell wall metabolism (Baek et al., 2014). While PBP4 expression has been shown to be important for maintaining resistance to oxacillin and nafcillin among community acquired strains of MRSA, knocking out PBP4 in N315, a classic nosocomial strain of the United States 100 lineage, did not impact nafcillin susceptibility; therefore, the contribution of this mutation is unclear (Memmi et al., 2008).

Like other *in vitro* studies with a similar design, this study has some limitations. We analyzed a set of 4 isogenic strains, which allows for better comparison across genotypes but does not allow for universal claims to be made about the relationship between beta-lactam synergy and the beta-lactam seesaw effect. However, our conclusion that synergy between glyco-/lipo-/lipoglyco-peptides and beta-lactams is independent of the seesaw effect between these agents in MRSA is robust and was demonstrated with several beta-lactams and glyco-/lipo-/lipoglycopeptide combinations among our strains. Furthermore, we are confident that beta-lactams are likely synergistic with glyco-/lipo-/lipoglyco-peptides, in part, because of beta-lactam effects on lipid metabolism, which enhances the activity of these drugs. Another potential limitation is that we exposed each strain to beta-lactam concentrations equal to 0.5x the MIC in time kills and prior to lipid analysis. Since these concentrations varied from strain to strain, some strains were exposed to absolute beta-lactam concentrations over 10 times greater than other strains, which could underestimate effects of higher concentrations on strains exhibiting the seesaw effect. Conversely, by using similar relative exposures among strains, we avoided underestimating effects in strains that did not exhibit the seesaw effect. With these limitations and tradeoffs in mind, we caution against readers who may be tempted to extrapolate these findings to determine the optimal beta-lactam/peptide combination for clinical use.

Future studies are needed to understand the roles of *vraTSR* and *walKR* in manifesting the seesaw effect and to uncover the molecular mechanisms by which *norA* and/or *asp1* affect cell envelope metabolism. Additional work is also needed to unveil the underlying mechanism(s) by which beta-lactams modulate lipidomic phenotypes and how the lipidomic changes affect the synergies between VAN/DAP/DAL and beta-lactams in MRSA.

DATA AVAILABILITY STATEMENT

The datasets presented in this study can be found in online repositories. The names of the repository/repositories and accession number(s) can be found below: http://www.ncbi.nlm.nih.gov/sra under BioProject number PRJNA547605.

AUTHOR CONTRIBUTIONS

BJW and LX conceived of and designed the study. RZ and KMH performed the lipidomic analysis. IAB, and NKA, performed the time-kill synergy studies, and susceptibility testing. NKA and BJW performed the *in vitro* serial passage, and resistance screening. KP, AW, EAH, and SJS performed the WGS and analysis. RZ wrote the first draft and all authors reviewed the data, prepared the manuscript and approved the final version.

FUNDING

This study was supported by the National Institute of Allergy and Infectious Diseases of the National Institutes of Health under the award numbers 1R01AI136979, 1R21AI132994, and SINGH19R0 from the Cystic Fibrosis Foundation.

SUPPLEMENTARY MATERIAL

The Supplementary Material for this article can be found online at: https://www.frontiersin.org/articles/10.3389/fmolb.2021.688357/full#supplementary-material

REFERENCES

Bæk, K. T., Gründling, A., Mogensen, R. G., Thøgersen, L., Petersen, A., Paulander, W., et al. (2014). β-Lactam Resistance in Methicillin-Resistant *Staphylococcus aureus* USA300 Is Increased by Inactivation of the ClpXP Protease. *Antimicrob. Agents Chemother.* 58, 4593–4603. doi:10.1128/AAC.02802-14

Bayer, A. S., Mishra, N. N., Chen, L., Kreiswirth, B. N., Rubio, A., and Yang, S.-J. (2015). Frequency and Distribution of Single-Nucleotide Polymorphisms withinmprFin Methicillin-Resistant *Staphylococcus aureus* Clinical Isolates

and Their Role in Cross-Resistance to Daptomycin and Host Defense Antimicrobial Peptides. *Antimicrob. Agents Chemother.* 59, 4930–4937. doi:10.1128/aac.00970-15

Boudjemaa, R., Cabriel, C., Dubois-Brissonnet, F., Bourg, N., Dupuis, G., Gruss, A., et al. (2018). Impact of Bacterial Membrane Fatty Acid Composition on the Failure of Daptomycin to Kill Staphylococcus aureus. *Antimicrob. Agents Chemother.* 62. e00023-18. doi:10.1128/AAC.00023-18

Camargo, I. L. B. d. C., Neoh, H.-M., Cui, L., and Hiramatsu, K. (2008). Serial Daptomycin Selection Generates Daptomycin-Nonsusceptible *Staphylococcus aureus* Strains with a Heterogeneous Vancomycin-Intermediate Phenotype. *Antimicrob. Agents Chemother.* 52, 4289–4299. doi:10.1128/aac.00417-08

Chong, J., Soufan, O., Li, C., Caraus, I., Li, S., Bourque, G., et al. (2018). MetaboAnalyst 4.0: towards More Transparent and Integrative Metabolomics Analysis. *Nucleic Acids Res.* 46, W486–W494. doi:10.1093/nar/gky310

Cingolani, P., Platts, A., Wang, L. L., Coon, M., Nguyen, T., Wang, L., et al. (2012). A Program for Annotating and Predicting the Effects of Single Nucleotide Polymorphisms, SnpEff. *Fly* 6, 80–92. doi:10.4161/fly.19695

CLSI (2017). *Performance Standards for Antimicrobial Susceptibility Testing: Twenty-Fifth Informational Supplement M100-S27*

Engman, J., Rogstam, A., Frees, D., Ingmer, H., and Von Wachenfeldt, C. (2012). The YjbH Adaptor Protein Enhances Proteolysis of the Transcriptional Regulator Spx in *Staphylococcus aureus*. *J. Bacteriol.* 194, 1186–1194. doi:10.1128/jb.06414-11

Foster, T. J. (2019). Can β-Lactam Antibiotics Be Resurrected to Combat MRSA? *Trends Microbiol.* 27, 26–38. doi:10.1016/j.tim.2018.06.005

Göhring, N., Fedtke, I., Xia, G., Jorge, A. M., Pinho, M. G., Bertsche, U., et al. (2011). New Role of the Disulfide Stress Effector YjbH in β-Lactam Susceptibility of *Staphylococcus aureus*. *Antimicrob. Agents Chemother.* 55, 5452–5458. doi:10.1128/aac.00286-11

Gu, Z., Eils, R., and Schlesner, M. (2016). Complex Heatmaps Reveal Patterns and Correlations in Multidimensional Genomic Data. *Bioinformatics* 32, 2847–2849. doi:10.1093/bioinformatics/btw313

Hines, K. M., Waalkes, A., Penewit, K., Holmes, E. A., Salipante, S. J., Werth, B. J., et al. (2017b). Characterization of the Mechanisms of Daptomycin Resistance Among Gram-Positive Bacterial Pathogens by Multidimensional Lipidomics. *mSphere* 2, e00492–00417. doi:10.1128/mSphere.00492-17

Hines, K. M., Herron, J., and Xu, L. (2017a). Assessment of Altered Lipid Homeostasis by HILIC-Ion Mobility-Mass Spectrometry-Based Lipidomics. *J. Lipid Res.* 58, 809–819. doi:10.1194/jlr.d074724

Hines, K. M., May, J. C., Mclean, J. A., and Xu, L. (2016). Evaluation of Collision Cross Section Calibrants for Structural Analysis of Lipids by Traveling Wave Ion Mobility-Mass Spectrometry. *Anal. Chem.* 88, 7329–7336. doi:10.1021/acs.analchem.6b01728

Hines, K. M., Shen, T., Ashford, N. K., Waalkes, A., Penewit, K., Holmes, E. A., et al. (2020). Occurrence of Cross-Resistance and β-lactam Seesaw Effect in Glycopeptide-, Lipopeptide- and Lipoglycopeptide-Resistant MRSA Correlates with Membrane Phosphatidylglycerol Levels. *J. Antimicrob. Chemother.* 75, 1182–1186. doi:10.1093/jac/dkz562

Jiang, J.-H., Bhuiyan, M. S., Shen, H.-H., Cameron, D. R., Rupasinghe, T. W. T., Wu, C.-M., et al. (2019). Antibiotic Resistance and Host Immune Evasion inStaphylococcus Aureusmediated by a Metabolic Adaptation. *Proc. Natl. Acad. Sci. USA* 116, 3722–3727. doi:10.1073/pnas.1812066116

Jorth, P., Mclean, K., Ratjen, A., Secor, P. R., Bautista, G. E., Ravishankar, S., et al. (2017). Evolved Aztreonam Resistance Is Multifactorial and Can Produce Hypervirulence in *Pseudomonas aeruginosa*. *mBio* 8, e00517–17. doi:10.1128/mBio.00517-17

Jousselin, A., Manzano, C., Biette, A., Reed, P., Pinho, M. G., Rosato, A. E., et al. (2015). The *Staphylococcus aureus* Chaperone PrsA Is a New Auxiliary Factor of Oxacillin Resistance Affecting Penicillin-Binding Protein 2A. *Antimicrob. Agents Chemother.* 60, 1656–1666. doi:10.1128/AAC.02333-15

Kebriaei, R., Rice, S. A., Stamper, K. C., and Rybak, M. J. (2019). Dalbavancin Alone and in Combination with Ceftaroline against Four Different Phenotypes of *Staphylococcus aureus* in a Simulated Pharmacodynamic/Pharmacokinetic Model. *Antimicrob. Agents Chemother.* 63, e01743–18. doi:10.1128/AAC.01743-18

Khan, A., Davlieva, M., Panesso, D., Rincon, S., Miller, W. R., Diaz, L., et al. (2019). Antimicrobial Sensing Coupled with Cell Membrane Remodeling Mediates Antibiotic Resistance and Virulence in *Enterococcus faecalis*. *Proc. Natl. Acad. Sci. U S A.* 116 (52), 26925–26932. doi:10.1073/pnas.1916037116

Lentz, B. R. (1989). Membrane "Fluidity" as Detected by Diphenylhexatriene Probes. *Chem. Phys. Lipids* 50, 171–190. doi:10.1016/0009-3084(89)90049-2

Lew, C., Mishra, N. N., Bayer, A. S., and Rose, W. E. (2021). Beta-lactam-induced Cell Envelope Adaptations, Not Solely Enhanced Daptomycin Binding, Underlies Daptomycin-Beta-Lactam Synergy in Methicillin-Resistant *Staphylococcus aureus*. *Antimicrob. Agents Chemother.* 14, AAC0035621. doi:10.1186/s13036-020-00243-4

Mehta, S., Singh, C., Plata, K. B., Chanda, P. K., Paul, A., Riosa, S., et al. (2012). β-Lactams Increase the Antibacterial Activity of Daptomycin against Clinical Methicillin-Resistant *Staphylococcus aureus* Strains and Prevent Selection of Daptomycin-Resistant Derivatives. *Antimicrob. Agents Chemother.* 56, 6192–6200. doi:10.1128/aac.01525-12

Memmi, G., Filipe, S. R., Pinho, M. G., Fu, Z., and Cheung, A. (2008). *Staphylococcus aureus* PBP4 Is Essential for β-Lactam Resistance in Community-Acquired Methicillin-Resistant Strains. *Antimicrob. Agents Chemother.* 52, 3955–3966. doi:10.1128/aac.00049-08

Metsalu, T., and Vilo, J. (2015). ClustVis: a Web Tool for Visualizing Clustering of Multivariate Data Using Principal Component Analysis and Heatmap. *Nucleic Acids Res.* 43, W566–W570. doi:10.1093/nar/gkv468

Mishra, N. N., Bayer, A. S., Baines, S. L., Hayes, A. S., Howden, B. P., Lapitan, C. K., et al. (2021). Cell Membrane Adaptations Mediate β-Lactam-Induced Resensitization of Daptomycin-Resistant (DAP-R) *Staphylococcus aureus In Vitro*. *Microorganisms* 9(5):1028. doi:10.3390/microorganisms9051028

Molina, K. C., Morrisette, T., Miller, M. A., Huang, V., and Fish, D. N. (2020). The Emerging Role of β-Lactams in the Treatment of Methicillin-Resistant *Staphylococcus aureus* Bloodstream Infections. *Antimicrob. Agents Chemother.* 64. e00468-2. doi:10.1128/AAC.00468-20

Müller, A., Wenzel, M., Strahl, H., Grein, F., Saaki, T. N. V., Kohl, B., et al. (2016). Daptomycin Inhibits Cell Envelope Synthesis by Interfering with Fluid Membrane Microdomains. *Proc. Natl. Acad. Sci. USA* 113, E7077–E7086. doi:10.1073/pnas.1611173113

Oku, Y., Kurokawa, K., Ichihashi, N., and Sekimizu, K. (2004). Characterization of the *Staphylococcus aureus* mprF Gene, Involved in Lysinylation of Phosphatidylglycerol. *Microbiology (Reading)* 150, 45–51. doi:10.1099/mic.0.26706-0

Ortwine, J. K., Werth, B. J., Sakoulas, G., and Rybak, M. J. (2013). Reduced Glycopeptide and Lipopeptide Susceptibility in *Staphylococcus aureus* and the "seesaw Effect": Taking Advantage of the Back Door Left Open? *Drug Resist. Updates* 16, 73–79. doi:10.1016/j.drup.2013.10.002

Peleg, A. Y., Miyakis, S., Ward, D. V., Earl, A. M., Rubio, A., Cameron, D. R., et al. (2012). Whole Genome Characterization of the Mechanisms of Daptomycin Resistance in Clinical and Laboratory Derived Isolates of *Staphylococcus aureus*. *PLoS One* 7, e28316. doi:10.1371/journal.pone.0028316

Peschel, A., Jack, R. W., Otto, M., Collins, L. V., Staubitz, P., Nicholson, G., et al. (2001). *Staphylococcus aureus* Resistance to Human Defensins and Evasion of Neutrophil Killing via the Novel Virulence Factor MprF Is Based on Modification of Membrane Lipids with L-Lysine. *J. Exp. Med.* 193, 1067–1076. doi:10.1084/jem.193.9.1067

Renzoni, A., Kelley, W. L., Rosato, R. R., Martinez, M. P., Roch, M., Fatouraei, M., et al. (2017). Molecular Bases Determining Daptomycin Resistance-Mediated Resensitization to β-Lactams (Seesaw Effect) in Methicillin-Resistant *Staphylococcus aureus*. *Antimicrob. Agents Chemother.* 61. doi:10.1128/AAC.01634-16

Roach, D. J., Burton, J. N., Lee, C., Stackhouse, B., Butler-Wu, S. M., Cookson, B. T., et al. (2015). A Year of Infection in the Intensive Care Unit: Prospective Whole Genome Sequencing of Bacterial Clinical Isolates Reveals Cryptic Transmissions and Novel Microbiota. *Plos Genet.* 11, e1005413. doi:10.1371/journal.pgen.1005413

Roch, M., Gagetti, P., Davis, J., Ceriana, P., Errecalde, L., Corso, A., et al. (2017). Daptomycin Resistance in Clinical MRSA Strains Is Associated with a High Biological Fitness Cost. *Front. Microbiol.* 8, 2303. doi:10.3389/fmicb.2017.02303

Ross, D. H., Cho, J. H., Zhang, R., Hines, K. M., and Xu, L. (2020). LiPydomics: A Python Package for Comprehensive Prediction of Lipid Collision Cross Sections and Retention Times and Analysis of Ion Mobility-Mass

Spectrometry-Based Lipidomics Data. *Anal. Chem.* 92 (22), 14967–14975. In Press. doi:10.1021/acs.analchem.1020c02560

Salipante, S. J., Sengupta, D. J., Cummings, L. A., Land, T. A., Hoogestraat, D. R., and Cookson, B. T. (2015). Application of Whole-Genome Sequencing for Bacterial Strain Typing in Molecular Epidemiology. *J. Clin. Microbiol.* 53, 1072–1079. doi:10.1128/jcm.03385-14

Sieradzki, K., and Tomasz, A. (1997). Inhibition of Cell wall Turnover and Autolysis by Vancomycin in a Highly Vancomycin-Resistant Mutant of *Staphylococcus aureus*. *J. Bacteriol.* 179, 2557–2566. doi:10.1128/jb.179.8.2557-2566.1997

Silverman, J. A., Oliver, N., Andrew, T., and Li, T. (2001). Resistance Studies with Daptomycin. *Antimicrob. Agents Chemother.* 45, 1799–1802. doi:10.1128/aac.45.6.1799-1802.2001

Ulmer, C. Z., Koelmel, J. P., Ragland, J. M., Garrett, T. J., and Bowden, J. A. (2017). LipidPioneer : A Comprehensive User-Generated Exact Mass Template for Lipidomics. *J. Am. Soc. Mass. Spectrom.* 28, 562–565. doi:10.1007/s13361-016-1579-6

Unsay, J. D., Cosentino, K., Subburaj, Y., and García-Sáez, A. J. (2013). Cardiolipin Effects on Membrane Structure and Dynamics. *Langmuir* 29, 15878–15887. doi:10.1021/la402669z

Vignaroli, C., Rinaldi, C., and Varaldo, P. E. (2011). Striking "Seesaw Effect" between Daptomycin Nonsusceptibility and β-Lactam Susceptibility in Staphylococcus Haemolyticus. *Antimicrob. Agents Chemother.* 55, 2495–2497. doi:10.1128/aac.00224-11

Werth, B. J. (2017). Exploring the Pharmacodynamic Interactions between Tedizolid and Other Orally Bioavailable Antimicrobials against *Staphylococcus aureus* and Staphylococcus Epidermidis. *J. Antimicrob. Chemother.* 72 (5), 1410–1414. doi:10.1093/jac/dkw588

Werth, B. J., Barber, K. E., Tran, K.-N. T., Nonejuie, P., Sakoulas, G., Pogliano, J., et al. (2015). Ceftobiprole and Ampicillin Increase Daptomycin Susceptibility of Daptomycin-Susceptible and -resistant VRE. *J. Antimicrob. Chemother.* 70, 489–493. doi:10.1093/jac/dku386

Werth, B. J., Steed, M. E., Kaatz, G. W., and Rybak, M. J. (2013a). Evaluation of Ceftaroline Activity against Heteroresistant Vancomycin-Intermediate *Staphylococcus aureus* and Vancomycin-Intermediate Methicillin-Resistant *S. aureus* Strains in anIn VitroPharmacokinetic/Pharmacodynamic Model: Exploring the "Seesaw Effect". *Antimicrob. Agents Chemother.* 57, 2664–2668. doi:10.1128/aac.02308-12

Werth, B. J., Vidaillac, C., Murray, K. P., Newton, K. L., Sakoulas, G., Nonejuie, P., et al. (2013b). Novel Combinations of Vancomycin Plus Ceftaroline or Oxacillin against Methicillin-Resistant Vancomycin-Intermediate *Staphylococcus aureus* (VISA) and Heterogeneous VISA. *Antimicrob. Agents Chemother.* 57, 2376–2379. doi:10.1128/aac.02354-12

Xhemali, X., Smith, J. R., Kebriaei, R., Rice, S. A., Stamper, K. C., Compton, M., et al. (2018). Evaluation of Dalbavancin Alone and in Combination with β-lactam Antibiotics against Resistant Phenotypes of *Staphylococcus aureus*. *J. Antimicrob. Chemother.* 74 (1), 82–86. doi:10.1093/jac/dky376

Conflict of Interest: BW has received research grants from commercial sources, including Shionogi Inc.

The remaining authors declare that the research was conducted in the absence of any commercial or financial relationships that could be construed as a potential conflict of interest.

Publisher's Note: All claims expressed in this article are solely those of the authors and do not necessarily represent those of their affiliated organizations, or those of the publisher, the editors and the reviewers. Any product that may be evaluated in this article, or claim that may be made by its manufacturer, is not guaranteed or endorsed by the publisher.

frontiers in Molecular Biosciences

ORIGINAL RESEARCH
published: 22 December 2021
doi: 10.3389/fmolb.2021.758228

Degradation of Components of the Lpt Transenvelope Machinery Reveals LPS-Dependent Lpt Complex Stability in *Escherichia coli*

Alessandra M. Martorana[1], Elisabete C. C. M. Moura[1], Paola Sperandeo[1], Flavia Di Vincenzo[1], Xiaofei Liang[2], Eric Toone[2], Pei Zhou[2,3] and Alessandra Polissi[1]**

[1]*Dipartimento di Scienze Farmacologiche e Biomolecolari, Università Degli Studi di Milano, Milan, Italy,* [2]*Department of Chemistry, Duke University, Durham, NC, United States,* [3]*Department of Biochemistry, Duke University School of Medicine, Durham, NC, United States*

OPEN ACCESS

Edited by:
Heidi Vitrac,
Tosoh Bioscience LLC, United States

Reviewed by:
Candice Klug,
Medical College of Wisconsin, United States
Denice C. Bay,
University of Manitoba, Canada

***Correspondence:**
Alessandra M. Martorana
alessandra.martorana@unimi.it
Alessandra Polissi
alessandra.polissi@unimi.it

Specialty section:
This article was submitted to Cellular Biochemistry, a section of the journal Frontiers in Molecular Biosciences

Received: *13 August 2021*
Accepted: *23 November 2021*
Published: *22 December 2021*

Citation:
Martorana AM, Moura ECCM, Sperandeo P, Di Vincenzo F, Liang X, Toone E, Zhou P and Polissi A (2021) Degradation of Components of the Lpt Transenvelope Machinery Reveals LPS-Dependent Lpt Complex Stability in Escherichia coli. *Front. Mol. Biosci. 8:758228. doi: 10.3389/fmolb.2021.758228*

Lipopolysaccharide (LPS) is a peculiar component of the outer membrane (OM) of many Gram-negative bacteria that renders these bacteria highly impermeable to many toxic molecules, including antibiotics. LPS is assembled at the OM by a dedicated intermembrane transport system, the Lpt (LPS transport) machinery, composed of seven essential proteins located in the inner membrane (IM) ($LptB_2CFG$), periplasm (LptA), and OM (LptDE). Defects in LPS transport compromise LPS insertion and assembly at the OM and result in an overall modification of the cell envelope and its permeability barrier properties. LptA is a key component of the Lpt machine. It connects the IM and OM sub-complexes by interacting with the IM protein LptC and the OM protein LptD, thus enabling the LPS transport across the periplasm. Defects in Lpt system assembly result in LptA degradation whose stability can be considered a marker of an improperly assembled Lpt system. Indeed, LptA recruitment by its IM and OM docking sites requires correct maturation of the $LptB_2CFG$ and LptDE sub-complexes, respectively. These quality control checkpoints are crucial to avoid LPS mistargeting. To further dissect the requirements for the complete Lpt transenvelope bridge assembly, we explored the importance of LPS presence by blocking its synthesis using an inhibitor compound. Here, we found that the interruption of LPS synthesis results in the degradation of both LptA and LptD, suggesting that, in the absence of the LPS substrate, the stability of the Lpt complex is compromised. Under these conditions, DegP, a major chaperone–protease in *Escherichia coli*, is responsible for LptD but not LptA degradation. Importantly, LptD and LptA stability is not affected by stressors disturbing the integrity of LPS or peptidoglycan layers, further supporting the notion that the LPS substrate is fundamental to keeping the Lpt transenvelope complex assembled and that LptA and LptD play a major role in the stability of the Lpt system.

Keywords: bacterial cell envelope, lipopolysaccharide, Lpt system, outer membrane stability, LpxC inhibitor

INTRODUCTION

Gram-negative bacteria are surrounded by two distinct lipid bilayers: the inner membrane (IM) and the outer membrane (OM). The IM and OM together delimit an aqueous compartment called periplasm which contains the peptidoglycan (PG), a continuous polymer that protects the cell from osmotic lysis. The outermost layer of the cell envelope, the OM, endows it with highly selective permeability properties (Silhavy et al., 2010). The asymmetric configuration of the OM, with phospholipids in the inner leaflet and lipopolysaccharide (LPS) in the outer leaflet, greatly hampers the permeation of many toxic molecules into the bacterium. The complex architecture of the Gram-negative bacterial cell envelope poses a great challenge to the development of novel antimicrobial molecules (Nikaido, 2003; Tacconelli et al., 2018). Therefore, the disruption of the LPS biosynthetic pathway has long been explored by pharmaceutical companies (Erwin, 2016). Over the last decade, targets in the LPS transport pathway have emerged providing innovative approaches for antibiotic development (Srinivas et al., 2010; Werneburg et al., 2012; Andolina et al., 2018; Vetterli et al., 2018; Moura et al., 2020; Zhang et al., 2019).

LPS is a complex glycolipid with six saturated acyl chains that insert into the OM (Raetz and Whitfield, 2002; **Figure 1A**). Thanks to its peculiar structure, LPS largely contributes to the permeability barrier function of the OM (Raetz and Whitfield, 2002; Nikaido, 2003).

LPS must be transported across the periplasm, from its final site of synthesis at the IM, to the cell surface. From the IM, the Lpt (lipopolysaccharide transport) transenvelope multiprotein machinery transports LPS to the outer leaflet of the OM. In *Escherichia coli*, the Lpt machine is composed of seven essential proteins (LptA-G) that work together as a single complex to extract LPS from the IM, transport it across the periplasm, and insert it into the OM (**Figure 1B**) (Sperandeo et al., 2019). The ABC transporter $LptB_2CFG$ powers the LPS extraction from the IM and its transport across the periplasm to the cell surface (Okuda et al., 2012; Li et al., 2019; Owens et al., 2019). LptA is the soluble protein connecting the IM and OM Lpt sub-complexes (Sperandeo et al., 2007; Suits et al., 2008; Tran et al., 2008; Sperandeo et al., 2011), and exactly how many LptA monomers compose the periplasmic Lpt bridge is not yet known. LPS flows from the periplasmic domain of LptC to LptA, and at the OM, the LptDE translocon receives LPS and inserts it into the outer leaflet (Tran et al., 2010; Freinkman et al., 2011; Dong et al., 2014; Qiao et al., 2014). According to the proposed PEZ model, the IM $LptB_2CFG$ ABC transporter loads and pushes a continuous stream of LPS monomers into the Lpt bridge in a mechanism resembling a PEZ candy dispenser (Okuda et al., 2016).

The Lpt bridge is formed by the shared β-jellyroll fold architecture of the periplasmic domains of LptF and LptC, the LptA protein, and the periplasmic domain of LptD, which all assemble in a C-to-N terminal configuration (Villa et al., 2013; Tran et al., 2010; Qiao et al., 2014; Suits et al., 2008; Dong et al., 2017; Luo et al., 2017; Okuda et al., 2016). The hydrophobic lumen of the bridge shields the LPS acyl chains from the hydrophilic periplasmic environment. When the LPS transport is compromised via the depletion of Lpt components or via the disruption of protein–protein interactions, LPS molecules accumulate at the outer leaflet of the IM, the Lpt bridge disassembles, and LptA is degraded. The LptA stability has thus been considered a sensor for the correct Lpt complex assembly (Sperandeo et al., 2008; Sperandeo et al., 2011; Moura et al., 2020).

The assembly of the Lpt machinery is carefully monitored by the cells to avoid LPS mistargeting. At the IM, recruitment of LptA by

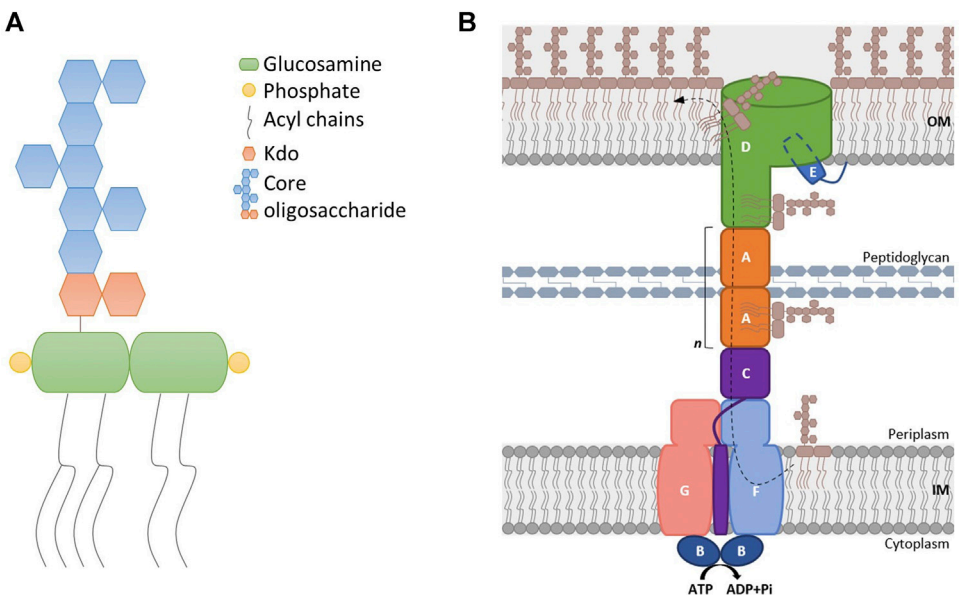

FIGURE 1 | Structure of LPS and the Lpt complex. **(A)** The lipopolysaccharide (LPS) molecule consists of three parts: (i) the lipid A moiety, comprising a phosphorylated glucosamine disaccharide linked to saturated acyl chains that insert into the outer membrane (OM); (ii) the core oligosaccharide formed by non-repeating sugar units; and (iii) the O antigen (not depicted), a long oligosaccharide chain that varies highly between species and strains. **(B)** LPS is extracted from the inner membrane (IM) by the IM complex $LptB_2FG$ and translocated through the hydrophobic cavity of the protein bridge formed by LptC, LptA, and the N-terminal region of LptD. The C-terminal domain of LptD forms the β-barrel that, together with LptE, inserts LPS into the OM.

TABLE 1 | *Escherichia coli* strains.

Strain	Genotype	Source or reference
BW25113	*lacI*^{q} *rrnB*$_{T14}$ Δ*lacZ*$_{WJ16}$ *hsdR514* Δ*araBAD*$_{AH33}$ Δ*rhaBAD*$_{LD78}$	Datsenko and Wanner (2000)
BB3	BW25113 (*kan araC araB*p-*yrbK*)*1*	Sperandeo et al. (2006)
JW0157	F-, Δ (*araD-araB*)*567*, Δ*degP775:kan*, Δ*lacZ4787* (:rrnB-3), λ$^-$, *rph-1*, Δ (*rhaD-rhaB*)*568*, *hsdR514*	Keio collection, Baba et al. (2006)
JW2479	F-, Δ (*araD-araB*)*567*, Δ*lacZ4787* (:rrnB-3), λ$^-$, Δ*yfgC742:kan*, *rph-1*, Δ (*rhaD-rhaB*)*568*, *hsdR514*	Keio collection, Baba et al. (2006)
AMM92	BW25113 Δ*degP*	This work
AMM93	BW25113 Δ*yfgC*	This work

the LptC protein does not occur unless the $LptB_2CFG$ complex is correctly formed (Villa et al., 2013). The correct formation of the LptDE complex is another key regulatory checkpoint in the assembly of the Lpt machinery. The OM translocon comprises LptD, with an N-terminal β-jellyroll domain and a large C-terminal β-barrel domain, and the lipoprotein LptE buried inside the barrel (Freinkman et al., 2011; Dong et al., 2014; Qiao et al., 2014). For the translocon to be functional, two disulfide bonds connect the N-terminal and the β-barrel domains of LptD, ensuring correct orientation of these domains which is essential for the recruitment of LptA (Ruiz et al., 2010; Freinkman et al., 2012). If the LptDE translocon is not correctly assembled, LptA fails to interact and the β-jellyroll oligomerization process for bridge formation does not occur (Freinkman et al., 2012). This ensures that the Lpt bridges do not couple with defective OM translocons, which would mistarget LPS to periplasm and cause toxicity problems (Chng et al., 2010; Freinkman et al., 2012; Zhang et al., 2013).

We have previously showed that LptA stability in the cell can be considered a sensor of the correct assembly of the Lpt complex (Sperandeo et al., 2011). In this work, we sought to clarify whether the stability of the Lpt complex is also dependent on the presence of its substrate. To this purpose, we analyzed the steady-state level of LptA in cells in which the LPS biosynthesis is blocked. We treated the cells with LPC-058, a compound known to inhibit the activity of LpxC, which catalyzes the first essential step of LPS biosynthesis and we show that not only LptA but also LptD steady-state levels decrease in the cell upon LPS biosynthesis blockage. Since LptD folding and turnover are dependent on two major chaperones/proteases that act at different points of the LptD assembly pathway, namely, DegP and BepA, we investigated their role in the decrease of the LptD level in cells with defective LPS synthesis. Overall, our results provide evidence that LPS is required to keep the machinery assembled, and when absent, due to the interruption of LPS synthesis, the Lpt bridge disassembles, and LptA and its anchor at the OM, the LptD protein, are degraded. Under these conditions, the stability of LptD, but not LptA, is controlled by the periplasmic chaperone/protease DegP.

METHODS

Bacterial Strains and Growth Conditions

E. coli strains used in this work are described in **Table 1**. Luria-Bertani-Lennox (LB-Lennox) medium (Ghisotti et al., 1992) has been described. 25 mg/ml kanamycin and 0.2% arabinose were added when required. Solid media contained 1% agar. Cells of BB3 strain were grown in 50 ml of LB-Lennox medium supplemented with 0.2% arabinose until OD_{600} 0.2. Then, the cells were harvested, washed three times with fresh LB-Lennox, diluted one hundredfold in fresh medium either with arabinose (permissive condition) or without arabinose (non-permissive condition), and incubated with aeration at 37°C. Cell growth was monitored by OD_{600} measurements.

TABLE 2 | Minimum inhibitory concentrations (MICs) of antibiotics/chemicals against *E. coli* strains.

	MIC[a]		
	BW25113	**AMM92**	**AMM93**
LPC-058	0.031 μg ml^{-1}	0.031 μg ml^{-1}	0.031 μg ml^{-1}
EDTA	20 mM	NT	NT
Polymyxin B	1.2 μg ml^{-1}	NT	NT
NH_4VO_3	25 mM	NT	NT
Aztreonam	30 μg ml^{-1}	NT	NT
Cefsulodin	20 μg ml^{-1}	NT	NT

[a]*MIC, minimum inhibitory concentration; NT, not tested.*

Strain Construction

degP and *bepA* deletion strains were obtained by P1 phage transduction (Silhavy et al., 1984) moving *kan*-marked alleles from the Keio *E. coli* single-gene knockout library (Baba et al., 2006). The *kan* cassette was removed by pCP20-encoded Flp recombinase to generate unmarked deletions (Datsenko and Wanner, 2000). The removal of the *kan* gene was verified by replica plating and colony PCR.

Growth Conditions of *E. coli* Cells Treated With Several Chemicals/Antibiotics

E. coli cells were grown in the LB-Lennox medium. At OD_{600} of 0.1, the cells were treated with 0.031 μg/ml of LPC-058, 20 mM ethylene-diaminetetraacetic acid (EDTA) (Falchi et al., 2018), 0.6 μg/ml polymyxin B, 25 mM ammonium metavanadate (NH_4VO_3) (Tam and Missiakas 2005), 30 μg/ml aztreonam (Georgopapadakou et al., 1982), and 20 μg/ml cefsulodin (Curtis et al., 1979). The minimum inhibitory concentration (MIC) for each compound was determined using the broth micro-dilution method (Wiegand et al., 2008; **Table 2**). Cell growth was monitored by OD_{600} measurements. When treated cells decreased the growth rate compared to untreated cells (indicated in the figures with an arrow), samples for western blot analysis were collected after 5, 10, 20, and 60 min, from both

cell cultures, and processed as described in *SDS-PAGE and Immunoblotting*.

Analysis of Outer Membrane Protein Profiles

The analysis of outer membrane protein (OMP) profiles by SDS-PAGE was performed as described by Yethon et al. (2000) with some modifications. After treatment with LPC-058 as described above, equal numbers of cells (standardized by measuring the optical density at 600 nm) of LPC-058–treated and untreated cultures were harvested by centrifugation. After resuspension in 20 mM Tris buffer (pH 8), the cells were lysed by a passage through a High Pressure Cell Disruptor (Constant Systems) at 21,000 psi and centrifuged (3,500 × g, for 10 min) to remove the cell debris. The total membrane fractions were collected by centrifugation (100,000 × g, for 1 h) and then resuspended in 20 mM Tris (pH 8) 2% Sarkosyl buffer. The Sarkosyl-insoluble OM fraction was collected by centrifugation (100,000 × g, for 1 h), then washed with 20 mM Tris buffer (pH 8), and recentrifuged. The resulting pellet was resuspended in 250 µL of 20 mM Tris buffer (pH 8) and analyzed by sodium dodecyl sulfate–polyacrylamide gel electrophoresis (SDS-PAGE). Input samples from each cell culture were processed to obtain the cell crude extract and analyzed by western blot, as described in *SDS-PAGE and Immunoblotting*.

SDS-PAGE and Immunoblotting

LptA, LptD, LptB, LptE, LptC, and OmpA steady-state levels were assessed in the BW25113, BB3, and *degP* and *bepA* deletion strains (**Table 1**) by western blot analysis using polyclonal antibodies against LptA, LptD, LptB, LptE, LptC, and OmpA raised in rabbit. Crude-cell extracts for protein analysis were collected and harvested by centrifugation at the time points indicated in *Growth Conditions of E. coli Cells Treated With Several Chemicals/Antibiotics*. The cell pellets were resuspended in a volume (in mL) of SDS sample buffer equal to 1/24 of the total optical density of the sample. The samples were processed for immunoblotting as previously described (Moura et al., 2020).

LPS Analysis From Whole-Cell Extracts

Whole-cell extract samples for LPS analysis were obtained as described in the previous section and then separated by 18% Tricine SDS-PAGE (Lesse et al., 1990). Immunodecoration was performed using anti-LPS core WN1 222-5 monoclonal antibodies (Hycult Biotech) at a dilution of 1:1,000 and using anti-LptE antibodies as the loading control. Goat anti-mouse immunoglobulin Alexa Fluor® 788 conjugate and goat anti-rabbit immunoglobulin Alexa Fluor® 688 conjugate (Li-Cor) were used as secondary antibodies at a dilution of 1:15,000.

RESULTS

Improper Assembly of the Lpt Machine Causes Selective LptA Degradation

We previously reported that, in *E. coli* cells, LptA is degraded in the absence of the correct IM and OM docking sites, as depletion of LptC, LptD, or LptE (involved in proper LptD folding) (Chng et al., 2012) results in decreased LptA levels (Sperandeo et al., 2011). To understand whether the lack of LptA interaction with its IM docking site affects the stability of other Lpt proteins, we evaluated the stability of representative components of the IM and OM sub-complexes upon depletion of LptC. For this purpose, the BB3 strain, in which *lptC* expression is under the control of the inducible *araBp* promoter (Sperandeo et al., 2006), was grown under permissive conditions, namely, in the presence of 0.2% arabinose, to the exponential phase and then washed to remove arabinose and shifted to media lacking arabinose to deplete LptC. Samples for protein analyses were taken from cultures grown in the presence or in the absence of arabinose at 240, 300, and 360 min after the shift to non-permissive conditions and then processed for analysis with anti-LptA, anti-LptD, anti-LptC, anti-LptE, and anti-LptB antibodies (**Figure 2**). We observed a decrease in the steady-state level of

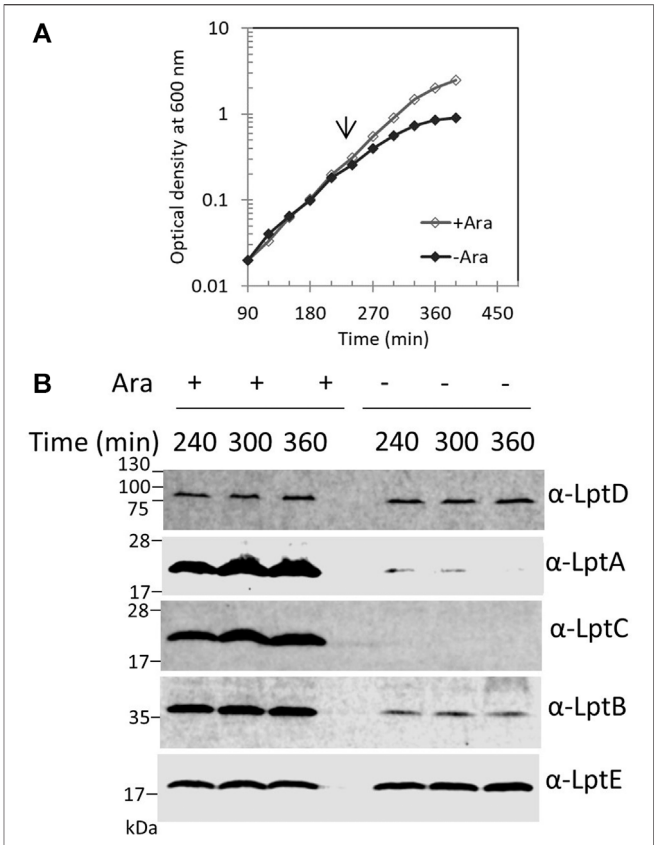

FIGURE 2 | Depletion of LptC does not affect the stability of the IM and OM Lpt sub-complexes. **(A)** Cells of BB3 were grown with 0.2% arabinose until OD_{600} 0.2; the cells were then harvested, washed three times, and resuspended in an arabinose-supplemented (+ Ara) or arabinose-free (no Ara) medium. Samples for analysis of protein stability were collected at the time points indicated. **(B)** Whole-cell extracts were prepared and analyzed by western blot with anti-LptA, anti-LptD, anti-LptC, anti-LptB, and anti-LptE (as the loading control) antibodies. An equal number of cells (0.67 OD_{600}) were loaded into each lane. Growth curves and western blot analyses shown are representative of at least three independent experiments.

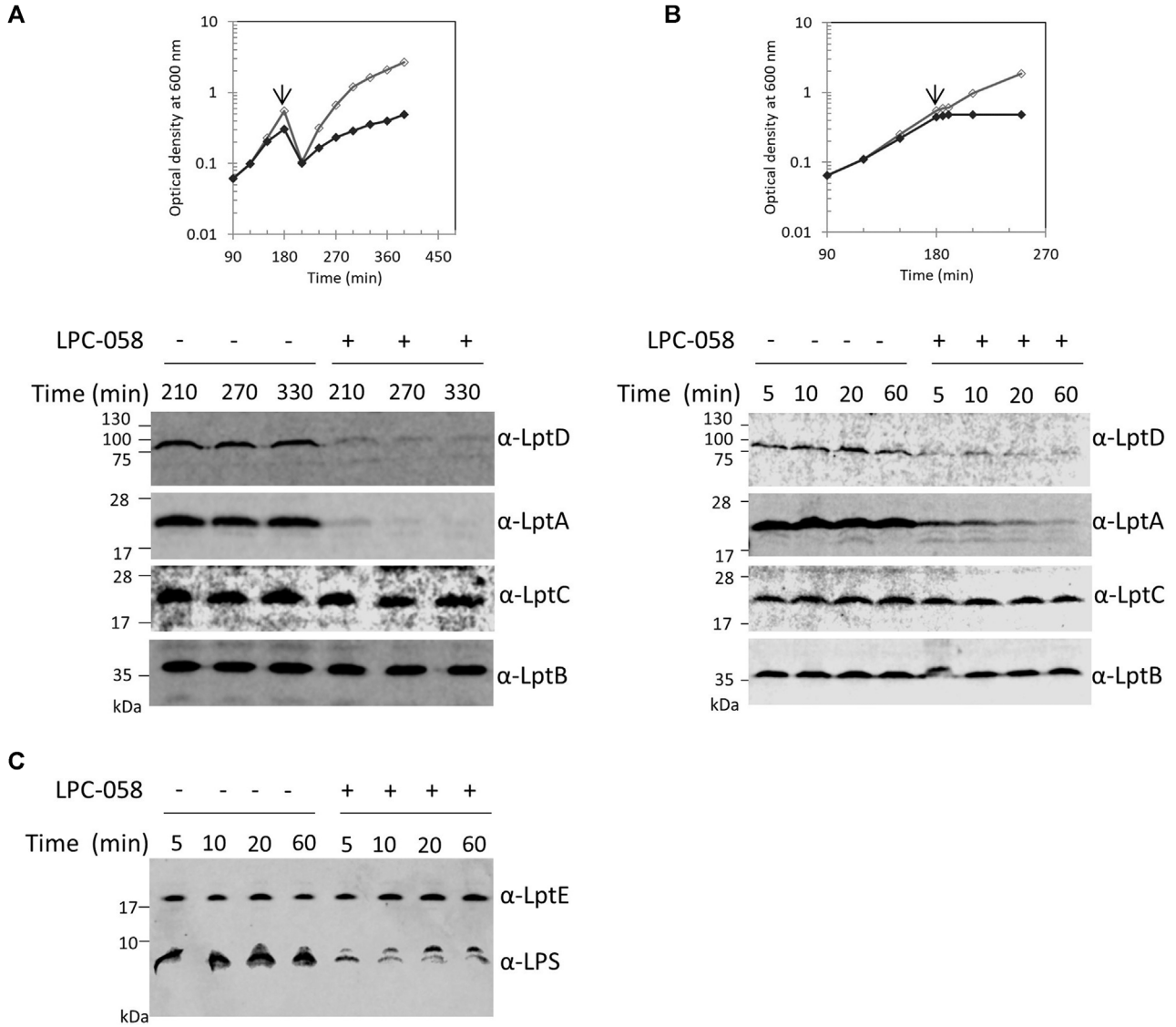

FIGURE 3 | Inhibition of LPS synthesis affects LptA and LptD stability. **(A)** *Escherichia coli* wild-type cells were grown in the LB-Lennox medium. When cells reached OD_{600} of 0.1, they were treated with 1xMIC of LPC-058 (LpxC inhibitor). Untreated cells were used as the control. Cell growth was monitored by OD_{600} measurements. When cultures reached OD_{600} of 1.0, they were diluted 10-fold, and samples for western blot analysis were taken after culture dilution at the indicated times. **(B)** Cells were treated or not treated with LPC-058 as indicated in panel **(A)** but not diluted. When the growth curves of treated and untreated cells separate (arrow), samples for western blot analysis were collected. Time points indicate the minutes after the growth curves separated. **(C)** LPS profiles of wild-type cells treated or not treated with LPC-058. Whole-cell extracts obtained at the same time point as in panel **(B)** were analyzed by western blot with anti-LPS and anti-LptE antibodies. An equal number of cells (0.67 OD_{600} in panels **(A)** and **(B)** and 0.17 OD_{600} in panel **(C)**) were loaded into each lane. Growth curves and western blot analyses shown are representative of at least three independent experiments.

LptA but not of other Lpt components. Under non-permissive conditions, LptB displays a lower but stable level than that observed under permissive conditions. It should be noted that, in the presence of arabinose, *lptCAB* are transcribed from the *araB*p promoter. Therefore, under this condition, the level of LptC, LptA, and LptB is higher than that expressed from the native chromosomal promoters (Sperandeo et al., 2011; Martorana et al., 2011). Indeed, under non-permissive conditions, namely, when *lptC* is not transcribed, the expression of the downstream *lptAB* genes is driven by the *lptA* promoter situated within the *lptC* coding region (Sperandeo et al., 2006, 2008; Martorana et al., 2011) resulting in a lower expression of LptA and LptB, and while LptA undergoes degradation, LptB has a lower but stable level (**Figure 2**). These data suggest that when the Lpt machinery is not functional due to the lack of either IM or OM components, LptA is selectively degraded because of the improperly assembled Lpt complex.

Blockage of LPS Synthesis Causes LptA and LptD Degradation

The Lpt machinery functions as a single device, and blocking the LPS transport causes accumulation of LPS at the outer leaflet of the IM (Sperandeo et al., 2008; Sperandeo et al., 2011). To test whether accumulation of LPS at the outer leaflet of IM affects the assembly of the Lpt machinery, and therefore LptA stability, we assessed the LptA steady-state level in cells where LPS synthesis is blocked. For this purpose, we treated wild-type cells with LPC-058. This molecule targets the essential uridine diphosphate-3-O-(R-3-hydroxymyristoyl)-N-acetylglucosamine deacetylase (LpxC), the enzyme that catalyzes the first committed step of the lipid A biosynthetic pathway (Lee et al., 2006; Titecat et al., 2016). We observed that cells treated with 1xMIC of LPC-058 arrested growth and LptA underwent degradation (**Figures 3A,B**). As expected for inhibitors of LPS synthesis, the total amount of LPS in cells treated with LPC-058 decreases compared to that of non-treated cells (**Figure 3C**). Surprisingly, the LptD level also decreased. The degradation of LptA and LptD in treated cells was very rapid as at 210 min of growth the two proteins were already undetectable in the crude extracts. To test the kinetics of LptA and LptD degradation, we collected the treated and untreated cells just after the two growth curves separated (**Figure 3B**). LptA and LptD steady-state levels decreased immediately after the treated cells arrested the growth and are barely detectable after 60 min, suggesting that the two proteins underwent degradation immediately after the LPS level in the cells became insufficient to support growth. Overall, these data suggest that the accumulation of LPS at the IM due to the blockage of transport does not affect the stability and the assembly of the Lpt machinery. Moreover, these results show that, in the absence of the LPS-cargo, both LptA and LptD are degraded, suggesting that, under these conditions, the Lpt machine disassembles.

Perturbing the LPS Outer Layer Does Not Affect the Stability of the Lpt Complex

Blocking LPS transport results in the alteration of the LPS layer with local loss of OM asymmetry and compensatory accumulation of glycerophospholipids at the outer leaflet of the OM (Nikaido, 2003). We therefore examined whether perturbation of the LPS layer by chemicals or antimicrobial peptides would affect the Lpt complex assembly or stability. We monitored the steady-state level of LptA, LptB, LptC, and LptD in cells treated with ethylene-diaminetetraacetic acid (EDTA), polymyxin B, and ammonium metavanadate (NH_4VO_3). The ion chelator EDTA disrupts OM asymmetry by removal of LPS from the OM's outer layer with consequent flipping of glycerophospholipids from the inner to the outer leaflet of the OM (Nikaido, 1996). Ammonium metavanadate triggers changes in the LPS structure and increases OM permeability (Zhou et al., 1999; Vinés et al., 2005; Tam and Missiakas, 2005; Martorana et al., 2011). Moreover, as metavanadate is an inhibitor of the ATP-binding proteins, it likely interferes with the LptB ATPase (Li et al., 2019). Polymyxin B disrupts the OM by interacting with LPS and displacing cations that are required for the maintenance of membrane integrity (Schindler and Osborn, 1979).

Surprisingly, none of the compounds affected the steady-state level of LptA, LptB, LptC, and LptD in treated cells in comparison with that of untreated cells (**Figure 4**). These data suggest that defects in LPS biogenesis, but not perturbations or disruption of the LPS layer, specifically affect the stability and assembly of the Lpt machine.

Perturbing the Peptidoglycan Does Not Affect the Lpt Complex Stability

We recently showed that defects in LPS biogenesis affect the PG structure, as blocking LPS synthesis or transport activates a PG remodeling program that results in the introduction of 3-3 crosslinks in PG to avoid cell lysis (Morè et al., 2019). These data highlight the importance of synchronizing growth and division of the different cell envelope layers to preserve the structural integrity of the cell (Gray et al., 2015). Based on these data, we tested whether altering the PG layer might compromise the Lpt machinery stability. We therefore treated cells with antibiotics that target PG at different stages of cell growth, namely, aztreonam and cefsulodin. Aztreonam targets PBP3 and affects cell division (Georgopapadakou et al., 1982), while cefsulodin targets PBP1A and PBP1B, the two major bifunctional peptidoglycan synthases, and affects cell elongation (Curtis et al., 1979). Under these conditions, neither LptA nor LptD stability is affected (**Figure 5**), suggesting that conditions affecting the PG structure and stability do not impair the assembly of the Lpt system.

The DegP Periplasmic Endoprotease Is Involved in LptD Degradation Upon Blockage of LPS Biosynthesis

LptD stability in the cell relies on two major proteases that act at different points of the LptD assembly pathway: the periplasmic chaperones/proteases DegP and BepA (Soltes et al., 2017; Narita et al., 2013). DegP degrades LptD to prevent initial contact with the β-barrel-assembly machinery (BAM) complex (Tomasek and Kahne, 2021), thus avoiding accumulation of non-functional proteins in the periplasm. BepA, instead, degrades the LptD mutant substrate that has engaged the BAM complex but is not fully functional or not properly folded (Soltes et al., 2017). To determine whether these proteases are involved in the degradation of LptD upon blockage of LPS biosynthesis, we tested LptD stability following LPC-058 treatment in mutants deleted for *degP* and *bepA* (**Figure 6A**). We found that the deletion of *bepA* does not increase the LptD steady-state level which is comparable to that observed in the non-treated bepA mutant (left panel) and in LPC-058–treated wild-type cells (right panel). On the contrary, the LptD level increases in degP mutant cells treated with LPC-058 (middle panel) compared to that observed in LPC-058–treated wild-type cells. These data suggest that DegP plays a major role in the degradation of

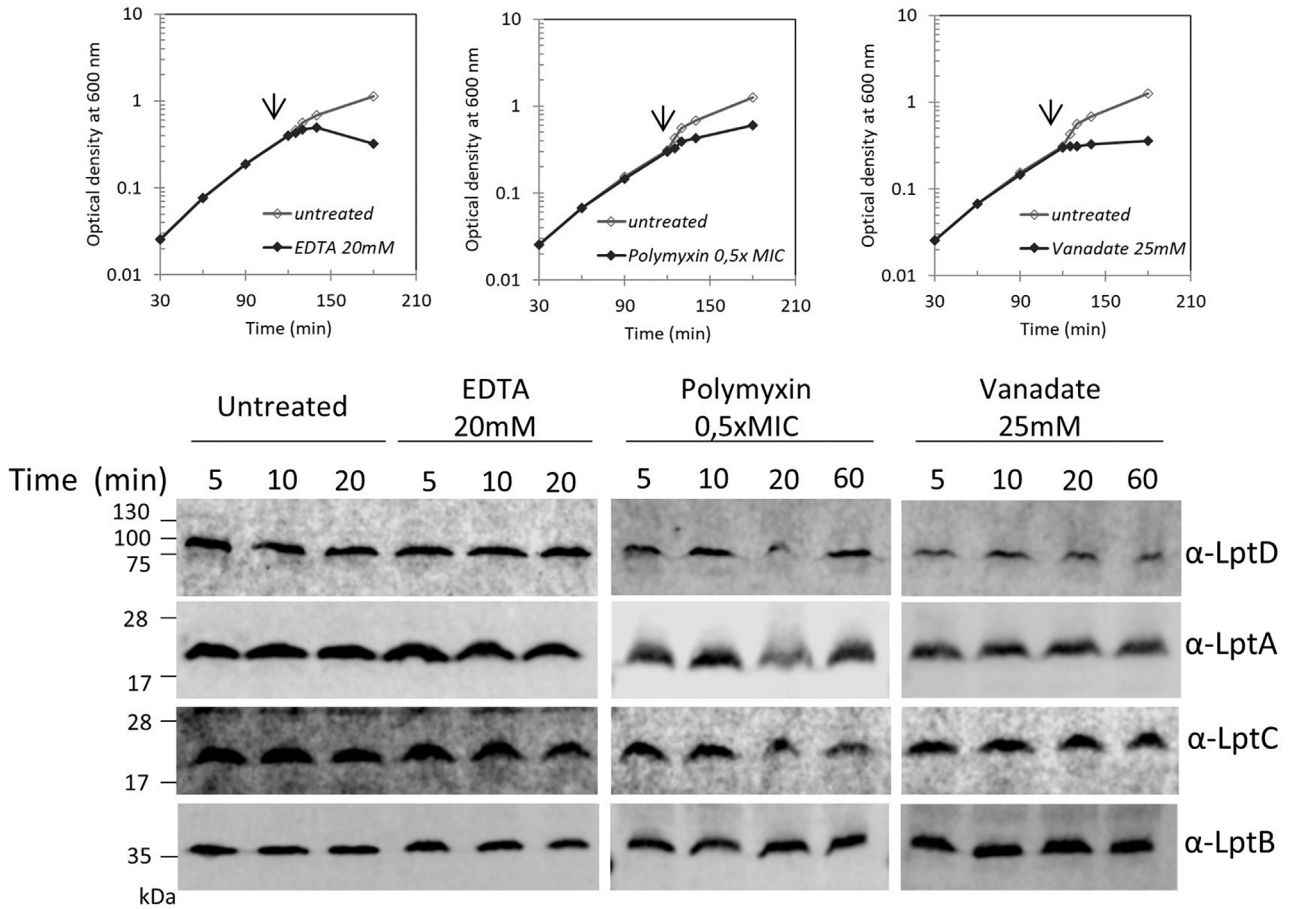

FIGURE 4 | Disrupting the LPS layer at the OM does not affect LptA and LptD levels. *Escherichia coli* wild-type cells were grown in the LB-Lennox medium. When cells reached OD_{600} = 0.1, they were treated with EDTA, polymyxin B, or ammonium metavanadate at the concentration indicated. Untreated cells were used as the control. Cell growth was monitored by OD_{600} measurements. When the growth curves of treated and untreated cells separate (arrow), samples for western blot analysis were collected. Time points indicate the minutes after the growth curves separated. An equal number of cells (0.67 OD_{600}) were loaded into each lane. Growth curves and western blot analyses shown are representative of at least three independent experiments.

LptD upon blockage of LPS biosynthesis. Interestingly, neither single *degP* nor bepA deletions affected LptA degradation.

To address whether LPC-058–induced Lpt protein changes are accompanied by alterations in the protein content of the OM, we examined the OMP profile in wild-type, Δ*degP*, and Δ*bepA* cells grown in the presence or absence of LPC-058. Equal numbers of cells were collected and processed for OM purification with sarkosyl (Yethon et al., 2000) and analyzed by Coomassie-stained SDS-PAGE (**Figure 6B**, upper panel). The overall OMP profile was very similar among the three untreated strains, and disruption of *degP* gene had little impact on the steady-state levels of OMPs, as already shown by Krojer et al. (2008). The OMP profile shows few minor changes in the LPC-058–treated wild-type cells, where the abundance of the major OMPs is slightly lower in the treated samples and one high-molecular-weight band disappears, whereas one low-molecular-weight band increases. Changes in the protein profile are more evident in the Δ*degP* strain, with the levels of OmpC/F and OmpA decreasing compared to those of wild-type and Δ*bepA*-treated samples.

Finally, we assessed the level of OmpA, a representative major OMP, in whole-cell lysates by western blot. The level of OmpA does not change in wild-type, *degP*, and *bepA* null strains, treated or not with the LpxC inhibitor (**Figure 6B**, lower panel). This suggests that blockage of LPS synthesis does not affect the overall OMP production and that the observed OMP reduction in the OM of LPC-058–treated cells is likely due to degradation by periplasmic proteases.

DISCUSSION

Previous work showed that the tight control of LptA level plays a fundamental role in the Lpt machinery assembly and stability (Benedet et al., 2006; Sperandeo et al., 2011; Sperandeo et al., 2019; Moura et al., 2020).

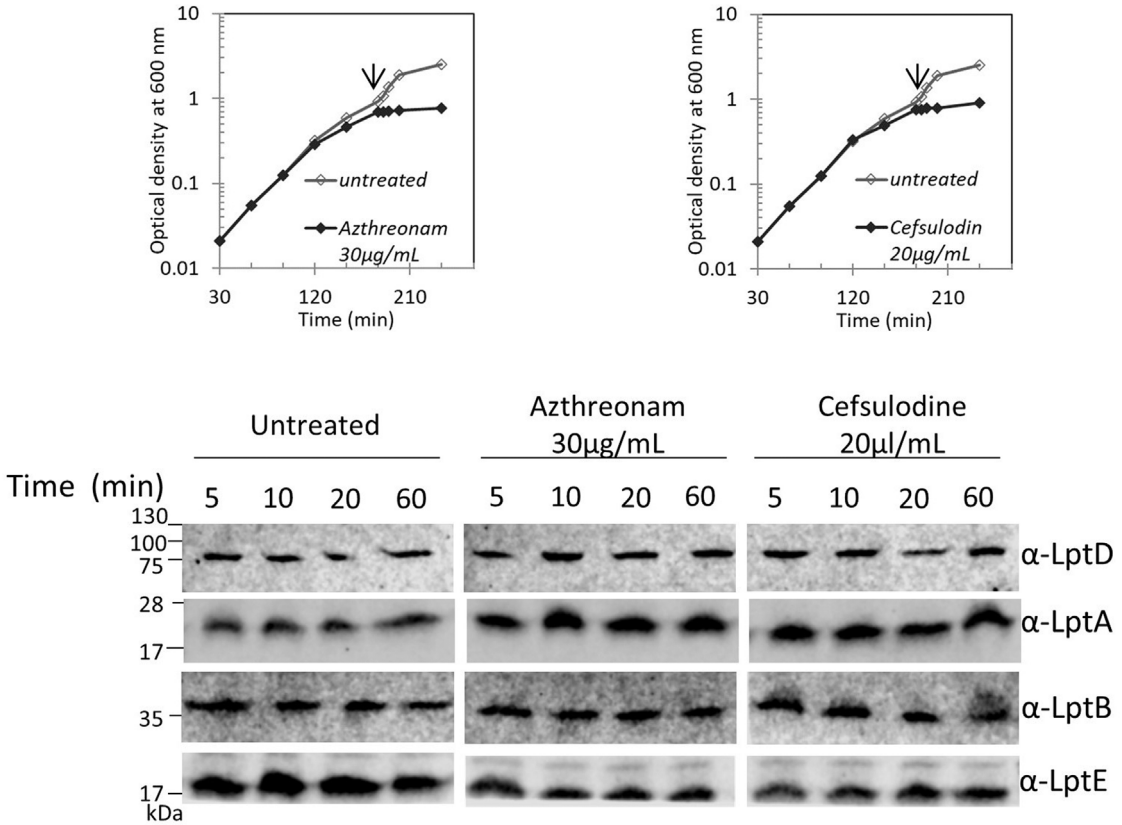

FIGURE 5 | Disturbing the PG layer does not affect LptA and LptD levels. *Escherichia coli* wild-type cells were grown in the LB-Lennox medium. When cells reached OD_{600} = 0.1, they were treated with aztreonam or cefsulodin at the concentrations indicated. Untreated cells were used as the control. Cell growth was monitored by OD_{600} measurements. When the growth curves of treated and untreated cells separate (arrow), samples for western blot analysis were collected. Time points indicate the minutes after the growth curves separated. An equal number of cells (0.67 OD_{600}) were loaded into each lane. Growth curves and western blot analyses shown are representative of at least three independent experiments.

Here, we have further investigated the Lpt assembly requirements. We show that LptA degradation occurs also when LPS synthesis is blocked (**Figure 3**). Since the LptA level is a proxy for a correctly assembled Lpt complex, we propose that LPS synthesis is fundamental for the assembly of a functional Lpt export machinery. Moreover, using a specific inhibitor of LpxC, the enzyme that catalyzes the first committed step of LPS biosynthesis (Titecat et al., 2016), we discovered that not only LptA but also LptD undergoes degradation, suggesting that a proper LPS biosynthesis is a prerequisite for the assembly of LptD into the OM.

The analysis of the LptA steady-state level upon treatment with agents altering the LPS layer, such as EDTA, polymyxin B, and vanadate, is in line with our hypothesis, as disrupting the LPS layer does not affect the protein level of any of the Lpt components (**Figure 4**). Interestingly, vanadate treatment, which is known to inhibit LPS transport, as demonstrated by LPS decoration with colanic acid (Martorana et al., 2011), does not affect the LptA steady-state level in the cell. These data suggest that, in the presence of vanadate, the Lpt system is assembled but not functional. This effect could be due to the inhibition of LPS transport caused by vanadate trapped in the $LptB_2FG$ IM complex (Li et al., 2019). Therefore, upon vanadate treatment, LPS might be jammed in the hydrophobic interior of the Lpt proteins, supporting the idea that the LptA level and, as a consequence, the transenvelope bridge stability correlates with the availability of the LPS substrate.

We recently discovered a PG remodeling pathway essential for survival in cells with defective LPS biogenesis (Morè et al., 2019), thus highlighting the importance of synchronizing growth of these two different cell envelope layers. While it appears that disrupting the LPS biogenetic pathway has a severe impact on the PG structure, the reverse is not true. Indeed, here we show that disturbing PG biosynthesis is not detrimental to the stability of the Lpt system, as the steady-state level of the Lpt proteins is not affected (**Figure 5**). This result further reinforces the hypothesis that the Lpt system stability depends on the availability of its own cargo. A similar mechanism of substrate-induced assembly of a transenvelope complex is adopted by the HlyA Type 1 secretion system of *E. coli*, where the interaction of the sub-complex composed by the IM ABC transporter HlyB and the membrane fusion protein HlyD with the OM porin TolC is

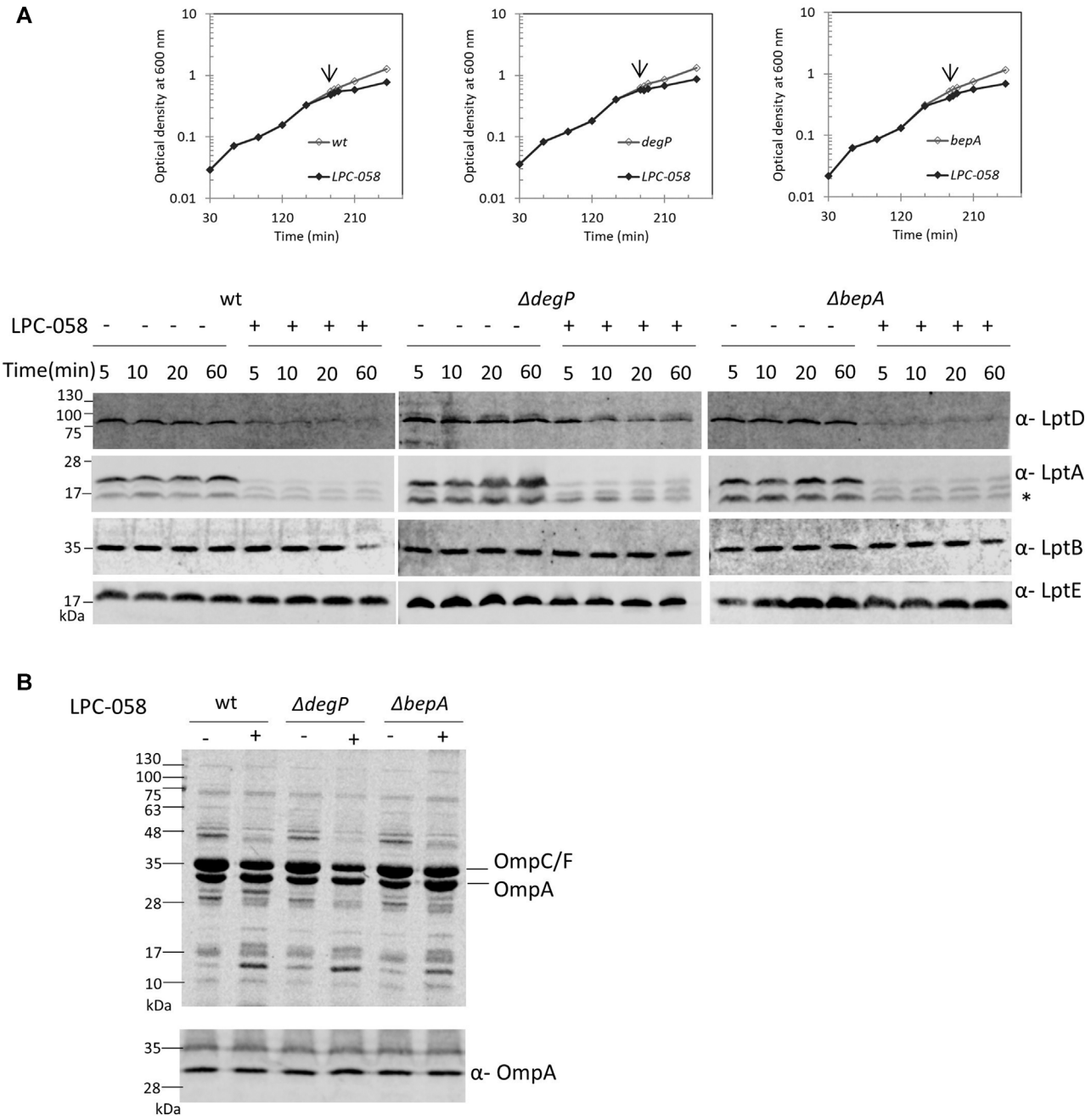

FIGURE 6 | DegP degrades LptD when the LPS biosynthesis is inhibited. *Escherichia coli* wild-type (wt), Δ*degP*, and Δ*bepA* cells were grown in the LB-Lennox medium at 30°C. When cells reached OD_{600} = 0.1, they were treated with 1xMIC of LPC-058 (LpxC inhibitor). Untreated cells were used as the control. **(A)** For the analysis of the steady-state level Lpt proteins, cell growth was monitored by OD_{600} measurements. When the growth curves of treated and untreated cells separate (arrow), samples for western blot analysis were taken. Time points indicate the minutes after the growth curves separated. * indicates the degradation product of LptA. **(B)** OM fractions were purified from cells treated for 2 h with LPC-058. Equal amounts of proteins were loaded (upper panel). Crude extracts of the same cultures were analyzed by western blot, using anti-OmpA antibodies, and equal amounts of cells were loaded (lower panel, 0.67 OD_{600}). Growth curves and western blot analyses shown are representative of at least three independent experiments.

dependent on the presence of the substrate toxin HlyA (Thanabalu et al., 1998). In *E. coli*, additional tripartite (IM, periplasmic, and OM subunits) transenvelope systems exist, which are involved in phospholipid trafficking (Ekiert et al., 2017; Isom et al., 2020). These systems employ two distinct strategies for substrate trafficking: the LetAB system employs the so-called "tunnel" strategy with a single polypeptide bridging the IM and OM, whereas the Mla system employs the "chaperon-

like" mechanism in which a soluble periplasmic protein shuttles the substrate from the OM to the IM (Malinverni and Silhavy, 2009; Powers and Trent, 2018). The Lpt system differs in that bridging between the IM and the OM is achieved by interaction of small proteins sharing the β-jellyroll fold architecture (Tefsen et al., 2005; Wu et al., 2006; Sperandeo et al., 2007, 2008; Ruiz et al., 2008; Suits et al., 2008; Okuda et al., 2012) with the LPS substrate playing a key role in maintaining the intermembrane bridge assembled.

The Lpt system assembly is finely regulated at several levels (Sperandeo et al., 2019). Our data suggest the existence of an additional control mechanism occurring when LPS biosynthesis is defective. Indeed, under such conditions, we observed the decrease of both the LptA and LptD levels. It was previously shown that only a correctly folded LptDE OM translocon allows the assembly of a functional Lpt system, since LptD mutant proteins that lack native disulfide bonds do not interact with LptA, thus preventing the formation of the transenvelope bridge (Chng et al., 2012; Freinkman et al., 2012; Okuda et al., 2016). Clearly, the proper maturation of LptD is carefully monitored by the cell and represents a key control step in the formation of the Lpt protein bridge. Here, we show that LPS biosynthesis is also a prerequisite for a proper LptD folding into the OM, and in turn for Lpt system assembly. Alongside the discovery that the OM translocon could communicate with the IM complex to arrest the LPS transport, in OM proteoliposomes that have reached the saturating amount of LPS (Xie et al., 2018), our data unveil that there are multiple control steps of assembling and functioning of the Lpt system.

We show that the stability of LptD in the *degP* null strain upon LPS biosynthesis blockage is increased (**Figure 6**), suggesting that DegP is the primary protease responsible for degrading LptD when the OM undergoes severe LPS depletion. The biogenesis and assembly of OMPs are tightly regulated processes at transcriptional and post-translational levels (Rhodius et al., 2006; Guisbert et al., 2007; Sklar et al., 2007; Merdanovic et al., 2011). The LptD biogenesis is carefully monitored in the cell, and its folding is assisted by several chaperones (Schwalm et al., 2013; Ruiz et al., 2010). In case of maturation defects, LptD is degraded by DegP to prevent initial contact with the BAM, preventing the unfolded protein from accumulating in the periplasm. In case the defective LptD has engaged the BAM complex, it is degraded by BepA to block the formation of a defective complete β-barrel (Soltes et al., 2017; Daimon et al., 2020). These quality control factors help ensure the integrity of the OM, since defective OMPs could compromise the permeability barrier properties of the OM (Ruiz et al., 2006). We hypothesize that DegP degrades LptD in order to prevent the assembly of LptD in a defective OM. LptD is the OMP with the largest lumen in *E. coli* (Braun and Silhavy, 2002; Botos et al., 2016); hence, its decreased level in a condition in which its lumen is empty (i.e., devoid of its cargo) can be a strategy to counteract the altered permeability of an LPS-depleted OM. Our results underscore the importance of the regulatory network controlling OM homeostasis: while defects in LPS induce the σ^E stress response to increase LptD transcription and counteract OMP assembly defects, as LPS is required for efficient OMP folding (Schnaitman and Klena, 1993; Missiakas et al., 1996; Klein et al., 2009), the control of LptD at a post-translational level is a fine-tuning system not only to correct defects in its maturation but also to correct OM permeability defects when the amount of LPS to be transported to the cell surface is limiting.

The LptD level in the cells does not decrease in the absence of DegP, but LptA degradation still occurs even when LptD is correctly maturated and can act as the LptA OM docking site, implying that DegP is not responsible for LptA degradation. We do not know what is the event that triggers LptA degradation; however, our data support that the LptA stability and thus Lpt protein bridge formation are correlated with the availability of LPS to be transported. It has been proposed that the Lpt machinery functions like a PEZ "candy dispenser" where the LPS "candies" are continuously pushed by $LptB_2FG$, using the energy provided by ATP hydrolysis, into the periplasmic channel formed by LptCAD up to the LptDE translocon, which finally assembles LPS at the OM (Okuda et al., 2016). The data presented here suggest that the LPS might trigger the assembly of the Lpt system/candy dispenser, and the LPS molecules/candies pushed through the protein bridge might act as a sort of "glue" to maintain the system assembled.

DATA AVAILABILITY STATEMENT

The original contributions presented in the study are included in the article/Supplementary Material, and further inquiries can be directed to the corresponding authors.

AUTHOR CONTRIBUTIONS

AM, EM, FD, and PS performed experiments. XL, ET, and PZ designed and synthetized LPC-058. AM, PS, and AP designed the *in vivo* experiments. AM, EM, and AP wrote the manuscript. AM, EM, PS, PZ, and AP reviewed the manuscript.

FUNDING

AP was supported by the European Commission *via* the International Training Network Train2Target (721484). PS was supported by "Azione A Linea2 PSR 2020 (PSR2020_PSPER)." The synthesis of LpxC inhibitor was in part supported by NIH grants AI055588 and GM115355 awarded to PZ.

ACKNOWLEDGMENTS

We are grateful to Prof. JF Collet (Institut de Duve, Bruxelles) that kindly gifted anti-OmpA antisera.

REFERENCES

Andolina, G., Bencze, L.-C., Zerbe, K., Müller, M., Steinmann, J., Kocherla, H., et al. (2018). A Peptidomimetic Antibiotic Interacts with the Periplasmic Domain of LptD from *Pseudomonas aeruginosa*. *ACS Chem. Biol.* 13 (3), 666–675. doi:10.1021/acschembio.7b00822

Baba, T., Ara, T., Hasegawa, M., Takai, Y., Okumura, Y., Baba, M., et al. (2006). Construction of *Escherichia coli* K-12 In-Frame, Single-Gene Knockout Mutants: The Keio Collection. *Mol. Syst. Biol.* 2 (1), 2006–0008. doi:10.1038/msb4100050

Benedet, M., Falchi, F. A., Puccio, S., Di Benedetto, C., Peano, C., Polissi, A., et al. (2006). The Lack of the Essential LptC Protein in the Trans-envelope Lipopolysaccharide Transport Machine Is Circumvented by Suppressor Mutations in LptF, an Inner Membrane Component of the *Escherichia coli* Transporter. *PLoS One* 11 (8), e0161354. doi:10.1371/journal.pone.0161354

Botos, I., Majdalani, N., Mayclin, S. J., McCarthy, J. G., Lundquist, K., Wojtowicz, D., et al. (2016). Structural and Functional Characterization of the LPS Transporter LptDE from Gram-Negative Pathogens. *Structure* 24 (6), 965–976. doi:10.1016/j.str.2016.03.026

Braun, M., and Silhavy, T. J. (2002). Imp/OstA Is Required for Cell Envelope Biogenesis in *Escherichia coli*. *Mol. Microbiol.* 45 (5), 1289–1302. doi:10.1046/j.1365-2958.2002.03091.x

Chng, S.-S., Gronenberg, L. S., and Kahne, D. (2010). Proteins Required for Lipopolysaccharide Assembly in *Escherichia coli* Form a Transenvelope Complex. *Biochemistry* 49 (22), 4565–4567. doi:10.1021/bi100493e

Chng, S.-S., Xue, M., Garner, R. A., Kadokura, H., Boyd, D., Beckwith, J., et al. (2012). Disulfide Rearrangement Triggered by Translocon Assembly Controls Lipopolysaccharide export. *Science* 337 (6102), 1665–1668. doi:10.1126/science.1227215

Curtis, N. A., Orr, D., Ross, G. W., and Boulton, M. G. (1979). Affinities of Penicillins and Cephalosporins for the Penicillin-Binding Proteins of *Escherichia coli* K-12 and Their Antibacterial Activity. *Antimicrob. Agents Chemother.* 16 (5), 533–539. doi:10.1128/AAC.16.5.533

Datsenko, K. A., and Wanner, B. L. (2000). One-step Inactivation of Chromosomal Genes in *Escherichia coli* K-12 Using PCR Products. *Proc. Natl. Acad. Sci.* 97, 6640–6645. doi:10.1073/pnas.120163297

Daimon, Y., Narita, S. I., Miyazaki, R., Hizukuri, Y., Mori, H., Tanaka, Y., et al. (2020). Reversible autoinhibitory regulation of *Escherichia coli* metallopeptidase BepA for selective β-barrel protein degradation. *Proc Natl Acad Sci U S A* 117 (45), 27989–27996. doi:10.1073/pnas.2010301117

Dong, H., Xiang, Q., Gu, Y., Wang, Z., Paterson, N. G., Stansfeld, P. J., et al. (2014). Structural Basis for Outer Membrane Lipopolysaccharide Insertion. *Nature* 511 (7507), 52–56. doi:10.1038/nature13464

Dong, H., Zhang, Z., Tang, X., Paterson, N. G., and Dong, C. (2017). Structural and Functional Insights into the Lipopolysaccharide ABC Transporter LptB2FG. *Nat. Commun.* 8 (1), 222. doi:10.1038/s41467-017-00273-5

Ekiert, D. C., Bhabha, G., Isom, G. L., Greenan, G., Ovchinnikov, S., Henderson, I. R., et al. (2017). Architectures of Lipid Transport Systems for the Bacterial Outer Membrane. *Cell* 169 (2), 273–285. doi:10.1016/j.cell.2017.03.019

Erwin, A. L. (2016). Antibacterial Drug Discovery Targeting the Lipopolysaccharide Biosynthetic Enzyme LpxC. *Cold Spring Harb Perspect. Med.* 6 (7), a025304. doi:10.1101/cshperspect.a025304

Falchi, F. A., Maccagni, E. A., Puccio, S., Peano, C., De Castro, C., Palmigiano, A., et al. (2018). Mutation and Suppressor Analysis of the Essential Lipopolysaccharide Transport Protein LptA Reveals Strategies to Overcome Severe Outer Membrane Permeability Defects in *Escherichia coli*. *J. Bacteriol.* 200, e487. doi:10.1128/jb.00487-17

Freinkman, E., Chng, S.-S., and Kahne, D. (2011). The Complex that Inserts Lipopolysaccharide into the Bacterial Outer Membrane Forms a Two-Protein Plug-And-Barrel. *Proc. Natl. Acad. Sci.* 108 (6), 2486–2491. doi:10.1073/pnas.1015617108

Freinkman, E., Okuda, S., Ruiz, N., and Kahne, D. (2012). Regulated Assembly of the Transenvelope Protein Complex Required for Lipopolysaccharide export. *Biochemistry* 51 (24), 4800–4806. doi:10.1021/bi300592c

Georgopapadakou, N. H., Smith, S. A., and Sykes, R. B. (1982). Mode of Action of Azthreonam. *Antimicrob. Agents Chemother.* 21 (6), 950–956. doi:10.1128/AAC.21.6.950

Ghisotti, D., Chiaramonte, R., Forti, F., Zangrossi, S., Sironi, G., and Deho, G. (1992). Genetic Analysis of the Immunity Region of Phage-Plasmid P4. *Mol. Microbiol.* 6 (22), 3405–3413. doi:10.1111/j.1365-2958.1992.tb02208.x

Gray, A. N., Egan, A. J., Van't Veer, I. L., Verheul, J., Colavin, A., Koumoutsi, A., et al. (2015). Coordination of Peptidoglycan Synthesis and Outer Membrane Constriction during *Escherichia coli* Cell Division. *Elife* 4, e07118. doi:10.7554/eLife.07118

Guisbert, E., Rhodius, V. A., Ahuja, N., Witkin, E., and Gross, C. A. (2007). Hfq Modulates the σ E -Mediated Envelope Stress Response and the σ 32 -Mediated Cytoplasmic Stress Response in *Escherichia coli*. *J. Bacteriol.* 189 (5), 1963–1973. doi:10.1128/JB.01243-06

Isom, G. L., Coudray, N., MacRae, M. R., McManus, C. T., Ekiert, D. C., and Bhabha, G. (2020). LetB Structure Reveals a Tunnel for Lipid Transport across the Bacterial Envelope. *Cell* 181 (3), 653–664. doi:10.1016/j.cell.2020.03.030

Klein, G., Lindner, B., Brabetz, W., Brade, H., and Raina, S. (2009). *Escherichia coli* K-12 Suppressor-free Mutants Lacking Early Glycosyltransferases and Late Acyltransferases. *J. Biol. Chem.* 284, 15369–15389. CrossRef Medline. doi:10.1074/jbc.m900490200

Krojer, T., Sawa, J., Schäfer, E., Saibil, H. R., Ehrmann, M., and Clausen, T. (2008). Structural Basis for the Regulated Protease and Chaperone Function of DegP. *Nature* 453 (7197), 885–890. doi:10.1038/nature07004.8

Lee, C.-J., Liang, X., Wu, Q., Najeeb, J., Zhao, J., Gopalaswamy, R., et al. (2016). Drug Design from the Cryptic Inhibitor Envelope. *Nat. Commun.* 7, 10638. doi:10.1038/ncomms10638

Lesse, A. J., Campagnari, A. A., Bittner, W. E., and Apicella, M. A. (1990). Increased Resolution of Lipopolysaccharides and Lipooligosaccharides Utilizing Tricine-Sodium Dodecyl Sulfate-Polyacrylamide Gel Electrophoresis. *J. Immunological Methods* 126, 109–117. doi:10.1016/0022-1759(90)90018-q

Li, Y., Orlando, B. J., and Liao, M. (2019). Structural Basis of Lipopolysaccharide Extraction by the LptB2FGC Complex. *Nature* 567 (7749), 486–490. doi:10.1038/s41586-019-1025-6

Luo, Q., Yang, X., Yu, S., Shi, H., Wang, K., Xiao, L., et al. (2017). Structural Basis for Lipopolysaccharide Extraction by ABC Transporter LptB2FG. *Nat. Struct. Mol. Biol.* 24 (5), 469–474. doi:10.1038/nsmb.3399

Malinverni, J. C., and Silhavy, T. J. (2009). An ABC transport system that maintains lipid asymmetry in the Gram-negative outer membrane. *Proc Natl Acad Sci U S A* 106, 8009–8014.

Martorana, A. M., Sperandeo, P., Polissi, A., and Dehò, G. (2011). Complex Transcriptional Organization Regulates an *Escherichia coli* Locus Implicated in Lipopolysaccharide Biogenesis. *Res. Microbiol.* 162 (5), 470–482. doi:10.1016/j.resmic.2011.03.007

Merdanovic, M., Clausen, T., Kaiser, M., Huber, R., and Ehrmann, M. (2011). Protein Quality Control in the Bacterial Periplasm. *Annu. Rev. Microbiol.* 65, 149–168. doi:10.1146/annurev-micro-090110-102925

Missiakas, D., Betton, J.-M., and Raina, S. (1996). New Components of Protein Folding in Extracytoplasmic Compartments ofEscherichia coliSurA, FkpA and Skp/OmpH. *Mol. Microbiol.* 21 (4), 871–884. doi:10.1046/j.1365-2958.1996.561412.x

Morè, N., Martorana, A. M., Biboy, J., Otten, C., Winkle, M., Serrano, C. K. G., et al. (2019). Peptidoglycan Remodeling Enables *Escherichia coli* to Survive Severe Outer Membrane Assembly Defect. *mBio* 10 (1), e02729. doi:10.1128/mBio.02729-18

Moura, E. C. C. M., Baeta, T., Romanelli, A., Laguri, C., Martorana, A. M., Erba, E., et al. (2020). Thanatin Impairs Lipopolysaccharide Transport Complex Assembly by Targeting LptC-LptA Interaction and Decreasing LptA Stability. *Front. Microbiol.* 11, 909. doi:10.3389/fmicb.2020.00909

Narita, S.-i., Masui, C., Suzuki, T., Dohmae, N., and Akiyama, Y. (2013). Protease Homolog BepA (YfgC) Promotes Assembly and Degradation of -barrel Membrane Proteins in *Escherichia coli*. *Proc. Natl. Acad. Sci.* 110, E3612–E3621. doi:10.1073/pnas.1312012110

Nikaido, H. (2003). Molecular Basis of Bacterial Outer Membrane Permeability Revisited. *Microbiol. Mol. Biol. Rev.* 67 (4), 593–656. doi:10.1128/mmbr.67.4.593-656.2003

Nikaido, H. (1996). Multidrug Efflux Pumps of Gram-Negative Bacteria. *J. Bacteriol.* 178 (20), 5853–5859. doi:10.1128/jb.178.20.5853-5859.1996

Okuda, S., Freinkman, E., and Kahne, D. (2012). Cytoplasmic ATP Hydrolysis powers Transport of Lipopolysaccharide across the Periplasm in *E. coli*. *Science* 338 (6111), 1214–1217. doi:10.1126/science.1228984

Okuda, S., Sherman, D. J., Silhavy, T. J., Ruiz, N., and Kahne, D. (2016). Lipopolysaccharide Transport and Assembly at the Outer Membrane: the PEZ Model. *Nat. Rev. Microbiol.* 14 (6), 337–345. doi:10.1038/nrmicro.2016.25

Owens, T. W., Taylor, R. J., Pahil, K. S., Bertani, B. R., Ruiz, N., Kruse, A. C., et al. (2019). Structural Basis of Unidirectional export of Lipopolysaccharide to the Cell Surface. *Nature* 567 (7749), 550–553. doi:10.1038/s41586-019-1039-0

Powers, M. J., and Trent, M. S. (2018). Phospholipid Retention in the Absence of Asymmetry Strengthens the Outer Membrane Permeability Barrier to Last-Resort Antibiotics. *Proc. Natl. Acad. Sci. USA* 115, E8518–E8527. doi:10.1073/pnas.1806714115

Qiao, S., Luo, Q., Zhao, Y., Zhang, X. C., and Huang, Y. (2014). Structural Basis for Lipopolysaccharide Insertion in the Bacterial Outer Membrane. *Nature* 511 (7507), 108–111. doi:10.1038/nature13484

Raetz, C. R. H., and Whitfield, C. (2002). Lipopolysaccharide Endotoxins. *Annu. Rev. Biochem.* 71, 635–700. doi:10.1146/annurev.biochem.71.110601.135414

Rhodius, V. A., Suh, W. C., Nonaka, G., West, J., and Gross, C. A. (2006). Conserved and Variable Functions of the σE Stress Response in Related Genomes. *Plos Biol.* 4 (1), e2. doi:10.1371/journal.pbio.0040002

Ruiz, N., Wu, T., Kahne, D., and Silhavy, T. J. (2006). Probing the barrier function of the outer membrane with chemical conditionality. *ACS Chem Biol.* 1 (6), 385–395.

Ruiz, N., Chng, S.-S., Hiniker, A., Kahne, D., and Silhavy, T. J. (2010). Nonconsecutive Disulfide Bond Formation in an Essential Integral Outer Membrane Protein. *Proc. Natl. Acad. Sci.* 107 (27), 12245–12250. doi:10.1073/pnas.1007319107

Ruiz, N., Gronenberg, L. S., Kahne, D., and Silhavy, T. J. (2008). Identification of Two Inner-Membrane Proteins Required for the Transport of Lipopolysaccharide to the Outer Membrane of *Escherichia coli*. *Proc. Natl. Acad. Sci.* 105 (14), 5537–5542. doi:10.1073/pnas.0801196105

Schindler, M., and Osborn, M. J. (1979). Interaction of Divalent Cations and Polymyxin B with Lipopolysaccharide. *Biochemistry* 18 (20), 4425–4430. doi:10.1021/bi00587a024

Schnaitman, C. A., and Klena, J. D. (1993). Genetics of Lipopolysaccharide Biosynthesis in Enteric Bacteria. *Microbiol. Rev.* 57 (3), 655–682. doi:10.1128/mr.57.3.655-682.1993

Schwalm, J., Mahoney, T. F., Soltes, G. R., and Silhavy, T. J. (2013). Role for Skp in LptD Assembly in *Escherichia coli*. *J. Bacteriol.* 195 (16), 3734–3742. doi:10.1128/JB.00431-13

Silhavy, T. J., Berman, M. L., and Enquist, L. W. (1984). *Experiments with Gene Fusions*. 1st ed. New York: Cold Spring Harbor Laboratory Press. ISBN 0 87969 163 8.

Silhavy, T. J., Kahne, D., and Walker, S. (2010). The Bacterial Cell Envelope. *Cold Spring Harbor Perspect. Biol.* 2 (5), a000414. doi:10.1101/cshperspect.a000414

Sklar, J. G., Wu, T., Kahne, D., and Silhavy, T. J. (2007). Defining the Roles of the Periplasmic Chaperones SurA, Skp, and DegP in *Escherichia coli*. *Genes Dev.* 21 (19), 2473–2484. doi:10.1101/gad.1581007

Soltes, G. R., Martin, N. R., Park, E., Sutterlin, H. A., and Silhavy, T. J. (2017). Distinctive Roles for Periplasmic Proteases in the Maintenance of Essential Outer Membrane Protein Assembly. *J. Bacteriol.* 199 (20), e00418. doi:10.1128/JB.00418-17

Sperandeo, P., Cescutti, R., Villa, R., Di Benedetto, C., Candia, D., Dehò, G., et al. (2007). Characterization of lptA and lptB , Two Essential Genes Implicated in Lipopolysaccharide Transport to the Outer Membrane of *Escherichia coli*. *J. Bacteriol.* 189 (1), 244–253. doi:10.1128/JB.01126-06

Sperandeo, P., Lau, F. K., Carpentieri, A., De Castro, C., Molinaro, A., Dehò, G., et al. (2008). Functional Analysis of the Protein Machinery Required for Transport of Lipopolysaccharide to the Outer Membrane of *Escherichia coli*. *J. Bacteriol.* 190 (13), 4460–4469. doi:10.1128/JB.00270-08

Sperandeo, P., Martorana, A. M., and Polissi, A. (2019). Lipopolysaccharide Biosynthesis and Transport to the Outer Membrane of Gram-Negative Bacteria. *Subcell Biochem.* 92, 9–37. doi:10.1007/978-3-030-18768-2_2

Sperandeo, P., Pozzi, C., Dehò, G., and Polissi, A. (2006). Non-essential KDO Biosynthesis and New Essential Cell Envelope Biogenesis Genes in the *Escherichia coli* yrbG-yhbG Locus. *Res. Microbiol.* 157 (6), 547–558. doi:10.1016/j.resmic.2005.11.014

Sperandeo, P., Villa, R., Martorana, A. M., Šamalikova, M., Grandori, R., Dehò, G., et al. (2011). New Insights into the Lpt Machinery for Lipopolysaccharide Transport to the Cell Surface: LptA-LptC Interaction and LptA Stability as Sensors of a Properly Assembled Transenvelope Complex. *J. Bacteriol.* 193 (5), 1042–1053. doi:10.1128/JB.01037-10

Srinivas, N., Jetter, P., Ueberbacher, B. J., Werneburg, M., Zerbe, K., Steinmann, J., et al. (2010). Peptidomimetic Antibiotics Target Outer-Membrane Biogenesis in *Pseudomonas aeruginosa*. *Science* 327 (5968), 1010–1013. doi:10.1126/science.1182749

Suits, M. D. L., Sperandeo, P., Dehò, G., Polissi, A., and Jia, Z. (2008). Novel Structure of the Conserved Gram-Negative Lipopolysaccharide Transport Protein A and Mutagenesis Analysis. *J. Mol. Biol.* 380 (3), 476–488. doi:10.1016/j.jmb.2008.04.045

Tacconelli, E., Carrara, E., Savoldi, A., Harbarth, S., Mendelson, M., Monnet, D. L., et al. (2018). Discovery, Research, and Development of New Antibiotics: the WHO Priority List of Antibiotic-Resistant Bacteria and Tuberculosis. *Lancet Infect. Dis.* 18 (3), 318–327. doi:10.1016/S1473-3099(17)30753-3

Tam, C., and Missiakas, D. (2005). Changes in Lipopolysaccharide Structure Induce the σE-dependent Response of *Escherichia coli*. *Mol. Microbiol.* 55 (5), 1403–1412. doi:10.1111/j.1365-2958.2005.04497.x

Tefsen, B., Geurtsen, J., Beckers, F., Tommassen, J., and de Cock, H. (2005). Lipopolysaccharide Transport to the Bacterial Outer Membrane in Spheroplasts. *J. Biol. Chem.* 280 (6), 4504–4509. doi:10.1074/jbc.M409259200

Thanabalu, T., Koronakis, E., Hughes, C., and Koronakis, V. (1998). Substrate-induced Assembly of a Contiguous Channel for Protein export from E.Coli: Reversible Bridging of an Inner-Membrane Translocase to an Outer Membrane Exit Pore. *EMBO J.* 17 (22), 6487–6496. doi:10.1093/emboj/17.22.6487

Titecat, M., Liang, X., Lee, C.-J., Charlet, A., Hocquet, D., Lambert, T., et al. (2016). High Susceptibility of MDR and XDR Gram-Negative Pathogens to Biphenyl-Diacetylene-Based Difluoromethyl-Allo-Threonyl-Hydroxamate LpxC Inhibitors. *J. Antimicrob. Chemother.* 71 (10), 2874–2882. doi:10.1093/jac/dkw210

Tomasek, D., and Kahne, D. (2021). The Assembly of β-barrel Outer Membrane Proteins. *Curr. Opin. Microbiol.* 60, 16–23. doi:10.1016/j.mib.2021.01.009

Tran, A. X., Dong, C., and Whitfield, C. (2010). Structure and Functional Analysis of LptC, a Conserved Membrane Protein Involved in the Lipopolysaccharide Export Pathway in *Escherichia coli**. *J. Biol. Chem.* 285 (43), 33529–33539. doi:10.1074/jbc.M110.144709

Tran, A. X., Trent, M. S., and Whitfield, C. (2008). The LptA protein of *Escherichia coli* is a periplasmic lipid A-binding protein involved in the lipopolysaccharide export pathway. *J. Biol. Chem.* 283, 20342–20349. doi:10.1074/jbc.M110.144709

Vetterli, S. U., Zerbe, K., Müller, M., Urfer, M., Mondal, M., Wang, S.-Y., et al. (2018). Thanatin Targets the Intermembrane Protein Complex Required for Lipopolysaccharide Transport in *Escherichia coli*. *Sci. Adv.* 4 (11), eaau2634. doi:10.1126/sciadv.aau2634

Villa, R., Martorana, A. M., Okuda, S., Gourlay, L. J., Nardini, M., Sperandeo, P., et al. (2013). The *Escherichia coli* Lpt Transenvelope Protein Complex for Lipopolysaccharide export Is Assembled via Conserved Structurally Homologous Domains. *J. Bacteriol.* 195 (5), 1100–1108. doi:10.1128/JB.02057-12

Vinés, E. D., Marolda, C. L., Balachandran, A., and Valvano, M. A. (2005). Defective O-antigen polymerization in *tolA* and *pal* mutants of *Escherichia coli* in response to extracytoplasmic stress. *J Bacteriol.* 187, 3359–3368.

Werneburg, M., Zerbe, K., Juhas, M., Bigler, L., Stalder, U., Kaech, A., et al. (2012). Inhibition of Lipopolysaccharide Transport to the Outer Membrane in *Pseudomonas aeruginosa* by Peptidomimetic Antibiotics. *Chembiochem* 13 (12), 1767–1775. doi:10.1002/cbic.201200276

Wiegand, I., Hilpert, K., and Hancock, R. E. (2008). Agar and Broth Dilution Methods to Determine the Minimal Inhibitory Concentration (MIC) of Antimicrobial Substances. *Nat. Protoc.* 3, 163–175. doi:10.1038/nprot.2007.521

Wu, T., McCandlish, A. C., Gronenberg, L. S., Chng, S.-S., Silhavy, T. J., and Kahne, D. (2006). Identification of a Protein Complex that Assembles Lipopolysaccharide in the Outer Membrane of *Escherichia coli*. *Proc. Natl. Acad. Sci.* 103, 11754–11759. doi:10.1073/pnas.0604744103

Xie, R., Taylor, R. J., and Kahne, D. (2018). Outer Membrane Translocon Communicates with Inner Membrane ATPase to Stop Lipopolysaccharide Transport. *J. Am. Chem. Soc.* 140 (40), 12691–12694. doi:10.1021/jacs.8b07656

Yethon, J. A., Vinogradov, E., Perry, M. B., and Whitfield, C. (2000). Mutation of the Lipopolysaccharide Core Glycosyltransferase Encoded by waaG Destabilizes the Outer Membrane of *Escherichia coli* by Interfering with Core Phosphorylation. *J. Bacteriol.* 182 (19), 5620–5623. doi:10.1128/JB.182.19.5620-5623.2000

Zhang, G., Meredith, T. C., and Kahne, D. (2013). On the Essentiality of Lipopolysaccharide to Gram-Negative Bacteria. *Curr. Opin. Microbiol.* 16 (6), 779–785. doi:10.1016/j.mib.2013.09.007

Zhang, X., Li, Y., Wang, W., Zhang, J., Lin, Y., Hong, B., et al. (2019). Identification of an Anti-gram-negative Bacteria Agent Disrupting the Interaction between Lipopolysaccharide Transporters LptA and LptC. *Int. J. Antimicrob. Agents* 53 (4), 442–448. doi:10.1016/j.ijantimicag.2018.11.016

Zhou, Z., Lin, S., Cotter, R. J., and Raetz, C. R. (1999). Lipid A Modifications Characteristic of *Salmonella typhimurium* Are Induced by NH4VO3 in *Escherichia coli* K12. Detection of 4-Amino-4-Deoxy-L-Arabinose, Phosphoethanolamine and Palmitate. *J. Biol. Chem.* 274, 18503–18514. doi:10.1074/jbc.274.26.18503

Conflict of Interest: The authors declare that the research was conducted in the absence of any commercial or financial relationships that could be construed as a potential conflict of interest.

Publisher's Note: All claims expressed in this article are solely those of the authors and do not necessarily represent those of their affiliated organizations, or those of the publisher, the editors, and the reviewers. Any product that may be evaluated in this article, or claim that may be made by its manufacturer, is not guaranteed or endorsed by the publisher.

frontiers in Molecular Biosciences

ORIGINAL RESEARCH
published: 02 February 2022
doi: 10.3389/fmolb.2022.795212

Cell-Free Expression to Probe Co-Translational Insertion of an Alpha Helical Membrane Protein

*Laura R. Blackholly, Nicola J. Harris, Heather E. Findlay and Paula J. Booth**

Department of Chemistry, King's College London, London, United Kingdom

The majority of alpha helical membrane proteins fold co-translationally during their synthesis on the ribosome. In contrast, most mechanistic folding studies address refolding of full-length proteins from artificially induced denatured states that are far removed from the natural co-translational process. Cell-free translation of membrane proteins is emerging as a useful tool to address folding during translation by a ribosome. We summarise the benefits of this approach and show how it can be successfully extended to a membrane protein with a complex topology. The bacterial leucine transporter, LeuT can be synthesised and inserted into lipid membranes using a variety of *in vitro* transcription translation systems. Unlike major facilitator superfamily transporters, where changes in lipids can optimise the amount of correctly inserted protein, LeuT insertion yields are much less dependent on the lipid composition. The presence of a bacterial translocon either in native membrane extracts or in reconstituted membranes also has little influence on the yield of LeuT incorporated into the lipid membrane, except at high reconstitution concentrations. LeuT is considered a paradigm for neurotransmitter transporters and possesses a knotted structure that is characteristic of this transporter family. This work provides a method in which to probe the formation of a protein as the polypeptide chain is being synthesised on a ribosome and inserting into lipids. We show that in comparison with the simpler major facilitator transporter structures, LeuT inserts less efficiently into membranes when synthesised cell-free, suggesting that more of the protein aggregates, likely as a result of the challenging formation of the knotted topology in the membrane.

Keywords: protein folding, membrane proteins, co-translational folding, cell-free, cell-free (CF) protein synthesis, lipids, membranes

OPEN ACCESS

Edited by:
Heidi Vitrac,
Tosoh Bioscience LLC, United States

Reviewed by:
Gunnar Von Heijne,
Stockholm University, Sweden
Innokentiy Maslennikov,
Chapman University, United States

****Correspondence:***
Paula J. Booth
paula.booth@kcl.ac.uk

Specialty section:
This article was submitted to Cellular Biochemistry, a section of the journal Frontiers in Molecular Biosciences

Received: *14 October 2021*
Accepted: *11 January 2022*
Published: *02 February 2022*

Citation:
Blackholly LR, Harris NJ, Findlay HE and Booth PJ (2022) Cell-Free Expression to Probe Co-Translational Insertion of an Alpha Helical Membrane Protein. Front. Mol. Biosci. 9:795212. doi: 10.3389/fmolb.2022.795212

INTRODUCTION

Membrane proteins constitute approximately 30% of the proteome (Doerr, 2009) and command considerable attention due to their physiologically important roles and dominance of drug targets (Fagerberg et al., 2010; Lunn, 2010). Currently, most studies aimed at garnering high resolution structural or functional information on these proteins require significant amounts of pure protein sample. Classical overexpression of membrane proteins *in vivo* can result in experimental difficulties due to the complex topological nature, tedious preparation, low protein yields and potential toxicity (Wagner et al., 2007; Gubellini et al., 2011). Protein overexpressed *in vivo* can be probed using *in vitro* techniques. The details applicable to the native conformational states, folding pathways, mechanisms

and functions that classical refolding *in vitro* techniques provide can be limited (Booth, 2003). In classical *in vitro* folding, a full length polypeptide chain is usually available via artificial denaturation for refolding, which is not representative of co-translational protein folding *in vivo* (Booth et al., 2001). *In vitro* investigations where a near-native lipid membrane environment is considered will provide experimental results more applicable to native protein states (Booth, 2005; Booth and Curnow, 2009). Membrane protein folding in non-native lipid environments must not overlook how the orientation and architectures of multispanning membrane proteins are determined during translation.

In vivo, most membrane protein biosynthesis starts on the ribosome where translation of the polypeptide chain and subsequent co-translational integration of nascent α-helices into a membrane environment is aided by the translocon (Serdiuk et al., 2019). This process occurs simultaneously whereby, in the majority of instances, a protein is co-translationally inserted *via* a membrane-embedded translocon apparatus into the bilayer during synthesis on the ribosome and as such a protein will fold upon biosynthesis (Skach, 2009; Liutkute et al., 2020). When using *in vitro* folding methods, these co-translational processes are hard to mimic (Harris and Booth, 2012; Hingorani and Gierasch, 2014). The hydrophobicity of membrane proteins, propensity to aggregation, and the chemically complex lipid composition of the surrounding native membrane environment makes experimental investigations into co-translational insertion of these proteins complicated (Bowie, 2005; Marinko et al., 2019). Probing co-translational folding is complex and the tool kits we have available to investigate this are limited.

Cell-free systems have recently provided excellent alternative techniques with the capacity to overcome the traditional problems of membrane protein production as they are not hindered by the same complications and variabilities as overexpression (Carlson et al., 2012; Findlay and Booth, 2013; Harris, 2017; Harris and Charalambous, 2018; Harris et al., 2020). We can exploit cell-free approaches to investigate membrane proteins - notably to probe co-translational folding *in vitro* as the nascent chain is being synthesized by the ribosome. These methods enable us to move from the current biophysical approaches employing artificially-denatured, full-length proteins to a situation that is more representative of cellular biosynthesis. This has afforded new opportunities to remedy the deficit of membrane protein folding studies (Schneider, 2010; Silverman et al., 2020).

Cell-free systems are frequently based on cellular extracts, such as the S30 *Escherichia coli* extract. Comprising an ensemble of the *E. coli* translation machinery, in addition to other chaperones, active enzymes and the T7 RNA polymerase to facilitate transcription, translation and protein folding *in vitro* (Kwon and Jewett, 2015; Terada et al., 2016). An issue with such extracts is that they can contain a large number of components, making it difficult to probe the influence of particular constituents (Zemella et al., 2015; Komar, 2018), as well as showing high variability (Takahashi et al, 2015), especially in extracts synthesized in non-commercial settings (Dopp and Reuel, 2018; Dopp et al., 2019).

Commercially synthesized extracts or cell-free systems containing purified elements tend to show less variability (Shimizu, 2001; Chong, 2014; Tuckey et al., 2014). As such, we have successfully utilized a defined system of purified components, namely the commercially available PURExpress system developed by the Ueda group (Swartz, 2001; Shimizu et al., 2005; Gregorio et al., 2019), and the Expressway kit; a commercial S30 system. PURExpress® constitutes purified tRNAs, amino acids, rNTPs and other small molecules, ribosomes, the T7 RNA polymerase, aminoacyl-tRNAs, translation factors, and energy regeneration enzymes. A drawback of this particular purified system is that necessary accessory proteins like SecA, FtsY, and the signal recognition particle (SRP) are not included. In the Expressway™ commercial kit, the *E. coli* extract contains all necessary machinery required for transcription and translation, as well as accessory proteins required by the translocon. Both systems enable the addition of membrane vesicles alongside large complexes to facilitate folding, and can enable the rapid synthesis of membrane proteins, in a variety of synthetic lipid envrionments (**Figure 1B**) (Shimizu, 2001; Kuruma and Ueda, 2015; Khambhati, 2019).

Utilizing cell-free techniques to investigate co-translational folding and insertion of membrane proteins is an emerging field. Previous work has focused on the insertion of functional membrane proteins in liposome-assisted or nanodisc synthetic systems with cell-free methodologies, probing topogenesis using techniques such as proteolysis, substituted cysteine accessibility (SCAM), and functional assays (Sahin-Toth et al., 1995; van Geest and Lolkema, 2000; Kalmbach et al., 2007; Cappuccio et al., 2009). Further investigations are emerging, focusing on how the lipid bilayer effects nascent chain insertion using a cell-free approach, proving that these techniques are viable in probing co-translational folding *in vitro* (Roos et al., 2013; Harris, 2017; Harris and Charalambous, 2018; Sanders et al., 2018; Harris and Booth, 2019; Eaglesfield et al., 2021).

Lipid properties such as headgroup charge, mechanical properties and chain lateral pressures exerted by lipids can affect the insertion, folding and topology of a membrane protein (Bogdanov et al., 2014; Findlay and Booth, 2017; Vitrac et al., 2017). Manipulation of bilayer mimics by varying lipid composition of liposomes provided into *in vitro* transcription and translation (IVTT) cell-free systems allows for the direct investigation of lipid: protein interactions, focusing on how changes to bilayer lateral chain pressure, fluidity, polarity, charge and thickness may affect protein folding and insertion (Rigaud and Lévy, 2003; Allen et al., 2004a; Junge, 2011; Pellowe and Booth, 2019). Although liposome membrane mimics cannot be directly compared to entire membrane lipid extracts or novel polymer based nanodiscs like those produced using the developing SMALP polymer and associated techniques (Dörr, 2016; Simon et al., 2018), liposomes provide us with a system that bridges the middle ground between native environment and application of use.

Utilizing IVTT cell-free systems supplemented with liposomes also offers the potential to probe how insertion efficiency is

affected by the presence of the translocon machinery. Biogenesis of nearly all alpha helical membrane proteins is governed by insertases and translocases, which provide a lower free-energy barrier for correct protein insertion and folding within a membrane (Cymer et al., 2015; Serdiuk et al., 2019). In *E. coli* this insertion is governed by SecYEG, a multimeric complex protein conducting channel (Veenendaal et al., 2004). Transmembrane helices of polytopic membrane proteins insert sequentially into the membrane utilizing the translocon machinery (Cymer et al., 2015; Pellowe and Booth, 2019; Mercier et al., 2021), and the SRP mediates ribosome targeting by coupling the synthesis of the translating nascent chain to correct cellular localization, ensuring integral membrane proteins are bought to the SecYEG translocon for correct co-translational integration into the membrane (Skach, 2011; Akopian et al., 2013; Saraogi and Shan, 2014).

SecYEG has previously been itself synthesized in PURE IVTT systems(Matsubayashi et al., 2014a; Matsubayashi et al., 2014b; Kuruma and Ueda, 2015), and liposomes containing reconstituted SecYEG have been implemented with the cell-free synthesis of the multidrug transporter EmrE (Ohta et al., 2016). We were subsequently interested to investigate the effect of the SecYEG translocon on the folding of the NSS transporter LeuT, looking at co-translational insertion utilizing reconstituted liposomes containing purified SecYEG (**Figure 1D**). This helps us ascertain how the presence of the translocon, with or without the necessary accessory factors, affects the overall percentage of LeuT inserted into liposomes during IVTT synthesis.

We target the leucine transporter LeuT, not previously investigated in cell-free, extending this co-translational approach to a protein with a complex topology, and advancing these successful investigations into the thermodynamics of folding in the co-translational arena. We do this employing the PURExpress® and Expressway™ IVTT systems.

$LeuT_{Aa}$ functions as a sodium/leucine transporter in *Aquifex aeolicus* and is a member of the neurotransmitter sodium symporter (NSS or SLC6) family (Yamashita et al., 2005; Krishnamurthy et al., 2009; Navratna and Gouaux, 2019). In humans, NSS proteins are responsible for the re-uptake of neurotransmitters involved in synaptic transmission (Joseph et al., 2019; Möller et al., 2019). LeuT has been widely used as a blueprint to provide insights into the organization, mechanisms and functions of mammalian NSS transporters, as it is an orthologue of eukaryotic proteins such as the Dopamine active transporter (DAT) and the Serotonin transporter (SERT) (Torres and Amara, 2007; Cheng and Bahar, 2019). Eukaryotic NSS proteins are physiologically important in humans with NSS dysfunction being related to various chronic neurological disorders such as depression, epilepsy and Parkinson's disease (Gotfryd et al., 2020). LeuT contains 12 transmembrane helices arranged in a coupled figure-eight (4 1) trefoil (31) slipknot (**Figure 1A**) (King et al., 2007; Yeates et al., 2007; Sułkowska et al., 2012), which has been postulated to be important for protein stability (Sanders et al., 2018). Knotted proteins account for 1% of known high resolution structures in the Protein Data Bank (PDB), although since membrane proteins remain underrepresented in the PDB, the extent of knotting in helical membrane proteins is unknown (Lim and Jackson, 2015a; Jarmolinska et al., 2019). Studies of knotted proteins are currently focused almost exclusively on a small number of water soluble proteins and have suggested that knots may be important for activity or increasing protein stability (Sułkowska et al., 2012; Faísca, 2015; Xu et al., 2018).

The hyperthermophile *Aquifex aeolicus* from which LeuT has been derived presents diverse lipid membrane structures (Braakman and Smith, 2014; Siliakus et al., 2017). Little is known about the lipid headgroups in this eubacterial species, although they are known to be vastly different to those found in *E. coli* membranes (Sturt et al., 2004; Jain et al., 2014; Sohlenkamp and Geiger, 2015). In addition to this, other lipids associated with eubacteria are significantly more branched (Sohlenkamp and Geiger, 2015), believed to be linked to adaptations to high temperature (Koga, 2012; Siliakus et al., 2017). Lipids, in particular sphingolipids, cholesterol and other anionic lipid species, are thought to play a significant role in regards to transporter conformational dynamics, structural stabilization, and modulating substrate interactions for eukaryotic NNS transporters (Magnani et al., 2004; Hong and Amara, 2010; Khelashvili and Weinstein, 2015; Joseph et al., 2019). An example of this is cardiolipin (CL), thought to be important in the stabilization of LeuT dimers *in vitro* (Gupta et al., 2017).

Our previous work concerning the cell-free synthesis of multidomain membrane proteins has involved developing a methodology in which to purify spontaneously inserted protein from cell-free kit components, to probe the effects of the lipid bilayer on co-translational folding (**Figures 1B,C**). (Harris et al., 2020; Findlay and Booth, 2013; Harris, 2017; Harris and Booth, 2019; Harris and Booth, 2017) Thus far, we have successfully applied this cell-free approach to multi-domain proteins such as the rhomboid protease, GlpG (Harris, 2017), and the major facilitator transporters, LacY and XylE (Harris and Booth, 2019). Our aim is to develop these methodologies and ascertain their broader applicability. We herein discuss our studies extending this to a protein with a more complex, knotted structure.

The lipid membrane environment impacts the insertion (Meijberg and Booth, 2002; Allen et al., 2004a; Lorch and Booth, 2004), folding (Allen et al., 2004b; Seddon, 2008; Findlay and Booth, 2017; Sanders et al., 2018), and function of membrane proteins (Bogdanov and Dowhan, 1999; Lee, 2004; Lee, 2005; Bogdanov et al., 2008). We have exploited this lipid influence to optimize the efficiency of our cell-free co-translational folding systems, and to provide a system more similar to that of native membranes. Here, we were interested to explore whether manipulation of synthetic lipid mixtures is sufficient to ensure efficient co-translational insertion and folding of a protein with a complex structure, or if additional cellular factors such as the translocon would be required by LeuT for insertion in cell-free systems (Phillips et al., 2009). Notably, through manipulation of the lipid composition, we show herein that on average ≤ 24% of all LeuT protein synthesized inserts and folds correctly in a synthetic lipid membrane in IVTT systems.

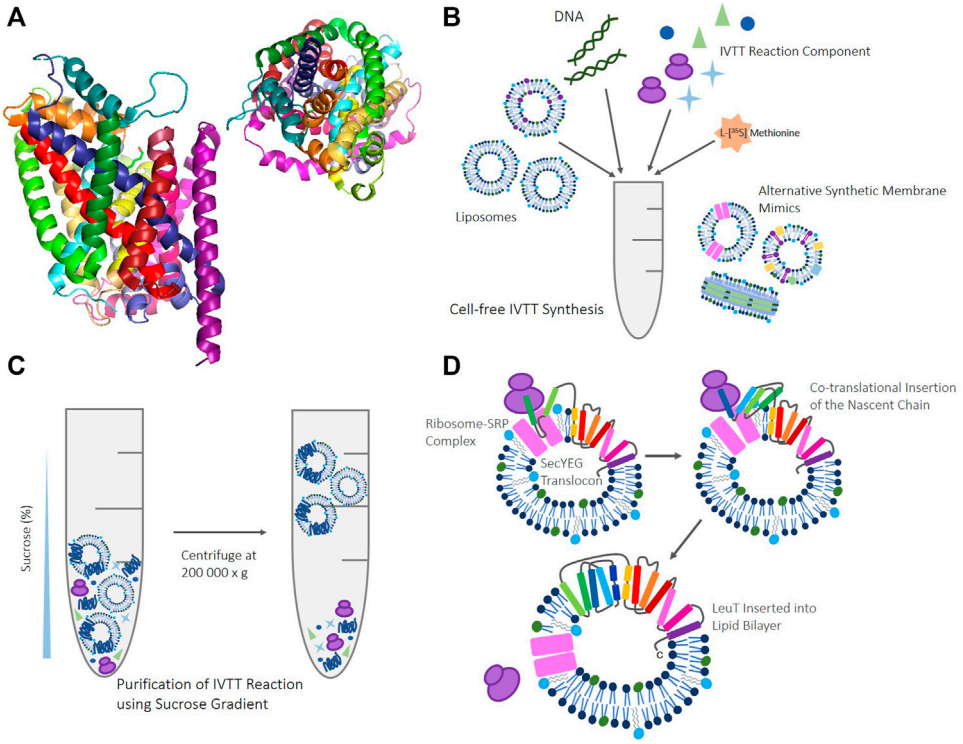

FIGURE 1 | (A) LeuT crystal structure (3GJD) (Quick et al., 2009) in a monomeric conformation. LeuT seen from the side (left), and from above (right) to highlight the complex knotted conformation. **(B)** Schematic of reagents and components required for IVTT cell-free reactions, such as; template DNA in the form of either PCR product, RNA or dsDNA, ribosomes, rNTPs, tRNA, amino acids. In addition to IVTT components, synthetic membrane mimics like that provided by liposomes are required. Various other alternative synthetic membrane mimics can be supplemented into these reactions such as; liposomes reconstituted with other proteins, inner/inverted membrane vesicles, and nanodiscs. **(C)** Schematic of the sucrose gradient methodology (Harris, 2017) used to purify IVTT reactions. Upon completion, cell-free reactions are suspended with 60% (w/v) sucrose. 30% (w/v) sucrose and buffer are layered on top to provide gradient, before centrifugation at 200,000 x g. Proteoliposomes and empty liposomes float to the 30% sucrose: buffer interface, and any unreacted IVTT kit components and aggregated, truncated, or non-inserted protein remains at the bottom of the gradient. **(D)** Cartoon schematic to illustrate how co-translational insertion of LeuT in IVTT systems where the translocon has been reconstituted into liposomes may occur. *In vivo*, protein knotting like that seen in LeuT is thought to be established and promoted by cellular machinery, including the ribosome(Chwastyk and Cieplak, 2015), providing new folding routes (Dabrowski-Tumanski et al., 2018), modulating hydrophobic reactions (Especial et al., 2019), and stabilising folding intermediates during co-translation (Lim and Jackson, 2015b; Faísca, 2015). Translation may occur via the SecYEG translocon when reconstituted and present, but we have also shown that spontaneous insertion occurs when the translocon is absent.

MATERIALS AND METHODS

All standard reagents were purchased from Sigma. The EXPRESSway™ Mini Cell-Free Expression system was purchased from ThermoFisher Scientific. The PURExpress® *In Vitro* Protein Synthesis kit and all molecular biology reagents were purchased from New England Biolabs unless stated otherwise. Methionine, L-[35S] was purchased from PerkinElmer. Lipids were purchased from Avanti Polar lipids, and the EnzCheck™ Phosphate Assay Kit, and NuPAGE Bis-Tris Gels were purchased from ThermoFisher Scientific.

Wild type $LeuT_{Aa}$ was modified with a C-terminal 10x Histidine tag (10x His) (WT CHis-LeuT) in a pET28a vector. The LeuT gene was adapted and codon optimized for expression in heterologous *E. coli* systems using the GENEius tuning tool (Eurofins Genomics) (Sanders et al., 2018). For use in cell-free expression systems WT CHis-LeuT was further modified to include a C-terminal V5 tag (14aa) with a GSSG linker between the coding regions and the 10x His tag. SecYEHisG (donated by Prof. Ian Collinson, University of Bristol), was in a pBAD vector for *in vivo* overexpression, with a 6x His tag on the N-terminus of the SecE subunit coding region.

Preparation of Lipids

5 mg of 1,2-dioleoyl-sn-glycero-3-phosphoethanolamine (DOPE), 1,2-dioleoyl-snglycero-3-phosphocholine (DOPC), 1,2-dioleoyl-sn-glycero-3-phospho-(1′-rac-glycerol) (sodium salt) (DOPG), *E. coli* Polar Lipid Extract, Cardiolipin (*E. coli*) (sodium salt) ($CL_{E.\ coli}$), 1′,3′-bis[1,2-dipalmitoyl-sn-glycero-3-phospho]-glycerol (sodium salt) ($CL_{16:0}$), 1′,3′-bis[1,2-dioleoyl-sn-glycero-3-phospho]-glycerol (sodium salt) ($CL_{18:1}$), 1,2-diphytanoyl-sn-glycero-3-phosphocholine (DPhPC) and 1,2-diphytanoyl-sn-glycero-3-phospho-(1′-rac-glycerol) (sodium salt) (DPhPG) lipids were dissolved in cyclohexane at 45°C. Required ratios of lipids were mixed and flash frozen in liquid N_2 before freeze drying overnight. Lipids were stored at -20°C upon removal from the freeze dryer, and N_2 gas was passed over lipid films to prolong storage life and for preservation.

Liposomes were prepared for IVTT using preparation as previously described (Harris, 2017), and lipid films were resuspended at 10 mg ml^{-1} in 40 mM HEPES-KOH (pH 7.6) and suspensions extruded through 200 nm or 400 nm Millipore filters using a mini-extruder with a minimum of 25 pushes. Liposomes were used immediately in IVTT.

Cell-free Synthesis and Insertion of LeuT

The PURExpress® *In Vitro* Protein Synthesis Kit and EXPRESSway™ Mini Cell-Free Expression system were used following manufacturer's instructions. Liposomes were supplemented instead of buffer to make up to the required reaction volume, and in each case provided a final concentration of lipids at 3 mg ml^{-1} in both cell-free kits. The total reaction volume for the EXPRESSway™ commercial kit is larger than that of PURExpress®; 25 µl volume for PURExpress®, and 50 µl for EXPRESSway™. Reactions were initiated with the addition of 50 ng µl^{-1} of plasmid DNA before incubation at 30°C for 2–4 h. DNA was added after liposomes into the kit to prevent early initiation of protein synthesis. Methionine, L-[35S], 0.04–0.1 mCi ml^{-1} was added at the start of each reaction, being supplemented before the addition of plasmid DNA. Protein synthesized was quantified following the PURExpress® *In Vitro* protein Synthesis Kit manual, using the Ultima Gold MV scintillation cocktail (PerkinElmer), with a 1600 TR Tri-Carb® Liquid Scintillation Counter (Packard) as previously described (Harris, 2017).

Insertion of LeuT

All sucrose and urea solutions used were prepared in 40 mM HEPES-KOH at pH 7.6. Following IVTT using the PURExpress® *In Vitro* Protein Synthesis Kit, the reaction mix was resuspended in 80 µl 60% sucrose, before 100 µl of 30% sucrose layered on top, followed by 50 µl of 40 mM HEPES-KOH pH 7.6 buffer to complete the gradient. Gradients were then centrifuged at 200,000 x g (70,000 RPM, Beckman TLA 100 rotor) to float liposomes and proteoliposomes to the interface between the 30% sucrose: 40 mM HEPES-KOH buffer, leaving unreacted IVTT kit components to pellet to the bottom of the gradient (**Figure 1C**). The layers of sucrose were then separated in two aliquots; top and bottom fractions, for use in further investigation and for visualization using SDS-PAGE gel analysis as previously described (Harris, 2017). When using the EXPRESSway™ Mini Cell-Free Expression System, 200 µl 6M Urea was added to each 50 µl reaction before liposomes were pelleted via centrifugation at 350,000 x g (90,000 RPM, Beckman TLA-100 rotor) for 45 min. Liposomes were resuspended in 100 µl 60% sucrose before continuing with gradient steps as above. For detection of proteoliposomes, sucrose gradient top and bottom fractions were directly run on a 12% Nu-PAGE Bis-TRIS SDS-PAGE gel before wet transferring to a nitrocellulose membrane. Membranes were placed in a cassette with phosphor screen to develop and were imaged using a Typhoon™ FLA 7000 Biomolecular Imager. To calculate radiolabeled counts using Methionine, L-[35S], a 3 µl sample from each sucrose gradient layer, and 2 × 2 µl sample from the reaction upon completion were taken and pipetted onto MF-Millipore™ 0.5 µm membrane filter (Merck Millipore) before quantification of protein within each sample could be calculated using LSC.

Calculation of Insertion Efficiencies

In each lipid condition insertion efficiencies for LeuT are calculated as a percentage of protein yielded in the top fraction of the sucrose gradient after purification (Harris, 2017). This is done using protein yields obtained via LSC counts as described above. 0% insertion is where empty liposomes reside in the top fraction, and all cell-free synthesized protein aggregated in the bottom fraction, and 100% insertion is where all protein is incorporated into proteoliposomes in the top fraction, and no cell-free synthesized protein is aggregated in the bottom fraction.

The average yield from PURExpress® IVTT reactions ranges between 0.1–1 µg protein per 25 µl reaction. In EXPRESSway™ a total protein yield of approximately 1–10 µg per 50 µl reaction is synthesized. Where ≥80% of total protein is lost during sucrose gradient purification, the experimental result is disregarded. There is a negative correlation between high initial IVTT expression yields and low proteoliposome recovery after purification (**Supplementary Figure S4**). A threshold was set so as to reject datasets where high aggregation and low protein recovery interferes with accurate calculation of any insertion efficiencies. Liposome aggregation during expression and purification is likely to reduce the amount of protein floated on the sucrose gradient. Low proteoliposome recovery, and the poor quality of such samples meant that individual IVTT reactions where ≥80% of total protein is lost during sucrose gradient purification was not compared to IVTT reactions where larger yields of protein was recovered.

Statistical analysis was performed using GraphPad Prism 9. Brown-Forsyth and Welch ANOVA tests were conducted with raw data sets when comparing average insertion efficiencies for each group of lipids investigated (DO, DPh, and CL mixes). Where individual p values are presented directly comparing two lipid conditions, Welch's t test was calculated using complete data sets.

Isolation and Purification of the SecYEG Translocon

A colony from a fresh transformation of pBAD SecYEG plasmid construct in c43 competent *E. coli* cells was grown in LB containing 100 µg ml^{-1} ampicillin overnight, shaking at 37°C. This was seeded into 6 x 1L smooth flasks in LB media (100 µg ml^{-1} ampicillin) and grown at 37°C, shaking, till OD ~ 0.6–0.8 before induction with 0.1% (w/v) L-(+)-arabinose. After induction the cells were grown until stationary, and then harvested by centrifugation at 4,900 x g (4,200 RPM, Beckman JS-4.2SM) at 4°C for 45 min. Cell pellets were resuspended and washed in 200 ml phosphate-buffered saline (PBS) at 4°C at 9,000 x g (6,000 RPM, Avanti JLA-8.1000) for 10 min. Supernatant was then discarded and the pellet resuspended in 50 ml PBS with cOmplete™ protease inhibitor tablet, after which 1 µl of benzonase was added to sample, before incubation at room temperature on a roller shaker for 10 min. The sample was homogenized, and cells lysed using a constant systems cell

disruptor; 1 pass, before ultracentrifugation at 148,000 x g at (38,000 RPM, Beckman Type 70 Ti rotor) 4°C, for 45 min to pellet cellular membranes. The supernatant was discarded, and the pellet was resuspended in 35 ml solubilization buffer (20 mM TRIS-HCl (pH 8), 300 mM NaCl, 10% (w/v) glycerol, 0.1 mM phenylmethylsulfonyl fluoride (PMSF), 2% (w/v) n-Dodecyl β-D-maltoside (DDM), 1x cOmplete™ EDTA-free protease Inhibitor Tablet, and 20 mM imidazole) to solubilize, left to stir at 4°C for 2 h.

For affinity purification, a HisTrap™ HP column (Ni^{2+}-chelated Sepharose prep-packed, 1 ml) was connected to an AKTA prime chromatography system (GE Healthcare) equilibrated with 0:100 Buffer B: Buffer A. Buffer A: 20 mM TRIS-HCl (pH 8), 300 mM NaCl, 10% (w/v) glycerol, 0.1 mM PMSF, (0.1% w/v) DDM, Buffer B: 20 mM TRIS-HCl (pH 8), 300 mM NaCl, 10% (w/v) glycerol, 0.1 mM PMSF, 0.1% (w/v) DDM, 500 mM Imidizole, 1 mM 2-Mercaptoethanol. Solubilized, filtered sample was loaded onto HisTrap™ HP column, and after protein binding the column was washed with 10 CV 0:100 Buffer B: Buffer A, then 25 CV 15:85 Buffer B: Buffer A. Protein was eluted with 100% Buffer B and directly injected onto a HiLoad® 16/600 Superdex® gel filtration column before fractions collected using peak fractionation and then pooled and concentrated where required. Pooled fraction concentration determined *via* a NanoDrop™ spectrophotometer at UV280. A sample of protein was visualized using SDS-PAGE, run on a NuPAGE Bis-Tris Protein Precast gel with MES SDS running buffer, before protein was stored at −80° (**Supplementary Figure S2**).

Reconstitution of SecYEG

1.2% n-Octyl-β-D-glucopyranoside (OG) was added to liposomes pre-extruded at 400 nm diameter, prepared as described above in 40 mM HEPES pH 7.6, before incubation using a rotator mixer for 30 min at room temperature. SecYEG was then subsequently added at a predetermined concentration before further incubation in a rotator mixer for 1 h, again at room temperature. Detergent was then removed using a Pierce™ Detergent Removal Spin Column (ThermoFisher). Reconstitution efficiency and protein concentration in the liposomes was then determined using a Markwell-Lowry assay (Markwell et al., 1978) before use in subsequent cell-free experiments.

Where SecYEG was reconstituted at a SecYEG: lipid ratio (w/w) of 1:50, this equates to a composition of approximately 1.7% of heterotrimeric SecYEG per liposome, assuming a theoretical 100% reconstitution efficiency and in 400 nm liposome vesicles. For conditions where SecYEG was reconstituted into 400 nm liposomes at 1 in 25, approximately 3.4% of the liposome surface area was heterotrimeric SecYEG monomers, and at 1 in 100 only 0.86%. In IVTT where the effect of SecYEG was investigated and in liposome conditions where SecYEG was absent, liposomes were mock reconstituted with the addition and removal of detergent, following the same methodology as the SecYEG condition. Liposomes were immediately used in ATPase assay after reconstitution and in IVTT experiments.

SecYEG ATPase Activity

The EnzChek™ Phosphate Assay kit (ThermoFisher) was utilized to investigate SecYEG reconstituted protein when bound with SecA. SecA was donated by Prof. Ian Collinson (Collinson Group, University of Bristol) in a pET28 plasmid. SecA was purified following methods as previously described (Gold et al., 2007). The reaction mix was set up, initially omitting the experimental substrate, ATP. Reaction mix: 10 µL 20x Reaction Buffer, 40 µl MESG substrate solution, 2 µl purine nucleoside phosphorylase (PNP), 0.05–0.03 µM SecA, 50–100 µl liposomes, X µl nuclease free water (to make up 200 µl total reaction volume). Reaction mix was preincubated for 15 min at room temperature before initiation by the addition of 1 mM ATP. Sample was inverted to mix before immediately reading the A360 in a spectrophotometer as a function of time. Reactions were run for 30 min, or until no further change in A360 was observed, where no more SecA dependent ATPase activity by SecYEG present in liposomes occurred. Only functionally active SecYEG was used in insertion IVTT cell-free experiments.

Inverted Membrane Vesicle (IMV) Preparation

Halophilic archaeal strains of *Halobacterium salinarium*, wild type (S9) and L33 (bR knockout) were grown aerobically in 50 ml basal salt liquid media, pH 7.2 (4 M NaCl, 100 mM $Mg.SO_4.7H_20$, 10 mM $Na_3C_6H_5O_7$, 25 mM KCl, 1% (w/v) Oxoid peptone) at 39°C in a shaking incubator at 150 RPM till an OD (A600) of 1.0. 10 ml of preliminary culture was subsequently seeded into a 1 L flask containing 700 ml basal salt liquid media, grown as before for another 4 days or until stationary growth was reached at an OD (A600) between 1–1.5. The crude vesicles were then harvested via centrifugation at 4,900 x g (4,200 RPM, Beckman JS-4.2SM) for 45 min. The supernatant was subsequently discarded and the pellet resuspended in buffer A (50 mM Tris-HCl (pH 7.2, 1.75 M NaCl) at v:w, buffer: pelleted cell weight of 1:1. Sample homogenized using a OneShot consistent systems cell-disruptor at 4°C, 20,000 psi, performing a total of 3 passes, keeping the crude vesicle pellet on ice at all times. Homogenized sample ultracentrifuged at 170,000 x g (40,000 RPM, Beckman Type 70 Ti rotor) for 1 h at 4°C before pellet resuspended in 5 ml of buffer A. Inverted membrane vesicles were purified on a sucrose gradient. All gradient concentrations of sucrose were made up in 2 M NaCl, 50 mM Tris-HCl (pH 7.2). 1 ml of crude vesicle membrane pellet resuspension was carefully pipetted onto a sucrose cushion comprising six steps. Sucrose density gradient composition; 1.5 ml 1 (1.5 M), 2.5 ml B (1.4 M), C (1.3 M), D (1.2 M), 2.0 ml E (1.1 M), and 1 ml F (0.9 M). Gradients centrifuged at 187,000 x g (32,000 RPM, Beckman SW 32.1 Ti rotor) for 24 h at 4°C, rotor acceleration and deceleration speed set at maximum. Bands containing IMV's were collected and diluted into 20 ml of buffer B (50 mM Tris-HCl pH 7.2, 2 M NaCl) before centrifuging at 230,000 x g (45,000 RPM, Beckman Type 60 Ti rotor) for 2 h at 4°C. Pellets resuspended again 0.5 ml of buffer B and stored at −80°C until use.

TABLE 1 | Lipid compositions and their respective molar ratios investigated for LeuT spontaneous insertion 1–10. In each lipid condition the average mean insertion efficiency is provided, calculated as a percentage of protein in the top fraction of the sucrose gradient after purification. 0% insertion is where proteoliposomes reside solely in the top fraction, and all protein aggregated in the bottom fraction, and 100% insertion where all protein is incorporated into proteoliposomes in the top fraction, and no protein aggregated in the bottom fraction. Average total yields for each condition are presented as the total amount of protein synthesized during IVTT before purification. Protein lost between the total yield and the yield after purification ranges from 0–0.25 μg, equating to an average loss of ≤ 25%. All mean insertion efficiencies are thus calculated from the total protein yield. The total protein yields after purification are presented in **Supplementary Table S1**. Both the average yield and mean insertion efficiency (%) were calculated from a minimum of three repeats ($n \geq 3$), and experimental errors for mean insertion are presented as SEM. The only condition where less than 3 repeats were conducted was in the IMV condition, where $n = 2$. All experiments were conducted in PURExpress® except the IMV condition where Expressway™ was used.

	Lipid Composition	*Lipid Molar Ratio*	*Mean Insertion (%)*	*SEM*	*Average Yield (μg/25 μl)*
1	DOPC	**1**	**20**	**6.9**	**0.56**
2	DOPC:DOPG	**50:50**	**24**	**6**	**0.62**
3	DOPC:DOPE	**50:50**	**18.4**	**5.8**	**0.59**
4	DOPE:DOPG	**50:50**	**17.6**	**3.5**	**0.61**
5	DOPC:DOPE:DOPG	**24.5:50.5:25**	**16.5**	**3.6**	**0.56**
6	DPhPC	**1**	**17.5**	**2.1**	**0.42**
7	DPhPG:DPhPC	**34:66**	**12.5**	**4.0**	**0.30**
8	DPhPG:DPhPC	**50:50**	**16.3**	**4.1**	**0.40**
9	DPhPG:DPhPC	**66:34**	**21.4**	**4.8**	**0.53**
	IMV		**19.8**	**1.9**	**2.7**

RESULTS

Cell-free Synthesis and Insertion of LeuT Into Liposomes

Cell-free IVTT of LeuT was initially performed using the PURExpress® system, in the presence of liposomes comprising five lipid mixes (1–5) (**Table 1**). Following reaction incubation and IVTT, liposomes were floated on a gradient of sucrose and the insertion efficiency was calculated. Insertion efficiency is represented as a percentage of protein in the top fraction over the total protein synthesized, using liquid scintillation counts (LSC) from incorporated Methionine, L-[35S] during protein cell-free synthesis.

LeuT was found to insert into liposomes with a mean insertion efficiency of 16.5–24% (**Table 1**). This is in a consistent range with other membrane transporters previously investigated (Long et al., 2012; Ando, 2016; Harris, 2017; Harris et al., 2020). The highest percentage of spontaneous insertion occurred in liposomes with a lipid composition of a 50:50 M ratio (DOPC: DOPG) at an insertion yield of 24 ± 6%. The lowest percentage insertion efficiencies could be seen in DOPE lipid mixes; DOPC: DOPE, DOPG:DOPE, and DOPC:DOPE:DOPG at 18.4 ± 5.8%, 17.6 ± 3.5%, and 16.5 ± 3.6% respectively. Insertion of LeuT in all mixes of DOPC, DOPG, and DOPE lipids does not appear to be heavily dictated by liposome properties, and preference to a particular bilayer is not apparent. The average insertion efficiencies for the individual DiOleoyl (DO) lipid mixes tested are unlikely to be statistically significant ($p < 0.85$) where each lipid composition is directly compared.

Insertion of LeuT Into Liposomes Constituting Near-Native Lipids

As LeuT is natively expressed in the hyperthermophillic, chemolithotrophic eubacterium; *Aquifex aeolicus* (Deckert et al., 1998; Singh and Pal, 2015), the native environment in which this protein resides is vastly different to the DO lipid environment provided in these experiments for spontaneous insertion in IVTT conditions. Isoprenoids are a major component in archaea (and eubacterium) membranes (Lange et al., 2000; Koga and Morii, 2007). Liposomes comprising DiPhytanoyl (DPh) lipids, a synthetic lipid comprising two methyl-branched acyl chains attached to a glycerol moiety to mimic the lipid physiological properties of both eubacterial and eukaryotic origin (Panov et al., 2014; Tsuchikawa et al., 2020), were subsequently employed. These lipids have been shown to produce a stable planar lipid membrane, and DPhPC forms excellent stable model bilayers (Hung et al., 2000). Various liposome conditions comprising branched lipids were studied for LeuT insertion to mimic a nearer-native membrane environment (6–10) (**Table 1**).

The percentage insertion of LeuT into liposomes containing DPh lipids remains in a comparable range to that with DO lipids; between 12–22% (**Table 1**). There is no statistical difference in the mean insertion efficiencies for these lipid conditions ($p < 0.80$). The highest insertion efficiency into DPh containing liposomes is seen in 66:34 DPhPG:DPhPC at 21.4 ± 4.8%. Insertion into 50:50 DPhPG:DPhPC liposomes was lower than 50:50 DOPG:DOPC liposomes at 16.3 ± 4.1%. The insertion efficiency into pure DPhPC is also lower than pure DOPC liposomes, where the percentage mean insertion efficiency for DPhPC was 17.5 ± 2.1% compared to 20 ± 6.9% in DOPC albeit these results are not within error.

The total protein yields were lower than that seen with DO lipids (**Table 1**). This was particularly apparent with 100% DPhPG liposomes where only 0.06–0.19 μg of total protein was synthesized in each IVTT reaction, notably lower compared to 0.3–72 μg in other lipid conditions (**Supplementary Table S2**). Such low yields were not reliably quantifiable above background, therefore 100% DPhPG insertion efficiencies were not compared further to conditions where protein IVTT expression yields were higher.

TABLE 2 | Lipid compositions and their respective molar ratios investigated for LeuT spontaneous insertion in PURExpress® 1–6. Mean insertion efficiencies (%) and average total yields with each condition are shown for each lipid condition tested. The total protein yields after purification are presented in **Supplementary Table S3**. The average protein yield after sucrose gradient purification is consistent with the total yields immediately after IVTT reaction, so protein is not lost during purification steps. The average total yield and mean insertion efficiencies (%) were calculated from three repeats (n = 3) except condition 6 where n = 5. Experimental errors for mean insertion are presented as SEM.

	Lipid Composition	Lipid Molar Ratio	Mean Insertion Efficiency (%)	SEM	Average Yield (μg/25 μL)
1	**DOPC:$CL_{E.\ coli}$**	99.5:0.5	**8.3**	**1.0**	**0.55**
2	**DOPC:$CL_{E.\ coli}$**	95:5	**12.9**	**1.8**	**0.56**
3	**DOPC:DOPE:DOPG:$CL_{E.\ coli}$**	24:51.5:24:0.5	**13.9**	**1.6**	**0.57**
4	**DOPC:DOPG:$CL_{18:1}$**	50.5:49:0.5	**19.1**	**1.7**	**0.60**
5	**DOPC:DOPG: $CL_{18:1}$**	53:41.5:5.5	**16.2**	**1.9**	**0.62**
6	**DOPE:DOPG:$CL_{18:1}$**	72:27.5:0.5	**17.4**	**3.7**	**0.72**

Insertion of LeuT Inverted Membrane Vesicles

To further investigate if a nearer-native lipid environment would increase the percentage of protein to spontaneously insert during IVTT, inverted membrane vesicles (IMVs) from *Halobacterium salinarium* L33 were produced. Although *H. salinarium* is a halophilic archaeon and not considered hyperthermophillic nor chemolithotrophic like *A. aeolicus*, this extremophile can be cultivated and grown using relatively standard, well documented lab conditions (Ring and Eichler, 2001; Eichler, 2019; Vauclare et al., 2020). The lipid environment of IMVs was hoped to provide a nearer-native environment than that provided by DO and DPh lipid compositions.

Purified *H. salinarium* IMVs were supplemented into the Expressway™ system, where the sucrose gradient was adapted for variability in IMV flotation as noted in methods. Spontaneous insertion of LeuT into IMVs using LSC counts gave a percentage insertion of 19.8 ± 1.9% (**Table 1**), which initially appears consistent with other IVTT reactions in Expressway™ (**Table 2**). It should be noted that the 2.7 μg yield of average total protein calculated using LSC counts cannot be distinguished as corresponding solely to spontaneously inserted LeuT, on account of non-specific reactions with Methionine, L-[35S] and IMV components (**Supplementary Figure S1**). Optimizing the use of IMVs in IVTT was thus not undertaken and different avenues of investigation were pursued.

Insertion of LeuT Into Cardiolipin Containing Liposomes

The effect of CL on the spontaneous insertion of LeuT in IVTT was also investigated as CL is postulated to play a stabilizing role in LeuT dimers (Gupta et al., 2017; Corey et al., 2019). CL has also been implicated in playing a stabilizing role for other membrane proteins, including the Na^+/H^+ antiporter NhaA (Gupta et al., 2017; Rimon et al., 2019). Two commercially available CL extracts were used to investigate this effect: natural *E. coli* CL ($CL_{E.\ coli}$) and purified trans18:1 CL ($CL_{18:1}$). The former has a varied fatty acid distribution within the natural extract, although the two most common acyl chain structures present are 16:0 (33.3%) and cyclo17:0 (27%), with trans18:1 representing 14.4% of this natural lipid extract mixture (Macias et al., 2019). DO lipid mixes at ratios previously investigated were doped with 0.5–5% of either $CL_{E.\ coli}$ or $CL_{18:1}$ to investigate any effects on spontaneous protein insertion. Liposomes constituting various lipid mixes were supplemented into IVTT (**Table 2**). 72:22.5:5.5 DOPE:DOPC:$CL_{18:1}$ was a particularly interesting composition to test as is comparable to that of an *E. coli* total lipid extract (Raetz and Dowhan, 1990; Sohlenkamp and Geiger, 2015; Hoyo et al., 2020).

Spontaneous insertion of LeuT into CL liposome mixes remained consistent, albeit slightly lower than that seen with DO lipids, and with greater variability comparatively across individual CL lipid conditions ($p < 0.09$) (**Figure 2**). Percentage insertion of LeuT into CL lipid mixes was found to be between 8–19% (**Table 2**). This general decrease in insertion can be observed in direct comparison with DO lipid mixes with and without doped CL. The most significant effect can be seen with pure DOPC bilayers where spontaneous insertion is reduced 8.3 ± 1% with 0.5% $CL_{E.\ coli}$ ($p < 0.16$) (**Figure 2**). The reduction in spontaneous insertion from lipid mixes without CL to with CL is less prominent with 5% $CL_{E.\ coli}$ where spontaneous insertion is reduced from 20 ± 6.9% in pure DOPC bilayers, to 12.9 ± 1.8%, and in 50:50 DOPC:DOPG bilayers, where the percentage insertion is 24 ± 6%, compared to 19.1 ± 1.7% in 50.5:49:0.5 DOPC:DOPG:$CL_{18:1}$ and 16.2 ± 1.9% in 53:41:5.5 DOPC:DOPG:$CL_{18:1}$ ($p < 0.27$–0.47). CL with a saturated acyl chain structure of $CL_{18:1}$ does not appear to reduce the spontaneous insertion of LeuT as much as that seen with natural $CL_{E.\ coli}$, containing a mixed distribution of acyl chain structures.

SecYEG Reconstituted Liposomes to Improve LeuT Insertion in Cell-free Systems

The EXPRESSway™ system was used for investigations into the effect of the SecYEG translocon on LeuT insertion over the PURExpress® system employed for earlier lipid optimization investigations. This system was chosen to investigate the effect of the translocon on LeuT insertion as it is an *E. coli* extract, and as such, contains all the necessary cellular machinery required for transcription and translation, as well the associated accessory proteins required by the translocon for co-translational insertion.

SecYEG was prepared (Collinson et al., 2001) and reconstituted into liposomes at various concentrations. Liposomes contained differing amounts of CL to test the efficiency of insertion in the presence of SecYEG (**Table 3**).

TABLE 3 | The individual lipid compositions used for conditions where SecYEG was either present or absent 1–4. SecYEG was reconstituted at a ratio of 1 in 50 (w/w) protein: lipid in conditions where present. Average total yields refer to the total amount of protein synthesized during IVTT, and average yield purified refers to the amount of protein recovered after sucrose gradient purification. We can consider the protein lost between synthesis and purification to be aggregated or non-inserted. The mean insertion efficiencies (%) are presented for each condition with SecYEG absent or present. Errors presented are SEM calculated from a minimum of 3 repeats, any experimental results disregarded can be found in **Supplementary Table S5 and S6**. All experiments were conducted in Expressway™.

	Lipid Composition	Lipid Molar Ratio	SecYEG	Mean Insertion Efficiency (%)	SEM	Average Total Yield (μg/50 μL)	Average Yield Purified (μg/50 μL)
1	**DOPE:DOPG:$CL_{18:1}$**	72:27.5:0.5	**no**	**18.7**	**2.7**	**4.6**	**1.4**
1	**DOPE:DOPG:$CL_{18:1}$**	72:27.5:0.5	**yes**	**20.1**	**1.1**	**4.4**	**1.4**
2	**DOPE:DOPG:$CL_{18:1}$**	72:22.5:5.5	**no**	**23.8**	**2.9**	**4.3**	**1.7**
2	**DOPE:DOPG:$CL_{18:1}$**	72:22.5:5.5	**yes**	**21.8**	**2.4**	**4.4**	**1.4**
3	**DOPE:DOPG:$CL_{E.\ coli}$**	72:27.5:0.5	**no**	**20.3**	**2.1**	**4.2**	**1.9**
3	**DOPE:DOPG:$CL_{E.\ coli}$**	72:27.5:0.5	**yes**	**16.3**	**5.9**	**4.2**	**1.5**
4	**DOPE:DOPG:$CL_{E.\ coli}$**	72:22.5:5.5	**no**	**28.3**	**3.7**	**4.0**	**1.7**
4	**DOPE:DOPG:$CL_{E.\ coli}$**	72:22.5:5.5	**yes**	**21.1**	**0.1**	**2.3**	**0.8**

CL is required for the *in vivo* stability and function of the bacterial translocon, as well as DOPG (Collinson, 2019; Ryabichko et al., 2020). SecYEG activity in reconstituted liposomes was investigated using an ATPase assay, yielding consistent activity comparable with other investigations (**Supplementary Figure S3**, **Supplementary Table S8**) (Robson et al., 2009). Lipid mixes containing SecYEG were supplemented into IVTT reactions.

The percentage insertion of LeuT in EXPRESSway™ remains consistent with efficiencies seen in PURExpress® IVTT systems, where the insertion was between 16–28% in both "empty" and SecYEG conditions (**Table 3**). In all lipid conditions, insertion was not improved by the presence of SecYEG, where SecYEG was reconstituted at a 1 in 50 (w/w) protein: lipid ratio. For each condition investigated, the presence of the SecYEG translocon did not alter the insertion efficiencies, and any changes are not likely to be statistically significant ($p < 0.14–0.64$). In 72:22.5:5.5 DOPE:DOPG:$CL_{E.\ coli}$, the insertion efficiency of 28.3 ± 3.7% was reduced to 21.1 ± 0.1% in SecYEG containing liposomes (**Table 3**).

Increased SecYEG Reconstitutions to Improve LeuT Insertion in Cell-free Systems

SecYEG did not induce a significant improvement of LeuT insertion into liposomes in IVTT systems. To further investigate the effects of SecYEG on spontaneous insertion, SecYEG was reconstituted into liposomes at both 1 in 25 and 1 in 100 (w/w) protein: lipid ratios.

In both lipid mixes where SecYEG was reconstituted at 1 in 25 (w/w) protein: lipid ratio, there was an increase in LeuT insertion (**Table 4**). In 72:27.5:0.5 mol ratios of DOPE:DOPG:$CL_{18:1}$, we see a spontaneous insertion of 23.6 ± 1.7% for 1 in 25 SecYEG conditions, compared to 20.1 ± 1.1% and 21.8 ± 0.8% for 1 in 50 and 1 in 100 conditions respectively ($p < 0.17–0.31$). In 72:22.5:5.5 DOPE:DOPG:$CL_{18:1}$, we see a similar, yet more pronounced effect where spontaneous insertion is found to be at 32.3 ± 0.1% for 1 in 25 SecYEG, compared to 21.8 ± 2.4% and 22.8 ± 0.5% for 1 in 50 and 1 in 100 conditions respectively (**Table 4**). The increase in insertion for 1 in 25 SecYEG in this lipid condition is statistically significant ($p < 0.040$) when compared with empty liposomes of the same composition (**Figure 3**). In addition to the mean insertion rates, the yield of protein produced remains consistent across all SecYEG reconstitutions and are comparable to other EXPRESSway™ IVTT yields.

DISCUSSION

The lipid compositions chosen for study struck a balance between lipids that would yield the formation of a stable bilayer, lipids required for SecYEG functionality, and lipids that would provide a membrane mimic suitable for protein insertion (Van Dalen and

TABLE 4 | Investigations were conducted in lipid conditions comprising 72:27.5:0.5 and 72:22.5:5.5 mol ratios of DOPE:DOPG:$CL_{18:1}$, with each protein: lipid ratio of SecYEG. The mean insertion efficiencies (%) are presented for each lipid condition where SecYEG is present at each concentration. Errors presented are SEM calculated from a minimum of 2 repeats. The total protein yields after purification are presented in **Supplementary Table S4**. All experiments were conducted in Expressway™.

	Lipid Composition	Lipid Molar Ratio	SecYEG	Mean Insertion Efficiency (%)	SEM	Average Total Yield (μg/50 μL)
1	**DOPE:DOPG:$CL_{18:1}$**	72:27.5:0.5	**1 in 25**	**23.6**	**1.7**	**3.8**
1	**DOPE:DOPG:$CL_{18:1}$**	72:27.5:0.5	**1 in 50**	**20.1**	**1.1**	**4.4**
1	**DOPE:DOPG:$CL_{18:1}$**	72:27.5:0.5	**1 in 100**	**21.8**	**0.8**	**4.4**
2	**DOPE:DOPG:$CL_{18:1}$**	72:22.5:5.5	**1 in 25**	**32.3**	**0.1**	**4.0**
2	**DOPE:DOPG:$CL_{18:1}$**	72:22.5:5.5	**1 in 50**	**21.8**	**2.4**	**4.4**
2	**DOPE:DOPG:$CL_{18:1}$**	72:22.5:5.5	**1 in 100**	**22.8**	**0.5**	**4.7**

De Kruijff, 2004; Phillips et al., 2009; Sachse et al., 2014; Kuruma and Ueda, 2015). Insertion of LeuT was independent of the lipid compositions investigated, where changes in lateral pressure and charge had little to no effect. We show that percentage insertion remains consistent in DO lipid mixes, where insertion appeared to not favor any of the compositions tested. This lack of dependence on membrane lipids remains in the DPh lipids tested, where changes in bilayer properties with the addition of DPhPG to DPhPC made little difference to LeuT insertion. In contrast to this we show that liposomes containing small amounts of CL such as 0.5 and 5.5%, appeared to be less favored for LeuT insertion, especially when directly compared to DO lipid mixes. Improvement of LeuT insertion was not obtained; regardless of lipid composition, or *via* the presence of the bacterial translocon SecYEG at low concentrations.

The lack of lipid dependency contrasts with previous *in vitro* folding work with LeuT that was partly denatured in the presence of urea, where unfolding was measured in reconstituted proteoliposomes. Both lateral chain pressure and the presence of negatively charged headgroups was found to increase the thermodynamic stability of LeuT and the unfolding free energy in liposomes (Sanders et al., 2018). The results we show for LeuT also contrasts with other membrane proteins investigated using this IVTT methodology which exhibit greater dependence on the lipid membrane environment provided (Findlay and Booth, 2013; Harris, 2017; Harris et al., 2020). The percentage incorporation of LeuT into proteoliposomes was lower than other transporters such as XylE and LacY, where ≥ 5% improvement in insertion can be obtained through lipid optimization. It was shown that spontaneous insertion of LacY increased from 17.0 ± 2.7% in pure DMPC bilayers, to 25.9 ± 1.6% in pure DOPC bilayers, and then to 32.7 ± 1.7% in 50:50 DOPC:DOPE bilayers, suggesting that an increase in lateral pressure led to an improvement in the insertion yield. Conversely with XylE, spontaneous insertion was lowest in pure DOPC liposomes. Insertion efficiencies were reduced as lateral pressure was introduced by the addition of DOPC, and the greatest insertion efficiency was in pure DOPG bilayers where a spontaneous insertion of 58.7 ± 2.4% was seen (Harris et al., 2020).

There is a comparative difference between higher insertion yields previously seen with major facilitator superfamily (MFS) transporters, and lower yields seen with LeuT. This may be due to an increased propensity for aggregation during insertion linked to the complexity in LeuT conformation and the knotted topology (Harris, 2017; Harris and Booth, 2019). The lack of improvement of insertion efficiencies through lipid optimization may be due to the complex structure of LeuT hindering insertion. In addition to this, LeuT is derived from eubacterium whereas the other transporters previously investigated are integral membrane proteins found in *E. coli*. The native membrane conditions required by such proteins are thus inherently different and we are limited further by the complexity in simulating a near-native environment for LeuT. More is known about the lipid architectures of *E. coli*, and much less about the lipid species and arrangements in the eubacterium *A. aeolicus*.

Further investigations into function would be required to investigate the functionality of cell-free synthesized and spontaneously incorporated protein. The low yields obtained for LeuT when synthesized in cell-free IVTT systems mean that functional assays are not viable methods to probe folding and activity. With yields of ≤ 0.7 μg (PURExpress®) or ≤ 2.3 μg (EXPRESSway™) per reaction of purified LeuT proteoliposomes, it was not feasible to calculate protein activity using the functional assay as previously devised for LeuT where at least 40 μg of protein was reconstituted into liposomes for each assay (Sanders et al., 2018). Despite this, previous work with other membrane proteins such as GlpG, DsbB and LacY has shown that functional protein can be synthesized in cell-free systems using our methodologies (Findlay et al., 2016; Harris, 2017). Radiolabeled gels or western blot analysis can also be used to qualitatively ascertain the quality, purity and overall proportion of spontaneously inserted protein. Our previous work has shown that protein can be considered to be folded, and therefore likely to be functional, when incorporated into proteoliposomes, present in the top fraction on a gel after sucrose gradient purification (Harris, 2017).

Low yields of protein synthesised in IVTT are incompatible with our method of quantifying insertion efficiencies using LSC counts, as these cannot distinguish above background (**Supplementary Table S2**). In Expressway™, low amounts of inserted protein were recovered in sucrose gradient fractions with cardiolipin containing liposomes. In some cases, as much as ~95% of the protein is lost. The quality of some CL samples with very low protein recovery meant that the data could not be compared, and therefore for our analysis we used a cut-off of (80%) recovered protein. This is highlighted by the negative correlation seen with high initial total protein yields, and low protein yields recovered after gradient purification in EXPRESSway™ (**Supplementary Figure S4**), with liposomes containing cardiolipin, in particular $CL_{E.\ coli}$ lipid species. This effect is not observed with cardiolipin containing liposomes in the PURExpress® system so is a result of an interaction between the liposomes and the reaction components (**Supplementary Figure S5**).

In EXPRESSway™, protein yields tend to be higher, possibly as a result of larger reaction volumes. However, because the yield of protein recovered in the gradient after purification remains consistent across both IVTT systems, it shows that high initial yields do not always equate to more inserted protein being produced. IVTT systems still prove to be useful methodologies to probe protein insertion into liposomes in a range of lipid compositions (Cheng and Bahar, 2019; Chong, 2014; Collinson, 2019; Harris and Booth, 2017; Quick et al., 2009).

LeuT Lipid Dependency

Liposomes comprising DO lipids enabled us to probe the various effects lipids can have on the synthetic lipid bilayer, and to measure what effect this has on LeuT insertion efficiency. For example, DOPC lipids assemble naturally into bilayers, and DOPE lipids do not, instead forming non-lamellar structures. Using DOPC as a standard for comparison, this lipid species has a neutral headgroup, unsaturated fatty acid chains and forms fluid

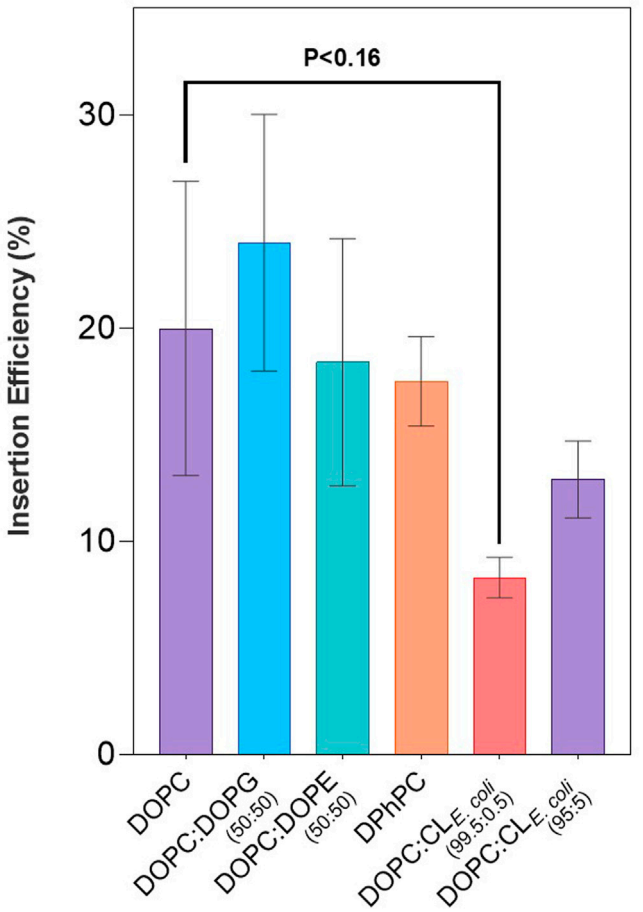

FIGURE 2 | LeuT expressed in PURExpress® IVTT systems in the presence of liposomes comprising various lipid compositions as presented in **Table 1** and **Table 2**. Spontaneously inserted protein was quantified using LSC counting of Methionine, L-[^{35}S] incorporated into LeuT. Insertion efficiency is represented as a percentage of protein in the top fraction over the total yield of protein synthesized. Highlighted here are the results of lipid optimization on LeuT spontaneous insertion efficiencies, comparing various lipid species derived from DO, DPh and Cardiolipin liposome compositions. Errors presented are SEM calculated from ≥3 repeats.

bilayers. Introducing DOPE into a bilayer of DOPC is known to increase the outward lateral chain pressure, and to reduce the laterally exerted pressure in the headgroup region to create bilayers that show an increase in activation energy associated with insertion of a protein helix across a bilayer (Lorch and Booth, 2004). Addition of DOPG, a lipid species with a negatively charged headgroup introduces charge to the bilayer without significantly impacting bilayer fluidity or lateral chain pressure. Such manipulations of bilayer properties were hypothesized to affect the spontaneous insertion of LeuT, and yet we find little dependence of insertion yield on lipid composition when either DOPG or DOPE are introduced into the bilayer (**Figure 2**).

DPh lipids were used to provide bilayers with nearer-native properties to the *A. aeolicus* eubacterium. In these lipid conditions, low yields and an absence of improvement for insertion efficiency was seen. Although DPh branched lipids have a shorter fatty acid chain tail length, the thickness of bilayer produced is comparable to that of DO lipid bilayers (Tristram-Nagle et al., 2010; Kučerka et al., 2011). DOPC and DPhPC bilayers yielded comparable percentage insertion of LeuT (**Figure 2**). In DPhPG, the average initial total protein yield was significantly lower than yields seen in other DPh lipid mixes suggesting inhibition of protein expression when using pure DPhPG. A lack of lipid dependency is further illustrated by LeuT insertion into IMVs, where no improvement was present. The 2.7 µg of total protein in this condition (**Table 1**) is comparatively low to other total protein yields in Expressway™ (**Table 3**), even when we consider that these LSC counts correspond to both spontaneously inserted LeuT as well as other IMV components.

In PURExpress®, addition of cardiolipin species hindered LeuT insertion (**Table 2**). Comparing pure DOPC lipid bilayers to liposomes comprised of DOPC and either 0.5% or 5.5% $CL_{E.\ coli}$, there is a decrease in LeuT insertion efficiency (**Figure 2**). Anionic phospholipids, such as CL, are understood to have a higher tendency to aggregate within IVTT buffers (Kuruma and Ueda, 2015), which is likely to increase the amount of protein lost during purification. With 0.5 and 5.5% concentrations of CL, the direct propensity for aggregation on insertion efficiency is likely to be minimal in PURExpress®. It would be more reasonable to suggest that the result seen with certain species of CL show that CL is less favored for insertion by LeuT. We would expect to see a marked decrease in insertion in liposome conditions containing 5.5% CL when compared with 0.5% CL if this was the case. $CL_{E.\ coli}$ comprises a mix of various CL species, containing only 14% $CL_{18:1}$. If insertion is less negatively affected when this lipid is present than when other CL species in the natural CL extract are present, this may account for the increase in insertion efficiency between 0.5 and 5.5% $CL_{E.\ coli}$, as more $CL_{18:1}$ would be present in the latter liposome composition.

In the natural $CL_{E.\ coli}$ extract the general alkyl chain length of fatty acid tails is ≤ 19 carbons, with the most prevalent CL species being 16:0 at 33% and cyclo17:0 at 27%. Purified 16:0 CL ($CL_{16:0}$) was tested in EXPRESSway™ at 0.5 and 5.5% concentrations with and without SecYEG, but there was poor proteoliposome recovery after purification (**Supplementary Table S7**), as seen with other $CL_{E.\ coli}$ IVTT reactions. These low recovery yields meant that LeuT insertion could not be reliably compared to the other samples in EXPRESSway™. An increase in sample loss during purification was a feature of all liposome reactions using this IVTT kit, however the type of CL present had some impact, with $CL_{18:1}$ least affected. As cardiolipin is essential to the function of many membrane proteins, including the translocon (Collinson, 2019; Ryabichko et al., 2020), it is not always possible to do without it entirely. Where required, optimizing CL type to reaction conditions can help reproducibility.

SecYEG Effects on LeuT Insertion

Our previous work utilizing IVTT for the synthesis of membrane proteins has focused on spontaneous insertion in the absence of the

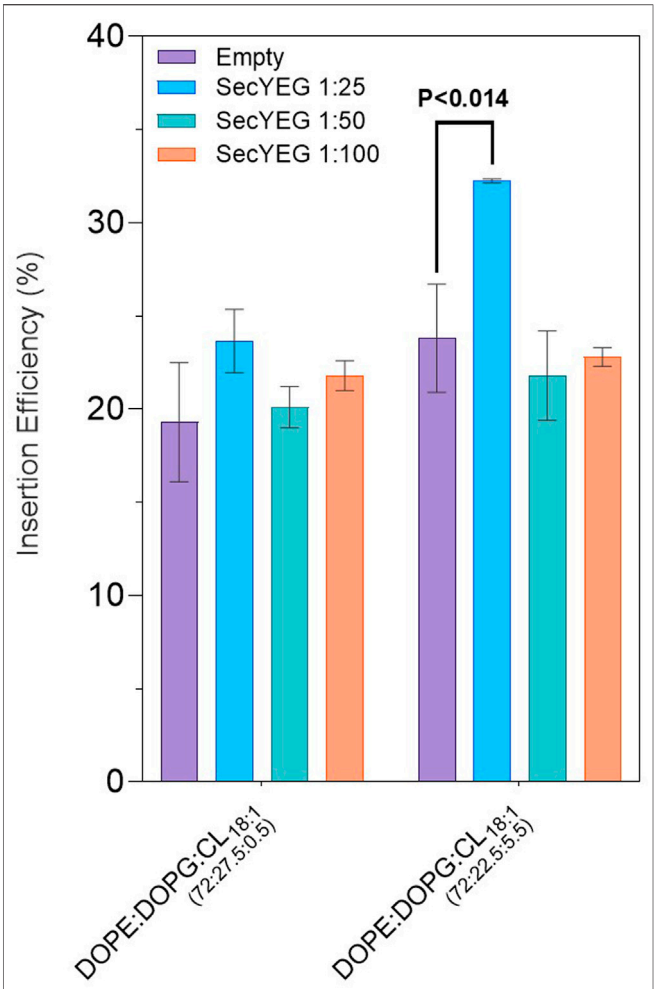

FIGURE 3 | LeuT expression in EXPRESSway™ IVTT systems with SecYEG reconstituted liposomes, as presented in **Table 3** and **Table 4**. $CL_{18:1}$ was added into DOPE:DOPC lipid mixes at either 0.5 or 5.5% concentrations. In empty conditions, SecYEG was absent. In SecYEG conditions, SecYEG was reconstituted at a 1 in 25, 1 in 50, or 1 in 100 (w/w) protein: lipid concentration. Errors presented are SEM calculated from ≥2 repeats for 1 in 25 and 1 in 100 SecYEG conditions, and from ≥5 repeats for all other conditions.

translocon machinery. We were interested in whether insertion could be improved above that of bilayer manipulations, through the reconstitution of SecYEG into liposomes supplemented into cell-free IVTT systems. Reconstitution of SecYEG for investigating the effect of the translocon on LeuT insertion needed to strike a balance between a high enough concentration to yield an effect, whilst also leaving enough surface lipid so as not to restrict incorporation *in vitro*.

Initial experiments with SecYEG showed no improvement in the insertion efficiency of LeuT during IVTT. The question this poses is thus; does the presence of SecYEG directly influence or inhibit LeuT incorporation into liposomes, or does the presence of SecYEG induce other effects which make the liposomes more or less suitable for spontaneous incorporation? This would equally remain a point of contention if the results showed an improvement in LeuT insertion. Although SecYEG is present in our membrane mimics, we cannot conclude that LeuT insertion is being facilitated *in vitro* and indeed using this protein conducting channel for insertion. Incorporation may still occur spontaneously, avoiding the translocon altogether. It may be that reconstituted SecYEG prompts a change in the surrounding lipids, affecting the fluidity and or curvature of the liposome lipid bilayer, which in turn may be behind any observed changes to the final percentage insertion of LeuT. Although this is less likely as LeuT shows little lipid dependency. Another important point to address would be that SecYEG is part of the *E. coli* translocon machinery, and is thus non-native to the eubacterium *A. aeolicus*, even as eubacterial proteins are transported through a homologous complex (Trueman et al., 2012).

Our results showed that higher concentrations of reconstituted SecYEG (1 in 25 w/w protein: lipid) in some lipid conditions improved insertion. We highlight that 5.5% $CL_{18:1}$ yielded the best improvement in LeuT insertion when the SecYEG translocon was present at the highest protein: lipid ratio investigated, where we saw the highest insertion efficiency for LeuT at 32.3 ± 0.1% (**Figure 3**) (**Table 4**). All other concentrations of SecYEG in both cardiolipin species lipid mixes showed no improvement in LeuT insertion, and in $CL_{E.\ coli}$, spontaneous insertion appeared hindered by the presence of SecYEG (**Table 3**). Is the effect of SecYEG on insertion concentration dependent? When a certain concentration of SecYEG is present, is LeuT more efficiently and effectively incorporated into proteoliposomes, or, does having more or less SecYEG per liposome alter conditions for bilayer insertion? Any lipid effects instigated by the presence of SecYEG could change when variable amounts of SecYEG is reconstituted per liposome, which would require further detailed study.

CONCLUSION

We have shown that it is possible to use an *in vitro* cell-free approach for studies on the co-translational insertion of LeuT, which extends the applicability of this cell-free method to an important membrane protein transporter class. The resulting yields of insertion of LeuT are however lower than those previously reported for other membrane proteins. This may be due to the lipid composition being suboptimal and/or the knotted structure of LeuT. LeuT is a topologically complex protein that does not definitively require SecYEG for incorporation into liposomes under the conditions that were probed here. It is possible that the thermodynamics of insertion are as such that if a membranous environment is present, regardless of a complex topology, insertion is more favorable than aggregation in solution.

It appears that LeuT is also resilient to perturbations in the lipid composition, although further studies into a wider range of lipid compositions may start to reveal a dependence. Our results showed that co-translational insertion efficiency could not be improved above 24 ± 6% regardless of the lipid composition in the liposomes tested. The low insertion efficiencies can equally be explained by the minimal cell-free *in vitro* conditions not being optimized for protein insertion. We show that for DO and DPh lipids the

insertion of LeuT remains consistent, and we see a general decrease in these efficiencies when CL is added at the concentrations we tested. In addition to this we show that the presence of the bacterial translocon did not consistently improve the insertion efficiency of LeuT, a result that was unexpected owing to the complex topological nature of this transporter. We can however increase the insertion efficiency to 32.3 ± 0.1% with the addition of SecYEG, above what can be achieved with lipid optimization. This builds upon previous work investigating the lipid dependency of other transporters insertion in IVTT cell-free, and contrasts with this former work which showed a high dependency on lipid environment (Harris et al., 2020; Harris, 2017; Harris and Booth, 2012; Harris and Booth, 2019).

Insertion was less favored when we included nearer-native lipids into our liposome membrane mimics. As so little is known about the lipid species and compositions of eubacterial membranes, our synthetic mimics are unlikely to be entirely representative to the native membrane environment of *A. aeolicus*. The membrane lipid architectures and structures favored by LeuT may be different to those tested here, or LeuT may have less dependance on an optimal lipid composition for insertion and folding. Lipids are known to play key roles in modulating protein insertion folding and function and we anticipate that while LeuT inserted is likely to be folded, this folding is likely to be fine-tuned by a lipid environment more native than that tested within the scope of this investigation.

We build upon our previous investigations using cell-free IVTT systems, expanding to include the first such study on a transporter with a topologically complex structure. By finding new avenues in which to probe this protein *in vitro*, we are expanding the toolkits available to investigate the co-translational folding of more complex proteins, adding to the knowledge of how these proteins may fold *in vivo*.

DATA AVAILABILITY STATEMENT

The raw data supporting the conclusion of this article will be made available by the authors, without undue reservation.

AUTHOR CONTRIBUTIONS

Experiments were conceived and devised by PB, LB, NH, and HF. All experiments presented and data analyses were completed by LB. This manuscript was written and revised by all authors, and all authors read and approved the final article.

FUNDING

We acknowledge funding from the Wellcome Trust Investigator Award 214259/Z/18/Z to PB, and LB acknowledges financial support from King's College, London.

SUPPLEMENTARY MATERIAL

The Supplementary Material for this article can be found online at: https://www.frontiersin.org/articles/10.3389/fmolb.2022.795212/full#supplementary-material

REFERENCES

Akopian, D., Shen, K., Zhang, X., and Shan, S. O. (2013). Signal Recognition Particle: An Essential Protein-Targeting Machine. *Annu. Rev. Biochem.* 82, 693. doi:10.1146/annurev-biochem-072711-164732

Allen, S. J., Curran, A. R., Templer, R. H., Meijberg, W., and Booth, P. J. (2004). Controlling the Folding Efficiency of an Integral Membrane Protein. *J. Mol. Biol.* 42, 1293. doi:10.1016/j.jmb.2004.07.041

Allen, S. J., Curran, A. R., Templer, R. H., Meijberg, W., and Booth, P. J. (2004). Folding Kinetics of an α Helical Membrane Protein in Phospholipid Bilayer Vesicles. *J. Mol. Biol.* 42, 1279. doi:10.1016/j.jmb.2004.07.040

Ando, M. (2016). Liposome Chaperon in Cell-free Membrane Protein Synthesis: One-step Preparation of KcsA-Integrated Liposomes and Electrophysiological Analysis by the Planar Bilayer Method. *Biomater. Sci.* 4, 258. doi:10.1039/c5bm00285k

Bogdanov, M., and Dowhan, W. (1999). Lipid-assisted Protein Folding. *J. Biol. Chem.* 24, 274. doi:10.1074/jbc.274.52.36827

Bogdanov, M., Dowhan, W., and Vitrac, H. (2014). Lipids and Topological Rules Governing Membrane Protein Assembly. *Biochim. Biophys. Acta - Mol. Cel Res.* 1843, 1875. doi:10.1016/j.bbamcr.2013.12.007

Bogdanov, M., Mileykovskaya, E., and Dowhan, W. (2008). Lipids in the Assembly of Membrane Proteins and Organization of Protein Supercomplexes: Implications for Lipid-Linked Disorders. *Subcell. Biochem.* doi:10.1007/978-1-4020-8831-5_8

Booth, P. J., and Curnow, P. (2009). Folding Scene Investigation: Membrane Proteins. *Curr. Opin. Struct. Biol.* 19, 8–13. doi:10.1016/j.sbi.2008.12.005

Booth, P. J., Templer, R. H., Meijberg, W., Allen, S. J., Curran, A. R., and Lorch, M. (2001). In VitroStudies of Membrane Protein Folding. *Crit. Rev. Biochem. Mol. Biol.* 36, 501–603. doi:10.1080/20014091074246

Booth, P. J. (2003). The Trials and Tribulations of Membrane Protein Folding *In Vitro*. *Biochim. Biophys. Acta - Biomembranes.* doi:10.1016/S0005-2736(02)00714-9

Booth, P. (2005). Sane in the Membrane: Designing Systems to Modulate Membrane Proteins. *Curr. Opin. Struct. Biol.* 15, 435–440. doi:10.1016/j.sbi.2005.06.002

Bowie, J. U. (2005). Solving the Membrane Protein Folding Problem. *Nature* 438, 581–589. doi:10.1038/nature04395

Braakman, R., and Smith, E. (2014). Metabolic Evolution of a Deep-Branching Hyperthermophilic Chemoautotrophic Bacterium. *PLoS One* 9, e87950. doi:10.1371/journal.pone.0087950

Cappuccio, J. A., Hinz, A., and Kuhn, A. (2009). Cell-free Expression for Nanolipoprotein Particles: Building a High-Throughput Membrane Protein Solubility Platform. *Methods Mol. Biol.* doi:10.1007/978-1-59745-196-3_18

Carlson, E. D., Gan, R., Hodgman, C. E., and Jewett, M. C. (2012). Cell-free Protein Synthesis: Applications Come of Age. *Biotechnol. Adv.* 30, 1185. doi:10.1016/j.biotechadv.2011.09.016

Cheng, M. H., and Bahar, I. (2019). Monoamine Transporters: Structure, Intrinsic Dynamics and Allosteric Regulation. *Nat. Struct. Mol. Biol.* 26, 545. doi:10.1038/s41594-019-0253-7

Chong, S. (2014). Overview of Cell-free Protein Synthesis: Historic Landmarks, Commercial Systems, and Expanding Applications. *Curr. Protoc. Mol. Biol.* 108, 16. doi:10.1002/0471142727.mb1630s108

Chwastyk, M., and Cieplak, M. (2015). Cotranslational Folding of Deeply Knotted Proteins. *J. Phys. Condensed Matter* 30, 1185. doi:10.1088/0953-8984/27/35/354105

Collinson, I., Breiton, C., and Duong, F. (2001). Projection Structure and Oligomeric Properties of a Bacterial Core Protein Translocase. *EMBO J.* 20, 2462. doi:10.1093/emboj/20.10.2462

Collinson, I. (2019). The Dynamic ATP-Driven Mechanism of Bacterial Protein Translocation and the Critical Role of Phospholipids. *Front. Microbiol.* 19, 1217. doi:10.3389/fmicb.2019.01217

Corey, R. A., Vickery, O. N., Sansom, M. S. P., and Stansfeld, P. J. (2019). Insights into Membrane Protein-Lipid Interactions from Free Energy Calculations. *J. Chem. Theor. Comput.* 15, 5727. doi:10.1021/acs.jctc.9b00548

Cymer, F., Von Heijne, G., and White, S. H. (2015). Mechanisms of Integral Membrane Protein Insertion and Folding. *J. Mol. Biol.* 427, 999. doi:10.1016/j.jmb.2014.09.014

Dabrowski-Tumanski, P., Piejko, M., Niewieczerzal, S., Stasiak, A., and Sulkowska, J. I. (2018). Protein Knotting by Active Threading of Nascent Polypeptide Chain Exiting from the Ribosome Exit Channel. *J. Phys. Chem. B* 122, 11616. doi:10.1021/acs.jpcb.8b07634

Deckert, G., Warren, P. V., and Gassterland, A. (1998). The Complete Genome of the Hyperthermophilic Bacterium Aquifex Aeolicus. *Nature* 392, 353. doi:10.1038/32831

Doerr, A. (2009). Membrane Protein Structures. *Nat. Methods* 6, 35. doi:10.1038/nmeth.f.240

Dopp, J. L., Jo, Y. R., and Reuel, N. F. (2019). Methods to Reduce Variability in E. Coli-Based Cell-free Protein Expression Experiments. *Synth. Syst. Biotechnol.* 4, 204. doi:10.1016/j.synbio.2019.10.003

Dopp, J. L., and Reuel, N. F. (2018). Process Optimization for Scalable *E. coli* Extract Preparation for Cell-free Protein Synthesis. *Biochem. Eng. J.* doi:10.1016/j.bej.2018.06.021

Dörr, J. M. (2016). The Styrene–Maleic Acid Copolymer: a Versatile Tool in Membrane Research. *Eur. Biophys. J.* 345, 3. doi:10.1007/s00249-015-1093-y

Eaglesfield, R., Madsen, M. A., Sanyal, S., Reboud, J., and Amtmann, A. (2021). Cotranslational Recruitment of Ribosomes in Protocells Recreates a Translocon-independent Mechanism of Proteorhodopsin Biogenesis. *iScience* 24, 102429. doi:10.1016/j.isci.2021.102429

Eichler, J. (2019). Halobacterium Salinarum. *Trends Microbiol.* 27, 651. doi:10.1016/j.tim.2019.02.005

Especial, J., Nunes, A., Rey, A., and Faísca, P. F. N. (2019). Hydrophobic Confinement Modulates thermal Stability and Assists Knotting in the Folding of Tangled Proteins. *Phys. Chem. Chem. Phys.* 21, 11764. doi:10.1039/c9cp01701a

Fagerberg, L., Jonasson, K., Von Heijne, G., Uhlén, M., and Berglund, L. (2010). Prediction of the Human Membrane Proteome. *Proteomics*, 10, 1141–1149. doi:10.1002/pmic.200900258

Faísca, P. F. N. (2015). Knotted Proteins: A Tangled Tale of Structural Biology. *Comput. Struct. Biotechnol. J.* 13, 459. doi:10.1016/j.csbj.2015.08.003

Findlay, H. E., and Booth, P. J. (2013). Folding Alpha-Helical Membrane Proteins into Liposomes *In Vitro* and Determination of Secondary Structure. *Methods Mol. Biol.*, 117–124. doi:10.1007/978-1-62703-583-5_6

Findlay, H. E., and Booth, P. J. (2017). The Folding, Stability and Function of Lactose Permease Differ in Their Dependence on Bilayer Lipid Composition. *Sci. Rep.* 7, 13056. doi:10.1038/s41598-017-13290-7

Findlay, H., Harris, N., and Booth, P. (2016). *In Vitro* synthesis of a Major Facilitator Transporter for Specific Active Transport across Droplet Interface Bilayers. *Sci. Rep.* 6, 39349. doi:10.1038/srep39349

Gold, V. A. M., Robson, A., Clarke, A. R., and Collinson, I. (2007). Allosteric Regulation of SecA: Magnesium-Mediated Control of Conformation and Activity. *J. Biol. Chem.* 282, 17474. doi:10.1074/jbc.M702066200

Gotfryd, K., Bosen, T., and Mortensen, J. (2020). X-ray Structure of LeuT in an Inward-Facing Occluded Conformation Reveals Mechanism of Substrate Release. *Nat. Commun.* 11, 1005. doi:10.1038/s41467-020-14735-w

Gregorio, N. E., Levine, M. Z., and Oza, J. P. (2019). A User's Guide to Cell-free Protein Synthesis. *Methods Protoc.* 2, 24. doi:10.3390/mps2010024

Gubellini, F., Verdon, G., Karpowich, N. K., Luff, J. D., Boël, G., Gauthier, N., et al. (2011). Physiological Response to Membrane Protein Overexpression in *E. coli*. *Mol. Cell Proteomics* 10, M111.007930. doi:10.1074/mcp.M111.007930

Gupta, K., Donland, J. A. C., and Hopper, J. T. C. (2017). The Role of Interfacial Lipids in Stabilizing Membrane Protein Oligomers. *Nature* 541, 421. doi:10.1038/nature20820

Harris, N. J., and Booth, P. J. (2017). Investigating the Insertion and Folding of Membrane Transporters into Lipid Bilayers Using a Cell Free Expression System. *Biophys. J.* 112, p204a.

Harris, N. J., and Booth, P. J. (2019). Co-Translational Protein Folding in Lipid Membranes. *Trends Biochem. Sci.* 44, 729. doi:10.1016/j.tibs.2019.05.002

Harris, N. J., and Booth, P. J. (2012). Folding and Stability of Membrane Transport Proteins *In Vitro*. *Biochim. Biophys. Acta (Bba) - Biomembranes* 1818, 1055–1066. doi:10.1016/j.bbamem.2011.11.006

Harris, N. J., and Charalambous, K. (2018). Lipids Modulate the Insertion and Folding of Alpha Helical Membrane Proteins. *Biochem. Soc. Trans.* 46, 1355. doi:10.1042/BST20170424

Harris, N. J., Pellowe, G. A., and Booth, P. J. (2020). Cell-free Expression Tools to Study Co-translational Folding of Alpha Helical Membrane Transporters. *Sci. Rep.* 10. doi:10.1038/s41598-020-66097-4

Harris, N. J. (2017). Structure Formation during Translocon-Unassisted Co-translational Membrane Protein Folding. *Sci. Rep.* 7, 8021. doi:10.1038/s41598-017-08522-9

Hingorani, K. S., and Gierasch, L. M. (2014). Comparing Protein Folding *In Vitro* and *In Vivo*: Foldability Meets the Fitness challenge. *Curr. Opin. Struct. Biol.* 24, 81–90. doi:10.1016/j.sbi.2013.11.007

Hong, W. C., and Amara, S. G. (2010). Membrane Cholesterol Modulates the Outward Facing Conformation of the Dopamine Transporter and Alters Cocaine Binding. *J. Biol. Chem.* 285, 32616. doi:10.1074/jbc.M110.150565

Hoyo, J., Torrent-Burgués, J., and Tzanov, T. (2020). Lipid-lipid Interactions of escherichia Coli Mimetic Inner Membrane at Human Physiological Temperature. *Gen. Physiol. Biophys.* doi:10.4149/gpb_2019063

Hung, W. C., Chen, F. Y., and Huang, H. W. (2000). Order-disorder Transition in Bilayers of Diphytanoyl Phosphatidylcholine. *Biochim. Biophys. Acta - Biomembr.* doi:10.1016/S0005-2736(00)00221-2

Jain, S., Caforio, A., and Driessen, A. J. M. (2014). Biosynthesis of Archaeal Membrane Ether Lipids. *Front. Microbiol.* 5, 641. doi:10.3389/fmicb.2014.00641

Jarmolinska, A. I., Perlinska, A. P., and Runkel, R. (2019). Proteins' Knotty Problems. *J. Mol. Biol.* 431, 244. doi:10.1016/j.jmb.2018.10.012

Joseph, D., Pidathala, S., Mallela, A. K., and Penmatsa, A. (2019). Structure and Gating Dynamics of Na+/Cl– Coupled Neurotransmitter Transporters. *Front. Mol. Biosciences* 6, 80. doi:10.3389/fmolb.2019.00080

Junge, F. (2011). Advances in Cell-free Protein Synthesis for the Functional and Structural Analysis of Membrane Proteins. *N. Biotechnol.* 28, 262. doi:10.1016/j.nbt.2010.07.002

Kalmbach, R., Chizhuo, I., and Schumacher, M. C. (2007). Functional Cell-free Synthesis of a Seven Helix Membrane Protein: *In Situ* Insertion of Bacteriorhodopsin into Liposomes. *J. Mol. Biol.* 371, 689. doi:10.1016/j.jmb.2007.05.087

Khambhati, K. (2019). Exploring the Potential of Cell-free Protein Synthesis for Extending the Abilities of Biological Systems. *Front. Bioeng. Biotechnol.* 28, 262. doi:10.3389/fbioe.2019.00248

Khelashvili, G., and Weinstein, H. (2015). Functional Mechanisms of Neurotransmitter Transporters Regulated by Lipid-Protein Interactions of Their Terminal Loops. *Biochim. Biophys. Acta - Biomembranes* 1848, 1765. doi:10.1016/j.bbamem.2015.03.025

King, N. P., Yeates, E. O., and Yeates, T. O. (2007). Identification of Rare Slipknots in Proteins and Their Implications for Stability and Folding. *J. Mol. Biol.* 373, 153. doi:10.1016/j.jmb.2007.07.042

Koga, Y., and Morii, H. (2007). Biosynthesis of Ether-type Polar Lipids in Archaea and Evolutionary Considerations. *Microbiol. Mol. Biol. Rev.* 28, 262. doi:10.1128/mmbr.00033-06

Koga, Y. (2012). Thermal Adaptation of the Archaeal and Bacterial Lipid Membranes. *Archaea* 2012, 789652. doi:10.1155/2012/789652

Komar, A. A. (2018). Unraveling Co-translational Protein Folding: Concepts and Methods. *Methods* 137, 71. doi:10.1016/j.ymeth.2017.11.007

Krishnamurthy, H., Piscitelli, C. L., and Gouaux, E. (2009). Unlocking the Molecular Secrets of Sodium-Coupled Transporters. *Nature* 459, 347. doi:10.1038/nature08143

Kučerka, N., Nieh, M. P., and Katsaras, J. (2011). Fluid Phase Lipid Areas and Bilayer Thicknesses of Commonly Used Phosphatidylcholines as a Function of Temperature. *Biochim. Biophys. Acta - Biomembr.* 1808, 2761. doi:10.1016/j.bbamem.2011.07.022

Kuruma, Y., and Ueda, T. (2015). The PURE System for the Cell-free Synthesis of Membrane Proteins. *Nat. Protoc.* 10, 1238. doi:10.1038/nprot.2015.082

Kwon, Y. C., and Jewett, M. C. (2015). High-throughput Preparation Methods of Crude Extract for Robust Cell-free Protein Synthesis. *Sci. Rep.* 5, 8663. doi:10.1038/srep08663

Lange, B. M., Rujan, T., Martin, W., and Croteau, R. (2000). Isoprenoid Biosynthesis: The Evolution of Two Ancient and Distinct Pathways across Genomes. *Proc. Natl. Acad. Sci. U. S. A.* 97, 13172. doi:10.1073/pnas.240454797

Lee, A. G. (2004). How Lipids Affect the Activities of Integral Membrane Proteins. *Biochim. Biophys. Acta - Biomembranes* 1666, 62. doi:10.1016/j.bbamem.2004.05.012

Lee, A. G. (2005). How Lipids and Proteins Interact in a Membrane: A Molecular Approach. *Mol. BioSystems* 1, 203. doi:10.1039/b504527d

Lim, N. C. H., and Jackson, S. E. (2015b). Mechanistic Insights into the Folding of Knotted Proteins *In Vitro* and *In Vivo*. *J. Mol. Biol.* 427, 248. doi:10.1016/j.jmb.2014.09.007

Lim, N. C. H., and Jackson, S. E. (2015a). Molecular Knots in Biology and Chemistry. *J. Phys. Condens. Matter*. doi:10.1088/0953-8984/27/35/354101

Liutkute, M., Samatova, E., and Rodnina, M. V. (2020). Cotranslational Folding of Proteins on the Ribosome. *Biomolecules* 10, 97. doi:10.3390/biom10010097

Long, A. R., O'Brien, C. C., and Alder, N. N. (2012). The Cell-free Integration of a Polytopic Mitochondrial Membrane Protein into Liposomes Occurs Cotranslationally and in a Lipid-dependent Manner. *PLoS One* 7, e46332. doi:10.1371/journal.pone.0046332

Lorch, M., and Booth, P. J. (2004). Insertion Kinetics of a Denatured α Helical Membrane Protein into Phospholipid Bilayer Vesicles. *J. Mol. Biol.* 344, 1109. doi:10.1016/j.jmb.2004.09.090

Lunn, C. A. (2010). Membrane Proteins as Drug Targets. *Preface. Prog. Mol. Biol. Transl. Sci.* doi:10.1016/S1877-1173(10)91012-0

Macias, L. A., Feider, C. L., Eberlin, L. S., and Brodbelt, J. S. (2019). Hybrid 193 Nm Ultraviolet Photodissociation Mass Spectrometry Localizes Cardiolipin Unsaturations. *Anal. Chem.* 91, 12509. doi:10.1021/acs.analchem.9b03278

Magnani, F., Tatell, C. G., Wynne, S., Williams, C., and Haase, J. (2004). Partitioning of the Serotonin Transporter into Lipid Microdomains Modulates Transport of Serotonin. *J. Biol. Chem.* 279, 38770. doi:10.1074/jbc.M400831200

Marinko, J. T., Huang, H., Penn, W. D., Capra, J. A., Schlebach, J. P., and Sanders, C. R. (2019). Folding and Misfolding of Human Membrane Proteins in Health and Disease: From Single Molecules to Cellular Proteostasis. *Chem. Rev.* 119, 5537–5606. doi:10.1021/acs.chemrev.8b00532

Markwell, M. A. K., Haas, S. M., Bieber, L. L., and Tolbert, N. E. (1978). A Modification of the Lowry Procedure to Simplify Protein Determination in Membrane and Lipoprotein Samples. *Anal. Biochem.* doi:10.1016/0003-2697(78)90586-9

Matsubayashi, H., Kuruma, Y., and Ueda, T. (2014q). Cell-Free Synthesis of SecYEG Translocon as the Fundamental Protein Transport Machinery. *Orig. Life Evol. Biosph.* 44, 331. doi:10.1007/s11084-014-9389-y

Matsubayashi, H., Kuruma, Y., and Ueda, T. (2014b). Vitro Synthesis of the *E. coli* Sec Translocon from DNA. *Angew. Chem. - Int. Ed.* 34534, 7535. doi:10.1002/anie.201403929

Meijberg, W., and Booth, P. J. (2002). The Activation Energy for Insertion of Transmembrane α-helices Is Dependent on Membrane Composition. *J. Mol. Biol.* doi:10.1016/S0022-2836(02)00342-X

Mercier, E., Wang, X., Maiti, M., Wintermeyer, W., and Rodnina, M. V. (2021). Lateral Gate Dynamics of the Bacterial Translocon during Cotranslational Membrane Protein Insertion. *Proc. Natl. Acad. Sci. U. S. A.* 118, e2100474118. doi:10.1073/pnas.2100474118

Möller, I. R., Silvacka, M., and Neilson, A. K. (2019). Conformational Dynamics of the Human Serotonin Transporter during Substrate and Drug Binding. *Nat. Commun.* 10, 1687. doi:10.1038/s41467-019-09675-z

Navratna, V., and Gouaux, E. (2019). Insights into the Mechanism and Pharmacology of Neurotransmitter Sodium Symporters. *Curr. Opin. Struct. Biol.* 54, 161. doi:10.1016/j.sbi.2019.03.011

Ohta, N., Kato, Y., Watanabe, H., Mori, H., and Matsuura, T. (2016). *In Vitro* membrane Protein Synthesis inside Sec Translocon-Reconstituted Cell-Sized Liposomes. *Sci. Rep.* 6, 36466. doi:10.1038/srep36466

Panov, P. V., Akimov, S. A., and Batishchev, O. V. (2014). Isoprenoid Lipid Chains Increase Membrane Resistance to Pore Formation. *Biochem. Suppl. Ser. A. Membr. Cel Biol.* doi:10.1134/S1990747814050067

Pellowe, G. A., and Booth, P. J. (2019). Structural Insight into Co-translational Membrane Protein Folding. *Biochim. Biophys. Acta - Biomembranes* 1862, 183019. doi:10.1016/j.bbamem.2019.07.007

Phillips, R., Ursell, T., Wiggins, P., and Sens, P. (2009). Emerging Roles for Lipids in Shaping Membrane-Protein Function. *Nature* 459, 379. doi:10.1038/nature08147

Quick, M., Lund Winther, A. M., and Shei, L. (2009). Binding of an Octylglucoside Detergent Molecule in the Second Substrate (S2) Site of LeuT Establishes an Inhibitor-Bound Conformation. *Proc. Natl. Acad. Sci. U. S. A.* 106, 5563. doi:10.1073/pnas.0811322106

Raetz, C. R. H., and Dowhan, W. (1990). Biosynthesis and Function of Phospholipids in *Escherichia coli*. *J. Biol. Chem.* 344, 1109. doi:10.1016/s0021-9258(19)40001-x

Rigaud, J. L., and Lévy, D. (2003). Reconstitution of Membrane Proteins into Liposomes. *Methods Enzymol.* 344, 1109. doi:10.1016/S0076-6879(03)72004-7

Rimon, A., Mondal, R., Friedler, A., and Padan, E. (2019). Cardiolipin Is an Optimal Phospholipid for the Assembly, Stability, and Proper Functionality of the Dimeric Form of NhaA Na+/H+ Antiporter. *Sci. Rep.* 9, 17662. doi:10.1038/s41598-019-54198-8

Ring, G., and Eichler, J. (2001). Characterization of Inverted Membrane Vesicles from the Halophilic Archaeon Haloferax Volcanii. *J. Membr. Biol.* 183, 195. doi:10.1007/s00232-001-0067-4

Robson, A., Gold, V. A. M., Hodson, S., Clarke, A. R., and Collinson, I. (2009). Energy Transduction in Protein Transport and the ATP Hydrolytic Cycle of SecA. *Proc. Natl. Acad. Sci. U. S. A.* 106, 5111. doi:10.1073/pnas.0809592106

Roos, C., Kai, L., and Proverbio, D. (2013). Co-translational Association of Cell-free Expressed Membrane Proteins with Supplied Lipid Bilayers. *Mol. Membr. Biol.* 30, 75. doi:10.3109/09687688.2012.693212

Ryabichko, S., Feraria, V. D. M., and Vitrac, H. (2020). Cardiolipin Is Required *In Vivo* for the Stability of Bacterial Translocon and Optimal Membrane Protein Translocation and Insertion. *Sci. Rep.* 10, 6296. doi:10.1038/s41598-020-63280-5

Sachse, R., Dondapati, S. K., Fenz, S. F., Schmidt, T., and Kubick, S. (2014). Membrane Protein Synthesis in Cell-free Systems: From Bio-Mimetic Systems to Bio-Membranes. *FEBS Lett.* 588, 2774. doi:10.1016/j.febslet.2014.06.007

Sahin-Toth, M., Dunten, R. L., and Kaback, H. R. (1995). Design of a Membrane Protein for Site-specific Proteolysis: Properties of Engineered Factor Xa Protease Sites in the Lactose Permease of *Escherichia coli*. *Biochemistry* 34, 1107. doi:10.1021/bi00004a001

Sanders, M. R., Findlay, H. E., and Booth, P. J. (2018). Lipid Bilayer Composition Modulates the Unfolding Free Energy of a Knotted α-helical Membrane Protein. *Proc. Natl. Acad. Sci. U. S. A.* 115, E1799. doi:10.1073/pnas.1714668115

Saraogi, I., and Shan, S. u. (2014). Co-translational Protein Targeting to the Bacterial Membrane. *Biochim. Biophys. Acta - Mol. Cel Res.* 1843, 1433. doi:10.1016/j.bbamcr.2013.10.013

Schneider, B. (2010). Membrane Protein Expression in Cell-free Systems. *Methods Mol. Biol.* doi:10.1007/978-1-60761-344-2_11

Seddon, A. M. (2008). Phosphatidylglycerol Lipids Enhance Folding of an α Helical Membrane Protein. *J. Mol. Biol.* 380, 548. doi:10.1016/j.jmb.2008.05.001

Serdiuk, T., Steudle, A., Mari, S. A., Manioglu, S., Kaback, H. R., Kuhn, A., et al. (2019). Insertion and Folding Pathways of Single Membrane Proteins Guided by Translocases and Insertases. *Sci. Adv.* 5, eau6824. doi:10.1126/sciadv.aau6824

Shimizu, Y. (2001). Cell-free Translation Reconstituted with Purified Components. *Nat. Biotechnol.* 19, 751. doi:10.1038/90802

Shimizu, Y., Kanamori, T., and Ueda, T. (2005). Protein Synthesis by Pure Translation Systems. *Methods* 36, 299. doi:10.1016/j.ymeth.2005.04.006

Siliakus, M. F., van der Oost, J., and Kengen, S. W. M. (2017). Adaptations of Archaeal and Bacterial Membranes to Variations in Temperature, pH and Pressure. *Extremophiles* 21, 651. doi:10.1007/s00792-017-0939-x

Silverman, A. D., Karim, A. S., and Jewett, M. C. (2020). Cell-free Gene Expression: an Expanded Repertoire of Applications. *Nat. Rev. Genet.* 344, 1109. doi:10.1038/s41576-019-0186-3

Simon, K. S., Pollock, N. L., and Lee, S. C. (2018). Membrane Protein Nanoparticles: The Shape of Things to Come. *Biochem. Soc. Trans.* 46, 1495. doi:10.1042/BST20180139

Singh, S. K., and Pal, A. (2015). "Biophysical Approaches to the Study of LeuT, a Prokaryotic Homolog of Neurotransmitter Sodium Symporters," in *Methods in Enzymology*. doi:10.1016/bs.mie.2015.01.002

Skach, W. R. (2009). Cellular Mechanisms of Membrane Protein Folding. *Nat. Struct. Mol. Biol.* 16, 606–612. doi:10.1038/nsmb.1600

Skach, W. R. (2011). Cellular Mechanisms of Membrane Protein Folding. *FASEB J.* doi:10.1096/fasebj.25.1_supplement.194.2

Sohlenkamp, C., and Geiger, O. (2015). Bacterial Membrane Lipids: Diversity in Structures and Pathways. *FEMS Microbiol. Rev.* 40, 133. doi:10.1093/femsre/fuv008

Sturt, H. F., Summons, R. E., Smith, K., Elvert, M., and Hinrichs, K. U. (2004). Intact Polar Membrane Lipids in Prokaryotes and Sediments Deciphered by High-Performance Liquid Chromatography/electrospray Ionization Multistage Mass Spectrometry - New Biomarkers for Biogeochemistry and Microbial Ecology. *Rapid Commun. Mass. Spectrom.* 18, 617–628. doi:10.1002/rcm.1378

Sułkowska, J. I., Rawdon, E. J., Millett, K. C., Onuchic, J. N., and Stasiak, A. (2012). Conservation of Complex Knotting and Slipknotting Patterns in Proteins. *Proc. Natl. Acad. Sci. U. S. A.* 109, e1715. doi:10.1073/pnas.1205918109

Swartz, J. A. (2001). PURE Approach to Constructive Biology. *Nat. Biotechnol.* 19, 723. doi:10.1038/90773

Takahashi, M. k., Hayes, C. A., and Chapell, J. (2015). Characterizing and Prototyping Genetic Networks with Cell-free Transcription-Translation Reactions. *Methods* 86, 50. doi:10.1016/j.ymeth.2015.05.020

Terada, T., Kusano, S., Matsuda, T., Shirouzu, M., and Yokoyama, S. (2016). *Cell-Free Protein Production for Structural Biology*. doi:10.1007/978-4-431-56030-2_5

Torres, G. E., and Amara, S. G. (2007). Glutamate and Monoamine Transporters: New Visions of Form and Function. *Curr. Opin. Neurobiol.* 17, 304. doi:10.1016/j.conb.2007.05.002

Tristram-Nagle, S., Kim, D. J., and Akunzada, N. (2010). Structure and Water Permeability of Fully Hydrated diphytanoylPC. *Chem. Phys. Lipids* 163, 630. doi:10.1016/j.chemphyslip.2010.04.011

Trueman, S. F., Mandon, E. C., and Gilmore, R. (2012). A Gating Motif in the Translocation Channel Sets the Hydrophobicity Threshold for Signal Sequence Function. *J. Cel Biol.* 199, 907. doi:10.1083/jcb.201207163

Tsuchikawa, H., Ona, T., and Yamagami, M. (2020). Conformation and Orientation of Branched Acyl Chains Responsible for the Physical Stability of Diphytanoylphosphatidylcholine. *Biochemistry* 59, 3929. doi:10.1021/acs.biochem.0c00589

Tuckey, C., Asahara, H., Zhou, Y., and Chong, S. (2014). Protein Synthesis Using a Reconstituted Cell-free System. *Curr. Protoc. Mol. Biol.* 108, 16. doi:10.1002/0471142727.mb1631s108

Van Dalen, A., and De Kruijff, B. (2004). The Role of Lipids in Membrane Insertion and Translocation of Bacterial Proteins. *Biochim. Biophys. Acta - Mol. Cel Res.* 11, 1694. doi:10.1016/j.bbamcr.2004.03.007

van Geest, M., and Lolkema, J. S. (2000). Membrane Topology and Insertion of Membrane Proteins: Search for Topogenic Signals. *Microbiol. Mol. Biol. Rev.* 64, 13. doi:10.1128/mmbr.64.1.13-33.2000

Vauclare, P., Natali, F., Kleman, J. P., Zaccai, G., and Franzetti, B. (2020). Surviving Salt Fluctuations: Stress and Recovery in Halobacterium Salinarum, an Extreme Halophilic Archaeon. *Sci. Rep.* 10, 3298. doi:10.1038/s41598-020-59681-1

Veenendaal, A. K. J., Van Der Does, C., and Driessen, A. J. M. (2004). The Protein-Conducting Channel SecYEG. *Biochim. Biophys. Acta - Mol. Cel Res.* 1694, 81. doi:10.1016/j.bbamcr.2004.02.009

Vitrac, H., Maclean, D. M., and Karlsteadt, A. (2017). Dynamic Lipid-dependent Modulation of Protein Topology by post-translational Phosphorylation. *J. Biol. Chem.* 2292, 1613. doi:10.1074/jbc.M116.765719

Wagner, S., Baars, L., Ytterberg, A. J., Klussmeier, A., Wagner, C. S., Nord, O., et al. (2007). Consequences of Membrane Protein Overexpression in *Escherichia coli*. *Mol. Cell Proteomics* 6, 1527–1550. doi:10.1074/mcp.M600431-MCP200

Xu, Y., Li, S., and Yan, Z. (2018). Stabilizing Effect of Inherent Knots on Proteins Revealed by Molecular Dynamics Simulations. *Biophys. J.* 115, 1681. doi:10.1016/j.bpj.2018.09.015

Yamashita, A., Singh, S. K., Kawate, T., Jin, Y., and Gouaux, E. (2005). Crystal Structure of a Bacterial Homologue of Na+/Cl --dependent Neurotransmitter Transporters. *Nature* 437, 215. doi:10.1038/nature03978

Yeates, T. O., Norcross, T. S., and King, N. P. (2007). Knotted and Topologically Complex Proteins as Models for Studying Folding and Stability. *Curr. Opin. Chem. Biol.* 11, 595. doi:10.1016/j.cbpa.2007.10.002

Zemella, A., Thoring, L., Hoffmeister, C., and Kubick, S. (2015). Cell-Free Protein Synthesis: Pros and Cons of Prokaryotic and Eukaryotic Systems. *ChemBioChem* 16, 2420. doi:10.1002/cbic.201500340

Conflict of Interest: The authors declare that the research was conducted in the absence of any commercial or financial relationships that could be construed as a potential conflict of interest.

Publisher's Note: All claims expressed in this article are solely those of the authors and do not necessarily represent those of their affiliated organizations, or those of the publisher, the editors, and the reviewers. Any product that may be evaluated in this article, or claim that may be made by its manufacturer, is not guaranteed or endorsed by the publisher.

Advantages of publishing in Frontiers

OPEN ACCESS
Articles are free to read for greatest visibility and readership

FAST PUBLICATION
Around 90 days from submission to decision

HIGH QUALITY PEER-REVIEW
Rigorous, collaborative, and constructive peer-review

TRANSPARENT PEER-REVIEW
Editors and reviewers acknowledged by name on published articles

Frontiers
Avenue du Tribunal-Fédéral 34
1005 Lausanne | Switzerland

Visit us: www.frontiersin.org
Contact us: frontiersin.org/about/contact

REPRODUCIBILITY OF RESEARCH
Support open data and methods to enhance research reproducibility

DIGITAL PUBLISHING
Articles designed for optimal readership across devices

FOLLOW US
@frontiersin

IMPACT METRICS
Advanced article metrics track visibility across digital media

EXTENSIVE PROMOTION
Marketing and promotion of impactful research

LOOP RESEARCH NETWORK
Our network increases your article's readership